THE JOURNAL OF CHEMICAL PHYSICS

VOLUME 22 NUMBER 9

SEPTEMBER, 1954

UNIVERSITY OF MICHIGAN

Published by the

AMERICAN INSTITUTE OF PHYSICS

Lancaster, Pa., and New York, N. Y.

THE JOURNAL
OF
CHEMICAL PHYSICS

VOLUME 22, NUMBER 9 SEPTEMBER, 1954

On the Temperature Dependence of the Molecular Polarization of Ammonia

MIKIO KATAYAMA
Department of Chemistry, Faculty of Science, Tokyo University, Bunkyo-ku, Tokyo, Japan
(February 8, 1954)

The molecular polarization of ammonia is calculated quantum mechanically by taking account of the dipole matrix elements of inversion doubling in the first excited state as well as in the ground state of the symmetric deformation vibration. It is found to be reasonable that the dipole moment of this molecule decreases at higher temperatures. The atomic polarization is also calculated and the result, $P_A=0.65$ cc, is in good agreement with the observed value.

INTRODUCTION

IT was confirmed by the analysis of vibrational spectra that the ammonia molecule belongs to the symmetry group C_{3v}, with the nitrogen atom at the top.[1] If the coordinates of all the nuclei of this molecule are inverted at the center of mass, the resulting configuration is also an equilibrium structure for the molecule. It was observed that infrared absorption spectra of the symmetrical deformation vibration of this molecule are composed of doublet lines. This doubling is due to the fact that there are two equilibrium positions for the nitrogen atom at the side of the plane of three hydrogen atoms. The experimental results of the spectra were analyzed in detail by assuming suitable double minimum potential.[2,3] M. Mizushima[4] suggested that the orientation polarization of ammonia is entirely due to the dipole matrix elements of the inversion doubling and succeeded in explaining the experimental facts that the dipole moment measured by the dielectric constants[5] is 1.45 D, while that measured by the molecular beam method[6] is 0.56 D. He did not, however, consider the temperature dependence of the dipole moment. In this article the matrix elements are calculated for the purpose of obtaining the temperature dependence of the dipole moment. At the same time the contribution of the matrix element of the symmetrical deformation vibration 950 cm^{-1} to the atomic polarization is also calculated.

CALCULATION OF DIPOLE MOMENT AND ATOMIC POLARIZATION

If the molecule possesses a permanent dipole moment, there is a contribution to the polarization arising from a partial orientation of the molecule with its dipole moment pointing along the direction of electric field. In the ammonia molecule, which is the pyramidal form with a finite dipole moment, there is no contribution to the orientation polarization mentioned above because of the rapid inversion motion of the nitrogen atom. On the other hand, the transitions between the rotational and vibrational energy states including the inversion doubling give rise to the orientation polarization of the molecule. According to Van Vleck[7] the electric susceptibility due to the transitions between the rotational and vibrational states is given by the following expression:

$$\chi=\frac{N}{3kT}\frac{\sum_{j,m}[\mu(j:j')]^2\exp-W_{nj}/kT}{\sum_{j,m}\exp-W_{nj}/kT}+\tfrac{2}{3}N\sum_{n'(n'\neq n)}\frac{|\mu(n:n')|^2}{h\nu(n:n')},\quad(1)$$

where n, j, m are the vibrational, rotational, and axial quantum numbers, respectively, $\mu(j:j')$ and

[1] G. Herzberg, *Molecular Spectra and Molecular Structure II. Infra-red and Raman Spectra of Polyatomic Molecule* (D. Van Nostrand Company, Inc., New York, 1945), p. 294.
[2] M. F. Manning, J. Chem. Phys. **3**, 136 (1935); F. T. Wall and G. Glockler, J. Chem. Phys. **5**, 314 (1937).
[3] D. M. Dennison and G. E. Uhlenbeck, Phys. Rev. **41**, 313 (1932).
[4] M. Mizushima, J. Phys. Soc. Japan **4**, 11 (1949).
[5] H. E. Watson, Proc. Roy. Soc. (London) **A117**, 43 (1927).
[6] H. Schaeffer, Physik Z. **41**, 89, 98 (1940).
[7] J. H. Van Vleck, *The Theory of Electric and Magnetic Susceptibilities* (Clarendon Press, Oxford, 1932), p. 193.

$\mu(n:n')$ the matrix elements of dipole moment, N Avogadro's number, and W_{nj} the energy of the state (n,j). Here we neglect the excitation of electric states and assume that kT/h is much greater than the rotational frequencies. It was confirmed by Wright and Randall that[8] the frequencies of the inversion doubling are so small that they may be treated with sufficient accuracy as a part of rotational ones. There are four distinct vibrational frequencies for ammonia molecule. Two of the normal coordinates associated with these frequencies belong to the total symmetric representation A_1, the other two belong to the doubly degenerate representation E. These frequencies are listed in Table I. The equation of motion for the totally symmetric vibration contains the changes of N−H bond lengths and that of bond angles. The former corresponds to ν_1, and the latter to ν_2. The totally symmetric deformation vibration, which is to be discussed here with the inversion doubling, belong to A_1. The frequency of ν_1, 3334 cm^{-1}, is so large that it can be ignored for the time being. And inversion motion may be regarded as an extention of the symmetrical deformation vibration.

The double minimum problem of ammonia has been solved by Manning, Glockler,[2,3] and others. Though several forms of potential have been used by them, it has been found that there is little difference in their results. Therefore, a simple method suitable for the calculation of the matrix elements is followed by assuming the potential suggested by Dennison. According to him, the inversion motion is approximately described by the following wave equation:

$$\frac{h^2}{8\pi^2\mu}\frac{d^2\psi(q)}{dq^2}+(E-V)\psi(q)=0, \tag{2}$$

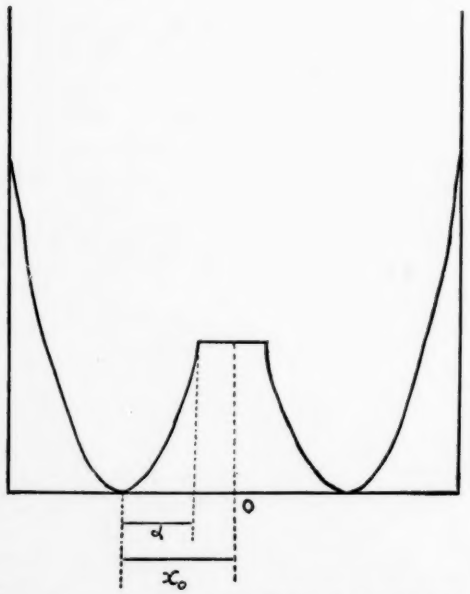

FIG. 1. Dennison's potential function of ammonia.

[8] N. Wright and H. H. Randall, Phys. Rev. 44, 391, (1933).

where μ is the reduced mass, $1/M+1/3m$. The potential V, which is shown in Fig. 1, is expressed as follows:

$$\begin{aligned} 2V/h&=(x-x_0)^2 && x_0-\alpha<x<+\infty \\ &=(x+x_0)^2 && -\infty<x<\alpha-x_0 \\ &=\alpha^2 && \alpha-x_0<x<x_0-\alpha, \end{aligned} \tag{3}$$

where ν_0 is the frequency of the symmetrical deformation vibration. Putting $q=[h/4\pi^2\mu\nu_0]^{\frac{1}{2}}x$, Eq. (2) is reduced to the following expression:

$$\frac{d^2\psi(x)}{dx^2}+2\frac{(E-V)}{h\nu_0}\psi(x)=0. \tag{4}$$

In the regions above $x=x_0-\alpha$, or below $x=\alpha-x_0$, particularly in the neighborhood of the potential minima, the zeroth-order wave functions are approximated by those of a harmonic oscillater,

$$\psi_n=N\exp[-\tfrac{1}{2}(x\pm x_0)^2]H_n(x+x_0), \tag{5}$$

with the eigenvalue,

$$E=(n+\tfrac{1}{2})h\nu_0, \quad (n=0, 1, 2, \cdots), \tag{6}$$

where $H(x)$ is a Hermite polynomial, and N the normalization coefficient.

TABLE I. The normal modes of molecular vibration of ammonia.

Symmetry	Normal frequencies
A_1	3334 cm^{-1}
	960
E	3414 cm^{-1}
	1628

It is easily shown that the zeroth order solution in the middle region of $\alpha-x_0<x<x_0-\alpha$ is a hyperbolic sine or cosine function,

$$\psi=A\cosh ax, \quad \text{or} \quad A\sinh ax, \tag{7}$$

where the constant a is equal to $(V-E)^{\frac{1}{2}}$, the potential V being a constant $\alpha^2h\nu_0/2$ in this region, and E the eigenvalue of energy. The constant A is the normalization coefficient.

Combining these functions we can obtain the wave function in the whole region. The constant a is so chosen that the energy E is equal to that of Eq. (6) obtained in the outer regions. At the same time A is fixed so as to fulfil the conditions of the continuity of the function at $x=x_0-\alpha$ and $x=\alpha-x_0$. For one value of E, two wave functions are obtained according to whether we use the hyperbolic cosine or sine function. The former gives a symmetric state, the latter an antisymmetric one. First-order wave function and energy level may be found by applying the usual method of variation principle. It is obvious that the degenerate energy level in the zeroth-order calculation splits into the symmetric and antisymmetric ones, and a calculated energy level is lower than the zeroth-order

calculated one. But these cumbersome calculations need not be considered, for in order to calculate the transition moments it is sufficient to use the zeroth-order approximation. As for the values of α and x_0, we may use the values, $\alpha=1.930$ and $x_0=3.182$, which were obtained by Dennison from the height of the pyramid and the potential barrier of the inversion doubling. It is supported by the fact that the same values of α and x_0 were obtained within the error of a few percent by the other methods for the solution of the double minimum problem. Thus the wave functions for a few lower states are found to be as follows: the symmetric wave function for $n=0_+$,

$$\psi_{0+}=\begin{cases}25.86A_0\exp[-(x-x_0)^2/2] & x\geq x_0-\alpha\\ A_0\cosh 1.65x & x_0-\alpha\geq x\geq\alpha-x_0;\\ 25.86A_0\exp[-(x+x_0)^2/2] & \alpha-x_0\geq x\end{cases} \tag{8}$$

the antisymmetric wave function for $n=0^-$,

$$\psi_{0-}=\begin{cases}25.05B_0\exp[-(x-x_0)^2/2] & x\geq x_0-\alpha\\ B_0\sinh 1.65x & x_0-\alpha\geq x\geq\alpha-x_0;\\ -25.05B_0\exp[-(x+x_0)^2/2] & \alpha-x_0\geq x\end{cases} \tag{9}$$

the symmetric wave function for $n=1_+$,

$$\psi_{1+}=\begin{cases}-5.42A_1(x-x_0)\\ \quad\times\exp[-(x-x_0)^2/2] & x\geq x_0-\alpha\\ A_1\cosh 0.85x & x_0-\alpha\geq x\geq\alpha-x_0;\\ 5.42A_1(x+x_0)\\ \quad\times\exp[-(x+x_0)^2/2] & \alpha-x_0\geq x\end{cases} \tag{10}$$

the antisymmetric wave function for $n=1_-$,

$$\psi_{1-}=\begin{cases}-4.27B_1(x-x_0)\\ \quad\times\exp[-(x-x_0)^2/2] & x\geq x_0-\alpha\\ B_1\sinh 0.85x & x_0-\alpha\geq x\geq\alpha-x_0;\\ -4.25B_1(x+x_0)\\ \quad\times\exp[-(x+x_0)^2/2] & \alpha-x_0\geq x.\end{cases} \tag{11}$$

The constants A_1, A_0, B_1, B_0 are the normalization coefficients. The calculation of the matrix elements for the transitions

$$\mu_{ij}=\epsilon\int_{-\infty}^{+\infty}\psi_i^*x\psi_j dx \tag{12}$$

is easily performed by use of these wave functions. The results are as follows*:

$$\begin{aligned}\mu_{0+0-}&=3.16\epsilon\\ \mu_{1+1-}&=2.90\epsilon\\ \mu_{0+1-}&=0.39\epsilon\\ \mu_{0-1+}&=0.43\epsilon,\end{aligned} \tag{13}$$

where ϵ denotes the effective charge. Needless to say, μ_{1+1+}, μ_{1-1-}, μ_{0+0+}, and μ_{0-0-} vanish. According to Eq. (1), the dipole moment of ammonia molecule is expressed in terms of the matrix elements by the following equation:

$$\mu^2=k^2(\mu^2{}_{0+0-}e^{-W_0/kT}+\mu^2{}_{1+1-}e^{-W_1/kT}+\cdots)/\times(e^{-W_0/kT}+e^{-W_1/kT}+\cdots). \tag{14}$$

This equation has an unknown constant k, in addition to an effective charge ϵ. If the value of the product $k\epsilon$ is fixed to be 3.87×10^{-10} e.s.u. cm by referring to an observed value of the dipole moment at a certain temperature 1.46 D at 27°C, the moment at all other temperatures are directly calculated from Eq. (14).† The calculated dipole moment and orientation polarization are listed in Table II.

TABLE II. The temperature dependence of dipole moment and orientation polarization of ammonia.

T°K	200	300	400	500	600	700	800	900
P_0T	13022	12966	12953	12891	12860	12745	12696	12631
P_0cc	65.11	43.32	32.39	25.79	21.38	18.21	15.86	14.01
μD	1.46	1.46	1.45	1.45	1.45	1.44	1.44	1.44

According to Eq. (1) the contribution to the atomic polarization of the dipole matrix elements of molecular vibration is expressed as follows:

$$P_A=\frac{8}{9}\pi N\sum_{n'(n')\neq n}\frac{|\mu(n,n')|^2}{h\nu(n,n')}=\frac{8}{9}\frac{\pi N}{h\nu_0}[\mu_{0+1-}{}^2+\mu_{0-1+}{}^2]. \tag{15}$$

The magnitude of P_A due to the symmetric deformation vibration $\nu_2=950$ cm^{-1} is found to be 0.65 cc by this equation. It is easily shown that the contribution of other normal frequencies, $\nu_1=3334$ cm^{-1}, $\nu_2=3314$ cm^{-1}, and $\nu_4=1628$ cm^{-1} are all negligibly small.

COMPARISON WITH THE EXPERMENTAL RESULTS

Many an experimental datum is available for the dipole moment of ammonia molecule. It was observed by Watson[5] that the moment is 1.51 D by the measurement of dielectric constants at the temperature between −47°C and 16°C, and 1.46 D at temperatures between 16°C and 100°C. This represents a downward tendency of the dipole moment with rise of temperature. But the temperature dependence of the observed dipole moment is so small and the experimental error takes part so seriously that it cannot safely be said whether the experimental results accord with the computation. The accurate measurement was carried out by De Bruyne and Smyth.[9] The relation between PT and T calculated by the use of their results is dotted in Fig. 2, where P denotes the total polarization at the temperature T°K. A relation $PT=AT+P_0T$ is also indicated by the curve (a), where P_0 is the calculated orientation

* The dimension of cm is used as a unit of length.

† It is assumed that the $k\epsilon$ is the same through the states.

[9] M. A. De Bruyne and C. P. Smyth, J. Am. Chem. Soc. **57**, 1203 (1935).

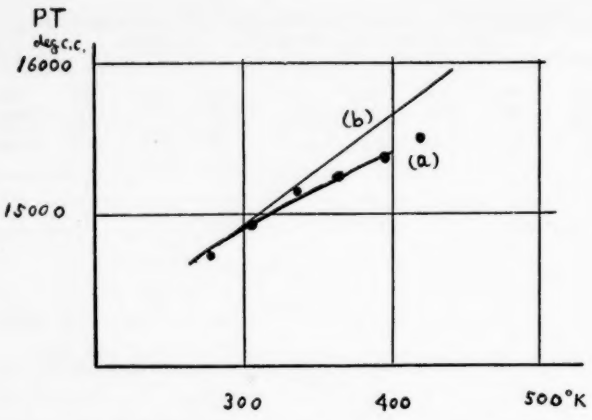

FIG. 2. The relation between PT and T of ammonia from the experimental results by Bruyne and Smyth. ●: observed value, (a): calculated curve.

polarization and A is a constant which is determined to agree with the observed value of polarization at 35°C, i.e., $A=6.13$ cc. The relation $PT\sim T$ would be linear as shown by a tangent (b) of the curve (a) provided that the dipole moment and A are independent of temperature. Actually it deviates from a straight line, indicating clearly the decrease in the dipole moment with rise of temperature. From the recent experimental results of Itterbeek and De Clippeleir[10] the same relation was obtained as shown in Fig. 3. The calculated curve is drawn so as to coincide with the observed value at 5.8°C. The deviation of the observed PT value from the straight line (b) is originated from the matrix elements of the transition between the symmetric and antisymmetric states belonging to the first excited states of the symmetrical deformation vibration. In fact, if we take into consideration the symmetric and antisymmetric states of the vibrational ground state alone, we are unable to get the temperature dependence of the dipole moment, though the finite magnitudes of the moment itself are obtained just as shown by M. Mizushima.

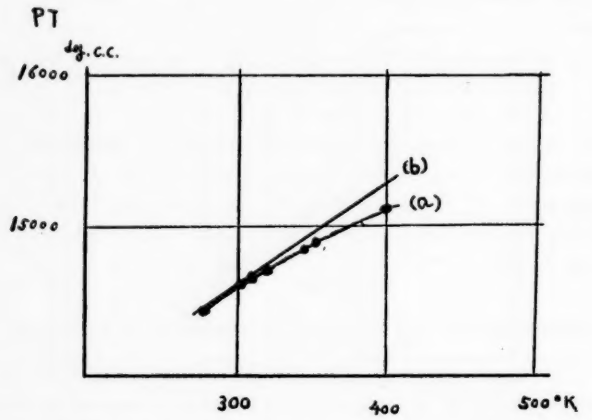

FIG. 3. The relation between PT and T of ammonia at 1 atm from the experimental results of Itterbeek and De Clippeleir. ● observed values. (a) calculated curve.

The dipole moment in the gaseous state was also observed by C. T. Zahn[11] and by Uhling, Keyes, and Kirkwood.[12] Their experimental values also deviate from the straight line (b) in Figs. 2 or 3. The smooth relation such as the curve (a) or dotted points in Fig. 2 or 3 were not obtained because the temperature ranges of their experiments were not suitable. Yet their results clearly showed that the higher the temperature the smaller the dipole moment.

The essential agreement between the observed and calculated values mentioned above indicates that abnormality of the temperature dependence of polarization of ammonia is mainly due to the matrix elements of the inversion doubling in the first excited state of the symmetrical deformation vibration.

The atomic polarization calculated above is also in accordance with the value 0.1∼0.5 cc obtained by Smyth and others.[9] As already stated, other vibrational frequencies of ammonia molecule are so high that these vibrations make far less contribution to atomic polarization.

The author is grateful to Professor Yonezo Morino and Assistant Professor Masashi Yasumi for their valuable suggestions and kind advice on this problem.

[10] A. van Itterbeek and De Clippeleir, Physica **14**, 349 (1948).
[11] C. T. Zahn, Phys. Rev. **27**, 455 (1926).
[12] H. H. Uhling and F. G. Kirkwood, J. Chem. Phys. **1**, 155 (1933).

THE JOURNAL OF CHEMICAL PHYSICS VOLUME 22, NUMBER 9 SEPTEMBER, 1954

Variation in the Quadrupole Coupling Constant with Vibrational State in the Methyl Halides*

J. KRAITCHMAN† AND B. P. DAILEY
Department of Chemistry, Columbia University, New York 27, New York
(Received January 4, 1954)

The $J=0\rightarrow1$ microwave rotational transitions in the states $v=1$ of the vibrations $\nu_3(a_1)$ and $\nu_6(e)$ in methyl chloride and the state $v=1$ of the vibration $\nu_3(a_1)$ in methyl bromide have been studied. The quadrupole coupling constants eqQ of chlorine and bromine in these states were determined. These were compared with the values determined for the ground state. No variation of the quadrupole coupling constants with vibrational state was observed. The accuracy of the measurements requires the variation of eqQ with vibrational state to be less than 0.07 percent in methyl bromide. The rotational constants and vibration-rotation constants for these states were also determined.

INTRODUCTION

THE problem of the nature of the changes of molecular electronic structure with a change in vibrational state is one of considerable general interest. Since variations in the quadrupole coupling constant with vibrational state are indicative of changes in the molecular electronic structure, a study of the methyl halides was undertaken in order to ascertain the magnitude of these variations.

In a recent molecular beam study of KCl, values of the quadrupole coupling constant for chlorine in several vibrational states were determined.[1] The quadrupole coupling constant eqQ was found to increase by approximately a factor of two in going from one vibrational state to the next higher one. While the absolute value of eqQ is very small in KCl, it has been suggested that comparable percentage variations in eqQ might also be observed in the large quadrupole coupling constants exhibited by more covalently bonded molecules. In fact, on the basis of the KCl results and the observed difference in eqQ for CH_3Cl and CD_3Cl in the ground state, Duchesne[2] has concluded that a rather large change in the quadrupole coupling constant of CH_3Cl with vibrational state would be expected.

Data on the $J=0\rightarrow1$ rotational transitions of methyl chloride[3] and methyl bromide[4] in the ground state have previously been reported. In this investigation the $J=0\rightarrow1$ transitions of CH_3Cl in the states $v=1$ of the vibrations $\nu_3(a_1)$ and $\nu_6(e)$, and in CH_3Br in the state $v=1$ of the vibration $\nu_3(a_1)$ have been observed.[5]

EXPERIMENTAL PROCEDURE

The instrument used in this investigation was a Stark modulation spectrometer[6] employing square wave modulation at 85 kc and phase sensitive detection. A sensitivity permitting the detection of a minimum absorption coefficient of approximately 2×10^{-9} cm^{-1} was obtained using a geared-down motor to drive the klystron resonator tuning screw and a recording milliammeter to observe the spectrometer output. For frequency measurements the klystron was electronically tuned by applying a sawtooth voltage to its reflector. The output was displayed on an oscilloscope; a sensitivity of approximately 4×10^{-9} cm^{-1} was obtained at a sweep rate of about 1 cps.

Frequency measurements were made using a frequency standard[7] which was monitored against WWV. In making frequency measurements minimum filtering of the output of the phase sensitive detector consistent with good signal to noise ratio was used. All frequency measurements were made by first sweeping over the line from low to high frequency and then from high to low frequency. It was found that the average obtained from such measurements effectively eliminated any errors due to different time delays in the spectrometer and frequency standard systems and any distortion of the line introduced by the small amount of filtering used.

THE SPECTRA

The $J=0\rightarrow1$ transition of the symmetric rotors CH_3Cl and CH_3Br in the ground state consists of three hyperfine components. The splitting of the transition into hyperfine components is due to the interaction between the nuclear quadrupole moment of the halogen nucleus and the electric field produced by the charges external to the halogen nucleus.[8] Except for reduced intensity, transitions in the excited vibrational states are qualitatively similar to those in the ground state.

In methyl chloride, because of the small quadrupole

* Work supported in part by a Signal Corps contract and a grant from the Research Corporation.
† Present address: Westinghouse Research Laboratories, East Pittsburgh, Pennsylvania.
[1] Lee, Fabricand, Carlson, and Rabi, Phys. Rev. **91**, 1395 (1953).
[2] J. Duchesne, J. Chem. Phys. **20**, 1804 (1952).
[3] Gordy, Simmons, and Smith, Phys. Rev. **74**, 243 (1948).
[4] A. H. Sharbaugh and J. Mattern, Phys. Rev. **75**, 1102(L) (1949).
[5] G. Herzberg, *Infrared and Raman Spectra of Polyatomic Molecules* (D. Van Nostrand Company, Inc., New York, 1945), pp. 312 ff.
[6] R. H. Hughes and E. B. Wilson, Jr., Phys. Rev. **71**, 562 (L) (1947); A. H. Sharbaugh, Rev. Sci. Instr. **21**, 120 (1950).
[7] L. C. Hedrick, Rev. Sci. Instr. **24**, 565 (1953).
[8] J. Bardeen and C. H. Townes, Phys. Rev. **73**, 97 (1948).

TABLE I. Hyperfine structure of the $J=0\rightarrow1$, $K=0$ rotational transition in CH_3Cl^{35}.

State	Transition F_i	Transition F_f	Frequency (Mc) Observed	Frequency (Mc) Calculated	eqQ (Mc)	ν_0 (Mc)	Intensity (cm^{-1})
$v=0$	3/2	1/2	26604.38±0.05	26604.37	−74.77±0.10	26585.68±0.03	2.4×10^{-6}
	3/2	5/2	26589.40	26589.42			7.1
	3/2	3/2	26570.73	26570.72			4.7
$v_3=1$	3/2	1/2	26373.96±0.05	26373.97	−74.87±0.10	26355.25±0.03	0.7×10^{-7}
	3/2	5/2	26359.01	26359.00			2.1
	3/2	3/2	26340.27	26340.28			1.4
$v_6=1$	3/2	1/2	26506.38±0.10	26506.38	−74.89±0.20	26487.65±0.05	2.2×10^{-8}
	3/2	5/2	26491.39	26491.40			5.4
	3/2	3/2	26472.68	26472.68			3.6

coupling constant, the spectrum is quite simple. At approximately 26.6 kMc three closely spaced lines due to the transition in the ground state of CH_3Cl^{35} occur. At approximately 0.1 kMc and 0.3 kMc lower, two other sets of three closely spaced lines occur due to transitions in the excited vibrational states $\nu_6(e)$ and $\nu_3(a_1)$. A similar pattern is repeated at a still lower frequency for CH_3Cl^{37}.

Identification of the lines was verified by intensity measurements at room and dry ice temperatures. Enhancement of the intensity of the ground-state transition and disappearance of the excited-state transitions was observed at dry ice temperature. Relative intensity measurements at room temperature gave results which agreed with the theoretical values within the precision of the measurements (±20 percent).

Because of the larger quadrupole coupling constant in CH_3Br the hyperfine components of the two isotopic species of the molecule in the ground and excited states of the transition $J=0\rightarrow1$ are intermingled. While this makes the interpretation of the spectrum somewhat more difficult than in CH_3Cl, identification could still be made in the manner described above for CH_3Cl. However, one complication did arise: the $F=3/2\rightarrow3/2$ component in the state $v=1$ of the vibration $\nu_3(a_1)$ of CH_3Br^{79} occurred very close to the $F=3/2\rightarrow5/2$ component in the ground state of CH_3Br^{79}. In order to completely resolve the two lines it was necessary to reduce the sample pressure in the wave-guide cell to such an extent that the signal to noise ratio of the excited state line became quite poor. As a result the frequency measurement of this line is less accurate than the others.

RESULTS

In addition to measuring the frequencies of the transitions in the excited vibrational states of CH_3Cl and CH_3Br, the ground-state transitions have been remeasured. The results of the measurements on CH_3Cl and CH_3Br are summarized in Tables I to IV. Included are the calculated value of the quadrupole coupling constant eqQ, the hypothetical unsplit frequency ν_0, and the theoretical intensities of the transitions assuming a half-width of 25 Mc at 1 mm pressure. The agreement between the observed and calculated frequencies is in all cases within the experimental accuracy.

The quadrupole coupling constant is such a sensitive function of the measured frequencies that even a small change in these frequencies is reflected in a relatively large change in eqQ. This accounts for the rather sizeable difference between the ground-state values reported here and the values of $eqQ(Cl^{35})=-75.13$ Mc and $eqQ(Cl^{37})=-59.03$ Mc reported by Gordy, Simmons, and Smith.[3] The values of $eqQ(Cl^{35})=-74.77$ Mc and $eqQ(Cl^{37})=-58.92$ Mc reported by Geschwind, Gun-

TABLE II. Hyperfine structure of the $J=0\rightarrow1$, $K=0$ rotational transition in CH_3Cl^{37}.

State	Transition F_i	Transition F_f	Frequency (Mc) Observed	Frequency (Mc) Calculated	eqQ (Mc)	ν_0 (Mc)	Intensity (cm^{-1})
$v=0$	3/2	1/2	26191.00±0.05	26190.99	−58.93±0.10	26176.26±0.03	0.7×10^{-6}
	3/2	5/2	26179.18	26179.20			2.2
	3/2	3/2	26164.48	26164.47			1.5
$v_3=1$	3/2	1/2	25966.37±0.05	25966.37	−58.89±0.10	25951.65±0.03	2.1×10^{-8}
	3/2	5/2	25954.60	25954.59			6.4
	3/2	3/2	25939.87	25939.87			4.4
$v_6=1$	3/2	1/2	26094.56±0.10	26094.57	−58.76±0.20	26079.88±0.05	0.5×10^{-8}
	3/2	5/2	26082.83	26082.82			1.7
	3/2	3/2	26068.83	26068.82			1.1

TABLE III. Hyperfine structure of the $J=0\rightarrow1$, $K=0$ rotational transition in CH_3Br^{79}.

State	Transition F_i	Transition F_f	Frequency (Mc) Observed	Frequency (Mc) Calculated	eqQ (Mc)	ν_0 (Mc)	Intensity (cm^{-1})
$v=0$	3/2	1/2	18992.47±0.05	18992.48	577.15±0.10	19136.41±0.03	0.5×10^{-6}
	3/2	5/2	19107.72	19107.70			1.6
	3/2	3/2	19252.11	19252.12			1.1
$v_3=1$	3/2	1/2	18846.88±0.05	18846.90	577.32±0.20	18990.87±0.05	2.9×10^{-6}
	3/2	5/2	18962.19±0.05	18962.15			8.6
	3/2	3/2	19106.60±0.10	19106.62			5.7

ther-Mohr, and Townes[9] are in excellent agreement with the values obtained here.

The measurements reported here on the ground-state transitions of CH_3Br are in satisfactory agreement with the values of $eqQ(Br^{79})=577.3$ Mc and $eqQ(Br^{81})=482.4$ Mc reported by Sharbaugh and Mattern.[4] Because of the large quadrupole coupling constant in CH_3Br, second-order quadrupole effects must be considered.[10] The results on CH_3Br reported here include both first- and second-order effects.

In Tables V and VI the various molecular constants obtained from the data in Tables I to IV are summarized. Listed are B_{v_i}, the rotational constant of the molecule in the state v_i of the vibration ν_i, and the vibration-rotation interaction constant α_i^B where

$$B_{v_i}=B_e-\Sigma_i\alpha_i^B(v_i+d_i/2).$$

The B_e is the equilibrium rotational constant and the d_i are the degeneracies of the vibrations ν_i.

It is well known that rotational energy levels in degenerate vibrational states can be perturbed by Coriolis interactions.[11] While the rotational levels in the degenerate vibrational state $v_6=1$ with $K=0$ cannot suffer any Coriolis-type splitting or l-type doubling, these levels can be shifted by this interaction. However, it can be shown that the levels with $J=0$ and 1 with $K=0$ are completely untouched by this interaction.[11] Consequently, the equation given above can also be used to obtain the vibration-rotation constant for the degenerate vibrational state $\nu_6(e)$.

The results obtained on the quadrupole coupling constants indicate no variation with vibrational state within the precision of measurements. In CH_3Br any such variation must be less than 0.07 percent, while in CH_3Cl, because of the smaller quardupole coupling constant, a variation of as much as 0.4 percent cannot be ruled out.

DISCUSSION

The results of this study indicate that the changes in the molecular electronic structure of CH_3Cl and CH_3Br with change in vibrational state are quite small. In CH_3Br the change in eqQ must be less than 0.07 percent in going from the ground state to the first excited state of the vibration ν_3. Although Duchesne has predicted a considerably larger change, the following discussion is designed to show that these results are in reasonable agreement with other data on the subject.

In a number of molecular beam studies on diatomic molecules, a variation in eqQ with vibrational state has been observed. In $TlCl^{35}$ and $TlCl^{37}$ the quadrupole coupling constants of Cl^{35} and Cl^{37} were found to be -15.788 Mc and -12.425 Mc in the ground state and increased in absolute magnitude by about $\frac{1}{2}$ percent from one vibrational state to the next higher one.[12] On the other hand in KCl^{35} the percentage variation in eqQ of Cl^{35} with vibrational state was found to be considerably larger.[1] Values of >-0.040, -0.075, -0.237, and -0.393 Mc were observed for the states $v=0$, 1, 2, and 3, respectively. In KBr^{79} the quadrupole coupling

TABLE IV. Hyperfine structure of the $J=0\rightarrow1$, $K=0$ rotational transition in CH_3Br^{81}.

State	Transition F_i	Transition F_f	Frequency (Mc) Observed	Frequency (Mc) Calculated	eqQ (Mc)	ν_0 (Mc)	Intensity (cm^{-1})
$v=0$	3/2	1/2	18943.38±0.05	18943.39	482.16±0.10	19063.68±0.03	0.5×10^{-6}
	3/2	5/2	19039.69	19039.68			1.6
	3/2	3/2	19160.30	19160.31			1.1
$v_3=1$	3/2	1/2	18798.72±0.05	18798.73	482.21±0.10	18919.02±0.03	2.8×10^{-6}
	3/2	5/2	18895.04	18895.02			8.4
	3/2	3/2	19015.66	19015.67			5.6

[9] Geschwind, Gunther-Mohr, and Townes, Phys. Rev. **81**, 288(L) (1951).
[10] J. Bardeen and C. H. Townes, Phys. Rev. **73**, 627 (1948).
[11] H. H. Nielsen, Revs. Modern Phys. **23**, 90 (1951).
[12] Carlson, Lee, and Fabricand, Phys. Rev. **85**, 784 (1952); H. J. Zeiger and D. L. Bolef, Phys. Rev. **85**, 788 (1952).

TABLE V. Molecular constants of CH_3Cl.

Constant (Mc)	CH_3Cl^{35}	CH_3Cl^{37}
$B_{v=0}$	13292.84±0.03	13088.13±0.03
$B_{v_3=1}$	13177.63±0.03	12975.82±0.03
$B_{v_6=1}$	13243.83±0.05	13039.94±0.05
α_3^B	115.21±0.05	112.30±0.05
α_6^B	49.01±0.06	48.19±0.06

constant of Br^{79} was found to be 10.244 Mc in the ground state and increased by about 1 Mc or 10 percent with vibrational state.[13]

Aside from the diatomic molecules the only other reported variation of eqQ with vibrational state is from the microwave study of Tentenbaum of the linear triatomic molecule cyanogen bromide.[14] Rotational transitions were observed for this molecule in both the ground state and the first excited state of the degenerate vibration ν_2. From an analysis of the hyperfine structure of these transitions Tentenbaum reported values of 686.06 Mc for the quadrupole coupling constant of Br^{79} in the ground state and 682.84 Mc for the excited vibrational state. These values result in a variation of over 3 Mc in eqQ in going from the ground to the first excited vibrational state. However, the reality of this rather large variation in eqQ with vibrational state is open to some question for the following reason. For the transitions occuring in the excited vibrational state a linear variation was observed in the l-type doublet splitting with the bromine quadrupole correction. To satisfactorily account for this variation of the doublet splitting it appears necessary to introduce certain additional terms in the quadrupole interaction energy which take into account the fact that the electric field gradient is not axially symmetric when the molecule is bent by the vibration. Since Tetenbaum neglected to include these additional terms in analyzing the hyperfine structure of the transitions occuring in the excited vibrational state, it is incorrect to interpret the value of 682.84 Mc as the bromine quadrupole coupling constant for the excited vibrational state. Inclusion of these additional terms leads to results which suggest that the excited state value of eqQ is probably not appreciably different from the ground-state value.

In order to understand the significance of an observed change in eqQ it is necessary to remember that this quantity is primarily determined by the number of electrons in p type valence orbitals.[15] The observed changes in eqQ presumably arise from the removal of a small fraction of an electron charge from a p orbital in going from the ground state to an excited vibrational state. The fraction of an electron charge removed from a valence p orbital of the halogen atom is just the ratio of the change in the quadrupole coupling constant with vibrational state to the quadrupole coupling constant of a single unbalanced p electron in a valence orbital. The fraction of an electron charge removed is approximately 0.06 percent for TlCl, 0.1 percent for KBr, and 0.02 percent for KCl. In all of these cases it may be seen that a change in vibrational state produces only a very small perturbation of the molecular electronic structure. Within the accuracy of this investigation such small perturbations of the electronic configurations of the methyl halides would probably produce no observable variation of eqQ with vibrational state.

The quadrupole coupling constants of various isotopic species of a molecule provide another important source of information, since observed differences among species with the same halogen nucleus presumably arises from zero-point vibrational effects in the molecule. A considerable body of data on the various isotopic

TABLE VI. Molecular constants of CH_3Br.

Constant (Mc)	CH_3Br^{79}	CH_3Br^{81}
$B_{v=0}$	9568.20±0.03	9531.84±0.03
$B_{v_3=1}$	9495.43±0.05	9454.51±0.03
α_3^B	72.77±0.06	77.32±0.05

[13] Fabricand, Carlson, Lee, and Rabi, Phys. Rev. **91**, 1403 (1953).
[14] S. J. Tetenbaum, Phys. Rev. **86**, 440 (1952).

TABLE VII. Quadrupole coupling constants of various isotopic species of CH_3Cl.

Molecule	State	eqQ (Mc)	Reference
$C^{12}H_3Cl^{35}$	$v=0$	−74.77±0.10	a
	$v_3=1$	−74.87±0.10	a
	$v_6=1$	−74.89±0.20	a
$C^{13}H_3Cl^{35}$	$v=0$	−74.88	b
$C^{12}D_3Cl^{35}$	$v=0$	−74.41	c
$C^{12}H_3Cl^{37}$	$v=0$	−58.93±0.10	a
	$v_3=1$	−58.89±0.10	a
	$v_6=1$	−58.76±0.20	a
$C^{13}H_3Cl^{37}$	$v=0$	−58.95	b
$C^{12}D_3Cl^{37}$	$v=0$	−58.58	c

[a] This paper.
[b] Matlack, Glockler, Bianco, and Roberts, J. Chem. Phys. **18**, 332 (1950).
[c] J. W. Simmons and J. H. Goldstein, J. Chem. Phys. **20**, 122 (1952).

TABLE VIII. Quadrupole coupling constants of various isotopic species of CH_3Br.

Molecule	State	eqQ (Mc)	Reference
$C^{12}H_3Br^{79}$	$v=0$	577.15±0.10	a
	$v_3=1$	577.32±0.20	a
$C^{13}H_3Br^{79}$	$v=0$	577.0	b
$C^{12}D_3Br^{79}$	$v=0$	574.6	c
$C^{12}H_3Br^{81}$	$v=0$	482.16±0.10	a
	$v_3=1$	482.21±0.10	a
$C^{13}H_3Br^{81}$	$v=0$	482.0	b
$C^{12}D_3Br^{81}$	$v=0$	479.8	c

[a] This paper.
[b] J. W. Simmons, Emory University (private communication).
[c] J. W. Simmons and J. H. Goldstein, J. Chem. Phys. **20**, 122 (1952).

[15] C. H. Townes and B. P. Dailey, J. Chem. Phys. **17**, 782 (1949).

species of the methyl halides is available; these data are summarized in Tables VII and VIII. It is of interest to note that the variation in eqQ with isotopic species is quite similar for all four halogen nuclei: a substitution of C^{12} for C^{13} produces no observable change in eqQ while substitution of deuterium for hydrogen decreases the absolute magnitude of eqQ by about 0.4 percent.

From the observed rotational constants of the various isotopic species of the methyl halides, best values of the structural parameters were obtained by assuming a shortening of the C−H bond by 0.009 A and an increase in the H−C−H angle by 12′ in the deuterated species.[16] Carbon mass changes were assumed to have negligible effect on the structural parameters. These assumptions correlate quite nicely with the change in eqQ observed on deuteration of the molecule and the lack of change on substitution of C^{13} for C^{12}; they do not require any large variation of eqQ with vibrational state such as Duchesne has predicted.

[16] Miller, Aamodt, Dousmanis, Townes, and Kraitchman, J. Chem. Phys. **20**, 1112 (1952).

THE JOURNAL OF CHEMICAL PHYSICS VOLUME 22, NUMBER 9 SEPTEMBER, 1954

Influence of a Magnetic Field on the Microwave Dielectric Constant of a Liquid Crystal*

E. F. Carr and R. D. Spence
Department of Physics, Michigan State College, East Lansing, Michigan

(Received September 29, 1953)

The real and imaginary parts of the complex dielectric constant of the liquid crystal and normal liquid phases of *para*-azoxyanisole and *para*-azoxyphenetole have been measured at a frequency of 15 300 Mc. A static magnetic field applied to the sample is capable of producing large changes in the observed values of the complex dielectric constant. The extent of this effect depends on the orientation and intensity of the static magnetic field and on the temperature.

INTRODUCTION

THE compounds *para*-azoxyanisole and *para*-azoxyphenetole are simple examples of substances which exhibit a liquid crystal phase.[1] As is the case with several other of the compounds which possess such a phase, their liquid crystal phases are characterized by the fact that they flow like ordinary liquids but in the presence of a static electric or magnetic field they show the anisotropy commonly associated with the crystalline state. This anisotropy can be partially understood by reference to the structure of the free molecules shown in Table I. The orienting effect of a magnetic field presumably arises from the diamagnetic anisotropy[2] of the benzene rings. The permanent electric dipole moment[3] of the molecule is transverse to the long axis of the molecule and appears to originate largely in the central azoxy group. The direction of the greatest polarizability is along the long axis of the molecule and accounts for the possibility of orienting these compounds by a static electric field. However, it does not appear possible to derive all the properties of these substances from the structure of the free molecule. It is generally considered necessary to introduce a postulate to the effect that in the liquid crystal phase the molecules are bound together in swarms[4] of the order of a million molecules, and that while in the individual swarms the orientation of the molecules is essentially identical, the orientation varies from swarm to swarm. While the concept of swarms suffers from lack of *direct* experimental verification and an adequate theoretical basis it has proved convenient in interpreting many experiments. It should be pointed out that there are other models[5] of the liquid crystal phase which have been successful in explaining many experiments.

As might be inferred from the previous remarks, the dielectric constant of the liquid crystal phase of these compounds can be influenced by the application of an external static magnetic or electric field. Thus, Jezewski[6] and Kast[7] have shown that a magnetic field applied parallel to the measuring electric field in a parallel plate condenser filled with these compounds produces a decrease of the dielectric constant. If the magnetic field is applied perpendicular to the electric field, no effect is observed. Maier[8] has studied the effect of a static magnetic field on the dielectric constant of a

* Submitted by E. F. Carr in partial fulfillment of requirements for the degree of Doctor of Philosophy in the Graduate School of Michigan State College. A preliminary report of these results was made at the January 1953 meeting of the American Physical Society [Phys. Rev. **90**, 339 (1953)].

[1] For a general discussion of the liquid crystal phase the reader is referred to the following books and papers. R. Schenck, *Kristalline Flüssigkeiten* (Leipzig, 1905); Liquid Crystals and Anisotropic Melts, Trans. Faraday Soc. **29**, 881–1085 (1933).

[2] P. Selwood, *Magnetochemistry* (Interscience Publishers Inc., New York, 1943).

[3] J. Errera, Physik. Z. **29**, 426 (1928).

[4] L. Ornstein and W. Kast, Trans. Faraday Soc. **29**, 931–944 (1933).

[5] H. Zocher, Trans. Faraday Soc. **29**, 945 (1933).

[6] M. Jezewski, J. phys. radium. **5**, 59–64 (1924).

[7] W. Kast, Ann. Physik **73**, 145–160 (1924).

[8] W. Maier, Z. Naturforsch. **2a**, 458–465 (1947).

TABLE I.

COMPOUND	STRUCTURE	MELTING POINT	CLEARING POINT
p-azoxyanisole	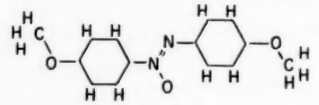	118°C	135.8°C
p-azoxyphenetole	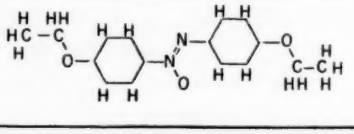	137°C	168°C

homologous series of compounds which exhibit the liquid crystal phase and has correlated the results with the electric dipole moments and polarizabilities. Jezewski[9] has found that a static electric field applied parallel to the measuring field decreases the dielectric constant of *para*-azoxyanisole and *para*-azoxyphenetole. Ornstein and Kast[4] have shown that in the absence of any external field the dielectric loss of *para*-azoxyanisole has a maximum at frequencies the order of one megacycle. The frequency at which the maximum loss was observed increased rapidly with temperature. A very striking experiment at optical frequencies is that of Pellet and Chatelain[10] who by orienting liquid crystals by mechanical means were able to form them into what behaved essentially like uniaxial crystals and were therefore able to measure the index of refraction for the ordinary and extraordinary rays with considerable precision. They found that the difference between the two indices completely disappeared at the transition from the liquid crystal to the normal liquid phase.

EXPERIMENTAL

Figure 1 shows a block diagram of the experimental setup. The klystron was a Varian X-12 which has a range from 12 400 Mc to 17 500 Mc. All the measurements reported in this paper were made at 15 300 Mc. The tube was modulated by a 1000-cycle square wave from a Hewlett-Packard Power Supply. The microwave power was transmitted through the attenuator to the second directional coupler where most of power was absorbed. A portion of the power was coupled into the cell containing the liquid crystal. By using a directional coupler in conjunction with the attenuator, the klystron was well isolated from the cell. The cell was a section of coin silver wave guide (inside dimensions 0.311 in. ×0.622 in.) with a thin mica window at the bottom, and was fitted with a movable short circuiting plunger. Power reflected from the cell was measured by a crystal detector connected to a recorder or tuned amplifier.

The cell was placed between the pole pieces of an electromagnet, and the entire assembly of the cell and magnet was immersed in a constant temperature bath. Peanut oil proved to be a convenient liquid for the bath. Oil was prevented from seeping into the cell through the flange at the bottom of the cell by baking on a coat of clear glyptal.

The real part of the dielectric constant was obtained by moving the short circuiting plunger with a micrometer screw, and thus determining the wavelength inside the cell. The imaginary part of the dielectric constant was obtained from the amplitude of the reflection maxima. The results for the imaginary part of the dielectric constant of *para*-azoxyanisole were further checked by measuring the transmission through a

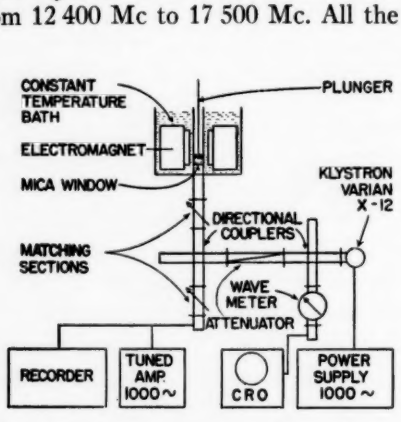

FIG. 1. Block diagram of experimental setup.

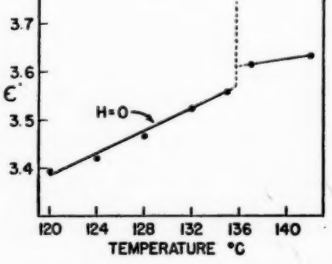

FIG. 2. Temperature dependence of the real part of the complex dielectric constant in a magnetic field of 2000 gauss parallel to the microwave electric field and in zero field for *para*-azoxyanisole. Results for ϵ' with a magnetic field of 2000 gauss perpendicular to the microwave field were found to be almost the same as for zero field. The liquid crystal range is 118–135.8°C.

[9] M. Jezewski, Z. Physik **51**, 159–164 (1928).
[10] O. Pellet and P. Chatelain, Bull. Soc. franc. Mineral **73**, 154–172 (1950).

section of sample. This was accomplished by replacing the plunger with a matched detector.

RESULTS AND DISCUSSIONS

A. Dielectric Constant—ϵ'

Figures 2 and 3 show the temperature dependence of the real part of the dielectric constant (in cgs units) of *para*-azoxyanisole and *para*-azoxyphenetole in zero magnetic field and in a field of 2000 gauss parallel to the microwave electric field. The error in measurement of ϵ' for $H=0$ and for $H=2000$ gauss is estimated at ± 0.2 percent and ± 0.1 percent, respectively, and the error in the temperature is ± 0.5°C. Results for a field of 2000 gauss perpendicular to the microwave electric field indicate that to within the experimental error ϵ' for this situation is indistinguishable from that obtained in zero field. Thus in our case the dielectric constant in a parallel magnetic field exceeds that in a perpendicular field. This situation is exactly opposite to that found by Jezewski[6] in his measurements of the low-frequency dielectric constant. Maier[8] has interpreted Jezewski's results as indicating that the contribution to the low-frequency dielectric constant from the permanent electric dipole moment, which is perpendicular to the axis of the molecule, is greater than the contribution from the induced polarization along the axis of the molecule. Our experiment appears to indicate that at microwave frequencies the induced polarization yields the predominant effect. The dielectric constant of the normal liquid phase in contrast to the liquid crystal phase shows no observable dependence on the magnetic field. This is in agreement with the optical measurement of Pellett and Chatelain[10] in that they observed no anisotropy for the index of refraction in the normal liquid phase.

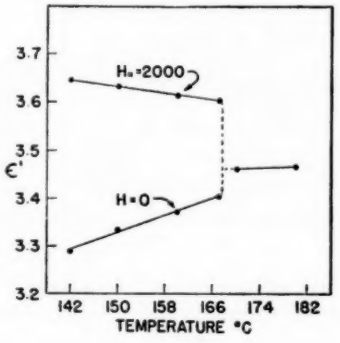

FIG. 3. Temperature dependence of the real part of the complex dielectric constant in a magnetic field of 2000 gauss parallel to the microwave electric field and in zero field for *para*-azoxyphenetole. The liquid crystal range is 138–168°C.

B. Dielectric Loss—ϵ''

As is shown in Fig. 4, the dielectric loss of the liquid crystal phase of *para*-azoxyanisole decreases in a static magnetic field parallel to the microwave electric field and increases if the magnetic field is perpendicular to the electric field. The estimated error in ϵ'' is 2 percent in this plot. A similar situation prevails for the liquid crystal phase of *para*-azoxyphenetole. Figure 5 shows

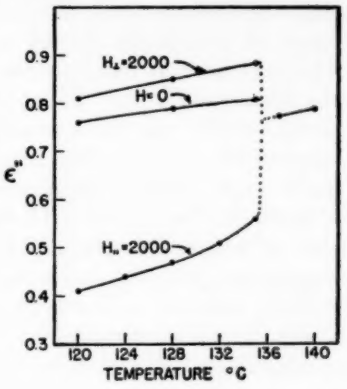

FIG. 4. The temperature dependence of the imaginary part of the complex dielectric constant in a magnetic field of 2000 gauss parallel and perpendicular to the microwave electric field, and in zero field for *para*-azoxyanisole.

the decrease in loss in a parallel magnetic field for this case. From Figs. 4 and 5 it is clear that regardless of the magnitude or orientation of the applied magnetic field, ϵ'' increases as the temperature of the liquid crystal phase increases. The total increase throughout the liquid crystal phase is approximately the same for corresponding values and orientations of the magnetic field for the two compounds. For the case $H=0$ the values of ϵ'' fluctuate in time and the results plotted for this case represent a time average of such values. This fluctuation will be referred to later in this paper.

It has been suggested that the imaginary part of the dielectric constant in zero magnetic field (ϵ_0'') should be related to the corresponding quantity in a perpendicular magnetic field ($\epsilon_\perp''$) and in a parallel field ($\epsilon_\parallel''$) by the relation

$$\epsilon_0''=\alpha\epsilon_\perp''+\beta\epsilon_\parallel''. \tag{1}$$

If we assume that for $H=0$ a state of random orientation exists then a naive picture based on the rod like shape of the molecule leads to

$$\alpha=\tfrac{2}{3},\quad \beta=\tfrac{1}{3},\quad \alpha/2\beta=1.$$

Table II shows the experimental values of these quantities. It is clear that the simple model fails to account for the observed results. Furthermore if we try to extend a similar model to the real part of the dielectric constant the results are even worse since our results show $\epsilon_0'\sim\epsilon_\perp'$ for this case. It might be argued

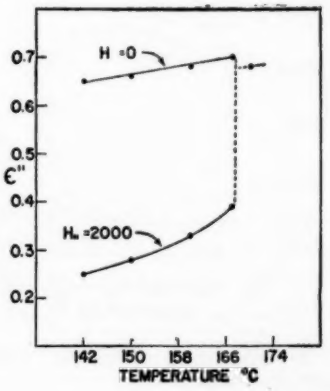

FIG. 5. The temperature dependence of the imaginary part of the complex dielectric constant in a magnetic field of 2000 gauss parallel to the microwave electric field and in zero field for *para*-azoxyphenetole.

that the failure of the model implied in Eq. (1) is a result of orientation by the walls of the wave guide. This may be true, but if so then it appears that most of the results on static dielectric constants suffer from similar defects since the sample size in most cases was comparable to ours. Experiments with larger wave guide might answer this question.

Since our frequency of 15 300 Mc was 15 000 times that at which Ornstein and Kast reported finding an absorption maxima in *para*-azoxyanisole, it seems unlikely that the microwave absorption which we have observed can be regarded as merely a high-frequency manifestation of the absorption which they found. It appears that these compounds possess another relaxation frequency higher than the one at one megacycle. In fact, Ornstein and Kast's data suggest the evidence of another absorption maxima at higher frequencies. It is reasonable to assume that our frequency of observation is considerably greater than $1/\tau$ where τ is the relaxation time of the postulated absorption. In the simple Debye theory the relaxation time should be proportional to η/T, where η is the viscosity and T is the absolute temperature. Therefore we might expect ϵ'' to be proportional to $1/\tau$ or T/η.

The viscosities of *para*-azoxyanisole and *para*-azoxyphenetole in the presence of a static magnetic field have been measured by Miesowicz[11] by observing the decrement of the vertical oscillations of a thin glass plate dipping into the liquid. From such observations he obtained the viscosity for various temperatures, for various values of the magnetic field intensity, and for different orientations of the magnetic field with respect to the measuring plate. Before we can apply his data to our problem we must form some picture of the relation between the molecular motion induced by dipping the plate at a given angle with respect to the magnetic field and that produced by the microwave electric field applied at a given angle with respect to the magnetic field. Since the long axis of *para*-azoxyanisole and *para*-azoxyphenetole molecules is the axis of least diamagnetic susceptibility, they tend to orient themselves with this axis parallel to the magnetic field. The permanent electric dipole moment for liquid crystals with a central azoxy group is transverse to the long axis of the molecule, and therefore the application of a microwave electric field parallel to the magnetic field tends to produce a rotation about an axis perpendicular to the plane of the permanent electric dipole moment and the magnetic field. The appropriate viscosity for the case in which the electric field is applied parallel to the magnetic field is that observed when the dipping plate is perpendicular to the magnetic field and therefore to the long axis of the molecules. In this case the motion induced in the molecules by the motion of the plate is also about an axis perpendicular to the magnetic field. In Fig. 6 we have plotted values of T/η for *para*-azoxyanisole calculated from Miesowicz's data as a function of temperature in zero field and in a field of 3800 gauss perpendicular to the dipping plate. Although a detailed comparison of Figs. 4 and 6 reveals certain numerical discrepancies, there is sufficient agreement in the general form of the two plots to suggest that such a simple model may have some validity. Unfortunately Miesowicz gives data on the viscosity for the case of the plate parallel to H only at the temperature of 122°C for *para*-azoxyanisole. At this temperature he finds for this case $\eta=0.034$ poise corresponding to $T/\eta=14\,600$. Thus it would appear that the curve of T/η for H parallel to the plate would be slightly below the curve for $H=0$ rather than slightly above as might be expected from our data. From the magnitude of the viscosity obtained from Miesowicz's data and from the radii of the molecule one finds that the value of the reciprocal relaxation time $1/\tau$ calculated on the basis of the Debye formula must lie between 10^7-10^9 sec^{-1}. T is is certainly too high to be identified with the absorption maxima found by Kast at one megacycle but might be responsible for the absorption which we have observed at 15 000 megacycles. However, other mechanismsin volving molecular distortion rather than molecular rotation may be responsible for the microwave absorption. The fact that the order of magnitude of ϵ'' in the liquid crystal state is the same as in the normal liquid suggests that the process responsible for the absorption is the same in both phases.

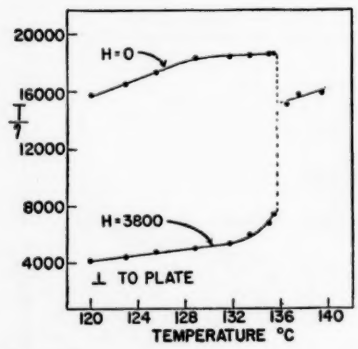

FIG. 6. Temperature dependence of the quantity T/η where T is the absolute temperature and η is the viscosity from Miesowicz's data.

TABLE II. The constants α and β for *para*-azoxyanisole.

Temp °C	α	β	$\alpha/2\beta$
120	0.875	0.125	3.5
128	0.842	0.158	2.7
135	0.77	0.23	1.7

Figure 7 shows the field dependence of the imaginary part of the complex dielectric constant for *para*-azoxyanisole at a temperature of 124°C. In *para*-azoxyphenetole we found that the results of the field dependence were quite similar to those of *para*-azoxyanisole. The general shape of this curve is very much like that

[11] M. Miesowicz, Bull. Acad. polon. d. Sciences et Lettres (serie A), p. 229 (1936).

observed by Miesowicz for the field dependence of the viscosity. Miesowicz's results show the region of saturation to be at a higher field than shown by our results, but this could be expected on the basis of the orientation phenomena to be discussed next.

C. Reorientation Phenomena

We have shown earlier that the microwave dielectric loss in the liquid crystal phase of *para*-azoxyanisole and *para*-azoxyphenetole is decreased by the application of a magnetic field parallel to the microwave electric field. If the magnetic field, which produces the anisotropy of the liquid crystal phase, is suddenly turned off, a length of time varying from a fraction of a minute to a few minutes is required for the liquid crystal to become isotropic. This can be shown by measuring the change of the dielectric loss after the external magnetic field is turned off. The time required to return to the zero-field distribution is dependent upon the temperature, and decreases as the temperature is increased. For any given temperature there is some variation in the "orientation" time. This variation appears to be related to the fluctuations observed in the measurements of ϵ'' in zero field. These may have their source in thermal currents in the liquid crystal phase.

By suddenly reversing an externally applied magnetic field of about 200 gauss, it can be shown that the aligning effect of the magnetic field is entirely due to the diamagnetic nature of these compounds. At the field and temperature, at which the observations were made, about one minute was necessary to produce the alignment in the liquid crystal, when the field was turned on. If the alignment were due to a permanent magnetic moment the molecules or swarms would have turned over when the field was reversed and while turning over they would pass through a state of random orientation. Because of the long time required for the alignment to take place, this random distribution would have caused a change in the dielectric loss as the magnetic field was reversed. Reversing the magnetic field showed that there was no turning over of the "particles" which implies that the magnetic moment in the liquid crystal *para*-azoxyanisole is induced.

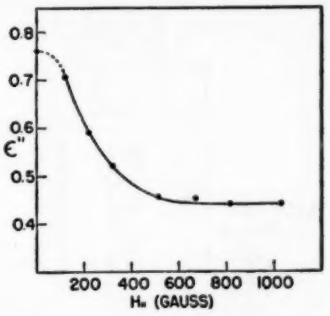

FIG. 7. Field dependence of the imaginary part of the complex dielectric constant for *para*-azoxyanisole at a temperature of 124°C.

It is interesting to consider the effect of this reorientation process on other measurements. For example, one might question whether the viscosities measured by an oscillating plate such as used by Miesowicz can actually be considered as the true viscosities if the period of oscillation is much less than the time for the disturbed liquid to return to its original orientation.

THE JOURNAL OF CHEMICAL PHYSICS VOLUME 22, NUMBER 9 SEPTEMBER, 1954

Velocity of One Megacycle Ultrasonic Waves in Benzene and Toluene Solutions of Polystyrene

WILLIAM M. FOX* AND GEORGE W. HAZZARD
St. Lawrence University, Canton, New York
(Received December 18, 1953)

A standing wave, single crystal interferometer was used to measure the ultrasonic velocity in polystyrene having molecular weights from 4100 to 159 000. Most of the measurements were made with 2 g of polystyrene per 100 ml of solution, benzene being the solvent. Some measurements used similar concentrations with toluene as the solvent. In the range of temperatures from 8.95°C to 54.45°C the velocity attributable to the polystyrene had a negative temperature coefficient below 35°C and a positive one above 35°C. At a given temperature the velocity attributable to the polystyrene showed two minima when plotted as a function of molecular weight. These minima occurred at polystyrene molecular weights of 17 000 and 53 000. Suggestions, but no conclusions, are given for the cause of these minima or dispersive regions.

INTRODUCTION

THE lack of dependence of ultrasonic absorption on the concentration of polystyrene in benzene and toluene has been shown previously.[1] The present work was carried out to study the behavior of polystyrene molecules in more detail. At a fixed frequency the velocity of ultrasonic waves in benzene and toluene was measured as a function of temperature and of the molecular weight of the polystyrene. The hope was that the use of dilute solutions at a fixed frequency would

* Now at The Franklin Institute, Philadelphia, Pennsylvaain.
[1] G. W. Hazzard, J. Acoust. Soc. Am. **22**, 29 (1950).

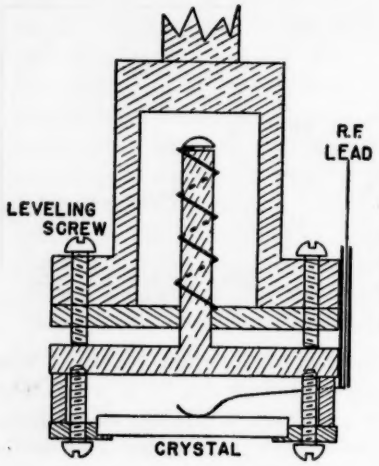

FIG. 1. Mounting of X-cut quartz crystal to show leveling and electrical connections. Both top and bottom surfaces of the crystal are chromium and silver plated with the bottom surface grounded.

make the effect of chain length on the vibration characteristics of the molecules most noticeable. A few absorption measurements were made, but their lack of precision precluded any reporting at this time.

EXPERIMENTAL PROCEDURE

Apparatus

The velocity measurements were made using a variable path interferometer similar to that described by McMillan and Lagemann.[2] The apparatus was modified so that the bottom of the cup containing the experimental liquid acted as a reflector and the quartz crystal transducer was carried up and down in the liquid by the micrometer screw. The mounting of the crystal is shown in Fig. 1. Working in this way we had no trouble exciting the crystal and obtaining excellent crevasses or dips in the crystal voltage.

The inside of the brass cup was covered with an evaporated film of SiO. The usual precautions of rising with pure benzene and drying between trials on different samples maintained consistency of results. Extreme sensitivity of the velocity to temperature variations required the immersion of the interferometer in a water constant temperature bath. The variations in temperature of the solution being tested were then never greater than ± 0.02°C. With these precautions velocity measurements were reproducible with a probable error of 0.2 m, sec^{-1} or about 0.02 percent.

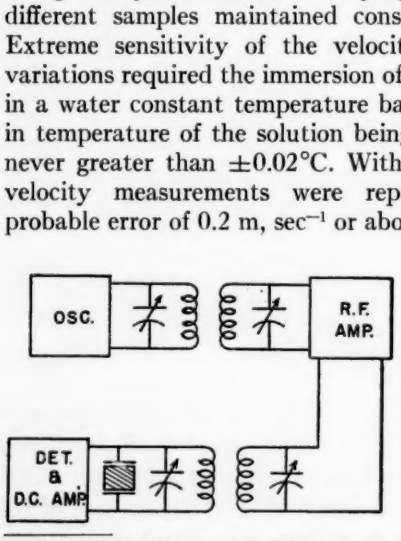

FIG. 2. Block diagram of the driving and detecting circuits for obtaining crystal voltage crevasses.

[2] D. R. McMillan and R. T. Lagemann, J. Acoust. Soc. Am. **19**, 956 (1947).

The variations of the rf voltage (nominal frequency = 1 mc, sec^{-1}) on the quartz crystal caused by resonance in the liquid column at half-wavelength intervals were detected and fed through a stage of dc amplification to a recording milliammeter. The micrometer screw carrying the crystal was driven by a 2-rpm synchronous motor. In this way the shape of the crevasses could be carefully and easily studied, and adjustment of oscillator frequency and coupling capacitance made in preliminary measurements. A block diagram of the electrical circuit is shown in Fig. 2.

Once the apparatus was adjusted the actual measurements were made manually. Crevasses were observed on a galvanometer in the detector circuit. Coasting of the recorder and motor made this necessary for highest precision. Normally, the distance traveled by the crystal for 20 crevasses was measured, and a series of such readings was taken over various portions of the micrometer screw. A check of the oscillator frequency against WWV was made before each set of readings.

Polystyrene

The polystyrene samples were obtained by precipitation fractionation from four broad fractions of Dow Styron. Since the preparation of the samples is important in deciding about the results, it will be summarized briefly.

Three percent by weight of Styron from one of the four samples was dissolved in benzene. Methanol was added in a thin stream under constant stirring at 25°C until the mixture became slightly cloudy. The system was then heated to 55°C or until complete solution occurred. It was then cooled to the mixing temperature and held at this temperature for 24 hours. The resultant heavy viscous "precipitate" was then redissolved in benzene, filtered to remove any foreign material, and slowly added in a thin stream to a large quantity of rapidly stirred methanol. The resulting precipitate or fraction was filtered under vacuum and dried at 40°C.

The weight average molecular weight of each fraction was obtained from viscosity and density measurements on small portions of each fraction, dissolved in varying concentrations in toluene. From these measurements we obtained the intrinsic viscosity and hence the molecular weight from the Mark-Houwick equation:[3]

$$M = k([\eta]/100)^b,$$

where $k = 293\,000$ and $b = 1.45$ are empirical constants, M = molecular weight, $[\eta]$ = intrinsic viscosity = $\lim_{c\to 0}(\eta-\eta_0)c/\eta_0$, η = viscosity of solution, η_0 = viscosity of solvent, c = concentration of solute. We feel that the molecular weight distribution in each sample should be fairly narrow since from five to ten fractions were made from each original sample.

It has been suggested[4] that the results may be in-

[3] L. Cragg and H. Hammerschlag, Chem. Revs. **39**, 79 (1946).
[4] A. Weissler (private communication).

conclusive because of retention of methanol by the polymer in the final precipitation. We feel this is not so because a series of fractions covering the molecular weight range from 4000 to 20 000 were all made from the same original sample and were consistent with fractions from other samples.

EXPERIMENTAL RESULTS

Temperature Variation

The variation of ultrasonic velocity with temperature for benzene and toluene is shown in Fig. 3. Although each of the curves is very slightly concave upward, the concavity is so slight that we computed the temperature coefficient for a linear variation. This coefficient is -4.7 m, sec^{-1}, °C^{-1} for benzene and -4.4 m, sec^{-1}, °C^{-1} for toluene, in good agreement with other published values.

The results for solutions of polystyrene in benzene (2 g/100 ml of solution) are presented in Fig. 4. If the

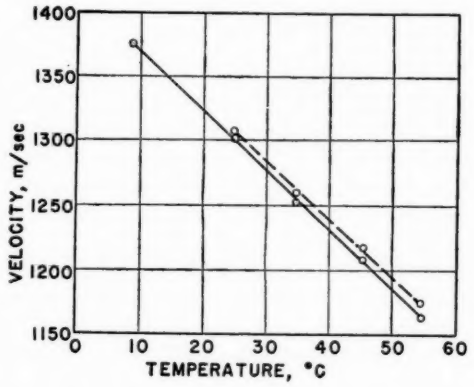

FIG. 3. Observed velocity of benzene(———) and toluene (– – –) *vs* temperature.

actual velocity of the solutions is plotted as a function of temperature, only the temperature variation of the solvent is seen. The variation of the "excess velocity" as a function of the temperature for different molecular weight samples of polystyrene is shown in Fig. 4. By "excess velocity" we mean the difference between the ultrasonic velocity in the solution at a given temperature and in the solvent at the same temperature. The excess velocity, which should represent the behavior of the polystyrene, then seems to have a more or less negative temperature coefficient below 35°C and a positive one above.

Solutions of polystyrene in toluene were studied only at 25°C so no temperature coefficient for excess velocity was obtainable.

Molecular Weight Variation

In presenting the variation of the ultrasonic velocity with molecular weight we again use the excess velocity

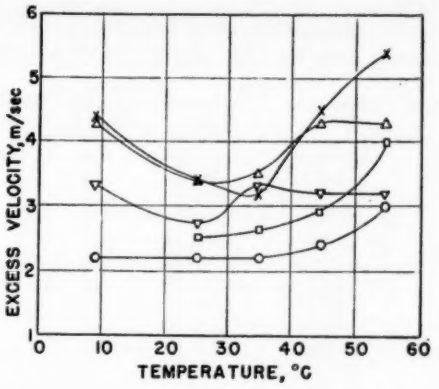

FIG. 4. Observed excess velocity (velocity in solution—velocity in solvent) *vs* temperature for various polystyrene molecular weights with benzene as solvent [△ 6820; ○ 16 400; □ 19 600; × 29 900; ▽ 51 800].

defined above. Figure 5 is a plot of the excess velocity of solutions of polystyrene in benzene as a function of the polystyrene molecular weight at five different temperatures. Data were taken first at 25°C, and include the greatest number of samples. Not shown are values for molecular weights of 109 000 and 159 000. Since interesting results appeared at the lower molecular weights (as perhaps might be expected), data at other temperatures were selected to cover these regions. The region above 74 000 molecular weight was not further investigated. The data on toluene solutions were a result of just trying another supposedly "good" solvent for polystyrene like benzene. The results were somewhat surprising and would merit further investigation along with a "poor" solvent like decalin.

The general characteristics of the plots for benzene at all temperatures are clearly a dip at about 15 000 and possibly 55 000 molecular weight or, conversely, two maxima at about 8000 and 30 000 molecular weight. It is interesting to observe that the excess velocity is, in general, greatest at 55°C, decreasing to a

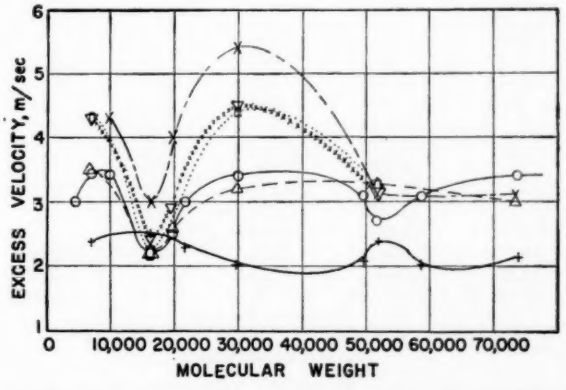

FIG. 5. Observed excess velocity (velocity in solution—velocity in solvent) *vs* molecular weight of polystyrene for various temperatures. [□ 8.95°C; ○ 25.00°C; △ 34.80°C; ▽ 44.55°C; × 54.45°C with benzene as solvent]. [+25.00°C with toluene as solvent.]

TABLE I. Ultrasonic velocity in polystyrene-benzene solutions (2 g polystyrene/100 ml solution).

Temperature (°C)	Molecular weight	Velocity (m/sec)	Excess velocity (m/sec)	Frequency (Mc/sec)
8.95	Benzene	1377.5	0.0	1.0400
	6820	1381.8	4.3	
	16 400	1379.7	2.2	
	29 900	1381.9	4.4	
	51 800	1380.8	3.3	
25.00	Benzene	1300.9	0.0	1.0144
	4100	1303.9	3.0	
	6820	1304.3	3.4	
	9910	1304.3	3.4	
	16 400	1303.1	2.2	
	19 600	1303.4	2.5	
	21 500	1303.9	3.0	
	29 900	1304.3	3.4	
	49 700	1304.0	3.1	
	51 800	1303.6	2.7	
	58 700	1304.0	3.1	
	73 700	1304.3	3.4	
	109 000	1304.1	3.2	
	159 000	1303.6	2.7	
34.80	Benzene	1253.6	0.0	1.0072
	6820	1257.1	3.5	1.0080
	16 400	1255.8	2.2	1.0088
	19 600	1256.2	2.6	1.0056
	29 900	1256.8	3.2	1.0088
	51 800	1256.9	3.3	
	73 700	1256.6	3.0	
44.55	Benzene	1209.0	0.0	1.0288
	6820	1213.3	4.3	1.0280
	16 400	1211.4	2.4	1.0240
	19 600	1211.9	2.9	1.0264
	29 900	1213.5	4.5	1.0352
	51 800	1212.2	3.2	1.0264
54.45	Benzene	1163.3	0.0	1.0056
	6820	1167.6	4.3	
	9910	1167.6	4.3	
	16 400	1166.3	3.0	1.0048
	19 600	1167.3	4.0	
	29 900	1168.7	5.4	1.0056
	51 800	1166.5	3.2	
	73 700	1166.4	3.1	
	109 000	1166.5	3.2	

TABLE II. Ultrasonic velocity in polystyrene-toluene solutions (2 g polystyrene/100 ml solution).

Temperature (°C)	Molecular weight	Velocity (m/sec)	Excess velocity (m/sec)	Frequency (Mc/sec)
25.00	Toluene	1306.3	0.0	1.0144
	6820	1308.7	2.4	1.0056
	16 400	1308.8	2.5	
	21 500	1308.6	2.3	
	29 900	1308.3	2.0	
	49 700	1308.4	2.1	
	51 800	1308.7	2.4	
	58 700	1308.3	2.0	
	73 700	1308.5	2.2	
	126 000	1308.6	2.3	
34.75	Toluene	1260.4	0.0	1.0088
44.65	Toluene	1218.0	0.0	1.0288
54.85	Toluene	1174.9	0.0	1.0056

minimum in the 25–30°C region, and increasing markedly at 90°C.

A general summary of the data is given in Table I and Table II.

DISCUSSION

As Fig. 4 showed, polystyrene samples of molecular weight from 6820 to 51 800 gave excess velocities which first decreased and then increased with increasing temperature. Since the normal viscous effect on velocity is to decrease the velocity with increasing temperature, it appears that a second mechanism swamps the viscous mechanism above a temperature of 35°C. This mechanism cannot be due to the slowness of energy exchange between external and internal degrees of freedom. For if increasing temperature resulted in higher internal specific heat, the net specific heat would be increased and the sound velocity decreased with increasing temperature. On the other hand, when the sound propagation occurs in a medium for which a relaxation frequency exists, there are competing effects which might cause a net increase in velocity. That is the bulk modulus, $-V(\partial\rho/\partial V)_s$, could increase explicitly with increasing temperature or implicitly through increases in the volume expansity and molar volume. Certainly the change from a negative to a positive temperature coefficient is unusual and provocative.

The results of the molecular weight study are also difficult to interpret simply. That relaxation processes occur is a reasonable conclusion. But the exact molecular weights at which they occur and the nature of the mechanisms are not obvious. For example, should one consider a region where the molecular weight is 9000 12 000, or 17 000 as the dispersive region? Similarly, should one talk about a second dispersive region as being at 30 000, 40 000, or 53 000 molecular weight?

On the basis of a relaxation mechanism there seems no easy way to decide about the dispersive region. If one looked at the problem from a classical point of view, as in optical dispersion, there might be some reason to believe we had passed through resonance at 17 000 and 53 000 molecular weight. Thus at the lower molecular weight we might have come to a twisting or rotating frequency which could be in resonance with the sound vibration. At the higher molecular weight there might exist an entanglement frequency. That the dispersive regions are not sharper is probably due to the distribution in molecular weights about its mean value in each sample.

The behavior of the same polystyrene samples in toluene makes one wonder if toluene is a good solvent. Apparently there is some hindering of the rotational or twisting relaxation at the lower molecular weight but none of the entranglement relaxation at the higher molecular weight.

ACKNOWLEDGMENTS

The authors wish to thank the Research Corporation for the grant which made this work possible. We also wish to thank R. F. Boyer of The Dow Chemical Corporation for supplying the polystyrene samples. To Alfred Romer and George E. Miller, Jr., go our thanks for many helpful discussions.

Free Radicals by Mass Spectrometry. VI. The Bond Dissociation Energies of Some Methyl, Allyl, and Benzyl Compounds by Electron Impact*

F. P. Lossing, K. U. Ingold,† and I. H. S. Henderson†
Division of Pure Chemistry, National Research Council, Ottawa, Canada

(Received July 10, 1953)

The appearance potentials for the radical ions from methyl, allyl, and benzyl halides and two other derivatives have been measured. Using previously measured values for the ionization potentials of the free radicals, the R−X bond dissociation energies in these compounds have been calculated. The results are in good agreement with published data for the methyl and allyl compounds, and in fair agreement for the benzyl halides.

INTRODUCTION

In an earlier paper[1] the method of determining bond dissociation energies from the appearance potentials of the radical ions was reviewed. The determination of the ionization potentials of methyl, allyl, and benzyl radicals by direct measurement on a stream of radicals of reasonably high purity was described. In this paper the appearance potentials of the radical ions from a number of derivatives have been measured and, using the new ionization potential values, dissociation energies of the bonds have been derived. These values have been compared with the data obtained from kinetic and thermochemical measurements which have been summarized in two recent reviews.[2,3]

EXPERIMENTAL

The method of measuring the appearance potentials was the same as that used in the earlier paper for the ionization potentials of the radicals. The compound examined, together with the acetylene used as a reference standard, was carried in a stream of helium at a few mm pressure past the high-pressure side of the mass spectrometer leak. The partial pressures were adjusted to make equal the net peak heights of the acetylene mass 26 ion and of the ion in question. Where necessary, the peak heights were corrected for isotopic or other contributions. Ionization efficiency curves were measured for the two ions and the logarithm of the percentage of the net peak height at 50 volts was plotted against the applied electron accelerating potential. The voltage difference (δV) between the two curves at given values of the ion current (I) was plotted against the ion current and the resulting curve or line was extrapolated to $I=0$. In general, greater curvature was found in the δV *vs* I curves from appearance potential measurements than in those from ionization potential measurements. Typical δV *vs* I relationships for $A(CH_3^+)$ from the methyl halides are plotted in Fig. 1. The increase in curvature from iodide to fluoride is marked. The limits of error shown in Table I were estimated from the uncertainty of the extrapolation of these curves. Curves similar to that of CH_3I in Fig. 1 were assigned a limit of error of ± 0.03 ev, those like $CH_3Br \pm 0.06$ ev, while curves like that for CH_3F, where the extrapolation was practically meaningless, were assigned an error of ± 0.6 ev. The value of the appearance potential was calculated by dividing the extrapolated value of δV by the slope of the calibration line described previously,[1]

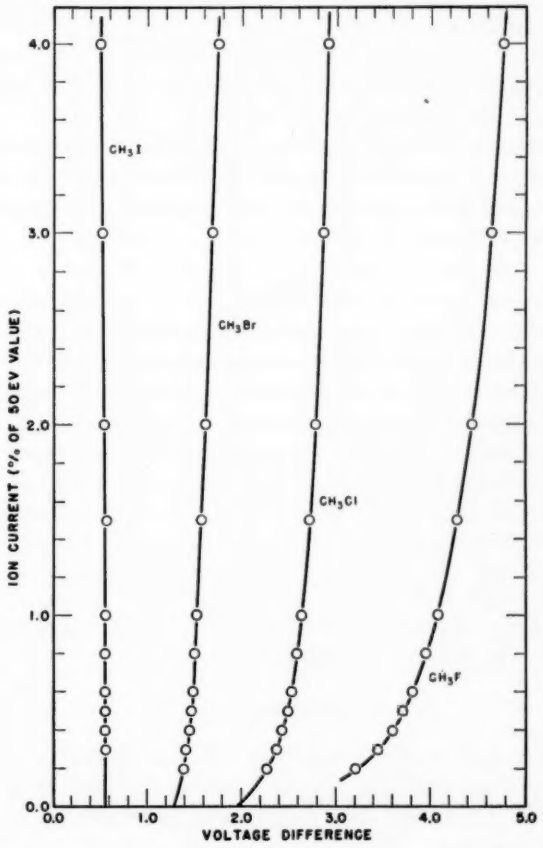

FIG. 1. δV *vs* I curves for the methyl ion from the halides. The voltage difference (δV) between the ionization efficiency curves for the methyl ion and for the acetylene standard is plotted against the ion current. There is a marked increase in the curvature of this relation from the iodide to the fluoride.

* National Research Council Contribution No. 3329.
† National Research Council Postdoctorate Fellows.
[1] Lossing, Ingold, and Henderson, J. Chem. Phys. **22**, 621 (1954).
[2] J. S. Roberts and H. A. Skinner, Trans. Faraday Soc. **45**, 339 (1949).
[3] M. Szwarc, Chem. Revs. **47**, 75 (1950).

TABLE I. Appearance potentials and bond dissociation energies.

Substance	Ion	Appearance potential (ev) This work	Literature	Ref.	Bond dissociation energy (kcal/mole) This work	Literature	Ref.
Methane	CH_3^+	14.41±0.03	14.5 ±0.4	5	102.8±1.5	102 ±1	11
			14.5 ±0.1	6		101.9±2	12
			14.4 ±0.3	7			
			14.57±0.05	8			
			14.5 ±0.3	9			
			14.39±0.02	10			
Methyl iodide	CH_3^+	12.15±0.03	12.36±0.02	13	50.7±1.5	55.0	2
			12.4 ±0.2	14		~54	3
	I^+	12.88±0.1	12.9 ±0.3	14	56.3±2.5		See also 13
Methyl bromide	CH_3^+	12.83±0.06	13.2 ±0.3	14	66.4±2	67.4	2
						~68	3
Methyl chloride	CH_3^+	13.44±0.15	13.5 ±0.5	14	80.5±3	80.7	2
Methyl fluoride	CH_3^+	14.6 ±0.6	—	—	107 ±12	high	15
Methanol	CH_3^+	13.90±0.15	14.0 ±0.5	16	91.1±4	91.2	2
						90–91	3
Allyl iodide	allyl$^+$	9.64±0.03	—	—	34.1±1.5	~34.4	2
	I^+	12.02±0.2	—	—	36.4±5	35–37	3
Allyl bromide	allyl$^+$	10.23±0.08	—	—	47.7±2.5	~45.5	2
						47.5±2	17
Allyl chloride	allyl$^+$	10.78±0.1	11.09±0.1	18	60.4±3	~59.3	2
						58	3
Benzyl iodide	benzyl$^+$	9.23±0.05	—	—	34.6±3	~36.5	2
						~39	3
Benzyl bromide	benzyl$^+$	9.67±0.05	—	—	44.7±3	~48.5	2
						50.5±2	17
Benzyl chloride	benzyl$^+$	10.35±0.1	11.13±0.1	18	60.4±4	—	—

and adding the result algebraically to the ionization potential of acetylene.

Two or three determinations of each appearance potential were made, the agreement between them being within the estimated limit of error.

The limits of error shown for the bond dissociation energies were estimated from the sum of the errors in the ionization potential and appearance potential measurements.

RESULTS

The measured appearance potentials of the radical ions are given in Table I together with data from the literature. The bond dissociation energies listed were calculated from these appearance potentials using the ionization potentials of the radicals which were reported previously, i.e., methyl, 9.95±0.03 ev; allyl, 8.16±0.03 ev; and benzyl, 7.73±0.08 ev.[1] In the cases where the appearance potential of the iodine atomic ion I^+ was measured, the spectroscopic ionization potential 10.44 ev of the iodine atom was used.[4] Bond dissociation energies obtained from kinetic and thermochemical data are shown for comparison.

DISCUSSION

The appearance potential of CH_3^+ from methane has been measured a number of times as can be seen from Table I,[5–10] and the results are generally in good agreement. The value of 14.41±0.03 ev found here is almost identical with the recent value of 14.39±0.02 ev found by McDowell and Warren.[10] This, combined with the ionization potential of methyl (9.95±0.03 ev) reported in the previous paper,[1] yields $D(CH_3-H) = 102.8\pm0.9$ kcal. This agrees well with the Kistiakowsky and Van Artsdalen[11] value of 102.1±1 kcal, and the average electron impact value of 101.9±0.9 kcal cited by Stevenson.[12] It may be noted that the Hipple and Stevenson values[6] of 14.5±0.1 ev for $A(CH_3^+)$ and 10.07±0.1 ev for $I(CH_3)$ are both about 0.1 ev higher than the corresponding values found in this work, and give almost the same dissociation energy (102.2±2 kcal) for the CH_3-H bond.

The appearance potential of CH_3^+ from methyl iodide is about 0.2 ev lower than that found previously,[13,14] and the derived value for the bond dissociation energy $D(CH_3-I) = 50.7\pm1.5$ kcal appears to be too low. The value of McDowell and Cox gives $D(CH_3-I) = 55.6\pm1.5$ kcal, which is in better agreement with other estimates for this bond and with the value obtained from the appearance potential of I^+. No reason for obtaining the low value of $A(CH_3^+)$ could be found, the spectrum of the CH_3I showing no evidence for the presence of impurities which could give

[4] G. Herzberg, *Atomic Spectra and Atomic Structure* (Dover Publications, New York, 1944), p. 200.
[5] L. G. Smith, Phys. Rev. **51**, 663 (1937).
[6] J. A. Hipple and D. P. Stevenson, Phys. Rev. **63**, 121 (1943).
[7] M. B. Koffel and R. A. Lad, J. Chem. Phys. **16**, 420 (1948).
[8] J. J. Mitchell and F. F. Coleman, J. Chem. Phys. **17**, 44 (1949).
[9] J. Geerk and H. Neuert, Z. Naturforsch. **5A**, 502 (1950).
[10] C. A. McDowell and J. W. Warren, Discussions Faraday Soc. **10**, 53 (1951).
[11] G. B. Kistiakowsky and E. R. Van Artsdalen, J. Chem. Phys. **12**, 469 (1944).
[12] D. P. Stevenson, Discussions Faraday Soc. **10**, 35 (1951).
[13] C. A. McDowell and B. C. Cox, J. Chem. Phys. **20**, 1496 (1952).
[14] H. Branson and C. Smith, J. Am. Chem. Soc. **75**, 4133 (1953).

CH_3^+ at a lower appearance potential. Further vacuum distillation of the methyl iodide had no effect.

In the case of the methyl halides, two processes leading to the formation of CH_3^+ are possible:

$$(1)\quad CH_3I+e\rightarrow CH_3^++X+2e,$$

$$(2)\quad CH_3I+e\rightarrow CH_3^++X^-+e.$$

Process (2) would have an appearance potential lower than that of process (1) by an amount approaching the electron affinity of X. In view of this possibility, a search was made for I^- ions from CH_3I and a small current of I^- ions was indeed found. Although the relative efficiency of collection for positive and negative ions for the instrument is not known, the current for I^- was only about 1/2000 of that found for CH_3^+. Even if all these I^- ions were produced by an ion-pair process, this amount could hardly lower the observed appearance potential of CH_3^+ significantly below that required for process (1). The possibility of the formation of a trace of CH_3 radicals by pyrolysis on the mass spectrometer filament was also considered. However, almost no curvature was found in the δV *vs* I relation, as would be the case if CH_3 were formed.

The appearance potential of CH_3^+ from methyl bromide, although lower than that found by Branson and Smith,[14] gave $D(CH_3-Br)=66.4\pm2$ kcal, in good agreement with the previous estimates.[2,3] The value of $D(CH_3-Cl)=80.5\pm3$ kcal is also in good agreement with the data of Roberts and Skinner.[2] The δV *vs* I relation for methyl fluoride had a large curvature (Fig. 1) and consequently a large uncertainty exists in the value for $D(CH_3-F)$. The dissociation energy for C–F bonds is thought to be large.[15]

In the case of methanol, good agreement was obtained with the results of Cummings and Bleakney,[16] and the derived value of $D(CH_3-OH)=91.1\pm4$ kcal, appears to indicate that the process is

$$CH_3OH+e\rightarrow CH_3^++OH+2e$$

rather than

$$CH_3OH+e\rightarrow CH_3^++O+H+2e.$$

Allyl Compounds

In conjunction with the previously measured ionization potential of the allyl radical, 8.16 ± 0.03 ev,[1] the values of $A(CH_2{:}CH\cdot CH_2^+)$ and $A(I^+)$ from allyl iodide give values for $D(CH_2{:}CH\cdot CH_2-I)$ in good agreement with each other and with the kinetic and thermochemical data.[2,3]

The results for $D(CH_2{:}CH\cdot CH_2-Br)$ and $D(CH_2{:}CH\cdot CH_2-Cl)$ are also in satisfactory agreement with previous estimates.[2,3,17] The value of 11.09 ± 0.11 ev for $A(CH_2{:}CH\cdot CH_2^+)$ from the chloride found by Franklin and Lumpkin[18] is about 0.3 ev higher than that reported here. It is of interest to note that in the present work their value corresponded to the voltage difference between the ionization efficiency curves for the allyl ion and for the acetylene molecular ion at an ion current equal to 1 percent of the 50-volt value. This suggests the possibility that the method used by Franklin and Lumpkin did not allow sufficiently for the curvature of the δV *vs* I relation.

As pointed out previously,[1] the appearance potential of the mass 41 peak in the spectrum of 1-butene, 11.65 ev,[8,19] is not compatible with the values of $I(CH_2{:}CH\cdot CH_2)$ and $A(CH_2{:}CH\cdot CH_2^+)$ found in the present work. It has been suggested that this process requires an excess energy term[19,20] and from this work this excess energy would amount to about 0.9 ev. Consequently the value of 9.05 ev predicted for the ionization potential of the allyl radical by Evans and Szwarc[21] would be too high by this amount.

Benzyl Compounds

The appearance potentials found for the benzyl ion from benzyl iodide and benzyl bromide, together with the value of $I(\text{benzyl})=7.73\pm0.08$ ev measured previously,[1] give $D(C_6H_5\cdot CH_2-I)=34.6\pm3$ kcal and $D(C_6H_5\cdot CH_2-Br)=44.7\pm3$ kcal. These bond dissociation energies are about 3–5 kcal lower than the previous estimates,[2,3,17] an amount just greater than the error of measurement in the present data. If the estimates are assumed to be correct, this difference suggests the possibility that the measured value of I(benzyl) is too high by about 0.2 ev, or that the appearance potentials are too low by the same amount. The possibility of ion-pair formation was investigated, but no iodine negative ions were found in excess of 1/2000 of the benzyl positive ion current. This result, as with CH_3I, would seem to rule out interference by the ion-pair process.

The appearance potential found for the benzyl ion from benzyl chloride, 10.35 ± 0.1 ev is considerably lower than that obtained by Franklin and Lumpkin, 11.13 ± 0.1 ev.[18] This difference would seem to arise from the same cause as in the case of allyl chloride. It is unfortunate that an unambiguous measurement of appearance potentials cannot be made in cases such as these, where a large curvature of the δV *vs* I relation is found. The use of a method of detecting fine detail in

[15] J. R. Dacey and J. W. Hodgins, Can J. Research **B28**, 173 (1950).
[16] C. S. Cummings and W. Bleakney, Phys. Rev. **58**, 787 (1940).
[17] Szwarc, Ghosh, and Sehon, J. Chem. Phys. **18**, 1142 (1950).
[18] J. L. Franklin and H. E. Lumpkin, J. Chem. Phys. **19**, 1073 (1951).
[19] D. P. Stevenson, J. Am. Chem. Soc. **65**, 209 (1943).
[20] F. H. Field, J. Chem. Phys. **20**, 1734 (1952).
[21] M. G. Evans and M. Szwarc, J. Chem. Phys. **19**, 1322(1951)

the lower portion of appearance potential curves, such as that described by Morrison[22] or by Fox *et al.*[23] would be of great help in such studies.

[22] J. D. Morrison, J. Chem. Phys. **19**, 1305 (1951).
[23] Fox, Hickam, and Kjeldaas, Phys. Rev. **89**, 555 (1953).

ACKNOWLEDGMENT

The authors are indebted to Dr. L. C. Leitch, Mr. A. T. Morse, and Mr. R. Renaud of these laboratories for preparing the allyl iodide and benzyl iodide used in this work.

THE JOURNAL OF CHEMICAL PHYSICS VOLUME 22, NUMBER 9 SEPTEMBER, 1954

Thermoelectric Power of Pure and Doped AgBr

LYLE PATRICK* AND A. W. LAWSON
Institute for the Study of Metals, University of Chicago, Chicago 37, Illinois
(Received April 27, 1954)

Measurements on the thermoelectric power of pure AgBr and AgBr doped with $CdBr_2$ have been interpreted in the light of the kinetic theories of Wirtz and de Groot. The ratio of the mobility of the interstitial silver ions to that of the vacancies as determined by Teltow is reasonably consistent with the data reported here on thermoelectric power. Estimates are given for the heats of transport of the various species of moving imperfections. No evidence of a contribution by Schottky defects to the thermoelectric power is found.

I. INTRODUCTION

OUR comprehension of ionic crystals has progressed to the point where, by coupling simple theoretical models with measurements on electrical conductivity and transport phenomena, we are able to specify the nature of the conductivity mechanism and make estimates of the number density and mobilities of the charge carriers. It is important to emphasize, however, that the models employed in such estimates are presently quite naive and, furthermore, are based on assumptions which are known to be incorrect in principle, although they may lead to good quantitative approximations.

As an example of this state of affairs, let us review the situation in AgBr. Transport experiments indicate that conduction is overwhelmingly controlled by transport of Ag^+ ions. It is assumed that this transport is either by the motion of Ag^+ interstitial ions or by motion of vacancies on positive sites, arising from so-called Frenkel type disorder. In order to find the number of these Frenkel defects, as well as the mobilities of the interstitial ions and the vacancies separately, it is necessary to know more than just the electrical conductivity. One procedure which yields the necessary information is as follows. Pure AgBr is doped with $CdBr_2$. It is assumed that the Cd^{++} ions replace Ag^+ ions substitutionally and that the introduction of each Cd^{++} ion introduces a positive ion vacancy to the lattice. If it further be assumed that the Cd^{++} ions and the vacancies do not cluster, but are completely dissociated, then by measuring the electrical conductivity of doped samples as well as pure samples it is possible to find ndependently the number density of defects as well as the mobilities of the two carriers. This procedure has been applied by Teltow[1] and Kurnick[2] to AgBr.

In addition, Teltow has made estimates of the corrections which are necessary if the assumption of complete dissociation of Cd^{++} ions and vacancies is invalid or if long-range forces (partially screened) between imperfections are important. He reaches the conclusion that both association and long-range forces play an appreciable role and shows that if these phenomena are taken into account the estimated mobilities are appreciably different from those estimated when such effects are neglected (see Fig. 3 and Table III). Unfortunately, at the present time, well-established independent information on the heat of association of Cd^{++} ions and vacancies is lacking, and it is difficult to know which of the two estimates is closer to the real state of affairs.

It is desirable, therefore, to obtain measurements of quantities which depend on the various parameters involved in electrical conductivity in a different way so that parameters variously estimated may be tested for self-consistency. Since the thermoelectric power of an ionic crystal may involve the mobilities of the moving ions as well as heats of activation related to those involved in electrical conductivity, a partial test of consistency of the estimated mobilities is provided by a measurement of this quantity.

For this reason, we present more extensive data than has previously been available on the thermoelectric power of both pure AgBr and AgBr doped with $CdBr_2$. These data are examined in the light of the theory of Wirtz[3] and de Groot[4] of the thermoelectric power of ionic crystals (briefly outlined in the next section). The

* Now at Westinghouse Research Laboratories, East Pittsburgh, Pennsylvania.

[1] J. Teltow, Ann. Physik **5**, 63 (1950).
[2] S. W. Kurnick, J. Chem. Phys. **20**, 218 (1952).
[3] K. Wirtz, Physik. Z. **44**, 221 (1943).
[4] S. R. de Groot, *L'Effet Soret* (Amsterdam, 1945).

predictions concerning the ratio of the mobility of Ag^+ ions to that of the vacancies in AgBr are compared with estimates of the same ratio derived from the electrical conductivity measurements of Teltow and Kurnick.

It is found that the two ratios are in better agreement if no corrections are introduced for association or long range forces between imperfections.

II. THEORY

As mentioned above, Wirtz has considered the thermoelectric power of ionic crystals from a kinetic point of view. This theory has been amended and extended by de Groot, who has shown how this theory is a special case in the more general framework of quasi-thermodynamics. In the case of pure AgBr, the appropriate formula for the thermoelectric power ϵ is

$$\epsilon=\frac{\varphi B-A}{eT(\varphi+1)}, \tag{1}$$

where e is the electronic charge, T the absolute temperature, φ the ratio of the mobility of the silver interstitial ions to that of the silver vacancies, and

$$B=(\omega/2)+Q_i \tag{2}$$

and

$$A=(\omega/2)-Q_v, \tag{3}$$

where ω is the heat of formation of an interstitial ion and a vacancy. A and B are the heats of transport of the interstitial ion and the vacancy, respectively, in the sense of de Groot. Q_i and Q_v are the contributions to these heats of transport arising from the activation energies involved in moving imperfections from one state of relative equilibrium to another.

The assumptions involved in the derivation of Eq. (1) are as follows:

(1) Frenkel defects are the predominant contributors to the thermoelectric power.

(2) Although the sample is in a temperature gradient, the defects are present in their equilibrium number at the local temperature. In other words, the formation and recombination time is very much less than the time required to drift to a significantly different temperature.

(3) The charge separation required to build up the electrical field present is negligibly small compared with the total number of defects.

If we assume that activation of the motion of a defect is a simple process with the fluctuation in energy inducing motion entirely localized at the initial position of the moving interstitial ion, or at the position of an ion which jumps into a vacancy, then $Q_i=U_i$ and $Q_v=U_v$ where U_i and U_v are the activation energies in the usual type of formula for the mobility μ of a defect, namely

$$\mu=C/Te^{-U/RT}. \tag{4}$$

Wirtz does not make such a restrictive assumption. He assumes that U's may be split into three parts such that

$$U=q_I+q_M+q_F, \tag{5}$$

where q_I is the energy which must be furnished to a particle at its initial position in order that it may detach itself from this position of relative equilibrium, q_M is the energy which must be supplied to ions on the plane between the initial and final positions to move them apart and permit the jump, and q_F is the energy which must be provided at the final plane to form a "hole" into which the jumping ion may fall. In this case $Q\neq U$ but $Q=q_I-q_F$ and will usually be smaller than U.

By using measured values of φ at two different temperatures in Eq. (1), it is possible to determine A and B. Then using the measured values of ω, one can determine Q_i and Q_v from Eqs. (2) and (3). The values of Q_i and Q_v should be less than U_i and U_v and should be consistent with an exponential dependence of φ on $1/T$ and the observed temperature variation of ϵ.

The situation in doped samples is somewhat different. In the range of temperature where the doping agent (say $CdBr_2$) controls the concentration of vacancies, the theory leads to the following expression for the thermoelectric power:

$$\epsilon=(Q_d+Q_v)/2eT, \tag{6}$$

where Q_d is the heat of transport of the doping ion. This formula will break down at higher temperatures where the intrinsic formation of Frenkel defects becomes competitive with the effect of the doping in controlling the number of charge carriers.

The principal difference between Eq. (6) and Eq. (1) is the absence of any mobility terms in Eq. (6). The reason the two equations differ is that in the case of the pure sample the silver ions may move by either of two alternative methods, i.e., as interstitials or via vacancies, and the steady-state condition is determined by requiring the sum of the interstitial and vacancy currents to vanish. In the doped case, however, in order to attain a steady state both the cadmium ion current and the vacancy current must vanish separately, and the mobility terms drop out.

III. MEASUREMENTS

Measurements of the thermoelectric power were made both on a pure single crystal of AgBr and a crystal grown from a melt containing 0.25 percent $CdBr_2$. These crystals were kindly furnished by Dr. R. W. Christy. The crystals were right circular cylinders approximately $\frac{1}{4}$ in. in diameter and 1 cm in height. Disks of silver were affixed to each end of the sample to serve as electrodes. Chromel and Alumel wires were silver-soldered to each electrode and served as thermocouples to measure both the temperature and temperature gradient in the sample.

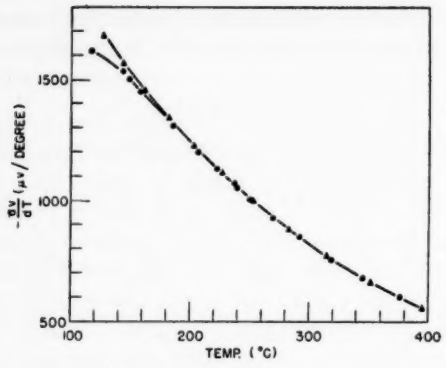

FIG. 1. The sum of the homogeneous and inhomogeneous thermoelectric powers of pure AgBr with Ag electrodes. The circles and triangles are results on two different crystals. The bending over at low temperatures is probably the effect of impurities.

A temperature gradient of approximately 10°C was established between the two electrodes and the emf between the two electrodes was observed by using the Chromel wires as leads. The emf so observed is then corrected to give absolute values of dV/dT by using known values[5] for Pt and Pt *versus* Chromel. This correction is relatively small, amounting to only about 20μv/°C in values of the order of 1000μv/°C.

It is also necessary to correct dV/dT for the variation of the contact potential of the silver electrodes with temperature. Originally, the authors had hoped to utilize the fact that ϵT for the doped samples should be independent of temperature over a reasonable range to estimate this correction. Unfortunately, however, the lack of precision in the data on doped samples precluded this possibility. We have therefore used the estimate of 140 μv/°C given by Reinhold and Blachny[6] for the inhomogeneous thermoelectric power of the Ag—AgBr junction.

The results obtained in this manner are shown in Fig. 1 and Fig. 2 and are listed in Table I.

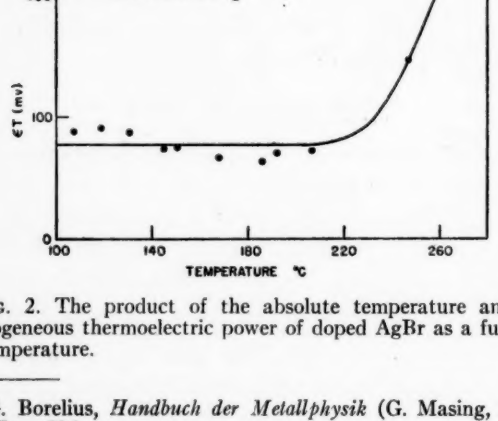

FIG. 2. The product of the absolute temperature and the homogeneous thermoelectric power of doped AgBr as a function of temperature.

[5] G. Borelius, *Handbuch der Metallphysik* (G. Masing, 1935), Part I, p. 396.
[6] H. Reinhold and A. Blachny, Z. Elektrochem. **39**, 290 (1933).

IV. DISCUSSION

The data for the thermoelectric power of pure AgBr are in excellent agreement with the earlier but more sparse data of Reinhold and Blachny, as may be seen by a comparison of Table I and Table II. At higher temperatures, the two sets of data deviate by only a few percent. At 400°K, the agreement is worse but at this temperature the thermoelectric power is sensitive to small amounts of impurities.

In an effort to check the consistency of the thermoelectric data with mobility estimates deduced from conductivity measurements, we have estimated the values of A and B in Eq. (1) by inserting the estimated values of ϵ and φ at two different temperatures. We have then calculated φ as a function of temperature using the

TABLE I. Thermoelectric power of pure and doped AgBr as a function of temperature.

$$\epsilon = -\frac{dV}{dT}\Big)_{\text{obs}} - 140$$

T°K	$-\frac{dV}{dT}$ μv/°C	$\epsilon_{\mu v/°C}$	$T\epsilon_{mv}$
Pure AgBr			
667	570	430	286
625	660	520	325
588	770	630	370
556	882	742	411
526	1000	860	451
500	1110	970	485
476	1230	1090	521
455	1330	1190	543
Doped AgBr			
381	373	233	88
391	370	230	91
404	358	218	88
418	315	175	74
424	315	175	75
441	290	150	67
459	278	138	63
465	290	150	70
480	290	150	72
519	418	278	144
539	510	370	199

remainder of the data available on ϵ to see whether the temperature variation of ϵ is consistent with an exponential dependence of the mobility ratio φ on $1/T$. This procedure was carried out using the values of φ estimated independently by Kurnick and Teltow, assuming no appreciable association of Cd^{++} ions and vacancies, and also using Teltow's estimate of φ when association effects are taken into account. The results of these calculations are shown in Fig. 3.

The best consistency between thermoelectric data and conductivity data is obtained with Teltow's estimate of φ, made by neglecting the effect of association between Cd^{++} ions and vacancies. In fact, considering various experimental errors and uncertainties in the correction for the inhomogeneous thermoelectric power, even the consistency with Kurnick's estimate of φ is not bad. The poorer consistency of the thermo-

electric data with Teltow's corrected estimate of φ indicates the heat of dissociation of Cd^{++} ion-vacancy complexes used by him is much too high. Teltow estimated the heat of dissociation of these complexes to be about 8 kcal/mole. Preliminary measurements by Reif and Cohen[7] on this quantity based on a nuclear resonance technique indicate this quantity may be at least an order of magnitude smaller.

From the values of A and B deduced according to the procedure described above, it is possible to estimate Q_i and Q_v, the heats of transport of the imperfections, by use of Eq. (2) and Eq. (3), once $\omega/2$ is known. Estimates of these quantities are given in Table III. The most striking aspect of these data is that, if one uses φ values uncorrected for association, Q_i is an order of magnitude less than U_i while Q_v is of the same order of magnitude as U_v. This result is comprehensible in view of the fact that considerable energy must be expended on the receiving plane of atoms to allow room for a jumping interstitial. Thus, one might expect $q_F \sim q_I$ and hence $Q_i \sim 0$. On the other hand, a moving vacancy can receive a jumping Ag^+ ion with little trouble, in which case one expects $q_F \sim 0$ and $q_I \sim Q_v \sim U_v$. On the other hand, the quantity $|Q_v|$ must be less than $|U_v|$. This condition is not satisfied by the Q_v estimated from Teltow's corrected φ and accordingly supports the suggestion made above that Teltow's corrected φ must be considerably overcorrected.

Kurnick's assumption of a large number of Schottky defects at 400°C would lead to a reversal of the sign of ϵ.

TABLE II. Thermoelectric power of pure AgBr after Reinhold and Blachny (see reference 6).

T°K	$\epsilon_{\mu v}$/°C
400	1340
500	990
600	650

TABLE III. Estimated values of Q_i and Q from Fig. 3.

	Teltow uncorrected	Kurnick	Teltow corrected
U_i	0.157 ev	0.208 ev	0.123 ev
U_v	0.368	0.497	0.253
A	0.250	0.120	1.28
B	0.652	0.603	0.705
$\omega/2$	0.635	0.605	0.506
Q_i	0.017	−0.002	0.199
Q_v	0.385	0.485	−0.774

[7] F. Reif and M. Cohen (private communication).

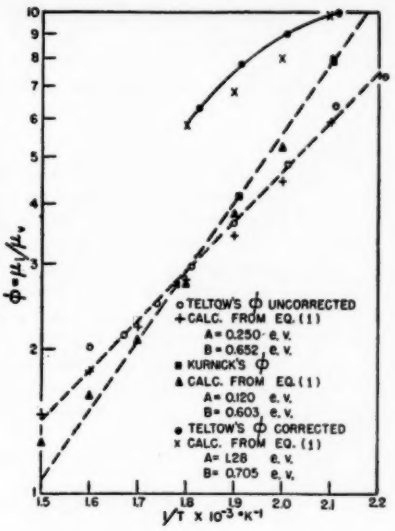
o TELTOW'S Φ UNCORRECTED
+ CALC. FROM EQ. (1)
A = 0.250 e.v.
B = 0.652 e.v.
■ KURNICK'S Φ
▲ CALC. FROM EQ. (1)
A = 0.120 e.v.
B = 0.603 e.v.
● TELTOW'S Φ CORRECTED
x CALC. FROM EQ. (1)
A = 1.28 e.v.
B = 0.705 e.v.
Φ = μi/μv
1/T x 10⁻³ °K⁻¹

FIG. 3. The ratio φ of the mobility of silver interstitial ions to that of silver vacancies as a function of the reciprocal of the absolute temperature.

For, if $\omega/2 > Q_v$, then the law of mass action would result in many more vacancies than interstitial ions. If also the Br^- vacancies do not diffuse readily without the electric field, the vacancy diffusion current would be larger and the cold end of the sample would become negative rather than positive. From Fig. 1, we see there is no tendency for ϵ to drop below a reasonable value for a Frenkel mechanism, even at 400°C. Accordingly, the anomalous conductivity at higher temperatures in AgBr, observed by both Teltow and Kurnick, appears presently to remain unexplained.

Turning now to the situation in doped samples, we observe that Eq. (6) would predict a constant value for ϵT over a reasonably low temperature range. The data plotted in Fig. 2 show some evidence that this is indeed true, although a slight tendency in this quantity to decrease with increasing temperature is certainly not ruled out. In order to obtain quantitative agreement between theory and experiment, assuming a value for Q_v of about 0.4 ev, we must make $Q_{Cd^{++}}$ slightly negative. This assumption would make $Q_{Cd^{++}}$ very small as compared to the estimate[8] for $U_{Cd^{++}}$ of about 0.8 ev. Such an assumption would be consistent with the result found above for Q_i if we assume that the Cd^{++} ions move as interstitial ions. This latter assumption appears reasonable.

ACKNOWLEDGMENT

We acknowledge with gratitude the partial support of the U. S. Office of Naval Research.

[8] Schone, Stasiw, and Teltow, Z. Physik Chem. **197**, 145 (1951).

Appearance Potential Studies. I. Determination of Excess Kinetic Energy*

RICHARD J. KANDEL
University of California, Los Alamos Scientific Laboratory, Los Alamos, New Mexico
(Received February 22, 1954)

The metastable ion suppressor on the Consolidated Engineering Corporation Model 21–103 mass spectrometer has been used as a retarding potential device to determine the excess kinetic energies possessed by the ions formed during appearance potential measurements. The suppressor setting at which an ion beam is extinguished is compared with the extinction setting for an ion beam with no excess energy. These settings are studied as a function of ionizing voltage, extrapolated back to the appearance potential, and converted into units of energy.

N^+ from N_2 was found to have no excess kinetic energy at the appearance potential. CH_3^+ from C_2H_6, CH_3^+ from C_3H_8, CN^+ from C_2N_2, and CH_3^+ from $C_6H_5CH_3$ were all formed with excess kinetic energy. The following quantities were deduced after taking the excess energy into account: $D(CH_3-CH_3)=3.87$ volts; $D(CH_3-C_2H_5)=3.70$ volts; $I(CN)=15.13$ volts; $I(C_6H_5)=9.90$ volts; $D(C_6H_5-CH_3)=3.80$ volts; $D(C_6H_5-H)=4.64$ volts.

INTRODUCTION

WHILE various methods have been suggested for predicting or qualitatively determining when an ion will be formed with excess kinetic energy in a mass spectrometer,[1–9] very little quantitative work has been done in this field.[7–9] Hagstrum[9] has incorporated retarding potential electrodes at the collector of a mass spectrometer and has thus obtained appearance potential and retarding potential curves for ions in the same apparatus under similar operating conditions. We have used the metastable ion suppressor slit system in the Consolidated Engineering Corporation Model 21–103 mass spectrometer in much the same manner.

The metastable suppressor, by applying a retarding potential almost equal to the initial ion accelerating voltage, filters out metastable ions formed past the ion source. If the metastable suppressor voltage is increased, the ion current is decreased in a manner dependent on the energy distribution of the ions. A cutoff point is finally attained at which the last noticeable ion current disappears. Molecular ions formed without dissociation possess no excess kinetic energy and have a common cutoff point while ions formed with excess kinetic energy have a higher cutoff point.

We have converted the arbitrary graduations on the metastable suppressor control potentiometer into units of excess kinetic energy and have studied the excess energy of a number of ions as a function of the ionizing voltage. All curves relating excess kinetic energy or metastable suppressor setting to the ionizing voltage have been extrapolated back to the appearance potential, and the final values for the excess kinetic energy have been determined at this voltage.

INSTRUMENT

The instrument used was a slightly modified Consolidated Engineering Corporation Model 21–103 mass spectrometer. A magnetic scan circuit which permitted a short scan of two to three mass units was incorporated into the instrument. Magnetic scanning was used in preference to voltage scanning for all appearance potential and excess energy determinations. The metastable suppressor and repeller circuits were slightly modified in order to obtain lower repeller voltages (0.25 percent of the ion accelerating voltage) and more accurately set and measured metastable suppressor voltages. In particular, a ten-turn, 100 000 ohm, 0.1 percent Beckman Helipot was installed as the control potentiometer in the metastable suppressor circuit. With this modification as little as 0.03 volt of excess kinetic energy could readily be detected.

EXCESS ENERGY DETERMINATION

The following symbols will be used throughout the remainder of this work: p—pressure; P—peak height; P_0—peak height with the metastable suppressor set at zero; S—metastable suppressor setting; S_x—metastable suppressor setting at which the ion beam is extinguished; S_x^0—extinction setting extrapolated back to the appearance potential; V_A—ion accelerating voltage; V_i—ionizing voltage; I_i—ionizing current; E—excess kinetic energy possessed by an ion; E_t—total excess kinetic energy of both the ion and the neutral fragments formed along with it; $A(X^+)$—appearance potential of X^+.

The value obtained for S_x in any particular experiment depends in a complex manner on the conditions under which it was determined. In particular, S_x varies with p, P_0, V_A, V_i, and I_i. There are two important reasons for this. One simply involves instrument sensitivity considerations. More sensitive gases run at higher

* This work was performed under the auspices of the U. S Atomic Energy Commission.

[1] W. Bleakney, Phys. Rev. **35**, 1180 (1930).
[2] H. D. Hagstrum and J. T. Tate, Phys. Rev. **59**, 354 (1941).
[3] R. E. Fox and J. A. Hipple, Rev. Sci. Instr. **19**, 462 (1948).
[4] J. A. Hipple, J. Phys. and Colloid Chem. **52**, 456 (1948).
[5] C. A. McDowell and J. W. Warren Discussions Faraday Soc. **10**, 53 (1951).
[6] D. P. Stevenson, Discussions Faraday Soc. **10**, 35 (1951).
[7] H. W. Washburn and C. E. Berry, Phys. Rev. **70**, 559 (1946).
[8] C. E. Berry, Phys. Rev. **78**, 597 (1950).
[9] H. D. Hagstrum, Revs. Modern Phys. **23**, 185 (1951).

pressures, ionizing currents, and voltages will naturally exhibit higher cutoff points than substances studied at lower pressures, currents, and voltages. The other includes all the factors which come under the heading of "space charge effects," and variations in any of the parameters listed above will affect the results for this reason. Consequently, as many of these quantities as possible are held constant during a determination. In particular, I_i is kept at 20 μa and V_A at 1002.5 volts. For any given set of determinations, p is held constant, the value selected depending on the nature of the substance being run and the abundance of the ion in question. P_0 is kept constant at 25 or 50 divisions, the choice again depending on the abundance of the ion.

In general, three types of behavior have been noted. Molecular ions typified by A^+, formed without fragmentation and having no excess kinetic energy, have cutoff points almost completely independent of V_i. Some fragments, typified by N^+ from N_2, have higher extinction points at high ionizing voltages but are extinguished at the same setting as A^+ in the vicinity of the appearance potential. These ions are formed with excess kinetic energy only at high ionizing voltages. The process taking place at the appearance potential, while it may involve the formation of fragments with excitational energy, does not involve the formation of ions with excess kinetic energy. Still other fragments, typified by CH_3^+ from C_2H_6, are formed with excess kinetic energy at the appearance potential and at all higher voltages.

Argon ions were the first to be investigated. V_A and I_i were set as mentioned above. V_i was set about three volts above the appearance potential and the pressure was adjusted to give a P_0 of 50 divisions. The suppressor potentiometer was turned up to the vicinity of the cutoff point, and the peak was repeatedly scanned at suppressor settings corresponding to ion energy increments of approximately 0.05 volt until the cutoff point had been passed. Peak heights were read with a calibrated cathetometer and could be measured reproducibly to within ± 0.04 division on the linagraph record paper (1 division = 2 mm). P was plotted against S, and S_x was determined by extrapolation.

This process was repeated at higher ionizing voltages. Compensation for the higher ionization probabilities was made as follows: The peaks were read on one of four galvanometers with sensitivities in the ratio 1:1/3:1/10:1/30. In addition, the sensitivity of the amplifier could be changed by a factor of fifteen. The choice of amplifier sensitivity and galvanometer was made in such a manner as to give a value of P_0 as near 50 divisions as possible. The observed peak heights were then adjusted to give $P_0 = 50$ divisions by multiplication by a constant factor. Those peaks which, after adjustment, would be too low to be read directly on the record (less than 0.1 division) were discarded.

With abundant ions such as argon S_x could be determined at ionizing voltages down to three volts above the appearance potential. Less sensitive ions, in some cases, could be studied only to within ten volts of the appearance potential without using excessively high sample pressures. S_x was then plotted against ΔV_i, the ionizing voltage increment above the appearance potential, and S_x^0 was obtained by extrapolation. Extrapolation of the argon curve was not necessary since S_x was constant over the range of voltages studied. The curve for A^+ is shown in Fig. 1.

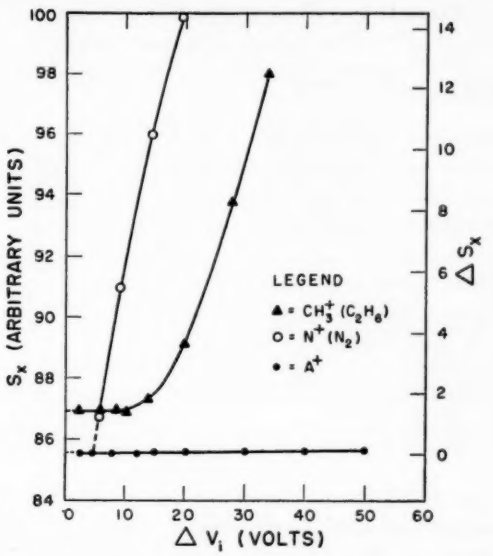

FIG. 1. Metastable suppressor curves for three ions. The S_x scale is arbitrary and applies to A^+. The ΔS_x scale refers to the extinction setting difference between the ions N^+ and CH_3^+ and their parent molecule ions N_2^+ and $C_2H_6^+$, the curves for the latter ions having been adjusted so as to coincide with the A^+ curve.

Similar studies were made on other ions formed without dissociation, among them Kr^+, Ne^+, N_2^+, CH_4^+, $C_2N_2^+$, and $C_6H_6^+$. The curves were all similar to the A^+ curve although S_x^0 varied as the nature of the chemical species studied was changed. For the above substances S_x^0 was between 85.0 and 86.0 in every case.

Ions formed by fragmentation were studied in a similar manner. I_i, V_A, p, and P_0 were held constant. S_x was determined at a series of ionizing voltages. In order to compensate for the variation of S_x with the material being run, the following procedure was adopted: After S_x had been determined at a given ionizing voltage for ion X^+, the magnetic field was changed so as to bring the parent ion XY^+ into focus, and S_x was determined for this ion. ΔS_x, the difference in extinction setting between X^+ and XY^+ was obtained and plotted against ΔV_i. ΔS_x^0 was determined by extrapolation. Curves for N^+ from N_2 and CH_3^+ from C_2H_6 are shown in Fig. 1. The values of S_x are arbitrarily chosen in order to present the three types of curves in the same figure for purposes of comparison.

The computation of E was made as follows: S_x^0 for A^+ was 85.5. The total ion accelerating voltage was 1002.5 volts (1000 volts from the ion accelerating

TABLE I. Appearance potentials of reference ions.

Ions	Appearance potential (volts)	Other reported values (volts)
He^+	24.40±0.10	24.47,[a] 24.58[b]
Ne^+	21.65±0.10	21.51,[a] 21.53,[c] 21.56,[b] 21.67[d]
Kr^+	14.08±0.02	13.96,[a] 14.01,[e] 14.03[e]
N_2^+	15.55±0.05	15.52,[d] 15.58,[b] 15.60,[f] 15.66[e]
CH_4^+	13.13±0.02	13.04,[f] 13.12,[h] 13.16[g]
$CH_3^+(CH_4)$	14.40±0.06	14.39,[h] 14.51,[i] 14.58[j]

[a] Dibeler, Mohler, and Reese, J. Research Natl. Bur. Standards **38**, 617 (1947).
[b] See reference 14.
[c] J. D. Morrison, J. Chem. Phys. **19**, 1305 (1951).
[d] F. H. Field, J. Chem. Phys. **20**, 1734 (1952).
[e] See reference 13.
[f] R. E. Honig, J. Chem. Phys. **16**, 105 (1948).
[g] J. D. Morrison and A. J. C. Nicholson, J. Chem. Phys. **20**, 102 (1952).
[h] See reference 5.
[i] See reference 15.
[j] See reference 12.

voltage and 2.5 volts from the repellers). The applied retarding potential, as deduced from the circuits, may be given as $1012.5+0.25S$, where S is defined above. Since S_x^0 is 85.5, the applied retarding potential at the cutoff point is 1033.9 volts. This potential is applied to the metastable suppressor slit system and produces a saddle point potential distribution through which the ions must pass before reaching the collector. Those ions which pass through the exact center of the field encounter only a fraction of the applied potential, that fraction being 0.966.[10] Since our beam has a finite width, we would expect a higher value for this fraction. The value actually obtained for several ions from the ratio of the applied accelerating to applied retarding potentials at the cutoff point is 0.969_6.

For any ion with excess kinetic energy, then,

$$E=0.969_6(1012.5+0.25S_x^0)-1002.5 \quad (1)$$

or

$$E=0.969_6(0.25\Delta S_x^0)=0.242_4\Delta S_x^0. \quad (1a)$$

Consider the reaction $XY+e\rightarrow X^+ + Y+2e$. It has been assumed[9] that equilibrium occurs during this simple fragmentation process to the extent that fragments may be considered to carry off excess kinetic energy in amounts inversely proportional to their masses as is required by the laws of conservation of mass, momentum, and energy in the case of an elastic collision. When such a reaction has taken place, therefore, and when $E(X^+)$ is known, E_t can be determined from the equation

$$E_t=E(X^+)M_{XY}/M_Y, \quad (2)$$

where M_{XY} and M_Y are the masses of the parent molecule and the uncharged fragment, respectively.

Where it appears evident from the energies involved that multiple fragmentation has taken place, no simple method can be used to determine E_t. The complete mechanism of fragmentation, including the sequence of steps, must be known before this quantity can be estimated. Consequently, in such cases only a minimum valve for E_t can be determined. In the examples that follow it is believed that fragmentation is of the simple kind described above.

[10] C. E. Berry, Consolidated Engineering Corporation (private communication).

APPEARANCE POTENTIAL DETERMINATION

Appearance potentials were determined by the method of initial breaks.[11,12] Argon and krypton were used as calibrating gases, and one of these gases was always mixed with the substance being studied. The ionization probability curves were investigated and the slopes of the linear portions of the curves above the exponential tails were determined. The pressures of the two components were then adjusted so that the curves were parallel in this region. At constant I_i and V_A the peaks were repeatedly scanned as the ionizing voltage was raised in 0.1 volt increments from a point below the first detectable ion current to the point where the peak height was approximately one division on the linagraph paper. The ion being studied and the calibrating ion were run alternately.

Peak heights were again read with the cathetometer. A straight line was fitted to the $P-V_i$ data by the Method of Least Squares. The appearance potential was determined from the intercept of the least squares line with the voltage axis.

Appearance potentials of several ions were determined in this manner as a means of checking the method. The results are given in Table I. Each appearance potential is the result of at least four determinations.

RESULTS

Values for appearance potentials and excess kinetic energies for several ions are summarized in Table II. The results are discussed below.

N^+ from N_2

$$A(N^+)=D(N_2)+I(N)=24.50\pm0.10 \text{ volts}. \quad (3)$$

Hagstrum[9] has shown that N^+ from N_2 is formed without excess kinetic energy at the appearance potential, and this work supports that contention. The ion is

TABLE II. Appearance potentials and excess kinetic energies of certain ions.

Substance	Ion	Appearance potential (volts)	Excess energy (volts)	Deduced quantity (volts)
N_2	N^+	24.50±0.10	0	
C_2H_6	CH_3^+	14.65±0.03	0.70	$D(CH_3-CH_3)=3.87$
C_3H_8	CH_3^+	15.77±0.12	1.99	$D(CH_3-C_2H_5)=3.70$
C_2N_2	CN^+	20.75±0.04	0.57	$I(CN)=15.13$
$C_6H_5CH_3$	CH_3^+	14.28±0.14	0.40	$D(C_6H_5-CH_3)=3.80$
$C_6H_5CH_3$	$C_6H_5^+$	13.70±0.05	0	$I(C_6H_5)=9.90$
C_6H_6	$C_6H_5^+$	14.54±0.02	0	$D(C_6H_5-H)=4.64$

[11] L. G. Smith, Phys. Rev. **51**, 263 (1937).
[12] J. J. Mitchell and F. F. Coleman, J. Chem. Phys. **17**, 44 (1949).

formed with excess energy at voltages above the appearance potential. This may account for the wide peaks observed by McDowell and Warren[5] indicating excess kinetic energy. Since $I(N)=14.55$ volts,[13] one obtains $D(N_2)=9.95\pm0.10$ volts. While this value is in agreement with the higher of the two acceptable spectroscopic values (9.756 volts),[14] the possibility of electronic excitation cannot be ruled out. Thus, a demonstration of the absence of excess kinetic energy in this process is not sufficient to provide a definitive value for the dissociation energy of nitrogen.

CH_3^+ from C_2H_6

$$A(CH_3^+)=D(CH_3-CH_3)+I(CH_3)+E_t=14.65\pm0.03 \text{ volts.} \quad (4)$$

ΔS_x^0 was determined by extrapolation to be 1.45. This corresponds to $E=0.35$ volt and, if one adds a like amount for the methyl radical, one obtains $E_t=0.70$ volt. Since $I(CH_3)=10.08$ volts,[15] then $D(CH_3-CH_3)=3.87$ volts. Van Artsdalen[16] obtained 3.71 volts for this dissociation energy from photobromination studies and Butler and Polanyi[17] obtained 3.77 volts from the pyrolysis of iodides.

CH_3^+ from C_3H_8

$$A(CH_3^+)=D(CH_3-C_2H_5)+I(CH_3)+E_t=15.77\pm0.12 \text{ volts.} \quad (5)$$

$\Delta S_x^0=5.4$. E, therefore, is 1.31 volts and E_t is 1.99 volts. This value, in conjunction with the aforementioned ionization potential of CH_3 and the measured appearance potential, gives $D(CH_3-C_2H_5)=3.70$ volts. By the same methods mentioned in connection with CH_3^+ from C_2H_6, Van Artsdalen[16] and Butler and Polanyi[17] obtained 3.63 and 3.69, respectively, for this bond energy. The ethyl ion from propane is formed without excess energy. Stevenson and Hipple[18] studied the appearance potential of this ion and deduced

$$D(CH_3-C_2H_5)=3.52 \text{ volts.}$$

CN^+ from C_2N_2

$$A(CN^+)=D(CN-CN)+I(CN)+E_t=20.75\pm0.04 \text{ volts.} \quad (6)$$

E_t is 0.57 volt and $D(CN-CN)$ at 25°C is 5.05 volts.[19] $I(CN)$, therefore, is 15.13 volts. McDowell and Warren[20] obtained $A(CN^+)=20.4\pm0.3$ volts, predicted excess kinetic energy, and set a maximum limit of 15.6 volts for $I(CN)$.

CH_3^+ and $C_6H_5^+$ from $C_6H_5CH_3$

$$A(CH_3^+)=D(C_6H_5-CH_3)+I(CH_3)+E_t=14.28\pm0.14 \text{ volts.} \quad (7)$$

$$A(C_6H_5^+)=D(C_6H_5-CH_3)+I(C_6H_5)=13.70\pm0.05 \text{ volts.} \quad (8)$$

$E_t=0.40$ volts. Hence, $D(C_6H_5-CH_3)$ is 3.80 volts, and $I(C_6H_5)$ is 9.90 volts. Szwarc[21] and Roberts and Skinner[22] estimated $D(C_6H_5-CH_3)$ as 3.95 and 3.90 volts, respectively.

$C_6H_5^+$ from C_6H_6

$$A(C_6H_5^+)=D(C_6H_5-H)+I(C_6H_5)=15.54\pm0.02 \text{ volts.} \quad (9)$$

No excess kinetic energy was found in studying this ion. A value of 4.64 volts for $D(C_6H_5-H)$ is obtained from this appearance potential and the above-listed value for $I(C_6H_5)$. Szwarc[21] and Roberts and Skinner[22] estimated 4.51 and 4.42 volts, respectively, for this bond energy.

ACKNOWLEDGMENTS

The author would like to express his thanks to Dr. Clifford E. Berry of Consolidated Engineering Corporation and Dr. Louis C. Smith of this laboratory for their many helpful suggestions during the course of this work. He would also like to thank Mr. Candelario Esquibel for his help in running the spectrometer and interpreting the records.

[13] R. F. Bacher and S. Goudsmit, *Atomic Energy States* (McGraw-Hill Book Company, Inc., New York, 1932).
[14] G. Herzberg, *Molecular Spectra and Molecular Structure. I. Diatomic Molecules* (Prentice-Hall, Inc., New York, 1935).
[15] J. A. Hipple and D. P. Stevenson, Phys. Rev. **63**, 121 (1943).
[16] E. R. Van Artsdalen, J. Chem. Phys. **10**, 653 (1942).
[17] E. T. Butler and M. Polanyi, Trans. Faraday Soc. **39**, 19 (1943).
[18] D. P. Stevenson and J. A. Hipple, J. Am. Chem. Soc. **64**, 2769 (1942).
[19] Brewer, Templeton, and Jenkins, J. Am. Chem. Soc. **73**, 1462 (1951).
[20] C. A. McDowell and J. A. Warren, Trans. Faraday Soc. **48**, 1084 (1952).
[21] M. Szwarc, Chem. Revs. **47**, 75 (1950).
[22] J. S. Roberts and H. A. Skinner, Trans. Faraday Soc. **45**, 339 (1949).

Thermal Relaxation in Gases*

ROBERT BROUT†
Department of Chemistry, Columbia University, New York, New York
(Received December 22, 1953)

The solution of the linearized equations appropriate for sound dispersion is presented. The limiting cases as the sound frequency becomes large or small is examined. The two state gas is exhibited as a special case and shown equivalent to previous work in the field when the appropriate assumptions are made.

I. INTRODUCTION

IN gases undergoing rapid compressions and rarefactions, there is insufficient time for equilibration of internal and external modes of motion of the molecules. Hence, the apparent heat capacity calculated from the velocity of sound is often lower than the equilibrium value indicating some of the internal molecular energy has been "frozen" in. This effect has been cast into the form of a relaxation time by Kneser[1] and others for the two state gas and has been extended by Landau and Teller[2] for the n-state harmonic oscillator, assuming only $n\rightarrow n\pm1$ transitions occur, these transitions depending on n only as the squares of the dipole matrix elements $X_{n,n}\pm1$. The general n-state gas has been treated by Bourgin[3] and Schaefer[4] and more recently by Schwartz, Slawsky, and Herzfeld.[5] It is the purpose of this article to cast the relaxation equations into a form in which matrix algebra may be used and to immediately demonstrate the existence of a weighting factor other than the Boltzmann factor to describe this nonequilibrium situation.

II

We begin with the following assumptions:

1. Only binary collisions occur.
2. Translation equilibrates instantaneously.

We let N=number of molecules/cm^3; N_i=number of molecules in state i/cm^3; N_i^0=number of molecules in state i/cm^3 at equilibrium; p_{ij}^{kl}=the probability that molecules in internal states i, j, upon colliding produce molecules in internal states k, l; Z_0=number of collisions/sec$\times N^2$. Then, taking into account the following facts:

(a) The number of collisions between molecules in states i and $j=Z_0N_iN_j$ if $i\neq j$, but $=\frac{1}{2}Z_0N_i^2$ $i=j$.

(b) $P_{ij}{}^{kk}$ and $P_{kk}{}^{ij}$ must be weighted doubly in an expression for (dN_k/dt) if i, $j\neq k$, but $P_{ik}{}^{kk}$ and $P_{kk}{}^{ik}$ are weighted singly. Then, taking into account

$$\sum_1 \sum_{k\leq l} P_{ij}{}^{kl}=1 \text{ all } i,\ j,$$

$$(1/Z_0)(dN_k/dt)=\tfrac{1}{2}\sum_{i,j,l}[(1+\delta_{kl})P_{ij}{}^{kl}-2\delta_{ik}\delta_{jl}]N_iN_j.$$

As we are interested in conditions near equilibrium, we will consider $N_i=N_i^0+n_i$, where N_i^0 is the equilibrium number of molecules per cm^3 in the state i and n_i is the deviation of N_i from equilibrium.

Further, as the process is one of thermal relaxation (i.e., rapid temperature fluctuations), $Z_0P_{ij}{}^{kl}$ will change with the temperature and therefore will be expanded about the equilibrium temperature.

$$Z_0P_{ij}{}^{kl}=Z_0P_{ij}{}^{kl}|_0+(\partial Z_0P_{ij}{}^{kl}/\partial\beta)|_0\delta\beta.$$

The subscript "0" will be dropped as it is needless.

Then, dropping second-order terms in n_i and $\delta\beta$ and remembering that

$$\tfrac{1}{2}\sum_{i,j,l}[(1+\delta_{kl})P_{ij}{}^{kl}-2\delta_{ik}\delta_{jl}]N_i^0N_j^0=0, \qquad (1)$$

(the definition of equilibrium) we have

$$\begin{aligned}\dot{n}_k/Z_0=\dot{N}_k/Z_0=\tfrac{1}{2}\{&\sum_{i,j,l}[(1+\delta_{kl})P_{ij}{}^{kl}\\&-2\delta_{ik}\delta_{jl}][N_i^0n_j+N_j^0n_i]\\&+\delta\beta\sum_{i,j,l}(\partial/\partial\beta)[Z_0(1+\delta_{kl})P_{ij}{}^{kl}\\&-2Z_0\delta_{ik}\delta_{jl}]N_i^0N_j^0\}. \qquad (2)\end{aligned}$$

If 1 is differentiated with respect to β, bearing in mind that $(\partial N_i^0/\partial\beta)=(\bar{\epsilon}-\epsilon_i)N_i^0$,

$$\begin{aligned}\sum_{i,j,l}(\partial/\partial\beta)&[(1+\delta_{kl})P_{ij}{}^{kl}-\delta_{ik}\delta_{jl}]N_i^0N_j^0\\&=\sum_{i,j,l}[(1+\delta_{kl})P_{ij}{}^{kl}-\delta_{ik}\delta_{jl}]N_i^0N_j^0(\epsilon_i+\epsilon_j). \qquad (3)\end{aligned}$$

We thus have the needed expression for the rather nebulous term containing $(\partial/\partial\beta)Z_0P_{ij}{}^{kl}$. This arises directly from the equilibrium equation. The customary work in all relaxation phenomena is to make use of detailed balance. It is here shown that this is an unnecessarily stringent condition; this derivation would include cyclic phenomena if such exist.

---

* Submitted in partial fulfillment for the degree of Doctor of Philosophy in the Faculty of Sciences, Columbia University.

† U. S. Atomic Energy Commission Predoctoral Fellow 1951–1953. Present address: Department of Chemistry, University of Rochester, Rochester, New York.

[1] See, for example, H. Kneser, *Ergebnisse der Exacten Naturwissenschaften* (Julius Springer, Berlin, 1949), Chap. XXII.

[2] L. Landau and E. Teller, Physik. Z. Sowjetunion **10**, 34 (1936).

[3] D. G. Bourgin, Phys. Rev. **34**, 821 (1929); **42**, 721 (1932); **50**, 355 (1936).

[4] K. Schaefer, Z. physik. Chem. **B46**, 212–228 (1940).

[5] Schwartz, Slawsky, and Herzfeld, J. Chem. Phys. **20**, 1519 (1952).

Substituting (2) into (1),

$$\dot{n}_k/Z_0=\tfrac{1}{2}\{\sum_{i,j,l}[(1+\delta_{kl})P_{ij}{}^{kl}-2\delta_{ik}\delta_{jl}][N_i{}^0n_j+N_j{}^0n_i]+\delta\beta\sum_{i,j,l}[(1+\delta_{kl})P_{ij}{}^{kl}-\delta_{ik}\delta_{jl}-\delta_{il}\delta_{jk}]N_i{}^0N_j{}^0\epsilon_i.$$

Using the condition $P_{ij}{}^{kl}=P_{ji}{}^{kl}$, one obtains

$$\dot{n}_k/Z_0=\sum_{i,j,l}[(1+\delta_{kl})P_{ij}{}^{kl}-\delta_{ik}\delta_{jl}-\delta_{il}\delta_{jk}]N_j{}^0n_i+\delta\beta\sum_{i,j,l}[(1+\delta_{kl})P_{ij}{}^{kl}-\delta_{ik}\delta_{jl}-\delta_{il}\delta_{jk}]N_j{}^0N_i{}^0\epsilon_i.$$

We now define what are analogous to first-order rate constants,

$$k_{ki}=Z_0\sum_{j,l}[(1+\delta_{kl})P_{ij}{}^{kl}-\delta_{ik}\delta_{jl}-\delta_{il}\delta_{jk}]N_j{}^0, \quad (4)$$

whence

$$\dot{n}_k=\sum_i k_{ki}n_i+\delta\beta\sum_i k_{ki}N_i{}^0\epsilon_i. \quad (5)$$

Two immediate facts about the k_{ki}'s present themselves:

$$\sum_i k_{ki}N_i{}^0=0, \text{ a restatement of (1)}; \quad (6a)$$

$$\sum_k k_{ki}=0, \quad (6b)$$

where (6b) is apparent from the normalization condition of $P_{ij}{}^{kl}$.

Let us now consider the special case of a periodic motion such that $\delta\beta=\delta\beta_0e^{i\omega t}$, where $(\omega/2\pi)$ is the frequency of the imposed sound field on the system undergoing collisions, whence (5) becomes

$$\dot{n}_k-\sum k_{ki}n_i=e^{i\omega t}\delta\beta_0\sum_i k_{ki}\epsilon_iN_i{}^0. \quad (7)$$

In the steady state, n_k is of the form $n_k{}^0e^{i\omega t}$, and hence

$$\dot{n}_k=i\omega n_k;$$

whence,

$$\sum_i(k_{ki}-i\omega\delta_k)n_i=-\delta\beta\sum_i k_{ki}\epsilon_iN_i{}^0. \quad (8)$$

If K denotes the matrix with elements k_{ij}, n and (ϵN) vectors with elements n_i and $\epsilon_iN_i{}^0$, respectively, (8) may be rewritten

$$(K-Ii\omega)n=-\delta\beta K(\epsilon N).$$

A solution of these equations is readily found

$$n=-\delta\beta[i\omega(K-Ii\omega)^{-1}(\epsilon N)+\epsilon N].$$

Letting

$$r_{ij}=i\omega(K-Ii\omega)_{ij}{}^{-1},$$

$$n_i=-\delta\beta[\sum_i r_{ij}\epsilon_jN_j{}^0+\epsilon_iN_i{}^0]=-\delta\beta N_i{}^0[\sum_j(1/N_i{}^0)r_{ij}\epsilon_jN_j{}^0+\epsilon_i]. \quad (9)$$

This is to be compared with the value of n_i if equilibration is instantaneous, *viz.*,

$$n_i=\delta\beta N_i{}^0(\bar{\epsilon}-\bar{\epsilon}_i). \quad (10)$$

It is seen that the r_{ij} is merely a new frequency dependent weighting factor other than the Boltzmann factor. In order to demonstrate the meaning and the validity of Eq. (9), limiting cases as $\omega\to0$ and $\omega\to\infty$ will now be calculated.

$$r_{ij}=\frac{(-1)^{i+j}i\omega M_{ji}}{|K-Ii\omega|}, \quad (11)$$

where M_{ji} is the ji minor of $|K-Ii\omega|$.

Now $\lim_{\omega\to0}|K-Ii\omega|=|K|=0$ from relations (6). It is therefore necessary to calulate $\lim_{\omega\to0}(i\omega/|K-Ii\omega|)$

$$|K-Ii\omega|=0-i\omega\sum M_{ii}+0(\omega^2,\omega^3,\cdots\omega^r),$$

where M_{ii} are the first-order diagonal minors of $|K|$ Hence,

$$\lim_{\omega\to0}(i\omega/|K-Ii\omega|)=(-1/\sum_l M_{ll}).$$

Thus,

$$\lim r_{ij}=-\frac{M_{ji}(-1)^{i+j}}{\sum_l M_{ll}}. \quad (12)$$

In order to evaluate the minors, we note

$$\sum_k k_{ki}M_{ki}(-1)^{i+k}=0, \quad \text{since} \quad |K|=0.$$

$$\sum_k k_{ki'}M_{ki}(-1)^{i+k}=0, \quad i\neq i', \quad (13)$$

by definition of a determinant. Now from (6b)

$$\sum_k k_{ki}=0, \quad \text{all } i.$$

Therefore the relations (13) state that $M_{ki}(-1)^{i+k}$ is independent of the index k; call it M_i.

Similarly,

$$\sum_i k_{ki}M_i=0 \quad \text{since} \quad |K|=0, \quad \text{all } k.$$

But (6a) states

$$\sum_i k_{ki}N_i{}^0=0, \quad \text{all } k.$$

Thus, $M_{ji}(-1)^{i+j}=\text{constant}\times N_i{}^0$. Whence from (11)

$$\lim_{\omega\to0} r_{ij}=-N_i{}^0/N. \quad (14)$$

In the limit as $\omega \to \infty$,

$$\lim_{\omega\to\infty} |K - I i\omega| = (-i\omega)^r;$$

$$\lim_{\omega\to\infty} M_{ii} = (-i\omega)^{r-1};$$

$$\lim_{\omega\to\infty} M_{ij} = (-i\omega)^{r-2}, \quad i \neq j.$$

Therefore

$$\lim_{\omega\to\infty} r_{ij} = \lim_{\omega\to\infty} \frac{i\omega M_{ij}(-1)^{i+j}}{|K - I i\omega|} = -\delta_{ij}. \tag{15}$$

Summarizing,

$$n_i = N_i^0 \delta\beta\Big[-\sum_j (1/N_i^0) r_{ij} \epsilon_j N_j^0 - \epsilon_i\Big]; \tag{16}$$

$$\lim_{\omega\to\infty} n_i = N_i^0 \delta\beta[\bar{\epsilon} - \epsilon_i]; \tag{17}$$

$$\lim_{\omega\to\infty} n_i = 0. \tag{18}$$

Both limits give the required behavior of n_i.

The effective heat capacity C_v is given by the equation

$$C_v = \tfrac{3}{2}R - (1/NkT^2)(d/d\beta)\sum n_i \epsilon_i. \tag{19}$$

But we have found, to our approximations, $dn_i/d\beta = n_i/\delta\beta$, as given by (15). Putting (16), (17), and (18) into (19), we find

$$C_v = \tfrac{3}{2}R + (1/NkT^2) \sum_{i,j} (r_{ij} + \delta_{ij}) \epsilon_i \epsilon_j N_j^0;$$

$$\lim_{\omega\to 0} C_v = \tfrac{3}{2}R + (1/NkT^2) \sum_{i,j} (\delta_{ij} - N_i^0/N) \epsilon_i \epsilon_j N_j^0 \tag{20}$$

$$= \tfrac{3}{2}R + (1/NkT^2)(\langle \bar{\epsilon}^2 \rangle_{Av} - \bar{\epsilon}^2);$$

$$\lim_{\omega\to\infty} C_v = \tfrac{3}{2}R.$$

Thus both limiting values are correct. In the general formula r_{ij} is given by (11). It is to be noted that the inverse of $(K - iI\omega)$ could be expressed in terms of the eigenvalues of K, each eigenvalue representing a relaxation time. This would create an analogy between the above general development and the often treated two state case, however it would not simplify the above equations, but rather complicate them.

III. TWO STATE GAS

An important illustration of the above is the two state gas, used in almost all interpretations of sound dispersion data. Our results are then exhibited using relations (6).

$$|K - I i\omega| = i\omega(k_{11} + k_{22}) + (i\omega)^2$$

$$r_{11} = -(k_{22} - i\omega)/k_{11} + k_{22} - i\omega; \quad r_{12} = -k_{22}/k_{11} + k_{22} - i\omega.$$

Substituting into (16) and (20) using relations (6),

$$n_1 = -n_2 = \delta\beta(N_1^0 N_2^0/N)((\epsilon_2 - \epsilon_1)/1 + i\omega\tau),$$

$$C = C_{\text{trans}} + \frac{C_{\text{int}}}{(1 + i\omega\tau)},$$

where $\tau^{-1} = -(k_{11} + k_{22})$ and $C_{\text{int}} = (\langle \bar{\epsilon}^2 \rangle_{Av} - \bar{\epsilon}^2)(1/NkT^2)$. Now, from (4),

$$k_{11} = -Z_0[-(P_{11}^{12} + 2P_{11}^{22})N_1^0 + (P_{12}^{11} - P_{12}^{22})N_2^0].$$

In most applications it is assumed that

$$P_{11}^{22} = P_{22}^{11} = 0;$$

$$\tfrac{1}{2}P_{11}^{12} = P_{12}^{22} = \alpha = \text{probability of activation};$$

$$\tfrac{1}{2}P_{22}^{12} = P_{12}^{11} = \gamma = \text{probability of deactivation},$$

whence

$$\tau^{-1} = Z_0 N(\gamma + \alpha).$$

Using relation (6a),

$$\gamma N_2^0 = \alpha N_1^0.$$

Hence

$$\tau^{-1} = Z_0 N \gamma (1 + N_2^0/N_1^0).$$

These are the customary relations previously derived from considerations of the two state gas alone. It is here shown that our general formulation is consistent with previous calculations.

IV. ACKNOWLEDGMENTS

I would like to express my gratitude to Professor George Kimball for his guidance of this research. Thanks are due to the U. S. Atomic Energy Commission for their financial support in the course of this research.

Dissociation Energy of N_2†

J. M. HENDRIE
Columbia University, New York, New York
(Received April 12, 1954)

An attempt has been made to observe the thermal dissociation of N_2 in order to choose between the two values, 7.385 ev and 9.765 ev, for the dissociation energy of N_2. At the highest available temperatures no dissociation could be observed, and a lower limit of 8.80 ev is set for $D(N_2)$.

INTRODUCTION

THE value of the dissociation energy of the nitrogen molecule, $D(N_2)$, has long been a subject of controversy.[1] Of the many values proposed by various authors, all but the values 7.385 ev and 9.765 ev have been eliminated as possibilities for $D(N_2)$. Until 1951 most writers preferred the lower value 7.385 ev but the recent experiments of Douglas[2] on the N_2^+ spectrum, of Carroll[3] on the N_2 spectrum, and of Kistiakowsky, Knight, and Malin,[4] and Thomas, Gaydon and Brewer[5] on cyanogen-oxygen mixtures now give very strong support to the higher value, 9.765 ev. The purpose of the present work is to choose between the values 7.385 ev and 9.765 ev for $D(N_2)$ by observation of the thermal dissociation of N_2 at high temperatures and low pressures.

The general procedure is as follows: Nitrogen at pressures of the order of 1 mm Hg is heated to temperatures up to the limit of a tungsten oven, about 3450° K. A beam of the hot gas, effusing from the tungsten oven mounted in the source chamber of a molecular beams apparatus, passes through the evacuated apparatus to a detector. A strong inhomogeneous magnetic field perpendicular to the beam may be turned on to deflect particles of large magnetic moment away from the detector. The field strength is adjusted so that nitrogen atoms, having magnetic moments of the order of one Bohr magneton, are deflected away from the detector, while nitrogen molecules, whose moments are of the order of a nuclear magneton are not sufficiently deflected to miss the detector. A comparison of the beam intensity at the detector with the magnetic field off and on permits the fractional content of nitrogen atoms in a beam of hot nitrogen gas to be determined. Nitrogen gas in thermal equilibrium with an oven at 3450°K temperature and 1 mm Hg pressure should be 20 percent dissociated if $D(N_2)=7.385$ ev, and only 0.5 percent dissociated if $D(N_2)=9.765$ ev. This considerable difference in the fractional dissociation of N_2 for the two values of $D(N_2)$, at the same temperature and pressure, makes it possible to choose the correct value from the data of these experiments.

It should be noted that the method used here is substantially less accurate than spectroscopic methods for the determination of the dissociation energy of a molecule. In the particular case of N_2, the spectroscopic method gives several values, each very accurately measured, but is unable to choose rigorously between them. The molecular beams method used in this experiment gives an unambiguous choice between the spectroscopic values, but can add nothing in the way of improved accuracy.

In order to check the validity of the whole procedure, particularly with regard to thermal equilibrium of the gas passing through the hot oven, several runs were made with hydrogen. The dissociation energy of hydrogen is 4.47 ev, and for pressures around 1 mm Hg, H_2 gas in thermal equilibrium should be 98 percent dissociated at 3000°K. The interesting portions of the hydrogen dissociation curves are therefore in a temperature region which is experimentally convenient for tungsten ovens.

APPARATUS

The oven in which the gas is heated, Fig. 1, is a tungsten tube 2.5 cm long, 0.25 cm o.d., and 0.15 cm i.d. The oven is made by grinding a solid 0.25-cm tungsten rod to a half cylinder. A 0.15 cm thick grinding wheel is then dressed to a round edge and is used to grind out the center of the half-cylinder. Two such half-cylinders are used together to form a tube. Into the edge of one of the half-cylinders a 0.32 cm long, 0.0076 cm wide slit is lapped. The two half-cylinders are ground to fit snugly into tungsten collars at either end. The tungsten collars are, in turn, brazed to water-cooled copper blocks. The oven is heated by passing current through it, 300 amp being sufficient to raise the oven to about 3300°K. The oven is supported in the source chamber of a molecular beams apparatus. Gas is fed into the oven through one end collar at pressures around 1 mm Hg, and effuses out into the vacuum through the slit

† This research was supported in part by the Office of Naval Research.

[1] For reviews of the subject and a list of the literature prior to 1948, see G. Herzberg, *Molecular Spectra and Molecular Structure, I. Diatomic Molecules* (Prentice-Hall Inc., New York, 1950), second edition, and A. G. Gaydon, *Dissociation Energies and Spectra of Diatomic Molecules* (Chapman and Hall, Ltd., London, 1947). More recent articles of interest are: J. Kaplan, Phys. Rev. **78**, 93 (1950); H. D. Hagstrum, Revs. Modern Phys. **23**, 185 (1951); G. Glocker, J. Chem. Phys. **19**, 124 (1951); A. E. Douglas and G. Herzberg, Can. J. Phys. **29**, 294 (1951); L. Pauling and W. F. Sheehan, Jr., Proc. Natl. Acad. Sci. **35**, 359 (1949); Brewer, Templeton, and Jenkins, J. Am. Chem. Soc. **73**, 1462 (1951).

[2] A. E. Douglas, Can. J. Phys. **30**, 302 (1952).

[3] P. K. Carroll (private communication).

[4] Kistiakowsky, Knight, and Malin, J. Am. Chem. Soc. **73**, 2972 (1951).

[5] Thomas, Gaydon, and Brewer, J. Chem. Phys. **20**, 369 (1952).

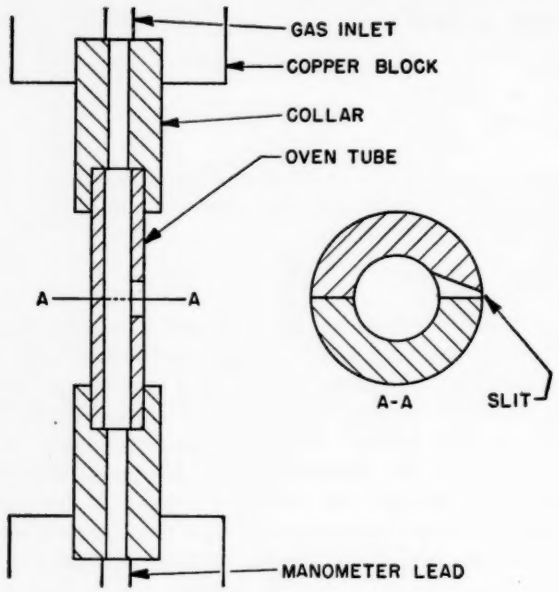

FIG. 1. Oven assembly.

at the center of the oven. The flow rate is controlled by a needle valve. A $\frac{1}{8}$ inch copper tube leads from the other end of the oven to an oil manometer. The manometer measures the pressure difference between the oven interior and the source chamber, which is at 2×10^{-5} mm Hg. A glass plate in the source chamber wall permits optical pyrometer measurements of the oven temperature.

In searching for dissociation in nitrogen, observations were taken at successively higher temperatures until the oven burned out. The highest temperature at which observations were made was 3530°K. In the oven mounting used, small stresses on the oven due to the mount could not be avoided. At temperatures at which the tungsten became plastic these stresses distorted the oven tube, producing a region of decreased cross section at which the local temperature rose to the melting point (3655°K). Efforts to reduce these stresses gave ovens with useful lives of perhaps 20 minutes at 3400° to 3450°K. Below 3300°K the ovens were quite stable.

The apparatus, Fig. 2, is divided into a source chamber and an interaction space. Some of the particles effusing from the oven slit pass through a 0.015-cm slit in the wall of the source chamber and continue on into the interaction space as a thin beam. Vacuum in the interaction space is of the order of 10^{-6} mm Hg. The beam passes between the poles of an iron electromagnet whose field direction is perpendicular to the beam. The magnetic field is strongly inhomogeneous, having a ratio of gradient to field of 3.2 cm^{-1} over the region of the beam. The field strengths used for deflection were 12 000–14 000 gauss.

The beam is collimated by a 0.0025-cm slit between the magnet and the detector and is detected in a Pirani gauge which is described in detail in a paper by Prodell and Kusch.[6] The entry slit of the detector is 0.0025 cm wide.

DEFLECTION OF THE BEAM

In the presence of the transverse, inhomogeneous field of the electromagnet, those particles in the beam which have magnetic dipole moments are subjected to a force tending to deflect them out of the beam. The field strength is so chosen that particles with magnetic moments of the order of μ_0 are removed from the beam, while particles of moments of the order of a nuclear magneton are only slightly effected and remain in the beam.

For temperatures up to 3500°K, the only molecular state of N_2 sufficiently populated to enter into the discussion is the $^1\Sigma$ ground state. Contributions to the magnetic moment of N_2 in the $^1\Sigma$ state come from the nitrogen nuclei, whose moments are 0.403 nuclear magneton and from the molecular rotational moment, which is presumably less than a nuclear magneton. The reduction in the observed intensity at the detector of the molecular component of a beam of nitrogen at 3000°K due to deflection in the magnetic field is calculated to be only 0.1 percent. Similar considerations apply to the hydrogen molecule, which also has a $^1\Sigma$ ground state. The state of the nitrogen atom of interest in the dissociation process is the $^4S_{\frac{3}{2}}$ ground state, which has a magnetic moment of $\pm\mu_0$ or $\pm3\mu_0$, depending on the m_J value. The reduction in the atomic component of a beam of nitrogen at 3000°K resulting from deflection in the magnetic field is calculated to be larger than 99.4 percent. Again the same remarks apply to the hydrogen atom, which has a $^2S_{\frac{1}{2}}$ ground state.

PROCEDURE

The procedure used in all runs was to set the potential applied across the oven at some value and allow the oven to come to equilibrium at a corresponding temperature. The beam intensities with magnetic field off and on were observed alternately several times. The oven temperature was read with the optical pyrometer, and the total pressure in the oven was measured with the manometer. The oven potential was then increased, and the observations repeated at a higher temperature. Each new oven was used in a run on hydrogen before it was tried with nitrogen. The hydrogen runs were generally terminated around 3000°K, while the nitrogen runs were continued until the oven burned out.

The oven temperature was measured with an optical pyrometer through a glass plate at the end of the source chamber. In order to remove uncertainties in the temperature measurement caused by the glass plate, the pyrometer was calibrated against a solid tungsten rod heated by a known current. A 0.25-cm diameter solid tungsten rod 10.8 cm long was mounted in the source chamber in the position of the oven. Heating current was supplied from four two-volt submarine

[6] A. G. Prodell and P. Kusch, Phys. Rev. 88, 184 (1952).

storage cells and measured by observing the potential developed across a Leeds and Northrup standard high current milliohm resistance. The temperature of the solid rod was determined at each setting of current by use of the Jones-Langmuir tungsten tables, and corresponding readings of the optical pyrometer were noted. The pyrometer was thus calibrated in the identical setup in which oven temperatures were measured during runs. Several calibrating runs with the solid rod were made at various times during the experiment and all were in good agreement. At temperatures above 2600°K the oven came to a uniform temperature over the central section, no substantial temperature difference being observed with the pyrometer over the whole hot region of the oven between the end collars.

CALCULATIONS

Fractional Dissociation in the Oven

For a given temperature and pressure in the oven the measured quantities are the intensity of the beam with magnetic field off I and the reduction in beam with magnetic field on i. These quantities must be related to the equilibrium partial pressures of molecules $p(N_2)$ and atoms, $p(N)$, in the oven. In particular, the fractional dissociation,

$$X=p(N)/[p(N)+p(N_2)] \tag{1}$$

must be determined from the quantities I and i. For internal pressures in the oven of the order of 1 mm Hg, the number of particles effusing per unit time through a narrow slit will be

$$n(N_2)=\beta p(N_2)/(2M)^{\frac{1}{2}} \tag{2}$$

for nitrogen molecules, and

$$n(N)=\beta p(N)/M^{\frac{1}{2}} \tag{3}$$

for nitrogen atoms. Here β is a constant involving the dimensions of the slit, and M is the atomic weight of nitrogen. The intensity I and the differential intensity i observed at the detector are

$$I=k_2 n(N_2)+k_1 n(N), \tag{4}$$

$$i=k_1 n(N), \tag{5}$$

where the k's are constants involving the geometrical properties of the apparatus and the response of the detector to unit incident particle. Since two atoms combine to form a single molecule in the detector it might be expected that $k_1=0.5k_2$. In fact, in experiments on the detector response for atomic hydrogen compared to that for hydrogen molecules, it has been found that $k_1=0.46k_2$, in satisfactory agreement with predictions based on elementary considerations. A Wood's discharge tube was used as a source in this measurement instead of the tungsten oven. By turning the discharge on and off it was possible to obtain beams of molecules plus atoms or of molecules alone. A comparison of the detector responses and the pressures of the gas with the discharge tube on and off yields the relative detection efficiency of hydrogen atoms and molecules under the conditions of these experiments.

The agreement between the relative predicted response for atoms and molecules 0.5 and that measured 0.46 indicates that atoms entering the Pirani gauge cavity recombine to molecules almost immediately, and that the heat of recombination of the molecules thus formed is not liberated on the temperature sensitive resistance elements of the gauge to a degree which significantly effects the equilibrium temperature of the elements. Finally, there is no large difference in the scattering of atoms and molecules over the length of the beam. In view of these considerations the relative atom-molecule detection efficiency may be assumed to be the same for nitrogen as for hydrogen.

It is to be noted that reasonable deviations from the ideal relative detection efficiency have no significant effect on any results obtained in the present research.

Equation (5) for the atomic signal may then be rewritten as

$$i=0.46k_2 n(N). \tag{6}$$

After rearrangement of the above equations, the partial pressures become

$$\begin{aligned} p(N_2)&=(2M)^{\frac{1}{2}}(I-i)/k_2\beta, \\ p(N)&=M^{\frac{1}{2}}i/0.46k_2\beta, \end{aligned} \tag{7}$$

and the fractional dissociation in terms of the observed quantities is

$$X=i/[i+0.46\sqrt{2}(I-i)] \tag{8}$$

This expression is free of the unknown constants β and k_2 and is used to calculate fractional dissociation in the oven. It is used for both nitrogen and hydrogen. The fractional dissociation in the oven may be expressed

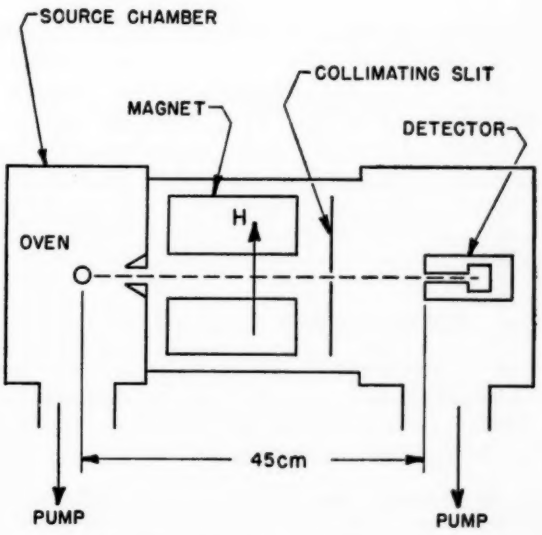

FIG. 2. Diagram of the molecular beams apparatus.

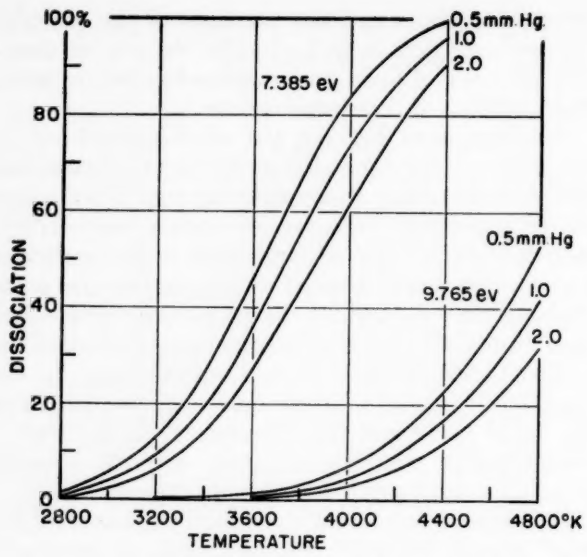

FIG. 3. The calculated dissociation of N_2 for each of the two proposed values for $D(N_2)$, 7.385 ev and 9.765 ev.

in terms of the fractional reduction in beam with magnetic field, which is just $\theta \equiv i/I$. Equation (8) then becomes:

$$X=\theta/[0.46\sqrt{2}+(1-0.46\sqrt{2})\theta]. \quad (9)$$

Theoretical Dissociation

The fractional dissociation of a diatomic gas in thermal equilibrium at a temperature T may be calculated from the equilibrium constant, $K(T)$. Where $p(N)$ and $p(N_2)$ are the partial pressures of atomic and molecular components in the reaction

$$N_2 \rightleftharpoons 2N,$$

the equilibrium constant is defined as

$$K(T)=[p(N)]^2/p(N_2). \quad (10)$$

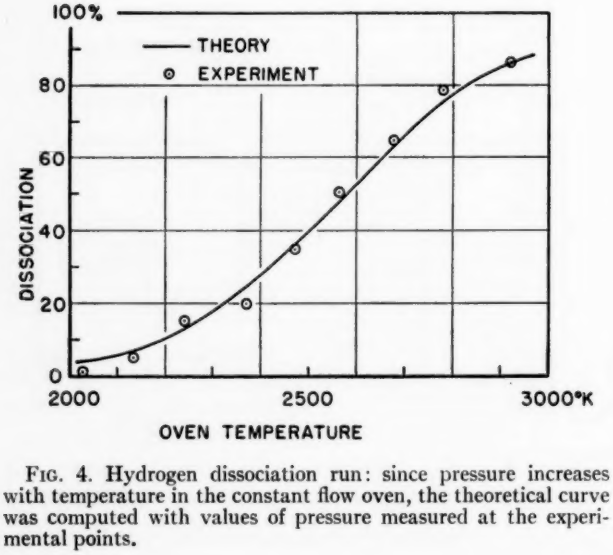

FIG. 4. Hydrogen dissociation run: since pressure increases with temperature in the constant flow oven, the theoretical curve was computed with values of pressure measured at the experimental points.

If the total pressure P is given by

$$P=p(N)+p(N_2)$$

and the fractional dissociation X by

$$X=p(N)/P,$$

then

$$K(T)=X^2P/(1-X). \quad (11)$$

The equilibrium constant may be calculated from the equation[7]

$$R\ln K(T)=-\Delta(F^0-E_0^0)/T-\Delta E_0^0/T, \quad (12)$$

where R is the gas constant and $(F^0-E_0^0)$ is the Lewis and Randall free energy of the components of the reaction. For the diatomic gases N_2 and H_2 of interest, the quantity ΔE_0^0 is just the dissociation energy, $D(N_2)$ or $D(H_2)$. Values of the function $(F^0-E_0^0)$ have been calculated from spectroscopic data for both nitrogen and hydrogen, and are available in the literature.[8–11] In calculating the theoretical dissociation of nitrogen two sets of calculations were made; one using the $D(N_2)$ value 7.385 ev (59 566 cm^{-1}) and one using 9.765 ev (97 970 cm^{-1}). These results are graphed in Fig. 3.

In calculating the theoretical dissociation of hydrogen, the value of Beutler[12] for $D(H_2)$ was used (36 116 cm^{-1}). The recent calculations of Wooley, Scott, and Brickwedde[11] for $(F^0-E_0^0)$ at 1500°, 2000°, and 3000°K were used to correct the older values of Giauque[9] (as corrected by Davis and Johnston[10]). Giauque's table gives the function $(F^0-E_0^0)$ for hydrogen every hundred degrees.

RESULTS

The experimental dissociation curves for hydrogen, obtained with Eq. (8) from observed beam intensities, agreed with the calculated ones. Five runs were made at pressures from 1 to 4 mm Hg. The general agreement with the theoretical dissociation supports the assumption that thermal equilibrium at the oven temperature is reached by the gas in the oven. Results of a single run are shown in Fig. 4.

Two high-temperature runs were made with nitrogen. No measureable dissociation was observed in either of them. These runs reached the following oven conditions: 3410°K at 0.61 mm Hg and 3530°K at 1.11 mm Hg. At these points the theoretical dissociations using $D(N_2)=7.385$ ev are 25 percent and 28 percent, re-

[7] See, for example, G. N. Lewis and M. Randall, *Thermodynamics and the Free Energy of Chemical Substances* (McGraw-Hill Book Company, Inc., New York, 1923), Chap. 24.
[8] W. F. Giauque and J. O. Clayton, J. Am. Chem. Soc. **55**, 4875 (1933).
[9] W. F. Giauque, J. Am. Chem. Soc. **52**, 4816 (1930).
[10] C. O. Davis and H. L. Johnston, J. Am. Chem. Soc. **56**, 1045 (1934).
[11] Wooley, Scott, and Brickwedde, J. Research Natl. Bur. Standards **41**, 379 (1948).
[12] H. Beutler, Z. physik. Chem. **B29**, 315 (1935).

spectively. From Eq. (9), the corresponding reductions in beam with magnetic field on are found to be 17.6 percent and 20 percent. These are very substantial changes in beam intensity and failure to observe them means that the dissociation energy of N_2 cannot be 7.385 ev. The theoretical dissociation for the above points using $D(N_2)=9.765$ ev is 0.5 percent, and the expected reduction in beam with magnetic field is then 0.35 percent. This effect was unobservable against the noise in the detector signal.

In attempting to set a lower limit to $D(N_2)$ the effect of noise in the detector must be considered. The rms noise throughout the experiment was 0.4 cm on the detector scale independent of the total beam intensity. In the run most favorable for the observation of small dissociation effects ($T=3410°K$, $p=0.61$ mm Hg) the beam intensity was 24.8 cm on the detector scale. For this beam the rms noise level was 1.6 percent of the beam. For the purpose of setting a lower limit to $D(N_2)$ any reduction in beam with magnetic field of this amount or less is assumed to be unobservable. A beam reduction of 1.6 percent corresponds to a dissociation in the oven of 2.5 percent, by Eq. 9. From Eqs. (11) and (12) a value for $D(N_2)$ may be computed which gives a dissociation of 2.5 percent for nitrogen at 3410°K and 0.61 mm Hg. The value thus obtained is 8.80 ev, and the lower limit of $D(N_2)$ is set at that value.

With elimination of the value 7.385 ev, the dissociation energy of N_2 is presumably 9.765 ev without any ambiguity. It should be pointed out, however, that the present experiment does not confirm the 9.765 ev value, but only sets a lower limit to $D(N_2)$ at 8.80 ev.

The author would like to thank Professor P. Kusch for his advice and guidance throughout the experiment.

THE JOURNAL OF CHEMICAL PHYSICS VOLUME 22, NUMBER 9 SEPTEMBER, 1954

Van Der Waal's Adsorption as a Determinant of Joshi Effect

N. A. RAMAIAH
Department of Chemistry, University of Delhi, Delhi, India

(Received March 1, 1954)

The significance as a determinant of Joshi effect Δi in H_2O vapor of the predischarge adsorption consisting of an instantaneous uptake of molecules due to van der Waal's forces and slow process of sorption on Langmuir sites was investigated. Joshi effect corresponding to 15–20-percent reversible current suppression was detected with a predischarge interval = ½ min; it was not altered by increase of this last to 5 hr or favored by "aging" under discharge, which indicated that the instantaneous process, *viz*, van der Waal's adsorption, which was quite distinct from Langmuir sorption formed during the predischarge interval and/or under discharge, was the chief seat of Δi. It was suggested that under light, surface molecules dissociated into atoms and/or radicals which possessed large electron affinity, to increase the work function of the cathode and, therefore, to give Δi. Observation of Δi even with longer wavelengths than those corresponding to dissociation energy of H_2O suggested that the adsorbed molecules possessed, prior to irradiation, certain energy $h(\nu_d-\nu)$ obtained by ionic bombardment under applied fields (ν_d is the frequency corresponding to dissociation energy of a molecule, and ν is that employed for observing Δi).

JOSHI effect* (Δi) occurs chiefly in gases and vapors, which give under discharge atoms and/or radicals with appreciable electron affinity, like chlorine and water vapor;[1,2] the electron affinity of Cl atom and of OH radical, a dissociation product of H_2O vapor,[3–5] is 88 kcal.[6,7] Further, the effect Δi is primarily surface dependent,[8,9] as illustrated by the observation that it is markedly affected by any alteration in the nature of the electrode surface by "aging" (see herein), coating materials, etc.[8,10] It has been pointed out[1] that the adsorbed layers, especially those held by van der Waal's forces on a Langmuir layer on the electrodes, of the electronegative gas or vapor like H_2O vapor, are responsible for the production of Δi. The detailed evidence supporting this point of view will be presented in this paper.

THEORY OF THE INVESTIGATION

For the occurrence of the phenomenon Δi, Joshi[11] postulates that (a) an adsorption-like layer consisting of excited particles, ions and electrons, and characterized by a low work function, is formed under

*For a brief introductory account of this phenomenon, see Ramaiah, Bhatawdekar, and Subrahmanyam, J. Chem. Phys. **21**, 1160 (1953).

[1] Ramaiah, J. Sci. Ind. Research (India) **10A**, 182 (1951); Saxena and Ramaiah, J. Chem. Phys. **20**, 1342 (1952).

[2] Ramaiah, J. Phys. Chem. **56**, 218 (1951).

[3] Frost and Oldenberg, J. Chem. Phys. **4**, 627 (1936).

[4] Bonhoeffer and Reichardt, Z. physik. Chem. **139**, 75 (1928).

[5] Risse, Z. physik. Chem. **140**, 133 (1929).

[6] West, J. Phys. Chem. **39**, 503 (1935).

[7] Laderle, Z. physik. Chem. **17B**, 368 (1932).

[8] Ramaiah, Ratnam, and Devi, J. Sci. Ind. Research (India) **11B**, 524 (1952).

[9] Saxena and Ramaiah, J. Chem. Phys. **12A**, 130 (1953).

[10] Joshi, Proc. Indian Sci. Congr., Presidential Address, Chem. Sec. (1943).

[11] Joshi, Current Sci. (India) **16**, 19 (1947).

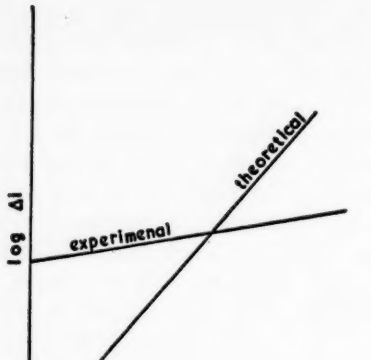

FIG. 1. Variation of log$i$ with log$t$.

discharge on the electrode surface; (b) light releases electrons from this boundary layer; and (c) space charge due to, say, negative ion formation on account of capture of photoelectrons by excited neutral particles reduces the current i to give Δi. Postulate (a) was found helpful in elucidating the observed influence on Δi of "aging," *viz.*, continued exposure to discharge due to a fixed potential:[2,12,13] Δi increased initially rapidly with time (t) of exposure to discharge and attained saturation at large t. This time development of Δi is attributed to the progressive formation of the boundary layer,[2] since (b) and (c) are sensibly instantaneous and completely reversible, and it is argued that the time-rate of increase of Δi is determined practically entirely by the extent to which the adsorption-like layer (a) is formed. Bangham and Burt[14] observed that the rate at which sorption of gases takes place on glass surface is given, in early stages of the process, by

$$S^m = kt, \qquad \text{(i)}$$

where S is the amount adsorbed up to time t; k and m are constants. It is, therefore, anticipated on Joshi's theory that

$$(\Delta i)^m = k't. \qquad \text{(ii)}$$

Suggestively enough, (ii) was applicable to the data on the influence of "aging" on Δi in H_2O vapor and to earlier published results for chlorine, iodine, and oxygen,[2,13] as illustrated by the sensibly linear graphs obtained when $\log(\Delta i)$ was plotted against log$t$. Further, while, according to Joshi's theory, the lines $\log(\Delta i)$ *versus* log$t$ should pass through the origin, the graphs representing the data in H_2O, Cl_2, I_2, and O_2 in "untreated"† discharge tubes gave a Y-axis intercept (see Fig. 1). This last was a measure of the effect observed immediately and might be due to the predischarge adsorption[2] which decreased appreciably by the removal of surface alkali by washing the vessels with chromic acid and boiling distilled water, such that a definite amount of "aging" was found necessary to initiate Δi (at relative pressures of $H_2O < 0.6$).[13] It appeared desirable, therefore, to investigate in some detail the role of the predischarge adsorption caused by van der Waal's forces on a Langmuir layer on the electrodes (see herein) in determining the magnitude of Δi in water vapor.

METHOD OF INVESTIGATION

When a gas is brought in contact with a *nude* surface, frequently there is a practically instantaneous uptake, corresponding to van der Waal's adsorption, which requires no energy of activation, followed by a slow process of adsorption.[15,16] In the former, the quantity of the gas is held mainly in the form of molecules in multilayers by weak nonspecific forces, and depends upon the pressure and temperature of the system. The slow rate characteristic of the subsequent phase of adsorption (referred to as chemisorption or activated adsorption) is attributed to the low probability of "activation" of Langmuir sites by excited gas particles arriving from the gas phase before their actual combination with gas atom or molecules takes place.[17] This view is substantiated by the observation that while a few hours to years is necessary for saturation under normal conditions[17,18] where excitation is mainly due to kinetic collisions, the rate of adsorption under discharge is markedly rapid.[13] Johnson[19] found that adsorption of hydrogen under discharge was complete in 4–5 min; Taylor[20] observed that the uptake of hydrogen content in hydrogen-neon tubes was accomplished in ~5 min; and Willows and George[21] showed that sorption of gases in vacuum tubes attained saturation in 8–10 min. The predischarge adsorption, therefore, consists of gas molecules held by van der Waal's forces and those combined with Langmuir sites;[22] the greater the time interval between the introduction of a gas into a vessel and the onset of discharge, the larger is the chemi-sorption. The dependence of Δi on the amount of predischarge adsorption was investigated by observing the change in magnitude of Δi due to a fixed quantity of H_2O vapor

[12] Ramaiah, J. Sci. Research (Benares Hindu Univ.) **1**, 91 (1950).
[13] Ramaiah, J. chim. phys. **46**, 328 (1952).
[14] Bangham and Burt, Proc. Roy. Soc. (London) **A105**, 481 (1924).
† Discharge tubes like Siemen's type vessels, which were employed in this work and which were washed with cleaning solutions to remove surface free-alkali, were referred to as "acid treated" ozonizers; those which were not washed similarly were referred to as "untreated" vessels. This process of washing had a marked influence on the phenomenon (see reference 13).
[15] Laidler, J. Phys. & Colloid Chem. **53**, 713 (1949).
[16] Miller, *Adsorption of Gases on Solids* (Cambridge University Press, New York, 1948).
[17] Bangham, Phil. Mag. **5**, 737 (1928).
[18] Swan and Urquhart, J. Phys. Chem. **31**, 252 (1927).
[19] Johnson, Proc. Roy. Soc. (London) **123**, 603 (1923).
[20] Taylor, Nature **121**, 708 (1928).
[21] Willows and George, Proc. Phys. Soc. (London) **28**, 124 (1916).
[22] McBain, *Sorption of Gases on Solids* (Routledge, London, 1939).

led into a degassed vessel, by increasing the predischarge interval. During this work the aim was to maintain, as far as practicable, conditions unfavorable for the formation under discharge of any surface alkali, since this last influenced markedly the predischarge adsorption and the corresponding Δi.

DESCRIPTION OF THE APPARATUS

The apparatus employed and the electrical circuit are shown in Fig. 2. Siemen's type discharge tubes made of soft soda glass were used. This kind of vessel is specially favored for the present studies, since it does not possess any metal surface which is known to complicate the results on the disappearance of gas under discharge and the allied phenomena. The dimensions of a typical one of the ozonizers were as follows:

Inner diameter of the inner cylinder	=	10 mm
Outer diameter of the inner cylinder	=	13 mm
Inner diameter of the outer cylinder	=	18 mm
Outer diameter of the outer cylinder	=	20.5 mm
Length of the cylinders (average)	=	420 mm
Volume of the vessel	=	~52.5 cc
(Effective) surface area	=	~405.1 sq cm.

The other vessels employed had roughly the same measurements. The ozonizers were washed repeatedly with chromic acid and boiling distilled water. They were connected through stopcock T_1 to a liquid air trap (L), a sensitive manometer having a low-pressure (Apiezon) oil, and a train of P_2O_5 tubes leading to evacuating pump, and through taps T_2 and T_3 to a reservoir (R) containing twice-distilled water. This served as the source of water vapor; a required quantity of H_2O could be admitted into the ozonizer by careful manipulation of T_2 and T_3 and also by controlling the temperature of R.

OUTGASSING TEMPERATURE

Razouk and Salem[23] determined adsorption isotherms of water vapor on a sample of glass outgassed at increasing temperatures, say 25°, 100°, 200°, and 300°C for 15 hours; their results showed that as the degassing temperature was raised, the glass surface became clearer, so that the adsorbed quantities increased for the same pressure; outgassing at temperatures >200°C did not alter the adsorption isotherms. It is therefore concluded that baking out of glass vessels at 200°C for a period of 15 hours is most suitable for the removal of adsorbed films from glass surface. This is in agreement with the findings of Sherwood[24] and Harries and Schumacher[25] that when soda glass was outgassed at increasing temperatures, the surface layers (mainly H_2O and CO_2) were removed at about 200°C; and at higher temperatures, *viz.*, 300–500°C, there was a continuous evolution of gases and vapors due to a change in the composition, presumably on account of decomposition, of the glass, leading to subsequent diffusion through, and adsorption by, the solid. In the present series of experiments, it appeared "desirable to leave the interior of the glass unaltered and to have the changes confined to the removal and replacement of superficial layers."

The discharge tubes, were, therefore, degassed at 210°C maintained roughly constant for 15 hours by passing a suitable current through the heater coils (H, Fig. 2) of the asbestos chamber in which the ozonizers were enclosed. The evolved gases were condensed in the trap L cooled by liquid air (the stopcock T_3 being kept closed and the pump being in operation to maintain complete vacuum). After closing the tap T_1 and removing liquid air, they were pumped out. The discharge tubes were maintained at a desired temperature and filled with water vapor.

WORKING VOLTAGE

Single-phase alternating potentials of 50 cycles/sec were obtained from rotary converters worked off 200-v dc mains. They were fed to the primary of the stepup transformer to give secondary potentials kV measured by a Kelvin-White electrostatic voltmeter. The potential kV was kept constant at a required value by hand regulation of the resistance included in the primary circuit (not shown in Fig. 2). One of the secondaries of the transformer was introduced into the inner cylinder of the ozonizer, containing closely packed Cu turnings and a little mercury which served as an electrode; the other end was earthed. A helix of bright Cu wire surrounding the outer surface of the ozonizer was also

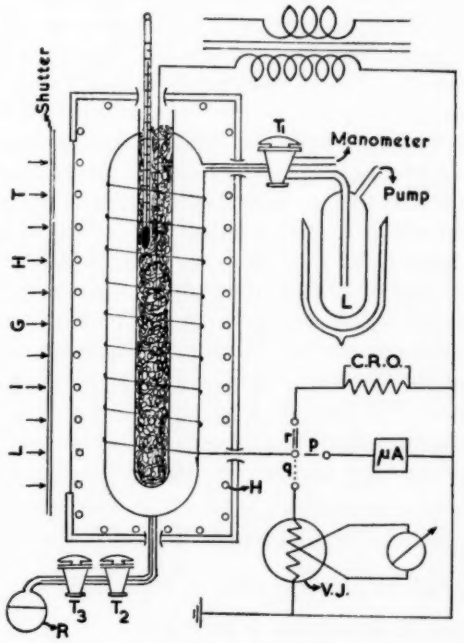

FIG. 2. Experimental setup for investigation of the dependence of Joshi effect on van der Waal's adsorption in water vapor.

[23] Razouk and Salem, J. Phys. & Colloid Chem. **52**, 1208 (1948).
[24] Sherwood, Phys. Rev. **12**, 448 (1918)
[25] Harries and Schumacher, Trans. Ind. Inst. Chem. Engrs. **15**, 176 (1923).

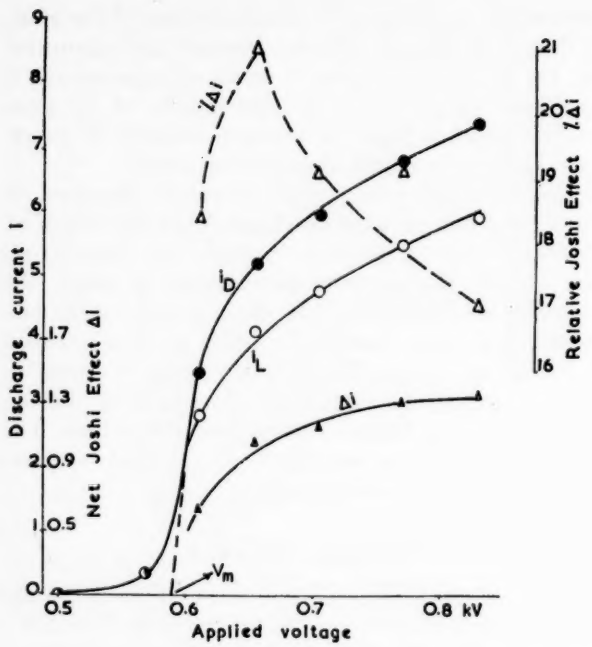

FIG. 3. Determination of the threshold potential V_m (i_D=current in dark; i_L=current under light).

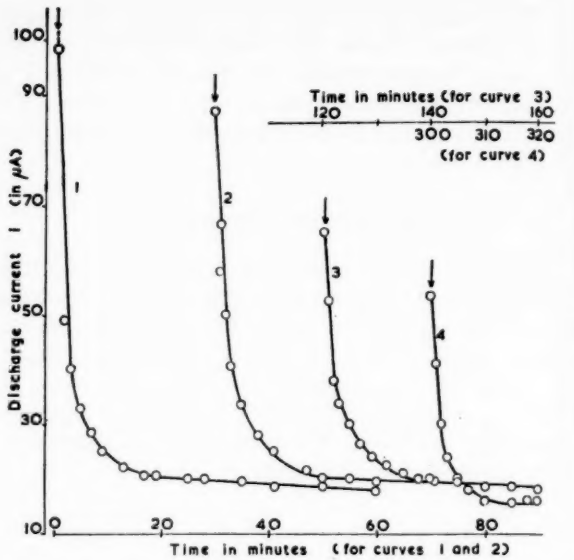

FIG. 4. Variation of the discharge conductivity with adsorption under discharge. (The arrow indicates the instant of excitation.)

earthed through a current-measuring instrument, *viz.*, a double-wave rectifier-type microammeter (μA, *p*) or a galvanometer actuated by a Cambridge vacuo-junction (V.J., *q*, Fig. 2). The galvanometer deflections were proportional to the square of the current *i*. The current structure was investigated by a cathode-ray oscillograph (*r*, Fig. 2).

The formation under discharge of surface compounds, especially in glass vessels, is well known. Rodebush and Klingelhoeffer[26] observed a white deposite on the walls of the vessels containing chlorine under hf excitation and attributed it to a compound formed by the union of Cl atoms with glass. Kellner[27] found a yellow deposit on glass when bromine was subjected to ozonizer discharge. Ludeking[28] estimated the amount of sodium iodide formed under spark discharge in iodine vapor. The formation of surface alkali, as indicated by the yellow color given by zinc uranyl acetate solution and the washings of the ozonizers filled with water vapor and exposed to intense discharge (see herein) for a long time, had been observed.[8] These results follow from the fact that the electrical conduction in glass is essentially electrolytic.[20,29] Further, it was found that the formation of surface alkali was appreciable when the voltage applied was well above a "threshold" value V_m, the fundamental importance of which as a necessary antecedent for the occurrence of any chemical reaction under discharge had been pointed out by Joshi.[30] The rate of a discharge reaction depends upon the difference $V-V_m$: the larger the voltage above V_m, the more appreciable is the reaction. The potential V_m is indicated by a sudden increase, due to the dielectric breakdown of the medium, of the discharge current *i* by but a small rise of *V*, and determined by the extrapolation of $V-i$ curves to the potential axis (Fig. 3). It corresponded roughly to 0.60 kv for a Siemen's ozonizer of the dimensions given above and for 31.8 mm Hg (30°C) of H_2O vapor. The series of experiments described below were carried out at a potential just above this value, *viz.*, 0.66 kv, such that the formation of surface alkali, known to affect markedly the predischarge adsorption and the associated Δi, was at a minimum.

IRRADIATION OF THE OZONIZER

A 200-w 200-v incandescent glass bulb was used for irradiating the excited system. At a desired interval of time and/or applied voltage, the discharge currents i_{dark} and i_{light} (Fig. 3) were noticed; and the net Joshi effect $\Delta i = i_{\text{dark}} - i_{\text{light}}$ and the relative effect percent $\Delta i = 100\Delta i/i_{\text{dark}}$ were calculated.

EXPERIMENTAL PROCEDURE AND RESULTS

In the first one of a series of experiments water vapor at a pressure of 31.8 mm Hg (30°C) was introduced into the system, which was previously evacuated and outgassed as described above. Variation of the discharge current *i* and the effect Δi with "aging" under discharge caused by a constant exciting potential 0.66 kv was studied immediately, i.e., the predischarge interval being $\sim\frac{1}{2}$ min. Later, the discharge vessel was opened to atmosphere and re-evacuated, tested for complete

[26] Rodebush and Klingelhoeffer, J. Am. Chem. Soc. **55**, 130 (1933).
[27] Kellner, Z. Elektrochem. **8**, 500 (1902).
[28] Ludeking, Chem. News **61**, 1 (1890).
[29] Morey, *Properties of Glass* (Reinhold Publishing Corporation, New York, 1948).
[30] Joshi, Trans. Faraday Soc. **25**, 127, 140 (1929).

vacuum for 24 hr, and rebaked out as described earlier. Enclosing the same amount of H_2O vapor in the degassed vessel, further experiments were carried out in which the predischarge interval was increased up to $\frac{1}{2}$ hr, 2, and 5 hr. The above series was repeated in a set of new ozonizers. Table I gives a typical series of results obtained with the ozonizer of which the dimensions were given above.

CURRENT FATIGUE DIAGRAMS

Figure 4 represents the time variation of the discharge current i in one series of experiments. It may be mentioned that when H_2O vapor was introduced and excited with predischarge interval=$\frac{1}{2}$ min (curve 1, Fig. 4, Table I), the current values were too large, and the decrease thereof was too rapid to be measured within the first 50 sec after the admittance of H_2O vapor into the vessel. This difficulty was not, however, noticed in other experiments in which the predischarge interval was $\frac{1}{2}$ hr or longer. The curves 1–4, Fig. 4, further showed that "aging" under discharge diminished the current rapidly to a minimum. Thus i was 98 and 15 μA at 1 and 15 min of "aging" (curve 1, Fig. 4); it was unaltered with prolonged exposure to discharge. This time

TABLE I. Dependence of Joshi effect in water vapor on the predischarge interval. p_{H_2O}=31.8 mm Hg Temp=30°C. Applied potential=0.66 kv.

Time of exposure to discharge in min	Vacuo-junction i_D^2	i_L^2	i_D	i_L	Δi	$\%\Delta i$	Microammeter i_D	i_L
	(a) Predischarge interval = $\frac{1}{2}$ min							
1	475	313	21.79	17.69	4.10	18.8	98.0	85.5
2	339	234	18.41	15.30	3.11	16.8	49.5	43.5
3	290	208	17.02	14.42	2.60	15.2	40.0	35.0
4	266	198	16.30	14.07	2.23	13.7		
5							33.0	29.0
6	242	180	15.55	13.42	2.13	13.7		
7							28.5	25.5
8	228	169	15.09	13.00	2.09	13.9		
9							25.0	22.0
10	213	157	14.59	12.53	2.06	14.1		
12	202	152	14.21	12.33	1.88	13.2		
13							22.0	19.5
15	197	148	14.03	12.17	1.86	13.2		
17							20.5	18.0
18	196	146	14.00	12.08	1.92	13.7		
19							20.5	17.5
20	196	141	14.00	11.79	2.13	15.2		
22							20.0	17.5
25	195	140	13.96	11.83	2.16	15.4		
28							20.0	17.5
30	193	139	13.99	11.79	2.10	15.1		
35	190	139	13.78	11.79	1.99	14.5	19.5	16.5
40	189	139	13.74	11.79	1.95	14.2		
41							18.5	16.5
45	185	139	13.60	11.79	1.81	13.4		
50	185	139	13.60	11.79	1.81	13.4	18.5	16.5
55	185	140	13.60	11.83	1.79	13.0		
60	184	142	13.56	11.91	1.65	12.1	18.0	16.5
	(b) Predischarge interval = $\frac{1}{2}$ hr							
0	572	366	23.92	19.13	4.79	20.0	87.0	76.0
1	400	267	20.00	16.34	3.66	18.3	66.5	58.0
2	310	208	17.60	14.42	3.08	17.5	50.0	43.0
3	283	194	16.82	13.93	2.83	17.2	40.5	35.5
4	264	185	16.25	13.60	2.65	16.3		
5							33.5	39.5
6	244	123	15.60	13.15	2.47	15.8		
8	231	165	15.20	12.84	2.36	15.5	28.0	25.0
10	224	160	14.96	12.65	2.31	15.4		
11							25.0	22.0
15	205	146	14.32	12.08	2.24	15.6		
17							21.5	19.0
18	196	138	14.00	11.75	2.25	16.1		
20	197	138	14.03	11.75	2.28	16.2	20.0	18.0
25	196	139	14.00	11.79	2.21	15.7	20.0	17.5
30	195	140	13.96	11.83	2.13	15.2	19.5	17.5
35	192	140	13.86	11.83	2.03	14.6	19.5	17.5
40	192	141	13.86	11.87	1.99	14.3	20.0	18.0
45	192	142	13.86	11.92	1.94	14.0	19.5	17.5
50	189	142	13.74	11.92	1.82	13.2	18.5	16.5
55	189	141	13.74	11.87	1.87	13.6	18.5	16.5
60	192	143	13.86	11.95	1.71	12.3	18.0	16.0

Time of exposure to discharge in min	Vacuo-junction i_D^2	i_L^2	i_D	i_L	Δi	$\%\Delta i$	Microammeter i_D	i_L
	(c) Predischarge interval = 2 hr							
0	400	265	20.00	16.28	3.72	18.6	65.0	56.0
1	317	215	17.80	14.66	3.14	18.2	53.0	47.0
2	272	191	16.50	13.82	2.68	16.2	38.0	34.0
3	257	181	16.03	13.45	2.58	16.1	34.0	30.5
4	244	175	15.62	13.23	2.39	15.3		
5							30.0	27.0
6	228	188	15.10	13.71	2.39	15.2		
7							26.5	23.5
8	221	158	14.87	12.57	2.30	15.5		
9							24.0	21.5
10	213	151	14.59	12.29	2.30	15.7		
12							22.5	20.0
13	203	142	14.25	11.92	2.33	16.2		
15							21.0	19.0
16	201	141	14.18	11.87	2.31	16.3		
18							20.0	18.0
20	195	136	13.96	11.66	2.30	16.4		
21							19.5	17.5
25	194	136	13.93	11.66	2.27	16.2	19.0	17.0
30	193	136	13.89	11.66	2.23	16.7	18.5	16.5
35	189	136	13.75	11.66	2.09	15.2	18.5	16.5
40	189	136	13.75	11.66	2.09	15.2	19.0	16.5
45	192	139	13.86	11.79	2.07	14.9		
50	189	139	13.75	11.79	1.96	14.2	19.5	17.0
60	191	139	13.82	11.79	2.03	14.7	19.5	17.5
	(d) Predischarge interval = 5 hr							
0	331	233	18.19	15.26	2.93	16.1	53.7	47.0
1	292	205	17.09	14.32	2.77	16.2	41.0	36.0
2	243	171	15.59	13.08	2.51	16.1	30.0	26.0
3	227	162	15.07	12.73	2.34	15.5	24.0	21.5
4	210	149	14.49	12.21	2.28	15.7		
5	197	141	14.04	11.87	2.17	15.4	20.0	17.5
6	190	137	13.78	11.70	2.08	15.1		
7							18.0	16.0
8	188	135	13.71	11.62	2.09	15.3		
10	182	132	13.49	11.49	2.00	14.8	16.0	14.0
12	186	127	13.26	11.27	1.99	15.0		
15	178	126	13.34	11.22	2.12	15.8	15.5	15.0
17	177	128	13.30	11.31	1.99	14.9		
18							16.0	14.0
20	176	128	13.27	11.31	1.96	14.7	16.0	14.0
25	175	128	13.23	11.31	1.92	14.5	15.5	13.5
30	175	129	13.23	11.33	1.87	14.1	15.0	13.0
35	177	129	13.30	11.36	1.94	14.6	16.0	14.0
40	176	128	13.27	11.31	1.96	14.7	16.0	14.0
45	180	136	13.42	11.41	2.01	15.0		
50							16.0	14.0

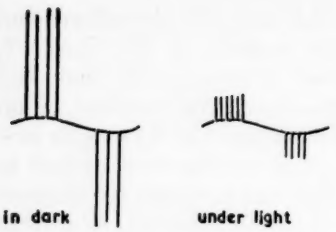

FIG. 5. Oscillograms representing the current structure in dark and under light.

variation of i was exceedingly rapid: i attained saturation with "aging" in about 15–20 min. This decrease of i appeared to be permanent in the sense that when the discharge was discontinued and restarted, the reduced i persisted. The initial large i could be noticed after degassing and refilling the vessel with water vapor. For a fixed quantity of H_2O vapor the minimum current observed after saturation was roughly the same in all experiments whether the predischarge interval was $\frac{1}{2}$ min or 5 hr (Fig. 4).

NONDEPENDENCE OF JOSHI EFFECT ON THE PREDISCHARGE INTERVAL

It was of interest to observe appreciable Joshi effect corresponding to 15–20-percent current suppression under light in water vapor (31.8 mm Hg, 30°C, i.e., at relative pressure = 1)‡ enclosed in a degassed vessel and excited immediately (predischarge interval = $\frac{1}{2}$ min). This was accompanied by marked suppression of the current pulses observed on the cathode-ray oscillograph (see Fig. 5). The effect percent Δi was sensibly unaffected by increasing the predischarge interval as illustrated by the data in Fig. 6 (Table I), which showed that the points for percent Δi in different experiments with increasing predischarge intervals fell roughly on the same curve. No enhancement of percent Δi with "aging" under discharge could be noticed; on the other hand, percent Δi decreased somewhat appreciably in the first 15–20 min of "aging"; in this time period, it may be recalled, the current i decreased to a minimum (see the foregoing). Later, the effect regained its initial value partially; further prolongation of "aging" appeared to have detrimental influence on Δi (Fig. 6).

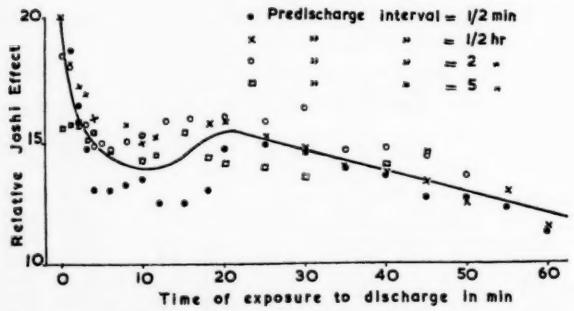

FIG. 6. Nondependence of Joshi effect on predischarge interval.

‡ Earlier work of numerous investigators has shown that adsorption (mainly of van der Waal's type which is shown later to be the chief seat of Δi), on alkali-free glass, of water vapor is appreciable at relative pressures >0.9. For a review of the literature on adsorption of water vapor on glass, see reference 23.

DISCUSSION

The instantaneous current i in a discharge is roughly given by[31,32]

$$i=\frac{i_0(\alpha-\beta)e^{(\alpha-\beta)x}}{\alpha-\beta\cdot e^{(\alpha-\beta)x}}, \qquad \text{(iii)}$$

where i_0, the primary electronic current, is equal to $n_0\cdot e$; n_0 is the number of electrons of charge e emitted from the cathode. When the well-known Townsend first coefficient α, which depends upon position x in nonuniform field, is much greater than the second coefficient β, (iii) is written as

$$i=\frac{i_0\alpha\exp\int\alpha dx}{\alpha-\beta\exp\int\alpha dx}. \qquad \text{(iv)}$$

Since at a fixed potential and pressure,§ α and β are sensibly constant, the current i at any time interval is determined fundamentally by n_0. In ozonizer-type excitation, the electrons deposited during the antecedent half-cycle, which remain unneutralized on the electrode because of its dielectric nature, constitute n_0; this last is controlled by the work function ϕ of the surface. The greater the ϕ, the less is the emission. The observed *permanent* decrease of i with time of exposure to discharge (Fig. 4) might be due to increase of ϕ on account of adsorption of H_2O and/or its dissociation products, mainly OH, of large electron affinity.[2] This agrees with the general decrease of photoelectric and thermoelectric currents due to adsorbed films of electronegative gases.[33–35] The atoms and radicals of the latter adsorbed on Langmuir sites, as suggested by Hallawachs,[36] retard the escape of electrons from the surface, leading to an increase in its work function ϕ. If A represents a Langmuir site on clean glass surface, adsorption of OH can be written as

$$A^*+\mathrm{OH}\rightarrow \mathrm{A-OH};\ \mathrm{A-OH}+\text{electron}\rightarrow A-\mathrm{OH}^-.$$

This follows from the observed decrease of i due to adsorption under discharge which is, however, incomprehensible with the current view that atoms adhere by Langmuir adsorption by electron-sharing with alkali atom in glass.[37]

Although the discharge current i was influenced markedly by the activated adsorption formed either

[31] Loeb, *Fundamental Processes of Electric Discharge in Gases* (John Wiley and Sons, Inc., New York, 1939).

[32] Townsend, *Electron in Gases* (Hutchison's Scientific and Technical Publications, London, 1947).

§ Calculations showed that the decrease of pressure due to formation of monomolecular Langmuir layer under discharge was 0.15 mm Hg, and negligible when compared with the pressure of H_2O vapor employed, *viz.*, 31.8 mm Hg (see reference 37).

[33] Langmuir, Phys. Rev. **2**, 450 (1913).

[34] Richardson, Phil. Mag. **23**, 266, 615 (1912).

[35] Bosworth, J. Roy. Soc. (New South Wales) **79**, 53, 166 (1945).

[36] Hallawachs, see Hughes and DuBridge, *Photochemistry of Gases* (McGraw-Hill Book Company, Inc., New York, 1932).

[37] Saxena, Bhatawdekar, and Ramaiah, Nature **171**, 929 (1953).

before or during discharge, Δi was not favored thereby (Fig. 6), especially when the conditions were maintained sensibly unfavorable for the formation of surface alkali. Further, the results suggested that the type of sorption which takes place in $\frac{1}{2}$ min or almost instantaneously i.e., van der Waal's adsorption in which the gas exists in the form of molecules is responsible for Δi. This is in good agreement with the finding[1] that Δi is undetectable at temperatures $>180°C$, where, suggestively enough, sorption in the form of molecules of water vapor is negligible.[38] The observed favorable influence on Δi of "aging" at intense fields follows from the fact that surface compounds like NaOH are produced. Faraday[39] observed that the presence of alkali would cause deposition of water owing to the lowering of vapor pressure brought about by its dissolution. The catalytic activity of such polar substances, in general, was attributed by Norrish[40] to increased concentration, due to sorption, of gases. Of the various forces available at the surface of a polar substance, those responsible for sorption of a molecule or an atom, are essentially of van der Waal's type.||

Based on these results, it has been suggested by the author[1] that van der Waal's sorption on Langmuir layer on the electrodes is the chief seat of Δi.[41] In the dark, under applied fields, ionic bombardment causes excitation leading to dissociation of surface molecules, as distinct from the dissociation of Cl_2 assumed[41] to be due to metastable atoms and resonance radiation. The produced atoms and/or radicals with greater electron affinity retain electrons on the surface, to increase ϕ. Furthermore, irradiation (depending upon the extent of excitation and/or vibrational energy levels, even under red light) enhances the dissociation of surface molecules, which augments ϕ; the effect Δi, therefore, follows. Photodissociation of H_2O occurs at $\lambda=2250$A,[42] however, it has been observed[2,43] that Δi in water vapor is appreciable over the range 6600–2537A; and varies sensibly linearly with frequency (ν) of irradiation. Extrapolation of $\Delta i-\nu$ plots to ν axis has shown that the threshold (ν_0) for Δi in H_2O vapor is at $\lambda=7750$A. Employing the same method, it has been found that ν_0 for Δi in iodine vapor[44] is at $\lambda=8500$A, while dissociation of I_2 occurs at $\lambda=8000$A[45]; and it has been found independently by Deo[46] and Tawde and Gopalakrishnan[47] that ν_0 for Δi in Cl_2 is at $\lambda=8100$A, indicating thereby that Δi is detectable not only with light of $\lambda\leq 4800$A[41] corresponding to dissociation energy of Cl_2, but also with longer wavelengths, say 7070–6060A. The finding that Δi occurs even with red light suggests that the adsorbed molecule possesses, prior to irradiation, the difference of energy $h(\nu_d-\nu)$ obtained by ionic bombardment under applied fields (ν_d is the frequency corresponding to dissociation energy of a normal molecule). In other words, if Δi is observed with monochromatic radiation of frequenct ν, it follows from the foregoing theory that $h(\nu_d-\nu)$ gives excitation energy of the adsorbed molecule.

[38] Itterbeck and Vereycken, Z. physik. Chem. **48**, 139 (1941).
[39] Faraday, Phil. Trans. **1**, 49 (1830).
[40] Norrish, J. Chem. Soc. **123**, 3006 (1923).
|| The adverse influence on Δi of "aging" under discharge (Fig. 6) especially under conditions unfavorable for formation of surface alkali, is in agreement with the author's data in H_2O vapor obtained with fused silica ozonizer; in this last where production of surface compounds under discharge is negligible, Δi decreased with "aging." This finding, however, appears inexplicable and needs further consideration.
[41] Harries and von Engel, J. Chem. Phys. **19**, 514 (1951); Proc. Phys. Soc. (London) **64B**, 916 (1951).
[42] Bonhoeffer and Harteck, see Wiley, *Collisions of the Second Kind* (Edward Arnold and Company, London, 1937).
[43] Ramaiah, J. Sci. Research (Benares Hindu Univ.) **2**, 1 (1951–52).
[44] Ramanamurti, J. Sci. Research (Benares Hindu Univ.) **2**, 50 (1951–52).
[45] Noyes and Leighton, *Photochemistry of Gases* (Reinhold Publishing Corporation, New York, 1941).
[46] Deo, Proc. Indian Acad. Sci. **29**, 28 (1949).
[47] Tawde and Gopalkrishnan, Proc. Indian Acad. Sci. **29**, 171 (1949).

Fluorescence and Thermoluminescence of Ice*

LEONARD I. GROSSWEINER AND MAX S. MATHESON
Chemistry Division, Argonne National Laboratory, Lemont, Illinois
(Received February 8, 1954)

Experiments on the x-ray excited fluorescence and thermoluminescence of pure ice and ice containing certain additives are described. The luminescent spectra are explained by a model in which the primary process is the radiative capture of electrons by impurity cations. The first-order buildup of fluorescence and temperature dependence of luminous intensity are interpreted by the breakdown and formation of the dipole sheath surrounding the dissolved ions. From this viewpoint, the activation energy for rotation of a sheath ice dipole from the normal lattice position to the aligned configuration is calculated to be 0.07 ev. The principal trap depth determined from the glow curve is 0.32 ev, a correction for the luminous efficiency being incorporated in the calculation; the corresponding s value is 2×10^8 sec^{-1}. Possible mechanisms for the first-order thermoluminescence are given.

INTRODUCTION

THE radiation chemistry of aqueous solutions has been extensively studied in recent years because of the importance of this subject in biological systems and reactor technology.[1] The investigation of the effects of ionizing radiations in ice should contribute to our understanding of the processes occurring in aqueous systems. For example, certain transient species postulated for aqueous systems may be sufficiently stable in ice at low temperatures to permit their detection. Moreover, processes such as diffusion and dipole relaxation, which are considerably slower in ice at low temperatures, may be manifest in a different behavior of water and ice under ionizing radiations.

Irradiation effects are also of intrinsic interest as ice is an important example of a molecular crystal with strong intermolecular hydrogen bonds. It is transparent to light over a wide range of wavelengths and is particularly suitable for such studies as the x-ray-induced fluorescence and thermoluminescence reported in this paper. The chemical effects of radiation in ice have been reported[2] but only recently have the physical effects been studied.

I. X-RAY-EXCITED FLUORESCENCE OF ICE

A. Pure Ice

Some characteristics of the fluorescence of pure ice under x-irradiation were reported previously.[3] These experiments have been extended with new apparatus, and a description of the fluorescence based on the earlier and new work will be presented.

1. Experimental Details

(*a*) *Samples.*—The ice samples were prepared from triply distilled water[4] which had been degassed by repeated freezing with pumping, and thawing to obtain a final pressure over the ice of about 5 microns at −78°C. This degassed water was placed in a $\frac{3}{8}$-inch diameter precision-bore Pyrex tube and was slowly frozen, under vacuum, by placing the tube on a cooled metal rod. The ice formed from the bottom and was transparent with no evidence of cracks or bubbles. Samples were stored under vacuum for at least 24 hours at −25°C before use and were rapidly transferred to the sample holder, under dry conditions, immediately before the experiments.

(*b*) *Sample holder.*—The sample holder was a double-walled metal vessel supporting internally a solid copper block bored out to receive the sample (Fig. 1). By this means the $\frac{3}{8}$-in.×$\frac{3}{8}$-in. cylindrical ice sample could be held at low temperature and irradiated with x-rays with simultaneous measurement of luminescence. The x-rays were passed through a 2-mil aluminum foil which sealed the vacuum chamber, while the luminescence was transmitted through a 2-mm quartz optical window. The temperature was measured with a copper-constantan thermocouple soldered into the solid copper block.

(*c*) *Optical system.*—The light transmitted through the quartz window was reflected by a right-angle fused-quartz prism and focused on the detector by two concave, aluminized mirrors. The mirrors and lead shields to prevent stray x-rays from reaching the detector were contained in a light-tight box adjacent to the lead-lined chamber in which the x-ray tube was located (Fig. 2).

* By arrangement with Professor Paul L. Copeland this research has been submitted by L. I. Grossweiner to the Graduate School of Illinois Institute of Technology in partial fulfillment of the requirements for the degree of Doctor of Philosophy.

[1] For example, see papers in "Radiation Chemistry," Discussions Faraday Soc., No. 12 (The Aberdeen University Press, Aberdeen, Scotland, 1952).

[2] W. Duane and O. Scheuer, Le Radium **10**, 33 (1913); P. Gunther and L. Holzapfel, Z. physik Chem. **B44**, 374 (1939); P. Bonet-Maury and M. Lefort, Compt. rend. **226**, 1445 (1948).

[3] L. I. Grossweiner and M. S. Matheson, J. Chem. Phys. **20**, 1654 (1952).

[4] The triply distilled water was kindly made available to us by E. J. Hart of this Laboratory and was prepared as described in E. J. Hart, J. Am. Chem. Soc. **73**, 69 (1951). We wish to thank John Faris who made a spectroscopic analysis of the water by evaporating 500 ml to dryness in a Pyrex beaker in about 36 hours and analyzing by the copper spark method. The maximum total impurities were 29 μg/liter, of which 7 μg/liter was sodium ion and 20 μg/liter was silicon, probably as silicate. Since our samples are handled in Pyrex at or below room temperature, the concentration of alkali cation is certainly less than 3×10^{-7} molar.

(*d*) *Photometry.*—The luminescence was measured with a 1P28 photomultiplier tube whose output was connected to a Hewlett-Packard Model 404A vacuum tube voltmeter. (The x-ray tube, being half-wave rectified, excited an ac fluorescence that could be observed on an oscilloscope.) The emission spectra were taken with a Gaertner L234 (small) quartz spectrograph, with either photographic or phototube detection.

(*e*) *Excitation.*—The source of x-rays was a 50-kv tungsten tube with a beryllium window manufactured by Machlett Laboratories, Inc. To limit the luminescence of residual air, excited principally by soft x-rays.

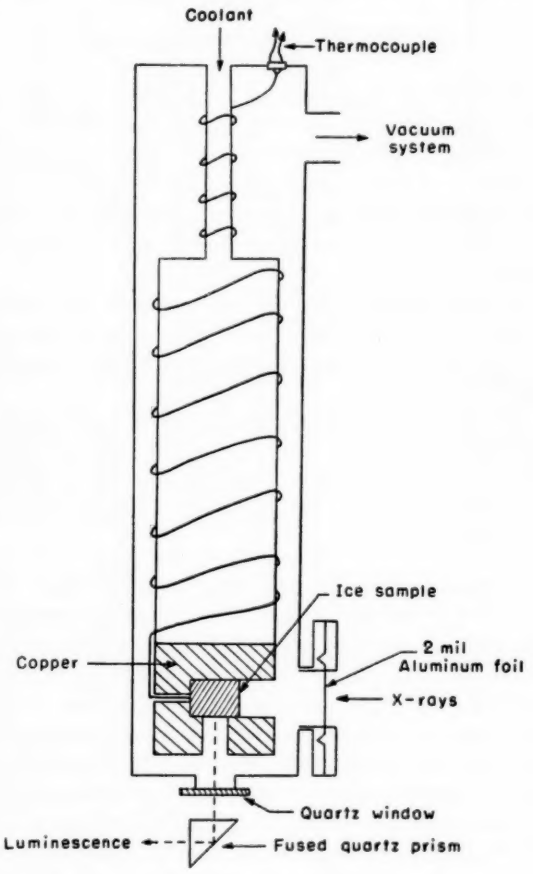

FIG. 1. Sample holder for fluorescence experiments.

a 100 mg/cm² aluminum filter was placed between the x-ray tube window and the sample holder. The x-ray dosage was measured by the oxidation of aqueous ferrous sulfate[5] located in the sample position. At 45 ma and 50 kv it was 1.8×10^{17} ev/g-min.

2. *Results on Steady Fluorescence*

A striking feature of the ice fluorescence is that a slow buildup in luminous intensity is observed following the start of irradiation. The effect of several variables on the fluorescence of pure ice, when steady conditions

[5] C. J. Hochanadel and J. A. Ghormley, J. Chem. Phys. **21**, 880 (1953).

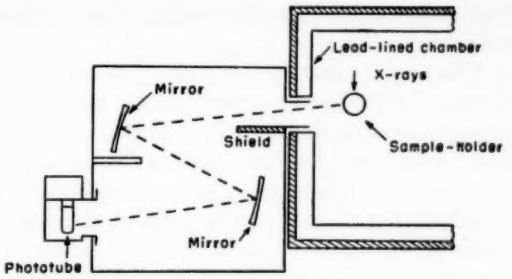

FIG. 2. Optical system for fluorescence experiments.

have been attained, will be described in this section, There was a small background fluorescence from the empty sample holder which may be due to emission from the metal or quartz excited by the x-rays. It was sometimes found expedient to reduce this background with a Corning No. 5970 filter in front of the photomultiplier. This attenuated the background considerably more than the luminescence as the latter is concentrated in a relatively narrow wavelength region.

(*a*) *Spectrum.*—This was measured with an apparatus similar to that described in a previous publication[3] except that no quartz window was used. Exposures of the order of six hours on Eastman Type 103-O and 103-D plates, at a dose rate of 1.0×10^{17} ev/g-min, were necessary for usable images since earlier work[3] showed the luminescent efficiency to be only 3×10^{-5} quanta emitted per ion pair formed. The spectrum of pure ice at −183°C is a single, almost symmetrical, peak at 385 mμ with a half-width of 75–90 mμ.

(*b*) *Effect of x-ray intensity.*—For a given condition of the ice the steady-state luminous intensity is linear with x-ray intensity up to at least 10^{17} ev/g-min. Measurements taken with several sizes of ice samples in different sample holders with temperatures between

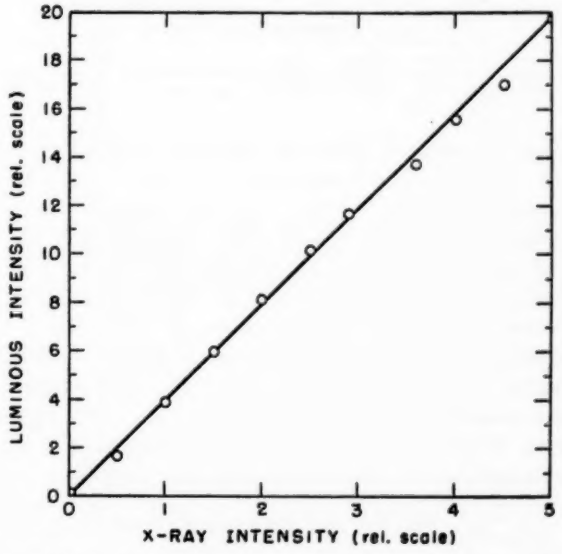

FIG. 3. Variation of luminous intensity with x-ray intensity for pure ice at −195°C.

$-30°C$ and $-195°C$ showed no significant departure from linearity (Fig. 3).

(*c*) *Effect of temperature.*—This was measured by irradiating the sample at $-195°C$ for a time sufficient to attain a steady fluorescent intensity, followed by warming with continued irradiation. In one case, however, a 5-second x-ray pulse at one minute intervals was used during warming. The general appearance of the luminous intensity-temperature curve was the same for various steady x-ray intensities and the run using pulsed excitation showed no perceptible differences (Fig. 4). We conclude that for the heating rates used (several degrees per minute) the behavior of the luminescence during warming is not dependent on the dose rate over a wide range.

A distinct and reproducible difference was found,

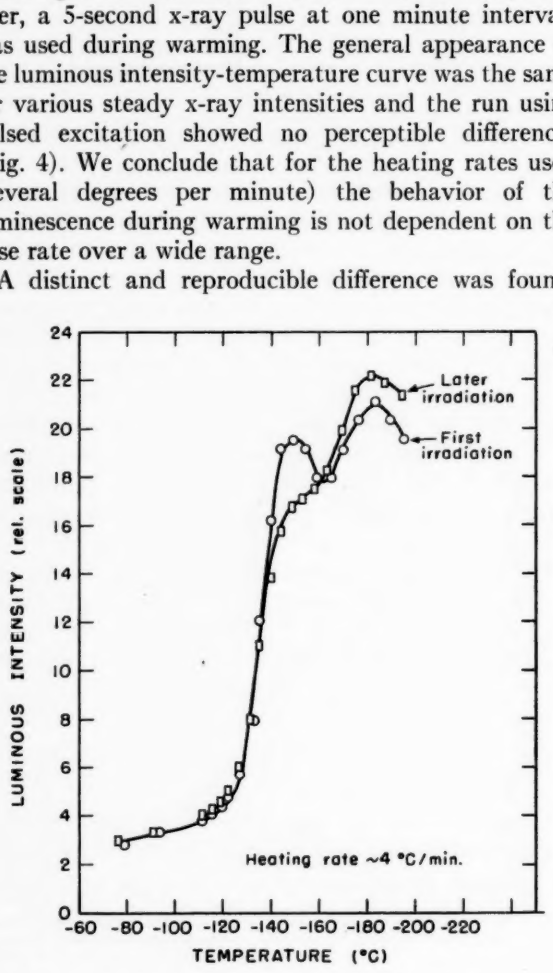

FIG. 4. Variation of luminous intensity with temperature for pure ice.

however, between fresh ice samples and those which had received some irradiation at $-195°C$ followed by warming to about $-70°C$. The fresh samples showed a distinct peak near $-150°C$, while the previously irradiated sample this peak was attenuated or absent (Fig. 4). (In fact, successive runs with an initially fresh sample showed a gradual disappearance of the peak.) The difference is due to irradiation and not successive cooling and warming of the ice, as a sample which had been cooled to $-195°C$ and warmed to $-70°C$ several times before the first irradiation showed the same behavior as that of a freshly prepared sample.

3. *Buildup of Fluorescence Intensity*

The following summarizes the general nature of the buildup process.

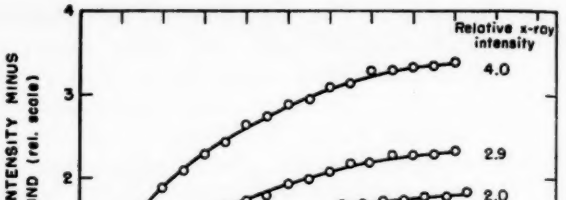

FIG. 5. Buildup of fluorescence at $-145°C$.

(1) The luminous intensity reaches a steady value after about 10 minutes of irradiation at $-145°C$ (Fig. 5), while at $-195°C$ the intensity slowly increases for at least one hour although about 90 percent of the maximum intensity is reached after 30 minutes (Fig. 6).

(2) No buildup occurs while the x-ray excitation is interrupted.

(3) The degree of buildup is "frozen in" at $-195°C$, decays slowly at $-145°C$, and is completely lost when the ice is warmed to temperatures in the vicinity of $-100°C$.

(4) The previously discussed linearity of fluorescent intensity with x-ray intensity applies closely for any given degree of buildup. This was shown by abruptly changing the x-ray intensity after irradiating at a given intensity.

It appears that certain changes are wrought in the ice by the initial irradiation which enable it to fluoresce, and that the stability of these changes decreases as the ice is warmed. The temperature range in which the buildup process reverses is the same as that in which the luminous intensity, under steady irradiation, shows the greatest temperature dependence. This suggests that the changes which occur when the buildup reverses are those which control the temperature dependence of the fluorescence in this range; i.e., the buildup process involves the activation of luminescent centers while the effect of warming is the deactivation of these centers. This deactivation would simultaneously cause a de-

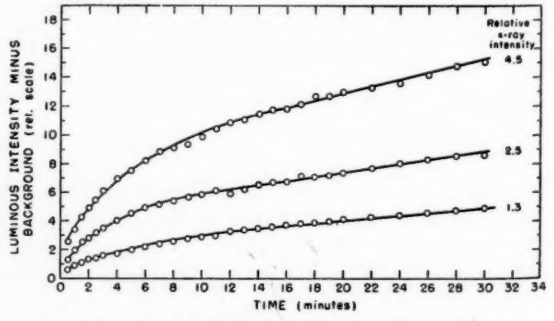

FIG. 6. Buildup of fluorescence at $-195°C$.

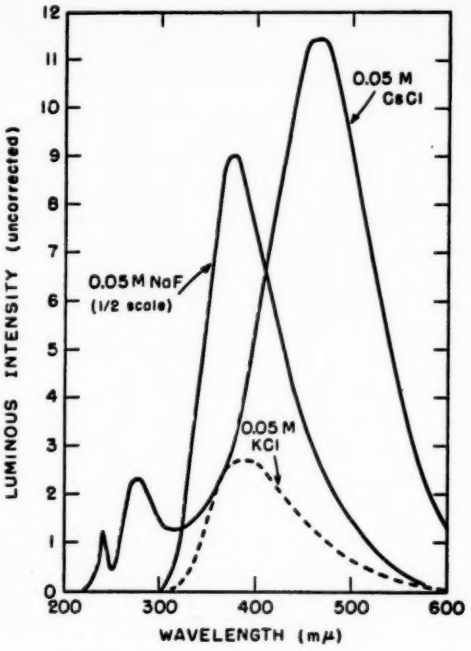

FIG. 7. Fluorescence of ice containing some salts. (Phototube detection.)

crease in luminous intensity with rising temperature under steady irradiation and allow renewed buildup when the ice is recooled and irradiated. This will be discussed in greater detail.

No phosphorescence of intensity comparable to the fluorescence was observed. At all temperatures, the fluorescence dropped to zero as rapidly as the General Radio type 715-A dc amplifier could follow when the excitation was removed.

B. Fluorescence of Ice Containing Additives

1. Effect of Ionic Additives

A series of ice samples containing various ionic additives was prepared, and the luminescent spectra were determined for x-ray excitation at −183°C. Slow freezing (about 1 cm per hour) was necessary, or the frozen sample appeared cloudy and did not exhibit the spectral shift (see 2 following). A check of the spacial distribution of the salt for one sample was made by dividing a 0.05 *M* LiOH sample into ten aliquots and analyzing for lithium ion. The lithium concentration decreased about fourfold from bottom to top, which should not affect the results appreciably as the luminescent properties vary very slowly with salt concentration.

Some representative spectra are shown in Fig. 7, and Table I summarizes the experimental data. The luminous intensities are very approximate as they were determined from average photographic plate or phototube characteristics and are based on one or two runs, at most. The following conclusions were drawn from these data.

TABLE I. Fluorescence of ice containing different salts (−183°C).

Sample	Peak emission energy (ev)	Detection	Approximate peak intensity[a]
xxx-H_2O	3.3 ±0.1	103-O(plates)	1½
0.001 *M* NaCl	3.2 ±0.1	103-O	5
0.005 *M* NaCl	3.2 ±0.1	103-O	6
0.01 *M* NaCl	3.2 ±0.1	103-O	9
	3.30±0.05	1P28(phototube)	
0.05 *M* NaCl	3.2 ±0.1	103-O	9
	3.30±0.05	1P28	
0.05 *M* NaOH	3.2 ±0.1	103-O	9
0.05 *M* NaF	3.2 ±0.1	103-O	12
	3.30±0.05	1P28	
0.05 *M* LiOH	3.3 ±0.1	103-O	1½
	3.30±0.05	1P28	
0.05 *M* KCl	3.17±0.05	1P28	3
0.05 *M* RbF	2.5 ±0.2[b]	103-D(plates)	
	2.7 ±0.2[b]	103-O	6
	2.6 ±0.2[b]	1P28	
0.05 *M* CsCl	2.7 ±0.1	103-D	
	2.8 ±0.1[c]	103-O	
	2.67±0.05[c]	1P28	18
0.05 *M* $CaCl_2$	3.1 ±0.1	103-O	6

[a] These values are not corrected for the spectral sensitivity of the detector.
[b] The band consists of two distinct overlapping peaks of about equal intensity near 3.2 and 2.6 ev. An analysis of our salt showed 2 percent potassium as the only significant contaminant and, in view of the usual slow increase of intensity with salt concentration, it is probable that the peaks are due to K^+ and Rb^+.
[c] In addition to the main peak, two others of considerably lower intensity were observed at 4.5 and 5.1 ev; these may be due to small amounts of impurities.

(1) The luminous intensity increases slowly with the salt concentration for a given additive but varies markedly with the specific additive present.

(2) The position of the emission band shifts with the addition of ionic impurities, but the shift is primarily a function of the cation. The emission band for pure ice, in which the ion present in highest concentration is 10^{-7} molar Na^+, resembles that for ice containing NaCl. A luminescent mechanism based on radiative

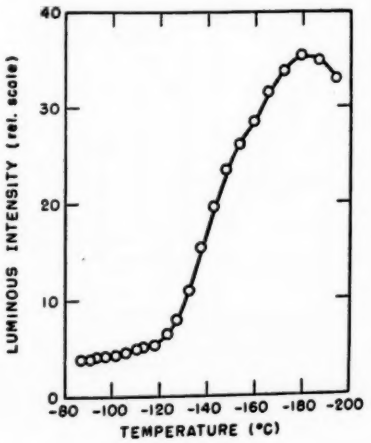

FIG. 8. Variation of luminous intensity with temperature for ice containing 0.001 *M* sodium chloride.

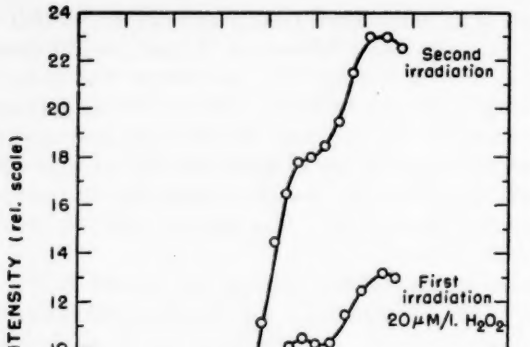

FIG. 9. Variation of luminous intensity with temperature for ice containing hydrogen peroxide.

capture of electrons by impurity cations will be discussed in a later section.

The temperature dependence of the fluorescence was also investigated for fresh, 0.001 *M* NaCl and the result is shown in Fig. 8. One distinct difference from pure ice is the absence of the peak at −150°C. The dependence on x-ray intensity and the nature of the buildup curves for 0.001 *M* NaCl are very similar to pure ice.

2. *Effect of Hydrogen Peroxide and Oxygen*

The fluorescence of ice containing 20 μmole/liter hydrogen peroxide showed some interesting differences from pure ice. The luminous intensity was suppressed markedly by the additive during the first irradiation, but for later irradiations the luminous intensity rose to that observed for pure ice. An analysis of the hydrogen peroxide concentration after the experiment showed that most of it had been decomposed, and presumably this accounts for the return to the normal luminous intensity (Fig. 9). Two other properties of the additive may be noted: (a) hydrogen peroxide does not affect the peak at −150°C; (b) hydrogen peroxide almost completely suppresses the luminous intensity above −130°C. The presence of air or oxygen was found to be without effect on the intensity of fluorescence or the nature of the buildup.

II. X-RAY-EXCITED THERMOLUMINESCENCE OF ICE

The absence of phosphorescence following the ice fluorescence suggested the possibility that irradiated ice exhibits thermoluminescence. A weak, but reproducible, thermoluminescence was detected and was reported previously,[6] and its properties have been further studied with an improved apparatus.

1. *Experimental Details*

The ice samples were prepared as described previously, except that they were nitrogen-washed to lower the residual oxygen content since oxygen, contrary to its behavior in fluorescence, does affect the thermoluminescence while nitrogen does not. The new sample holder was designed to permit irradiation of the sample with x-rays at −196°C and subsequent warming. As seen in Fig. 10, the sample was located at the bottom of a well in a brass rod and was warmed with an electrical heating tape. The temperature was measured with a copper-constantan thermocouple which contacted the base of the well. Calibration to ±1°C was made by comparing this thermocouple to one frozen into an ice sample during warming under experimental conditions. The samples were loaded in a cold dry-box after which the closure washer provided a virtually moistureproof seal. After irradiation the closure washer was removed, and the sample holder promptly attached to the detection apparatus.

The luminescence was measured with scintillation techniques using a 1P28 photomultiplier tube maintained at −196°C. The signal was taken off with a 6J6 cathode follower into an Atomic Instrument Company model 205-A preamplifier followed by a modified Atomic Instrument Company model 204-B linear amplifier and was measured with a standard decade scaler.

2. *Results on Thermoluminescence*

In the experiments reported here, the dosage was 4.1×10^{18} ev/g. All samples were annealed for 24 hours

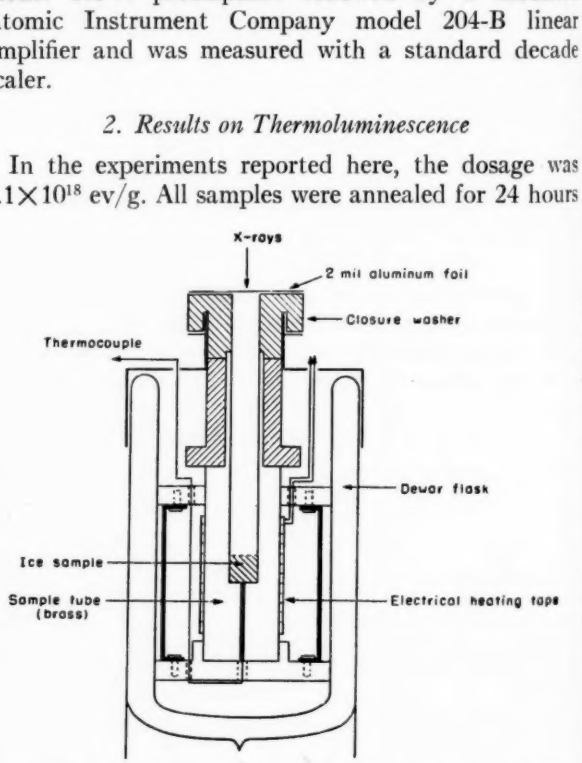

FIG. 10. Thermoluminescence of ice; cross section of sample holder.

[6] E. C. Avery and L. I. Grossweiner, J. Chem. Phys. **21**, 372 (1953).

at −25°C before the irradiation which was performed at −196°C. The thermoluminescence of ice irradiated immediately after freezing was considerably weaker than from annealed ice, which may be due to annealing of quenching sites associated with crystalline imperfections or to the creation of traps by annealing. Approximately one hour elapsed between the end of the irradiation and the beginning of the warming.

(*a*) *Pure ice.*—Earlier data on the thermoluminescence of pure ice irradiated with x-rays at −183°C showed that the glow curve consists of a single prominent peak at about −118°C with evidence of other peaks at higher and lower temperatures.[6] The trap depth for simple first-order decay was estimated as 0.25 ev. Further work using the earlier apparatus showed that the location of the main glow peak is independent of dosage over a wide range. For a series of 14 runs with a range in x-ray dosage of 7×10^{16} to 2×10^{18} ev/g, the average peak temperature was 155 ±2°K for an average heating rate of 2.8±0.2°K/min. This is good evidence of the validity of over-all first-order decay for the thermoluminescence.

The light sum corresponding to the main glow peak increases with increasing x-ray dosage. It was found that the decomposition product hydrogen peroxide suppresses the thermoluminescence (as well as the fluorescence) and only comparisons between samples which received the same total dosage are unambiguous. The light sum as a function of dosage for previously unirradiated ice samples is shown in Fig. 11. The relative x-ray intensities for each run are adjacent to the corresponding experimental point. To a first approximation the light sum is linear with total dosage.

A typical glow curve is shown in Fig. 12. In addition to the main glow peak several others are resolved. Since the work on the dependence of luminous intensity on temperature showed that the fluorescence intensity decreased with increasing temperature in the range of the main glow curve, we believe this variation should

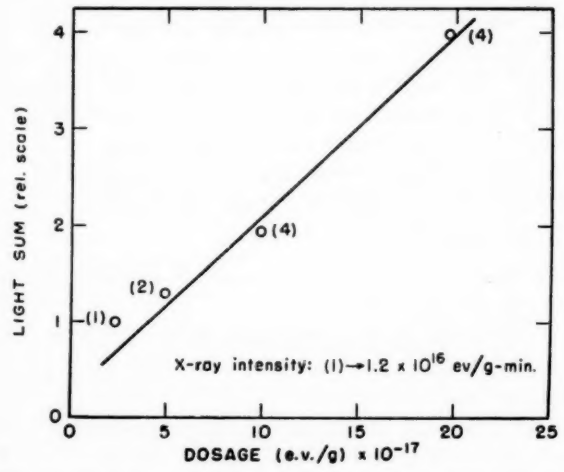

FIG. 11. Variation of thermoluminescent light sum with x-ray dosage for fresh ice.

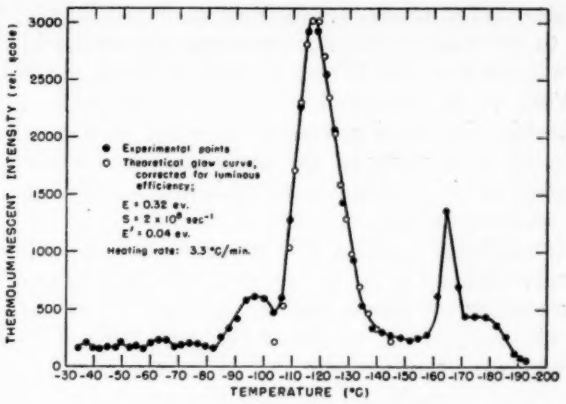

FIG. 12. Thermoluminescence of pure ice.

be incorporated into the calculation for the trap depth. If there exists a temperature-dependent luminous efficiency, the equation of the first-order glow curve is [Appendix A, Eq. (4)]

$$I=C(T)n_0 s\exp\left[-\int_0^T (s/\beta)\exp(-E/kT)dT\right]\times\exp(-E/kT),$$

where E is the trap depth, β the heating rate, n_0 the total light sum, $C(T)$ the luminous efficiency, s the frequency factor, and I the measured intensity. It is shown in Fig. 15 that above −125°C the luminous efficiency varies as $\exp(E'/kT)$ where $E'=0.04$ ev. For an exponential variation of luminous efficiency, it is shown in Appendix A that the trap depth E is related to E' and the temperatures at the maximum (T^*) and half-height of the glow curve (T') by the equation

$$(E-E')\Delta-0.693=[1-(E'/E)][1-(T'/T^*)^2\exp(-E\Delta)],$$

where Δ equals $(1/k)(1/T'-1/T^*)$. This equation can be solved for E by trial and error with values of T' from either side of the glow peak, and the results should agree.

For the glow curve of Fig. 12, Δ is 5.08 and −2.75 on the low and high temperature sides, respectively, and both values yield $E=0.32$ ev. The frequency factor, calculated from Eq. (8) of Appendix A, is 2×10^8 sec^{-1}. The theoretical glow curve for these parameters is shown in the figure and the agreement with the experimental glow curve is good.

A detailed calculation of the trap depth for the other peaks was not practical, but if it is assumed that the frequency factor does not vary widely, the trap depths are approximately in the ratio of the absolute temperatures of the maxima. It is possible that the peaks at −180°C and −95°C are associated with residual oxygen in the ice since the storage of samples in air accentuates these peaks. The peak at −165°C was not always resolved. However, this peak may be related to the

augmented luminescent efficiency at −150°C (Fig. 4) or to the disappearance of paramagnetic species in ice irradiated at −196°C and warmed to about −170°C. (Work to be published by Smaller, Matheson, and Yasaitis.) It should be noted that if the glow curve of Fig. 12 were corrected for the luminescent efficiency plotted in Fig. 4 all luminescence below −140°C would be relatively weak.

(*b*) *Effect of additives.*—It was observed that experimental factors such as the x-ray dosage previously received by the sample and the storage time of the ice in air changed the nature of the glow curves. These effects were shown to be caused by accumulation of hydrogen peroxide and diffusion of atmospheric oxygen into the ice. This was checked by measuring the thermoluminescence of ice containing dissolved oxygen or hydrogen peroxide. In addition, thermoluminescence of ice containing sodium chloride or hydrogen chloride was measured to determine the effects of additive ions and *p*H; the results are as follows:

(1) Hydrogen peroxide: This suppresses all glow peaks and the amount of suppression varies with the concentration; e.g., 90 μmole/liter attenuates the main glow peak 10 times.

(2) Oxygen: Ice frozen in the presence of one-fifth of an atmosphere of oxygen gas exhibits thermoluminescence over a broad temperature range with no evidence of clearly resolved peaks. A possible explanation is that oxygen acts as a competing electron trap. There is theoretical evidence for formation of O_2^- in the gas phase with binding energies of less than one electron volt.[7]

(3) 0.01 *M* NaCl and 0.05 *M* HCl: Both markedly suppressed all thermoluminescence. The contrast of this result with the effects of ionic additives on fluorescence during irradiation indicates that the electron traps are not associated with the impurity ions. Further, since the decomposition products H_2O_2 and O_2 suppress the thermoluminescence of the main glow peak we conclude the trapping in this peak is associated directly with the ice.

III. THEORY AND DISCUSSION

For greater clarity in the discussion of our proposed luminescent model it seems desirable to present a brief outline of the model at this point, with the details and the evidence for them to be taken up in succeeding sections. According to current theory, the absorption of x-rays eventually leads to the generation of secondary electrons with energies ranging from almost the incident photon energy to thermal energies. It is proposed in this paper that the observed luminescence is due to the radiative capture of thermalized secondary electrons by impurity cations in the ice.

When the ice is initially formed we assume that the impurity ions are surrounded by a shield of ice dipoles oriented towards the ions (alignment I). A cation with this alignment of the dipole sheath should act as an electron trap of low binding energy as the external electric field is well shielded. It is suggested that when an electron is trapped in this field the cationic field is partially neutralized and, as a result, the sheath dipoles may rotate into the normal lattice configuration (alignment *N*). In the new alignment the cation is weakly shielded and the previously trapped electron should now emit light as it is captured in the ground state of the atom corresponding to alignment *N*. (An alternate sequence is the capture of the trapped electron in an atomic state inside the dipole sheath with subsequent dipole rotation to alignment *N*.) The net result is the formation in the ice lattice of a free atom which is stable if the temperature is sufficiently low that reaction with ice does not occur. We associate the buildup with the time required to convert the hydrated cations (inactive luminescent centers) into free atoms (active luminescent centers). It is proposed that during steady fluorescence the energetic secondary electrons reionize the free atoms and the resulting cations, in the normal ice lattice, capture other electrons with light emission.

The experiments suggest that the electron traps emptied during thermoluminescence are not directly associated with ionic impurities. However, it is proposed that in the thermoluminescence experiments the detrapped electrons are captured by activated cations in a radiative process similar to that described above. With this introduction we will discuss some of the individual steps in more detail.

A. Primary Radiative Process

In this discussion it is assumed that the cations occupy ideal ice lattice positions and are not shielded by aligned dipoles after buildup (alignment *N*). The first assumption is made for convenience and the alternate assumption that the cations are in interlattice positions would change the calculated energies only slightly. The second assumption is essential to obtain results in agreement with experiment. The luminous energy can be estimated with a simple cycle.

Consider a large ice crystal at low temperature, a free electron and gaseous cation, all initially distant from one another:

(1) Remove an interior ice molecule and replace the cation in the vacancy;

(2) Place the electron in the ice, distant from the ion;

(3) Allow the ion to capture the electron with optical emission $h\nu$;

(4) Permit the relaxation of the polarized lattice about the atom, since the Franck-Condon principle requires that the atomic polarization remains after the optical transition;

[7] H. S. W. Massey, *Negative Ions* (University Press, Cambridge, 1950), pp. 28–31, 71–74, 89–92.

(5) Transfer the atom to vacuum and replace the ice molecule;

(6) Ionize the free atom, and the cycle is complete.

The emission energy is given by

$$h\nu = I - L - X - (S_a - S_i) - L_e,$$

where I is the ionization potential of the gaseous atom, L is the solvation energy of the cation in ice, L_e is the electron affinity of an ice crystal at low temperatures, X is the energy emission due to lattice relaxation, and S_i and S_a are strain energies in ice of the ion and atom, respectively.

The solvation energy of the cation in ice was calculated with the Born[8] formula,

$$L = (ze)^2(1 - 1/D_s)/2R,$$

where D_s is the "static" dielectric constant of ice, and R is the distance from the center of the assumed spherical ion to the dielectric. In this calculation, it was assumed that only the atomic component of polarization is significant, and the low-frequency dielectric constant of ice at −185°C, 2.43, was used.[9] The distance R was taken as the sum of the ionic radius and the ice molecular radius of 1.38 A. The lattice relaxation energy was estimated with the Platzman-Franck[10] formula,

$$X = (ze)^2(1/D_{op} - 1/D_s)^2/2R,$$

where D_{op} is the square of the ultraviolet refractive index of ice, 1.76.[11] This term is small for monovalent cations. The difference in strain energies was neglected, as was the electron affinity, L_e.[12] The calculation for monovalent ions is summarized in Table II, where comparison is made to experimental values. With the exception of K^+ the agreement between observed and calculated values of $h\nu$ is satisfactory. Although some assumptions used are necessarily arbitrary, it is believed that the correct magnitude of the calculated emission energies and their proper trend with increasing ionic size support the suggested mechanism. Extension of the calculation to multivalent ions is complicated by the uncertainty in the radius R which could be considerably smaller due to the strong attraction between the ion and dipoles. In the case of Ca^{++}, a choice of R between 1.4 and 2.3 A yields values of $h\nu$ from 2.7 to 6.4 ev as compared to the observed 3.1 ev. Thus, even with the high ionization potential (11.9 ev) the calculation gives reasonable results.

TABLE II. Calculation of average emission energies.

Ion	R_{ion}[a]	R	L	X	I[b]	$h\nu$ calc.	$h\nu$ obs.
Li^+	0.68	2.06	2.06	0.09	5.39	3.2	3.30±0.05
Na^+	0.98	2.36	1.80	0.08	5.14	3.3	3.30±0.05
K^+	1.33	2.71	1.56	0.07	4.34	2.7	3.17±0.05
Rb^+	1.48	2.86	1.48	0.06	4.18	2.6	2.6 ±0.2
Cs^+	1.67	3.34	1.27	0.05	3.89	2.6	2.67±0.05

[a] C. Kittel, *Introduction to Solid State Physics* (John Wiley and Sons, Inc., New York, 1953), p. 40.
[b] G. Herzberg, *Atomic Spectra and Atomic Structure* (Dover Publications, New York, 1944), p. 200.

B. The Nature of the Electron Traps in Ice

The simplest model for the thermoluminescence is one in which an electron is liberated in the ice during warming and subsequently migrates to an impurity center where radiative capture occurs. It was pointed out in the description of the effects of additives on the thermoluminescence that it is unlikely that ionic impurities are associated with the thermoluminescence electron traps. The mechanism of electron release should be consistent with the following experimental observations:

(1) Most of the thermoluminescence occurs between −130 and −110°C;

(2) The observed decay is first-order;

(3) The trap depth is about 0.3 ev. There are two simple first-order processes:

(a) An electron is detached from a single species by thermal activation;

(b) Reaction occurs between adjacent species in the ice, the reaction rate being limited by a thermal barrier, with a free electron as a product. Possible thermoluminescent processes of either type consistent with the above experimental observations are difficult to specify. Processes of type (a) may be represented, in general, by:

$$R^- + \text{heat} = R^0 + e.$$

The energy required for reaction is $(L+A)$, where L is the solvation energy of R^- in ice, and A is the electron affinity of R^0. Since the solvation energy of a species whose molecular size is about that of an ice molecule is greater than one electron volt, then even for a low electron affinity the trap depth would be much greater than 0.3 ev. It appears unlikely that the thermoluminescence involves electron detachment from such species as H^-, OH^-, O^-, and HO_2^-, since both L and A are greater than 0.3 ev. The absence of sharp peaks in the thermoluminescence glow curve of ice containing oxygen suggests that electron traps of different depths are present, which may indicate that oxygen molecules

[8] M. Born, Z. Physik **1**, 45 (1920).
[9] N. E. Dorsey, *Properties of Ordinary Water-Substance in All Its Phases* (Reinhold Publishing Corporation, New York, 1940), p. 500.
[10] R. Platzman and J. Franck, L. Farkas Memorial Volume, Research Council of Israel, Special Publication No. 1, Jerusalem, 1952, p. 34.
[11] Reference 9, p. 485.
[12] The "electron affinity" of an ice crystal should not be greater than the difference between the photoelectric threshold and the edge of the ultraviolet absorption band. Available experimental values for this difference yield a negative electron affinity which suggests that the light used in the older photoelectric experiment was not sufficiently pure. [E. J. Cassel, Proc. Roy. Soc. (London) **A153**, 534 (1936); W. Obolensky, Ann. Physik (4) **39**, 961 (1912).] A very rough estimate for this energy using the Born formula and the DeBroglie wavelength of a thermal electron for R gives less than 0.1 ev.

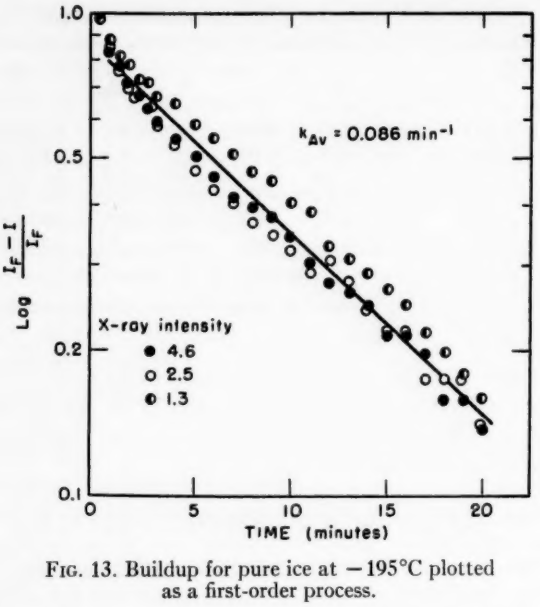

FIG. 13. Buildup for pure ice at −195°C plotted as a first-order process.

are located in a variety of environments. If the gas collects in crystal imperfections, the effect of solvation energy on the trap depth might be negligible.

Possible mechanisms of type (b) might result from the occurrence of the following reactions at irradiation temperatures:

$$e + H_2O = OH^- + H \quad (1)$$

$$e + H_2O = OH + H^-. \quad (2)$$

The electron energies necessary for the above are about 1 and 3 ev, respectively, using the Born formula for the solvation energies of OH^- and H^- in ice and Pritchard's[13] values for the electron affinities. We require then that fast secondary electrons interact with ice molecules and that the products of the reaction, which remain adjacent in the lattice, are prevented from recombining by a barrier equal to the observed trap depth. However, paramagnetic measurements show that atomic hydrogen formed in ice by γ irradiation at −196°C disappears below −170°C, and the reverse of reaction (1) possibly is ruled out as a source of electrons for thermoluminescence. It is not inconceivable that reaction (2) reverses at higher temperatures as the products are less mobile, but the cross section for this reaction must be very low, and further evidence is required.

Another possibility is that electrons are trapped at imperfections in ice. For example, Bjerrum[14] has proposed the existence of orientation fault sites where two protons are found between adjacent oxygen atoms. A captured electron at such a site is crudely equivalent to an excited state of the hydrogen molecular ion. Using Teller's[15] calculated energy for the $2s\sigma$ state and an effective atomic number of 0.17, a trap depth of about 0.35 ev was calculated. The thermal trap depth in this case would be lower by about 0.05 ev, or 0.3 ev. Although this is the order of the observed trap depth, confirmation of such a structure, perhaps by the magnetic measurements, is necessary before this model can receive serious consideration.

The work to date has not permitted an unambiguous specification of the thermoluminescent mechanism but some of the more likely possibilities have been discussed. It is hoped that further experimental work will bring the problem nearer to solution.

C. Discussion of the Fluorescent Buildup

It has been shown that the ice fluorescence builds up from an initial intensity near zero to a steady luminous intensity, the process requiring at least 30 minutes at −195°C and less time at higher temperatures. If the buildup is a first-order process, i.e., the rate of buildup is proportional to the number of inactive luminescent centers, it could be represented by $I = I_f(1 - e^{-kt})$, where I_f is the final luminous intensity, which is proportional to the x-ray intensity. The validity of this equation was checked by plotting $\log[(I_f - I)/I_f]$ against t, where the intensity after 30 minutes was used for I_f. The data for −195°C and −145°C are shown in Figs. 13 and 14, respectively. In each case the data for different x-ray intensities fall on approximately the same straight line, and the average rate constants at these temperatures are 0.086 min^{-1} and 0.31 min^{-1}, respectively. The deviation of the initial points from the line is equivalent to a nonzero initial luminescent efficiency. If the rate of first-order buildup is independent of the x-ray intensity, we must assume that the excitation at the lowest x-ray intensity used is sufficient to enable the process to proceed at the maxi-

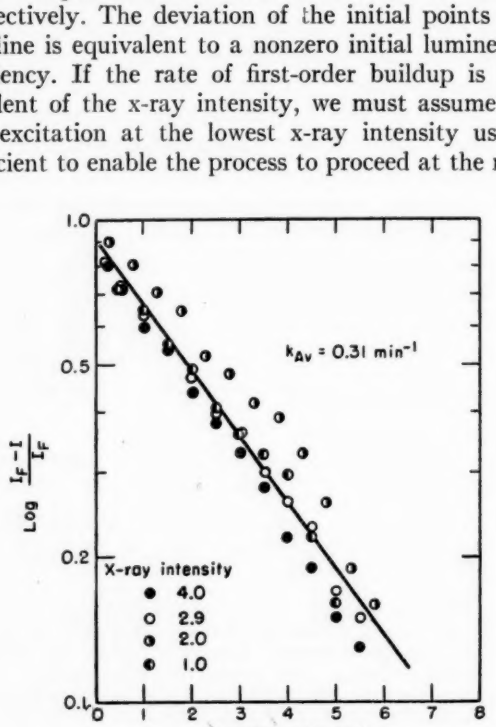

FIG. 14. Buildup for pure ice at −145°C plotted as a first-order process.

[13] H. O. Pritchard, Chem. Revs. **52**, 529 (1953).
[14] N. Bjerrum, Kgl. Danske Videnskab. Selskab Mat.-fys. Medd. **27**, No. 1 (1951), p. 31 (in Eng.).
[15] E. Teller, Z. Physik **61**, 458 (1930).

mum rate. Other experimental observations pertinent to this discussion are that no detectable buildup occurs while the excitation is interrupted, the buildup is completely reversible on warming the ice to about −100°C, and the character of the buildup is not changed on adding salts to the ice, although, in this case, the luminous intensity at each point in the buildup is several times larger than for pure ice.

If our luminescent mechanism is correct it is clear that most alkali ions are not active in luminescence. The maximum concentration of Na^+ in our pure ice is 10^{-7} molar. The addition of 10^{-3} molar NaCl increases the luminous intensity only several times and higher concentrations are correspondingly less effective. It is probable that most of the additive exists as ionic clusters and only a small fraction is situated in isolated lattice positions suitable for luminescence.

It has been proposed that the buildup process is the reorientation of the dipole sheath surrounding the cations and that the energy required comes from electrons trapped in the field of solvated ions. The bond energy of a sodium ion to an adjacent water dipole is about 0.8 ev while the energy bonding such an ice dipole to the normal lattice is about 0.6 ev.[16] Partial neutralization of the ion's electric field by a trapped electron would permit dipole rotation to the normal lattice position with little or no activation energy. When the dipole rotates and bonds with three adjacent ice molecules it seems probable that the reverse process cannot proceed spontaneously, after reionization, until the ice is warmed. The rotated dipole must overcome an energy barrier between the normal lattice position and the more stable position oriented toward the ion before realignment is possible.

The nondependence of the buildup rate on x-ray intensity and the absence of continued buildup during interruption of irradiation may be clarified by some order-of-magnitude calculations. In pure ice, where the alkali ion concentration is about 10^{-7} molar, we may set 1×10^{14} per cc as the maximum luminescent center concentration, although the slow increase of luminous intensity with additive concentration suggests it is considerably lower. At the lowest x-ray intensity used, about 2×10^{14} ev/g-sec, it requires a maximum of 10 seconds to activate one electron for each cation, assuming 20 ev per electron. If a reasonable fraction of the excited electrons is trapped at solvated cations, the buildup would proceed at a rate independent of x-ray intensity for all higher intensities, because every possible inactive luminescent center would hold a trapped electron. (It should be re-emphasized that it is unlikely that these bound electrons are involved in the thermoluminescence at −118°C as the addition of cations decreases the intensity of thermoluminescence.)

If one assumes that the above rapid saturation of inactive centers occurs, the slow process in the buildup must be the rotation of the dipoles so that the energy barrier for rotation, after electron capture, is the activation energy for the temperature dependence of the buildup. Based only on two temperatures, this is about 0.02 ev assuming that the buildup does not reverse rapidly at −145°C (Fig. 4).

To explain the absence of buildup when the x-rays are stopped, we assume that the lifetime of a trapped electron at a cation (inactive luminescent center) is short. If this lifetime is so short that all centers consist of either neutral atoms or cations within 30 seconds after the interruption of excitation, the expected buildup would be too small to be experimentally observed at −195°C. For this lifetime to be less than $10^{-8}\exp(E/kT)$ seconds, the maximum binding energy is 0.16 ev. Using the simplest model for a monovalent cation imbedded in a high dielectric medium, this binding energy corresponds to an effective dielectric constant greater than 9. Thus, for any significant degree of dipole alignment around a hydrated cation, the electronic binding energy would be sufficiently low to permit rapid release of the electron when the irradiation is stopped. The large increase in the low-frequency dielectric constant of ice caused by the addition of low concentrations of ionic salts is further evidence for the existence of augmented dipole mobility.[17]

To summarize, the lifetime of the electron trapped at the hydrated cation is (1) long enough that all inactive luminescent centers are saturated at the lowest x-ray intensity which yielded measurable fluorescence; (2) and short enough that no detectable buildup occurred after the x-irradiation was interrupted.

It has been pointed out that the steady fluorescence and thermoluminescence are suppressed by hydrogen peroxide concentrations greater than about 10 μmole/liter. The mechanism for this might be the reaction of hydrogen peroxide with the alkali atoms formed during the irradiation. The alkali metal hydroxide is stable and should not luminesce when excited with x-rays. On warming the ice, hydration would occur with the subsequent regeneration of the luminescent centers. The reaction of alkali atoms with hydrogen peroxide is almost certainly exothermic in ice while the reaction with ice itself is endothermic. For example, the heat of reaction (in ice) of sodium with hydrogen peroxide is about −30 kcal, while its heat of reaction with ice is about +40 kcal. In both cases the heats of formation of atoms are for the gaseous state as we neglect the small hydration energy of molecular species in ice, while for the ions, the heats of solvation in ice are included.[18] Thus, whenever there is a sufficient concentration of hydrogen peroxide present, either added or formed by the decomposition of ice, we might expect

[16] Haggis, Hasted, and Buchanan, J. Chem. Phys. **20**, 1452 (1952).

[17] C. P. Smyth and G. S. Hitchcock, J. Am. Chem. Soc. **54**, 4631 (1932).

[18] An estimate of −46 kcal was used for the heat of formation of NaOH(g).

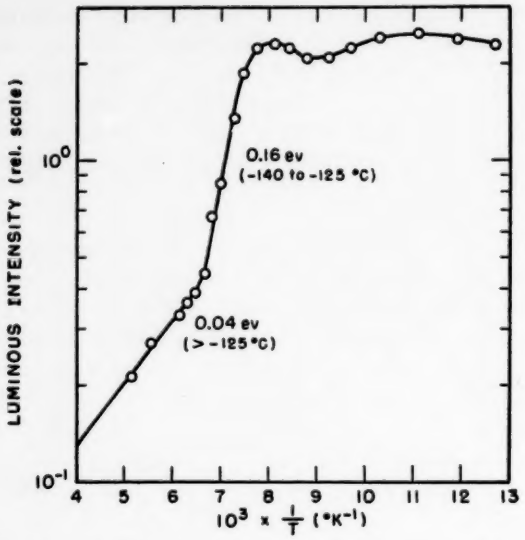

FIG. 15. Fluorescence of pure ice as an exponential function of temperature.

suppression of the luminescence by the reaction with the luminescent centers.

D. Interpretation of the Temperature Dependence of the Luminous Efficiency

One frequently represents the change in luminous intensity with temperature by the relationship $I = C \exp(E/kT)$. Agreement with this equation is taken to indicate that the controlling factor in the luminous efficiency is a competition between a temperature-independent radiative process and a nonradiative process controlled by thermal activation. In this case, the luminous efficiency is expressed as

$$I = 1/[1 + C^{-1} \exp(-E/kT)],$$

which reduces to the above for low efficiencies. It was found that there is good agreement with this equation for higher temperatures and only fair agreement below -130°C (Fig. 15). Since our data were taken at a slow heating rate and might not represent true equilibrium values, the simple exponential dependence was considered only as an empirical luminescent efficiency in the thermoluminescence experiment for comparable heating rates.

According to our luminescent model, the variation of luminous intensity with temperature is due to the decrease in the number of active luminescent centers during warming and not a competition as described above. If first-order decay of active centers and a single controlling activation energy are assumed, the differential equation for decay is

$$-(dN/dt) = aN \exp(-E/kT),$$

where N is the number of active centers at time t, E is the activation energy for decay, and a is a frequency factor. It is shown in Appendix B that integration gives the approximate equation

$$\log_{10}[(1/T^2)\log_{10}(I^0/I)] = \log_{10}(ak/2.3\beta E) - (E/2.3kT),$$

where I is the observed luminous intensity at T and β is the constant heating rate. Thus, a plot of $[(1/T^2)\log_{10}(I^0/I)]$ against $(1/T)$ on semilog coordinates should be a straight line with a slope of $(-E/2.3k)$.

The data for pure ice (previously irradiated) and 0.001 M NaCl (fresh) are shown in Fig. 16, where it is seen the above equation is obeyed. The activation energy in both cases is 0.074 ev. The equation is valid between -175°C and -125°C, a considerably wider range than was found for the simple exponential plot. The interpretation of the constant a is difficult as it probably involves the jump frequency and a transmission coefficient. It is much smaller than one expects for electronic transitions.

In terms of the proposed model, this activation energy is taken as the energy barrier for rotation of an ice molecule, adjacent to an alkali cation, from a position where it is bonded to three neighboring ice molecules to a position where it is aligned towards and bonded to the cation. Using the estimates of the respective bond strengths for Na^+ and the activation energy, we might represent these states on an energy level diagram (Fig. 17). The abscissa is a function of the angle between the axis of the dipole and a radius of the alkali cation, and the dashed line represents the energy of the water-cation bond when an electron is trapped in the field of the ion.

In conclusion, it must be pointed out that there are many questions concerning these effects which are unanswered at present. Some of the more important

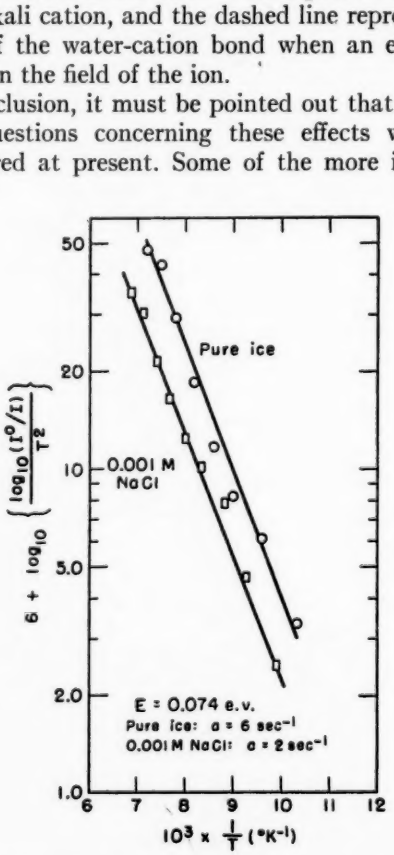

FIG. 16. Calculation of activation energy for decay of luminescent centers.

are: (a) What determines the number of potentially luminescent ions that freeze into ice, and how is this number and the chemical nature of the ion related to the luminous intensity under given conditions? (b) What are the electron traps corresponding to thermoluminescence in pure ice? (c) How does one interpret the two maxima in the steady-state luminescence *vs* temperature characteristics? It is hoped that current research on such topics as radiation chemistry of ice, paramagnetism of irradiated ice, electrification of ice containing salts, etc., will eventually aid in an understanding of some of the phenomena presented here.

SUMMARY

(1) The x-ray excited fluorescence of pure ice varies linearly with x-ray intensity and decreases in intensity with increasing temperature.

(2) There is an x-ray intensity independent buildup of fluorescence which obeys first-order kinetics with rate constants of 0.086 min^{-1} and 0.31 min^{-1} at $-195°C$ and $-145°C$, respectively.

(3) The spectrum of the pure ice fluorescence consists of a single band, about 80 mμ wide, at 385 mμ. The band location is shifted, and the luminescence intensified by the presence of ionic additives, and the effects are due principally to the cation.

(4) The principal thermoluminescence of pure ice consists of a single peak near $-117°C$ which is described by first-order decay with a trap depth of 0.32 ev and frequency factor of 2×10^{8} sec^{-1}.

(5) Both the steady fluorescence and thermoluminescence are suppressed by hydrogen peroxide. Oxygen suppresses the thermoluminescence but not the steady fluorescence. Ionic additives which intensify the fluorescence act to suppress the thermoluminescence.

The above observations and calculations are interpreted by a model in which the primary process is the radiative capture of electrons by impurity cations. The buildup is associated with the breakdown of the sheath of aligned ice dipoles surrounding the ions, and in terms of this model, an activation energy for alignment of such a dipole is found to be 0.07 ev. The experimental observations are qualitatively consistent with the proposed model.

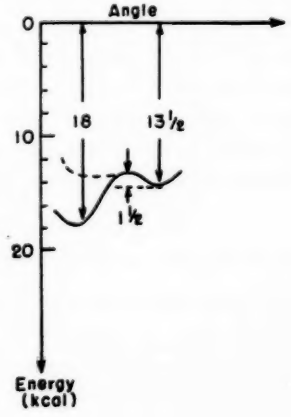

FIG. 17. Possible energy levels of the H_2O-Na^+ system in ice.

APPENDIX A

Analysis of Thermoluminescence Data

The analysis of a thermoluminescent glow curve requires (a) the determination of the order of the decay and (b) the calculation of the trap depth and frequency factor from the appropriate rate equation. If there is a temperature-dependent luminescent efficiency, the differential equation of the luminescent decay is

$$I=-C(T)(dn/dt)=C(T)sn^{p}\exp(-E/kT), \quad (1)$$

where n is the number of electrons in traps of depth, E, s is the frequency factor, $C(T)$ is the combined luminous efficiency and geometry factor, and p is a number defining the order of the decay. If the decay is first-order, $p=1$, the temperature of the glow curve maximum T^* will not vary with the light sum n^*, which is easily seen by differentiating Eq. (1) with respect to temperature and equating to zero

$$E/kT^{*2}=[(1/\beta)p(n^*)^{p-1}s\exp(-E/kT^*)] -[C'(T^*)/C(T^*)], \quad (2)$$

where β is the heating rate during the experiment, and the * refers to the glow peak.

In general, the order of the decay may be found from a logarithmic plot of I against n at any given temperature. The light sum n is calculated from the glow curve by

$$n(T)=(1/\beta)\int_{T}^{\infty}[I(T)/C(T)]dT. \quad (3)$$

In order to perform the integration $C(T)$ must be known and for decay other than first-order it is often assumed to be independent of T.

When the decay is first-order, Eq. (1) may be integrated to give

$$I=C(T)n_0 s\exp\left[-\int_{0}^{T}(s/\beta)\exp(-E/kT)dT\right] \times\exp(-E/kT). \quad (4)$$

The solution in terms of the temperatures of the maximum (T^*) and half-height (T') of the glow curve can be found using the procedure and approximations of Grossweiner[19] and is

$$(E/k)(1/T'-1/T^*) =\ln 2C(T')/C(T^*)+[skT^{*2}\exp(-E/kT^*)/E\beta] \times[1-(T'/T^*)^2\exp(-E/k)(1/T'-1/T^*)]. \quad (5)$$

Substitution of (2) in (5) gives

$$E\Delta=\ln 2C(T')/C(T^*)+\{1+[kT^{*2}C'(T^*)/EC(T^*)]\} \times[1-(T'/T^*)^2\exp(-E\Delta)], \quad (6)$$

[19] L. I. Grossweiner, J. Appl. Phys. **24**, 1306 (1953).

where Δ equals $(1/k)(1/T'-1/T^*)$. If, as in our case, $C(T)$ has the form $A\exp(E'/kT)$, Eq. (6) reduces to

$$(E-E')\Delta-0.693 = [1-(E'/E)][1-(T'/T^*)^2\exp(-E\Delta)]. \quad (7)$$

Thus, using two temperatures from the glow peak and E', the trap depth E is easily calculated by trial and error. The frequency factor s may be calculated from Eq. (2) when E and β are known. For first-order decay with the exponential dependence of luminous efficiency, this reduces to:

$$(E-E')/k=sT^{*2}\exp(-E/kT^*)/\beta. \quad (8)$$

APPENDIX B

Calculation of Activation Energy of Luminous Efficiency

Assume that the luminous intensity under steady irradiation conditions is proportional to the number of active luminescent centers N and that the decay of active luminescent centers is first-order in time and varies exponentially with temperature. Thus, the differential equation for decay is

$$-(dN/dt)=aN\exp(-E/kT), \quad (1)$$

where E is the activation energy for decay, and a is a frequency factor. Integration of (1) yields

$$N=N_0\exp\left[-\int_0^T(a/\beta)\exp(-E/kT)dT\right], \quad (2)$$

where β is the heating rate, which is assumed constant. We assume the observed luminous intensity I is proportional to N and take the logarithm of (2):

$$\ln(I/I^0)=-\int_0^T(a/\beta)\exp(-E/kT)dT. \quad (3)$$

The integral may be expanded as in Appendix A, Eq. (5), and the above equation is approximately

$$\log_{10}(I^0/I)=[T^2a\exp(-E/kT)/2.3\beta(E/k)]. \quad (4)$$

It is convenient to use the form

$$\log_{10}[(1/T^2)\log_{10}(I^0/I)] = \log_{10}(ak/2.3E\beta)-(E/2.3kT), \quad (5)$$

since a plot of the left-hand side against $(1/T)$ has a slope proportional to the activation energy E.[20] The rate constant a may be determined from the intercept of this plot.

ACKNOWLEDGMENTS

We take pleasure in acknowledging the valuable assistance of P. L. Copeland, Department of Physics, Illinois Institute of Technology and O. C. Simpson, Chemistry Division, this laboratory, who encouraged this research and discussed many phases of it at length with the authors. We wish to thank R. Platzman, Department of Physics, Purdue University and J. E. Robinson, Chemistry Division, this laboratory, for discussions on the interpretation of some of the experiments and E. C. Avery, Chemistry Division, this laboratory, who collaborated in the design of the thermoluminescence apparatus. Finally, we are indebted to P. Pringsheim, Chemistry Division, this Laboratory, for cooperation in making available to us certain research facilities.

[20] For $(E/kT)<10$ the approximation to the above integral using only the first two terms of the asymptotic expansion for $Ei(-E/kT)$ is poor. However, the error in the slope [Eq. (5)] is less than 3 percent for $(E/kT)>5$.

Decomposition of Methanol Induced by Methoxy Radicals

YOSHIMASA TAKEZAKI AND CHISATO TAKEUCHI
Kodama Laboratory, Institute for Chemical Research, Kyoto University, Kyoto, Japan
(Received February 10, 1953)

Kinetical studies were made at 167°C on the decomposition of methanol induced by methoxy radicals, by pyrolyzing a small amount of dimethyl peroxide in methanol. A considerable amount of ethylene glycol was found. The following mechanism was proposed, and the kinetical equations derived therefrom could express the most part of the reaction quantitatively:

$$\begin{aligned}
&CH_3OOCH_3 \rightarrow 2CH_3O,\\
&CH_3O+CH_3OH \rightarrow CH_3OH+CH_2OH, \quad (a)\\
&CH_3O \rightarrow CH_2OH,\\
&CH_3O+CH_2OH \rightarrow CH_3OH+HCHO,\\
&2CH_3O \rightarrow CH_3OH+HCHO,\\
&CH_3O+HCHO \rightarrow CH_3OH+CHO, \quad (b)\\
&CH_3O+CHO \rightarrow CH_3OH+CO \quad \text{or} \quad 2CHO \rightarrow HCHO+CO,\\
&2CH_2OH \rightarrow CH_2OH-CH_2OH.
\end{aligned}$$

The dissociation rate constant of dimethyl peroxide is represented by $4.1\times10^{15}\exp(-36.9\ \text{kcal}/RT)\ \text{sec}^{-1}$, and the activation heat of (a) is 3.0~4.3 kcal higher than that of (b).

INTRODUCTION

IN the previous report on the methyl radical induced decomposition of methanol at 309°C,[1,2] one of the authors (Y.T.) postulated the following consecutive reactions and succeeded in a quantitative explanation of observed facts:

$$CH_3+CH_3OH \rightarrow CH_4+CH_2OH,$$

$$CH_3+CH_2OH \rightarrow CH_4+HCHO,$$

$$CH_3+HCHO \rightarrow CH_4+CHO,$$

$$CH_3+CHO \rightarrow CH_4+CO.$$

Similar mechanism would be found as to the mode of the degradation of methanol when the methyl radical is replaced with methoxy radical, for both radicals are likely to behave in the same manner as to the abstraction of hydrogen atom from molecule or radical. When dimethyl peroxide is used for the source of methoxy radicals, the formation of ethylene glycol, which is a good evidence of the presence of CH_2OH as an intermediate and accordingly may serve as a proof for the occurrence of the first dehydrogenation of methanol at C−H, might be observed, because in this case the reaction temperature can be lowered far below that of the previous case where the formation of glycol was not ascertained. Furthermore, the dissociation rate constant of dimethyl peroxide, whose numerical value, it seems, has not been given heretofore,* would be obtained in this experiment.

With these expectations the present work has been performed, and the results have met them satisfactorily.

EXPERIMENTAL

Static method was used; a small amount of dimethyl peroxide was introduced into the methanol kept at the reaction temperature, then the pressure change was pursued, and at the required moment a major part of the reaction mixture was withdrawn and analyzed.

The reaction equipment was almost the same as illustrated in the previous report.[2] A 310-cc glass bulb (surface/volume≒1 cm^{-1}) installed in an electric copper block furnace (temperature constancy ±0.1°C) was connected by electrically heated (*ca* 100°C) capillary tubes to mercury cutoffs and to the head of the mercury in one branch of an inclined manometer (accuracy 0.1 mm), (total dead space 0.5 cc), both of which were heated to 100°C by steam jackets to prevent ethylene glycol from condensing. The mercury vapor slowly diffusing from the cutoffs and the manometer (≤0.3 mm) does not seem to affect the reaction, for, the presence of 5.4-mm mercury vapor caused by the introduction of a few drops of mercury before the reaction did not alter the features of the reaction.

The reaction mixture was withdrawn into an evacuated vessel of 500 cc (70 percent of the total reaction mixture was collected) and shaken with 15-cc water before and after it was brought to normal pressure by means of mercury, then the total gaseous products in this sampling vessel (*ca* 1 cc) were analyzed by a modified Ambler's apparatus (accuracy in reading 0.005 cc) and the quantity of formaldehyde in the aqueous solution (aliquot 5 cc) was measured according to the Clausen's method[3] by microtitration with 1/100 *N* iodine solution. On some samples colorimetric determination of formaldehyde was made with Schiff's

[1] Kodama, Takezaki, and Yoshida, J. Chem. Soc. Japan **71**, 173 (1950).
[2] Y. Takezaki, Bull. Inst. Chem. Research Kyoto Univ. **26**, 1 (1951).
* The authors could not refer to the report of M. B. Neiman [Uspekhi. Khim. **7**, 341 (1938)], in which the rate constant might be given.
[3] F. P. Clift and R. P. Cook, Biochem. J. **26**, 1788 (1932).

reagent under strongly acid condition (H_2SO_4 15 percent by weight).

As for ethylene glycol, about a half of the reaction mixture was condensed in a small trap and the entire condensate (*ca* 0.1 cc) was treated with periodic acid solution for 1 hour at 100°C under reflux and the consumed periodic acid was measured micro-iodometrically with 1/10 *N* thiosulfate solution.[4]

Methanol of cp grade, free from formaldehyde and acetone, was dried with magnesium-iodine mixture[5] and rectified; the center $\frac{1}{3}$ fraction of the total distillate was used.

Dimethyl peroxide was prepared according to Rieche;[6] after the removal of hydroperoxide with saturated calcium chloride solution, it was collected in a trap at 0°C through tubes filled with calcined calcium chloride, then rectified (top temperature 13.8°C at 759 mm; Rieche, bp 13.5°C at 740 mm). The vapor pressure of the peroxide thus obtained was 433 mm at 0.0°C and 767 mm at 14.0°C. The purity of peroxide was not determined; it was absorbed in water of fivefold volume quickly and completely.[6] As shown later, the only impurity, if any, is supposed to be dimethyl ether produced in large quantities in the preparation of peroxide, which still remains owing to the insufficient distillation, and the content of ether does not seem to exceed 3 percent.

RESULTS

Table I and Fig. 1 show the results obtained under the following standard conditions: the initial pressure of methanol $(CH_3OH)_0=400\pm5$ mm; the initial pressure of dimethyl peroxide $(DMP)_0=23\pm0.5$ mm; accordingly the ratio of initial pressures (referred to as I.P.R., hereafter), $(CH_3OH)_0/(DMP)_0=17.4\pm0.6$; and the reaction temperature 166.7°C. The numerical values concerning the amount of pressure rise or of products are given by the ratio to $(DMP)_0$ throughout the paper.

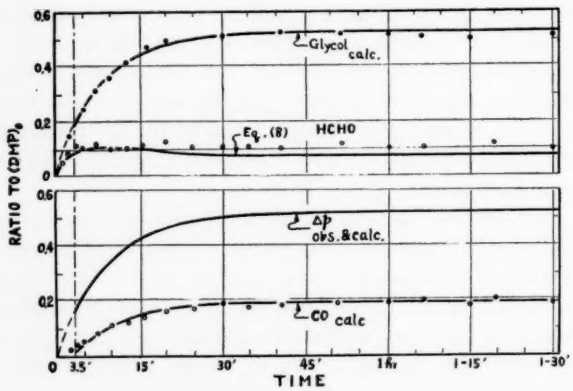

FIG. 1. Plot for the observed and calculated values of products 166.7°C, $(CH_3OH)_0=400$ mm, $(DMP)_0=23$ mm. Open and closed circles represent the observed values.

No CO_2 and olefins were found; the amount of H_2 was 0.02–0.03 between 10 min and 1.5 hr, and CH_4 was less than 0.02. Acetaldehyde was not detected by iodoform reaction. Ethylene glycol was detected by the method given Feigl,[7] *viz.*, the above-mentioned condensate was mixed with a few drops of concentrated $NaHSO_3$ solution and distilled, then the distillate was divided into two portions and the one was treated with periodic acid and the produced formaldehyde was tested with Schiff's reagent in the presence of sulfric acid. The development of color was quite remarkable, while the other, used as a control, remained almost colorless with Schiff's reagent.

Formation of glyoxal and glycolaldehyde is supposed to be negligible (0.01 or so) because of the fairly good coincidence of both aldehyde determinations shown in Table I, since it was found in the preliminary tests that glyoxal and glycolaldehyde can be measured within an error of a few percent by the Clausen method under the present analytical condition, i.e., observed "HCHO" $=HCHO+2(CHO)_2+CH_2OHCHO$ if the latter two exist, while they produce no color with Schiff's reagent under the strongly acid condition, and furthermore, that the dissolved dimethyl peroxide, a very weak oxidant,[6] does not destroy them and also formaldehyde. In the experiment in the reactor of very high surface-to-volume ratio† (glass-wool-filled bulb) the amount of glyoxal and glycolaldehyde was still small.

The amount of glycol decreases as $(CH_3OH)_0$ is reduced, and reaches 0.09 at I.P.R.$=0$ for $(DMP)_0=23$ mm; other products in the latter case were CO (0.43), HCHO (0.02), CH_3OH (1∼2, semiquantitatively analyzed by permanganate oxidation followed by colorimetry), H_2 (0.01) and CH_4 (0.03).

The final amount of pressure rise, $\Delta p_f/(DMP)_0$, decreases as the I.P.R. is raised, in the manner shown in Fig. 2; higher $(DMP)_0$ results in somewhat lower $\Delta p_f/(DMP)_0$. In the case of I.P.R.$=0$, $\Delta p_f/(DMP)_0$ was 0.93, 0.83, and 0.72, respectively, for $(DMP)_0=23$, 33, and 44 mm. But all the pressure curves obtained for the I.P.R's shown in Fig. 2 follow the first-order law exactly and have the same apparent rate constant, i.e., 1.85×10^{-3} sec^{-1} at 166.7°C.

In the range of the reaction temperature examined

[4] M. L. Malaprade, Bull. Soc. Chim. **43**, 683 (1928).
[5] N. Bjerrum and Z. Zechmeister, Ber. deut. chem. Ges. **64**, 210 (1931).
[6] A. Rieche, Ber. deut. chem. Ges. **61**, 951 (1928) and **62**, 218 (1929).
[7] F. Feigl, *Qualitative Analyse mit Hilfe von Tüpfelreaktionen* (Akademische Verlagsgesellschaft, Leipzig, 1938), p. 383.

† In the bulb filled with glass-wool the decomposition of peroxide proceeded faster; the results are as follows: Peroxide alone (23 mm, 166.7°C): time of $\frac{1}{4}$ completion of pressure rise, $t_{1/4}=1'40''$, $t_{1/2}=4'25''$, $t_{3/4}=9'$, $t_{99\ \text{percent}}=21'$; at the end of the reaction $\Delta p=0.90$, CO$=0.37$, $H_2=0.03$, $CH_4=0.02$, HCHO$=0.06$ (Clausen) and 0.06 (colorimetry), glycol$=0.03$. Methanol+peroxide (standard condition): $t_{1/4}=1'20''$, $t_{1/2}=4'00''$, $t_{3/4}=7'45''$, $t_{99\text{percent}}=21'$; at the end of the reaction $\Delta p=0.71$, CO$=0.20$, $H_2=0.05$, $CH_4=0.02$, HCHO$=0.19$ (Clausen) and 0.15 (colorimetry), hence 2 glyoxal +glycolaldehyde$=0.04$, glycol+glyoxal+glycolaldehyde$=0.21$. (Glyoxal and glycolaldehyde were found to consume one atom o of HIO_4 per molecule of each.)

TABLE I. Reaction products. 166.7°C, $(CH_3OH)_0=400$ mm, $(DMP)_0=23$ mm, surface/volume=1 cm^{-1}. Numerical values are the ratios to $(DMP)_0$.

Time \ Accuracy[a]	Δp ±0.009	CO ±0.012	HCHO ±0.013	HCHO ±0.01[b]	Glycol ±0.015
1.25 min	0.063	...	0.06	...	...
2.5	0.128	0.02	0.09	0.08	0.15
3.75	0.179	0.04	0.12	...	...
5.0	0.229	0.05	0.11	0.10	0.25
7.5	0.297	0.08	0.12	...	0.32
10	0.358	0.11	0.10	0.10	0.36
13	0.412	0.12	0.10	...	0.42
16.5	0.443	0.14	0.12	...	0.48
20	0.464	0.16	0.13	0.13	0.50
25	0.493	0.17	0.11	...	...
30	0.506	0.19	0.11	...	0.51
35	0.511	0.17	0.11	0.10	...
41	0.510	0.18	0.10	...	0.53
52	0.520	0.19	0.12	...	0.52
1 hr 00	0.525	0.19	0.10	0.09	0.51
1 07	0.521	0.20	0.10	...	0.51
1 15	0.514	0.18	...	0.09	0.50
1 20	0.520	0.20	0.10	...	...
1 30	0.528	0.19	0.10	0.10	0.51

[a] Maximum possible error for each single observation, calculated from the accuracy of pressure measurement or from the accuracy of the analysis and the amount of aliquot.
[b] Colorimetric determination with Schiff's reagent in acid medium.

(154.8~180.0°C), $\Delta p_f/(DMP)_0$ remained constant for the same I.P.R. and $(DMP)_0$.

DISCUSSION

Elementary Reactions

These observations on the pressure rise and the shape of the curves in Fig. 1 suggest the following nonchain mechanism analogous to that which was obtained in the reaction of methyl radicals with methanol:[1,2]

	Rate constant	
$CH_3OOCH_3 \rightarrow 2CH_3O,$	k_0	(0)
$CH_3O+CH_3OH \rightarrow CH_3OH+CH_2OH,$	k_1	(1)
$CH_3O+CH_2OH \rightarrow CH_3OH+HCHO,$ formation of O−H bond	k_2	(2)
$CH_3O+HCHO \rightarrow CH_3OH+CHO,$	k_3	(3)
$CH_3O+CHO \rightarrow CH_3OH+CO,$	k_4	(4)
$2CH_2OH \rightarrow CH_2OH-CH_2OH.$	k_5	(5)

Likewise, the reactions of CH_2OH which compete with those of CH_3O,

$CH_2OH+CH_3O \rightarrow CH_3OH+HCHO,$ formation of C−H bond	k_2'	(2[a])
$CH_2OH+CH_2OH \rightarrow CH_3OH+HCHO,$	k_2''	(2[b])
$CH_2OH+HCHO \rightarrow CH_3OH+CHO,$	k_3'	(3[a])
$CH_2OH+CHO \rightarrow CH_3OH+CO,$	k_4'	(4[a])

and the disproportionation of CHO

$$2CHO \rightarrow HCHO+CO \qquad k_4'' \ (4^b)$$

may be present; the extent of their contribution will be discussed later from the kinetical viewpoint.

As for the formation of formaldehyde, the reaction

$$2CH_3O \rightarrow CH_3OH+HCHO^8 \qquad k_2''' \ (2^c)$$

should be taken into consideration, since, as described above, methanol formation was observed in the experiment at I.P.R.=0, though it is possible to think that all the methanol was produced by the chain decomposition of peroxide,

$$CH_3O+CH_3OOCH_3 \rightarrow CH_3OH+CH_2OOCH_3, \qquad k_0' \ (0^a)$$

$$CH_2OOCH_3 \rightarrow CH_3O+HCHO, \qquad k_0'' \ (0^b)$$

and the subsequent reactions of formaldehyde, (3) and (4). The reactions $CH_3O \rightarrow H+HCHO$ and $2CH_3O \rightarrow H_2+2HCHO$ can be entirely ruled out in the present case because of the absence of H_2 in the experiment at I.P.R.=0, in which the concentration of CH_3O is supposed to be fairly higher than that of the present, since the amounts of methanol and formaldehyde in the former are much smaller.

The glycol must have been derived from (1) and, possibly, from the isomerization of CH_3O,

$$CH_3O \rightarrow CH_2OH, \qquad k_1' \ (1^a)$$

followed by the dimerization of CH_2OH. The occurrence of (1) is evident, because, otherwise the over-all reaction would be independent of the presence of methanol, which is contrary to the observed variation of Δp_f with I.P.R. (Fig. 2). Thus, the presence of the H atom abstraction reaction from methanol occurring primarily at the C−H bond is confirmed. However, the relative velocity of this reaction to that of the first dehydrogena-

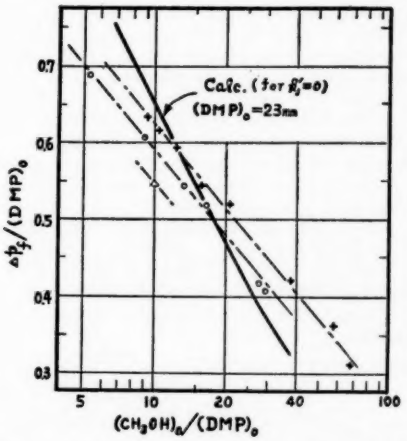

FIG. 2. Variation of final pressure rise with the initial pressure ratio. 166.7°C. △: $(DMP)_0=51$ mm. ○: $(DMP)_0=23$ mm. +: $(DMP)_0=11$ mm.

[8] Raley, Porter, Rust, and Vaughan, J. Am. Chem. Soc. **73**, 15 (1951).

tion at the O−H bond cannot be obtained from this experiment, as the intervention of the latter reaction, $CH_3O+CH_3OH \rightarrow CH_3OH+CH_3O$,‡ a superfluous one in the present case, does not affect the features of the whole reaction.

It is very plausible that (1[a]), an exothermic reaction, takes place as well as the other competing reactions of CH_3O under the present experimental condition. The presence of glycol in the products of the experiment at I.P.R.=0, where only a small amount of methanol was present, is suggestive of the occurrence of this reaction even in the present experiment, though the relative extent to (1) must be fairly less.

It seems impossible to explain the formation of methane by the reactions between above-mentioned reactants, inclusive of glycol. Probably it was derived from the induced decomposition of dimethyl ether contained in the peroxide as an impurity.§

Now, besides the numbered reactions given above, assuming some hydrogen and methane formation reactions|| and furthermore the presence of the reactions $CH_3O+CH_2OH \rightarrow CH_3OCH_2OH$ and $CH_3O+CHO \rightarrow HCOOCH_3$, we get the following relations from the material balance:

$$\Delta p = (HCHO)+2(CO)+(HCOOCH_3),$$

$$(\text{Decomposed DMP}) = \Delta p+(\text{glycol})+(HCOOCH_3) + (CH_3OCH_2OH)-(H_2)-(CH_4).$$

By the introduction of the observed values at the end of the reaction [(reacted DMP)=0.97] we have $(HCOOCH_3)=0.02$ and $(HCOOCH_3)+(CH_3OCH_2OH)=-0.01$, hence we may say that the formation of these products is also negligible in the empty reactor.¶

‡ This reaction must be far slower than (1), as discussed by Phibbs and Darwent [J. Chem. Phys. **18**, 495 (1950)], and also by us [J. Chem. Soc. Japan **73**, 440 (1952)] in the paper on the methyl radical induced decomposition of ethanol at 312°C, in which the first dehydrogenation of ethanol was concluded to occur almost exclusively at the αC−H bond, from the consideration on the steady concentration of formaldehyde and actaldehyde.

§ The content of ether is supposed to be 3 percent from the amount of methane in the experiment at I.P.R.=0; therefore all the numerical values about the amount of Δp or of products should be raised by 3 percent so as to be relative to the true $(DMP)_0$, but this correction and the terms which are to be introduced into the kinetical equations due to the reaction of ether and of CH_3 affect the kinetics of the proper reactions only slightly, i.e., to the magnitude less than the influence of the approximation used to integrate the rate equations.

|| The reactions assumed here are $CHO \rightarrow H+CO$, $CH_2OH \rightarrow H+HCHO$, $2CHO \rightarrow H_2+2CO$, $2H \rightarrow H_2$, $CH_3O+CH_3OCH_3 \rightarrow CH_3OH+CH_2OCH_3 \rightarrow CH_3+HCHO$ and the H atom abstraction reactions by H or CH_3 analogous to (1)–(4).

¶ When glyoxal and glycolaldehyde are present, the above balances become

$$\Delta p = (HCHO)+2(CO)+2(CHO)_2 + (CH_2OHCHO)+(HCOOCH_3),$$

$$(\text{decomposed DMP}) = \Delta p+(\text{glycol})+(HCOOCH_3) + (CH_3OCH_2OH)+(CHO)_2+(CH_2OHCHO)-(H_2)-(CH_4).$$

Introducing the results on the reaction in high surface/volume reactor, we get

peroxide alone: $(CH_3OCH_2OH)=0.00$, $(HCOOCH_3)=0.10$;
methanol+peroxide: $(CH_3OCH_2OH)=0.00$, $(HCOOCH_3)=0.12$.

Kinetics

As to the reaction in the unpacked reactor, two representative cases are treated mathematically at first, then the intermediate cases are considered qualitatively based on these results.

The one is the course in which the abstraction of H atom of CH_3OH, CH_3O, CH_2OH, HCHO, and CHO proceeds by the attack of CH_3O, i.e., the sequence of the reactions (0), (1), (1[a]), (2), (2[c]), (3), (4), and (5) (mechanism I) or (0), (1), (1[a]), (2), (2[c]), (3), (4[b]), and (5) (mechanism II; the seventh step being the disproportionation of CHO), and the other is the course in which CH_2OH acts as the H acceptor, i.e., (0), (1), (1[a]), (2[a]), (2[b]), (3[a]), (4[a]), and (5) (mechanism III) or (0), (1), (1[a]), (2[a]), (2[b]), (3[a]), (4[b]), and (5) (mechanism IV).

Discussion on the presence of the chain decomposition of peroxide will be given later for both cases.

The side-reactions such as the formation of H_2, CH_4, $(CHO)_2$, etc., are ignored to get the time-variation of main products. Peroxide is assumed to be 100 percent pure for simplicity.

The differential equations derived therefrom can be solved for the reaction stage where the formaldehyde concentration can be regarded practically as constant. This stage begins at about 3.5 min after the beginning of the reaction at 166.7°C and covers the major part of the reaction period, which corresponds to the latter $\frac{2}{3}$ of the peroxide decomposition.

The origin of time t in the following rate equations is, unless otherwise stated, taken at a definite time $\tilde{t}$ (from the beginning of the reaction) when $d(HCHO)/dt=0$ becomes available.

(A) *Case 1. Degradation by CH_3O [Mechanism I or II, (0), (1), (1[a]), (2), (2[c]), (3), (4) or (4[b]), and (5)]*

From (0) it follows

$$(DMP) = (\mathbf{DMP})\exp(-k_0 t) = (DMP)_0 \exp(-k_0\tilde{t})\cdot\exp(-k_0 t),$$

where (**DMP**), black type in parentheses, denotes the partial pressure of dimethyl peroxide at $t=0$ (and so on for (**HCHO**) etc.).

Applying the steady-state method to the concentration of radicals we get

$$(CH_3O) = 2k_0(DMP)_0\exp(-k_0\tilde{t})\cdot\exp(-k_0 t)/\{k_1(CH_3OH)+k_1'+3k_3(HCHO)/n + k_2'''(CH_3O)\}, \quad (6)$$

$$d\Delta p/dt = 2d(CO)/dt = 2k_3(HCHO)(CH_3O)/n,$$

$$d(\text{glycol})/dt = \{k_1(CH_3OH)+k_1'-k_3(HCHO)/n\}\times(CH_3O)/2,$$

where $n=1$ for mechanism I and $n=2$ for II, and the condition

$$d(\mathrm{HCHO})/dt=k_2'''(CH_3O)^2+k_2(CH_3O)(CH_2OH)+k_4''(CHO)^2-k_3(CH_3O)(HCHO)=0$$

(as compared with the rate of CO formation) is used.

We now subdivide the case into two with regard to the relative velocity of two competitive reaction (2) and (2^c).

(A-1) If $k_2(CH_3O)(CH_2OH)\gg 2k_2'''(CH_3O)^2$ almost in the entire period of the reaction.—Integration of the foregoing equations, noting

$$(CH_3OH)\fallingdotseq \text{const}\ (\fallingdotseq (\mathbf{CH_3OH})\fallingdotseq (CH_3OH)_0)$$

and $(HCHO)=(\mathbf{HCHO})=\text{const}$, gives

$$\Delta p/(\mathrm{DMP})_0=2(\mathrm{CO})/(\mathrm{DMP})_0=4\exp(-k_0\bar{t})\times\{1-\exp(-k_0t)\}/(nA+3), \quad (7)$$

$$(\mathrm{glycol})/(\mathrm{DMP})_0=\exp(-k_0\bar{t})(nA-1)\times\{1-\exp(-k_0t)\}/(nA+3),$$

where $A=\{k_1(CH_3OH)+k_1'\}/k_3(\mathbf{HCHO})=$ a constant for a fixed $(\mathrm{DMP})_0$ and I.P.R.

Hence, every curve should be of the first order in the reaction stage after $\bar{t}$, and its rate constant be k_0. This is well-proved in Fig. 3 with respect to Δp's at several temperatures, where every point, till 90 percent completion at least, falls within the experimental error calculated from the accuracy of pressure measurement. For 166.7°C, we get $k_0=1.87\times10^{-3}$ sec^{-1} (mean of 19 runs, average error $=0.05\times10^{-3}$ sec^{-1}) and $nA=4.82$, by the use of $\bar{t}=210$ sec and the observed value for $\Delta\bar{p}$ and Δp_f, respectively, 0.175 and 0.520. With the obtained values of k_0, nA and the final amount of CO (=0.195), curves for CO and glycol can be drawn. As shown in Fig. 1 (solid lines) the calculated values agree well with the observed ones.

(A-2) If $k_2(CH_3O)(CH_2OH)\gg 2k_2'''(CH_3O)^2$ does not hold.—Transformation of (6) gives as the second approximation

$$(CH_3O)=2k_0(\mathrm{DMP})_0\exp(-k_0\bar{t})\cdot\exp(-k_0t)/[k_1(CH_3OH)+k_1'+\{3/n+B\exp(-k_0t)\}k_3(\mathbf{HCHO})],^{**}$$

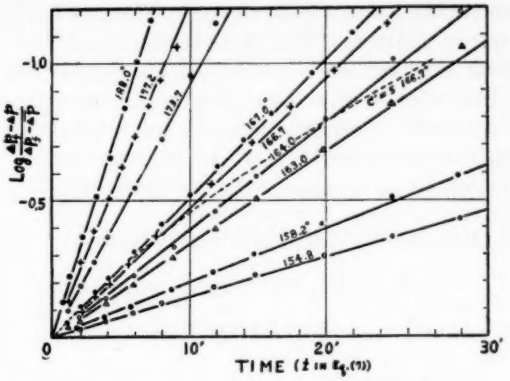

FIG. 3. First-order nature of pressure curve. $(CH_3OH)_0=400$ mm, $(\mathrm{DMP})_0=23$ mm.

Temp. °C	180.0	177.2	173.7	167.0	166.7	164.0	163.0	158.2	154.8
$\bar{t}$	0'50"	1'05"	2'00"	3'20"	3'30"	5'07"	5'10"	9'20"	12'10"
$k_0\times10^3$ sec^{-1}	6.20	4.72	3.51	1.96	1.88	1.49	1.29	0.779	0.565

$\bar{t}$ is taken to be the time when $\Delta p/(\mathrm{DMP})_0$ reaches 0.175 at all temperatures. $\Delta\bar{p}$ represents the pressure rise at $\bar{t}$. As for the broken line see the text.

where $B(0<B\leq1)$ is a parameter concerning the relative rate of (2^c) and (2) at $t=0$. Then we get

$$\frac{\Delta p}{(\mathrm{DMP})_0}=\frac{2(\mathrm{CO})}{(\mathrm{DMP})_0}=\frac{-4\exp(-k_0\bar{t})}{nB}\times\ln\frac{nA+3+nB\exp(-k_0t)}{nA+3+nB},$$

$$\frac{(\mathrm{glycol})}{(\mathrm{DMP})_0}=\exp(-k_0\bar{t})\left\{1-\exp(-k_0t)+\frac{4}{nB}\ln\frac{nA+3+nB\exp(-k_0t)}{nA+3+nB}\right\}.$$

Now, we know from the material balance $(\mathbf{DMP})/(\mathrm{DMP})_0=0.65$ irrespective of the mechanism assumed and it is equal to $\exp(-k_0\bar{t})$ when the chain decomposition of peroxide is absent; then on calculation using this value and $k_0=1.87\times10^{-3}$ sec^{-1} obtained before [this value is nearly the same as derived from $0.65=\exp(-k_0\bar{t})$ $(\bar{t}=210$ sec)] we see that both equations coincide, respectively, almost exactly with those of (A-1). The maximum deviations from the correct first-order expressions appear at $t=2.6$ min, and they are 0.008 for $nB=1$ and 0.012 for $nB=2$. Therefore, we may say that both mechanism I and II, with or without (2^c), can express the behaviors of Δp, CO and glycol curves

---

** In this case we have

$$k_2'''(CH_3O)^2=k_3(CH_3O)(\mathbf{HCHO})/n-k_2(CH_3O)(CH_2OH)\leq d(\mathrm{CO})/dt,$$

$$\{k_1(CH_3OH)+k_1'+3k_3(\mathbf{HCHO})/n\}(CH_3O)\geq 2k_5(CH_2OH)^2+3k_3(HCHO)(CH_3O)/n=3d(\mathrm{CO})/dt+2d(\mathrm{glycol})/dt.$$

On the other hand, we know that the observed curves are expressed formally by

$$(\mathrm{CO})/(\mathrm{DMP})_0=0.17\{1-\exp(-Kt)\}$$

and

$$(\mathrm{glycol})/(\mathrm{DMP})_0=0.33\{1-\exp(-Kt)\}.$$

Insertion of these values into the foregoing two relations gives that the last term of the denominator of (6) is at most 1/7 of the sum of the first three. Then dropping this last term from (6) we get, as the first approximation,

$$(CH_3O)\fallingdotseq 2k_0(\mathbf{DMP})\exp(-k_0t)/\{k_1(CH_3OH)+k_1'+3k_3(\mathbf{HCHO})/n\}=(\mathbf{CH_3O})\exp(-k_0t).$$

Introduction of this relation again into (6) gives the second approximation with the use of

$$k_2'''(\mathbf{CH_3O})^2=k_3(\mathbf{HCHO})(\mathbf{CH_3O})/n-k_2(\mathbf{CH_2OH})(\mathbf{CH_3O})=k_3B(\mathbf{HCHO})(\mathbf{CH_3O}).$$

at one $(DMP)_0$ and I.P.R. As to the effect of I.P.R., we will return again to it in a later section.

These mechanisms, however, are not complete in that they intrinsically give the expression for formaldehyde that decreases again through a maximum point. For instance, in the case of (A-1), the differential equation for formaldehyde is approximately represented by

$$d(\mathrm{HCHO})/dt=\{k_2(\mathrm{CH_2OH})-k_3(\mathrm{HCHO})/n\}(\mathrm{CH_3O})$$
$$\fallingdotseq\frac{2(\mathrm{HCHO})k_0\exp(-k_0t_m)\cdot\exp(-k_0\Delta t)}{nA'+3(\mathrm{HCHO})}$$
$$\cdot\left[\frac{(\mathrm{HCHO})_m}{(\mathrm{HCHO})}\left\{\frac{nA'+3(\mathrm{HCHO})_m}{nA'+3(\mathrm{HCHO})}\right\}^{\frac{1}{2}}\times\exp(-\tfrac{1}{2}k_0\Delta t)-1\right], \quad (8)$$

where

$$(\mathrm{CH_2OH})=[-k_2(\mathrm{CH_3O})+\{k_2^2(\mathrm{CH_3O})^2+8k_5[k_1(\mathrm{CH_3OH})+k_1'](\mathrm{CH_3O})\}^{\frac{1}{2}}]/4k_5$$
$$\fallingdotseq[\{k_1(\mathrm{CH_3OH})+k_1'\}/2k_5]^{\frac{1}{2}}(\mathrm{CH_3O})^{\frac{1}{2}}\dagger\dagger \quad (9)$$

is used, and $A'=\{k_1(\mathrm{CH_3OH})+k_1'\}/k_3$, $(\mathrm{HCHO})_m$ = maximum value of formaldehyde, t_m = time (from the beginning of the reaction) when $(\mathrm{HCHO})_m$ is reached, and Δt = time from t_m.

This equation is sufficiently accurate for the period after t_m ($\Delta t>0$), but less so for $\Delta t<0$, especially for $\Delta t\approx -t_m$. The result of numerical integration is represented by the curve denoted by "Eq. (8)" in Fig. 1 (the same curve for both mechanisms); it has the maximum point (assumed to be 0.11) at 8.5 min and decreases to 0.08 at $\Delta t=40$ min, whereas no decrease is actually recognized in the amount of formaldehyde.

If (2^c) is predominant in the neighborhood of $\bar{t}$, a steeper decline of formaldehyde curve would be seen after the maximum point (t_m shifts to the smaller value; this is favorable for the observed $\bar{t}$); therefore this reaction must be predominant, if at all, only in the very beginning of the reaction (before $\bar{t}$).

First-order rate equations are not obtained in the case where (4) and (4^b) take place concurrently, though it cannot be determined if the deviation from the first-order law attains to the recognizable amount under the present experimental conditions.

(B) *Case 2. Degradation by CH_2OH [Mechanism III or IV, (0), (1), (1^a), (2^a), (2^b), (3^a), (4^a) or (4^b), and (5)]*

In this case we have

$$(\mathrm{CH_3O})=2k_0(\mathbf{DMP})\exp(-k_0t)/\{k_1(\mathrm{CH_3OH})+k_1'\},$$
$$d\Delta p/dt=2d(\mathrm{CO})/dt=2k_3(\mathbf{HCHO})(\mathrm{CH_2OH})/m,$$
$$d(\mathrm{glycol})/dt=k_5(\mathrm{CH_2OH})^2,$$
$$(\mathrm{CH_2OH})=\frac{-k_2'(\mathrm{CH_3O})-2k_3'(\mathbf{HCHO})/m+\{[k_2'(\mathrm{CH_3O})+2k_3'(\mathbf{HCHO})/m]^2+8(k_2''+k_5)[k_1(\mathrm{CH_3OH})+k_1'](\mathrm{CH_3O})\}^{\frac{1}{2}}}{4(k_2''+k_5)}, \quad (9a)$$

where $m=1$ for mechanism III and $m=2$ for IV.

The last equation is transformed into

$$(\mathrm{CH_2OH})=\varphi_{(t)}\left[\frac{k_1(\mathrm{CH_3OH})+k_1'}{2(k_2''+k_5)}\right]^{\frac{1}{2}}(\mathrm{CH_3O})^{\frac{1}{2}}$$
$$=\varphi_{(t)}\left[\frac{k_0(\mathrm{DMP})_0\exp(-k_0\bar{t})}{k_2''+k_5}\right]^{\frac{1}{2}}\exp(-\tfrac{1}{2}k_0t),$$

$\varphi_{(t)}=0.85$, practically constant for

$$k_2''(\mathrm{CH_2OH})^2\gg k_2'(\mathrm{CH_3O})(\mathrm{CH_2OH}),\ddagger\ddagger$$

$\varphi_{(t)}=0.71$, practically constant for

$$k_2''(\mathrm{CH_2OH})^2\ll k_2'(\mathrm{CH_3O})(\mathrm{CH_2OH}),$$

$0.85>\varphi_{(t)}>0.71$, varies with t for the cases between above two extremes, if these mechanisms agree with the truth.

the condition $d(\mathrm{HCHO})/dt=0$:

$$\frac{\text{First term}}{\text{Second term}}\begin{cases}=\left\{\frac{d(\mathrm{CO})}{dt}\right\}^2\Big/2\left\{\frac{d(\mathrm{CO})}{dt}+\frac{d(\mathrm{glycol})}{dt}\right\}\\ \quad\times\left\{4\frac{d(\mathrm{CO})}{dt}+2\frac{d(\mathrm{glycol})}{dt}\right\}=\frac{1}{46} & \text{for the first case,}\\ =\left\{3\frac{d(\mathrm{CO})}{dt}\right\}^2\Big/8\left\{\frac{d(\mathrm{glycol})}{dt}\right\}\\ \quad\times\left\{3\frac{d(\mathrm{CO})}{dt}+2\frac{d(\mathrm{glycol})}{dt}\right\}=\frac{1}{12} & \text{for the second case,}\\ <\left\{3\frac{d(\mathrm{CO})}{dt}\right\}^2\Big/8\left\{\frac{d(\mathrm{glycol})}{dt}\right\}\\ \quad\times\left\{3\frac{d(\mathrm{CO})}{dt}+2\frac{d(\mathrm{glycol})}{dt}\right\}=\frac{1}{12} & \text{for the third case.}\end{cases}$$

†† The right side of (9) is derived by the use of

$$k_2^2(\mathrm{CH_3O})^2(\mathrm{CH_2OH})^2/8k_5(\mathrm{CH_2OH})^2\cdot\{k_1(\mathrm{CH_3OH})+k_1'\}(\mathrm{CH_3O})=1/120$$

calculated as in reference (**).

‡‡ The following relations are obtained as to the relative amount of the two terms in the root sign of (9a) by the use of the observed velocities of CO and glycol formation as before and with

That is, (CH_2OH) is (or almost is, at worst) proportional to $(CH_3O)^{\frac{1}{2}}$; hence we get

$$d\Delta p/dt = \text{constant}\cdot\exp(-\tfrac{1}{2}k_0 t)$$
$$d(\text{glycol})/dt = \text{constant}\cdot\exp(-k_0 t).$$

This result conflicts strongly with the observed fact that both curves have a same first-order rate constant, even if we allow the slight deviation from the first-order law which may arise in some cases.

(C) *Intermediate Cases*

(*C*-1).—Mechanisms constructed by replacing any one or two of (2^e), (3), and (4) by (2^b), (3^a), and (4^a), respectively [e.g., {(0), (1), (1^a), (2), (2^b), (3), (4) or (4^b), (5)}, etc.], seem improbable, because if $k_2''(CH_2OH) \gg k_2'''(CH_3O)$ as assumed in this example, $k_3'(CH_2OH) \gg k_3(CH_3O)$ and $k_4'(CH_2OH) \gg k_4(CH_3O)$ are also expected to hold simultaneously, since the value of the ratio of k's, for two H acceptors CH_3O and CH_2OH, of the same H abstraction reaction from one common molecule or radical, i.e., k_2''/k_2''', k_3/k_3', or k_4/k_4', must not reciprocate remarkably one after the other in these three pairs (these are all exothermic).

(*C*-2): The possibility that the reaction passes through the stage where all the above elementary reactions take place to the comparable extents seems improbable from the next consideration.

We have seen $(CH_2OH) \propto (CH_3O)^{\frac{1}{2}}$ in two extreme cases; the same expression can be shown to hold near the point where all the reactions have the same velocities. Therefore, if $k(CH_3O)(M)$ is not much greater than $k'(CH_2OH)(M)$ (M = radicals and HCHO) at t the change of mechanism from somewhat like I (or II) to somewhat like III (or IV) would appear in the meantime of the reaction and this would cause an appreciable deviation of Δp curve from the first order. If $k(CH_3O)(M) \approx k'(CH_2OH)(M)$ at t the reaction would assume more and more the mechanism III (or IV) as the time elapses and the inconsistency between pressure and glycol curves would be seen.

(D) *Chain Decomposition of Peroxide*

The presence of the chain decomposition of peroxide, (0^a), (0^b), and $CH_2OH + CH_3OOCH_3 = CH_3OH + CH_2OOCH_3$ k_0''' (0^c), can be excluded as calculated below.

When (0^a) and (0^b) are added to the mechanism I or II [(2^c) being dropped for simplicity; the conclusion is the same since the contribution of (2^c) is only slight in the expression of CH_3O as shown before], we get

$$(\mathbf{DMP})/(\mathrm{DMP})_0 = \exp(-k_0 t)/[1+C\{1-\exp(-k_0 t)\}],$$

$$\frac{2k_0'(\mathrm{DMP})_0}{k_1(CH_3OH)+k_1'} > C > \frac{2k_0'(\mathrm{DMP})_0}{k_1(CH_3OH)+k_1'+3k_3(\mathbf{HCHO})/n} > \frac{k_0'(\mathrm{DMP})_0}{2\{k_1(CH_3OH)+k_1'\}},$$

$$\Delta p = 4(\mathbf{DMP})\ln[1+C'\{1-\exp(-k_0 t)\}]/C'(nA+3),$$

$$C' = 2k_0'(\mathbf{DMP})/\{k_1(CH_3OH)+k_1'+3k_3(\mathbf{HCHO})/n\}.$$

By C or C' we can express the relative rate of (0^a) to those of other competing reactions at the respective origin of time. As shown in Fig. 3 (broken line, at 166.7°C) the deviation of this equation from the first order can be recognized sufficiently well if the extent of the contribution of (0^a) is corresponding to $C' \geq 5$ under the present experimental condition (166.7°C and I.P.R. = 17.4) and the accuracy of pressure measurement. Also we get $k_0 \doteqdot 1\times10^{-3}$ sec^{-1} for $C'=5$ as the lower limit of the true k_0 which is to be used in the above equation so that the calculated pressure curve coincides approximately with the observed one in the aerly stage.

On the other hand, we known $(\mathbf{DMP})/(\mathrm{DMP})_0 = 0.65$ from the material balance, then introducing this value and the lower limit of k_0 ($=10^{-3}$) into the first relation we get $C=0.02$, that is, the rate of (0^a) is less than 4 percent of the sum of the rates of (1) and (1^a) even at the beginning of the reaction.

Similar equations are obtained for the mechanism composed of III (or IV) and (0^c) and (0^b),§§ and the ratio [rate of (0^c)]/2[rate of $(2^b)+(5)$] is less than 0.03 at the beginning of the reaction, therefore we cannot expect by assuming the presence of the chain decomposition of peroxide to get the equations for pressure rise and glycol which are consistent with the observed fact.

From the arguments so far it seems the most probable that the mechanism I or II, with or without (1^a) and (2^c), is operative in the most part of the reaction period after t; near the end of the reaction the relative concentration of CH_2OH to CH_3O becomes high and (2^a), (2^b), (3^a), and (4^a) may contribute to some extent or more, but they would affect the whole reaction only slightly as judged from the constancy of the rate constant in the range of 0–90 percent completion.

§§ In this case we get

$$\{(\mathbf{DMP})/(\mathrm{DMP})_0\}^{\frac{1}{2}} \doteqdot \exp(-\tfrac{1}{2}k_0 t)/[1+D(\mathrm{DMP})_0^{\frac{1}{2}}\{1-\exp(-\tfrac{1}{2}k_0 t)\}],$$

$$\Delta p = 4k_3'(\mathbf{HCHO})\ln[1+D(\mathbf{DMP})^{\frac{1}{2}}\{1-\exp(-\tfrac{1}{2}k_0 t)\}]/mk_0''',$$

where

$$D = \varphi_{(t)}k_0'''/\{k_0(k_2''+k_5)\}^{\frac{1}{2}}.$$

(E) *Isomerization of CH_3O, and the Activation Heats*

To see the variation of Δp_f with I.P.R, the following approximations are adopted in the mechanism I or II of (A-1):

(i) $(\mathbf{HCHO})=(\mathrm{HCHO})_m$

(ii) t_m is assumed to be the same for all I.P.R.'s.

(iii) Equation (7) is applicable from the beginning of the reaction; this may be reasonable since the extrapolation of (7) to $t<0$ coincides with the observed curve quite well, and as described before pressure curves for all I.P.R.'s are of the first order from the beginning of the reaction.

Then, from (8), using (6) and (9), we get

$$\frac{(\mathbf{HCHO})}{(\mathrm{DMP})_0}=\frac{nk_2}{k_3}\left\{\frac{k_0\exp(-k_0t_m)}{k_5(\mathrm{DMP})_0}\right\}^{\frac{1}{2}}\left\{\frac{k_1(\mathrm{I.P.R.})/k_3+k_1'/k_3(\mathrm{DMP})_0}{k_1(\mathrm{I.P.R.})/k_3+k_1'/k_3(\mathrm{DMP})_0+3(\mathbf{HCHO})/n(\mathrm{DMP})_0}\right\}^{\frac{1}{2}},$$

and from (7)

$$\frac{\Delta p_f}{(\mathrm{DMP})_0}=\frac{4(\mathbf{HCHO})/(\mathrm{DMP})_0}{k_1(\mathrm{I.P.R.})/k_3+k_1'/k_3(\mathrm{DMP})_0+3(\mathbf{HCHO})/n(\mathrm{DMP})_0}.$$

At first the absence of (1^a) is assumed, then on calculation using $nk_1/k_3=0.030$ (given later) the change in (**HCHO**) is found to be quite small for the wide variation of I.P.R. [e.g., 0.086 (observed 0.08±0.01) for I.P.R.=5, and 0.119 for 30, both at $(\mathrm{DMP})_0=23$ mm]. The result on Δp_f is shown in Fig. 2 by the thick line for the case of $(\mathrm{DMP})_0=23$ mm. (The same line is obtained for both mechanisms.)

The slope of this line differs somewhat from that of the observed one, presumably because of the omission of (1^a) and/or the assumption (ii) on t_m. If the discrepancy of slope is assumed to be caused solely by the omission of (1^a), good coincidence of both lines can be attained by the assignment of proper values to nk_1/k_3 and nk_1'/k_3, respectively, 0.021 and 3.5 mm ($=1.3\times10^{-7}$ mole/cc) at 166.7°C, that is, 29 percent of total CH_2OH is produced by (1^a) at I.P.R.=17.4. This value 29 percent is considered to be the upper limit of the contribution of (1^a) in the present case, as it can be shown that the slope of the calculated line for $k_1'=0$ approaches the observed one to some extent when the change of t_m with I.P.R. is taken into account.

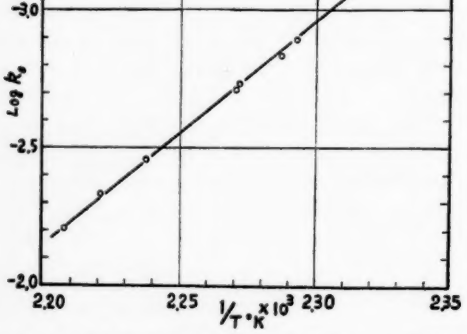

FIG. 4. Activation heat plot for the dissociation of dimethyl peroxide.

From the value of nA given before, in which $(\mathbf{HCHO})/(\mathrm{DMP})_0=0.11$ and $(\mathbf{CH_3OH})/(\mathrm{DMP})_0=17.6$, we get $nk_1/k_3=0.030$ for the case of $k_1'=0$ [$+0.004\sim-0.008$ with sufficient allowance for the change of (CH_3OH) during the reaction, fluctuation of I.P.R. in each run, precision of pressure measurement and HCHO analysis, and the presence of glyoxal and glycolaldehyde amounting to 0.02 which might be involved in (**HCHO**) =0.11], hence the difference of the activation heats, E_1-E_3, is obtained to be $3.1\begin{Bmatrix}+0.3\\-0.1\end{Bmatrix}$ kcal for the mechanism I, or $3.7\begin{Bmatrix}+0.3\\-0.1\end{Bmatrix}$ kcal for II [each value is raised by 0.3 kcal when (1^a) takes place to the maximum], assuming that the collision numbers and the steric factors of these two reactions are respectively the same.

Also, we get $k_0'/k_1<0.7$ or <1.0 at 166.7°C, respectively, for $k_1'=0$ or $nk_1'/k_3=3.5$ mm, from the value of C obtained before.

From the plot of $\log k_0$ *vs* $1/T$ (Fig. 4), the activation heat for (0) is found as 36.9 kcal (accurate within ±1.1 kcal), and finally we have $k_0=4.1\times10^{15}\exp(-36.9\ \mathrm{kcal}/RT)\ \mathrm{sec}^{-1}$, and the entropy of activation $=+10.2$ eu at 166.7°C.

We may regard the value 36.9 kcal as a good approximation of the dissociation heat of the O—O bond in dimethyl peroxide. It is of interest to note that this value is close to those of di-*t*-butyl peroxide [39.1 kcal, frequency factor $=3.2\times10^{16}$;[9] 36 kcal, $(4\sim7)\times10^{14}$ [10]] and di-*t*-amyl peroxide (37~41 kcal[9]), and *not less* than that of dipropyl (~35 kcal[11,12]) or diethyl (31.7 kcal, 2.1×10^{13} [11]) peroxide.

[9] Raley, Rust, and Vaughan, J. Am. Chem. Soc. **70**, 88 (1948).
[10] Murawski, Roberts, and Szwarc, J. Chem. Phys. **19**, 698 (1951).
[11] R. E. Rebbert and K. J. Laidler, J. Chem. Phys. **20**, 574 (1952).
[12] E. J. Harris, Proc. Roy. Soc. (London) **A173**, 126 (1939).

THE JOURNAL OF CHEMICAL PHYSICS VOLUME 22, NUMBER 9 SEPTEMBER, 1954

Thermodynamics of Phase Transitions in Compressible Solid Lattices*

O. K. RICE
University of North Carolina, Chapel Hill, North Carolina
(Received November 4, 1953)

The calculations on the Ising lattice and the order-disorder phenomenon indicate that the specific heat may become infinite at the λ temperature or transition point. The general thermodynamics of such a system in a variable magnetic field is considered, and the relation to the generalized theories of critical points of Tisza and of Semenchenko is indicated. The general import of these theories is that infinite values of the heat capacity at constant pressure C_p, or the analogous heat capacity in a system with variables other than p, V, and T, can become infinite in a one-phase system only at a critical point. The existence of a locus of points where $C_p=\infty$ is thermodynamically possible in the pVT system, and equations analogous to the Clapeyron and Ehrenfest equations may be derived. However, the thermodynamic requirements show that such a locus is not likely to occur. Interesting possibilities occur where there is an interaction between several sets of variables. If an Ising lattice is compressible, for example, the transition temperature will depend on the lattice distance. In this case, the infinite heat capacity is to be considered as a singularity in C_v rather than in C_p. The effect of the compressibility is to change any transition in which infinite specific heats occur to a first-order transition. If there is already a first-order transition, even for an assumed incompressible lattice, the introduction of compressibility increases the latent heat and a discontinuity in lattice distance appears. This situation appears to arise in the order-disorder transformation of an alloy like $AuCu_3$, and the phases may also be expected to have different compositions; this latter phenomenon has also been considered from the point of view of this paper. If there is a λ point without infinite specific heats, the introduction of compressibility may or may not change it to a first-order transition; in any event, the λ point is made "sharper." There may be a critical point in this case. Various thermodynamic relationships are deduced, and the nature of the isotherms in all these cases is considered.

1. INTRODUCTION

OF recent years there has been considerable interest in the Ising lattice.[1] Originally designed as a model for ferromagnetism, it is possible to show that the order-disorder phenomenon of a binary alloy with equal molal quantities of the two components is mathematically equivalent to the Ising lattice in vanishing magnetic field, and so the functional relation between specific heat and temperature is the same for the two cases. There has been, of course, a great deal of work, both experimental and theoretical, on the order-disorder problem; however, the great interest in the Ising lattice arises from the fact that Onsager has shown that it is possible to make an exact analysis of the two-dimensional case. It has been found in this case that the specific heat becomes logarithmically infinite at the transition point where long-range order appears upon cooling. Work using series expansions makes it probable that an infinite specific heat occurs also in the three-dimensional case, at least with some lattice types.[2] This appearance of an infinite heat capacity has caused speculation regarding the possibility of discovering an infinite specific heat in actual thermodynamic systems. There have also been attempts to find a theoretical scheme into which these infinite specific heats can be fitted. Tisza[3] has recently developed a general theory of classical critical points, and has shown that the phenomena observed in the case of ferroelectricity fit in with the theory. Similar ideas have been advanced by Semenchenko.[4] This theory amounts, in large part, to a generalization of familiar ideas. It is well-known that the heat capacity at constant pressure C_p becomes infinite at the critical point (or perhaps in a critical region—see end of Sec. 3, below) for the liquid-vapor equilibrium of a pure substance. The heat capacity at constant magnetic field, C_H, in the system for which the thermodynamic variables are T, H, and I (I being the intensity of magnetization) is quite analogous to C_p in the pVT system. C_H might be expected to become infinite at a critical point, and Tisza has, indeed, indicated that the infinite specific heat of the Ising lattice fits into the picture. The thermodynamic properties of the Ising lattice are sufficiently peculiar to warrant some special discussion, and we shall consider them, by way of introduction, in Sec. 2 of this paper.

Our principal concern, however, will be the discussion of the interaction of various sets of variables. A part of this would appear to be hidden in the generalized formalism of Tisza; however, this does not seem to cover all the possibilities, and in any event the situation is clarified by considering some specific examples. Some discussion of this sort would seem to be necessary if one is to understand how experimental observations can be correlated with such phenomena as the infinite heat capacity of the Ising lattice.

In the discussion of the Ising lattice or the order-disorder phenomenon in any approximation, the lattice

* Work supported by the U. S. Office of Naval Research.

[1] For reviews with references see G. F. Newell and E. W. Montroll, Revs. Modern Phys. **25**, 353 (1953); G. S. Rushbrooke, *Changements de Phases* (Comptes Rendus 2e Réunion Annuelle, Société de Chimie Physique, Paris, 1952), p. 177.

[2] A. J. Wakefield, Proc. Cambridge Phil. Soc. **47**, 419, 799 (1951).

[3] L. Tisza, in *Phase Transformations in Solids*, R. Smoluchowski, Editor (John Wiley & Sons, Inc., New York, 1951), p. 1.

[4] V. K. Semenchenko, Zhur. Fiz. Khim. **21**, 1461 (1947); **25**, 121 (1951).

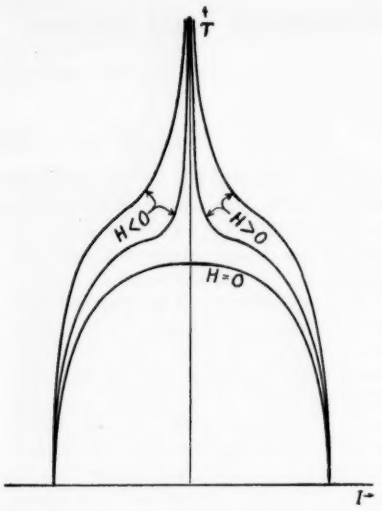

FIG. 1. Schematic magnetization curves for Ising lattice.

constant is supposed to be a fixed quantity, which does enter into the calculation in any essential way. It has been pointed out, however, that the lattice constant, or (in the three-dimensional case, which is the one we shall consider) the molal volume can be a variable parameter;[5] then the interaction between spins or the interaction producing order depends on this parameter. However, if the parameter were held fixed, the calculation would go through in the same manner as before.[6] The critical temperature T_c at which the singularity in C_H (for $H=0$) occurs would then depend on the molal volume V. C_H would become identical to (or at least be closely related to) C_v in the compressible lattice. C_v would appear to have a much more fundamental significance than C_p, and one is driven to find out what happens at the locus in the p-V plane or T-V plane at which C_v is infinite. The question also arises, can C_p become infinite in a case like this, and can we have a locus of points where C_p is infinite, or is $C_p=\infty$ confined to a critical point, or at most to a critical region? This question cannot, perhaps, be unequivocally answered, but we shall essay a discussion of it in Sec. 3. The case of $C_v=\infty$ will be discussed in Sec. 4, and we shall show that such points actually become unstable in a compressible lattice, and the transition turns into a first-order transition. The case of transitions which are first order to start with are considered in Sec. 5, and second-order transitions will be dealt with in Sec. 6. It will be seen that all these phenomena arise because we have to consider the interaction of a pair of variables like H and I, with the ordinary thermodynamic variables p and V.

2. THERMODYNAMICS OF THE INCOMPRESSIBLE ISING LATTICE

To introduce the subject we shall first discuss the thermodynamics of the Ising lattice, considering the temperature T, the magnetization I, and the magnetic field H, as the sole thermodynamic variables. A couple of diagrams will clarify the thermodynamic position of the infinite specific heat at the transition temperature which marks the appearance or disappearance of long-range order.

An Ising lattice is, of course, a somewhat artificial construction. It is assumed that the spin vectors are always directed along a fixed direction, and that there are only two states, the spin being either positive or negative. This considerably simplifies the situation, since we do not need to consider the vector properties of the magnetic field. H may be considered to have the same direction as the line along which the spins are oriented; it can have any positive or negative value.

In Fig. 1 we show an I-T diagram. The curves are for constant H. For $H=0$ we know that I is zero above the critical temperature, T_c. Below this temperature long-range order sets in, and the system acquires a permanent magnetic moment, which can be in either the positive or the negative direction. If H is not zero, but positive, for example, then I will always be positive, and will only vanish asymptotically as T becomes infinite. This behavior is illustrated in Fig. 1.

Figure 2, which is an H-I diagram, with isotherms, can be readily constructed from Fig. 1. I is analogous to V in the ordinary p-V diagram, H to $-p$. It will be seen that these isotherms indicate a first-order transition if $T<T_c$. T_c is a true critical temperature and there is no first-order transition for $T>T_c$. The remarkable feature of this diagram is the fact that the transition always takes place at the same H. This can be readily understood from the equation analogous to the

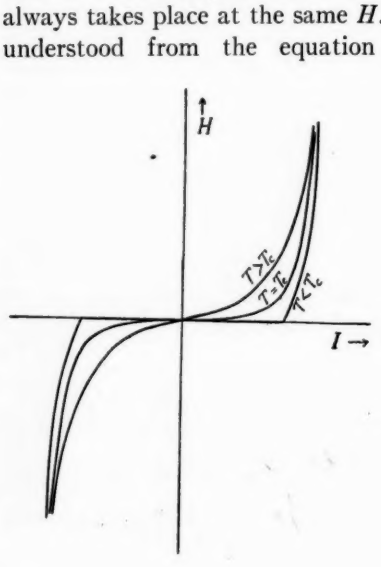

FIG. 2. Schematic isotherms for Ising lattice.

[5] R. Eisenschitz, Proc. Roy. Soc. (London) **168A**, 546 (1938); H. A. Bethe and J. G. Kirkwood, J. Chem. Phys. **7**, 578 (1939); H. Sato, Proc. Phys. Soc. (Japan) **2**, 17 (1947) [Chem. Abstracts **44**, 9206h (1950)]; L. Kholodenko, Zhur. Eksptl. Teort. Fiz. **20**, 1083 (1950) [Chem. Abstracts **45**, 5999g (1951)]; L. Saroléa, Physica **19**, 615 (1953).

[6] This, of course, assumes that there is no local variation in the lattice constant, depending upon statistical fluctuations in the degree of order from place to place in the system, an effect which might have to be considered in some real systems.

Clapeyron equation.

$$dH/dT=-\Delta S/\Delta I. \tag{1}$$

The isotherms are entirely symmetrical with respect to the origin, and the entropy will not depend on the sign of I, as this is merely a question of the direction of the spins. Thus $\Delta S=0$, and hence $dH/dT=0$. Aside from this peculiarity the isotherms are quite analogous to those found in the p-V diagram, assuming a classical type of critical point.

The situation at the critical point may be understood by the aid of some other thermodynamic equations. In analogy to the well-known equation

$$\partial C_v/\partial V)_T=T(\partial^2 p/\partial T^2)_V \tag{2}$$

we can write

$$(\partial C_I/\partial I)_T=-T(\partial^2 H/\partial T^2)_I. \tag{3}$$

Now clearly, from Fig. 2, $(\partial H/\partial T)_I$ and $(\partial^2 H/\partial T^2)_I$ are both zero at the critical point, and there is no reason to suppose that $(\partial^2 H/\partial T^2)_I$ will be infinite anywhere. There should, therefore, be no singularities in C_I. For C_H we may write

$$C_H=C_I-T(\partial H/\partial T)_I(\partial I/\partial T)_H, \tag{4}$$

which is quite analogous to the equation

$$C_p=C_v+T(\partial p/\partial T)_V(\partial V/\partial T)_p \tag{5}$$

which applies to the case where p and V are the variables. It can be seen from the figures that $(\partial H/\partial T)_I$ and $(\partial I/\partial T)_H$ have opposite signs, so C_H is always greater than C_I. Furthermore, $(\partial I/\partial T)_H$ is infinite at the critical point, so C_H *may* become infinite. As far as the thermodynamics is concerned, however, this is not necessary, since $(\partial H/\partial T)_I$ is zero. Only the statistical calculation shows that C_H does become infinite for the Ising lattice. The possibility of an infinite specific heat is certainly consistent with Tisza's general thermodynamic formalism, and it is quite in accord with the usual ideas about a critical point. However, whether it will actually occur cannot be determined by thermodynamics alone.

Also it would be thermodynamically quite possible to have points of zero slope in other isotherms than the critical one, and this would lead to infinities in C_H at other points. This seems extremely unlikely, however, and the corresponding situation when the variables are p and V will be discussed in detail in the next section. Domb[7] has conjectured from statistical calculations that C_H will not become infinite if $H\neq 0$.

We may recall again at this point that the order-disorder phenomenon for a binary alloy with equal molal parts of the two components is mathematically equivalent to the Ising lattice. A disorder parameter, which is called a quasi-thermodynamic variable, can be introduced[8] to take the place of the variable I. The difference, as Tisza has pointed out, is that the binary alloy corresponds just to the case $H=0$, and there is no way whereby we can exert a force on it to remove it from the condition corresponding to $H=0$. However, it is just for $H=0$ that the infinite value of C_H occurs. Thus we will have the infinite specific heat to deal with in the case of the binary alloy, and if the alloy is a compressible system, we see that this corresponds to an infinity in C_v.

3. THERMODYNAMICS OF A SYSTEM WITH INFINITE VALUES OF C_p

The results of the last two sections lead to the preliminary inference that an infinite value of C_v might arise and that the temperature at which this would happen would be a function of the volume of the system. C_p appears to be a much less fundamental quantity than C_v. C_p is of course, in general, infinite at a critical point, or in a critical region, and it appears to be infinite in a two-phase region; that is, the heat capacity, including the heat required for phase transition, is infinite at constant pressure for the two-phase system as a whole. Usually we expect to find an infinite C_p nowhere else. It would, however, be thermodynamically quite possible for the condition $C_p=\infty$ to define a locus in, say, the p-V plane. A brief investigation of the thermodynamics of such a situation will show why it rarely or never occurs. We start with the equation

$$(\partial C_p/\partial T)_p=-(\partial C_p/\partial p)_T(\partial p/\partial T)_{C_p} \tag{6}$$

which by use of the thermodynamic relation

$$(\partial C_p/\partial p)_T=-T(\partial^2 V/\partial T^2)_p \tag{7}$$

becomes

$$(\partial C_p/\partial T)_p=T(\partial^2 V/\partial T^2)_p(\partial p/\partial T)_{C_p}. \tag{8}$$

Let us now define $T_0(p)$ as the temperature at the pressure p at which C_p becomes infinite. Then it is seen that

$$\lim_{C_p=\infty}(\partial p/\partial T)_{C_p}=dp/dT_0 \tag{9}$$

so that Eq. (8) gives a thermodynamic expression for dp/dT_0. We shall consider the case where dp/dT_0 and dV/dT_0 are both finite, this being essentially the only case of interest to us. If either one were infinite, then there would be only one temperature of "transition" in the finite range of pressure or of volume.

Equation (8) is analogous to the Clapeyron equation. If $(\partial p/\partial T)_{C_p}$ is to remain finite when $C_p\to\infty$, $(\partial C_p/\partial T)_p$ and $(\partial^2 V/\partial T^2)_p$ must become infinite together and in the same way, and hence C_p and $(\partial V/\partial T)_p$ will also behave similarly. It is not necessary that C_p and $(\partial V/\partial T)_p$ should become infinite in the same way above and below T_0, but it is necessary by Eqs. (8)

[7] C. Domb, Proc. Roy. Soc. (London) **A199**, 199 (1949).

[8] See, e.g., L. Landau, Physik. Z. Sowjetunion **11**, 26 (1937); L. Landau and E. Lifshitz, *Statistical Physics* (Oxford University Press, London, 1938), Chap. XI.

and (9) that the ratio of $(\partial C_p/\partial T)_p$ and $(\partial^2 V/\partial T^2)_p$, and hence of C_p to $(\partial V/\partial T)_p$ should be the same,[9] in the region where they are very large. Since $(\partial C_p/\partial T)_p/(\partial^2 V/\partial T^2)_p$ is constant and equal to $C_p/(\partial V/\partial T)_p$ everywhere in the immediate neighborhood of T_0 for the particular p, it is also true that (where H stands for enthalpy, *not* magnetic field)

$$\frac{(\partial C_p/\partial T)_p}{(\partial^2 V/\partial T^2)_p}=\frac{\int_{T'}^{T''} C_p dT}{\int_{T'}^{T''} (\partial V/\partial T)_p dT}=\frac{\Delta H}{\Delta V}. \tag{10}$$

Here T'' and T' are two temperatures very close to T_0 and such that $T''>T_0$ and $T'<T_0$. This integration is to be performed at constant pressure. Thus ΔH is the "heat of transition" for a very small range around T_0 and ΔV is the "volume change of the transition." The analogy of Eq. (8) to the Clapeyron equation is now obvious. By integrating $(\partial C_p/\partial T)_p$ and $(\partial^2 V/\partial T^2)_p$ instead of C_p and $(\partial V/\partial T)_p$ we get the analogy of the Ehrenfest equation for a second-order transition.

It is clear from the preceding paragraph that $(\partial V/\partial T)_p$ becomes infinite when C_p does. Since

$$(\partial V/\partial T)_p=-(\partial V/\partial p)_T(\partial p/\partial T)_V \tag{11}$$

we see that either $(\partial V/\partial p)_T$ is infinite or else $(\partial p/\partial T)_V$ must be. To decide which one is infinite let us use the equation

$$dV/dT_0=(\partial V/\partial T)_p+(\partial V/\partial p)_T dp/dT_0. \tag{12}$$

Since $(\partial V/\partial T)_p$ becomes infinite at the transition line $(\partial V/\partial p)_T$ must also become infinite if dV/dT_0 and dp/dT_0 are to be finite. If we invert Eq. (12),

$$dp/dT_0=(\partial p/\partial T)_V+(\partial p/\partial V)_T dV/dT_0. \tag{13}$$

Since $(\partial p/\partial V)_T$ is zero, we must have

$$dp/dT_0=(\partial p/\partial T)_V. \tag{14}$$

The isotherms will look as shown in Fig. 3. Since $(\partial V/\partial T)_p$ and $(\partial p/\partial T)_V$ do not in general change sign at the singular point, we see from Eq. (11) that $(\partial V/\partial p)_T$ should not change in sign there, in conformity with the curves shown in Fig. 3.

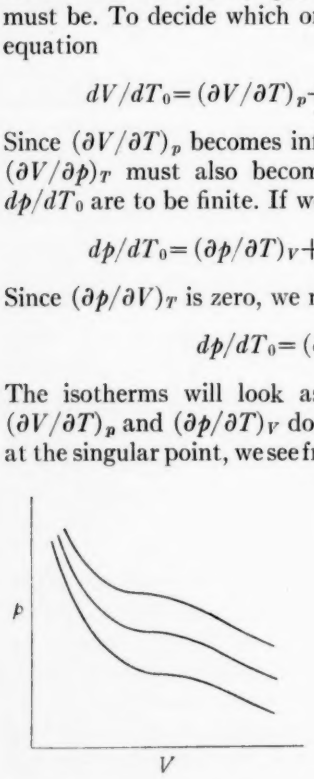

FIG. 3. Isotherms, C_p having an infinity.

We can now see why we do not expect to have a locus of points where C_p is infinite. If $(\partial p/\partial V)_T$ does become zero we should expect it usually to change sign; only in a special case would we anticipate that a zero value and a maximum would coincide. If $(\partial p/\partial V)_T$ becomes positive the system is unstable and we have separation of phases. Thus Tisza seems justified in supposing that a point where C_p becomes infinite is a special point; i.e., a critical point, though as already noted, there may be a critical region. It has been suggested that, in the liquid-vapor transition just above the point of disappearance of the meniscus, there is an anomalous first-order transition, with $(\partial p/\partial V)_T$ equal to zero, and C_p, hence, infinite over a finite range of the p-V plane.[10] It has also been suggested[10] that the liquid-vapor coexistence curve has a flat horizontal portion along the top, but with no region of anomalous first-order transition. This would make C_p infinite along the flat horizontal line, though not infinite in a finite region. This would actually be a case in which dV/dT_0 is infinite, with $(\partial p/\partial V)_T=0$ along the transition line, and with $(\partial p/\partial T)_V$ finite. Though our other proof that $(\partial p/\partial T)_V$ is finite would not hold in this case, it certainly could not be infinite along the entire line, for $(\partial p/\partial T)_V=(\partial S/\partial V)_T$, and so this would imply an infinite change in entropy for a finite change in volume.

4. THERMODYNAMICS OF A SYSTEM WITH INFINITE VALUES OF C_v; THE COMPRESSIBLE ISING LATTICE

Though the considerations of Sec. 3 indicate that we will be unlikely to find infinite values of C_p, except those associated with a first-order transition and the corresponding critical point, we have seen that the Ising lattice calculations make it appear likely that loci of infinite C_v could exist in a thermodynamic variable.[11] We shall now show that this is not to be expected to this case, either.

Since the interaction between the spins, which causes them to line up at the lower temperatures (or, in the binary alloy case, the interaction which tends to produce order) will undoubtably be greater the smaller the volume, we expect T_0 to be greater the smaller V, i.e.,

$$dT_0/dV<0. \tag{15}$$

This, of course, is a nonthermodynamic assumption, which we believe to be justified in this case. However, the results of the opposite assumption could be readily enough worked out, and they would not be very different.

[9] It is to be noted that C_p and $(\partial V/\partial T)_p$ will not change in sign as T goes through T_0, while the opposite will be true of $(\partial C_p/\partial T)_p$ and $(\partial^2 V/\partial T^2)_v$.

[10] For reviews see J. E. Mayer, *Changements de Phases* (Comptes Rendus 2e Réunion Annuelle, Société de Chimie Physique, Paris, 1952), p. 35; O. K. Rice, J. Phys. & Colloid Chem. **54**, 1293 (1950).

[11] As noted in Sec. 1, we shall assume that we are dealing with a three-dimensional Ising lattice, but we shall assume that the specific heat curve has an infinity at the transition point, as in the two-dimensional case.

We proceed much as in Sec. 3, writing

$$(\partial C_v/\partial T)_V = -(\partial C_v/\partial V)_T(\partial V/\partial T)c_v \qquad (16)$$

which, by Eq. (2) becomes

$$(\partial C_v/\partial T)_V = -T(\partial^2 p/\partial T^2)_V(\partial V/\partial T)c_v. \qquad (17)$$

In analogy to Eq. (9)

$$\lim_{C_v=\infty}(\partial V/\partial T)c_v = dV/dT_0. \qquad (18)$$

Since dV/dT_0 is finite, and since $(\partial C_v/\partial T)_V$ must become infinite when the transition line is approached, $(\partial^2 p/\partial T^2)_V$ must also become infinite. Then, since C_v itself becomes infinite, $(\partial p/\partial T)_V$ will become infinite. Of course, we can also see directly that if C_v is infinite only along the transition line, $(\partial C_v/\partial V)_T$ [and, hence, $(\partial^2 p/\partial T^2)_V$] must become infinite as well as $(\partial C_v/\partial T)_V$, for C_v becomes infinite whether the transition line is approached along a path of constant volume or a path of constant temperature.

Since dV/dT_0 is negative, we see from Eq. (17) that in the neighborhood of the transition line $(\partial p^2/\partial T^2)_V$ must have the same sign as $(\partial C_v/\partial T)_V$ and $(\partial p/\partial T)_V$ must have the same sign as C_v, i.e., it is positive and infinite at the transition line. Writing Eq. (11) in the form

$$(\partial p/\partial T)_V = -(\partial p/\partial V)_T(\partial V/\partial T)_p \qquad (19)$$

we see that one or the other of the two factors on the right-hand side must become infinite at the transition line. We can see which factor this should be by considering Eq. (13). If $(\partial p/\partial V)_T$ remains finite then dp/dT_0 is determined by $(\partial p/\partial T)_V$ and becomes infinite. This means essentially that at all finite pressures (it is difficult to see how such a condition could exist over a limited range) there will be only one temperature at which the transition can occur, and hence only one volume. This is not a case of interest to us. Therefore, we must suppose that $(\partial p/\partial V)_T$ becomes infinite.

It will be noted that the result is just the opposite to that which is obtained when C_p is infinite, and where we found that $(\partial p/\partial V)_T$ must become zero. Therefore a locus of infinite C_v could not coincide with or even cross a locus of infinite C_p.

Since $(\partial V/\partial p)_T$ will be zero for infinite C_v we see from Eq. (12) that

$$dV/dT_0 = (\partial V/\partial T)_p. \qquad (20)$$

Therefore, along the locus $(\partial V/\partial T)_p$ is negative, and since $(\partial p/\partial T)_V$ is positive then $(\partial p/\partial V)_T$ is positive by Eq. (19). Of course, far from the transition $(\partial p/\partial V)_T$ must have the normal negative sign. These rather queer relationships with regard to sign can be understood from the p-V diagram (Fig. 4). From this figure the behavior of the coefficient $(\partial V/\partial T)_p$ can also be understood.

Of course the striking feature of Fig. 4 is the fact

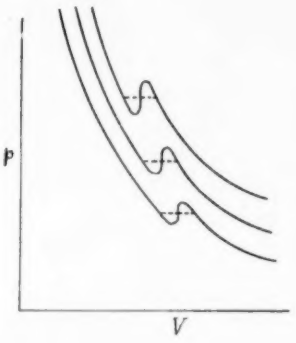

FIG. 4. Isotherms, C_v having an infinity.

that the isotherms have the familiar S shape such as is given by the van der Waals equation in the condensation region of a gas, and we see at once that the transition will be changed into a first-order transition taking place along the dotted line. The only exception to this will occur if dV/dT_0 is infinite, or $dT_0/dV=0$. This of course, is the case we have excluded by assuming that the interaction between neighbors changes with V, but can be thought of as the limiting case where the dependence on V is very weak. In this case the transition line coincides with an isotherm, and the transition will not turn into a first-order transition. In general the less the transition temperature depends on the volume, the less marked we expect the first-order transition to be. Also the less compressible the substance, the less marked the first-order transition; for the greater the normal value of $-(\partial p/\partial V)_T$, the smaller the volume range along any given isotherm along which it will be counteracted by the abnormal negative contribution to $-(\partial p/\partial V)_T$.

The general qualitative reason for the shape of the isotherms shown in Fig. 4 may be worth a word of explanation, though it is actually intuitively obvious. Since the interactions which result in the transition to the state of greater order become greater the smaller the volume, and since they are forces which lower the energy, it is obvious that they should have a net attractive effect. An attraction lowers the pressure, and since the attraction will be increasing very rapidly with decreasing volume near the transition, it will result, in this region, in a marked negative contribution to $-(\partial p/\partial V)_T$, which in fact becomes infinite just at the transition line. This results in the S-shaped curve, and of course means that the transition line itself is in an unstable region which could never be realized in any experiment.

In the above we have assumed that $(\partial p/\partial T)_V$ is everywhere positive, as is usual. If $(\partial p/\partial T)_V$ should be negative outside the transition region, a situation which rarely if ever occurs in the solid state, the isotherms will be as shown in Fig. 5, those corresponding to higher temperatures being at the lower part of the diagram outside the transition region. The transition will still turn into a first-order transition.

The considerations of this Section may appear to

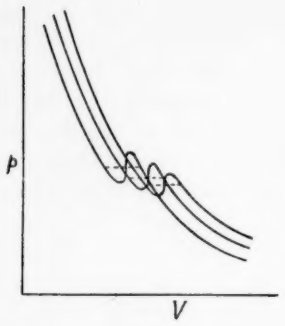

FIG. 5. Isotherms, C_v having an infinity, $(\partial p/\partial T)_V$ negative except near the singularity.

imply a restriction, in that we have assumed that the interactions between the sites of the lattice depend wholly on the volume. For it might be supposed that they would not depend on the volume itself, but rather on some parameter Y which is a function of V and T. Then the specific heat C_H would, when considering the expansion of the lattice, go over into C_y, the specific heat at constant Y, rather than to C_v. It seems reasonable to assume that $(\partial Y/\partial V)_T$ and $(\partial Y/\partial T)_V$ are everywhere finite and $(\partial Y/\partial V)_T$ is nonvanishing. Furthermore, it can be supposed that lines of constant Y in the T-V plane will not cross. We can then define Y in such a way that $(\partial Y/\partial V)_T$ is always positive. Then the inequality

$$dT_0/dY<0$$

would take the place of (15), but it is not to be expected that the situation would be sufficiently altered to cause (15) to fail.

On the basis of these assumptions we can show that our argument will go through exactly as before. We write

$$(\partial S/\partial T)_Y=(\partial S/\partial T)_V+(\partial S/\partial V)_T(\partial V/\partial T)_Y$$

or, multiplying through by T and setting $(\partial S/\partial V)_T=(\partial p/\partial T)_V$,

$$C_y=C_v+T(\partial p/\partial T)_V(\partial V/\partial T)_Y.$$

Since $(\partial V/\partial T)_Y=-(\partial V/\partial Y)_T(\partial Y/\partial T)_V$ cannot be infinite we see that if C_y is infinite either $(\partial p/\partial T)_V$ is infinite or both $(\partial p/\partial T)_V$ and C_v are infinite [if C_v is infinite we know that $(\partial p/\partial T)_V$ must be]. Let us suppose that $(\partial p/\partial T)_V$ is infinite, but C_v is finite. Then C_p must be infinite, unless $(\partial V/\partial T)_p=0$, by Eq. (5). It is most unlikely that $(\partial V/\partial T)_p$ should vanish along the whole locus[12] or any extended portion of it, and this situation may for practical purposes be excluded; however, if C_p is infinite then we have seen that in all normal circumstances $(\partial p/\partial T)_V$ will be finite, so we are forced into a contradiction. We can therefore conclude that if C_y is infinite C_v must be also, at least if there is a locus of infinities, and the converse, that C_y is infinite if C_v is, is easily proved. We see that all our previous deductions as to the behavior of the system when C_v is infinite will be valid when C_y is infinite.

If Y should be set equal to $-p$, it is seen that a special case occurs, in that C_y is then equal to C_p, and if C_p is infinite C_v is not. However, it must be noted that in this case $(\partial Y/\partial V)_T$ becomes equal to zero at the transition line, and so contradicts our original hypothesis. Such a situation will not be expected to occur, and lends added weight to our contention that a locus of points for which C_p is infinite will not be expected under any normal circumstances.

Since the behavior of C_y depends upon the conditions on the partial derivatives of Y rather than upon the physical interpretation, it is seen that there is a whole category of specific heats which become infinite together. As we have just seen, C_p does not belong in this category, and it is finite when they are infinite.

Although exceptions to the conditions assumed are thermodynamically imaginable, we believe that, from a practical point of view, it has been shown that a locus of infinite C_v changes over to a set of first-order transitions.

5. CASE WITH FIRST-ORDER TRANSITION ALREADY PRESENT

In some cases, for example, the order-disorder transition in the $AuCu_3$ alloy, in which the two components are not present in equal molal quantities, and even in AuCu, which has a face-centered lattice, theory indicates that the transition will be first-order,[13] even when only a constant-volume lattice is considered. It will be of interest to consider how such a transition will be affected if the compressibility of the lattice is taken into account. We make the same general assumptions as to the dependence of the interaction forces on the volume, so that the inequality (15) will again hold.

If the first-order transition takes place at constant volume, and with the density of each of the two phases remaining constant throughout the transformation, we must in general suppose that the two phases which are in equilibrium with each other are at different pressures. Of, course, any such effect is taken up by the lattice when the lattice is supposed to be incompressible. In a real system, it would be necessary to have some machine to maintain the difference in pressure. Let the difference in pressure be Δp, the difference in entropy be ΔS, and the difference in energy be ΔE. The amount of work done by the system on the machine when the phase which has the lower pressure changes to the phase which has the higher pressure is $V\Delta p$. The condition of equilibrium is

$$\Delta E-T\Delta S+V\Delta p=0. \tag{21}$$

However, the theories ignore pressure effects entirely,

[12] Furthermore, if $(\partial p/\partial T)_V$ is infinite and $(\partial V/\partial T)_p=0$, then $(\partial V/\partial p)_T=0$, and by Eq. (12) either $dV/dT_0=0$ or $dp/dT_0=\infty$, which are excluded cases.

[13] See E. A. Guggenheim, *Mixtures* (Oxford University Press, London, 1952), Chapter VII; F. C. Nix and W. Shockley, Revs. Modern Phys. **10**, 1 (1938).

and they take as the condition of equilibrium

$$\Delta E - T\Delta S = \Delta A = 0 \tag{22}$$

where ΔA is the change in Helmholtz free energy. This is the equation, then, which actually determines the supposed T_0 as a function of V.

Since $(\partial\Delta A/\partial T)_V = -\Delta S$ and $(\partial\Delta A/\partial V)_T = -\Delta p$ we can write, to get the effect of change of temperature on the transition,

$$d\Delta A = -\Delta S dT_0 - \Delta p dV = 0$$

or[14]

$$dV/dT_0 = -\Delta S/\Delta p. \tag{23}$$

This will hold for the artificial transition determined by Eq. (22), even though there is no true equilibrium between the phases. Now, according to our assumptions dT_0/dV is negative, therefore ΔS and Δp have the same signs. If Δ indicates a change from an ordered to a disordered system ΔS and Δp are positive. Therefore, the isotherms, assuming an artifically induced transition where Eq. (22) holds, will appear as shown in Fig. 6. Once again the actual transition will take place at a constant pressure along the dotted line. Since the transition from A to B involves no change in A the change in G is given by $V\Delta P$ and along the other lines $dG = Vdp$, so the position of the dotted line is determined by the usual equal-area criterion. Since the transitions from A' to A, from A to B, and from B to B' all involve positive changes in entropy, the actual transition will be a transition with greater latent heat than the calculation based on Eq. (22) would indicate.

The close resemblance between Fig. 4 and Fig. 6 and the general similarity of the ideas involved in obtaining these figures will be evident at once. The second case may be said to be a somewhat more extreme example of the same type of effect considered in the first one, and as such the nature of the phenomena involved are perhaps more obvious.

In the above we have assumed that the composition of an alloy like $AuCu_3$, which we have used as an example showing the type of transition considered, remains uniform throughout. This will presumably be the case if diffusion is slow enough. Shockley,[15] however, has pointed out that if two phases are in equilibrium they will actually have different compositions, and such an effect has been demonstrated experimentally in at least one case.[16] The thermodynamics of this situation has been discussed by direct use of the free energy function by Shockley, but can also be handled by the method used in this paper, as we shall briefly demonstrate.

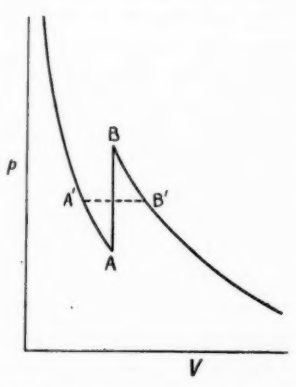

FIG. 6. Isotherm for first-order order-disorder transition.

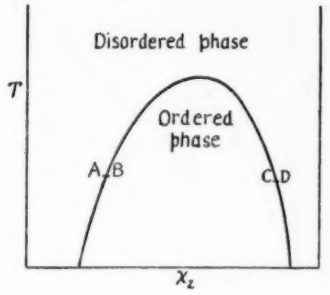

FIG. 7. Temperature-composition diagram for first-order order-disorder transition.

We deal now with the variables T, x_2, and μ_2, where x_2 and μ_2 are the mole fraction and chemical potential of one of the components, instead of T, V, and p. We shall not attempt to consider the case with all five variables. If we should assume x_2 to be uniform throughout the system, and the same in coexisting ordered and disordered phases, we might expect to have a phase diagram with a transition line such as is shown in Fig. 7. Equation (22) is again taken as determining this artificial transition line. Essentially we assume in this treatment that both p and V are constant, so A and G are identical.

To get the slope of the transition line we introduce as an auxilliary variable n_2, the number of molecules of component 2, which can take the place of x_2 if n_1 is held constant. We then have, for the transition line,

$$d\Delta A = 0 = (\partial\Delta A/\partial T)_{n_2} dT_0 + (\partial\Delta A/\partial n_2)_T dn_2 = -\Delta S dT_0 + \Delta\mu_2 dn_2. \tag{24}$$

Consider now the transition from the point A to point B, Fig. 7. (Essentially the same ultimate results would be found for points like C and D.) Here $dn_2/dT_0 > 0$, hence ΔS and $\Delta\mu_2$ have the same sign. If Δ indicates a change from ordered to disordered system ΔS is positive and $\Delta\mu_2$ is positive. In general $(\partial\mu_2/\partial x_2)_T$ is positive, but it will be seen that μ_2 decreases from A to B. Hence the μ_2-x_2 diagram will be as shown in Fig. 8. Since in a true equilibrium the value of μ_2 must be equal on the two-sides of the transition line, the concentrations of the two phases will be given by the ends of some dotted line such as is shown in Fig. 8. The exact position of the dotted line is determined by the condition that μ_1 does not change across the transition. The point at which the conditions on both μ_2 and μ_1 are fulfilled may be found by plotting μ_1 against μ_2. μ_1, of course

[14] Equation (23) is given by Semenchenko (see reference 4) but the exact meaning and application of it is not clear.

[15] W. Shockley, J. Chem. Phys. **6**, 130 (1938).

[16] Newkirk, Smoluchowski, Geisler, and Martin, J. Appl. Phys. **22**, 290 (1951).

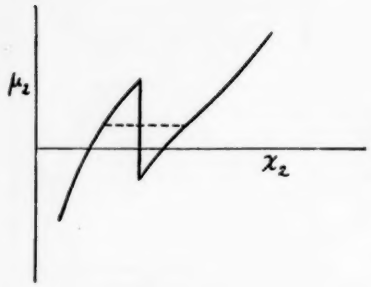

FIG. 8. Isotherm, chemical potential *vs* mole fraction, for first-order order-disorder transition.

decreases as μ_2 increases, and by the Gibbs-Duhem equation $d\mu_1/d\mu_2 = -x_2/x_1$. Also, at the transition line of Fig. 7 we will have $\Delta\mu_1/\Delta\mu_2 = -x_2/x_1$. The curve which will be found will thus be somewhat as shown in Fig. 9, and the encircled intersection is the point desired.

As we have remarked, essentially the same results would be obtained on the right-hand branch of the curve in Fig. 7. At the top of the curve $dT/dn_2 = 0$, and so $\Delta\mu_2 = 0$, by Eq. (24). Thus in this case, only, there is no tendency for the two phases to take on different compositions. The phase diagram of Fig. 7 is replaced by the usual type of phase diagram in which the transition line of Fig. 7 is "broadened out" into an area which indicates over-all compositions in which two phases of different composition (as well as having different degrees of order) are in equilibrium with each other.

6. ISING LATTICE WITH $H \neq 0$; TRANSITION WITH A FINITE λ POINT

In Sec. 4 we considered in some detail the case of the Ising lattice with $H = 0$. The case for $H \neq 0$ is a situation in which one of the magnetic orientations is favored over the other, and it also has analogies in other order-disorder phenomena. If Fig. 1 gives a correct view of the situation, it is seen that $(\partial I/\partial T)_H$ may become large in magnitude in a certain temperature range, but never infinite, for $H \neq 0$. Therefore, Eq. (4) indicates that C_H will probably show a maximum at a certain temperature, but will not become infinite.

We suppose again that the critical temperature is raised by decreasing V. As an approximation it seems reasonable to suppose that Fig. 1 remains unaltered when V changes, except for a change in the scale of the T axis. There will also be an equivalent change in the scale of H; thus if T_c doubles, a curve which previously

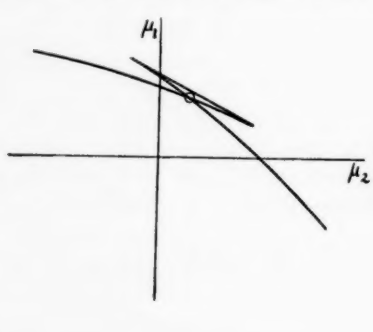

FIG. 9. Chemical potential diagram for first-order order-disorder transition.

had a given value of H would now correspond to twice that value. This occurs because a change in T_c by a given factor implies a change in spin interaction by the same factor, and to get a given value of I at a given reduced temperature T/T_c, the value of the magnetic field energy will have to be increased by the same factor. Let us consider now what happens if we hold H constant as V decreases and T_c increases. If $H = 0$ the curve for C_H is a function of T/T_c only.[1] But if H is not zero what happens is that by holding H constant and decreasing V we effectively approach, in Fig. 1, the curve for which $H = 0$. We, therefore, approach more closely the situation when $H = 0$, and the maximum in C_H, which is equivalent to C_v in the pVT system, goes up. A system of contours of constant C_v in the V-T plane will look somewhat as shown in Fig. 10. The dotted line shows the locus of the maximum of C_v with respect to T at constant V. The higher the value of T at which a C_v contour crosses this locus the higher the value of C_v. We see that there will be one point in any isotherm where $(\partial V/\partial T)_{C_v}$ is infinite, and $(\partial C_v/\partial V)_T$ is zero. From Eq. (2), then, we see that at such a point $(\partial^2 p/\partial T^2)_V$ will be zero, so that $(\partial p/\partial T)_V$

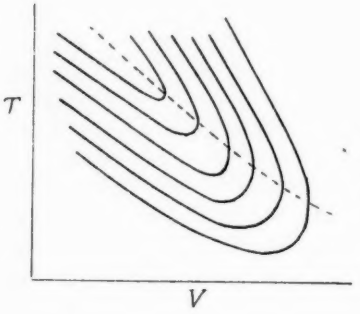

FIG. 10. Curves of constant C_v when C_v along an isochore has a maximum but no singularity.

will be a maximum along the isochore at this point. There will thus be a "ridge" of high values of $(\partial p/\partial T)_V$ and the maximum for any given value of V will occur at a certain value of T, again called T_0. We may thus expect an isotherm to show a behavior more or less similar to that described in Sec. 4, but less marked in its peculiarities. Since Eq. (20) will not hold in this case, it is harder to draw definite conclusions. However, when the maximum in C_v is marked we may at least expect $(\partial V/\partial T)_p$ and dV/dT_0 to have the same sign in the neighborhood of the maximum of C_v. Then $(\partial p/\partial V)_T$ will be positive in a certain region, and we will have a first-order transition as before. On the other hand, if the maximum of C_v is not so steep the situation need not be so extreme. We may see from Fig. 11, which shows two isotherms and the transition curve in such a less extreme case (assuming $(\partial p/\partial T)_V$ is everywhere positive) that the two isotherms may be farthest apart in the neighborhood of the transition, and hence $(\partial p/\partial T)_V$ largest there, with $(\partial p/\partial V)_T$ remaining negative. In this case there will be no first-order transition. This will be the case likely to exist at low

temperatures where the maximum in C_v is not so extreme (though there is an opposing factor, for at low temperatures and large volumes the isotherms will be less steep and hence more affected by induced changes in slope). We thus may expect a critical temperature in the pVT system above which there is a first-order transition, and below which there is none.

At the critical point, of course, we expect an infinite value of C_p, and below the critical point where there is no first-order transition we expect a maximum in C_p to be induced which is more marked than the maximum of C_v. This appears from the thermodynamic equation

$$C_p=C_v-T(\partial p/\partial T)_V^2(\partial V/\partial p)_T \qquad (25)$$

and from Fig. 11, from which we see that both $(\partial p/\partial T)_V$ and $-(\partial V/\partial p)_T$ are abnormally large in the neighborhood of the transition.

The type of transition which we have just discussed is of course radically different from condensation. In condensation the ordering phenomenon is accompanied by a marked change in volume, and if clusters of liquid-like material appear in the vapor before actual condensation takes place they have a markedly different density from the surrounding material. Nevertheless, we might suppose that if we could arrest the precipitate formation of liquid, and could observe the gradual appearance of order in the forbidden region between liquid and vapor we would find a maximum in C_v in this region. Certainly, a very marked maximum in C_v has been observed[17] just above the critical point. The thermodynamics of the situation in the liquid-vapor equilibrium may thus have some resemblance to that of the Ising lattice, except of course that in vaporization the first-order transition occurs below the critical point and the curves of Fig. 10 face the other way. Though one must be cautious in attempting to push an analogy in the direction of molecular mechanisms, it is of interest that the simple van der Waals theory of condensation indicates no anomaly whatsoever in $(\partial^2 p/\partial T^2)_V$ and hence in C_v near the critical point. The anomaly in C_v seems definitely to be linked with the ordering process.

In the case of a second-order transition, the specific heat generally rises in the neighborhood of the transition. The situation differs from that we have considered in the preceding portion of this section in that the specific heat shows a discontinuity in the transition. Such a discontinuity was found in the order-disorder problem for a binary alloy when approximate methods, such as the Bragg-Williams or the quasi-chemical approximations, were applied. Though the more exact analysis of Onsager indicated an infinite specific heat in the case of the two-dimensional Ising lattice, it is quite possible that other situations exist in nature

[17] A. Michels and J. Strijland, *Changements de Phases* (Comptes Rendus 2e Réunion Annuelle, Société de Chimie Physique, Paris, 1952), p. 87.

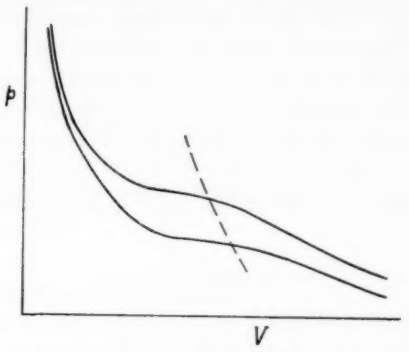

FIG. 11. Isotherms, specific heat having maximum but no singularity.

which would give rise to a λ point with a finite specific heat and a discontinuity.

The situation which arises in the case of a second-order transition is not fundamentally different from that which obtains when C_v shows a continuous maximum. The thermodynamics of this case has been previously considered; in particular Sato[5] has considered the effect of expansion of a lattice on C_p, Saroléa[5] has made a thorough statistical study of the Bragg-Williams approximation, and Eisenshitz[5] and Bethe and Kirkwood[5] have considered how ΔC_p differs from ΔC_v, where Δ indicates here the change across the transition line in the second-order transition.

C_p is, of course, greater than C_v, and ΔC_p is also, at least in the normal case, greater than ΔC_v. The following equation may be shown to hold[8]:

$$\Delta C_v=-T(dV/dT_0)\Delta(\partial p/\partial T)_V. \qquad (26)$$

Fig. 11 will be modified; instead the situation will be somewhat as shown in Fig. 12. Then it will be seen from Eq. (5) that the jump in C_p will be greater than that of C_v, because the jump in $(\partial V/\partial T)_p$ will contribute something extra to the jump in C_p. An increase in both $(\partial V/\partial T)_p$ and $(\partial p/\partial T)_V$ goes with a decrease in $-(\partial p/\partial V)_T$ as may be seen from Fig. 12; thus, since dV/dT_0 is negative the jump in C_v and the extra jump in C_p arising from the last term in Eq. (5) have the same sign.

If the maximum in the specific heats is large enough, it is quite possible that a second-order transition will

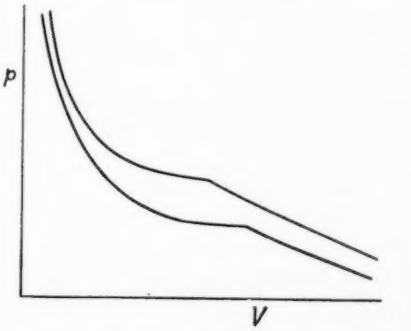

FIG. 12. Isotherms, second-order transition.

also be converted into a first-order transition. Again a critical temperature would be a possibility.

While Fig. 12 is about what we should expect for a solid lattice, showing a second-order transition, it should be remarked that it would be thermodynamically possible to get diagrams which look quite different. This happens, for example, in the λ transition in liquid helium.[18]

7. CONCLUSIONS

The results of this paper, besides being of interest themselves, may have some application in the consideration of experimental results, and the comparison of such results with theory. In the first place, it is to be noted that we never should expect to find any infinite specific heats, apart from a first-order transition, although the specific heats may rise to a large value if the solid is sufficiently incompressible, and if there is sufficiently little coupling between the interaction causing the transition and the degree of expansion of the solid. If a correct theory without compressibility predicts infinite specific heats we should look for a first-order transition, with discontinuous change of volume. If the theory predicts a first-order transition even at constant volume, we should still look for a change in volume at the transition. If the theory without compressibility predicts a λ point in the specific heat we may or may not actually have a first-order transition. If not, the sharpness of the λ point will be enhanced.

[18] O. K. Rice, Phys. Rev. **93**, 1161 (1954).

THE JOURNAL OF CHEMICAL PHYSICS VOLUME 22, NUMBER 9 SEPTEMBER, 1954

Vibrational Spectrum of Hexafluoro-2-Butyne*

FOIL A. MILLER, *Department of Research in Chemical Physics, Mellon Institute, Pittsburgh, Pennsylvania*

AND

ROBERT P. BAUMAN, *Department of Physics, University of Pittsburgh and Mellon Institute, Pittsburgh 13, Pennsylvania*

(Received January, 13, 1954)

Infrared and Raman spectra have been obtained for hexafluoro-2-butyne, including qualitative depolarizations and gaseous state frequencies for the stronger Raman lines. The data provide good evidence that D_{3d} selection rules are followed. From this it appears that there must be hindered rotation between the CF_3 groups, with the "staggered" configuration being stable. An assignment of fundamental frequencies has been made for this model. The origin of the potential barrier is not known. (See note added in proof at end of paper.)

INTRODUCTION

THE synthesis of hexafluoro-2-butyne, $CF_3-C\equiv C-CF_3$, has been reported in the literature[1–3] and its chemical properties have been described.[2,3] The compound melts at −117°C[2] and boils at −25°C. The infrared spectrum has been reported[2–4] but no attempt has been made to interpret the spectrum or identify impurity bands. An electron diffraction study has given the molecular dimensions, but has not established the symmetry.[5] The present paper describes the infrared and Raman spectra of the compound and their interpretation.

EXPERIMENTAL

Hexafluoro-2,3-dichloro-2-butene[6] was treated with zinc to give the acetylene:

$$CF_3-CCl=CCl-CF_3 \xrightarrow[EtOH]{Zn} CF_3-C\equiv C-CF_3.$$

After purification of the starting butene by fractional crystallization (mp −55.2±0.1°C), the reaction proceeded smoothly, giving a 30 percent yield in three hours. The butyne was purified by distillation at atmospheric pressure in a Podbielniak low temperature column. Comparison of the infrared spectra before and after distillation served to identify many of the bands as due to impurities.

The infrared spectrum was obtained from 4000 to 280 cm^{-1} with a Perkin-Elmer 12B spectrometer, using

* From a thesis submitted by R. P. Bauman in partial fulfillment of the requirements for the degree of Doctor of Philosophy at the University of Pittsburgh.

[1] C. I. Gochenour, U. S. Patent No. 2 546 997.

[2] A. L. Henne and W. G. Finnegan, J. Am. Chem. Soc. **71**, 298 (1949).

[3] R. N. Haszeldine, J. Chem. Soc. **1952**, 2508.

[4] (a) Smith, Alpert, Saunders, Brown, and Moran, Naval Research Laboratory, Washington, D. C., Report 3924, February 1, 1952; pp. 65, 74–75.
(b) American Petroleum Institute Research Project 44, Carnegie Institute of Technology. Catalog of Infrared Spectral Data. Serial Nos. 1366 and 1367, hexafluoro-2-butyne, submitted by the Naval Research Laboratory.

[5] W. F. Sheehan and V. Schomaker, J. Am. Chem. Soc. **74**, 4468 (1952).

[6] This compound was generously provided by the Hooker Electrochemical Company.

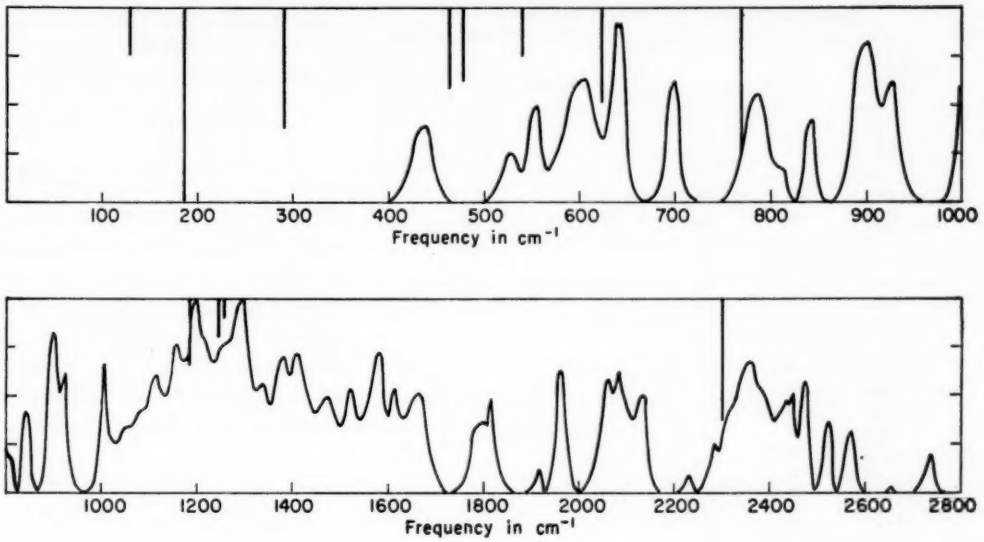

FIG. 1. Observed infrared and Raman frequencies for $CF_3-C\equiv C-CF_3$. Raman frequencies are indicated by vertical lines, with intensities estimated visually from the photographic plates. For infrared bands, intensities are plotted on a scale of $\log_{10}$ absorptivity. See Table II for numerical values.

a one-meter cell and CaF_2, NaCl, KBr, and KRS-5† prisms. Pressures ranged from less than a millimeter to half an atmosphere. Spectra obtained on a Baird instrument were useful in identifying impurity bands.

The Raman spectrograph has been described elsewhere.[7] It has been improved by the acquisition of a new Bausch and Lomb grating which gives markedly better performance and permits observation of Raman shifts down to about 125 cm^{-1}. Raman spectra of the liquid were obtained at approximately $-50°C$ using an unsilvered Dewar jacket similar to that described by Lord and Nielsen.[8] A stream of cold gas, obtained by bubbling dried cylinder nitrogen through liquid nitrogen, was used to cool the sample. Exposures of 6 and 12 hours were made on about 5 ml of liquid sample. Qualitative depolarizations were determined for the stronger lines by the method of Edsall and Wilson,[9] using 19-hour exposures. A one-week exposure on the gas gave four lines. Positions of the weakest lines were measured by the method of Joyner and Glockler,[10] using a thin filament of Duco cement to make the lines visible to the microdensitometer.

The results are shown in Fig. 1, and tabulated in Tables I and II.

ASSIGNMENT OF THE FREQUENCIES

Three possibilities concerning the internal rotation must be considered. The first (which was expected from analogy with the hydrocarbon analog, dimethylacetylene[11–14]) is free rotation of the CF_3 groups with respect to each other. This gives an instantaneous molecular symmetry of D_3, but a potential field symmetry of D_{3h}. Howard[15] has shown that the selection rules for this case, which he calls D_{3h}', are the same as for D_{3h}. The second possibility (and the most unlikely one) is that the rotation will be hindered, with the eclipsed configuration being stable. This symmetry is D_{3h}, so that the selection rules for it will be identical with those for the case of free rotation. The third alternative is hindered rotation with the staggered configuration being the stable one. Its symmetry is D_{3d}.

The selection rules for D_{3d} and D_{3h} are shown in Table III. (Herzberg's notation is used throughout.[16]) It will be observed that the only difference between them is in the degenerate species. For D_{3d}, because of

TABLE I. Observed Raman frequencies.

Liquid	Gas	Intensity	Polarization	Assignment
129		2		$f-186$,[a] $2\nu_{16}=130$
186		10	dp	ν_{12}
291		6	p	ν_3
464		4		ν_{11}
478		4		$\nu_3+\nu_{12}=477$
540		2		$\nu_{14}-\nu_{16}=540$
624		5		ν_{10}
771	771	8	p	ν_2
1170	1181	3		ν_1
1233	1245	2		ν_9
1257		1		$\nu_{13}+\nu_{16}=1260$
2305	2300	7	p	ν_4

[a] f = Hg 4047 A.

† The authors wish to express their appreciation to Dr. R. A. Friedel of the U. S. Bureau of Mines, Bruceton, Pennsylvania, for the loan of this prism.

[7] F. A. Miller and R. G. Inskeep, J. Chem. Phys. **18**, 1519 (1950).

[8] R. C. Lord and E. Nielsen, J. Opt. Soc. Am. **40**, 655 (1950).

[9] J. T. Edsall and E. B. Wilson, Jr., J. Chem. Phys. **6**, 124 (1938), method 1.

[10] P. Joyner and G. Glockler, J. Chem. Phys. **20**, 302 (1952).

[11] B. L. Crawford, Jr., and W. W. Rice, J. Chem. Phys. **7**, 437 (1939).

[12] G. B. Kistiakowsky and W. W. Rice, J. Chem. Phys. **8**, 618 (1940).

[13] Osborne, Garner, and Yost, J. Chem. Phys. **8**, 131 (1940).

[14] Yost, Osborne, and Garner, J. Am. Chem. Soc. **63**, 3492 (1941).

[15] J. B. Howard, J. Chem. Phys. **5**, 442, 451 (1937).

[16] G. Herzberg, *Infrared and Raman Spectra of Polyatomic Molecules* (D. Van Nostrand Company, Inc., New York, 1945), pp. 116, 117.

TABLE II. Observed infrared frequencies.

Frequency (cm^{-1})	Intensity[a]	Assignment
[65][b]		ν_{16}
[90][b]		ν_5
[234][b]		ν_{15}
437	0.4	$2\nu_{12}+\nu_{16}=437$
526	0.1	$\nu_{15}+\nu_3=525$; $\nu_{11}+\nu_{16}=529$
554	1.0	$\nu_5+\nu_{11}=554$; $\nu_{10}-\nu_{16}=559$
605	3.9	ν_{14}
642	50	ν_8
698	3.1	$\nu_{11}+\nu_{15}=698$; $3\nu_{15}=702$
786	1.7	$\nu_{12}+\nu_{14}=791$
813	0.05	
843	0.5	$\nu_3+\nu_5+\nu_{11}=845$
900	20	ν_7
926	2.8	$\nu_3+\nu_8=933$
1007	4.1	$\nu_{13}-\nu_{12}=1009$; $\nu_2+\nu_{15}=1005$
1055	0.2	$\nu_5+\nu_7+\nu_{16}=1055$; $\nu_1+\nu_6-\nu_{12}=1060$
1085	0.2	$\nu_7+\nu_{12}=1086$
1115	2.7	$\nu_1-\nu_{16}=1116$
1156	10	$\nu_9-\nu_5=1155$
1195	120	ν_{13}
1223	3	$\nu_{10}+\nu_{14}=1229$
1260	2	$\nu_8+\nu_{10}=1266$
1294	100	ν_6
1344	0.65	$\nu_9+\nu_{12}-\nu_5=1341$
1379	6.4	$\nu_{12}+\nu_{13}=1381$; $\nu_2+\nu_{14}=1376$
1410	7.5	$\nu_2+\nu_8=1413$; $\nu_1+\nu_{15}=1415$
1475	1	$\nu_9+\nu_{15}=1479$; $\nu_6+\nu_{12}=1480$
1522	1.4	$\nu_7+\nu_{10}=1524$
1582	7.7	$\nu_3+\nu_6=1585$
1618	1.3	$\nu_9+\nu_{11}-\nu_5=1619$
1669	1.1	$\nu_2+\nu_7=1671$
1800	0.3	$\nu_9+\nu_{10}-\nu_{16}=1804$
1822	0.6	$\nu_1+\nu_8=1823$; $\nu_{10}+\nu_{13}=1819$
1921	0.03	$\nu_6+\nu_{10}=1918$
1963	3.5	$\nu_2+\nu_{13}=1966$
2063	2.0	$\nu_2+\nu_6=2065$
2085	2.8	$\nu_1+\nu_7=2081$
2138	1.2	$\nu_7+\nu_9=2145$
2235	0.02	$\nu_4-\nu_{16}=2235$
2288	0.1	
2365	5	$\nu_1+\nu_{13}=2376$; $\nu_4+\nu_{16}=2365$
2432	0.9	$\nu_9+\nu_{13}=2440$
2450	1.1	$2\nu_{13}+\nu_{16}=2455$
2475	2.0	$\nu_1+\nu_6=2475$
2527	0.3	$\nu_6+\nu_9=2539$
2547	0.2	
2654	0.01	
2738	0.06	
2912	0.1	
2990	0.1	
3130	0.07	
3257	0.07	
ca 3530	0.3	
ca 3595	1	$\nu_4+\nu_6=3594$

[a] Absorptivity $\times 10^{+4}$: $a=[1/b(\text{cm})p(\text{mmHg})]\log_{10}(I_0/I)$.
[b] [ ] Estimated from combination tones.

its center of symmetry, there are no allowed infrared-Raman coincidences. For D_{3h}, on the other hand, the four E' fundamentals can be active in both. It will therefore be significant to observe whether or not the perpendicular infrared bands have Raman counterparts. Actually there is only one apparent coincidence, the weak bands at 1257 and 1260 cm^{-1}. These can be given an alternative explanation (see Tables I and II). D_{3d} symmetry will therefore be tentatively assumed in discussing the assignments, and more convincing evidence for it will be indicated later.

Table IV gives the notation, a schematic description of the vibrations, and the assignments of the fundamentals.

RAMAN-ACTIVE FUNDAMENTALS

1. Species A_{1g}

There is no doubt, because of their polarization, that 2300, 771, and 291 cm^{-1} should be assigned to ν_4, ν_2, and ν_3, respectively. For ν_1, the C—F stretch, there is a choice between 1181 and 1245 cm^{-1}. We have rather arbitrarily taken the former because of its somewhat greater intensity, and assigned the latter to the E_g stretching mode ν_9. These could be reversed without changing any of our subsequent conclusions.

2. Species E_g

In addition to 1245 as ν_9, the assignment of the very strong band at 186 to ν_{12} is straightforward. The remaining two fundamentals are then presumably to be chosen from among the four Raman lines at 464, 478, 540, and 624 cm^{-1}. 478 can be explained as $186+291=477$ (E_g). 464 is a reasonable E_g fundamental, and we assign it to ν_{11}. The remaining fundamental has been taken as 624 because of its greater intensity and because 540 can be explained otherwise (see Table I).

INFRARED-ACTIVE FUNDAMENTALS

1. Species A_{2u}

The infrared bands at 1294 and 642 cm^{-1} are intense parallel bands, with an observed separation of approximately 6 cm^{-1} compared to the calculated separation of 6.3 cm^{-1}, and are obviously to be attributed to ν_6 and ν_8, respectively. The band at 900 cm^{-1} is assigned to ν_7, the C—C stretching mode. Such an intense band must be a fundamental, and it must belong to A_{2u} because no E_u fundamental except ν_{13} will be this high.

2. Species E_u

ν_{13}, the C—F stretch, is readily assigned to 1195 cm^{-1} on the basis of position, intensity, and contour. ν_{15} and ν_{16} will certainly be low frequencies. Since no reasonably strong infrared bands were observed between 600 and 280 cm^{-1}, they must lie below the latter limit. Further discussion of them is temporarily deferred. ν_{14}, the CF_3 deformation, must be chosen from 526 (0.1),

TABLE III. Selection rules.

No. of fund. vibns.	Species	D_{3d} IR	Raman	Species	D_{3h} IR	Raman
4	A_{1g}	···	p	A_1'	···	p
1	A_{1u}	···	···	A_1''	···	···
0	A_{2g}	···	···	A_2'	···	···
3	A_{2u}	∥	···	A_2''	∥	···
4	E_g	···	dp	E'	⊥	dp
4	E_u	⊥	···	E''	···	dp

554 (1.0), 605 (3.9), 698 (3.1), and 786 (1.7) (intensities in parentheses). 605 has been selected on the basis of its intensity and its utility in explaining combination tones. One can also make a case for 554, but it does not seem as satisfactory.

ASSIGNMENT OF COMBINATION TONES

Assignments for the remaining combination tones have been made as shown in Tables I and II. In most cases only binary combinations have been considered. The infrared spectrum was rich in bands, as is characteristic of fluorocarbons, and a large proportion of the binary infrared-active combinations which can be calculated from the assignments of the fundamentals are actually observed. Because most of the calculated and observed values agree within 5 cm^{-1}, we feel that this constitutes a good test of the assignments, and that the unexplained combination bands can provide good evidence for the unobserved fundamentals.

ASSIGNMENT OF THE UNOBSERVED FUNDAMENTALS

Three fundamentals, ν_5, ν_{15}, and ν_{16}, have not been directly observed. It has been found that just three additional frequencies are required to make a complete assignment of all the observed infrared and Raman bands. The infrared bands at 526, 1115, and 2235, and the Raman band at 540 cm^{-1} are nicely explained by assuming a fundamental at 65 cm^{-1}. One might expect this to be the torsional frequency, but the selection rules forbid it. In particular, $\nu_4-65=2235$ is observed, and the torsional vibration is not allowed to combine with a totally symmetric vibration to give an infrared-active combination for either D_{3d} or D_{3h}'. Consequently, 65 cm^{-1} is assigned to ν_{16}. Because of the low frequency of this vibration and its twofold degeneracy, the lower excited levels are more highly populated than the ground state. Hence difference tones involving this frequency may be expected to be as intense as the corresponding summation bands.[17] This is actually observed.

The strong infrared band at 698 cm^{-1} is best explained in terms of a fundamental at 234 cm^{-1}; $234+464=698$. Alternative explanations of several other observed bands are also possible using this value for ν_{15}. Although it would be possible to reassign the Raman band at 464 cm^{-1} as the overtone of ν_{15}, $2\times234=468$, the intensities of the 464 cm^{-1} band and especially of the combination tones involving the 464 cm^{-1} value make this seem inadvisable.

The final fundamental to be assigned is ν_5, the torsional oscillation. For reasons set forth below this is believed to be different from zero, and it has been tentatively given the value 90 cm^{-1} in order to explain the very strong band at 1156 cm^{-1} and the moderately strong band at 554 cm^{-1} in the infrared. The significance of this assignment will be discussed below.

[17] See reference 16, p. 266.

TABLE IV. Fundamental frequencies.

Notation	Nature of vibration[a]	Assigned frequency, cm^{-1}
A_{1g}		
ν_1	C−F stretch	1181
ν_2	C−C stretch	771
ν_3	CF_3 deformation	291
ν_4	C≡C stretch	2300
A_{1u}		
ν_5	Torsion	[90][b]
A_{2u}		
ν_6	C−F stretch	1294
ν_7	C−C stretch	900
ν_8	CF_3 deformation	642
E_g		
ν_9	C−F stretch	1245
ν_{10}	CF_3 deformation	624
ν_{11}	C−CF_3 rocking	464
ν_{12}	C−C≡C bend	186
E_u		
ν_{13}	C−F stretch	1195
ν_{14}	CF_3 deformation	605
ν_{15}	C−CF_3 rocking	[234][b]
ν_{16}	C−C≡C bend	[65][b]

[a] The description is approximate and must not be taken too literally.
[b] [ ] Estimated from combination tones.

The case for the 65 cm^{-1} assignment seems quite convincing; that for 234 and 90 cm^{-1} is considerably less so.

CONCLUSIONS

Molecular Symmetry

It is now possible to marshal the arguments which show that the equilibrium symmetry is D_{3d} rather than D_{3h}' (or D_{3h}). There are three of them.

1. The lack of coincidences between infrared and Raman frequencies led to the initial, tentative assumption of D_{3d} symmetry upon which the assignment was made. Had D_{3h}' selection rules been assumed, the assignment of the fundamentals would be exactly the same. Then, however, it would have been necessary to explain why the four E' fundamentals were not also observed in the Raman spectrum. One is definitely at 1195, and another probably is at 605 cm^{-1}. There is certainly nothing in the Raman spectrum at these two frequencies. Furthermore, there is no unassigned Raman line below 450 cm^{-1} which could be attributed to ν_{15}. This suggests that these frequencies are forbidden to appear. An argument based on the nonappearance of Raman lines is seldom thoroughly satisfying, since they may merely be very weak but not strictly forbidden. This is especially true when dealing with fluorocarbons, for which Raman scattering is notoriously feeble. However, to accept D_{3h}' symmetry one would have to assume that all eight A_1' and E'' fundamentals had been observed, as well as four combination tones, but that not one of the allowed E' fundamentals had appeared

in the Raman spectrum. It would be difficult to make a convincing case for this.

2. A comparison of the direct products for D_{3d} and D_{3h}' shows that the rule of mutual exclusion holds for combination tones under D_{3d} but not under D_{3h}'. For instance, some combinations which are only infrared active under D_{3d} are also Raman active under D_{3h}'. Although none of these frequencies are found in the Raman spectrum, again suggesting D_{3d}, the evidence is not very convincing because of the weakness of Raman lines of fluorocarbons. A much more powerful argument for D_{3d} may be obtained from the infrared spectrum. If the configuration were D_{3h}', overtones and combination tones of the types $E'\times E'$ and $E''\times E''$ would be infrared active, whereas these combinations ($E_u\times E_u$ and $E_g\times E_g$) are infrared inactive under D_{3d} selection rules. Eighteen such binary combinations may be calculated that are within the experimentally observed region and not covered by strong fundamentals. Of these, twelve are definitely missing, four may be equally well explained as binary combinations allowed for both D_{3h}' and D_{3d}, and the remaining two bands, 1055 and 1800 cm^{-1}, which are both quite weak, may be satisfactorily explained as ternary combinations allowed in both D_{3h}' and D_{3d}.

This is a strong argument against D_{3h}' selection rules because infrared bands of fluorocarbons are characteristically intense, and a large number of combination tones are easily observed. The nonappearance of so many combinations is good evidence that they are strictly forbidden.

3. In all the discussion thus far the selection rules have been derived on the customary basis of transitions from the ground state (totally symmetric) to the first excited level. The evidence for a degenerate fundamental frequency at 65 cm^{-1} requires a more exact consideration of the selection rules. Because of the relatively high population of the lower excited levels for this vibration, "upper stage" bands such as $\nu_{16}+\nu_i-\nu_{16}$[17] are to be expected. For them, under D_{3d} symmetry, the selection rules are virtually unchanged except to mix very slightly the characters of the A_{1g} and E_g and the A_{2u} and E_u bands. In particular the rule of mutual exclusion still holds. Under D_{3h}' symmetry, however, the A_1' and E' species are mixed, as are the A_2'' and E'' species. As a result of this mixing *all* of the vibrational frequencies which are forbidden to appear as transitions originating from the ground state can appear as transitions originating from the first excited level of ν_{16}. They may be weaker in the latter case (by roughly the typical ratio of the intensity of a binary combination to a fundamental) but they should be clearly evident in at least the infrared spectrum. The predicted coincidences have not, of course, been observed. Thus if ν_{16} is low—and we are convinced that it is—this is a powerful argument against D_{3h}'.

These three arguments constitute a convincing case for D_{3d} symmetry. Hence we conclude that the internal rotation is not free, but is hindered, and that the equilibrium configuration is the staggered one.

NATURE OF THE POTENTIAL FIELD

The existence of an effective barrier to internal rotation in this molecule is quite unexpected because of the relatively large distance between the two CF_3 groups. It is therefore of interest to inquire into its origin. The free rotation in dimethyl acetylene[11–14] has shown, as predicted by valence theory, that there is no barrier to rotation in the carbon chain. Since the distance of closest approach of the fluorine atoms is 5.1 A[5] there can be no steric interaction between the CF_3 groups. This suggests an electrostatic interaction.

A simple Coulombic interaction, based on the amount of charge present on the fluorine atoms, gives a barrier which is too small by a factor of about 50. A higher approximation to the actual electrostatic field[18] should therefore be investigated.

EVIDENCE FROM RELATED MOLECULES

There is some support for hindered rotation in analogous molecules. 1,4-dichloro-2-butyne, $CH_2Cl-C\equiv C-CH_2Cl$, has been shown by means of the temperature dependence of the dipole moment in solution to have a barrier to internal rotation of 0.75 $\pm$0.20 kcal/mole.[19] More recently Bak, Hansen, and Rastrup-Andersen[20] have reported microwave results on a compound they believe to be $CH_3-C\equiv C-CF_3$. They find hindered rotation with a moderately low barrier.

An upper limit to the barrier height is set by the value in hexafluoroethane. Pace and Aston[21] have determined the barrier to internal rotation to be 4.35 kcal/mole, or 1520 cm^{-1}, and have concluded from the Raman spectrum that the configuration is D_{3d}. Nielsen, Richards, and McMurry[22] showed that the infrared spectrum was in agreement with this result.‡

[18] E. N. Lassettre and L. B. Dean, Jr., J. Chem. Phys. **17**, 317 (1949).

[19] Morino, Miyagawa, and Wada, J. Chem. Phys. **20**, 1976 (1952).

[20] Bak, Hansen, and Rastrup-Andersen, J. Chem. Phys. **21**, 1612 (1953).

[21] E. L. Pace and J. G. Aston, J. Am. Chem. Soc. **70**, 566 (1948).

[22] Nielsen, Richards, and McMurry, J. Chem. Phys. **16**, 67 (1948).

‡ *Note added in proof.*—A reinvestigation of the selection rules for a freely rotating ethane-type molecule has shown that they are D_{3d} and not D_{3h} as heretofore reported (R. P. Bauman, to be published). Hence the results of this paper (that C_4F_6 follows D_{3d} selection rules) show only that it has either free internal rotation or has the staggered configuration, but they are incapable of distinguishing between the two.

THE JOURNAL OF CHEMICAL PHYSICS VOLUME 22, NUMBER 9 SEPTEMBER, 1954

Silver-Activated Alkali Halides

H. W. ETZEL AND J. H. SCHULMAN
Chemistry Branch, Metallurgy Division, Naval Research Laboratory, Washington, D. C.
(Received February 12, 1954)

The emission, excitation, and absorption spectra of silver-activated alkali halides have been investigated. Three absorption bands due to ionic silver have been observed in NaCl, NaBr, KCl, and KBr, and the growth of these bands with silver concentration has been studied. In each of these crystals the two shorter-wavelength bands are ascribed to isolated silver ions, while the band of longest wavelength is ascribed to pairs of silver ions.

Upon x-ray irradiation as many as five new absorption bands arise in certain alkali halides in addition to the *F* band. Excitation into three of these bands (designated as the *B*, *C*, and *D* bands) produces luminescence, the emission spectrum being different for each band. The *B* band is attributed to a center consisting of an electron trapped at a silver ion adjacent to a halogen-ion vacancy; the *C* band to an electron trapped at a complex of two silver ions adjacent to a halogen-ion vacancy; and the *D* band to a hole trapped at an alkali-ion vacancy adjacent to a silver ion.

INTRODUCTION

THE earliest investigation of the silver-activated alkali halides appears to have been made by Smakula.[1] He found a single sharp absorption band with a peak at 2100A in NaCl:Ag. One of the more recent studies of the ionic bands is by Kato,[2] who investigated the emission as well as the absorption spectra. Kato's absorption data agree well with Smakula's, and he finds that excitation into the characteristic silver ion band gives principally an ultraviolet emission peaking at 2490A with a second emission band peaking at 4000A.

New bands in the silver-activated alkali halides which arise upon x-ray, γ ray, ultraviolet irradiation, additive coloring, or electrolysis, will be referred to as "induced" bands. Blau[3] and later Toporets[4] observed two induced bands in the absorption spectrum of NaCl:Ag, colored by heating the sodium chloride in a vapor of sodium. The work of Weyl, Schulman, Ginther, and Evans[5] showed that the system NaCl:Ag, is radiophotoluminescent. Such a system is originally nonluminescent under ultraviolet or visible light but is made responsive to such excitation by pretreatment with γ rays or x-rays. They suggested two possible configurations that might be responsible for the induced absorption bands: (a) the ionic silver may trap an electron and be reduced to atomic silver and (b) the center may be a silver ion adjacent to a vacancy which has trapped an electron. Within the last few years the silver-activated alkali halides have been studied by many investigators.[6–9] The nature of the centers responsible for the induced bands is still not certain. The present work represents additional experimental data on the silver-activated alkali halides. On the basis of this information an interpretation of the centers is proposed.

EXPERIMENTAL TECHNIQUES

All the crystals used in this investigation were single crystals grown by the Kyropoulos technique. Silver was introduced into the NaCl and KCl melts as silver chloride and into the NaBr and KBr melts as silver bromide. The concentration of silver in the single crystals of NaCl:Ag and KCl:Ag was determined by colorimetric chemical analysis. No chemical analysis was made of the NaBr:Ag and KBr:Ag series.

The absorption measurements were made using a split-beam single-detector automatic recording spectrophotometer[10] and also a Beckman Model DU spectrophotometer. The source was either a Beckman hydrogen lamp or a tungsten lamp depending on the wavelength range being investigated.

Measurements of luminescence excitation spectra were made using a Beckman Model DUR spectrophotometer modified as described by Klick.[11] For these measurements the single crystals of the silver-activated alkali halides were ground into powders.

Measurements of luminescence emission spectra were made using two Gaertner quartz monochromators in series to monochromatize the radiation from a quartz-envelope mercury H-4 lamp. The beam from the Gaertner was incident on a powder plaque of the specimen placed at the entrance slit of a Beckman

[1] A. Smakula, Nachr. Akad. Wiss. Göttingen Math.-physik. Kl. 110 (1929).
[2] M. Kato, Sci. Papers Phys. Chem. Research Tokyo **41**, 113 (1943).
[3] M. Blau, Nachr. Akad. Wiss. Göttingen Math.-physik Kl. 401 (1933).
[4] A. Toporets, Doklady Akad. Nauk S.S.S.R. **4**, 25 (1935); **15**, 245 (1937).
[5] Weyl, Schulman, Evans, and Ginther, J. Electrochem. Soc. **95**, 70 (1944).
[6] Schulman, Etzel, and Ginther, Conf. on Elec. and Opt. Prop. of Ionic Crystals, University of Illinois, October, 1951.
[7] Etzel, Schulman, Ginther, and Claffy, Phys. Rev. **85**, 1063 (1952).
[8] Burstein, Oberly, Henvis, and White, Phys. Rev. **86**, 255 (1952).
[9] R. Kaiser, Z. Physik **132**, 482 (1952).
[10] H. Etzel, J. Opt. Soc. Am. **43**, 87 (1953).
[11] Klick, Schumacher, and Stokes, Rev. Sci. Instr. **22**, 776 (1951).

Model DUR spectrophotometer. The beam emerging from the Beckman was reflected by an aluminum mirror on to a 1P28 photomultiplier tube. This modification to the Beckman has been described by Klick.[11]

For x-ray irradiation of the specimens a tungsten-target beryllium window Machlett AEG-50 was used. The specimens were placed about four inches from the target and the machine was run at 50 kvp and 15 ma.

The electrolysis of the silver-activated alkali halides was investigated to see if the same centers that arise upon x-raying would appear by electron injection. Single crystals 2 cm long and 1 cm by 1 cm in cross section were electrolyzed in air at 700°C. The field was approximately 125 volts/cm and parallel to the long axis of the crystal. The crystals were held between platinum electrodes, one in the form of a disk and the other a pointed wire. The electrolysis of the "pure" crystals was accomplished without difficulty. However, in NaCl:Ag containing as little as 0.05 nominal mole percent silver (i.e., added to the melt), the electrolysis would not continue long enough to allow sufficient penetration of the electrons into the crystal. The resulting spot of color was too small to be measured optically. The same difficulty was experienced in attempting to electrolyze KCl:Ag crystals having having more than 0.1 nominal mole percent silver. In the lower concentration KCl:Ag crystals the electrolysis was carried out without difficulty, and the F-center

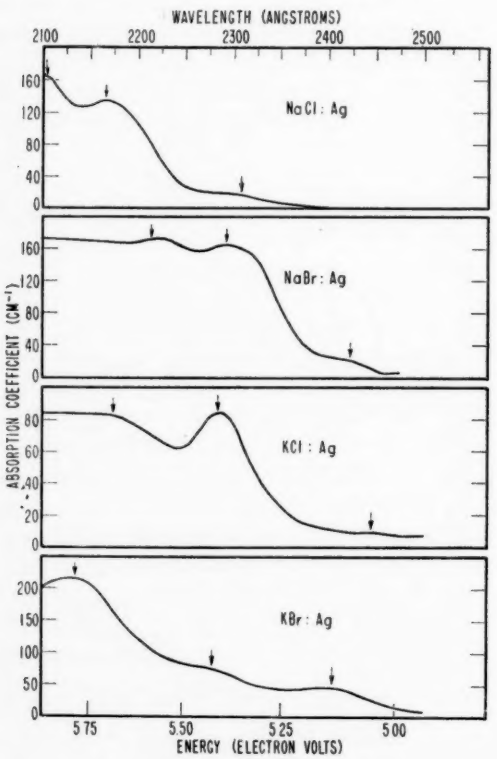

FIG. 1. Absorption of ionic silver centers in the alkali halides containing 1.0 nominal mole percent silver.

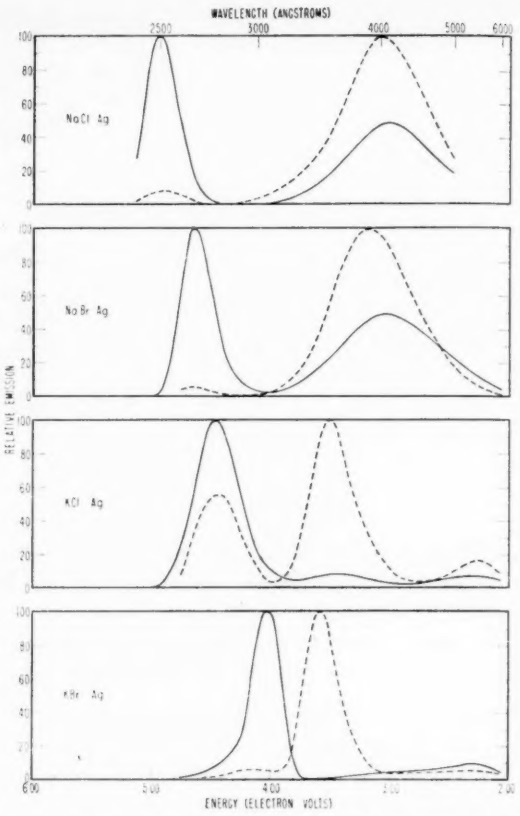

FIG. 2. Emission of ionic silver centers in the alkali halides containing 1.0 nominal mole percent silver. Solid curve—Excitation into bands due to isolated silver ions. Dashed curve—Excitation into band due to pairs of silver ions.

cloud, if desired, could be withdrawn leaving only induced centers in the crystals.

In order to study the effect of plastic deformation on the x-ray induced absorption bands, the crystals were deformed using a hydraulic press. A uniform loading rate of 1000 psi/min was applied until 1800 psi was reached. Crystals 1 cm² in area were used. After pressure was applied it was noted that the area increased by about 40 percent and the thickness of the crystals decreased by 40 percent. Both KBr:Ag and KCl:Ag single crystals were optically clear after being plastically deformed; however, NaCl:Ag crystals showed many minute cracks and were not as satisfactory for optical measurements. After being plastically deformed, the crystals were x-rayed under the conditions described above.

EXPERIMENTAL RESULTS

Ionic Silver Centers

The absorption bands introduced into the various alkali halides by silver in ionic form are shown in Fig. 1. Each of the four silver-activated alkali halides investigated shows at least three bands in the region of the tail of the fundamental absorption band. In all cases the longest wavelength band is the weakest, and in KCl:Ag it is barely perceptible. The absorption

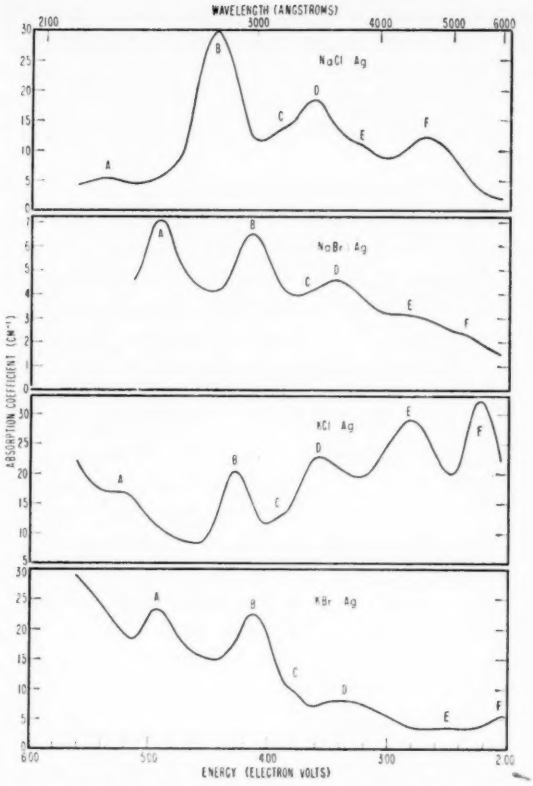

FIG. 3. Induced absorption bands which arise from x-ray irradiation of 1.0 nominal mole percent silver-activated alkali halides.

spectra of the "pure" alkali halides are not shown since they are essentially structureless and would not alter the curves shown. In a previous publication[7] it has been shown that in NaCl:Ag the two shorter wavelength bands are due to isolated silver ions in the lattice, and the longest wavelength band is due to pairs of silver ions. Although it has not been demonstrated experimentally, it seems reasonable to attribute the longest wavelength ionic absorption band in KCl:Ag, NaBr:Ag, and KBr:Ag also to pairs of silver ions in the host lattice. In all the silver-activated alkali halides investigated, excitation into the longest wavelength ionic band produces the longer wavelength emission. Exciting at the shorter wavelengths produces predominantly the shorter wavelength emission. The emission spectra shown in Fig. 2 are normalized phototube response. The shorter wavelength emission shifts toward the visible with increase in lattice constant, i.e., from NaCl (2.79A), to NaBr (2.96A), to KCl (3.14A), to KBr (3.29A), while the pair band emissions shift in the reverse sense.

Induced Silver Centers

When the silver-activated alkali halides are x-rayed, absorption bands appear in the region from 2200A to 6200A and are designated as the *A*, *B*, *C*, *D*, *E*, and *F* bands. The last is the well-known *F* band, characteristic of the "pure" alkali halides, first observed by Rose[12] and so named by Pohl.[13] Figure 3 shows the x-ray induced absorption bands in crystals containing 1 nominal mole percent of silver. In NaCl:Ag all six bands are observable. In NaBr:Ag the *C* band is barely observable. However, an emission characteristic of the *C* band in the other alkali halides is observed in NaBr:Ag, although the *C* band absorption is masked by the *B* and *D* bands in this material. In KCl:Ag all bands are observable and only the *C* band is weak. In KBr:Ag the *E* band is the only band not readily observable. In the host lattices investigated the presence of the silver suppresses the *F* band; i.e., if two crystals, one containing ionic silver and the other with no ionic silver, are x-rayed simultaneously, the *F* band will be more prominent in the "pure" crystal.

Four crystals of NaCl containing 2.0, 1.0, 0.1, and 0 nominal mole percent of silver were x-rayed for one hour, and after graphically resolving the overlapping induced absorption bands, the absorption of the individual bands was plotted as a function of the chemically determined concentration of silver. The result is shown in Fig. 4. All bands except the *F* band increased as the silver content increased. The *C* band appeared to grow more rapidly than the *B*, *D*, or *E* bands at high silver concentrations. The *A* band was not prominent enough in the lower concentration crystals to be plotted in this graph.

The *A* bands are near enough to the ionic silver bands that illumination into them produces the characteristic ionic emission. Illumination into the *E* band, which appears most prominently in KCl:Ag, does not give rise to an observable emission in the visible region. The emissions which result from excitation into the *B*, *C*,

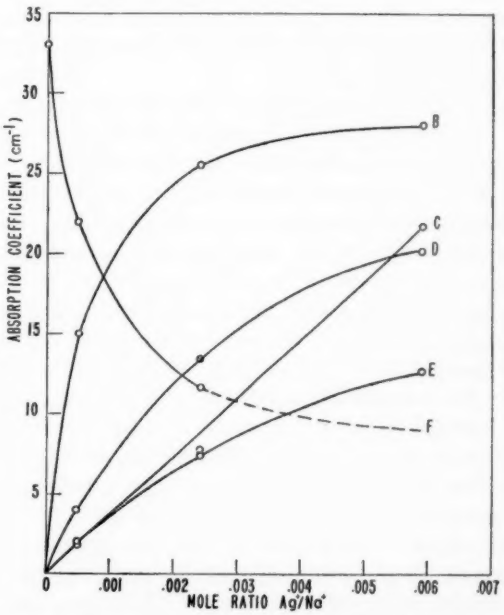

FIG. 4. Absorption coefficient of the induced bands in NaCl:Ag as a function of the chemically determined silver concentration.

[12] H. Rose, Ann. Physik **120**, 1 (1863).

[13] R. Pohl, Z. Physik **39**, 36 (1938).

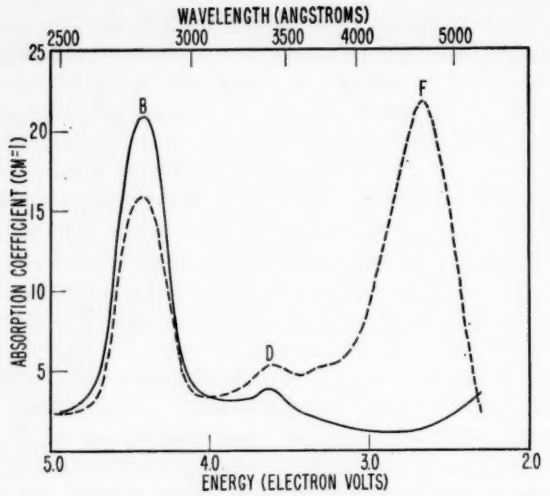

FIG. 5. Optical bleaching of the F band in 0.1 nominal mole percent NaCl:Ag using a tungsten source and a Corning No. 3389 filter. Dashed curve—Before bleaching. Solid curve—After bleaching.

and D bands are given in Table I. Excitation into the F band in NaCl:Ag and KCl:Ag bleaches it, and an emission identical in spectral distribution (within experimental error) to that obtained upon excitation into the B band is observed. An emission characteristic of ionic silver (at 2500A) is also produced by excitation into the F band in NaCl:Ag. Both emissions are due to an indirect excitation of the respective centers by the optical bleaching of the F center. That is to say, the electron released from the F center may recombine with a hole, and the energy dissipated by this recombination may excite the B center or ionic silver center. This process continues as long as there remain F centers to be bleached. On the other hand the B center emission may be due to the formation of the center itself by the capture of an electron.

Optical bleaching experiments indicate that irradiation into the F band of x-rayed NaCl:Ag and KCl:Ag bleaches the F band and enhances the B band. In KCl:Ag where the A band is fairly prominent there appears to be a bleaching of this band as the F band is bleached. The effect on the C and D bands of optically bleaching the F band in KCl:Ag is obscured by the simultaneous bleaching of the E band. However in NaCl:Ag the E band is very weak, and in Fig. 5 it is seen that the optical bleaching of the F band does not affect the D band. The effect, if any, on the C band was not detected in this experiment, because the silver concentration was too low to observe the C band before bleaching the F band. On the other hand, a crystal having a silver concentration high enough to permit one to detect the C band gives a barely perceptible F band. Although the B, C, and D bands do bleach slowly under ultraviolet irradiation at room temperature they are more stable than the E and F bands in all the alkali halides investigated. Since the B band is relatively stable it is difficult to determine experimentally whether any of the less stable bands (A, E, and F) are affected when the B band is bleached optically. Irradiation into the B band in NaCl:Ag and KCl:Ag is accompanied by a decrease of D band absorption; however, optical bleaching of the D band does not alter the B band absorption.

Thermal bleaching of the x-ray induced B and D bands in KCl containing 2, 1, 0.5 nominal mole percent silver shows that the rate of bleaching depends on the concentration of silver, the bleaching rate being faster for higher silver concentrations. Also the ratio of the percent decrease in B band absorption to the percent decrease in D band absorption for a given thermal bleach is independent of silver concentration. This ratio ($\Delta B/\Delta D$) is about 0.8. For NaCl containing 1.0 nominal mole percent silver the ratio of the decrease in B band absorption to the decrease in D band absorption is the same as in KCl:Ag. Thermal bleaching experiments were also carried out in NaCl:Ag crystals containing Ca^{++}. It has been shown that the introduction of divalent calcium into a monovalent lattice increases the number of free positive ion vacancies.[14] If a crystal containing 1 nominal mole percent silver and 0.2 nominal mole percent calcium is x-rayed and thermally bleached, it is found that the D band is enhanced relative to the B band.

Figure 6 shows the absorption spectrum of a single crystal of KCl:Ag which was x rayed for one hour and the absorption spectrum of one which was electrolyzed. These crystals were from the same Kyropoulos boule. The part of the electrolyzed crystal which was measured was the section through which the F center cloud penetrated. The B band in the electrolyzed crystal is some sevenfold greater than the B band in the x-rayed crystal.

From the work of Przibram[15] it appears that the concentration of vacancies in the alkali halides can be increased by plastic deformation. Single crystals of NaCl:Ag, KCl:Ag, and KBr:Ag containing 0.05 nominal mole percent of silver were plastically deformed as described in the preceding section. The absorption spectra of these crystals were measured before and after 90 minutes of x-ray irradiation. The results for KCl:Ag are shown in Fig. 7; the results for KBr:Ag are essentially the same. It is clear that the B band is most markedly influenced by the plastic deformation and by the presence of vacancies. In NaCl:Ag the

TABLE I. Emissions due to excitation into the B, C, and D bands.

Excitation into	B	C	D
NaCl:Ag	4420A	5560A	5820A
NaBr:Ag	4730A	5640A	5820A
KCl:Ag	4360A	5560A	5670A
KBr:Ag	4530A	5640A	5710A

[14] H. Etzel, Phys. Rev. **87**, 906 (1952).
[15] K. Przibram, Z. Physik **102**, 331 (1936).

effect of plastic deformation is to broaden all the bands (B, D, and F), and it is difficult to say which is influenced the most by the presence of the additional lattice defects. It does appear, however, that both the D and B bands are enhanced.

DISCUSSION

Since the concentration of silver ions in the lattice is known from the chemical analysis, the oscillator strength can be calculated for the ionic bands using Smakula's dispersion formula.[16] For NaCl:Ag and KCl:Ag the oscillator strength of the silver ions is found to be in the order of a few hundredths. It was not possible to determine the oscillator strengths for the induced bands by measuring the difference in ionic absorption before and after x-ray irradiation, because upon irradiation a broad V band arises in the region of the ionic silver absorption. (The growth of the V band was to be expected since the trapping of an electron by a negative ion vacancy or by a silver center leaves a hole free in the lattice to form a V center.) One can estimate the oscillator strength for the B band by electrolyzing an alkali halide crystal containing a known amount of silver, assuming that all of the ionic silver has been converted to B centers, and applying Smakula's dispersion formula. This requires a measurement of the width of the absorption band at half-maximum and the height of the band. Figure 6 shows the absorption spectrum obtained after electrolysis of a single crystal of KCl containing 0.0037 mole percent silver. It can be seen from the figure that the B band is the most prominent band. A calculation of the oscillator strength indicates it is of the order of 0.4. This is a minimum value. If all the ionic silver has not been converted to B centers the oscillator strength is greater than 0.4.

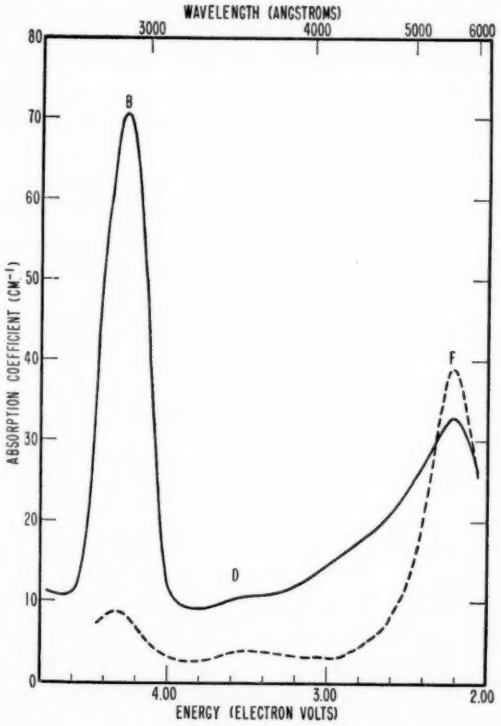

FIG. 6. Absorption spectra of electrolyzed (solid curve) and x-rayed (dashed curve) 0.05 nominal mole percent KCl:Ag.

[16] F. Seitz, *The Modern Theory of Solids* (McGraw-Hill Book Company, Inc., New York, 1940), p. 664.

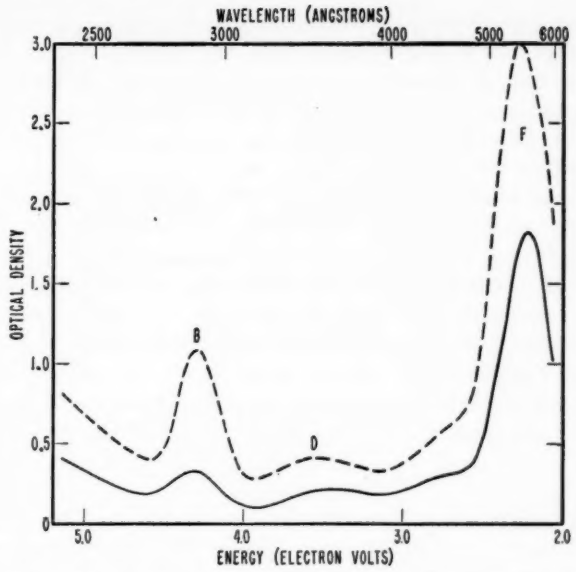

FIG. 7. Absorption spectra of 0.05 nominal mole percent x-rayed KCl:Ag. Solid curve—no plastic deformation. Dashed curve—after plastic deformation.

When the F band is optically bleached the A band bleaches. The bleaching of the A band, however, is not complete. The simultaneous bleaching of this band with the F band seems to indicate that the A band is a complex center involving at least a silver ion and a hole. The incomplete bleaching may be attributed to the fact that centers other than the F center have trapped electrons. Further evidence that the A band is of a trapped hole type is that this band is not observed in electrolysis in the F-center-colored portion.

The B band is attributed to silver ions in the lattice that have trapped an electron and have a negative ion vacancy as a nearest neighbor. This center can also be pictured as an F center with a silver ion replacing one of the alkali ions that surround the vacancy. In Fig. 4 it can be seen that the B band grows at the expense of the F band as the silver concentration is increased, and that the sum of the F and B band absorptions is very nearly constant. This indicates that a negative ion vacancy is a constituent common to both centers and that the oscillator strength of the B band is about equal to that of the F band. Supporting evidence for the presence of a negative ion vacancy is the prominence of the B band in crystals which have been plastically deformed (Fig. 7). In electrolysis of silver-activated alkali halides at 700°C B centers do not form, but at some intermediate temperature they do form as the electrolyzed crystal is cooled. This is verified by the follow-

ing experiment. If the electrolyzed crystal is quenched from 700°C the *B* band does not appear, but if the crystal is brought to room temperature slowly the prominent *B* band shown in Fig. 6 appears. This band can be thermally bleached by heating the crystal to 400 to 450°C for a few hours, and a hitherto unobserved band arises at 4500A and shifts to 4000A as the bleaching proceeds. This bleaching is attributed to the diffusion of the negative ion vacancy. The *B* band which arises under x-ray irradiation can be bleached at a much lower temperature (200°C). The bleaching in this instance is presumed due to the recombination of electrons from the *B* center with holes. It appears from the experimental data that the *B* center is formed by a preferential grouping of a negative ion vacancy, silver ion and electron, because on a probability basis the number of such centers should be exceedingly small. If one chooses the oscillator strength to be of the order of unity, the minimum number of silver centers responsible for the *B* band in Fig. 6 is of the order of 10^{17}/cc. From conductivity data[17] on the alkali halides one can estimate the number of vacancies present at the electrolysis temperature. Near the melting point there are about 10^{18}/cc. Thus if one were to assume a random distribution of silver ions and negative ion vacancies there would only be of the order of 10^{14} *B* centers/cc. Apparently at high temperatures where both the negative ion vacancy and the silver ion are mobile, a site nearest a negative ion vacancy is preferred by the silver ion rather than a normal lattice site since the lattice distortion due to the silver ion would be minimized. This configuration, composed of a silver ion and a negative ion vacancy, traps an electron and becomes a *B* center.

The *C* band is presumed to be due to a center consisting of two silver ions as nearest neighbors, an electron, and a negative ion vacancy. Figure 4 shows that the *C* band grows most rapidly at high silver concentrations, which suggests the configuration involving a pair of silver ions. It is observed, furthermore, that the *C* band appears only in those crystals in which the ionic band attributed to pairs is present. Because of the thermal stability of this band it is likely that this center has a negative ion vacancy as a constituent. A center having only two silver ions and an electron would be negatively charged and hence less stable than a neutral center, i.e., one which also contains a negative ion vacancy.

Experimental evidence indicates that the radiophotoluminescent *D* center is composed of at least a silver ion, a hole, and a positive ion vacancy. Since optical bleaching of neither the *F* band nor *B* band at room temperature enhances the *D* band it is difficult to visualize an electron as an intrinsic component of the center. When the crystals are electrolyzed, the *D* band does not appear; but the *F* and *B* bands, which are attributed to centers involving an electron, are easily observed. In the thermal bleaching experiment the *B* and *D* bands bleach at the same rate for a given silver concentration, indicating that the destruction of a *B* center is instrumental in the destruction of a *D* center. The same effect is observed when the *B* band is bleached optically, that is, the *D* band also bleaches. Furthermore, the thermal bleaching rate for NaCl:Ag increases with increasing silver concentration. This dependence appears to substantiate the assignment of the *D* center as one composed of at least a silver ion, positive ion vacancy, and hole. Finally, the presence of divalent calcium, which is known to introduce positive ion vacancies, changes the ratio of the *B* band to *D* band absorption (after x-ray treatment and a thermal bleach) in such a way as to enhance the *D* band with respect to the *B* band.

The *E* band, a relatively weak band in all the alkali halides except KCl:Ag, has not been studied in great enough detail to allow one to determine the nature of the center responsible for this band.

The *B*, *C*, and *D* bands in the silver-activated alkali halides have been found to be radiophotoluminescent. In the silver-activated phosphate glass emissions similar to those observed by exciting into the *C* and *D* bands in silver-activated alkali halides have been found.[5] In the glass the emission shifts from the red towards the blue as the silver concentration is increased. The same trend is observed in the alkali halides as the silver concentration is increased (the *C* band emission is at shorter wavelengths than the *D* band). The present work suggests that the radiophotoluminescent centers in this glass may have configurations similar to the *C* and *D* centers in the crystals, instead of being electrons trapped at isolated silver ions, as had been previously postulated. Further studies of the glass are planned to see if the suggested analogy between the radiophotoluminescent centers in the glass and the crystals is correct.*

The authors are indebted to Dr. C. C. Klick and Dr. D. L. Dexter for stimulating discussions, and to R. D. Kirk, Mrs. E. W. Claffy, and R. J. Ginther for the preparation and analysis of the crystals and for their help with many of the chemical aspects of the work.

[17] H. Etzel and R. Maurer, J. Chem. Phys. **18**, 1003 (1950).

* *Authors' note.*—Since the preparation of this manuscript, two papers have been brought to the attention of the authors. M. L. Katz [Doklady Akad. Nauk, S.S.S.R. **85**, 539 (1952); **85**, 757 (1952)], ascribes the *D* center (*A'* center, in his notation) to either an electron trapped at a silver ion in a normal lattice position, or to a silver ion in a lattice site adjacent to an *F'* center. Both these models involve the trapping of an electron in the formation of a *D* center, and hence on the basis of our experimental data, appear to be incorrect.

Ion-Pair Yield of the Tritium-Oxygen Reaction*

LEON M. DORFMAN AND B. A. HEMMER
Knolls Atomic Power Laboratory,† General Electric Company, Schenectady, New York
(Received April 24, 1954)

The rate of reaction of tritium and oxygen, initiated by the tritium beta radiation, has been investigated at 25°C, in the absence of mercury vapor, by using a sensitive Bourdon gauge as the manometer. The rate is not linear with time, but shows a small continual decrease as the reaction proceeds. The initial reaction rate was found to be directly proportional to the tritium pressure, and hence proportional to the radiation intensity. It was independent of the oxygen concentration over the range investigated. The reaction rate shows a slight dependence on the isotopic composition of the hydrogen reactant, tending to rise with increase in the mole fraction of protium. The initial reaction rate may be represented by

$$R_0 = 1.19 \times 10^{-4} C_{T_2}(1+0.3m_H),$$

where C_{T_2} is the tritium concentration in moles/liter or other absolute concentration units, and m_H is the mole fraction of protium in the hydrogen reactant. On the basis of a requirement of 33 ev per ion pair in the reactant mixture, the initial ion-pair yield for tritium disappearance or water formation is $(M/N)_0 = 3.2_5$ for the reaction of pure tritium with oxygen. Material balance measurements indicate that little or no peroxide appears in the product.

INTRODUCTION

THE combination of hydrogen and oxygen under various types of initiation and activation to form water and, under certain conditions, hydrogen peroxide, has been the subject of very extensive investigations over a period of years. The mechanism of the thermal reaction, which has received the greatest part of this attention, is reasonably well established.[1,2] A considerable amount of work has been done on the synthesis of water in various types of electric discharge[3,4] and reaction rates have also been determined for the combination of hydrogen and oxygen induced by alpha particles.[5] In an investigation of this latter effect Lind[5] found a water yield of 3.92 molecules per ion pair. Marshall[4] in his work on the hydrogen-oxygen combination under the effect of cathode rays reported yields similar to those of Lind. He found also, that in a flow system substantial amounts of hydrogen peroxide were obtained. Photochemical investigations[6] have been made both by absorption in the Schumann region and by mercury photosensitization. In the latter type of studies, quantum yields on the order of 2 have been obtained.

The isotopic hydrogen-oxygen system consisting of tritium and oxygen presents a rather interesting study since it has a self-contained source of ionizing radiation, the nuclear beta particles from the tritium decay, and will therefore undergo reaction at room temperature in the absence of any external excitation energy. The intensity of ionizing radiation is readily determinable from the tritium concentration since the radioactive half-life and the average energy of the beta spectrum are accurately known. In order to determine reaction yields, therefore, the rate of the beta particle induced reaction

$$T_2 + \tfrac{1}{2}O_2 = T_2O \qquad (1)$$

has been investigated at 25°C, in the absence of mercury vapor, by using a sensitive glass Bourdon gauge as the manometric device.

PRELIMINARY EXPERIMENTS

Complete details of four preliminary runs will not be given. These experiments are being mentioned here only insofar as they demonstrate the need for a mercury-free reaction cell in the investigation which followed. These preliminary runs were carried out in a cylindrical quartz cell connected to a mercury manometer. The reaction rate was determined by following the pressure drop. At the end of each run the condensible product was frozen out and its pressure subsequently measured to determine the material balance. If tritiated water is the only reaction product, complete material balance would be represented by $P_W/2\Delta P = 1$, where P_W is the pressure of the water product and ΔP the pressure drop. Substantial deficiencies were always found; the values for this ratio ranged from 0.70 to 0.87. During the runs a thin yellowish deposit accumulated on the walls of the cell and the mercury in the manometer became discolored, probably because of oxidation.

After these runs the occasion arose to store some tritium in this same cell, which had previously been degassed. At the end of a week the yellowish deposit on the walls of the cell had disappeared and the mercury

* Presented at the Annual Meeting of the American Physical Society, New York, New York, January, 1954.

† The Knolls Atomic Power Laboratory, Operated for the United States Atomic Energy Commission by the General Electric Company, Contract No. W-31-109 Eng-52.

[1] G. von Elbe and B. Lewis, J. Chem. Phys. **10**, 366 (1942).

[2] B. Lewis and G. von Elbe, *Third Symposium on Combustion and Flame and Explosion Phenomena* (Williams and Wilkins Company, Baltimore, 1949), p. 484.

[3] P. J. Kirkby, Proc. Roy. Soc. (London) **A85**, 151 (1911).

[4] A. L. Marshall, J. Am. Chem. Soc. **50**, 3197 (1928).

[5] S. C. Lind, J. Am. Chem. Soc. **41**, 531 (1919).

[6] W. A. Noyes, Jr., and P. A. Leighton, *The Photochemistry of Gases* (Reinhold Publishing Corporation, New York, 1941), p. 236 *ff* and p. 250*ff*.

appeared quite clean. Tritiated water had been formed from the reduction of the mercury oxide, probably through the action of the tritium atoms present:

$$H_gO+T=H_g+OT. \quad (2)$$

The water was frozen out and measured. The amount present was sufficient to bring the cumulative material balance for the four runs up to 0.94. It was clear, then, that oxidation of the mercury was the major reason for the material balance deficiency. Subsequent runs were therefore carried out in a mercury-free reaction cell.

EXPERIMENTAL METHODS

Pure reactants were obtained in the following manner. Oxygen was prepared by thermally decomposing potassium permanganate which had previously been warmed and degassed repeatedly in the vacuum system. The oxygen liberated was passed through a coil immersed in liquid nitrogen then into a storage bulb closed off by a Fugassi valve. Hydrogen was purified by sorption, pumping and subsequent desorption on a uranium bed. The hydrogen was stored in a Pyrex bulb connected to a Fugassi valve. The tritium was stored on a uranium bed and desorbed as required for each run. Krypton gas, used in one run, was degassed for a short time at −195°C and then pumped into the reaction cell through a trap immersed in a dry ice-acetone bath.

The H_2-T_2 mixtures used in the runs were analyzed on the General Electric analytical mass spectrometer in use here. Previous calibrations[7] had shown that the two isotopes have equal mass spectrometric sensitivities.

A modified glass Bourdon gauge with a tilting mirror attachment was used to follow the pressure drop during the run. The arrangement employed a lamp and translucent scale at a distance of 50 inches from the tilting mirror. Reproducible calibrations showed a gauge sensitivity of 27.9 mm scale deflection per mm pressure differential. The response was linear over a pressure difference of at least 10 mm, and the gauge could therefore be used either as a direct reading or a null instrument. The outside envelope of the Bourdon gauge was connected to a mercury bulb for sensitive pressure adjustment, and to a mercury manometer on which the pressure was read with a cathetometer. The inside of the gauge was connected to the reaction cell.

The reaction vessel was a spherical Pyrex bulb to which was connected a very small U tube for freezing out the water product at the end of a run. The actual bulb volume was 212 cc, the total reaction volume 248 cc. The reaction cell was closed by a 2-mm vacuum stopcock lubricated with Apiezon-*N* grease. The outlet arm of this stopcock was connected to a U tube and hence to the vacuum system. This outside U tube was kept in a dry ice-acetone bath to remove mercury vapor from the cell during degassing and to prevent its reentry during filling of the cell. At no time during the series of eleven runs was there any discoloration or deposit on the walls of the cell, which would have resulted from oxidation of the mercury.

The reactants were mixed in a separate bulb, transferred to the reaction cell by means of a Toepler pump and the pressure readings were started. The reaction cell was immersed in a water bath, which, although not thermostated, maintained a temperature of 25.0±2.0°C. Precise temperature readings, using a thermometer with 0.02°C graduations, were taken at the time of each pressure reading. The pressure was read intermittently for a period of 20 to 40 hours over a total pressure change of at least 3 mm and in no case more than 8 mm. The pressure of the water product was thus always below its equilibrium vapor pressure to ensure that the tritium would remain in the gas phase.

If, at the end of a run, material balance measurements were desired, the condensable product was frozen inside the cell using liquid nitrogen, and the remaining tritium-oxygen mixture removed. The pressure of condensable product could then be read. The tritium-oxygen mixture, and later the water product, were processed over a magnesium bed at 600°C to remove the oxygen and to permit the tritium to be taken up again on a uranium bed.

In the single run which contained krypton, the krypton was frozen in the cell at −195°C and the reactant gases were then added in the normal manner to start the run.

RESULTS AND DISCUSSION

A series of eleven runs was carried out involving varying amounts of the two hydrogen isotopes and oxygen. To avoid any confusion in nomenclature the normal stable isotope will be referred to as protium, and a mixture of the two isotopes, protium and tritium, will be referred to as hydrogen.

The tritium pressure covered a range of 30 to 104 mm, the oxygen pressure ranged from 69 to 218 mm. The mole fraction of protium in the hydrogen reactant ranged from 0.055, the purest tritium used, to 0.831. The details of these experimental conditions are listed in Table I. The results of material balance measurements for six of the runs are listed in Col. 5. They show that the over-all reaction may, indeed, be almost completely represented by Eq. (1). If water is the only condensable product, $P_w/2\Delta P=1$. This ratio attains values as high as 0.97 and 0.98, indicating that if any hydrogen peroxide is formed it must, in the static system involved here, have only a transitory existence, ultimately amounting to less than 2 to 3 percent of the condensible product.

The rate curves for two of the runs are shown in Fig. 1, in which the pressure, on a greatly expanded scale, is plotted against the time in minutes. It may be

[7] Mattraw, Pachucki, and Dorfman, J. Chem. Phys. **20**, 926 (1952).

seen that the rate is not independent of time, but shows a slight continual decrease as the reaction proceeds. The most definitive rate to be used in a correlation of the data is the initial rate, obtained from the slope of the rate curves at the ordinate axis. These initial slopes have been calculated for each run by fitting the third-degree polynomial,

$$y=a+bx+cx^2+dx^3, \qquad \text{(I)},$$

to each set of points. The limiting slope was obtained as the coefficient of the first degree term. These calculations were carried out by the machine calculations group. The results are listed in Col. 6 of Table I, which shows the initial rate of pressure decrease in mm/min. The initial reaction rate, in terms of hydrogen disappearance, or water formation, will be twice the rate of pressure decrease.

The intensity of beta radiation may be calculated directly from the tritium concentration. The tritium

TABLE I.

Run No.	Pressure of reactants (mm) Tritium	Protium	Oxygen	Material balance $P_w/2\Delta P$	$\left(-\frac{dP}{dt}\right)_{t=0}$ mm/min $\times 10^3$	$k=\frac{R_0}{C_{T_2}(1+0.3m_H)}$ min$^{-1}\times 10^4$
7	104.4	7.4	69.4	0.94	6.16	1.16
1	95.8	16.9	115.5	0.97	6.57	1.31
2	92.6	10.5	218.3	0.97	5.03	1.06
8	73.8	4.4	138.0	0.96	4.53	1.21
10[a]	56.9	3.3	93.7	···	2.90	1.00
9	45.2	127.3	99.9	···	3.26	1.18
4	42.2	16.4	106.8	0.98	2.62	1.14
11	39.8	195.9	68.9	···	2.80	1.13
6	37.5	72.2	90.2	···	2.94	1.31
5	32.4	82.1	103.0	···	2.12	1.08
3	30.2	18.5	184.0	0.96	2.24	1.30
						Mean[a]=1.19

[a] Run 10 contains, in addition to the reactants shown, krypton at a pressure of 85.6 mm. It has been omitted in averaging the values for k.

beta spectrum has an end-point energy of 18 kev[8,9] and an average energy of 5.69 kev.[10] The range[11] for these nuclear beta particles is 0.7 mg/cm^2. From the results of a recent determination[12] of the absorption curves for tritium beta particles in hydrogen and oxygen it can be shown that in the present investigation, with a reaction cell 73 mm in diameter, the gas density is sufficiently high in all runs so that practically all the beta-particle energy is absorbed in the gas phase. For the series of runs shown in Table I, therefore, the absorbed beta intensity is proportional to the tritium pressure.

It may be seen from the data that the reaction rate increases with increasing tritium pressure, or, in other words, with increasing intensity of the initiating beta

[8] Curran, Angus, and Cockcroft, Phil. Mag. **40**, 53 (1949).
[9] G. C. Hanna and B. Pontecorvo, Phys. Rev. **75**, 983 (1949).
[10] Jenks, Ghormley, and Sweeton, Phys. Rev. **75**, 701 (1949).
[11] L. E. Glendenin, Nucleonics, **2** (No. 1), 12 (1948).
[12] L. M. Dorfman, Phys. Rev. **95**, 393 (1954).

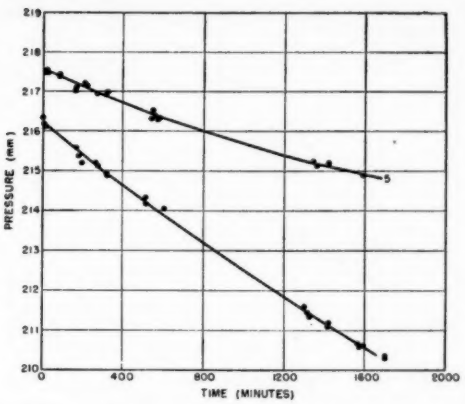

FIG. 1. Rate curves for runs No. 5 and No. 8, temperature=25 C.

radiation. It can be shown that the initial rate is directly proportional to the tritium pressure. There is, however, a small secondary effect which must be taken into account in this correlation. The reaction rate shows a slight dependence on the isotopic composition of the hydrogen reactant, tending to rise with increase in the mole fraction of protium. This may be seen from Fig. 2, in which the initial rate divided by the tritium pressure is plotted against the mole fraction of protium in the hydrogen. The ratio on the ordinate is proportional to the initial ion-pair yield. As an approximation this isotope effect has been represented as a linear trend. Evidence of such an effect was obtained in the preliminary experiments in which mass spectrometric analyses showed an isotopic fractionation in the reaction, with protium concentrating in the water product.

The initial reaction rate, for the conditions of this investigation, may be represented by the equation:

$$R_0=kC_{T_2}(1+bm_H), \qquad \text{(II)}$$

where R_0 is the initial reaction rate, with units determined by the units in which C_{T_2} is expressed. C_{T_2} is the tritium concentration in moles/liter or other absolute concentration units. k is the rate constant in min^{-1}. b, the isotope effect correction, has the value 0.3, and m_H is the mole fraction of protium in the hydrogen reactant.

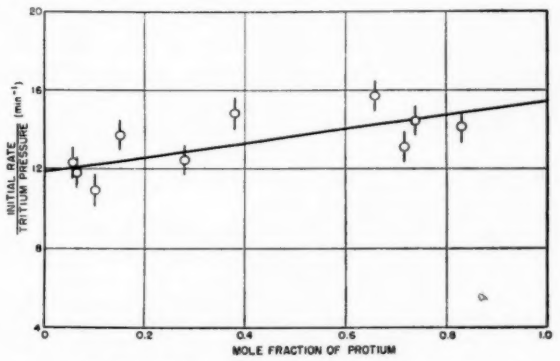

FIG. 2. The dependence of yield on the isotopic composition of the hydrogen.

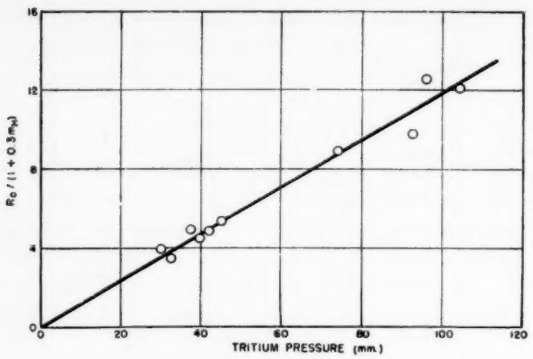

FIG. 3. Plot of Eq. (II).

The validity of Eq. (II) may be seen from Fig. 3, in which $R_0/(1+0.3m_H)$ is plotted against the tritium pressure. A straight line through the origin fits the data reasonably well over a $3\frac{1}{2}$-fold variation in tritium pressure. The values of k for each run are listed in Col. 7 of Table I. k has a mean value of 1.19×10^{-4} min^{-1}, with an average deviation from the mean of 0.076 or 6.4 percent.

Since the initial rate is directly proportional to the tritium pressure, and hence to the absorbed beta energy, the initial ion-pair yield $(M/N)_0$, for hydrogen disappearance will be independent of the tritium pressure. On the basis of an energy requirement[13] of 33 ev per ion pair in the reactant mixture Eq. (II) gives an initial yield of $(M/N)_0{}^T=3.2_5$ molecules/ion pair for the reaction of pure tritium with oxygen. On the basis of the observed isotope effect the initial yield for the beta-particle induced reaction of pure protium with oxygen is $(M/N)_0{}^H=4.2$ molecules/ion pair. This latter value compares very closely with the value 3.92 obtained by Lind[5] for the alpha-particle induced reaction. Lind's value is obtained directly from the measurement of a finite pressure change, and may be expected to be somewhat lower than the initial yield. The experimental yield values above correspond to G values of 9.8 and 12.7 molecules/100 ev respectively.

An extensive discussion of the reaction mechanism does not seem to be warranted, since it must be stated that examination of a number of mechanisms fails to meet the test of uniqueness. Several different reaction schemes lead to a rate equation of the form $R=f$ (intensity), with R independent of the reactant pressures as long as the total pressure is high enough for complete absorption of the beta radiation. Several significant factors pertaining to mechanism may, however, be pointed out.

It is clear from the values for the ion-pair yield that the reaction involves very short chains, but that branched chains do not occur. This is probably due, as in the case of the thermal reaction, to the fact that the reaction

$$T+O_2=OT+O \tag{3}$$

does not occur at room temperature, having an activation energy[14] of 17 kcal in the case of protium. The fate of the hydrogen atoms is then

$$T+O_2=TO_2. \tag{4}$$

Although little or no hydrogen peroxide appears in the product, it must be formed in the reaction, subsequently disappearing by reaction with atoms and radicals. This conclusion is a necessary consequence of the requirement for a chain terminating step of the type

$$TO_2+TO_2=T_2O_2+O_2. \tag{5}$$

Chain breaking steps which reform reactants, for example

$$T+T=T_2, \tag{6}$$

lead to a rate equation of the form $R=f(I_0)^{\frac{1}{2}}+f'(I_0)$ where I_0 is the beta intensity, and are therefore excluded.

A kinetic analysis of the data will not differentiate between the role of oxygen atoms or ozone in the reaction with hydrogen molecules. The possible role of excited ozone molecules is suggested in view of the high energy of the initiating radiation. And finally, the occurrence of an efficient energy transfer process is suggested by the fact that the presence of krypton seems to have little or no effect on the yield. The krypton would, however, markedly affect the primary absorption process.

ACKNOWLEDGMENT

The authors are indebted to Miss C. J. Hibbert and personnel of the Machine Calculations Unit and to Dr. W. S. Horton of the Chemistry and Chemical Engineering Section for their assistance in the curve-fitting computations.

[13] J. M. Valentine and S. C. Curran, Phil. Mag. **43**, 964 (1952).

[14] B. Lewis and G. von Elbe, *Combustion, Flames and Explosions of Gases* (Academic Press Inc., New York, 1951), p. 28.

Rotational Constants of SiH_3D*

SANTIAGO R. POLO AND M. KENT WILSON
Mallinckrodt Chemical Laboratory, Harvard University, Cambridge, Massachusetts

(Received March 2, 1954)

The analysis of the rotational structure of the Si−D stretching fundamental yields the following values:

$B''=2.11\pm0.01$ cm^{-1}, $B''-B'=0.019$ cm^{-1}, $\nu_0=1594.4\pm0.1$ cm^{-1}.

The value of the Si−H distance obtained under the assumption that it remains unchanged by isotopic substitution is

$d_{Si-H}=1.47_7\pm0.003$ A.

INTRODUCTION

THE infrared spectrum of SiD_4 has been investigated under prism dispersion[1] and that of SiH_4 has been studied under high resolution by Steward and Nielsen[2] and by Tindal, Straley, and Nielsen.[3] The latter authors obtained a value of 1.45_6 A for the Si−H distance. This determination required the rotational analysis of the two infrared-active fundamentals $\nu_3(f)$ and $\nu_4(f)$ which in SiH_4 is complicated by the existence of strong Coriolis perturbations.

The analysis of a parallel band of SiH_3D or SiD_3H is a more direct approach to the determination of the Si−H distance. In particular, the Si−D stretching fundamental ν_2 is far removed from the other fundamentals in SiH_3D and occurs in a region in which reasonable resolution can be obtained with prism instruments. The analysis of this band is the subject of the present paper.

EXPERIMENTAL

The sample of SiH_3D was prepared by the reaction of SiH_3Br† with $LiAlD_4$ in ether solution. Dry ethyl ether and the required SiH_3Br were condensed at liquid nitrogen temperature in an evacuated bulb containing the $LiAlD_4$ and the mixture allowed to warm to room temperature. The evolved SiH_3D was purified from ether vapor by several bulb-to-bulb distillations. The infrared spectrum shows a very small amount of SiH_2D_2 (presumably due to a trace of SiH_2Br_2 in the starting material) which in no way interferes with the analysis of the spectrum. Although a small amount of SiH_4 would be difficult to detect and might be present in the sample of SiH_3D, its presence would not interfere with measurements in the region of the Si−D stretch.

The ν_2 band at about 1600 cm^{-1} was recorded by means of a Perkin-Elmer Model 12C spectrograph modified for double-pass operation equipped with a CaF_2 prism. The instrument was calibrated in this region by means of the water vapor lines whose frequencies were taken from the work of Nielsen[4] and Benedict, Claassen, and Shaw.[5] The intense absorption due to water vapor was reduced to a tolerable value by flushing the entire instrument for several hours previous to the run with dry nitrogen.

In Fig. 1 is reproduced a record of the SiH_3D spectrum as well as a blank run illustrating the extent of water vapor absorption. The frequencies and assignments of the SiH_3D lines are given in Table I.

EXPERIMENTAL RESULTS

The frequencies of the rotational lines in a parallel band of a symmetric top when the effect of centrifugal distortion is neglected are given by

$$P(J)=\nu_0-(B'+B'')J+(B'-B'')J^2, \quad (1)$$

$$R(J)=\nu_0+(B'+B'')(J+1)+(B'-B'')(J+1)^2, \quad (2)$$

TABLE I. Observed frequencies of the rotational lines of the ν_2 fundamental of SiH_3D.

J	$R(J)$ (cm^{-1})	$P(J)$ (cm^{-1})
1	1602.1	...
2	06.8	...
3	10.9	1581.0
4	15.0	76.6
5	18.9	72.6
6	22.9	68.4
7	26.8	63.9
8	30.7	...
9	34.7	55.1
10	38.3	50.5
11	42.0	46.0
12	45.8	41.2
13	49.3	36.7
14	53.1	31.8
15	56.2	27.3
16	59.7	22.7
17	63.2	18.1
18	66.7	13.3
19	70.1	08.4
20	73.3	03.6
21	76.2	1498.7
22	79.8	93.9
23	...	89.0
24	89.2	84.0
25	...	78.6
26	...	73.5

* This work was supported in whole or in part by the U. S. Air Force under Contract AF18(600)-590 monitored by the Office of Scientific Research.

[1] J. H. Meal, Ph.D. thesis, Radcliffe, 1954.

[2] W. B. Steward and H. H. Nielsen, Phys. Rev. **47**, 828 (1935).

[3] Tindal, Straley, and Nielsen, Phys. Rev. **62**, 151 (1942).

† The sample of SiH_3Br was obtained from Professor John S. Peake of Indiana University.

[4] H. H. Nielsen, Phys. Rev. **59**, 565 (1941).

[5] Benedict, Claassen, and Shaw, J. Research Natl. Bur. Standards **49**, 91 (1952).

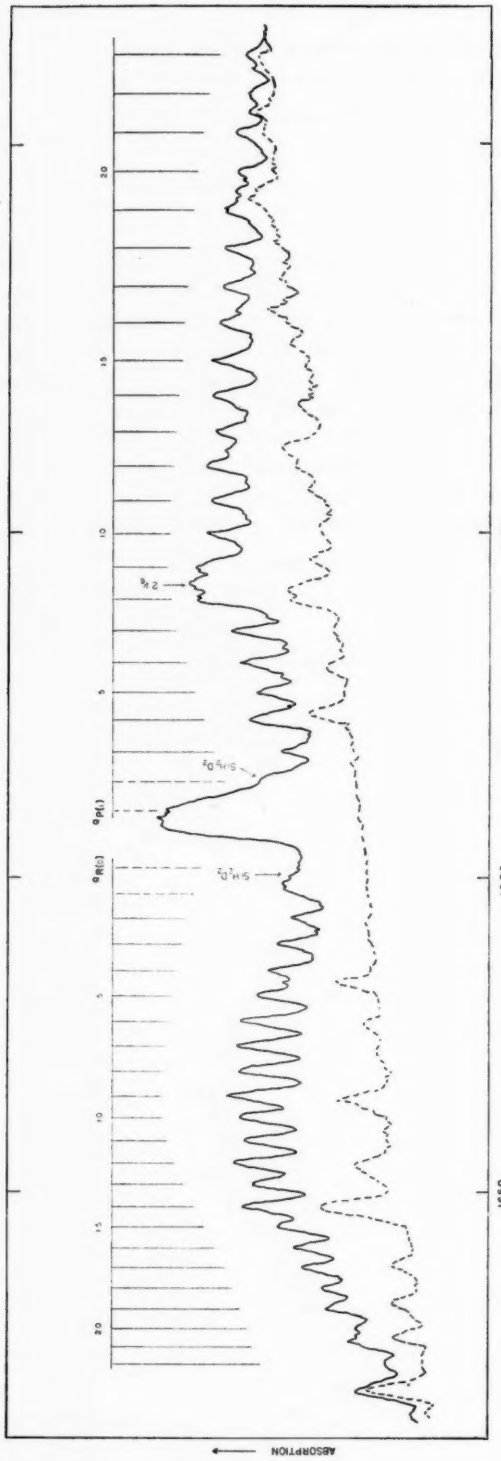

FIG. 1. The Si−D stretching fundamental, ν_2, of SiH_3D. The dotted curve indicates the absorption due to water vapor.

where B' and B'' refer to the upper and lower states, respectively, and J is the rotational quantum number in the lower state.

The values of B' and B'' can be obtained from the combination differences

$$\Delta_2F'(J)=R(J)-P(J),$$
$$=4B'(J+\tfrac{1}{2}), \quad (3)$$

$$\Delta_2F''(J)=R(J-1)-P(J+1),$$
$$=4B''(J+\tfrac{1}{2}), \quad (4)$$

and those of ν_0 and $(B'-B'')$ from the sum

$$R(J-1)+P(J)=2\nu_0+2(B'-B'')J^2. \quad (5)$$

The plot of $\Delta_2F''(J)-8.44(J+\frac{1}{2})$ *versus* $(J+\frac{1}{2})$ is represented in Fig. 2. The numerical values derived from the experimental data are listed in Table II. The SiH distance was calculated under the assumptions that the internuclear distances are unchanged by isotopic substitution and that the molecule is tetrahedral.

In order to visualize the effect of experimental errors on d_{SiH} the two dotted lines in Fig. 2 have been drawn. If the upper line is chosen instead of the full horizontal line to determine B'', the corresponding value of d_{SiH} is 1.47_3 A. Similarly, the lower dotted line corresponds to $d_{SiH}=1.48_1$ A.

In view of our present data, it seems then safe to conclude that the error in d_{SiH} is probably not greater than 0.003, as given above.

DISCUSSION

It is of interest at this point to compare the value of the Si−H distance obtained in the present work with those reported in the literature for SiH_4 and related molecules. It seems definite that the value of 1.45_6 A given in reference (3) is too low and therefore may be excluded. Further, it should be noted that the difference in zero-point energy between SiH_4 and SiH_3D would lead to a larger silicon-hydrogen distance in SiH_4 than in SiH_3D.

From a microwave investigation Dailey, Mays, and Townes[6] reported the Si−H distance in SiH_3Cl to be 1.50±0.03 A, while Bak, Bruhn, and Rastrup-Andersen[7] from a similar investigation report values which range from 1.40 to 1.45 A. These same authors report[8] that the Si−H distance in SiH_3F is the in range 1.45–1.47 A.

TABLE II. Molecular constants for SiH_3D.

$B''=2.11\pm0.01$ cm^{-1}
$B''-B'=0.019$ cm^{-1}
$d_{SiH}=1.47_7\pm0.00_3$ A
$\nu_0=1594.4\pm0.1$ cm^{-1}

[6] Dailey, Mays, and Townes, Phys. Rev. **76**, 136 (1949).
[7] Bak, Bruhn, and Rastrup-Andersen, J. Chem. Phys. **21**, 753 (1953).
[8] Bak, Bruhn, and Rastrup-Andersen, J. Chem. Phys. **21**, 752 (1953).

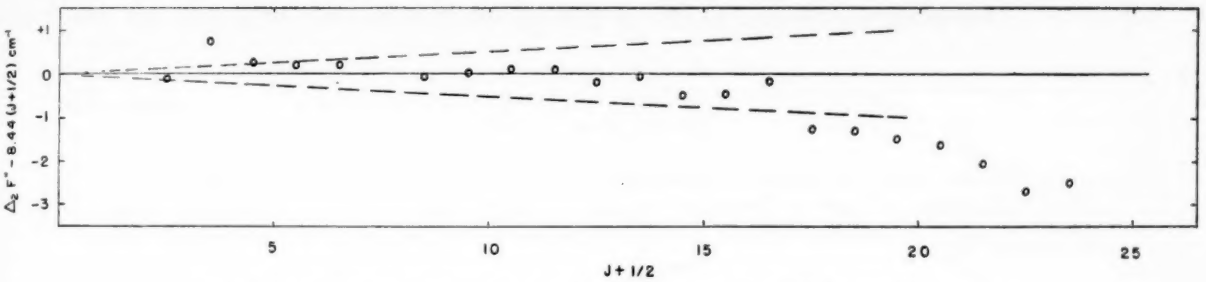

FIG. 2. Plot indicating the accuracy to which the value of B'' of SiH_3D was determined.

Preliminary data from our investigation of the infrared spectra of these compounds combined with the large moment of inertia as determined by the microwave investigations leads us to believe that the Si—H distance in these compounds is close to 1.48 A. In view of the discrepancies in the results just mentioned, we have critically examined the available data. Although our results will be discussed in detail in the publication reporting the infrared spectra of the halosilanes, some remarks may be anticipated.

In spite of the accuracy of the microwave data, the value obtained for d_{SiH} is quite sensitive to small errors in the microwave frequencies‡ and even to the values of the atomic masses used. The low d_{SiH} values given in reference (7) should perhaps be attributed to the use of improper values of the masses, since our calculations with their data on SiD_3Cl lead to a d_{SiH} value of 1.48 to 1.49 A.

Dailey, Mays, and Townes used a $M_{^{35}Cl}/M_{^{37}Cl}$ ratio of 0.945945. If instead one uses the more probable value[9] of 0.945980, the d_{SiH} value is reduced by 0.01 A.

In view of the present evidence, it seems probable to conclude that the SiH distance is about 1.48 A, the differences between different compounds being within the experimental error of the data available at present.

The authors wish to thank Professor John S. Peake for his kindness in supplying the sample of SiH_3Br used in this investigation.

‡ E.g.: When the isotopic species $^{28}SiH_3{}^{35}Cl$, $^{30}SiH_3{}^{35}Cl$, and $^{28}SiH_3{}^{37}Cl$ are used to determine the interatomic distances and angles, a simultaneous change of the B_0 values by 0.1 Mc, 0.1 Mc, and −0.1 Mc, respectively, decreases the value of d_{SiH} by 0.02 A.

[9] Smith *et al.*, Phys. Rev. **79**, 1007 (1949); Townes *et al.*, Phys. Rev. **73**, 1334 (1948); Townes and Schulman, Phys. Rev. **80**, 608 (1950); Gilbert and Roberts, Phys. Rev. **76**, 1723 (1949); E. Segrè, *Experimental Nuclear Physics* (John Wiley and Sons, Inc., New York, 1953).

Temperature Dependence of Ultrasonic Velocity in Plastics

S. V. SUBRAHMANYAM
Physical Laboratories, Osmania University, Hyderabad, India
(Received March 22, 1954)

The composite piezoelectric oscillator method has been employed to study the temperature dependence of the velocity of ultrasonic waves in Perspex and polystyrene plastics. While confirming a previously reported transition in Perspex at 60°C, the results show the existence of a transition in polystyrene also at 70°C for the first time.

1. INTRODUCTION

TEMPERATURE dependence of the velocity of longitudinal ultrasonic waves in methyl methacrylate has been studied by Protzman[1] and Melchor and Petrauskas[2] in the frequency range of 1 to 11 megacycles. Both of them have reported a sharp transition in the temperature-velocity curve. According to Protzman the transition temperature is strongly dependent on frequency, while the results of Melchor and Petrauskas show no such behavior. Hence it is thought desirable to find out whether the reported transition exists in the low-frequency range.

In the present investigation, a dynamic method developed by Balamuth[3] and Rose[4] has been employed to study the temperature variation of longitudinal and torsional velocities in methyl methacrylate (Perspex) and polystyrene plastics. The frequency range is 90–100 kc. This method has a special advantage over other methods, that the specimen does not come into contact with any liquid.

2. EXPERIMENTAL TECHNIQUE

As the experimental technique has been described in detail by Balamuth, Rose, and others, only the essential features of the method are given here. In this method, a composite cylinder, made by cementing the specimen to a suitably cut quartz rod of identical cross section, is set into vibration by applying an appropriate voltage. As the frequency of the voltage is varied in the neighborhood of the resonant frequency of the composite system, the current in the circuit containing the quartz crystal, at first rises, then shows a sharp dip, rises again, and finally falls, to form a symmetrical resonance curve. The resonant frequency f_0 of the system is given by

$$f_0 = f_{\max} + (f_{\min} - f_{\max}) \frac{I_{\min}}{I_{\max} + I_{\min}},$$

where $f_{\max}$ if the frequency at which the first maximum value of the current ($I_{\max}$) occurs and $f_{\min}$ that corresponding to the minimum value of the current ($I_{\min}$).

The fundamental resonant frequency f_s of the specimen is calculated by solving the equation

$$m_s f_s \tan(\pi f_0/f_s) + m_q f_q \tan(\pi f_0/f_q) = 0,$$

where f_q is the frequency of the quartz alone, m_q the mass of the quartz, and m_s the mass of the specimen.

The velocity V in the bar is evaluated using the formula

$$V = 2 f_s l,$$

where l is the length of the bar.

An X-cut quartz rod of 0.30-cm square cross section is used to excite the specimen in longitudinal vibration. To excite the torsional mode, a Y-cut quartz rod of circular cross section and 0.43 cm in diameter with electrode arrangement as suggested by Giebe and Scheibe[5] has been employed. The quartz is first cut to a square cross section, the edges are ground off, and the final form obtained by grinding in split cylindrical gadgets.

The adhesive used to cement the specimen consists of two parts of sodium silicofluoride and one part of barium sulfate mixed with a drop or two of water glass. The composite system works satisfactorily after it is kept under pressure for about twelve hours at room temperature.

In every case the specimen is excited at its third harmonic while the quartz is excited at its fundamental, so as to make the length of the specimen large when compared with its cross-sectional dimensions. The length of the specimen should be adjusted by trial so that its third harmonic and the individual frequencies of the quartz and the composite system lie within ten percent. This type of frequency matching minimizes the effect of the cement.

TABLE I. Elastic moduli of sodium chloride.

Temp °C	$S_{11}\times10^{13}$ (cm²/dyne) Author	Hunter and Siegel	$S_{44}\times10^{13}$ (cm²/dyne) Author	Hunter and Seigel
27	22.90	22.80	78.41	78.09
77	24.01	23.95	79.38	79.08
127	25.30	25.23	80.45	80.14
177	26.71	26.63	81.57	81.22
227	28.23	28.15	82.75	82.37
277	30.00	29.92	84.01	83.61

[1] T. F. Protzman, J. Appl. Phys. **20**, 627 (1949).
[2] J. L. Melchor and A. A. Petrauskas, Ind. Eng. Chem. **44**, 716 (1952).
[3] L. Balamuth, Phys. Rev. **45**, 715 (1934).
[4] F. C. Rose, Phys. Rev. **49**, 50 (1936).
[5] E. Giebe and A. Scheibe, Z. Physik **46**, 607 (1928).

The composite bar with its holder is placed in an electric furnace, the temperature of which is varied by controlling the heating current. Measurements of frequency and temperature are made after a steady state is reached.

It is observed that these plastics lose considerable weight during an individual temperature run, and to get reproducible results the specimens have to be annealed at 100°C for about ten hours.

3. RESULTS AND DISCUSSION

In order to check the accuracy of the experimental setup, elastic moduli S_{11} and S_{44} of sodium chloride have been determined at different temperatures. The results are compared with those of Hunter and Siegel[6] in Table I.

The results of measurements made on polystyrene and Perspex are given in Table II. Temperature variation of the velocity of longitudinal waves in the above plastics is represented graphically in Fig. 1.

TABLE II. Temperature dependence of ultrasonic velocity in Perspex and polystyrene. Here V_l and V_s denote longitudinal and torsional velocities, respectively. The units are in meters per second.

	Perspex		Polystyrene	
Temp °C	V_l	V_s	V_l	V_s
30	2205	1350	1842	1152
40	2157	...	1827	1141
50	2107	...	1811	1131
55	2018	...	...	...
60	2058	...	1796	1120
65	2014	...	1788	...
70	1972	...	1779	1109
75	...	...	1760	...
80	...	...	1743	...

A pronounced transition in the longitudinal velocity-temperature graphs of Perspex and polystyrene will be noticed at 60°C and 70°C, respectively. Hughes,

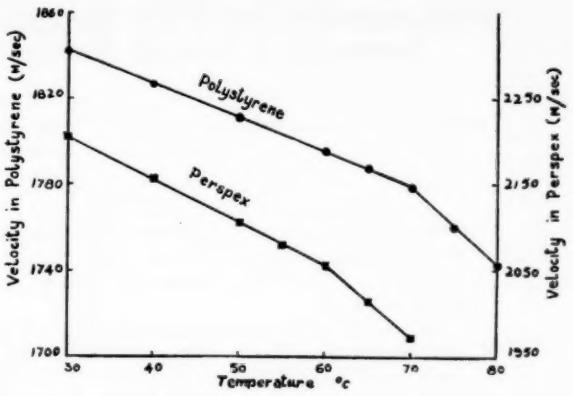

FIG. 1. Ultrasonic velocity as a function of temperature in plastics.

Blankenship, and Mims[7] studied the variation of ultrasonic velocities in polystyrene with temperature and pressure; however, their results do not show clearly the existence of the transition point. Recently Krishnamurthi and Sivarama Sastry of this laboratory have studied the same problem in the frequency range of 1 to 6 megacycles. The samples used by the author and the above workers are taken from the same sheet of material. It has been observed by them that both polystyrene and Perspex show a transition at 61°C and 70°C, respectively. From the above facts it can be concluded that, in the frequency range of 0.1 to 6 megacycles, the transition temperature is independent of frequency.

Torsional velocities are measured in polystyrene up to 70°C. As can be seen from Table II, they vary linearly with temperature. Above this temperature, the damping of the specimen becomes so great that measurements can no longer be carried out. This happened in the case of Perspex even at 35°C.

The author takes this opportunity to offer his grateful thanks to Professor S. Bhagavantam for suggesting the problem and giving necessary guidance.

[6] L. Hunter and S. Siegel, Phys. Rev. **61**, 84 (1942).

[7] Hughes, Blankenship, and Mims, J. Appl. Phys. **21**, 294 (1950).

Photoionization and Total Absorption Cross Section of Gases. I. Ionization Potentials of Several Molecules. Cross Sections of NH_3 and NO

K. WATANABE
Geophysics Research Directorate, Air Force Cambridge Research Center, Air Research and Development Command, Cambridge, Massachusetts

(Received April 14, 1954)

Ionization potentials determined by examining the long wavelength limit of the ionization continuum for H_2S, CS_2, C_6H_6, toluene, *p*-xylene, C_2H_4, butadiene, and CH_3I agreed with spectroscopic values obtained by Price and co-workers. Values are reported also for NH_3, NO, acetone, methyl-ethyl-ketone, CH_3OH, and C_2H_5OH.

Improved energy measurements showed that photoionization cross sections of NO in the region 1070–1340A obtained earlier were about 40 percent too low. At 1215.6A the photoionization and the total cross sections are 2.0×10^{-18} and 2.4×10^{-18} cm², respectively, the difference being ascribed to an absorption band. The photoionization cross section of NH_3 was found to rise rather gradually with decreasing wavelength in the region 1220–1060A and to reach a value of 9×10^{-18} cm² at 1060A.

INTRODUCTION

To provide a more quantitative description of photoionization processes in molecules, it is necessary to know the relevant transition probability as well as the ionization potential. The latter has been measured extensively by many investigators using the electron impact method, and furthermore, for a number of molecules very precise values are now available through spectroscopic determination, particularly by Price[1] and co-workers. On the other hand, both photographic plates of absorption spectra and ion-current curves[2] from electron impact have revealed very little regarding fine structures and absolute intensities of the ionization continuum from which to study transitions from neutral to ionic states of a molecule.

Preliminary photoionization experiments[3] with nitric oxide in the spectral region 1070–1340A showed that our apparatus with a resolution of about 1A is capable of detecting structures in the ionization continuum and of determining ionization cross sections and potentials with considerable accuracy. Similar measurements can be made in the more difficult region below 1000A as shown by Wainfan, Walker, and Weissler[4] who determined photoionization yields of O_2 and N_2 with a resolution of 10A. In both experiments ion currents were measured to separate photoionization from other absorption processes competing for the same photon.[5]

In the present work the total cross section was determined by a photoelectric method described previously using an absorption cell placed at the exit slit of a monochromator, and the ionization cross section was obtained by measuring, in addition, the rate of ion formation in the same cell. Data for about a dozen molecules will be described in several parts.

EXPERIMENTAL

The experiment consists of determining the total absorption cross section σ and the photoionization cross section σ_i in the spectral region 1050–2000A. The former is defined, as previously,[3] by $I=I_0\exp(-\sigma n_0 x)$, while the latter is the product of the former and the ionization yield (number of ions formed divided by total number of photons absorbed). Most of the experimental method has been described in earlier papers[3,6,7] but the following details regarding modifications in the apparatus and technique may be of interest. Values of detector sensitivities and available photon flux are included in view of the fact that some of the measurements would have been impossible had the grating efficiency[8] been lower by about one order of magnitude.

The main source of error in the first experiment on photoionization was in the calibration of a secondary detector, 1*P*21 tube coated with sodium salicylate. To obtain values of σ_i with an accuracy comparable with that for σ, it is necessary first to reduce the uncertainty in the thermocouple calibration. This was carried out by means of two compensated thermocouples mounted on a removable exit-slit mount of the monochromator each feeding into a separate breaker-type amplifier (Liston-Becker). A slit width of 0.33 mm instead of 1 mm was used so that only the middle third of their sensitive areas (1 mm×3 mm) was exposed to light during all calibrations. The absolute sensitivity in air and the vacuum-to-air ratio were measured[9] repeatedly. The absolute sensitivities in vacuum under typical experimental conditions were 6.25 and 7.25 microvolts

[1] W. C. Price, Chem. Revs. **41**, 257 (1947).
[2] J. D. Morrison, J. Chem. Phys. **21**, 1767 (1953).
[3] Watanabe, Marmo, and Inn, Phys. Rev. **91**, 1155 (1953).
[4] Wainfan, Walker, and Weissler, J. Appl. Phys. **24**, 1318 (1953).
[5] For atoms, the assumption that the absorption of light is due entirely to photoionization is usually made for the ionization region, and ion currents are not measured. Refer, e.g., to: Po Lee and G. L. Weissler, Proc. Roy. Soc. (London) **A219**, 71 (1953); Ditchburn, Justum, and Marr, *ibid*, **A219**, 89 (1953).
[6] K. Watanabe and E. C. Y. Inn, J. Opt. Soc. Am. **43**, 32 (1953).
[7] Watanabe, Inn, and Zelikoff, J. Chem. Phys. **21**, 1026 (1953); **20**, 1969 (1952).
[8] K. Watanabe, J. Opt. Soc. Am. **43**, 318 (1953).
[9] Details of the method, results and applications of the thermocouple calibration will be published elsewhere by Dr. H. E. Hinteregger.

per microwatt for the two thermocouples with an estimated error of about 5 percent. This estimate was consistent with the fact that the thermocouples in successive measurements always agreed within five percent on the spectral intensity of the hydrogen spectrum. Moreover, as will be pointed out later the above vacuum sensitivities gave most reasonable data on photoionization yields for a number of gases.

To obtain a resolution of 1A, a secondary detector had to be used, and several 1*P*21 tubes coated with sodium salicylate were calibrated[6] against both thermocouples in the spectral region 900–1700A. Throughout the experiment the operating voltage of the photomultiplier was kept constant at 667 volts ($\pm\frac{1}{4}$ percent). Under this condition, the detector used most frequently had a sensitivity of about 0.7 microamp per 10^{10} photons, the sensitivity being nearly independent[6] of wavelength in the above spectral region. Its absolute sensitivity, however, was found to decrease gradually when kept in vacuum and to recover when exposed to air. This effect, though negligible over a period of a day, became considerable in several days. Wainfan[10] observed a similar effect in the region below 1000A and suggested that the effect was due to dehydration of the sodium salicylate. Thus, this coating material is somewhat unsatisfactory, and it was necessary to repeat some of the measurements in terms of additional calibration against the thermocouples.

During the calibration the photomultiplier intercepted from 10^9 to 5×10^{10} photons per second, whereas during the ionization measurements it intercepted about 10^7 to 10^9 photons per second because a narrower slit (0.055 mm) and an absorption cell with LiF windows were used. Although linearity of the detector had to be assumed over the two intervals, this assumption was supported by the fact that in each interval the detector was quite linear. For example, data from neighboring source lines of quite different intensities gave smooth curves (σ *vs* λ) for an absorption continuum.

The absorption cell (length 7.04±0.02 cm) differed from the earlier model[3] in that the grounded, guard electrodes were omitted, and the two parallel plate electrodes, 15 mm apart, were extended over the entire cell length. This permitted measurements of the total ion current which was 2 to 10 times greater than the previously observed current, and also simplified the computation of the data. With the modified cell the curves for saturation current were still satisfactory as shown in Fig. 1. The flatness of the plateau suggests that the voltages used across the plates, about 15 volts, do not produce appreciable secondary effects. Tungsten electrodes were used in place of platinum because the former has a lower photoelectric yield[11] in the spectral region above about 1250A and therefore would be less

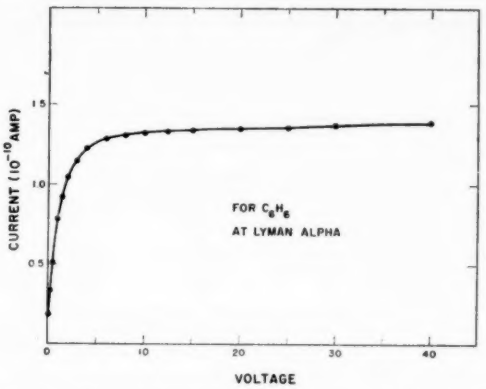

FIG. 1. Voltage-current diagram for photoionization of benzene at Lyman alpha (1215.6A).

sensitive to stray light. The photoelectric current produced by reflected and scattered light was small ($\sim3\times10^{-14}$ amp for Lyman alpha, the strongest line in the region studied) compared to the ion currents, 10^{-13} to 2×10^{-10} amp, which were measured with a Beckman micro-microammeter (Model V).

The gas-filling system differed from the previous one in that silicone grease was used for stopcocks, and pressures from 20 to 0.01 mm Hg were measured with an Alphatron gauge (National Research Corporation) and a silicone oil manometer to permit study of several organic vapors. The Alphatron gauge was calibrated for each gas against the oil manometer. The linearity of the gauge for lower pressures was measured by the expansion method for organic vapors and for permanent gases with a McLeod gauge. With the exception of methyl-iodide, all gases were analyzed with a mass spectrometer.

The error for ionization yields was estimated to be about 10 percent, and for σ, 5–10 percent in the case of permanent gases, and 5–20 percent for vapors depending on the uncertainty in the pressure measurements. Since the effect of scattered light from the grating was comparatively small (e.g., 0.8, 1.1, 0.2, and 1.4 percent of total current at 1443.5, 1335.9, 1215.6, and 1150.8A, respectively) and corrections were easy, this source of error was minor. Values of σ obtained earlier (for nitric oxide,[12] ethylene,[13] butane,[14] and oxygen[7]) and comparable ones in this series agreed within ±5 percent.

RESULTS AND DISCUSSION

Ionization Potentials

Our previous work[3,15] indicated that the photoionization method is capable of determining ionization potentials (*IP*) with an accuracy approaching that of the spectroscopic method and applies even to spectra which

[10] Private communication from N. Wainfan of the University of Southern California.
[11] H. E. Hinteregger and K. Watanabe, J. Opt. Soc. Am. **43**, 604 (1953).
[12] F. F. Marmo, J. Opt. Soc. Am. **43**, 1186 (1953).
[13] M. Zelikoff and K. Watanabe, J. Opt. Soc. Am. **43**, 756 (1953).
[14] Unpublished data.
[15] E. C. Y. Inn, Phys. Rev. **91**, 1194 (1953).

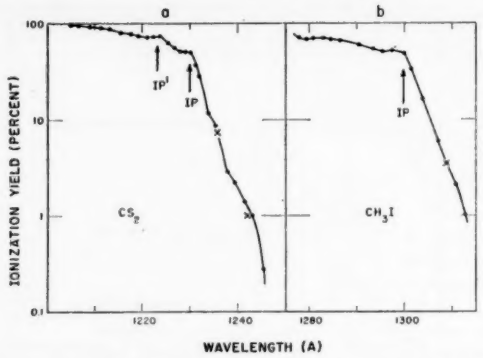

FIG. 2. Photoionization threshold of (a) CS_2 and (b) CH_3I.

are too complex or diffuse to identify Rydberg series. Additional data are presented below.

The sharpness of the photoionization threshold is expected to vary with molecules due to differences in fine structures and probabilities associated with the possible transitions between the molecular and ionic ground states. For example, if the change in molecular dimensions during ionization is rather large, σ_i at the threshold would be small according to the Franck-Condon principle so that it may be difficult to determine the adiabatic *IP*. Another source of difficulty is that some bands in the neighborhood of the threshold may be preionized and thereby distort the ionization continuum. Also, an experimental yield curve may show a long wavelength tail caused by impurities which have a lower *IP* than that of the gas being studied. Furthermore, the distribution of population in the ground state of a molecule is expected to appear as a wing on the long wavelength side of the threshold. In the case of nitric oxide a wing in the σ_i curve was observed[3] over an interval of only 5A due to the low light intensity available near the threshold. Inn[15] determined the longest wavelength at which the first ions *appeared*, without measuring the shape of the ionization continuum. Since the appearance wavelength is not necessarily equivalent to the first ionization potential, it is desirable to obtain curves for both σ_i and yield. From these curves it should be possible to measure the degree of "verticality" in the photoionization process and to decide whether an absorption band is preionized or not. Preionized bands will appear in the σ_i curve, while absorption bands which are not preionized will produce valleys in the yield curve.

Figure 2a shows a yield curve of CS_2 in semilog scale. The yield increases rapidly from an undetectable value at about 1247A to 50 percent at 1230A, and from there on it increases slowly to nearly 100 percent at about 1200A. At two points P and P' the curve changes direction somewhat abruptly, and the values 10.08 and 10.13 ev associated[16] with their wavelengths were taken as *IP* of CS_2, the two values being identified[17,18] as the doublet $^1\Sigma_g^+(CS_2) \rightarrow {}^2\Pi_g(CS_2^+)$. These values are exactly those obtained by Price and Simpson[18] (see Table I).

The wing of the yield curve for CS_2 could be followed over an interval of at least 15A, so an attempt was made to ascribe it to the thermal distribution of population in the ground state of CS_2. The points marked X in Fig. 2a correspond to values obtained using a simple Boltzmann factor, $\exp(-hc\Delta\nu/kT)$, and assuming a constant transition probability. These points fit the experimental curve rather closely, and in fact they should lie approximately on a straight line in this plot because $\Delta\nu$ is nearly proportional to $\Delta\lambda$ in the limited range. A more detailed analysis would require data obtained with higher resolution, and perhaps all that can be said at present is that the average slope of the wing follows approximately a continuous Boltzmann distribution of states for a temperature of about 300°K in nearly all cases observed.

The absorption curve for CS_2 in the region 1215–1245A shows several weak bands on a strong continuum which extends to longer wavelengths. Thus, ionization is accompanied by dissociation and excitation of CS_2, the latter two yielding to the first with decreasing wavelength. The diffuse bands below 1230A are not sufficiently intense to make the σ curve (not shown) very different from the yield curve so that it is difficult to determine whether they are preionized or predissociated. The high yield at the threshold indicates that photo-

TABLE I. A comparison of ionization potentials in ev.

Molecules	Present work		Previously reported spectroscopic value and observer		
CS_2	10.080	±0.01	10.079	±0.005	Price and Simpson[b]
	10.129	±0.01	10.134	±0.005	Price and Simpson[b]
CH_3I	9.537	±0.01	9.538	±0.002	Price[c]
			9.497	±0.007	Inn[d]
H_2S	10.458	±0.01	10.473[a]	±0.005	Price[c]
C_2H_4	10.516	±0.01	10.514[a]	±0.03	Price and Tutte[f]
			10.47	+0.02	Inn[d]
Butadiene	9.070	±0.01	9.063[a]	±0.01	Price and Walsh[g]
C_6H_6	9.245	±0.01	9.240[a]	±0.005	Price and Wood[h]
Toluene	8.821	±0.01	8.822[a]	±0.005	Price and Walsh[i]
p-Xylene	8.445	±0.015	8.48		Hammond *et al.*[j]
Acetone	9.690	±0.01	10.26		Duncan[k]
M-E-Ketone	9.54	±0.02			
CH_3OH	10.85	±0.05	10.52	±0.03	Inn[d]
C_2H_5OH	10.50	±0.05			
NO	9.25	±0.02	9.23	±0.02	Watanabe *et al.*[1]
NH_3	10.25	±0.1	10.13	±0.02	Inn[d]
			11.58		Duncan[m]

[a] Two values less than 0.02 ev apart were averaged.
[b] Reference 18.
[c] Reference 19.
[d] Reference 15.
[e] W. C. Price, J. Chem. Phys. **4**, 147 (1936).
[f] W. C. Price and W. T. Tutte, Proc. Roy. Soc. (London) **A174**, 207 (1940).
[g] W. C. Price and A. D. Walsh, Proc. Roy. Soc. (London) **A174**, 220 (1940).
[h] W. C. Price and R. W. Wood, J. Chem. Phys. **3**, 439 (1935).
[i] W. C. Price and A. D. Walsh, Proc. Roy. Soc. (London) **A191**, 22 (1947).
[j] Hammond, Price, Teegan, and Walsh, Discussions Faraday Soc. No. 9, 53 (1950).
[k] Reference 20.
[l] Reference 3.
[m] Reference 29.

[16] The wavelength associated with 1 ev is 1.2398×10^{-4} cm according to J. W. M. Du Mond and E. R. Cohen, Revs. Modern Phys. **25**, 691 (1953), and this conversion factor was applied throughout.

[17] R. S. Mulliken, J. Chem. Phys. **3**, 720 (1935).
[18] W. C. Price and D. M. Simpson, Proc. Roy. Soc. (London) **A165**, 272 (1938).

ionization here is nearly vertical as is expected in the case of removal of a nonbonding $p\pi$ electron of the sulfur atom.

Figure 2b shows the yield curve for CH_3I in the region 1275–1315A. As in the case of CS_2 the slope of the wing approximately follows a Boltzmann distribution. The calculated point marked X is a value for the vibrational level, $v=1$, using $\Delta\nu=533$ cm^{-1}.

The yield curve of CH_3I is rather smooth and flat in the region below 1300A where several strong bands with intensities as high as two times that of the underlying continuum appear in the σ curve. Thus, the σ_i curve is very similar to the σ curve and one may conclude that the bands are strongly preionized. Furthermore, the high yield and σ_i value ($\sim 5\times 10^{-17}$ cm^2) near the threshold is consistent with the interpretation that photoionization here is due to the removal of a nonbonding electron near the iodine atom.

The ionization potential 9.537±0.010 ev associated with point P in Fig. 2b is in excellent agreement with the value 9.538±0.002 ev obtained by Price.[19] The value obtained by Inn[15] from the "appearance wavelength" is 0.04 ev lower. A still lower threshold at 9.19 ev observed by the latter may be due to impurity. In the present study the CH_3I was obtained from a sealed bottle (Eastman Kodak) and precautions were taken to prevent its decomposition prior to measurement. No ion current was observed in the region corresponding to 9.19 ev although a more efficient ion cell was used.

Our value, 9.69±0.01 ev, for the IP of acetone (Fig. 3(a)) differs considerably from the value, 10.26 ev, obtained spectroscopically by Duncan.[20] Due to the complexity and diffuseness of the absorption spectra he was able to fit only three of the many observed bands into a Rydberg series as follows:

$$\nu=82\,767-\frac{R}{(n-0.495)^2}\ \text{cm}^{-1}\quad n=3,4,5. \qquad (1)$$

In view of the discrepancy, we have attempted to analyze the Rydberg series, assuming that our value is

TABLE II. Rydberg series for acetone.

n	Observed in cm^{-1} Duncan	This experiment	Calculated
2	65 213	65 260	65 840
3	71 308	71 310	71 317
4	73 834	73 880	73 838
5	75 376	75 230	75 201
6	76 030	76 020	76 021
7	76 563	76 500	76 553
8	...	76 940	76 916
9	...	77 180	77 176
10	77 360	...	77 368
11	77 483	...	77 515
12	77 646	...	77 628

[19] W. C. Price, J. Chem. Phys. **4**, 539 (1936).
[20] A. B. F. Duncan, J. Chem. Phys. **3**, 131 (1935); **8**, 444 (1940).

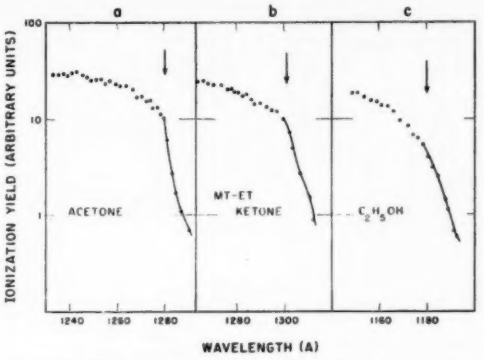

FIG. 3. Photoionization threshold of (a) acetone, (b) methyl-ethyl-ketone, and (c) ethyl alcohol.

the correct IP. For this purpose we have supplemented our data obtained with low resolution (1A) and a hydrogen source with the more accurate wave numbers reported by Duncan.[20] The result is summarized in Table II. Calculated values in the last column were obtained from the equation,

$$\nu=78\,280-\frac{R}{(n+0.97)^2}\ \text{cm}^{-1}\quad n=2,3,\ldots. \qquad (2)$$

The observed band $\nu=75\,376$ cm^{-1} obtained by Duncan listed in Table II may not be a member of this series. The IP, 9.705 ev, obtained from Eq. (2) is in good agreement with the value determined by the ionization method and is consistent with electron impact data.[21]

The IP of methyl-ethyl-ketone obtained from its yield curve, Fig. 3b, is 9.54±0.02 ev. There appears to be no accurate spectroscopic IP for comparison and we have not attempted as yet to locate a Rydberg series for this molecule.

In the case of C_2H_5OH, the yield curve (Fig. 3(c)) does not show a distinct break near the ionization threshold although the yield rises rather rapidly with decreasing wavelength. It is not possible to obtain an accurate value of IP; however, by comparison with curves for other molecules and by allowing for a long wavelength wing the IP of C_2H_5OH may be confined to the interval 10.45 to 10.55 ev. This is not unreasonable because the lower limit was taken as a point well along the long wavelength wing and the upper limit was taken as a point where the slope has departed considerably from that of the wing. The yield curve for CH_3OH (not shown) appeared very similar to that of C_2H_5OH, although a break in the yield curve was more apparent. By similar considerations the IP of CH_3OH was confined to the interval 10.80–10.90 ev. A weak, very long tail in the yield curve of CH_3OH was ascribed to impurity, about one percent acetone. These cases illustrate the limitation in the accuracy obtainable; although with improved technique and resolution it may be possible to reduce the uncertainty.

[21] J. D. Morrison and A. J. C. Nicholson, J. Chem. Phys. **20**, 1021 (1952).

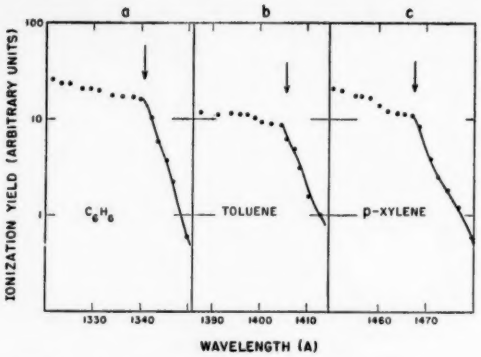

FIG. 4. Photoionization threshold of (a) benzene, (b) toluene, and (c) *para*-xylene.

Yield curves for benzene, toluene, *p*-xylene, H_2S, C_2H_4 and butadiene are shown in Figs. 4 and 5. In each case the break in the curve is distinct and the *IP* obtained is listed in Table I with others. This table shows that our results are in excellent agreement particularly with those obtained by Price and coworkers, and together they appear to constitute a consistent picture of the first ionization limit of these molecules.

PHOTOIONIZATION CROSS SECTION OF NO

The present data showed that the absolute value of σ_i for NO obtained earlier[3] was consistently too low by 35–40 percent throughout the spectral region 1070–1340. On the other hand, σ values agreed within about 5 percent with the values reported by Marmo.[12] The points in Fig. 6 are the revised σ_i values (estimated error$\pm$10 percent) and the solid curve represents the average of the σ curves obtained in the two observations. By subtracting the ionization continuum and the bands from the σ curve, Marmo[22] has obtained a smooth dissociation continuum extending from $\nu=71\,600$ to $\nu=83\,000$ cm^{-1}.

Three more steps in the σ_i curve were observed in addition to the three reported earlier. These steps indicated by arrows in Fig. 6 are almost certainly due to the vibrational level of NO^+ ground state: (a) the $\Delta\nu$'s between steps agree with those between the (0,0), (0,1), $\cdots$ and (0,5) members of the Miescher-Baer emission bands;[23,24] (b) the *IP* of NO obtained by a cycle[3] (average of Tanaka's γ-Rydberg series limits[25] minus (0,0) member of M-B bands equals 9.24 ev) agrees with our result (Table I). The transition probability for photoionization going to higher photon energies appears to be approximately cumulative at least in the wavelength region shown in Fig. 6, so that for ions with small vibrational $\Delta\nu$ the increments would be small and detection of vibrational structure in the ionization continuum would be difficult.

Recently, Sutcliffe and Walsh[26] have discussed the *A*, *C*, *D*, and *E* states of NO as involving Rydberg orbitals and suggested that transitions from the ground state to the *A* and *E* states represent the first two members of the Rydberg series, $(\pi_g 2p)^2\Pi \rightarrow (\sigma_g ns)^2\Sigma^+$. This suggestion is consistent with the ionization limit,

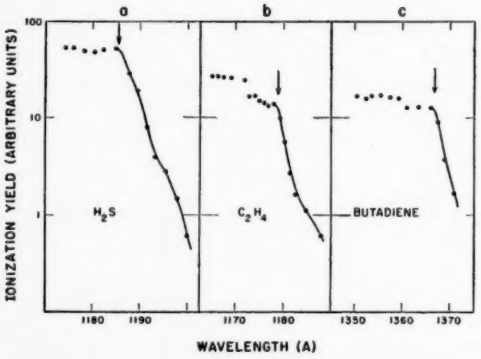

FIG. 5. Photoionization threshold of (a) H_2S, (b) C_2H_4 and butadiene.

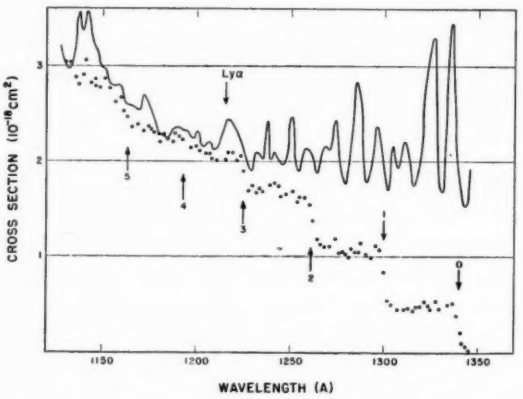

FIG. 6. Total absorption cross section (smooth curve) and photoionization cross section (points) of the NO molecule.

74 630 cm^{-1}, corresponding to the observed ionization threshold. It might be further suggested that the transition from the ground state to the *C* state and the *D* progression reported by Tanaka *et al.*[27] are the first two members of another Rydberg series converging to the same limit. Although it is possible to make predictions as to the approximate locations of the higher members, identification would be probably difficult because of the complexity of the NO absorption spectrum in the region below 1500A.

The σ_i value of NO at 1215.6A is of importance to the theory of *D*-layer formation.[28] As shown in Fig. 6, at this wavelength there is a diffuse absorption band

[22] F. F. Marmo, thesis, Department of Chemistry, Harvard University.

[23] R. Miescher and P. Baer, Nature **169**, 581 (1952).
[24] Y. Tanaka, J. Chem. Phys. **21**, 562 (1953).
[25] Refer to G. Herzberg, *Spectra of Diatomic Molecules* (D. Van Nostrand Company, Inc., New York, 1950), p. 558.
[26] L. H. Sutcliffe and A. D. Walsh, Proc. Phys. Soc. (London) **A66**, 209 (1953).
[27] Tanaka, Seya, and Mori, Science of Light (Japan) **1**, 80 (1951).
[28] Watanabe, Marmo, and Inn, Phys. Rev. **90**, 155 (1953).

which is not appreciably preionized, and the yield curve definitely shows that ionization yield here cannot be 100 percent. The σ and σ_i for this wavelength are 2.4×10^{-18} and 2.0×10^{-18} cm^2, respectively.

TOTAL AND PHOTOIONIZATION CROSS SECTION OF NH_3

The absorption spectrum of ammonia in the vacuum ultraviolet has been studied by several investigators. Duncan[29] made the most thorough study and extended the earlier observations of Leifson[30] (2400–1400A) and Dixon[31] (2400–1900A) down to 850A. Duncan classified four progressions (series I, II, III and IV) and fitted three of them into a Rydberg series converging to 93 380 cm^{-1} (11.58 ev).

Absorption intensities of NH_3 in the vacuum ultraviolet have been reported by Thompson and Duncan[32] in the region 1250–2200A, by Tannenbaum *et al.*[33] in the region 1700–2200A and Watanabe *et al.*[34] in the region 1050–2200A. Since the result of the last group is described in a report not widely circulated, two graphs with slight modifications are reproduced for convenience in Figs. 7 and 8. The k values ($k=\sigma n_0$ where n_0 is Loschmidt number) shown in Fig. 7 agree within about 10 percent with those obtained photographically by Tannenbaum *et al.* The f value, 0.088, for this region is about ten percent higher than their value, but much less than the value 0.13 reported by Thompson and Duncan. The spectrum in the region from 1600 to 1200A, Fig. 8, consists of many bands and the k values showed some apparent pressure effect which can be ascribed to lack of resolution of the rotational structure.[35]

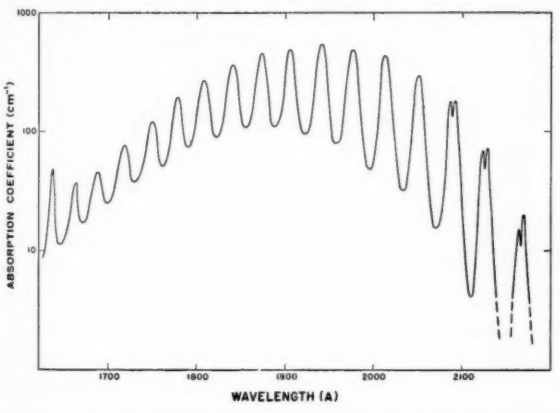

FIG. 7. Absorption coefficient of NH_3 in the region 1650–2200A.

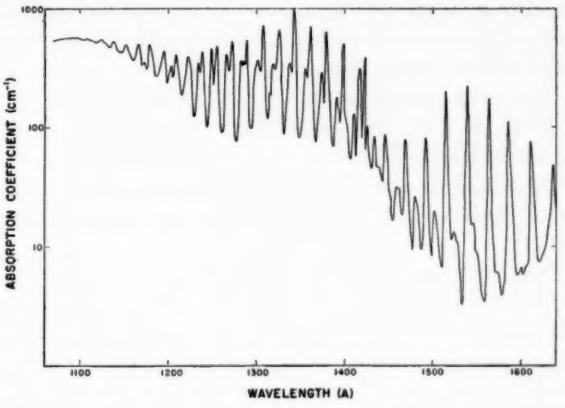

FIG. 8. Absorption coefficient of NH_3 in the region 1050–1650A.

In the region below about 1220A, the bands are weaker and apparently more diffuse as indicated by the constancy of the σ values (upper curve in Fig. 9) with respect to pressure. There appears to be a strong continuum underlying these bands and the possibility that this continuum may be partly due to photoionization was suggested earlier.[34] It is to be noted that the bands in this region were designated as series IV by Duncan.

The ionization yield of NH_3 was measured for seven pressures between 0.4 and 7 mm Hg. The yields for pressures below about 4 mm were independent of pressure, but at higher pressures they were somewhat pressure sensitive, probably due to recombination. The lower curve in Fig. 9 represents the mean σ_i values using only data for pressures less than 3 mm. The curve begins at about 1225A and rises gradually to shorter wavelengths, contributing about 40 percent of the σ value (2.1×10^{-17} cm^2) at 1100A. The lower curve shows indications of structure which probably represent contributions of preionization of the bands appearing in the upper curve; however, vibrational levels of the ionic state and experimental errors are not ruled out. The (0,0) member of series IV by Duncan lies near the

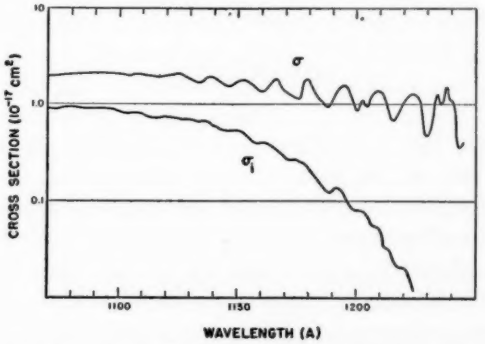

FIG. 9. Total cross section (σ) and photoionization cross section (σ_i) of NH_3 in the region 1070–1250A.

[29] A. B. F. Duncan, Phys. Rev. **47**, 822 (1935); **50**, 700 (1936).
[30] S. W. Leifson, Astrophys. J. **63**, 73 (1926).
[31] J. K. Dixon, Phys. Rev. **43**, 711 (1933).
[32] R. J. Thompson and A. B. F. Duncan, J. Chem. Phys. **14**, 573 (1946).
[33] Tannenbaum, Coffin, and Harrison, J. Chem. Phys. **21**, 311 (1953).
[34] Watanabe, Zelikoff, and Inn, Geophysical Research Paper, No. 21, Geophysics Research Directorate (1953).
[35] A. B. F. Duncan and G. R. Harrison, Phys. Rev. **49**, 211 (1936).

ionization threshold; therefore, it is possible that series IV is an extension of series III with the bands appearing more diffuse due to preionization.

The ionization potential of NH_3 obtained from Fig. 9 is 10.25±0.1 ev, the uncertainty being similar to that for the alcohols. This value is consistent with the value, 10.13±0.02 ev, obtained by Inn from appearance wavelength and is also consistent with the electron impact data.[21]

Duncan observed maximum intensity for bands with v' about 7 in series I, II, and III, and concluded that the molecular dimensions change considerably during the excitation of NH_3. A similar interpretation can be given for ionization because the vertical IP (corresponding to the position of the steepest slope of the σ_i curve plotted on a linear scale) appears to be about 0.5 ev higher than the adiabatic IP.

AN APPLICATION

Absorption processes are usually more complex in molecules than in atoms; however, absorption at some wavelengths may lead entirely to ionization of a molecule. In other words, photons may ionize a molecule much more readily than dissociate it, even if its IP is higher than its dissociation energy. By studying the maximum yield of a number of molecules such cases may be found for wavelengths above 1000A. Although our data are rather incomplete, hundred percent yields (±10 percent) were found in the case of NO (see Fig. 6) and CS_2, and nearly 100 percent for CH_3I. The fact that higher yields were not observed offers some assurance that secondary effects were negligible and that energy measurements were as reliable as stated.

The use of an ionization cell as a detector for absolute energies in the Schumann region appears practical. Its reproducibility was found to be better than that of the phosphor-coated photomultiplier tube. The high photoionization yield makes possible an efficient photon counter. In this respect, it is superior to a photoelectric cell because photoelectric yields of metals in this spectral region are rapidly changing with wavelength and about two orders of magnitude less than photoionization yields of certain molecules. Furthermore, the long wavelength cutoff of an ionization cell is sharp, and much better defined than the long wavelength cutoff for photoelectric detectors.

THE JOURNAL OF CHEMICAL PHYSICS VOLUME 22, NUMBER 9 SEPTEMBER, 1954

Influence of Rate of Shear on the Apparent Viscosity of A—Dilute Polymer Solutions, and B—Bulk Polymers

F. BUECHE*
Rohm and Haas Company, Philadelphia, Pennsylvania
(Received April 8, 1954)

The measured viscosity of bulk polymers and their solutions varies with the magnitude of the applied shearing stress. In this paper we show that this is a natural consequence of the fact that the molecules are caused to rotate by the shearing action. This rotation gives rise to sinusoidal forces which alternately stretch and compress the molecules. The viscous behavior of such a system is shown to be analogous to that of a spring immersed in a viscous medium and being acted upon by sinusoidal viscous forces. We have treated the problem quantitatively using the method of a previous paper. Good agreement is obtained between theory and experiment without the aid of adjustable parameters. It is found that, if the molecule is considered shielded, the theory accurately represents the experimental data for dilute solutions. The behavior of the bulk polymer is well represented by means of the free draining approach. It is pointed out that the variation of the viscosity of dilute polymer solutions with the rate of shear may provide a convenient method for determining molecular weights of coiling type polymers.

INTRODUCTION

IT is well known that the apparent viscosity both of high polymer solutions and of the pure polymer decreases as the rate of shear is increased. Several attempts have been made to interpret this phenomena both for dilute solutions of coiling polymers[1] and for the bulk polymer.[2] To our knowledge, no one has suggested that the effect of shear rate on the measured viscosity of bulk polymers is related to the dilute solution behavior. It is the purpose of this paper to present a unified treatment of both phenomena which shows they are intimately related. The approach followed here, using a method previously outlined,[3] leads to at least semiquantitative agreement with the available experimental data without introducing unknown adjustable parameters.

Before going into the details of our computation of the effects of rate of shear on the viscosity of polymer molecules, we shall outline a crude picture which will give some insight into the actual physical processes involved. Assume the molecule to be a porous spherical

* Present address: Department of Physics, University of Wyoming, Laramie, Wyoming.
[1] See, for example, A. Peterlin, J. Polymer Sci. 8, 621 (1952).
[2] R. S. Spencer, J. Polymer Sci. 5, 587 (1950).
[3] F. Bueche, J. Chem. Phys. 22, 603 (1954).

ball composed of polymer segments. When a shearing force is applied to a medium in which the molecule is imbedded, the solvent flows past the polymer segments and the resulting energy loss, due to the friction, is observed as an increase in the viscosity of the medium.

If we follow the approach of Debye[4] and refer to Fig. 1, it is clear that the motion of the solvent exerts a torque on the molecule and this will cause it to rotate. The friction losses are therefore a combination of the results of the motion of the solvent and the rotation of the molecule. Debye calculated what these friction losses would be and arrived at his well-known formula for the intrinsic viscosity of polymer solutions.

The effects of rate of shear upon the viscosity (or energy loss) are intimately connected with the details of such a model. One approach has been to consider the molecule to be rod-shaped. Then it is quite clear that the rod will try to line up in the solvent current in such a way as to decrease the viscosity. This approach has met with much success in interpreting data on the actual rod-like polymers. However, most coiling polymers do not behave like rods since they tend to remain in a ball-like form.

Such a ball of polymer segments will be somewhat deformable and as the solvent flows through the ball it will tend to be dilated and compressed. The solvent flow lines are such that the ball will tend to be stretched along the line $00'$ in Fig. 1 and compressed along II'. Actually, however, the molecule is rotating all the time and so the particular segments in the region of $00'$ and II' will change as the molecule rotates. Therefore, any single segment will go through a complete cycle such that it is first pulled out along $00'$ and then pushed in along II'. The frequency of the motion turns out to be proportional to the shear rate.

It may be shown that this alternate stretching and compressing movement does not change the energy loss per rotation and so the viscosity is not changed by including this effect. However, if the molecule is assumed to be somewhat stiff (as Peterlin has shown[1]) the viscous loss becomes a function of this compression-dilation process. To show how this comes about, consider for the moment that each polymer segment is tied to the center of mass of the molecule by a spring of stiffness σ. Although it is possible to relate this quantity to constants of the molecule, we shall be content for now to say that it is analogous to the spring constant one may assign to the statistical retractive forces on the ends of a polymer chain. The segment spring system, in our case, is being driven by the viscous drag of the solvent past it. As was pointed out above, this viscous drag alternately compresses and stretches the spring. If one works out this simple problem in mechanics it turns out that at low frequencies (or small shear rates) there is a great deal of viscous loss. However, at high frequencies the loss decreases to zero.

[4] P. Debye, J. Chem. Phys. 14, 636 (1946).

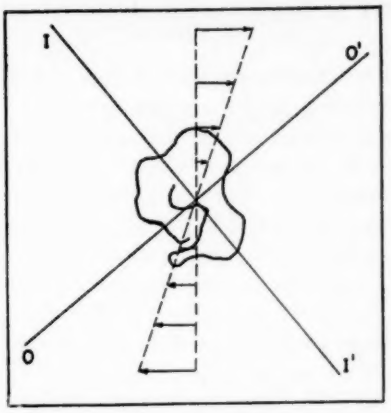

FIG. 1. This illustrates the forces which act upon a polymer molecule when the liquid in which it is immersed is sheared.

This change in viscous loss comes about because the phase between the applied force and the velocity of the end of the spring changes as the frequency increases. There is a particular characteristic frequency (proportional to a characteristic rate of shear) at which value the change is most rapid. It occurs when the frequency is approximately equal to σ/f where f is the friction constant between the segment and the solvent and σ is the spring constant. Above this frequency (or shear rate) the viscosity is rapidly decreasing, while below it, the viscosity approaches its maximum value.

It should not be thought that the magnitude of the stretching of the molecule is the important factor (unless the elongation becomes so large as to invalidate the assumptions made above). The important variable is the phase relationship between the stretching force and the displacement. This phase relationship is completely dependent upon the ratio of the frequency of the forces acting on the segments to the critical frequency of the molecule. For this reason, the same type of decrease in viscosity is found when a polymer solution is excited by oscillations of variable frequency even though these be of very small amplitude. This equivalence of frequency and shear rate forms the basis for the success of a macroscopic treatment presented by DeWitt[5] and extended by Ferry.[6] We shall show in the remainder of this paper how the critical frequency for the molecule may be calculated and we shall discover its relation to the observed experimental behavior.

In Part A of this paper we apply the method of a previous paper[3] to the case of dilute solutions of coiling polymer molecules. The result obtained is compared with the experimental data available for three polymers, polystyrene, polyisobutylene, and polymethyl methacrylate. In Part B we extend the treatment to the case of bulk polymers and compare the result with published experimental data for polystyrene.

[5] T. W. DeWitt, J. Appl. Phys. (to be published).
[6] J. D. Ferry, J. Phys. Chem. (to be published).

PART A: DILUTE SOLUTIONS OF HIGH POLYMERS

It has been shown elsewhere[3] that the motion of a polymer molecule under a given force can be reduced in a rigorous fashion to a mechanical problem involving the motion of $3N$ springs joined end to end in a particular arrangement. The first spring is to point in the $\pm x$ direction, the second in the $\pm y$, direction and so on. All forces acting on the molecule can be resolved into x, y, and z components and the motion resulting from each treated separately. We number the x directed segments from 1 to N. Then if $\Phi(i,x)$ is the x component force on the ith segment, the displacement of any segment, say the pth, from its average equilibrium position is

$$\xi_p=(2/mN)^{\frac{1}{2}}\sum_{n=1}^{N} q_n\cos(pk_n), \tag{1a}$$

with m being the mass of a segment, $k_n=n\pi/N$, and q_n being defined by the differential equation

$$\ddot{q}_n+(f/m)\dot{q}_n+\omega_n{}^2q_n=(2/mN)^{\frac{1}{2}}\sum_{i=0}^{N}\Phi(i,x)\cos(ik_n), \tag{1b}$$

where the dots signify derivatives with respect to time.

In the above expression $\omega_n{}^2\cong(3kT/\mathrm{ma}^2)(n^2\pi^2/N^2)$, where n is an integer $1\leqslant n\leqslant N$, and a is the average length of a segment. ω_n is essentially a natural frequency of the molecule when immersed in a liquid of zero viscosity. The quantity f is the friction factor for a segment defined in such a way that if the segment is moved with a velocity v it will experience a frictional retarding force equal to fv.

The method of normal coordinates was used in obtaining these relations. As such, the sum of Eq. (1a) represents the sum of the individual displacements of the segment resulting from vibration of the whole chain in its various normal modes of motion.

Using these equations it is possible to find the motion of the polymer molecule provided the forces acting on its segments are known. It should be mentioned that Φ does not include any friction forces which result directly from stretching of the molecular springs. These are already included in the friction term in Eq. (1b). Also, the above equations apply only to the cases where stretching of the molecule is small enough so that its behavior is Hookian. The theory is not expected to apply at such high frequencies of excitation (or equivalent short times of observation) that the structure of the individual segments becomes important.

In order to proceed with the calculation of the shear dependence of viscosity we must examine the picture of a polymer molecule in dilute solution when subjected to a shearing force. As is well known, the center of mass of the molecule will move with the velocity of the solvent at that point and so the translational motion of the molecule is obvious.

Debye[4] has shown that the solvent flow gradient gives rise to a torque on the molecule which causes it to rotate as illustrated in Fig. 1. Considering the molecule to be spherically symmetric it may be shown that the molecule will rotate with an angular velocity of $\gamma/2$ where γ is the shear rate. Because of this, the segments experience a clockwise torque when they are near either the top or the bottom of their rotation path and a counterclockwise torque when they are near the central portion of the path as illustrated in Fig. 1. To a first approximation these torques must balance and this results in the fact that the average angular velocity is $\gamma/2$.

It is now a simple matter to calculate the frictional force on any segment of the polymer molecule due to this rotation and the original shear gradient. Taking x, y, and z coordinates *fixed in the molecule* (that is, the coordinate system rotates with the molecule) we have that the x directed force on the ith segment is

$$\Phi(i,x)=\tfrac{1}{2}f\gamma[x_i\sin\gamma t+y_i\cos\gamma t], \tag{2}$$

and similarly

$$\Phi(i,y)=\tfrac{1}{2}f\gamma[-x_i\cos\gamma t+y_i\sin\gamma t],$$
$$\Phi(i,z)=0.$$

This shows at once that in the coordinate system of the molecule (neglecting centripetal forces) the molecule is being excited by sinusoidal type forces in the x and y directions as given above. Therefore, the solution to our problem reduces to the calculation of the viscous losses to be expected for a molecule imbedded in a viscous liquid when subjected to the sinusoidal forces of Eq. (2). We shall first obtain the losses due to the x directed motion. From the symmetry of Eqs. (2), the average viscous loss due to the motion in the y direction will be the same. If the viscous energy loss per unit volume is W, the viscosity increase due to the polymer molecules is given by W/γ^2.

Because of its motion in the x direction the ith segment will cause a viscous loss equal to the product of the force on the ith segment, that is $[\Phi(x,i)-f\dot{\xi}_i]$, and the velocity of the same segment, i.e., $1/f$ times the force. Therefore, the viscous energy loss of the whole molecule will be

$$W/\nu=2\sum_{i=0}^{N}(1/f)[\Phi(x,i)-f\dot{\xi}_i]^2, \tag{3}$$

where ν is the number of molecules per unit volume.

Making use of Eqs. (1) and (2) we find

$$\xi_i=(\gamma/N)\left\{\sum_{n=1}^{N}\frac{\tau_n\cos(i,k_n)}{1+\gamma^2\tau_n{}^2}\sum_{p=0}^{N}[x_p(\sin\gamma t-\gamma\tau_n\cos\gamma t)\right.$$
$$\left.+y_p(\cos\gamma t+\gamma\tau_n\sin\gamma t)]\cos pk_n\right\}, \tag{4}$$

where $\tau_n = fa^2N^2/3\pi^2n^2kT$, where n is an integer $1 \leqslant n \leqslant N$, and a is the length of a segment.

Actually, $x_p = x_{0p} + \xi_p$, where x_{0p} is the average equilibrium value of x_p. However, it turns out that even though ξ_p becomes fairly large in comparison to x_{0p}, the retention of this complication gives rise to small terms contributing at most only a few percent of the total viscous loss. This is a reflection of the fact that the elastic energy stored in the chain upon stretching is recovered without a net energy loss each time the molecule makes one complete rotation. With this fact in mind we shall consider x_p to have its average equilibrium value at all times thereby decreasing the complexity of the calculation.

To find the viscous energy loss we need only substitute the result of Eq. (4) into (3). Although the computation is laborious, the sums involved are not difficult. However, since the average values of $x_p x_q$ will occur in this evaluation, we must use the fact proven in reference 3 that

$$\langle x_p x_q \rangle = (a^2N/9)[1-(3q/N)+(3/2N^2)(q^2+p^2)],$$

where it is assumed that $q > p$.

After carrying out the computations indicated and averaging over a complete rotation of the molecule we find

$$\eta - \eta_s = \frac{W}{\gamma^2} = \left(\frac{fa^2N^2\nu}{36}\right)\left\{1 - \sum_{n=1}^{N} \frac{6\gamma^2\tau_1^2}{\pi^2n^2(n^4+\gamma^2\tau_1^2)} \times\left[2 - \frac{\gamma^2\tau_1^2}{n^4+\gamma^2\tau_1^2}\right]\right\}, \quad (5)$$

where $\tau_1 = fa^2N^2/3\pi^2kT$ and where η_s and η are the viscosities of the solvent and solution, respectively. The small inertia terms have been dropped.

For $\gamma \to 0$ the above expression reduces as it should to Debye's formula[4] for the viscosity of a dilute polymer solution composed of freely draining molecules. Calling $\eta_0 - \eta_s$ the viscosity increase due to the polymer when $\gamma \to 0$ one has

$$\frac{\eta - \eta_s}{\eta_0 - \eta_s} = 1 - \frac{6}{\pi^2}\sum_{n=1}^{N} \frac{\gamma^2\tau_1^2}{n^2(n^4+\gamma^2\tau_1^2)}\left[2 - \frac{\gamma^2\tau_1^2}{n^4+\gamma^2\tau_1^2}\right], \quad (6)$$

where $\tau_1 = (12/\pi^2\nu kT)(\eta_0 - \eta_s)$.

Equation (6) has no adjustable parameters and so it can be tested by comparing it with the available experimental data. To facilitate this test we have tabulated $(\eta - \eta_s)/(\eta_0 - \eta_s)$ as a function of $\gamma\tau_1$ in Table I.

TABLE I. Variation of viscosity with shear rate as predicted by Eq. (6).

$\gamma\tau_1$	0.050	0.100	0.400	0.700	1.000	2.000	4.000	10.00	50.00
$(\eta-\eta_s)/(\eta_0-\eta_s)$	0.997	0.988	0.847	0.667	0.526	0.356	0.261	0.160	0.088

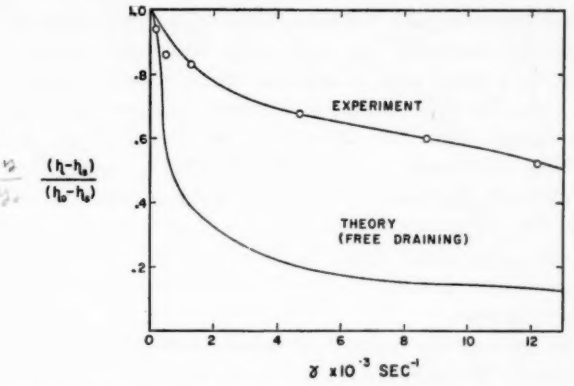

FIG. 2. The variation of viscosity with shear rate. Solid line is predicted from the free draining theory. Experimental points are for a polystyrene of $M = 6.6 \times 10^6$ in toluene (see reference 8).

As indicated in the introduction, the quantity τ_1 can be considered a characteristic relaxation time of the molecule and it is seen from the table that when the time taken for the molecule to make one complete rotation (i.e., $1/\gamma$) is comparable to it, the shear effects become important. Physically, thinking of the molecule as a spring, τ_1 is analogous to the relaxation period of the spring. If the rotation period of the molecule is slower than this, the molecule is being excited below its principal relaxation period and exhibits the viscous loss characteristic of all such damped spring-like systems. The decrease in viscous loss as one approaches the principal relaxation frequency of the molecule is analogous to the similar behavior exhibited by a spring. As shown by the sum of Eq. (6), our molecule actually has a large number of relaxation times which are given by τ_1/n^2 where n is an integer.

There are several reliable sets of experimental data with which we can compare our theoretical result. Of these we have chosen that of Fox, Fox, and Flory[7] for polyisobutylene, Sharman, Somes, and Cragg[8] for polystyrene, and Fox[9] for polymethyl methacrylate.

A comparison of the results of our theory with experiment is made in Fig. 2. It should be remembered that no unknown variables are used. The theoretical curve is completely determined by the solvent viscosity, polymer molecular weight, intrinsic viscosity and the temperature. No attempt has been made to correct the experimental data for the fact that it was obtained at a nonuniform rate of shear. Such a correction involves the slope of the experimental curve and could not be made with great accuracy. This neglect will not be serious for the present purposes.

Although some measure of agreement is obtained at low shear rates, the agreement is poor at the larger values. It is observed that the viscosity does not decrease as fast as theory would predict. The reason for

[7] Fox, Fox, and Flory, J. Am. Chem. Soc. **73**, 1901 (1951).
[8] Sharman, Somes, and Cragg, J. Appl. Phys. **24**, 703 (1953).
[9] T. G. Fox (unpublished results).

this is quite simple. We have assumed a freely draining molecule. Actually, at such high molecular weights there is a great deal of solvent immobilization within the coil. For this reason, an increase in shear increases the energy loss (and therefore the viscosity) by disturbing this formerly immobilized solvent. It would be an exceedingly formidable task to take account of this effect in a rigorous fashion. However, since the answer for the zero shear limit is known[10,11] we can get an approximate answer to the more general case in the following way.

We assume the shear rate is not constant inside the molecule. Instead, take the shear rate to vary within the molecule in the following manner;

$$\gamma' = \tfrac{1}{2}\{\exp[-\beta(N-i)]+\exp(-\beta i)\}\gamma,$$

where β is a parameter to be determined later.

Although the form of this function is certainly not correct, it does exhibit the general characteristics desired, namely, that the outer segments of the molecule experience the full solvent flow whereas those usually near the center experience nearly zero flow. It will be shown subsequently that $\beta^2 \sim 1/N$ and is of that order of magnitude.

It is a simple matter to include this shielding factor in our previous calculation. After dropping terms which are not important except at very large shear rates, we obtain the result

$$\eta-\eta_s = \nu(fa^2N/18\beta)\{1-Q(\gamma\tau_1/N)^{\frac{1}{2}}\}, \qquad (7)$$

where

$$\tau_1 = (\eta-\eta_s)(6\beta N/\pi^2 kT\nu)$$

and

$$Q = (\pi/2)\csc(3\pi/4)-(\tfrac{1}{4})(-\tfrac{3}{4}!)(\tfrac{3}{4}!) \cong 1.37.$$

To find β we need only compare the result of Eq. (7) for $\gamma \to 0$ with the more accurate calculations of Kirkwood and Riseman[10] or Debye and A. M. Bueche.[11] We have used the K. R. result since the model used there is more like our own. However, the D.B. treatment differs from it only by a factor of about two in this limit. After making this comparison we find that

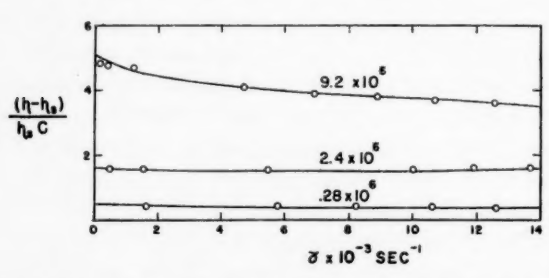

FIG. 3. The variation of viscosity with shear rate for polystyrene of various molecular weights in cyclohexane at 65°C. The points are from reference 8, the lines are calculated from Eq. (8).

[10] J. G. Kirkwood and J. Riseman, J. Chem. Phys. **16**, 565 (1948).
[11] P. Debye and A. M. Bueche, J. Chem. Phys. **16**, 573 (1948).

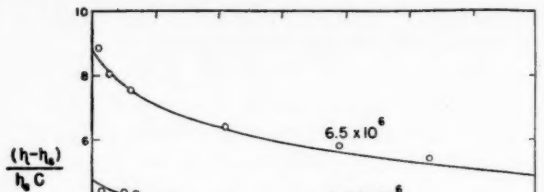

FIG. 4. The variation of viscosity with shear rate for polystyrene of various molecular weights in benzene at 25°C. The points are from reference 8, the lines are calculated from Eq. (8).

$\beta^2 \cong 4/Z$ and

$$\eta-\eta_s = (\eta_0-\eta_s)\{1-(\tau_0\gamma)^{\frac{1}{2}}\}, \qquad (8)$$

where

$$\tau_0 = 1.98(r/b)(\eta-\eta_s)(MM_0)^{\frac{1}{2}}/AkTc.$$

In the above expressions, c is the concentration of polymer in the solution (g/cc), M_0 is the molecular weight associated with each chain link (i.e., one-half the monomer molecular weight for vinyl type polymers), and A is Avogadro's number. The quantities r, b, and Z come in for the following reasons. We have replaced f by the friction factor for a Stokes' sphere, namely, $6\pi\eta_s r$. Kirkwood and Riseman, on the other hand, use a chain unit of length b, there being Z such units in a molecule. It is important to notice that the only quantity in Eq. (8) which is not directly measurable is the ratio (r/b). However, this quantity must be nearly constant for most polymer chains (possible exceptions being the cellulosics) and must be near unity. The exact value of (r/b) does not enter in a very sensitive fashion and so its choice is not critical. We have put it equal to 2.8 for the purposes of the figures but a closer examination of all the data when plotted against the square root of the shear rate indicates that a value of $(r/b) = 1.88$ is the most probable value. The important point is that we have considered it to be a constant independent of polymer type.

Equation (8) fits the available experimental data surprisingly well. This is shown in Figs. 3–6. Although the data were taken on different polymers at different temperatures in various solvents by independent investigators, they all agree almost within experimental error with our theoretical result. It should be emphasized that this good agreement is obtained without the aid of arbitrary parameters which can be varied as conditions vary. This fact allows us to predict in at least a semi-quantitative manner what the effect of shear rate will be on a given polymer solution at low concentrations. More precise data are needed at very low rates of shear in order to ascertain just how reliable the theory is in that region.

Equation (8) gives simple interpretations of several puzzling facts noticed by other investigators. One of the most important features of this theory is that it predicts the viscosity will decrease rather rapidly as the shear rate is increased. Other theories have predicted that the curve must begin at zero shear rate with a slope equal to zero. Experimental data on highly coiled polymers have indicated that this initial slope is different from zero as we predict. However, it should be noticed that even in our treatment a freely draining molecule should give rise to a zero initial slope.

Another question clarified by our result has to do with the change in shape of the viscosity *vs* rate of shear curves as the molecular weight of the polymer is increased. Some authors have speculated that the severe rate of shear dependence at low rates of shear observed for high molecular weight polymers might be the result of intermolecular entanglements. We have shown that such an interpretation is not necessary. The apparent change in shape of the curves with M is merely a manifestation of the fact that the decrease in viscosity is a function of $\gamma\tau_0$ and not of γ alone. Therefore, since τ_0 increases with M, an increase in M tends to compress the curve into the region of small shear rates. This results in an apparent change in shape of the curves.

Because of the fact that the decrease in viscosity with shear rate is a function of $\gamma\tau_0$ alone, we can make several additional predictions. We know that $\tau_0 \sim (\eta-\eta_s) \times (MM_0)^{\frac{1}{2}}/cT$ or in terms of the intrinsic viscosity $\tau_0 \sim [\eta]\eta_s(MM_0)^{\frac{1}{2}}/T$. From this, if the molecular weight, solvent viscosity, or intrinsic viscosity is increased, the viscosity will vary more rapidly with shear rate. The temperature dependence can become rather complicated, especially in poor solvents. This is clear from the fact that as T increases slightly, $[\eta]$ may increase a great deal in a poor solvent since the molecule will usually expand under such a change in conditions. We might therefore observe an increase in the rate of shear effect with temperature. However in a good solvent, the decrease in η_s/T with increasing temperature will usually outweigh any changes in $[\eta]$ and so the rate of shear effects will become less pronounced. This type of behavior has been found experimentally.[8]

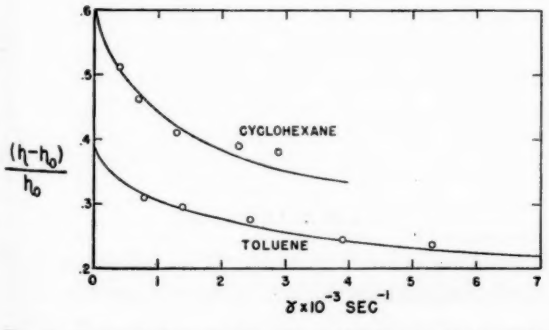

FIG. 5. The variation of viscosity with shear rate for polyisobutylene of $M=15\times10^6$ in two solvents. The points are from reference 7 and the lines are calculated from Eq. (8).

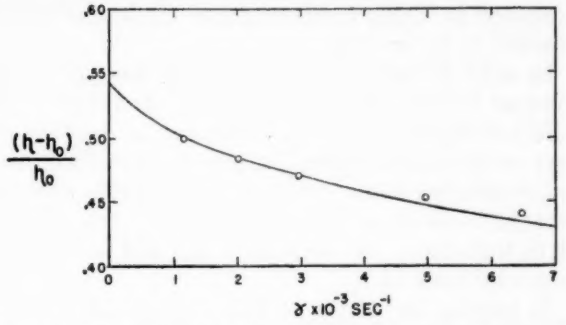

FIG. 6. The variation with shear rate for polymethyl methacrylate of $M=1.6\times10^6$ in chloroform at 30°C. The points are from reference 9, the line was calculated from Eq. (8).

It is also clear from the above result that polyelectrolytes and rather stiff cellulose type molecules will show very large rate of shear effects. Such large shear effects are a reflection of the well-known fact that these molecules are very large (in a geometrical sense) and therefore have large (η). We should be careful when applying our result to such problems because these very extended molecules may actually act more like rods than like balls. In that event, the complication of the orientation of the rods must also be considered.

PART B: BULK POLYMERS

We have previously presented reasons for thinking that viscous flow in the solid polymer is not basically different from the case of "free draining" dilute solutions of coiled polymers.[12] This applies only if the temperature is so high that the effect is largely viscous rather than elastic. In essence, it was pointed out that the free draining treatment of dilute solution viscosity assumes that the shape of the flow lines in the solution is not altered by the presence of the polymer molecule. This assumption should be reasonably valid in the case of the pure polymer. A theory for viscous flow in the pure polymer based upon this assumption has been presented and it was found to lead to a result in essential agreement with observed behavior.[12]

In view of the success of the free draining calculation when applied to the case of the bulk viscosity of polymers, it is tempting to apply it in the present instance to calculate the influence of the rate of shear on the observed viscosity of a bulk polymer. To this approximation Eq. (6) will lead at once to the fact that the bulk viscosity η of the pure polymer is given by

$$\frac{\eta}{\eta_0}=1-\frac{6}{\pi^2}\sum_{n=1}^{N}\frac{\gamma^2\tau_1^2}{n^2(n^4+\gamma^2\tau_1^2)}\left[2-\frac{\gamma^2\tau_1^2}{n^4+\gamma^2\tau_1^2}\right], \qquad (9)$$

where $\tau_1=12\eta_0/\nu\pi^2kT$, with ν being the number of polymer molecules per unit volume. This function is

[12] F. Bueche, J. Chem. Phys. **20**, 1959 (1952).

tabulated in Table I where η/η_0 is equivalent in this instance to $(\eta-\eta_s)/(\eta_0-\eta_s)$.

In order to test the validity of this formula we can compare it with the data of Spencer and Dillon[13] for bulk polystyrene. Since the experimental data are not very accurate, it is more convenient and perhaps more meaningful to make comparison, not with the raw data, but with the empirical relation Spencer and Dillon fit to their data. We have done this and the result is shown in Table II.

In making use of the empirical formula of Spencer and Dillon, we have used $M=360\,000$ and $K=3.70\times10^{-4}$ for 100 percent polymer and $K=5.70\times10^{-4}$ for 95 percent polymer. It should be noticed that there are no adjustable parameters in the theoretical relation of Eq. (9).

The agreement between theory and the empirical experimental relation is not perfect, but even so, the difference is no larger than the error in the raw experimental data. For example, because of the uncertainty in extrapolating the experimental data to zero shear rate, η_0 may be off by a factor of two. The empirical constant K, used in the experimental relation, is actually an average value and the experiments indicate that its value may be uncertain by as much as 30 percent. Also, in the last column of Table II we list the experimental result for a 95 percent mixture of polystyrene and isopropyl benzene. Spencer and Dillon state that K increases up to this limit as one adds plasticizer and remains at this value until at least 20 percent plasticizer has been added. Our theory predicts no such rapid change (although at *high* plasticizer contents a transition between the free draining and shielded models must occur) and so the variation may in itself be a measure of the experimental error. It would therefore appear that more accurate data are needed to obtain a real test of Eq. (9). At the present time it appears that the deviations between the theory and the experimental data are about the same size as the estimated errors in the experimental values.

Several general features of the shear behavior can be seen by referring to Eq. (9). First, since $\nu\sim M^{-1}$, we see that the decrease in η with shear rate will vary with the product of $\gamma\tau_1$ or γM. Therefore, increasing the molecular weight by a factor of two should be equivalent to doubling the shear rate. Such a behavior was observed by Spencer and Dillon. Secondly, experiment shows that the variation of η/η_0 with shear *stress* is independent of η_0, the zero shear viscosity. This is predicted from Eq. (9) since $\eta\gamma$ equals the shear stress and so the ratio η/η_0 may be thought of as being a function of shear stress times τ_1/η, rather than $\gamma\tau_1$. But since τ_1/η is independent of η we have at once the fact that the variation of η/η_0 with shear *stress* should be independent of η_0 as Spencer and Dillon observed.

TABLE II. A comparison of the results of experiment and theory for the variation of the bulk viscosity of polystyrene with the shear gradient.

γ (sec^{-1})	$(\eta/\eta_0)_{\text{theory}}$	$(\eta/\eta_0)_{\text{expt 100}}$	$(\eta/\eta_0)_{\text{expt 95}}$
0.000	1.00	1.00	1.00
0.100	0.66	0.78	0.66
0.636	0.25	0.43	0.37
1.302	0.17	0.30	0.24
7.850	0.087	0.098	0.092

[13] R. S. Spencer and R. E. Dillon, J. Colloid Sci. 4, 241 (1949).

CONCLUSIONS

The theory of the dynamic behavior of polymer molecules outlined in a previous paper has been applied to the problem of the effect of rate of shear on polymeric viscosity. For dilute polymer solutions, the free draining approach is not adequate and shielding must be taken into account. When this is done, good agreement is obtained between theory and experiment. The theory contains only one unknown parameter, the ratio of the Stokes' sphere substituted for a freely orienting chain segment to the bond length of a chain segment in the Kirkwood-Riseman sense. The actual value of this constant is not critical. When it is put equal to about 2, rather good agreement is obtained with all the rate of shear data available for polystyrene, polyisobutylene, and polymethyl methacrylate of various molecular weights, in good and poor solvents, and over a wide temperature range.

When the free draining approach is applied to the rate of shear behavior for the pure bulk polymer (polystyrene), substantial agreement is obtained between theory and experiment without the aid of any arbitrary parameters. For reasons previously discussed, we would expect the free draining approach to be valid in this instance. Whether or not the agreement is quantitatively correct is still in doubt because of the rather large uncertainty in the experimental data. In any event, the theory predicts the general behavior found by experiment.

Since only one unknown quantity, the ratio of the two radii, appears in the dilute solution result, the rate of shear dependence of dilute solution viscosity may prove a convenient means for determining molecular weights if this ratio were known. Examination of the experimental data now available indicates that the ratio of the two radii is a constant for most types of polymers. Its most probable value appears to be 1.88.

ACKNOWLEDGMENT

The author is indebted to Dr. T. G. Fox for numerous valuable suggestions during the course of this work.

THE JOURNAL OF CHEMICAL PHYSICS VOLUME 22, NUMBER 9 SEPTEMBER, 1954

Microwave Spectrum and Structure of Benzonitrile*

DAVID R. LIDE, JR.
Department of Chemistry, Harvard University, Cambridge, Massachusetts
(Received April 19, 1954)

The rotational spectrum of benzonitrile has been studied in the one-centimeter region, and approximately twenty absorption lines have been fitted to the rigid asymmetric-rotor theory. The principal moments of inertia are 89.370, 326.740, and 416.183 AUA². The evidence indicates a planar symmetric structure with ring dimensions essentially the same as in benzene. The dipole moment is 4.14±0.05 Debye units.

SINCE the addition of a CN group to the benzene ring results in a fairly long, rod-like molecule, the rotational spectrum of benzonitrile is expected to be characteristic of a near-prolate symmetric rotor with dipole moment in the small inertial axis. The principal transitions of such a rotor are of the type $J,K\rightarrow J+1, K$, where K is the quantum number of the limiting prolate symmetric rotor. While each transition of given J would appear as a single line in the limiting symmetric case, the molecular asymmetry produces a $(2J+1)$-fold splitting, corresponding to the various possible values of K. These $2J+1$ lines will be grouped about a central frequency given by $(b+c)(J+1)$, and it can be shown that the lines of higher K will converge toward this central frequency in a regular manner. It is thus predicted that the benzonitrile spectrum will consist of a series of bands in which successive band-heads are separated by roughly equal frequency intervals. There is, of course, nothing to prevent the overlapping of adjacent bands.

The microwave spectrum has been observed on a commercial sample of benzonitrile which had been distilled and dried over calcium sulfate. The spectrum was found to be quite rich, but the lines were extremely broad and seemed surprisingly weak, in view of the large reported dipole moment. An extended search revealed several regions of very dense absorption separated by intervals of about 2800 mc. These regions were assigned as band-heads of high K values, although they actually contained far more individual lines than could be expected from a single rigid rotor. On the basis of this framework, however, it was possible to pick out the lines of $K=0$, 1, and 2, which are shifted far away from the band-heads and can thus be chosen with less ambiguity. In this way an assignment consistent with the rigid asymmetric-rotor theory was arrived at. A set of rotational constants was calculated which gave a good fit for some twenty-odd lines of the $J=6\rightarrow7$, $7\rightarrow8$, and $8\rightarrow9$ systems. The agreement of all the calculated and observed frequencies within a few hundred kilocycles (which is not much greater than the uncertainty in frequency measurements) is adequate evidence for the assignment. The close agreement further indicates that centrifugal distortion is negligible, as is to be expected in such a heavy molecule. The rotational constants used in the assignment are given in Table I, and in Table II the assigned transitions are listed. While many additional lines could certainly be assigned, there seems little point in further experimental and computational labor.

Attempts to study the Stark effect of benzonitrile encountered a number of difficulties. In addition to the large line breadths and highly cluttered spectrum, intensity considerations made it necessary to work with lines of high J values, which increased the difficulties with resolution. It was possible, however, to obtain a partial resolution of the Stark effects of a few favorable lines. A detailed analysis was made on the $7_{25}\rightarrow8_{26}$ transition at 23 111.1 mc. The necessary direction-cosine matrix elements were calculated by approximating the asymmetric-rotor wave functions with elliptic cylinder functions.[1] It is interesting to note that a significant contribution to the Stark effect of this transition comes from the interaction of the nearly degenerate $7_{25}-8_{08}$ and $8_{26}-9_{09}$ pairs. While such levels with K values differing by two cannot interact in the symmetric limit, there is sufficient asymmetry in this molecule ($\varkappa=-0.850$) to permit an appreciable interaction. The dipole moment determined from this Stark effect is 4.14±0.05 Debye units. This value falls at the top of the rather wide range (3.61 to 4.14) of some two dozen reported measurements by the solution method;[2] a previous measurement in the vapor state gave 4.39. It is felt that the Stark effect should give the most reliable value, since all difficulties with molecular association are eliminated.

While a great many isotopic species would be required to give a complete determination of the structure of benzonitrile, a certain amount of information can be

TABLE I. Parameters of benzonitrile.

$b-c=$	332.45 mc
$b+c=$	2761.30
$a-\frac{1}{2}(b+c)=$	4274.7
$I_a=$	89.370 AUA²
$I_b=$	326.740
$I_c=$	416.183

*The research reported in this paper was made possible by support extended Harvard University by the U. S. Office of Naval Research under ONR Contract N5ori-76, Task Order V.

[1] S. Golden, J. Chem. Phys. **16**, 78 (1948).
[2] Everard, Kumar, and Sutton, J. Chem. Soc. **1951**, 2807.

TABLE II. Assigned lines in benzonitrile.

Transition	Calculated frequency	Observed frequency
$6_{25}\rightarrow 7_{26}$	19 179.4 mc	19 179.5 mc
$6_{61}\rightarrow 7_{62}$ $6_{60}\rightarrow 7_{61}$	19 383.4	19 383.5
$6_{52}\rightarrow 7_{53}$ $6_{51}\rightarrow 7_{52}$	19 397.9	19 398.1
$6_{43}\rightarrow 7_{44}$ $6_{42}\rightarrow 7_{43}$	19 425.6	19 426.0
$6_{34}\rightarrow 7_{35}$	19 448.9	19 449.2
$6_{33}\rightarrow 7_{34}$	19 535.4	19 534.8
$6_{24}\rightarrow 7_{25}$	20 096.2	20 096.3
$6_{15}\rightarrow 7_{16}$	20 193.1	20 193.7
$7_{17}\rightarrow 8_{18}$	20 453.2	20 453.3
$7_{07}\rightarrow 8_{08}$	20 828.6	20 829.0
$7_{26}\rightarrow 8_{27}$	21 856.3	21 856.4
$7_{62}\rightarrow 8_{63}$ $7_{61}\rightarrow 8_{62}$	22 163.5	22 163.1
$7_{53}\rightarrow 8_{54}$ $7_{52}\rightarrow 8_{53}$	22 185.2	22 184.7
$8_{18}\rightarrow 9_{19}$	22 938.1	22 937.9
$7_{16}\rightarrow 8_{17}$	22 943.8	22 943.7
$7_{25}\rightarrow 8_{26}$	23 111.2	23 111.1
$8_{08}\rightarrow 9_{09}$	23 228.1	23 227.9
$8_{27}\rightarrow 9_{28}$	24 509.9	24 509.3
$8_{72}\rightarrow 9_{73}$ $8_{71}\rightarrow 9_{72}$	24 929.9	24 929.1
$8_{63}\rightarrow 9_{64}$ $8_{62}\rightarrow 9_{63}$	24 948.1	24 948.7
$8_{54}\rightarrow 9_{55}$ $8_{53}\rightarrow 9_{54}$	24 978.9	24 978.6
$8_{36}\rightarrow 9_{46}$	25 033.0	25 032.7

drawn from the present data on the common species. First, the expected planarity of the molecule is confirmed by the smallness of the inertial defect ($I_c-I_a-I_b=0.073$); furthermore, the presence of a twofold axis (and hence, almost certainly, of C_{2v} symmetry) was demonstrated by observing the intensity alternation which results from the proton nuclear spins. If two pairs of protons can be exchanged by a 180° rotation about the small inertial axis, then the lines of even K will be enhanced over those of odd K by a factor of 10:6. An intensity alternation of this magnitude was found in the benzonitrile spectrum.

Since benzonitrile has been shown to have a planar symmetric structure, the moment of inertia about the symmetry axis should be comparable to the appropriate moment of benzene. The value of I_a determined here agrees quite closely with the benzene moment of 88.95 as determined from the rotational raman spectrum;[3] it seems likely, then, that the addition of the CN group causes no significant distortion of the ring dimensions. Thus if we assume hexagonal symmetry for the ring and a C−H distance of 1.080A, the value of I_a leads to a C−C distance in the ring of 1.402A. If it is further assumed that the C−N distance is 1.158A (the value found in several similar −CN compounds[4]) then the remaining experimental moment fixes the C−C single-bond distance as 1.419A. The decrease from the normal single-bond distance is clearly the result of resonance between the C−N triple bond and the ring, which tends to increase the bond order of the intervening C−C bond. In fact, the length of this bond in C_6H_5-CN falls in a logical position between the corresponding lengths in H_3C-CN (1.460) and HCC−CN (1.382).

Two further points should be mentioned. The unusual line widths in benzonitrile (at least 2 mc under the best experimental conditions) imply a very large collision cross section. In fact, rough measurements indicate an effective collision diameter of from 40 to 60A. While this diameter is much greater than normally encountered in microwave work, it is not too surprising when both the large physical size and the very high dipole moment of benzonitrile are taken into consideration. It should be noted that for the transitions studied here the calculated interaction of the nitrogen quadrupole moment results in a splitting of only about 0.05 mc, and thus makes a negligible contribution to the broadening.

Only about one-quarter of the observed lines were actually assigned, although these included all the strong lines. It is probable that the majority of the remaining lines are due to molecules in excited vibrational states. While there is little available vibrational data on benzonitrile, it seems likely that three or four fundamentals will be below 500 cm^{-1}, and at room temperature the population of each of these states will be ten percent or more of the ground state. Since each of these states will have a rotational spectrum which is as rich as the ground state, the number of observed lines seems a reasonable order of magnitude. Although an effort was made to find regularities among the unassigned lines, the spectrum was too dense to permit any progress in this direction.

[3] B. Stoicheff, J. Chem. Phys. **21**, 1410 (1953).

[4] Bond distances are taken from Gordy, Smith, and Trambarulo, *Microwave Spectroscopy* (John Wiley and Sons, Inc., New York, 1953), p. 371.

Lattice Vibrational Spectrum of Imperfect Crystals*†

KENNETH F. STRIPP‡ AND JOHN G. KIRKWOOD
Sterling Chemistry Laboratory, Yale University, New Haven, Connecticut
(Received January 7, 1954)

The influence of lattice defects on the normal modes of vibration of crystals is investigated by means of perturbation theory. The calculations have been carried to the second order, and the effect of holes on the vibrational partition function has been determined. It is found that through their influence on the lattice vibrational free energy, a pair of holes in a crystal attract each other with an average force whose potential diminishes asymptotically as $1/R^6$.

INTRODUCTION

IN the statistical-mechanical treatment of order-disorder equilibria in crystal lattices, it is usual to assume that the degree of order has only a negligibly small effect on the lattice waves and, hence, on the vibrational partition function.[1] This then reduces the problem to a purely static one. Now it is not *a priori* apparent that this neglect is always justifiable, and intuition suggests that in the case of Schottky (and Frenkel) defects the inadequacy of this procedure could be the most marked. We have, therefore, undertaken to calculate the influence of Schottky defects on the vibrational part of the crystal partition function.

For simplicity in this initial work we have limited our consideration to a classical, close packed, monatomic crystal in the nearest neighbor, harmonic approximation, but it will be apparent that the methods devised are capable of extension and elaboration. The results show that the influence of defects of this kind increases in relative importance with the absolute temperature. At temperatures comparable to $T=-zV/k$, where V is the static binding potential and z is the coordination number, the static and the vibrational parts of the partition function are equally sensitive.

DYNAMICS

We begin by considering a crystal consisting of $N-n$ atoms and n vacancies (holes) on N lattice sites:

$$\mathbf{R}_j=j_1\mathbf{a}_1+j_2\mathbf{a}_2+j_3\mathbf{a}_3;\quad 0\leqslant j_i<N^{\frac{1}{3}},\tag{1}$$

the $\mathbf{a}_i$ being the primitive lattice vectors. For convenience we choose $|\mathbf{a}_i|$ as our unit of length. In the nearest neighbor, harmonic approximation the potential energy can then be written:

$$U=\tfrac{1}{2}\sum_j\sum_{j'}\eta_j\eta_{j'}\times\left\{\lambda_{jj'}V-\frac{m}{2}(\mathbf{r}_{j'}-\mathbf{r}_j)\cdot\boldsymbol{\Omega}_{jj'}\cdot(\mathbf{r}_{j'}-\mathbf{r}_j)\right\},\tag{2}$$

$$\boldsymbol{\Omega}_{jj'}=-\frac{\alpha}{m}\lambda_{jj'}\mathbf{R}_{jj'}\mathbf{R}_{jj'},$$

where the j sums extend over all the lattice sites, V is the minimum interatomic potential, α is the second derivative of V at the minimum, m is the atomic mass, $\mathbf{R}_{jj'}$ is the vector distance between the equilibrium lattice sites j and j', $\mathbf{r}_j$ is the displacement from equilibrium at site j, $\lambda_{jj'}$ is the nearest neighbor selector factor defined as

$$\lambda_{jj'}=\begin{cases}1, \text{ for } j \text{ and } j' \text{ nearest neighbors,}\\ 0, \text{ all others,}\end{cases}\tag{3}$$

and the η_j are occupation variables defined as

$$\eta_j=\begin{cases}1, \text{ if site } j \text{ is occupied by an atom,}\\ 0, \text{ if site } j \text{ is vacant.}\end{cases}\tag{4}$$

With this form of potential we are ignoring, in addition to the anharmonic terms, the effects of thermal expansion and any relaxation of the structure about the defects. These factors would have to be included in a more refined treatment.

The kinetic energy of the system is simply

$$T=\frac{m}{2}\sum_j\eta_j\dot{\mathbf{r}}_j\cdot\dot{\mathbf{r}}_j.\tag{5}$$

The Lagrangian composed of (2) and (5) gives the equations of motion:

$$\eta_j\left\{\frac{d^2}{dt^2}\mathbf{r}_j+\sum_{j'}\eta_{j'}\boldsymbol{\Omega}_{jj'}\cdot(\mathbf{r}_j-\mathbf{r}_{j'})\right\}=0.\tag{6}$$

With a complementary occupation variable defined as

$$\rho_j=\begin{cases}1, \text{ if site } j \text{ is occupied by a hole,}\\ 0, \text{ if otherwise,}\end{cases}\tag{7}$$

* (Contribution No. 1202 from the Sterling Chemistry Laboratory, Yale University).

† From a dissertation submitted to the Graduate Faculty of Yale University in partial fulfillment of the requirements for the degree of Doctor of Philosophy.

‡ Present address, R.C.A. Laboratories, Princeton, New Jersey.

[1] See, for example, R. Fowler and E. A. Guggenheim, *Statistical Thermodynamics* (Cambridge University Press, Cambridge, 1949), Chap. XIII.

so that

$$\rho_j+\eta_j=1;\quad \sum_j \rho_j=n. \tag{8}$$

Equation (6) can be arranged in the more suggestive form:

$$\frac{d^2}{dt^2}\mathbf{r}_j+\sum_{j'}\mathbf{\Omega}_{jj'}\cdot(\mathbf{r}_j-\mathbf{r}_{j'})=H_j+F_j, \tag{9}$$

with

$$H_j=\rho_j\left\{\frac{d^2}{dt^2}\mathbf{r}_j+\sum_{j'}\mathbf{\Omega}_{jj'}\cdot(\mathbf{r}_j-\mathbf{r}_{j'})\right\},$$
$$F_j=\eta_j\{\sum_{j'}\rho_{j'}\mathbf{\Omega}_{jj'}\cdot(\mathbf{r}_j-\mathbf{r}_{j'})\}. \tag{10}$$

When all the ρ_j vanish, H_j and F_j are identically zero, and the resultant system of equations becomes exactly that for a defectless crystal. When holes are present, we shall regard the occasional nonvanishing right-hand member as a perturbation acting on the defectless system, whose eigenwaves we presume to know.

The perturbation has been written in two parts. F_j is due to the altered restoring forces on the atoms bordering a hole. H_j, which is an equation of motion for an apparent atom at a hole site, results from forcing the left-hand side of (9) to be completely identical in form with the equations for a defectless crystal. While the propriety of this latter device may seem questionable at this stage, it will be seen later that this term makes no contribution to the final result. Its inclusion here proves convenient in exploiting the orthonormality property of the unperturbed amplitudes.

FORMAL PERTURBATION TREATMENT

If periodic boundary conditions are imposed, the normal mode analysis of the unperturbed system can be carried out conveniently in terms of the running waves:[2,3]

$$\mathbf{r}_j=\mathbf{A}_j(\zeta,\mathbf{k})\exp[-i\omega_0(\zeta,\mathbf{k})t], \tag{11}$$

$$\mathbf{A}_j(\zeta,\mathbf{k})=N^{-\frac{1}{2}}\boldsymbol{\varepsilon}(\zeta,\mathbf{k})\exp(i\mathbf{k}\cdot\mathbf{R}_j), \tag{12}$$

where $\omega_0(\zeta,\mathbf{k})$ is the frequency of the wave with wave-number vector $\mathbf{k}$, $\boldsymbol{\varepsilon}(\zeta,\mathbf{k})$ is a unit polarization vector, and ζ takes the values 1, 2, 3 to distinguish the three polarizations associated with each $\mathbf{k}$. The wave number vector is restricted to the N values

$$\mathbf{k}=\frac{2\pi}{N^{\frac{1}{3}}}[k_1\mathbf{a}^1+k_2\mathbf{a}^2+k_3\mathbf{a}^3], \tag{13}$$

where the $\mathbf{a}^i$ are the primitive vectors in the reciprocal lattice and the k_i are integers in the range

$$-(N^{\frac{1}{3}})/2<k_i\leqslant(N^{\frac{1}{3}})/2. \tag{14}$$

The polarization vectors for a given $\mathbf{k}$ are mutually orthogonal:

$$\boldsymbol{\varepsilon}(\zeta,\mathbf{k})\cdot\boldsymbol{\varepsilon}(\zeta',\mathbf{k})=\delta_{\zeta\zeta'}, \tag{15}$$

$$\sum_\zeta \boldsymbol{\varepsilon}(\zeta,\mathbf{k})\boldsymbol{\varepsilon}(\zeta,\mathbf{k})=\mathbf{1}, \tag{16}$$

and the amplitudes (12) satisfy the orthonormality condition:

$$\sum_j \mathbf{A}_j^*(\zeta',\mathbf{k}')\cdot\mathbf{A}_j(\zeta,\mathbf{k})=\delta_{\zeta\zeta'}\delta_{\mathbf{k}\mathbf{k}'}. \tag{17}$$

Substitution of (11) into (9), with no perturbation, leads to

$$\omega_0^2(\zeta,\mathbf{k})\boldsymbol{\varepsilon}(\zeta,\mathbf{k})+\sum_{j'}\mathbf{\Omega}_{jj'}\cdot\boldsymbol{\varepsilon}(\zeta,\mathbf{k})[1-\exp(i\mathbf{k}\cdot\mathbf{R}_{jj'})]=0, \tag{18}$$

as the eigenvalue problem which determines the frequencies and the polarization vectors.

The waves (11) are highly degenerate, both from the equivalence of certain of them through crystal symmetry as well as from accidental degeneracies. The latter would be more difficult to recognize. To apply the perturbation method, we group the $3N$ amplitudes into S degenerate sets s:

$$s=1, 2, 3, \cdots S, \tag{19}$$

say in order of increasing frequency $\omega_0(s)$. The members of each set we assume suitably numbered

$$\mathbf{A}_j(n,s);\quad n=1, 2, \cdots\sigma_s, \tag{20}$$

where σ_s represents the number of waves in set s, and hence

$$\sum_s \sigma_s=3N. \tag{21}$$

For the perturbed amplitudes we write

$$\mathbf{B}_j(t,s)=\mathbf{B}_j^0(t,s)+\mathbf{B}_j^I(t,s)+\cdots, \tag{22}$$

with

$$\mathbf{B}_j^0(t,s)=\sum_{n=1}^{\sigma_s}\alpha_{tn}(s)\mathbf{A}_j(n,s);\quad t=1, 2, \cdots\sigma_s, \tag{23}$$

$$\mathbf{B}_j^I(t,s)=\sum_{s'\neq s}\sum_{n=1}^{\sigma_{s'}}\beta_{tn}(s,s')\mathbf{B}_j^0(n,s'); \tag{24}$$

and for the perturbed frequencies,

$$\omega^2(t,s)=\omega_0^2(s)+\omega_I^2(t,s)+\omega_{II}^2(t,s)+\cdots. \tag{25}$$

The implicit assumption is, of course, that $\mathbf{B}_j^I$ and the frequency shifts will be small. The proper zero-order amplitudes (23) are equally good solutions for the unperturbed system, and satisfy

$$\omega_0^2(s)\mathbf{B}_j^0(t,s)+\sum_{j'}\mathbf{\Omega}_{jj'}\cdot[\mathbf{B}_j^0(t,s)-\mathbf{B}_{j'}^0(t,s)]=0. \tag{26}$$

First-order perturbation treatment now gives

$$\omega_I^2(t,s)=F(t,s;t,s), \tag{27}$$

$$0=F(n,s;t,s);\quad n\neq t, \tag{28}$$

$$\beta_{tn}(s,s')=\frac{F(n,s';t,s)}{\omega_0^2(s)-\omega_0^2(s')}, \tag{29}$$

[2] M. Born and M. G. Mayer, *Handbuch der Physik* (1933), second edition, Vol. 24, part 2, p. 623 ff.

[3] F. Seitz, *Modern Theory of Solids* (McGraw-Hill Book Company, Inc., New York, 1940), Chap. III.

in terms of the matrix elements

$$F(n,s';t,s)=\sum_j\sum_{j'}\eta_j\rho_{j'}\mathbf{B}_j{}^{0*}(n,s')\cdot\mathbf{\Omega}_{jj'}\cdot[\mathbf{B}_j{}^0(t,s)-\mathbf{B}_{j'}{}^0(t,s)]. \quad (30)$$

The perturbation H_j makes no contribution here in view of (26). Diagonalization of the degenerate submatrix is represented by the $\sigma_s(\sigma_s-1)$ conditions (28), which, together with the σ_s normalization conditions

$$\sum_{n=1}^{\sigma_s}\alpha_{tn}{}^*(s)\alpha_{tn}(s)=1;\quad t=1,2,\cdots\sigma_s, \quad (31)$$

serve to evaluate the coefficients in (23). We shall see that it is not necessary to evaluate these coefficients explicitly.

The second-order calculation provides

$$\omega_{II}{}^2(t,s)=F(t,s;t,s)I(t,s;t,s)+\sum_{s'\neq s}\sum_{n=1}^{\sigma_{s'}}F(n,s';t,s)I(t,s;n,s')+\sum_{s'\neq s}\sum_{n=1}^{\sigma_{s'}}\frac{F(t,s;n,s')F(n,s';t,s)}{\omega_0{}^2(s)-\omega_0{}^2(s')}, \quad (32)$$

where the additional matrix element

$$I(t,s;n,s')=\sum_j\rho_j\mathbf{B}_j{}^{0*}(t,s)\cdot\mathbf{B}_j{}^0(n,s') \quad (33)$$

arises from H_j.

VIBRATIONAL PARTITION FUNCTION

If we write the perturbed frequencies as

$$\omega^2(t,s)=\omega_0{}^2(s)\left[1+\frac{\omega_I{}^2(t,s)}{\omega_0{}^2(s)}+\frac{\omega_{II}{}^2(t,s)}{\omega_0{}^2(s)}+\cdots\right], \quad (34)$$

the logarithm of the classical vibrational partition function[4] can be expanded as

$$\ln Q_v=\ln Q_v{}^0+\ln Q_v{}^I+\ln Q_v{}^{II}+\cdots, \quad (35)$$

with

$$\ln Q_v{}^0=3N\ln\frac{kT}{\hbar}-\tfrac{1}{2}\sum_s\sum_{t=1}^{\sigma_s}\ln\omega_0{}^2(s), \quad (36)$$

$$\ln Q_v{}^I=-\tfrac{1}{2}\sum_s\omega_0{}^{-2}(s)\sum_{t=1}^{\sigma_s}\omega_I{}^2(t,s), \quad (37)$$

$$\ln Q_v{}^{II}=-\tfrac{1}{2}\sum_s\omega_0{}^{-2}(s)\times\sum_{t=1}^{\sigma_s}\{\omega_{II}{}^2(t,s)-\tfrac{1}{2}\omega_0{}^{-2}(s)\omega_I{}^4(t,s)\}. \quad (38)$$

The use of the $3N$ frequencies (34) in (35)–(38) implies a system of $3N$ degrees of freedom, whereas our crystal of $N-n$ atoms and n holes has only $3(N-n)$. Since, in the Born-von Kármán crystal, the contribution per atom to the vibrational partition function is, for large systems, quite insensitive to the size of the system, we shall regard these expressions as correct if they are reduced by the factor $[1-(n/N)]$. Rather than make this adjustment explicitly, however, we shall use the results as they stand to apply, from here on, to a crystal of N atoms and

$$nN/(N-n)\approx n \quad (39)$$

holes.

Inserting (27) into (37) we have

$$\ln Q_v{}^I=-\tfrac{1}{2}\sum_s\omega_0{}^{-2}(s)\sum_{t=1}^{\sigma_s}F(t,s;t,s). \quad (40)$$

Now the t sum in (40) is just the trace of the degenerate submatrix of the set s, and this quantity is invariant to the transformation (23). Hence, it can be replaced by the sum of the analogous matrix elements formed with the plane waves of the set. Then, regrouping the total summation in (40), we have for the first-order term

$$\ln Q_v{}^I=-\tfrac{1}{2}\sum_{\mathbf{k}}\sum_{\zeta}\omega_0{}^{-2}(\zeta,\mathbf{k})F(\zeta,\mathbf{k};\zeta,\mathbf{k}). \quad (41)$$

Inserting (27) and (32) into (38), and using (28) for formally removing the restriction on some of the summations, we have

$$\ln Q_v{}^{II}=-\tfrac{1}{2}\sum_s\sum_{s'}\sum_{t=1}^{\sigma_s}\sum_{n=1}^{\sigma_{s'}}\omega_0{}^{-2}(s)F(n,s';t,s)I(t,s;n,s')-\tfrac{1}{2}\sum_s\sum_{t=1}^{\sigma_s}\left\{\frac{F^2(t,s;t,s)}{2\omega_0{}^4(s)}-\sum_{s'\neq s}\sum_{n=1}^{\sigma_{s'}}\frac{F(n,s';t,s)F(t,s;n,s')}{\omega_0{}^2(s)[\omega_0{}^2(s)-\omega_0{}^2(s')]}\right\}. \quad (42)$$

Since the total sum in (42) will not be altered by interchanging indices s and t with s' and n, we can replace (42) by half the sum of itself and the like expression with the interchange, and obtain

$$\ln Q_v{}^{II}=-\tfrac{1}{2}\sum_s\sum_{s'}\sum_{t=1}^{\sigma_s}\sum_{n=1}^{\sigma_{s'}}\left\{\omega_0{}^{-2}(s)F(n,s';t,s)I(t,s;n,s')-\frac{1}{2}\frac{F(n,s';t,s)F(t,s;n,s')}{\omega_0{}^2(s)\omega_0{}^2(s')}\right\}, \quad (43)$$

wherein we have succeeded in eliminating the "resonance denominator." Now the sums for a given s and s':

$$\sum_{t=1}^{\sigma_s}\sum_{n=1}^{\sigma_{s'}}F(n,s';t,s)I(t,s;n,s'), \quad (44)$$

$$\sum_{t=1}^{\sigma_s}\sum_{n=1}^{\sigma_{s'}}F(n,s';t,s)F(t,s;n,s'), \quad (45)$$

are also invariant under the transformation (23), so we

[4] For example, J. F. Mayer and M. G. Mayer, *Statistical Mechanics* (John Wiley and Sons, Inc., New York, 1940), p. 240.

can likewise use the plane wave matrix elements in (43):

$$\ln Q_v^{II} = -\tfrac{1}{2}\sum_{\mathbf{k}}\sum_{\mathbf{k}'}\sum_{\zeta}\sum_{\zeta'} \times\left\{\omega_0^{-2}(\zeta,\mathbf{k})F(\zeta',\mathbf{k}';\zeta,\mathbf{k})I(\zeta,\mathbf{k};\zeta',\mathbf{k}') -\tfrac{1}{2}\frac{F(\zeta',\mathbf{k}';\zeta,\mathbf{k})F(\zeta,\mathbf{k};\zeta',\mathbf{k}')}{\omega_0^2(\zeta,\mathbf{k})\omega_0^2(\zeta',\mathbf{k}')}\right\}. \quad (46)$$

By the property

$$N^{-1}\sum_{\mathbf{k}}\exp(-\mathbf{k}\cdot\mathbf{R}_{jj'}) = \delta_{jj'}, \quad (47)$$

and (4), (7), and (16), the first sum in (46) readily can be shown to vanish. Hence, H_j makes no contribution in second order, and

$$\ln Q_v^{II} = \tfrac{1}{4}\sum_{\mathbf{k}}\sum_{\mathbf{k}'}\sum_{\zeta}\sum_{\zeta'}\frac{F(\zeta',\mathbf{k}';\zeta,\mathbf{k})F(\zeta,\mathbf{k};\zeta',\mathbf{k}')}{\omega_0^2(\zeta,\mathbf{k})\omega_0^2(\zeta',\mathbf{k}')}. \quad (48)$$

Thus the degeneracy can be ignored in the evaluation of the partition function, and the virtually impossible diagonalization process (23) is not required.

FIRST ORDER, SPECIAL CASES

With the plane wave matrix elements in (41), the first-order correction is

$$\ln Q_v^{I} = \frac{\alpha}{2mN}\sum_{\mathbf{k}}\sum_{j}\sum_{j'}\eta_j\rho_{j'}\lambda_{jj'}\mathbf{R}_{jj'} \cdot\mathbf{M}^{-1}(\mathbf{k})\cdot\mathbf{R}_{jj'}[1-\exp(i\mathbf{k}\cdot\mathbf{R}_{jj'})], \quad (49)$$

$$\mathbf{M}^{-1}(\mathbf{k}) = \sum_{\zeta}\varepsilon(\zeta,\mathbf{k})\varepsilon(\zeta,\mathbf{k})\omega_0^{-2}(\zeta,\mathbf{k}). \quad (50)$$

Case 1

When no holes are contiguous neighbors, the η_j can be suppressed in (49). Summing over j by (18) we find the frequency in the denominator to be canceled. Then the remaining sums are readily performed, yielding

$$\ln Q_v^{I} = \tfrac{3}{2}n. \quad (51)$$

Case 2

If contiguous holes occur, but are in such array that their $\mathbf{R}_{jj'}$ are distributed uniformly over the z possible directions, we can substitute in (49)

$$\eta_j \rightarrow 1-(2p/zn), \quad (52)$$

where p is the total number of contiguous pairs. Then the same summation sequence as above gives

$$\ln Q_v^{I} = \tfrac{3}{2}\left(n-\frac{2p}{z}\right), \quad (53)$$

a result which will be found valid generally in the next section.

A simple physical deduction of (53) can be given. The unperturbed crystal may be regarded as consisting of $Nz/2$ springs and N masses, for a "total restoring force constant" $Nz\alpha/2$, and a total mass Nm. The geometric mean of the squares of the lattice frequencies we may take as proportional to the ratio of these latter two quantities:

$$\langle\omega_0^2\rangle_{Av} = c\frac{z\alpha}{2m}. \quad (54)$$

When n holes are present, the number of springs is reduced to $(N-n)z/2+p$, and the new mean of the squared frequencies, found from the new ratio, is

$$\langle\omega^2\rangle_{Av} = \langle\omega_0^2\rangle_{Av}\left[1-\frac{1}{N}\left(n-\frac{2p}{z}\right)\right]. \quad (55)$$

Using (55) in (34) and (37), we are led directly to (53).

FIRST ORDER, GENERAL CASE

The matrix inverse to (50) is shown readily, by (15), to be

$$\mathbf{M}(\mathbf{k}) = \sum_{\zeta}\varepsilon(\zeta,\mathbf{k})\varepsilon(\zeta,\mathbf{k})\omega_0^2(\zeta,\mathbf{k}). \quad (56)$$

We evaluate this quantity by substituting (18) and replacing the sum over nearest neighbors there by a surface integral. Then, with (56) in diagonal form, we invert to obtain a convenient power expansion for (50). The details are given in Appendix I; the result is

$$\mathbf{M}^{-1}(\mathbf{k}) = \frac{30m}{\alpha z}\Bigg[1\left(\frac{1}{k^2}+3.57143\times10^{-2} +6.14135\times10^{-4}k^2+7.36225\times10^{-6}k^4\cdots\right) -\frac{\mathbf{kk}}{k^2}\left(\frac{2}{3k^2}+1.58730\times10^{-2} -0.52490\times10^{-4}k^2 -9.21415\times10^{-6}k^4\cdots\right)\Bigg]. \quad (57)$$

In this expansion the inverse square terms in k are the equivalent of the Debye frequency approximation, and the higher terms represent corrections for the high-frequency dispersion in the discrete structure.

With (57) inserted into (49), we next replace, for simplicity, the sums over the rhombohedral domain in $\mathbf{k}$ space by an integral over an equal spherical volume. This reduces the $\mathbf{k}$ sum to terms of the form

$$N^{-1}\sum_{\mathbf{k}}\mathbf{M}^{-1}(\mathbf{k})\exp(i\mathbf{k}\cdot\mathbf{R}) = \frac{30m}{\alpha z}\left\{1\sum_{i=0}^{3}X_i(R)+\frac{\mathbf{RR}}{R^2}\sum_{i=0}^{3}Y_i(R)\right\}, \quad (58)$$

where the serial components in X and Y are the

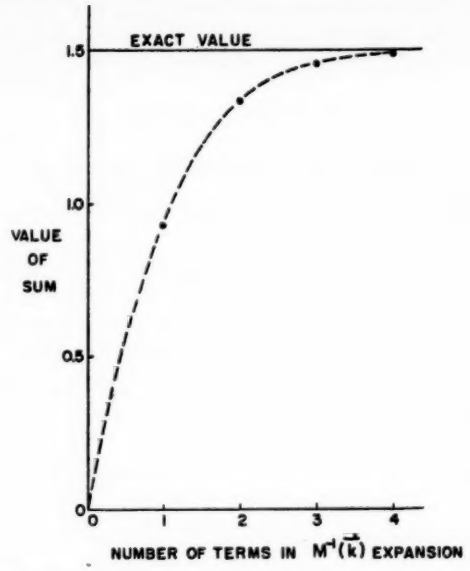

FIG. 1. Convergence rate of $\mathbf{M}^{-1}(\mathbf{k})$ in

$$-\tfrac{1}{2}\sum_{\mathbf{k}}\sum_{\zeta}\frac{F(\zeta,\mathbf{k};\zeta,\mathbf{k})}{\omega_0^2(\zeta,\mathbf{k})}=\tfrac{3}{2}.$$

counterparts of the Debye and dispersion terms in (57). The details of the operation and the forms of X and Y are given in Appendix II.

With the $\mathbf{k}$ sums thus performed in (49), the remaining j sums are simple, and give

$$\ln Q_v^{\,I}=\left(n-\frac{2p}{z}\right)\times\sum_{i=0}^{3}15\{X_i(0)+Y_i(0)-X_i(1)-Y_i(1)\}. \quad (59)$$

Table I contains the appropriate quantities for the evaluation of this expression. The partial sums are 0.9348, 1.341, 1.462, and 1.494. Thus, the Debye frequency approximation gives about $\frac{2}{3}$ the correct value, but with the inclusion of three orders of dispersion correction, the result is essentially exact (by comparison with (51) for $p=0$). This convergence is shown graphically in Fig. 1.

We have found, therefore, that each hole contributes equally and independently to the first-order correction, provided it is not a contiguous neighbor of another hole. Nearest neighbor pairs of holes, however, contribute to a different (lesser) extent. This is entirely analogous to the like *versus* unlike pair interactions in the static order-disorder problem.

SECOND ORDER

The second-order correction to $\ln Q_v$ depends on the interaction of pairs of holes, whether nearest neighbors or not. Using the plane wave matrix elements in (48), we can write the second-order term as

$$\ln Q_v^{\,II}=\sum_{j'}\sum_{l'}\rho_{j'}\rho_{l'}\ln Q_v^{\,II}(j',l'), \quad (60)$$

in which

$$\begin{aligned}\ln Q_v^{\,II}(j',l')&=\tfrac{1}{4}\sum_{\mathbf{k}}\sum_{\mathbf{k}'}\sum_{j}\sum_{l}\eta_j\eta_l\lambda_{jj'}\lambda_{ll'}\\&\times\mathbf{R}_{jj'}\cdot\mathbf{M}^{-1}(\mathbf{k})\cdot\mathbf{R}_{ll'}\mathbf{R}_{ll'}\cdot\mathbf{M}^{-1}(\mathbf{k}')\cdot\mathbf{R}_{jj'}\\&\times\{\exp(i\mathbf{k}\cdot\mathbf{R}_{ll'})-\exp[i(\mathbf{k}-\mathbf{k}')\cdot R_{ll'}]\}\\&\times\{\exp(i\mathbf{k}'\cdot R_{jj'})-\exp[i(\mathbf{k}'-\mathbf{k})\cdot\mathbf{R}_{jj'}]\}\\&\times\exp[i(\mathbf{k}-\mathbf{k}')\cdot(\mathbf{R}_{j'}-\mathbf{R}_{l'})], \quad (61)\end{aligned}$$

represents the contribution from a pair of holes at sites j' and l'. This interaction by hole pairs over a distance greater than the presumed effective interaction distance between the atoms comprising the crystal comes about through the mutual influence of the hole pair on the crystal vibrational wave field. The dependence of this interaction on the distance between the holes, $\mathbf{R}_{j'}-\mathbf{R}_{l'}$, is reflected in the final exponential term in (61).

Again applying the devices of Appendixes I and II, we reduce (61) to

$$\begin{aligned}\ln Q_v^{\,II}(j',l')&=\frac{900}{4z^2}\sum_{j}\sum_{l}\eta_j\eta_l\lambda_{jj'}\lambda_{ll'}\mathbf{R}_{ll'}\cdot\left\{\mathbf{1}[X(R_{lj'})-X(R_{lj})]\right.\\&\left.+\frac{\mathbf{R}_{lj'}\mathbf{R}_{lj'}}{|\mathbf{R}_{lj'}|^2}Y(R_{lj'})-\frac{\mathbf{R}_{lj}\mathbf{R}_{lj}}{|\mathbf{R}_{lj}|^2}Y(R_{lj})\right\}\cdot\mathbf{R}_{jj'}\\&\times\mathbf{R}_{jj'}\cdot\left\{\mathbf{1}[X(R_{jl'})-X(R_{jl})]\right.\\&\left.+\frac{\mathbf{R}_{jl'}\mathbf{R}_{jl'}}{|\mathbf{R}_{jl'}|^2}Y(R_{jl'})-\frac{\mathbf{R}_{jl}\mathbf{R}_{jl}}{|\mathbf{R}_{jl}|^2}Y(R_{jl})\right\}\cdot\mathbf{R}_{ll'}, \quad (62)\end{aligned}$$

which we shall evaluate for several cases of interest.

Self-Interaction

This arises from the terms in (60) for which $j'=l'$. One expects that this will be the largest contribution to (60), and that its relative smallness compared to the first-order term will indicate the validity of the perturbation treatment. Assuming first that the hole at site j' has no contiguous neighbor holes, the crystal geometry and the entries in Table II allow the ready evaluation of

TABLE I.

	$i=0$	$i=1$	$i=2$	$i=3$
$X_i(0)$	0.121898	0.030424	0.007254	0.001638
$Y_i(0)$	0.000000	0.000000	0.000000	0.000000
$X_i(1)$	0.040464	−0.000847	−0.000612	−0.000095
$Y_i(1)$	0.019131	0.004191	−0.000166	−0.000397

the expression, with the result‡

$$\ln Q_v^{II}(j',j')=0.225. \tag{63}$$

This is just 15 percent of the first-order term, and the perturbation treatment seems to have an adequate convergence.

When the hole has contiguous neighbors, the occupation variables in (62) delete some of the 144 terms. Since all terms are not equal in size, the sum depends on the arrangement of these neighbors as well as their number. The orientation effect is small, however, and the result is quite well represented by a linear decrease, as shown in Table III. The general self-interaction is then

$$\ln Q_v^{II}(\text{self})=\sum_{j'}\sum_{l'}\delta_{j'l'}\rho_{j'}\rho_{l'}\ln Q_v^{II}(j',l')$$

$$=0.225\left(n-\frac{2p}{z}\right), \tag{64}$$

which parallels the first-order term.

Pair at Large Distance

For a pair of isolated holes at a separation $|\mathbf{R}_{j'}-\mathbf{R}_{l'}|=R\gg 1$, we insert the asymptotic forms of X and Y, expand all quantities in powers of R^{-1}, and replace the nearest neighbor sums over j and l by surface integrals. The process is somewhat tedious, but the result is

$$\ln Q_v^{II}(j',l')\sim 0.1033/R^6, \tag{65}$$

with neglect of higher inverse powers.

Nearest Neighbor Pair

The asymptotic result suggests that we can expect the pair interactions to decrease rapidly with distance. We consider here, therefore, one more case, that of j' and l' on nearest neighbor sites, and otherwise isolated. By Table II and the crystal geometry, the result is

$$\ln Q_v^{II}(j',l')=0.0219. \tag{65}$$

TABLE II. $2\pi^2\Delta\times$.

R^2	$RX(R)$	$RY(R)$	$X(R)$	$Y(R)$
0	0.000000	0.000000	4.500400	0.000000
1	1.086189	0.635343	1.086189	0.635343
2	0.729292	0.716639	0.515687	0.506740
3	0.995857	0.547588	0.574958	0.316150
4	1.224227	0.444456	0.612113	0.222228
5	1.220849	0.458813	0.546000	0.205187
6	1.079996	0.529301	0.440907	0.216086
7	0.942767	0.589193	0.356332	0.222694
8	0.888622	0.606758	0.314175	0.214521
9	0.923832	0.583934	0.307944	0.194645
10	1.010501	0.540647	0.319548	0.170968
11	1.100431	0.499256	0.331792	0.150531
12	1.157716	0.475127	0.334204	0.137157
13	1.167894	0.473285	0.323916	0.131266
14	1.135715	0.490319	0.303533	0.131043
15	1.078265	0.517662	0.278407	0.133660
16	1.016373	0.545667	0.254093	0.136417
∞	1.047197	0.523598	0.000000	0.000000

‡ The value obtained is 0.223, which we increase by the factor $(1.5/1.494)^2$ in view of the behavior of this evaluation process in the first-order case.

VIBRATIONAL PARTITION FUNCTION

In the initial crystal model we assumed the interatomic forces to fall off sufficiently rapidly with distance so that only nearest neighbor interactions had to be considered. The interaction of hole pairs has been found to behave in just this way. Hence, it will be consistent to neglect all but the self and nearest neighbor interactions in evaluating (60). This can be indicated formally by altering that expression to

$$\ln Q_v^{II}\simeq\sum_{j'}\sum_{l'}\rho_{j'}\rho_{l'}\{\delta_{j'l'}+\lambda_{j'l'}\}\ln Q_v^{II}(j',l'). \tag{66}$$

By (63) and (65) this becomes

$$\ln Q_v^{II}\simeq 0.225n+0.0031\times 2p, \tag{67}$$

and together with (35) and (53) gives

$$\ln Q_v(N,n,c)=\ln Q_v^0(N)+1.725n-0.1221\times 2p_c, \tag{68}$$

as the vibrational partition function for N atoms and n holes on $N+n$ sites, in a configuration, c, which includes p_c nearest neighbor hole pairs.

ENTIRE PARTITION FUNCTION

We can now write down the entire partition function for our crystal of N atoms and n holes:

$$Q(N,n)=\sum_{\text{config.}}Q_s(N,n,c)Q_v(N,n,c). \tag{69}$$

The static term is

$$Q_s(N,n,c)=Q_s^0(N)\exp\left(\frac{nz}{2kT}V_{aa}\right)$$

$$\times\exp\left(-\frac{p_c}{kT}V_{aa}\right), \tag{70}$$

$$Q_s^0(N)=\exp\left(-\frac{Nz}{2kT}V_{aa}\right);\quad V_{aa}=V. \tag{71}$$

We can put the vibrational term, (68), in similar form

$$Q_v(N,n,c)=Q_v^0(N)\exp\left(-\frac{nz}{kT}V_{ah}\right)$$

$$\times\exp\left[-\frac{p_c}{kT}(V_{hh}-2V_{ah})\right], \tag{72}$$

by defining

$$V_{ah}=-0.1438kT,$$
$$V_{hh}=-0.0434kT. \tag{73}$$

In this way it is then possible to write (69) as

$$Q(N,n)=Q_s^0(N)Q_v^0(N)\exp\left[\frac{nz}{2kT}(V_{aa}-2V_{ah})\right]$$

$$\times\sum_{\text{config.}}\exp\left\{-\frac{p_c}{kT}[V_{aa}+V_{hh}-2V_{ah}]\right\}, \quad (74)$$

which is formally identical with the usual static order-disorder problem. The similarity has been achieved through formulating the influence of the defects on the lattice waves as apparent, attractive, temperature dependent potentials between nearest neighbor atom-hole pairs and nearest neighbor hole-hole pairs, V_{ah} and V_{hh}. By this device the thermodynamic properties of the dynamical model can now be obtained directly from the established methods and results for the static problem; e.g., the Bragg-Williams,[5] moment,[6] and quasi-chemical[7] methods.

Two important conclusions can be read directly from (74). First, from the exponential term $V_{aa}-2V_{ah}$, we see that the energy of the hole formation is lessened by the temperature dependent V_{ah}. Thus, the equilibrium hole concentration should exceed that for the static model, and this effect should become more pronounced as the temperature is raised. Second, the several methods for treating (74) predict phase changes when

$$\frac{z}{kT_c}[2V_{ah}-V_{aa}-V_{hh}]\simeq 4. \quad (75)$$

In the present case of Schottky defects this becomes

$$-\frac{z}{kT_c}V_{aa}-3\simeq 4, \quad (76)$$

so that, roughly speaking, the inclusion of the vibrational terms should halve the "melting temperature" calculated according to the hole theory.

APPENDIX I

By (16) and (18),

$$\mathbf{M}(\mathbf{k})=\frac{\alpha}{m}\sum_{j'}\lambda_{jj'}\mathbf{R}_{jj'}\mathbf{R}_{jj'}[1-\exp(i\mathbf{k}\cdot\mathbf{R}_{jj'})]. \quad (A1)$$

We substitute

$$\sum_{j'}\lambda_{jj'}f(\mathbf{R}_{jj'})\simeq\frac{z}{4\pi}\int_0^{2\pi}\int_0^{\pi}f(\mathbf{r})r^2\sin\vartheta d\vartheta d\varphi;$$

$$|\mathbf{r}|=1, \quad (A2)$$

[5] W. L. Bragg and E. J. Williams, Proc. Roy. Soc. (London) A151, 540 (1935).
[6] J. G. Kirkwood, J. Phys. Chem. 43, 97 (1939).
[7] R. Fowler and A. E. Guggenheim, see reference 1, Chap. VIII.

TABLE III. Self-interaction of a nonisolated hole; ratio to the value for an isolated hole.

Number of nearest neighbor holes	Maximum value	Minimum value	Linear decrease
0	1.000	1.000	1.000
1	0.906	0.906	0.917
2	0.816	0.806	0.834
3	0.723	0.710	0.750
4	0.626	0.614	0.667
5	0.558	0.516	0.583
6	0.480	0.425	0.500
7	0.405	0.341	0.417
8	0.327	0.256	0.334
9	0.250	0.190	0.250
10	0.167	0.117	0.167
11	0.083	0.056	0.083
12	0.000	0.000	0.000

with the normalization established by (3) with $f(\mathbf{R})\equiv 1$. If we take the polar axis in the $\mathbf{k}$ direction, the integration gives

$$\mathbf{M}(\mathbf{k})=M_{22}\mathbf{1}+\frac{\mathbf{kk}}{k^2}(M_{11}-M_{22});$$

$$M_{11}=\frac{\alpha z}{3m}[1-j_0(k)+2j_2(k)], \quad (A3)$$

$$M_{22}=\frac{\alpha z}{3m}[1-j_0(k)-j_2(k)],$$

where the j are the so-called spherical Bessel functions.[8] Then,

$$\mathbf{M}^{-1}(\mathbf{k})=M_{22}^{-1}\mathbf{1}+\frac{\mathbf{kk}}{k^2}(M_{11}^{-1}-M_{22}^{-1}), \quad (A4)$$

and inserting the power expansions for the functions and inverting the series, we get (57).

APPENDIX II

In evaluating

$$N^{-1}\sum_{\mathbf{k}}\mathbf{M}^{-1}(\mathbf{k})\exp(i\mathbf{k}\cdot\mathbf{R}), \quad (A5)$$

we see from (57) that we require sums of the type

$$N^{-1}\sum_{\mathbf{k}}\frac{\exp(i\mathbf{k}\cdot\mathbf{R})}{|\mathbf{k}|^2}k^{2t} \quad (A6)$$

$$t=0, 1, 2\cdots$$

$$N^{-1}\sum_{\mathbf{k}}\frac{\mathbf{kk}}{|\mathbf{k}|^4}\exp(i\mathbf{k}\cdot\mathbf{R})k^{2t}. \quad (A7)$$

[8] *Table of Spherical Bessel Functions* (Columbia University Press, New York, 1947).

We substitute

$$N^{-1}\sum_{\mathbf{k}} f(\mathbf{k}) \simeq \frac{1}{8\pi^3\Delta}\int_0^{2\pi}\int_0^{\pi}\int_0^{K} f(\mathbf{k})k^2\sin\vartheta dk d\vartheta d\varphi, \quad \text{(A8)}$$

where Δ ($\sqrt{2}$ in our case) is the volume of the unit cell in reciprocal space. In accordance with (47), we require (A6) to be unity when $\mathbf{R}=0$ and $t=1$, determining

$$K=(6\Delta\pi^2)^{\frac{1}{3}} \quad \text{(A9)}$$

in this way. With the polar axis in the $\mathbf{R}$ direction, the integrations give (58), with

$$X_0(R)=\frac{1}{K^3R}[2Si(KR)+j_1(KR)]$$

$$X_1(R)=\frac{10^{-2}}{KR}\left[10.71429j_1(KR)-4.76190\left\{\frac{Si(KR)-\sin(KR)}{(KR)^2}\right\}\right]$$

$$X_2(R)=\frac{K\times10^{-4}}{R}[11.36937j_1(KR)-7.05468j_3(KR)] \quad \text{(A10)}$$

$$X_3(R)=\frac{K^3\times10^{-6}}{R}[13.41468j_1(KR)-6.74496j_3(KR)+1.92714j_5(KR)]$$

$$X(R)=\sum_i X_i(R)$$

and

$$Y_0(R)=\frac{1}{K^3R}[Si(KR)-3j_1(KR)]$$

$$Y_1(R)=\frac{10^{-2}}{KR}\left[14.28570\left\{\frac{Si(KR)-\sin(KR)}{(KR)^2}\right\}-4.76190j_1(KR)\right] \quad \text{(A11)}$$

$$Y_2(R)=\frac{K\times10^{-4}}{R}[-1.57470j_3(KR)]$$

$$Y_3(R)=\frac{K^3\times10^{-6}}{R}[-21.49968j_3(KR)+6.14277j_5(KR)]$$

$$Y(R)=\sum_i Y_i(R).$$

For $R=0$ these reduce to

$$\begin{aligned} X_0(0)&=2.33333/K^2\\ X_1(0)&=3.04233\times10^{-2}\\ X_2(0)&=3.78978\times10^{-4}K^2\\ X_3(0)&=4.47156\times10^{-6}K^4\\ Y_i(0)&=0, \end{aligned} \quad \text{(A12)}$$

while for large R,

$$\begin{aligned} X(R)&\sim\pi/K^3R\\ Y(R)&\sim\pi/2K^3R. \end{aligned} \quad \text{(A13)}$$

THE JOURNAL OF CHEMICAL PHYSICS VOLUME 22, NUMBER 9 SEPTEMBER, 1954

Vibrational Spectra of Trifluoroethylene and Trifluoroethylene-d_1*†

D. E. MANN, N. ACQUISTA, AND EARLE K. PLYLER
National Bureau of Standards, Washington, D. C.

(Received April 16, 1954)

The infrared spectra of gaseous F_2C:CFH and F_2C:CFD have been investigated in the range 2–50μ. Complete and satisfactory vibrational assignments have been achieved. The a' fundamentals of the H compound are 3150, 1788, 1362, 1264, 1171, 929, 623, 485, 232; and the a'' modes occur at 750, 555, and 305 cm^{-1}. The corresponding fundamentals for the heavy molecule are 2347, 1767, 1323, 1200, 983, 855, 620, 480, and 228 in a', and 612, 528, and 291 cm^{-1} in species a''. Tables of the thermodynamic functions for the ideal gases are given.

INTRODUCTION

THE vibrational spectra of trifluoroethylene, F_2C:CFH, and trifluoroethylene-d_1, F_2C:CFD, are of considerable interest in a current investigation of the potential functions for various series of halogenated ethylenes. No prior studies of either their infrared or Raman spectra have been published. Because of the fortunate circumstance that all the fundamental vibrations of F_2C:CFH and F_2C:CFD are permitted to appear in the infrared, and obligingly occur in readily accessible spectral regions with adequate intensity and moderately well-defined band

* This work has been supported in part by the U. S. Office of Naval Research under contract NA ONR 112-51.

† Presented at the Symposium on Molecular Structure and Spectroscopy held at the Ohio State University in June, 1953.

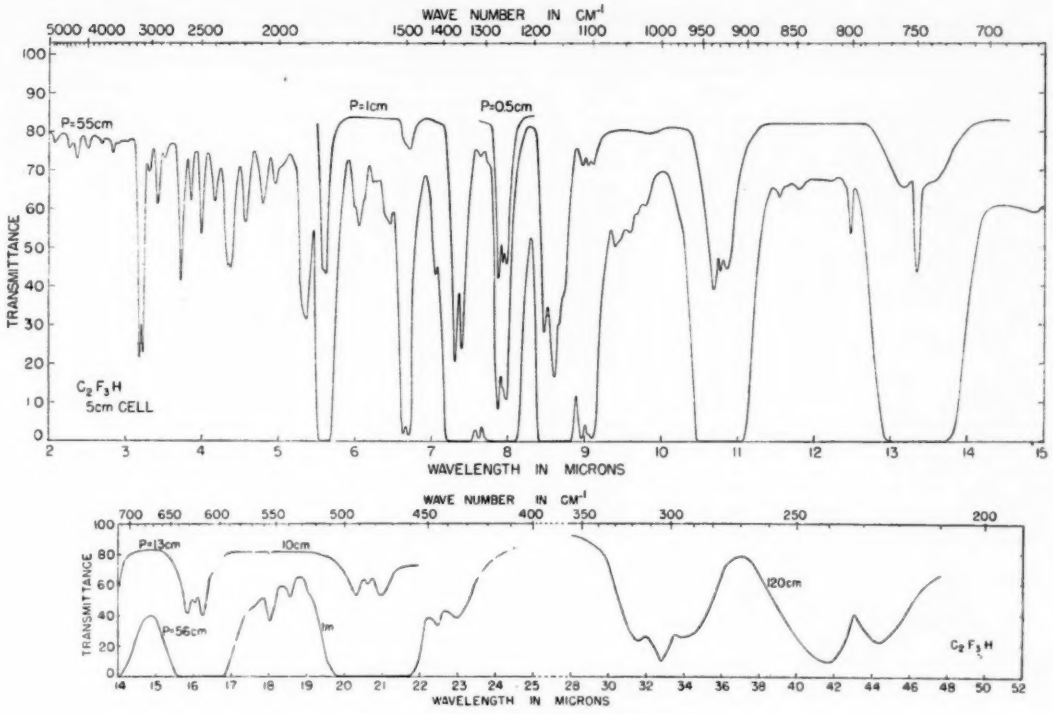

FIG. 1. Infrared spectrum of F_2C:CFH from 2 to 52μ.

envelopes, the need for Raman spectra was avoided. The present paper reports the infrared spectra of F_2C:CFH and F_2C:CFD for the region 2 to about 50μ. A complete vibrational analysis is given for each molecule.

EXPERIMENTAL

The samples of F_2C:CFH and F_2C:CFD were prepared at the National Bureau of Standards by Dr. R. E. Florin. A mass spectroscopic analysis indicated the presence of no more than one to two percent of contaminants, except that the heavy compound contained around 10 percent of F_2C:CFH.

For the infrared measurements the equipment and procedures previously described were used.[1] Prisms of LiF, NaCl, KBr, CsBr, and CsI were employed in appropriate spectral regions to ensure adequate resolution over the entire range. Interference by the light compound in the spectrum of F_2C:CFD was eliminated by subtracting the spectrum of the former for appropriate vapor pressures. It is evident from the dashed lines in Figs. 1–4 that even at the highest pressures employed for F_2C:CFD the overlap by the strongest bands of F_2C:CFH was not too troublesome. The regions in which interference occurred were examined a number of times sufficient to ensure the reliability of the correction for the presence of the hydrogen compound. Even so, it is readily admitted that in these overlap regions some very weak F_2C:CFD bands may have been missed, and the location of the bands given by dashed lines may be somewhat uncertain.

The complete infrared spectra of F_2C:CFH and

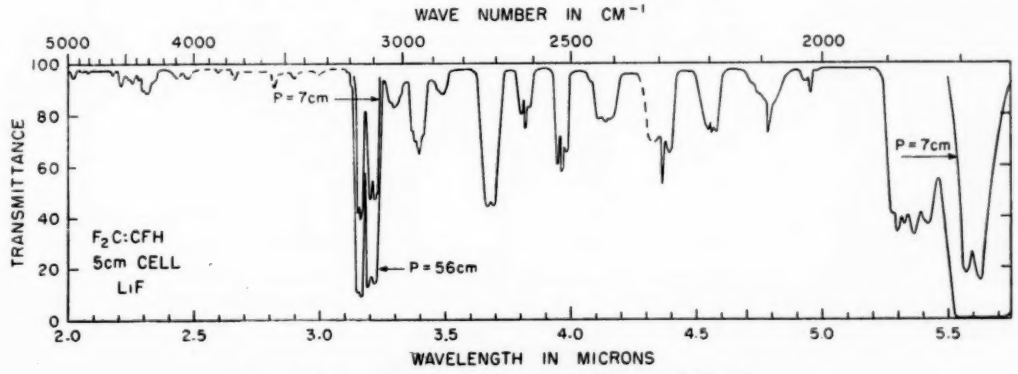

FIG. 2. Infrared spectrum of F_2C:CFH in the LiF region.

[1] Mann, Acquista, and Plyler, J. Chem. Phys. **21**, 1949 (1953).

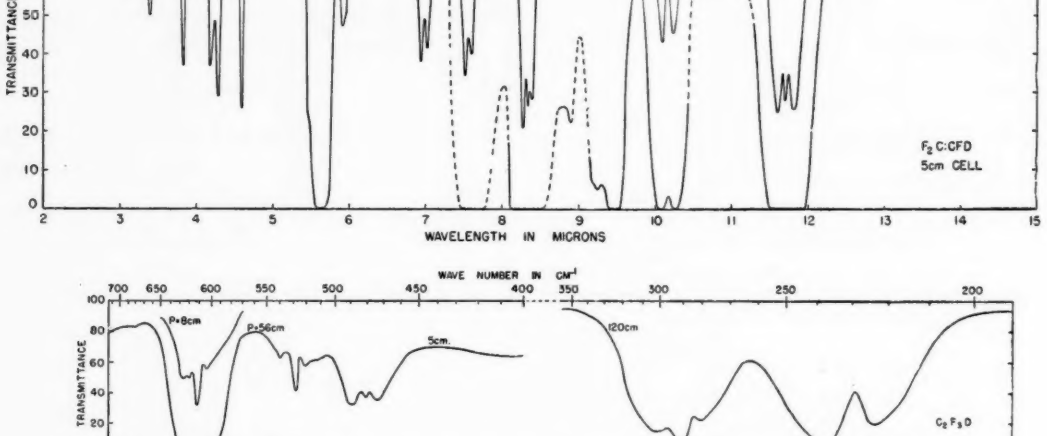

FIG. 3. Infrared spectrum of F_2C:CFD from 2 to 52μ.

F_2C:CFD are shown in Figs. 1 and 3, respectively. In Figs. 2 and 4 the corresponding LiF regions are presented with an expanded scale to reveal the structure not apparent in Figs. 1 and 3. The measured wave numbers are listed for the light and heavy molecules in Tables I and II, respectively.

INTERPRETATION

Preliminary Discussion of the Spectral Data

No electron-diffraction, x-ray, or microwave structural data are available for either F_2C:CFH or F_2C:CFD. The required parameters were guessed with the aid of the reasonable assumptions that both molecules are planar, and have distances and angles intermediate between those reported by Karle and Karle for F_2C:CF_2 and F_2C:CH_2.[2] The CC, CF, and CH (or CD) distances for both molecules are assumed to be 1.31A, 1.32A, and 1.07A, respectively. The CCF and CCH (or CCD) angles are taken to be 124° and 122°, respectively. The principal moments of inertia are then 78.345, 218.795, and 297.140×10^{-40} g cm² for F_2C:CFH, and 83.156, 220.029, and 303.185×10^{-40} g cm² for F_2C:CFD.

As a preliminary guide to the interpretation of the infrared spectra it is useful to consider what information may be gleaned from the band envelopes. The 12 normal vibrations of F_2C:CFH and F_2C:CFD are divided on the basis of symmetry into two distinct classes: nine planar modes in species a' of the point group C_s, and three out-of-plane motions in a''. The envelopes of the a' bands may be expected to have a hybrid character, each partaking in some degree of the conventional

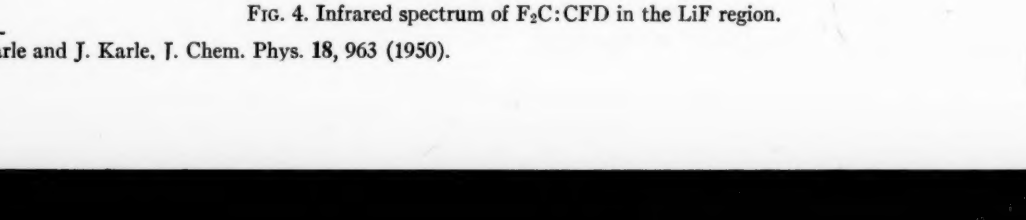

FIG. 4. Infrared spectrum of F_2C:CFD in the LiF region.

[2] I. L. Karle and J. Karle, J. Chem. Phys. 18, 963 (1950).

TABLE I. Infrared spectrum of $F_2C:CFH$ (gas).

Wave number (cm^{-1})	Intensity		Interpretation
225	~w[a]	P	
(232)[b,c]	~w		$\nu_9(a')$
240	~w	R	
296	~w	P	
305	~w	Q	$\nu_{12}(a'')$
318	~w	R	
435	vw		1362−929=433
445	vw		929−485=444
476	w	P	
485	w	Q	$\nu_8(a')$
495	w	R	
539	vw		232+305=537(A'')[c]
555	vw		$\nu_{11}(a'')$
~605 sh	vw		2×305=610
616	m	P	
623	m	Q	$\nu_7(a')$
631	m	R	
741	s	P	
750	s	Q	$\nu_{10}(a'')$
759	s	R	
803	vw		305+485=790(A'')
~823	vvw, b		?
836	vvw	P	
841	vvw	Q	232+2×305=842
846	vvw	R	
859	vvw		232+623=855
867	vvw		305+555=860
922	s	P	
929	s	Q	$\nu_6(a')$
935	s	R	
1022	vw		232+305+485=1022(A'')
1034	vw		1264−232=1032
1043	vw		485+555=1040(A'')
1060 sh	vw		?
1067	vw		?
1100	m	P	
1107	m	Q	2×555=1110; 485+623=1108
1116	m	R	
~1145 sh	vs	P	
~1153 sh	vs	Q	232+929=1161
1163	vs	P	
(1171)[c]	vs		$\nu_5(a')$
1181	vs	R	555+623=1178(A'')
1256	vs	P	
1264	vs	Q	$\nu_4(a')$
1272	vs	R	
1294 sh	w		232+305+750=1287
1312	w		555+750=1305
1355	vs	P	
(1362)[c]	vs		$\nu_3(a')$
1370	vs	R	
1422	w		485+929=1414
1495	m		232+1264=1496
(1504)[c]	m		
1511	m		2×750=1500
1553	vw		623+929=1552
1570 sh	vw		305+1264=1569(A'')
1590	vvw		232+1362=1594
1608	vvw		305+555+750=1610(A'')
~1639 sh	vw		232+485+929=1646
1656	vw		485+1171=1656
~1675 sh	vw		750+929=1679(A'')
1777	s	P	
(1788)[c]	s		$\nu_2(a')$
1795	s	R	
1845	w		485+1362=1847
1863	w		2×929=1858; 305+623+929=1857(A'')
1876	w		2×305+1264=1874
1888	w		623+1264=1887
1894	w		2×485+929=1899
~2008	vvw		
2022	vvw		750+1264=2014(A'')
2026	vvw		232+1788=2020
2092	vw		305+1788=2093(A'')
2184	vw	P	
2193	vw	Q	929+1264=2193
2199	vw	R	
2278	vw		2×555+1171=2281; 485+1788=2273; 485+623+1171=2279
2293	vw		305+623+1362=2290(A'') 929+1362=2291
~2313	vw		305+750+1264=2319
2402	vw	P	
2408	vw	Q	623+1788=2411
2414	vw	R	
~2444 sh	vvw		1171+1264=2435
2513	w	P	
2525	w	Q	2×1264=2528
2533	w	R	
2612	vw	P	
2621	vw	Q	1264+1362=2626
2630	vw	R	
2709	w	P	
(2717)[c]	w		2×1362=2724; 929+1788=2717
2724	w	R	
2860	vvw		232+1264+1362=2858
~2935 sh	vw		305+1264+1362=2931(A'')
2941	vw		650+929+1264=2943(A'')
~2956 sh	vw	Q	1171+1788=2959
~2961 sh	vw	R	
~3002 sh	vvw		485+2×1264=3013
3030	vvw		305+2×1362=3029(A'')
~3047 sh	vvw		1264+1788=3052
3115	m	P	
3120	m	Q	1362+1788=3150[d]
3132	m	R	
3160	m	P	
3170	m	Q	$\nu_1(a')$=ca 3150[d]
3179	m	R	
3333	vvw		623+929+1788=3340; 623+2×1362=3347
~3461	vvw		929+2×1264=3457
~3559	vvw		929+1264+1362=3555; 2×1788=3576
~3759	vvw		623+3120=3743
~3861	vvw		2×1264+1362=3890
4037	vvw		929+3120=4049
4098	vvw		929+3170=4099
4323	vvw		2×1264+1788=4316; 232+929+3170=4331
4348	vvw		1171+3170=4341
4384	vvw		1264+3120=4384
4423	vvw		1264+3170=4434
4456	vvw		555+750+3150=4455
4525	vvw		1362+3170=4532
4587	vvw		485+929+3170=4584
4787	vvw		485+1171+3120=4776
4871	vvw		485+1264+3120=4869
4941	vvw		1788+3170=4958

[a] The intensities of the bands observed in the cesium iodide region are uncertain relative to the remainder of the spectrum since the partial pressure of the absorbing gas, which was contained in the monochromator housing, was not determined.

[b] A wave number given in the form $(\ldots)_c$ is the measured value of the dip between P and R branches. The designation "sh" means shoulder, while "b" stands for broad. The tilde (~) is used to indicate that the measured quantity may be more than normally uncertain, and applies in particular to very weak shoulders or broad bands. In the following table the tilde may also apply to certain bands obtained upon correction for contaminant spectra.

[c] The species of the combination or overtone is understood to be A' unless A'' is given explicitly.

[d] Fermi resonance.

TABLE II. Infrared spectrum of F_2C:CFD (gas).

Wave number (cm^{-1})	Intensity		Interpretation
224	~w[a]	P	
(228)[b]e	~w		$\nu_9(a')$
238	~w	R	
282	~w	P	
291	~w	Q	$\nu_{12}(a'')$
304	~w	R	
472	w	P	
480	w	Q	$\nu_8(a')$
489	w	R	
521	vw		228+291=519(A'')[c]
528	w	Q	$\nu_{11}(a'')$
540	vw	R	
603	s	P	
612	s	Q	$\nu_{10}(a'')$
620	m	Q	$\nu_7(a')$
627	m	R	
~814 sh	vw	P	
~821 sh	vw	Q	291+528=819
845	s	P	
855	s	Q	$\nu_6(a')$
861	s	R	
977	s	P	
(983)e	s		$\nu_5(a')$
990	s	R	
1055	m	P	
1059	m	Q	2×528=1056
1066	m	R	
1083	m	P	
1088	m	Q	228+855=1083
~1127	w		528+612=1140; 228+291+612=1131
1192	vs	P	
1200	vs	Q	$\nu_4(a')$
1209	vs	R	
1316	vs	P	
(1323)e	vs		$\nu_3(a')$
1330	vs	R	
1425	w	P	
(1433)e	w		228+1200=1428
1441	w	R	
~1488	vw		291+1200=1491(A'')
~1508	vw		528+983=1511(A'')
1550	w		228+1323=1551
~1567 sh	w		228+480+855=1563
1603 sh	w		620+983=1603
1621	w	Q	291+1323=1614(A'')
1629 sh	w	R	
1681 sh	w		480+1200=1680
1698	w		2×855=1710; 228+612+855=1695(A'')
1756	s	P	
(1767)e	s		$\nu_2(a')$
1774	s	R	
1820	vw		620+1200=1820
1827	vw		228+620+983=1831
~1869	vvw		528+1323=1851(A'')
~1887	vvw		291+620+983=1894(A'')
~1930 sh	vw		612+1323=1935(A'')
1942	vw		228+2×855=1938
1947	vw		620+1323=1943
1955	vw		228+528+1200=1956(A'')
1960	vw		?
1972	vw		2×983=1966
2006	vvw		228+1767=1995
2058	vw	P	
2061	vw	Q	291+1767=2058(A'')
2171	w	P	
2182	w	Q	855+1323=2178; 983+1200=2183
2188	w	R	
~2294	vw		528+1767=2295(A'')
~2313	vw		983+1323=2306
~2347	w		$\nu_1(a')$
~2394	w	P	620+1767=2387
2403	w	Q	2×1200=2400
2410	w	R	
2516	vw	P	
2528	vw	Q	1200+1323=2523
2535	vw	R	
~2610 sh	vvw		228+620+1767=2615
2623 sh	w		855+1767=2622; 228+2×1200=2628
2638	w		291+2347=2638(A'')
~2644 sh	w	Q	2×1323=2646
2653 sh	w	R	
~2675 sh	vvw		620+855+1200=2675
2747	vvw	P	
(2756)e	vvw		983+1767=2750; 228+1200+1323=2751
2765	vvw	R	
2807	vvw		291+1200+1323=2814(A'')
~2857	vvw		228+855+1767=2850
2969	w		1200+1767=2967
~2980 sh	w		228+983+1767=2978
~3084 sh	vw	P	
3097	vw	Q	1323+1767=3090; 291+480+2347=3118(A'')
~3120 sh	vw		228+1323+1767=3118
~3332	vvw		983+2347=3330
~3559	vvw		1200+2347=3547
~3690	vvw		1323+2347=3670
~3802	vvw		855+1200+1767=3822
~3937	vvw		855+1323+1767=3945; 983+1200+1767=3950
4115	vvw		1767+2347=4114
~4170 sh	vvw		2×1200+1767=4167
4632	vvw		2×2347=4694

[a] See footnote a to Table I. [b] See footnote b to Table I. [c] See footnote c to Table I.

type A and type B contours. This is clearly evident on inspection of Figs. 1 and 3. The a'' bands have type C envelopes, and from Badger and Zumwalt's curves[3] it is apparent that the contours are characterized by very prominent Q branches with rather washed out wings. Indeed, the stronger and more clearly resolved a'' bands may be identified without hesitation. A beautiful example of the type C envelope expected in the present case is given by the 750 cm^{-1} band in Fig. 1. The relatively easy and certain identification of a'' bands in the spectra of F_2C:CFH and F_2C:CFD is a valuable aid in the subsequent vibrational analysis.

A preliminary examination of the spectra in Figs. 1 and 3 reveals several rather strong and well-defined bands which may reasonably be expected to represent fundamental modes. The envelopes of the bands at 750 and 305 cm^{-1} in the spectrum of F_2C:CFH clearly indicate their type C character. The much weaker though quite pronounced Q branch at 803 cm^{-1} must also represent a type C band, though not necessarily a fundamental. In Fig. 3 characteristic a'' contours are in evidence at 612, 528, and 291 cm^{-1}. In a similarly

[3] R. M. Badger and L. R. Zumwalt, J. Chem. Phys. 6, 711 (1938).

straightforward way bands which very probably represent planar fundamentals are indicated around 3150, 1788, 1362, 1264, 1171, 929, 623, 485, and 232 cm^{-1} in Fig. 1, and 2347, 1767, 1323, 1200, 983, 855, 480, and 228 cm^{-1} in Fig. 3. In the latter there is evidently some overlapping in the region of the *R* wing of the 612 cm^{-1} band. It is also interesting to notice the close resemblance of contours between certain of the stronger F_2C:CFH bands and those of the heavy molecule. The correspondence of the type *C* 750 and 305 cm^{-1} bands of the *H* compound with the 612 and 291 cm^{-1} bands, respectively, of F_2C:CFD is striking. No less remarkable are the *H*−*D* pairs 1362–1323, 1264–1200, 929–855, 485–480, and 232–228. A resemblance between the 1171 and 623 cm^{-1} bands of F_2C:CFH and those at 983 and 620 cm^{-1}, respectively, in Fig. 3 is also suggested.

Prior to discussing the assignment it is helpful to consider the spectral regions in which the fundamentals of F_2C:CFH and F_2C:CFD may be expected to occur. There can be no question that the modes primarily associated with the CH, CD, CC, and CF stretching motions may be sought in the vicinity of 3100, 2300, 1800, and 900–1400 cm^{-1}, respectively. For the light molecule the planar *H* deformation (δCFH) and out-of-plane *H* wagging (βCFH) vibrations may be expected around 1100–1300 and 800 cm^{-1}, respectively. The former mode may therefore be mixed with the CF stretching vibrations. In Cl_2C:CClH, where the CCl stretchings occur at appreciably lower frequencies than the *H* deformation mode, δCClH occurs at 1250 cm^{-1}.[4] In Cl_2C:CClD the δCClD mode appears at about 1020 cm^{-1}. Analogy with the present case suggests that the 1171 cm^{-1} band be ascribed to δCFH, and the 983 cm^{-1} band to δCFD.[5]

The spectrum of F_2C:CClH[6] also affords some interesting correlations with the trifluoroethylenes. The fundamentals listed by Nielsen, Liang, and Smith for 1, 1-difluoro-2-chloroethylene are 3130, 1745, 1333, 1199, 970, 845, 579, 433, and 201 for the planar modes, and 751, 572, and 243 cm^{-1} for *a″*. If the analogy with the data for F_2C:CFH, F_2C:CFD, Cl_2C:CClH, and Cl_2C:CClD has any meaning, then formally, at least, the 1199 cm^{-1} band of F_2C:CClH may be ascribed to δCClH, 751 to βCClH, while 3130, 1745, 1333, 970, and 845 may be assigned to νCH, νCC, νCF, νCF, and νCCl, respectively. It is noteworthy that the only other strong bands of F_2C:CFH that undergo quite large frequency shifts after deuterium substitution are the CH stretching, which goes from about 3150 to 2347, and the *H* wagging, which goes from 750 to 612 cm^{-1}. All the remaining fundamentals may be expected at lower frequencies.

Assignment of Fundamentals

On the basis of the preceding discussion the vibrational assignment may be developed. The pair of almost equally intense bands around 3150 cm^{-1} in Fig. 2 probably results from strong resonance of the CH stretching fundamental with the binary tone 1362 +1788=3150. It may therefore be supposed that if νCH occurred around 3150, it may appear as the slightly stronger band at 3170, while the sum occurs at 3120 cm^{-1}. The CD stretching vibration is seen at about 2347 in Fig. 4. Since it is partially obscured by the spectrum of the contaminating species, the precise value of the νCD frequency may be somewhat uncertain. There can be no doubt, however, of the reality and identification of the 2347 cm^{-1} band. Its strongest neighbor to lower frequencies occurs at 2182 cm^{-1}, and may be explained as 855+1323=2178 or 983+1200 =2183. The intense band at 2403 cm^{-1} must be ascribed to the overtone 2×1200=2400, although the *P* wing at 2394 may arise in part from 620+1767=2387.

The selection of the CC stretching modes is clear-cut for both the light and heavy compounds: in the former it occurs at 1788, and in the latter it is found at 1767 cm^{-1}. At lower frequencies we may expect to encounter first the four *a′* fundamentals which correspond more or less to the three CF stretchings and the *H* (or *D*) planar deformation. In the spectrum of F_2C:CFH the obvious choices are the strong bands at 1362, 1264, 1171, and 929 cm^{-1}; in the spectrum of the heavy compound the analogous bands occur at 1323, 1200, 983, and 855 cm^{-1}, respectively. The pairwise resemblance of envelopes, together with evidence previously adduced for trichloroethylene, suggests that 1171 and 983 correspond respectively to δCFH and δCFD, with the remaining fundamentals in this region ascribed to the CF stretching modes. It has been assumed that the

TABLE III. Fundamental vibration frequencies for F_2C:CFH and F_2C:CFD.

Species	Number	Designation[a]	F_2C:CFH	F_2C:CFD	Product calc'd.	Rule obs'd.
a′	1	νCH(D)	3150 cm^{-1}	2347 cm^{-1}	0.512	0.503
	2	νCC	1788	1767		
	3	νCF	1362	1323		
	4	νCF	1264	1200		
	5	δCFH(D)	1171	983		
	6	νCF	929	855		
	7	ρCF	623	620		
	8	δCF_2	485	480		
	9	ρCF_2	232	228		
a″	10	βCFH(D)	750	612	0.735	0.741
	11	βCF_2	555	528		
	12	τ	305	291		

[a] See reference 5.

[4] H. J. Bernstein, Can. J. Research **B28**, 132 (1950).

[5] It is worth emphasizing that the appellations CC stretching, CF stretching, CFH deformation, and so on are convenient labeling devices but have for F_2C:CFH, F_2C:CFD and related molecules only limited meaning and significance as descriptions of the most characteristic features of the corresponding normal modes. A more precise and meaningful picture of the fundamental vibrations must await the completion of the normal coordinate analyses currently being attempted. Nevertheless, the familiar tags (see reference 2) νCC, νCF, νCH, δCFH, ρCF, δCF_2, ρCF_2, βCFH, βCF_2, and τ are more perspicuous than the numbered frequencies $\nu_1-\nu_{12}$. They may, therefore, give some clue, if taken with the proper reservations, to the spectral range in which the fundamentals occur, and the nature of the vibrations they represent.

[6] Nielsen, Liang, and Smith, J. Chem. Phys. **20**, 1090 (1952).

TABLE IV. Calculated thermodynamic functions for F_2C:CFH in dimensionless units.

T°K	C_p°/R	$(H°-E_0°)/RT$	$-(F°-E_0°)/RT$	$S°/R$
200	6.631	4.936	27.285	32.221
300	8.352	5.796	29.449	35.245
400	9.758	6.617	31.230	37.847
500	10.864	7.361	32.788	40.149
600	11.723	8.019	34.190	42.209
700	12.394	8.598	35.470	44.068
800	12.925	9.107	36.652	45.759
900	13.353	9.556	37.751	47.307
1000	13.701	9.954	38.779	48.733
1100	13.989	10.308	39.745	50.052
1200	14.229	10.625	40.655	51.280
1300	14.431	10.910	41.517	52.427
1400	14.602	11.168	42.336	53.503
1500	14.748	11.402	43.114	54.516

1171 cm^{-1} of the light compound does in fact have the doublet structure displayed by the 983 cm^{-1} band of F_2C:CFD. The prominence of the peak at 1163 cm^{-1} and the shoulders at 1153 and 1145 cm^{-1} probably arise from overlapping by the combination 232+929=1161.

The type C bands at 750 cm^{-1} in Fig. 1 and 612 cm^{-1} in the spectrum of the heavy compound are obviously related to βCFH and βCFD, respectively. The asymmetry and R-branch structure of the latter band imply considerable overlapping around 620 cm^{-1}. The presence of an a' fundamental in the vicinity of 620 cm^{-1} is evident from the correlation of combination tones which involve the 623 cm^{-1} mode of F_2C:CFH with analogous bands of the heavy compound. The moderately intense bands at 485, 305, and 232 cm^{-1} in the spectrum of the hydrogen compound have almost identical counterparts at 480, 291, and 228 cm^{-1}, respectively, in the trace for the heavy molecule. The middle member of each group has evident type C character and may therefore be ascribed to an out-of-plane mode. The pairs 485, 232 and 480, 228 represent corresponding a' fundamentals for F_2C:CFH and F_2C:CFD, respectively.

A tally of the fundamentals assigned up to this point shows that only one a'' band remains to be determined for the H and D compounds. There can be little doubt that 528 represents the remaining type C fundamental for the heavy compound. This conclusion is borne out by an approximate force constant calculation[7] which not only confirms the present assignment of the 528 cm^{-1} band but also locates the corresponding fundamental in the F_2C:CFH spectrum at about 555 cm^{-1}. The product rule lends still further support to the present interpretation since the theoretical ratio for the a'' modes is 0.735 and the observed ratio (612×528×291)/(750×555×305) is 0.741. The prominent Q branch at 803 cm^{-1} in Fig. 1 may be due to the sum 305+485 =790(A''), or perhaps to the presence of F_2C:CH_2 as an impurity.

The assignments for both molecules are now complete, and are given in Table III, together with the calculated and observed product rule ratios. The present interpretation accounts satisfactorily for almost all the bands observed in the infrared spectra of F_2C:CFH and F_2C:CFD. The agreement of the product rule ratios for the planar modes is not quite as good as could be desired, though it appears impossible to justify enough of a change in the assignments to effect an appreciable improvement.

[7] Taken from an unpublished study by Mann and Shimanouchi.

THERMODYNAMIC FUNCTIONS

The molecular constants and moments of inertia for F_2C:CFH and F_2C:CFD have been given in a preceding section. The vibrational assignments are given in Table III. The thermodynamic functions, to the rigid-rotator, harmonic oscillator approximation, for the ideal gaseous state were computed with the aid of the SEAC at the National Bureau of Standards. Tables IV and V are abridged versions of the more complete tabulations available for F_2C:CFH and F_2C:CFD, respectively.

TABLE V. Calculated thermodynamic functions for F_2C:CFD in dimensionless units.

T°K	C_p°/R	$(H°-E_0°)/RT$	$-(F°-E_0°)/RT$	$S°/R$
200	6.870	5.017	27.381	32.398
300	8.712	5.954	29.592	35.546
400	10.146	6.830	31.427	38.258
500	11.249	7.609	33.037	40.646
600	12.102	8.289	34.486	42.775
700	12.768	8.883	35.809	44.693
800	13.292	9.403	37.030	46.433
900	13.710	9.859	38.165	48.024
1000	14.044	10.262	39.225	49.486
1100	14.316	10.618	40.220	50.838
1200	14.537	10.936	41.158	52.093
1300	14.720	11.220	42.044	53.264
1400	14.872	11.476	42.885	54.361
1500	14.999	11.707	43.685	55.392

ACKNOWLEDGMENTS

The authors are grateful to Dr. R. E. Florin for preparing the samples of F_2C:CFH and F_2C:CFD and to Dr. N. A. Narasimham for helpful suggestions.

Absolute Yield of the Ferrous Sulfate Oxidation Reaction*

J. WEISS, W. BERNSTEIN, AND J. B. H. KUPER
Brookhaven National Laboratory, Upton, New York

(Received March 24, 1954)

The absolute yield of the ferrous sulfate oxidation reaction, under the influence of ionizing radiation, has been determined. A polystyrene, parallel plate ionization chamber, filled with argon, nitrogen, or air, was used to measure the energy absorbed per unit volume of the solution through the application of the Bragg-Gray principle. The ionization current was extrapolated to zero changer spacing. In related experiments the average ionization potential of polystyrene was determined to be approximately 61.0 v; the value of W for air for electrons was determined to be 34.3 ev by comparison with argon and nitrogen. The G value obtained in this experiment using the three gases was 15.9±0.5 ions/100 ev, in good agreement with calorimetric and cathode-ray bombardment measurements.

INTRODUCTION

A VARIETY of values has been reported from the absolute yield of the ferrous sulfate oxidation reaction under the influence of ionizing radiation. The yield, G, is usually expressed in terms of ferrous ions oxidized per 100 electron volts absorbed in solution. When the absorbed energy was determined by calorimetry[1,2] and cathode-ray bombardment [2,3] methods, G values of approximately 15.6 were obtained. Published ionization chamber determinations,[1,4–8] on the other hand, have given a range of G values from 15 to 21, with most of the values grouped around 20. In view of the disagreement between the separate ionization chamber determinations, and their apparent disagreement with the other methods, it appeared worth while to reinvestigate the ionization chamber measurements thoroughly, using a chamber for which the Bragg-Gray principle[9] is valid.

THEORETICAL DISCUSSION

The energy absorbed per unit volume per second by the wall of a cavity ionization chamber, when irradiated by x-rays, is related to the ionization current produced in the gas by the Bragg-Gray equation,[10]

$$E_W = JW\frac{S_{\text{WALL}}}{S_{\text{GAS}}},$$

where E_w = energy absorbed per unit volume of wall material per second, J = ionizations per unit volume of the cavity per second, W = energy required to produce one ion pair in the gas, S = stopping power for electrons of the wall or gas. The energy absorbed per unit volume of the ferrous sulfate solution is related to the energy absorbed per unit volume of the chamber wall, provided the x-ray absorption probability is considered in each case. If the x-ray energy is high (~1 Mev) and low Z materials are used, the Compton interaction predominates. Therefore, the x-ray absorption per unit volume is proportional to the number of electrons per unit volume and the Bragg-Gray equation may be written as follows:

$$E_s = JW\frac{S_{\text{WALL}}}{S_{\text{GAS}}}\frac{(NZ)_{\text{SOL'N}}}{(NZ)_{\text{WALL}}},$$

where E_s = energy absorbed per unit volume of solution and (NZ) = number of electrons per unit volume.

A detailed evaluation of each of the factors in the Bragg-Gray equation and the necessary corrections will be discussed. The cavity ionization chamber used in this experiment was a parallel plate ionization chamber made of polystyrene. In a parallel plate chamber of finite spacing, the observed current must be corrected since some electrons generated in the side walls do not contribute fully. If the electrode spacing is extrapolated to zero, this edge effect is eliminated. Also the requirement of the Bragg-Gray principle that all electrons traverse the chamber is satisfied.

The stopping power, S, of any material for electrons may be calculated from the relativistic equation derived by Bethe.[11] This equation is valid for electron energies greater than the binding energies of the electrons in the wall or gas, and below 1 Mev, where no polarization effect[12] corrections are required. It may

* Work performed under the auspices of the U. S. Atomic Energy Commission.

[1] C. J. Hochanadel and J. A. Ghormley, J. Chem. Phys. **21**, 880 (1953).
[2] Lazo, Dewhurst, and Burton (private communication).
[3] J. Saldick and A. O. Allen, J. Chem. Phys. **22**, 438 (1954).
[4] N. Miller, J. Chem. Phys. **18**, 79 (1950).
[5] T. J. Hardwick, Can. J. Chem. **30**, 17 (1952).
[6] Todd and Whitcher, AECU 458 (UCLA 34).
[7] Riggs, Stein, and Weiss, Proc. Roy. Soc. (London) **A211**, 375 (1952).
[8] Cormack, Hummel, Johns, and Spinks, J. Chem. Phys. **22**, 6 (1954).
[9] L. H. Gray, Proc. Roy. Soc. (London) **A156**, 587 (1936).
[10] In order for this equation to be applicable several conditions must be satisfied [see for example, White, Marinelli, and Failla, Am. J. Roentgenol. **44**, 889 (1940)]. Except in the special case where the filling gas is of the same composition as the wall, these are: the thickness of the wall must be greater than the range of the most energetic secondary electron, the x-ray absorption in the wall must be negligible, there should be no x-ray interaction with the gas, the cavity must be small enough that only a negligible fraction of the electrons are stopped in the gas, and the geometrical conditions of the irradiation must be such that the entire assembly is immersed in a uniform, parallel beam.
[11] E. Segré, *Experimental Nuclear Physics* (John Wiley and Sons, Inc., New York, 1953), p. 254.
[12] R. Sternheimer, Phys. Rev. **88**, 851 (1952).

be written

$$S=-\frac{dE}{dX}=\frac{2\pi e^4(NZ)}{mv^2}[K],$$

where

$$K=\log\frac{mv^2E}{2I^2(1-\beta^2)}-[2(1-\beta^2)^{\frac{1}{2}}-1+\beta^2]\log 2+1-\beta^2+\tfrac{1}{8}[1-(1-\beta^2)^{\frac{1}{2}}]^2,$$

m = rest mass of the electron, v = velocity of electron, E = total energy—rest energy of the electron, $\beta=v/c$, and I = average ionization potential.

Since all the measurements involve the ratios of electron stopping powers, and these ratios are not very energy-dependent (see Table I) in the region from 100 kev to 1 Mev, the calculations were carried out for an electron kinetic energy of 128 kev corresponding to $\beta=0.6$. This is a reasonable assumption for an average incident x-ray energy of 1 Mev, since the average energy of the electrons existing in the polystyrene is somewhat lower than the average primary electron energy from the Compton interaction.

According to the Bragg rule, the average ionization potential of a compound is the geometric mean of the average ionization potentials of the constituent atoms: small corrections are necessary because of chemical binding. If 76.4 v and 15.6 v are the average ionization potentials[13] for carbon and hydrogen respectively, one obtains 61.0 v for polystyrene combined as C_8H_8. Experiments will be described in which the average ionization potential for polystyrene is determined with reference to aluminum.

Since a possible source of error in the yields based on ionization chamber measurements could be in the use of 32.5 ev for W for air, it was thought advisable to determine the energy absorbed per unit volume of the chamber wall using argon and nitrogen in addition to air as the chamber gas. As a result of these measurements, an experimental value of W for air can be calculated in terms of W for argon and nitrogen. The average ionization potentials[14] for air, argon, and nitrogen were taken to be 83.2 v, 195 v, and 80.5 v, respectively.

Since the experimental values for the average ionization potential of air and nitrogen are in good agreement with the values calculated from the equation $I=11.5\,Z$, it was thought advisable to use the calculated values in this determination. In the case of those elements with Z higher than 15, this equation is not verified by experiment and consequently an experimental value was used for argon.

TABLE I. Energy dependence of the stopping power correction.

Energy (kev)	$\frac{K_{poly}}{K_{air}}$
9.56	1.05
128	1.04
664	1.03

[13] See reference 11, p. 203.

[14] W. Siri, *Isotopic Tracers and Nuclear Radiations* (McGraw-Hill Book Company, Inc., New York, 1949), p. 79.

EXPERIMENTAL ARRANGEMENT

Measurements were made with the x-rays from a $\frac{1}{4}$-in. thick gold target in the 2-Mv electron Van de Graaff generator of the Chemistry Department operated at 150 μa. It was assumed that the average x-ray energy was of the order of 1 Mev.

The parallel plate ionization chamber used in this experiment is shown in Fig. 1. The front and rear plates of the chamber were coated with a thin layer of graphite; a circle was scribed in the rear plate to provide a collector and guard ring. The sensitive volume of the chamber, as defined by the scribed circle, was 3.99 cc; the spacing was 7.93 mm. Connections were made to the rear plate with thin shielded aluminum wire. The ionization currents were measured across a 1.013×10^6 ohm resistor with a calibrated vibrating reed electrometer. The saturation curve for the chamber, when filled with air, is shown in Fig. 2. All measurements were made with 450 volts across the chamber.

The polystyrene solution cell, which has the same sensitive volume as the ionization chamber, is shown in Fig. 3. The chemical solutions were made using reagent grade ferrous ammonium sulfate, cp sulfuric acid, and triply distilled water. In all cases the solutions were 3.0×10^{-3} M ferrous sulfate and 0.8 N sulfuric acid. Since it is known that oxidation of the ferrous ion may be promoted by the presence of certain organic impurities, and that the addition of chloride ion inhibits this oxidation,[15] samples were irradiated with and without

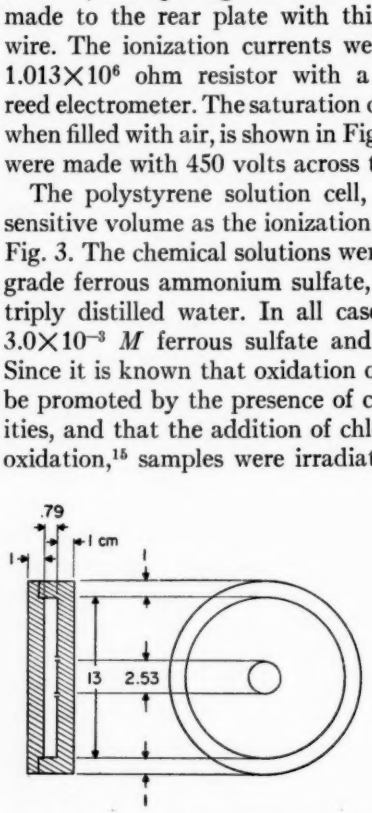

FIG. 1. Drawing of the polystyrene parallel plate ionization chamber.

10^{-3} M chloride ion present. In all cases the amount of iron oxidized was unchanged, indicating the absence of active organic impurities. Analyses[5] of the irradiated solutions were made with a Beckman quartz photoelectric spectrophotometer at a wavelength of 305 mμ using 2185 for the molar extinction coefficient of ferric ion at 24°C.

The ionization chamber and the solution cell were placed alternately, in the same position in the x-ray beam, 29 cm from the accelerator target. All solution exposures were for 500 seconds and several determina-

[15] H. Dewhurst, J. Chem. Phys. **19**, 1329 (1951).

tions were made to average out the small variations in the Van de Graaff x-ray intensity.

CORRECTIONS TO IONIZATION CHAMBER MEASUREMENTS

In order to determine the magnitude of the edge effect in the chamber, different graphite-coated polystyrene disks were inserted against the front face of the chamber to reduce the spacing. The collecting electrode remained in the same position throughout the measurements. Since most of the electrons are produced in the front surface, the insertion of the spacers effectively moved the sensitive region further away from the source. As a consequence, the current per unit volume had to be corrected for this change in

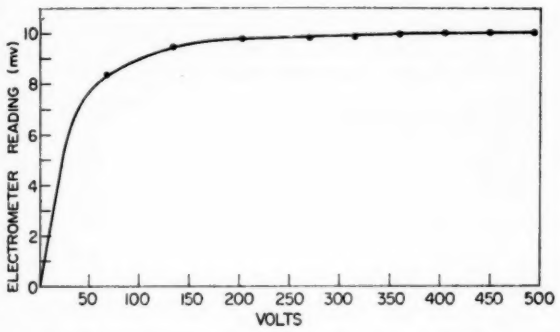

FIG. 2. Saturation curve for the chamber when filled with air.

solid angle, and also for attenuation of the x-rays, for each spacer. Figure 4 is a plot of corrected current per unit volume as a function of the spacing. Extrapolation to zero spacing gives a correction factor of 1.11 ± 0.02 to be applied to the current measured in the 7.93 mm deep experimental chamber.

The stopping power calculation for polystyrene is based on the use of the calculated value of its average ionization potential. This calculation was verified in the following manner. An identical ionization chamber was constructed of aluminum for which the theoretical and experimental determinations of the average ionization potential are in agreement at 150 v.[13] The front face of this chamber had the same number of electrons/cm^2 as the polystyrene chamber and the sensitive volumes of both chambers were located in the same position in the beam. In each case air was used as the gas. If the observed ionization currents are corrected for the different x-ray absorption probabilities, then for equal x-ray intensity, the energy absorbed per unit volume is equivalent for the polystyrene and aluminum chambers. Therefore, the Bragg-Gray equation may be rewritten as

$$\frac{J_{\text{POLY}}}{J_{\text{AL}}}=\frac{S_{\text{AL}}}{S_{\text{POLY}}}\frac{(NZ)_{\text{POLY}}}{(NZ)_{\text{AL}}}=\frac{K_{\text{AL}}}{K_{\text{POLY}}}.$$

The calculated value of this ratio is 0.89. The measured

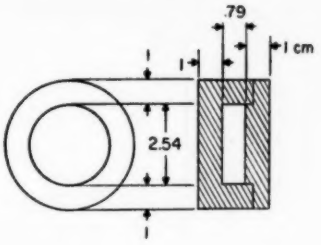

FIG. 3. Drawing of the polystyrene solution cell.

value was found to be 0.90. This indicates that the average ionization potential of polystyrene is not significantly different from 61.

The ionization currents were determined for the same x-ray intensity, using argon, nitrogen, and air as the chamber gas. The gases were allowed to flow through the polystyrene chamber; sufficient time was allowed to insure adequate flushing before the measurements were begun. No special precautions were taken to insure very high gas purity. In order to determine W for air in terms of the W of the other gases, the Bragg-Gray equation may be written as follows:

$$\frac{W_1}{W_2}=\frac{J_2S_1}{J_1S_2}=\frac{J_2(NZ)_1K_1}{J_1(NZ)_2K_2}.$$

The experimental results gave the ratios

$$\frac{W_{\text{air}}}{W_{\text{nitrogen}}}=0.93,\ \frac{W_{\text{air}}}{W_{\text{argon}}}=1.30,\ \text{and}\ \frac{W_{\text{nitrogen}}}{W_{\text{argon}}}=1.39.$$

The latter value is in good agreement with the ratio determined by Jesse[16] for polonium alpha particles, and all are in fair agreement with the β-particle measurements of Valentine.[17] If it is assumed that the value of W for argon and nitrogen is independent of the nature of the ionizing particle, and Jesse's alpha-particle values of 26.4 ev and 36.6 ev are adopted for argon and nitrogen, we obtain in each case a value of 34.3 ev for air under the laboratory conditions of humidity, etc.

RESULTS AND DISCUSSION

The energy absorbed per unit volume of solution/sec, E_s, is then calculated from the following equation:

$$E_s=\frac{PU}{R\times1.6\times10^{-19}(\text{COUL}/e)}\times\frac{W}{V}\times\frac{(NZ)_{\text{POLY}}K_{\text{POLY}}}{(NZ)_{\text{GAS}}K_{\text{GAS}}}\times\frac{(NZ)_{\text{SOL'N}}}{(NZ)_{\text{POLY}}},$$

where P=voltage observed on the electrometer, R=resistance from collecting electrode to ground, U=extrapolation correction, W=energy to form one ion pair in the gas, and V=sensitive volume of the chamber.

[16] W. P. Jesse and J. Sadauskis, Phys. Rev. **90**, 1120 (1953).
[17] J. M. Valentine, Proc. Roy. Soc. (London) A211, 75 (1952).

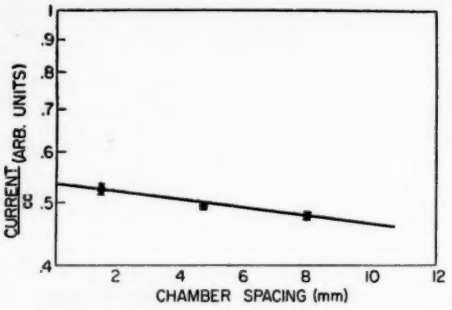

FIG. 4. Extrapolation plot of ionization current/unit volume *versus* chamber spacing.

The ferric ion yield (ions/ml/sec) is calculated from the following equation:

$$\frac{OD\times 457\times 10^{-9}\times 6.025\times 10^{23}}{\text{time}} = \text{ions/ml/sec},$$

where OD = optical density.

The experimental data are listed in Table II. The value of E_s is calculated to be 5.37, 5.37, and 5.33×10^{14} ev/ml/sec for argon, nitrogen, and air fillings; the ferric ion yield is 8.54×10^{13} ions/ml/sec.

The G value, ions oxidized/100 ev, is found to be 15.9 ± 0.5, in good agreement with the values around 15.6 determined by calorimetry and cathode-ray bombardment techniques. The main source of experimental error in this measurement is the extrapolation correction, since the use of spacers introduces an uncertainty in the determination of the sensitive volume. A further error is introduced in the correction for the x-ray attenuation. The construction of a better extrapolation chamber would eliminate this error.

It is evident that certain systematic errors may be present in this determination which have not been included in the assigned error. The relative electronic stopping power ratios depend upon two factors: the absence of any low-energy electrons (<10 kev) and the accuracy to which the values of the average ionization potentials are known. A search of the literature indicates a wide range of values of I for most materials and a possible breakdown of the Bragg rule for some compounds.

The good agreement between the determinations with the three gases and their agreement with the calorimetric and cathode ray bombardment determinations give support to the W values used for the three gases. However, these measurements were not intended to yield an absolute W for air, and in view of some of the assumptions which were made for argon and nitrogen, it would be desirable to obtain accurate absolute W values for the different gases. Although we feel that the ionization chamber measurements themselves are accurate within the assigned experimental error, the true yield of the ferrous sulfate reaction as determined by ionization chamber measurements is limited to the accuracy to which the product, $W(S_{\text{wall}}/S_{\text{gas}})$, is known. From our measurements we conclude that the high ionization chamber determinations of $G(\sim 20)$ are definitely outside all errors, and that the calorimetric value of 15.6 is more nearly correct.

The recent determination by Cormack *et al.*[8] appears to be in good agreement with our result, but this is to some extent fortuitous. They calculated a relative electronic stopping-power ratio of 1.09 for water and air, and used 32.5 ev for W of air. We have used a relative electronic stopping power ratio of 1.04 for polystyrene and air, and an experimentally determined W value of 34.3 ev. We believe that the conclusion of Cormack *et al.* that the equilibrium wall of the Victoreen R meter represented a water equivalent wall is not well founded, and that the relative electronic stopping power ratio of the wall itself and air should have been used. They based their conclusion on the fact that the currents obtained from the Victoreen R meter and an experimental "water equivalent" chamber showed the same energy dependence when exposed to Co^{60} and betatron radiation. It is quite probable that the average ionization potential of the wall is approximately 70, and if 83.2 v rather than 96 v is used for the average ionization potential of air, one would obtain an electronic stopping power ratio of 1.03. If our W value for air is used, the results are then in excellent agreement.

TABLE II. Summary of experimental data.

Temperature (°C)	24
Pressure (mm)	760
Number of ion current determinations	10
R (ohms)	1.013×10^{6}
U (extrapolation correction)	$1.11\ \pm 2\%$
V (cc) chamber volume	$3.99\ \pm 1\%$
NZ soln (electrons/cc)	$3.42\ \times 10^{23}$
P (millivolts) air filling	$9.1\ \pm 1\%$
P (millivolts) argon filling	$13.2\ \pm 1\%$
P (millivolts) nitrogen filling	$8.4\ \pm 1\%$
W air (ev/ion pair)	34.3
W argon (ev/ion pair)	26.4
W nitrogen (ev/ion pair)	36.6
K poly/K argon	1.18
K poly/K air	1.04
K poly/K nitrogen	1.04
(NZ) air (electrons/cc)	$3.57\ \times 10^{20}$
(NZ) argon (electrons/cc)	$4.49\ \times 10^{20}$
(NZ) nitrogen (electrons/cc)	$3.49\ \times 10^{20}$
Number of chemical determinations	10
Time of chemical determinations (sec)	500
OD	$0.155\pm 0.5\%$
Yield, air (ferric ions/100 ev)	16.0
Yield, argon (ferric ions/100 ev)	15.9
Yield, nitrogen (ferric ions/100 ev)	15.9
Total error	3%

ACKNOWLEDGMENT

The authors wish to thank Dr. A. O. Allen and his group for the use of the Van de Graaff machine, and to acknowledge many helpful discussions with them.

Cation Distribution and g Factors of Certain Spinels Containing Ni^{++}, Mn^{++}, Co^{++}, Al^{+++}, Ga^{+++}, and Fe^{+++}

SELMA GREENWALD, STANLEY J. PICKART, AND FREDERICK H. GRANNIS
U. S. Naval Ordnance Laboratory, White Oak, Maryland

(Received April 5, 1954)

X-ray measurements on $NiOAl_2O_3$, $MnOAl_2O_3$, and $CoOAl_2O_3$ show that the Ni spinel is almost completely inverted, the Mn partially so, and the Co compound almost completely normal. This information combined with the magnetic susceptibility *vs* temperature data yields a g-value of approximately 4.0 for both tetrahedrally coordinated Ni^{++} and for octahedrally coordinated Co^{++}. X-ray measurements indicate that the Ni^{++} ion also prefers the octahedral site in $NiOGa_2O_3$, $NiOFe_{1.00}Al_{1.00}O_3$, and $NiOFe_{0.25}Al_{1.75}O_3$.

INTRODUCTION

MANY materials with the chemical formula MON_2O_3, where M and N are divalent and trivalent ions, respectively, crystallize with the same arrangement of atoms as the mineral spinel ($MgOAl_2O_3$). The spinel structure with eight molecules per unit cell is characterized by an oxygen framework with tetrahedral and octahedral interstices—of these only eight and sixteen, respectively, are filled. When the tetrahedral or A sites are occupied by the eight divalent ions, and the octahedral or B sites by the sixteen trivalent ions, the spinel is called normal; on the other hand, if eight of the trivalent ions are located on the A sites, and the remaining trivalent and the eight divalent ions on the B sites, the spinel is called inverted. Partial inversions corresponding to intermediate distributions also occur.

Verwey and Heilmann[1] formulated a set of rules for predicting whether a spinel would be normal or inverted. These rules state that for a divalent-trivalent (2–3) spinel, the normal structure is the more stable with the following important exception: if the trivalent ion is Fe, Ga, or In, then the inverted structure is the more stable. There is the further exception that Zn^{++} and Cd^{++} spinels are normal, regardless of the trivalent ion.

Although the aluminates of Mn, Co, and Ni are known to be spinels,[2,3] it had never been clearly established whether they are normal or inverted; most of the available evidence [1,4] has suggested that they are normal as Verwey's rules predict. Recent theoretical work by Smart[5] on the series $NiOFe_{2-t}Al_tO_3$, where the parameter t is varied from 0 to 2 in small steps, indicated that $NiOAl_2O_3$ was nearly inverted; a reexamination of Holgersson's[2] work showed that this might indeed be the case. We have now therefore determined, by x-ray diffraction, the cation distribution in $NiOAl_2O_3$, $CoOAl_2O_3$, and $MnOAl_2O_3$.*

We have also made magnetic susceptibility measurements on these compounds. This will enable us, knowing the ion distribution, to obtain information on the g values of the divalent ions. Smart[5] and Wangsness[6] have suggested that the magnetic moments of the Ni atoms on the A and B sites might have different values because the effect of quenching due to the crystalline fields on the respective sites is different. Since the average effective moment per molecule is obtained from the susceptibility measurements, a knowledge of the ion distribution allows g values to be assigned to the Ni^{++} ions for each location. This work also includes similar calculations for cobalt and manganese aluminates, and nickel gallate.

In addition, we have determined the ion distributions in $NiOFe_{0.25}Al_{1.75}O_3$ and $NiOFe_{1.00}Al_{1.00}O_3$ by x-ray diffraction.

PREPARATION OF MATERIALS

The compounds were prepared using spectroscopically pure oxides in finely powdered form. After being mixed with water, they were rolled in a stone ball mill and dried. The samples underwent two preliminary heat treatments at 1000°C for an hour; following each heating, they were ground to a particle size of less than 74 microns. Finally, the compounds were heated at 1400°C for one or two hours, followed by quenching or by annealing at a 1°/minute rate.

X-RAY APPARATUS AND METHODS

Intensity *vs* 2θ curves were scanned at $\frac{1}{8}$°/min with a Norelco high angle goniometer spectrometer. Cu and Fe filtered radiations were used, and Lorentz polarization and geometrical factors were applied to the calculated intensities. In addition a temperature correction based on a Debye θ of 500°K, which was determined by Bacon *et al.*[7] for $MgOFe_2O_3$, was included.

Bertaut[8] has shown that the 400/220 and 400/224 intensity ratios in the spinels are very sensitive to the distribution of the cations and relatively insensitive to the oxygen parameter. The behavior of these calculated

[1] E. J. W. Verwey and E. L. Heilmann, J. Chem. Phys. **15**, 174 (1947).
[2] S. Holgersson Lunds, Univ. Arsskr. **23**, No. 9 (1927).
[3] Clark, Ally, and Badger, Am. J. Sci. **22**, 539 (1931).
[4] T. F. W. Barth and E. Posnjak, Z. Krist. **82**, 325 (1932).
[5] J. S. Smart, Phys. Rev. **94**, 847 (1954).
* F. C. Romeijn has also recently studied these spinels.
[6] R. K. Wangsness, Phys. Rev. **91**, 1085 (1953).
[7] G. E. Bacon and F. F. Roberts, Acta Cryst. **6**, 57 (1953).
[8] F. Bertaut, Compt. rend. **230**, 213 (1950).

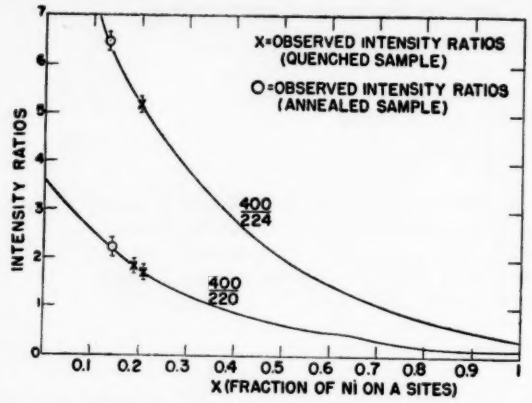

FIG. 1. Calculated curves of the 400/220 and 400/224 intensity ratios as a function of the fraction of Ni^{++} in $NiOAl_2O_3$ on the A sites.

intensity ratios as a function of x, the amount of Ni on the A sites, is shown in Figs. 1 and 2, for the cases of $NiOAl_2O_3$ and $NiOGa_2O_3$, respectively. The marked difference between the two figures can be ascribed to the fact that the scattering powers of the atoms are widely separated in the first case but nearly the same in the second. The intensity ratio curves calculated for $CoOAl_2O_3$ and $MnOAl_2O_3$ are similar to those shown in Fig. 1. By plotting the observed intensity ratios on these curves, the values of x for both quenched and annealed samples can be obtained.

It is more difficult to establish uniquely the distribution in the Ni ferrite-aluminate series for $t<2$, since there are now three kinds of atoms distributed between the A and B sites, and of them the Ni and Fe have nearly equal scattering powers. By solving the equations

$$F_{400}^2(x,z)/F_{220}^2(x,z) = \text{observed intensity ratio}$$

and (1)

$$F_{400}^2(x,z)/F_{224}^2(x,z) = \text{observed intensity ratio},$$

where z is the amount of Al on the A sites, for values of x and z which satisfy both expressions, the ion distribution is uniquely determined. The amount of Fe in the A sites can be found since it is $1-x-z$. Data for the compound with $t=1$ was analyzed in this way.

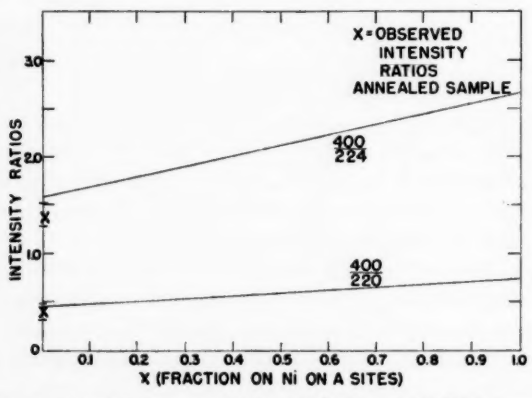

FIG. 2. Calculated curves of the 400/220 and 400/224 intensity ratios as a function of the fraction of Ni^{++} in $NiOGa_2O_3$ on the A sites.

In the case of $NiOGa_2O_3$, a value for the oxygen parameter, u, of 0.387 ± 0.003 had to be assumed to secure the rough agreement which has been obtained between the calculated and observed intensities. This value of u is comparable to the 0.387 ± 0.002 found for $NiOFe_2O_3$, an inverted spinel, by neutron diffraction.[9]

X-RAY RESULTS AND DISCUSSION

The results for the compounds studied are listed in Table I.

Our results for $NiOAl_2O_3$ agree roughly with Romeijn's.[10] He found x equal to 0.24 ± 0.02 but did not detect any distribution differences between quenched and annealed samples. Our data, however, when analyzed by the ratio method, indicated a more random ion distribution for quenched samples than for annealed ones, except in the case of $MnOAl_2O_3$. The ratio method probably attaches too much importance to the 400 peak but the differences in the intensity of this peak for the annealed and quenched samples were well beyond the limits of the experimental error in all cases except for $MnOAl_2O_3$. Annealing $MnOAl_2O_3$ in air results in the formation of Mn_3O_4 and a compound which is a tetragonal distortion of a spinel; if the heat treatments are carried out in an inert atmosphere, the cubic spinel structure is maintained.

The ion distributions for the Ni ferrite-aluminate series correspond within the limits of experimental error to those predicted by Smart[5] from the relation between the saturation moment and effective g factors of these materials. In addition, these results, coupled with those found for Ni gallate and Co and Mn aluminates, fit in very well with Romeijn's[10] suggestion that Ni^{++} has a strong preference for octahedral sites, Co^{++} for tetrahedral sites, and Mn^{++} no preference.

SUSCEPTIBILITY APPARATUS AND MEASUREMENTS

Magnetic susceptibility measurements were made by a body-force method[11] using a null-indicating electrodynamic torsion balance. The chamber housing the balance was evacuated and refilled with helium. All measurements were taken with the samples in a helium atmosphere; this precaution was important in the case of $MnOAl_2O_3$, which is unstable when heated in air. Initially the materials were annealed in helium, being cooled slowly from 1300°C to room temperature at a rate of approximately 1°C/minute. Then magnetic measurements were taken at various temperatures, as the temperature was either raised in steps from room temperature to 1200°C, or lowered progressively from 1200°C, after having been held at each temperature

[9] Corliss, Hastings, and Brockman, Phys. Rev. **90**, 1013 (1953).
[10] F. C. Romeijn, Philips Research Repts. **8**, 321 (1953).
[11] T. R. McGuire and C. T. Lane, Rev. Sci. Instr. **20**, 489 (1949).

TABLE I. X-ray data and ionic distribution results.

Material	Heat treatment	Observed intensity ratio $\frac{400}{220}$	Observed intensity ratio $\frac{400}{224}$	x = fraction of A sites occupied by M^{++}	z = fraction of A sites occupied by N^{+++}	$a_0(A)$
$NiOAl_2O_3$	annealed	2.21	6.49	0.15±0.03	0.85	8.043
	quenched	1.85	5.16	0.20±0.03	0.80	
$CoOAl_2O_3$	annealed	0.239	0.904	0.81±0.03	0.19	8.100
	quenched	0.336	1.33	0.69±0.03	0.31	
$MnOAl_2O_3$	annealed	0.490	1.78	0.66±0.04	0.34	8.241
	quenched	0.435	1.54	0.71±0.04	0.29	8.200[a]
$NiOFe_{0.25}Al_{1.75}O_3$	annealed	1.56	4.23	0.08±0.03	0.66±0.03	8.081
	quenched	1.33	4.08	0.18±0.03	0.64±0.03	
$NiOFeAlO_3$	annealed	0.775	2.38	0.02±0.01	0.23±0.04	8.185
	quenched	0.964	3.07	0.05±0.01	0.35±0.04	
$NiOGa_2O_3$	annealed	0.447	1.41	0.0 ±0.05	1.0	8.258

[a] The discrepancy between a_0 for the quenched and annealed samples may be due to the fact that the quenching was not done in an atmosphere of helium. Therefore, it is possible that even in the short time needed to quench the sample, some Mn_3O_4 was formed.

for at least one hour. The data shows no evidence of thermal hysteresis, indicating that an approximate equilibrium distribution of the magnetic ions was achieved for each measurement. Thus the high and the low temperature susceptibilities should correspond, at least roughly, to the distributions obtained from x-ray diffraction measurements on quenched and annealed samples, respectively.

The measured susceptibilities were corrected for diamagnetism to yield the paramagnetic susceptibility by considering the total diamagnetic susceptibility of the compound to be the sum of the free-ion susceptibilities. These were calculated by Dr. J. S. Smart using radial wave functions of a type first suggested by Slater.[12] The diamagnetic correction is small (-0.52×10^{-6} emu/g for $MnOAl_2O_3$, -0.43×10^{-6} emu/g for both the Co and Ni aluminates, and -0.37×10^{-6} emu/g for Ni gallate), but becomes relatively more important as the temperature is raised, since the diamagnetic susceptibility remains constant while the paramagnetic susceptibility decreases with temperature.

MAGNETIC SUSCEPTIBILITY RESULTS AND DISCUSSION

$MnOAl_2O_3$

The $1/\chi-T$ curve for this compound (Fig. 3) shows only a slight deviation from the Curie-Weiss behavior below room temperature where it probably begins to follow the more complicated Néel hyperbola.[13] The electron configuration of Mn^{++} is $3d^5$ with $6S_{5/2}$ lowest level. This state has no orbital magnetic moment and therefore there should be little difference in the magnetic moment for either the A or B sites. In addition, the g factor should be very close to 2, the spin-only value. The experimental value obtained from the susceptibility curve gives $g=1.94$.

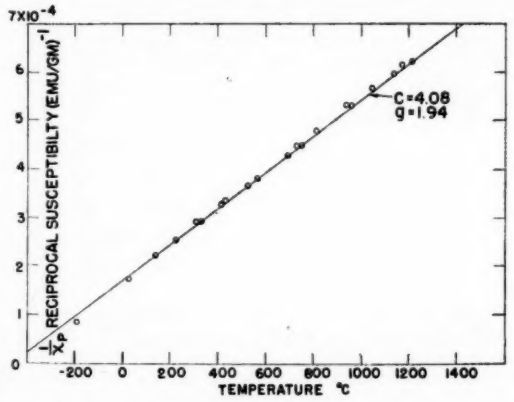

FIG. 3. Reciprocal magnetic susceptibility of $MnOAl_2O_3$ as a function of temperature.

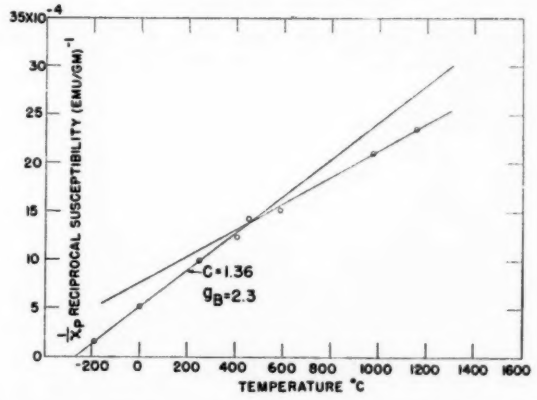

FIG. 4. Reciprocal magnetic susceptibility of $NiOGa_2O_3$ as a function of temperature.

[12] J. C. Slater, Phys. Rev. **36**, 52 (1930).

[13] L. Néel, Ann. phys. **3**, 137 (1948).

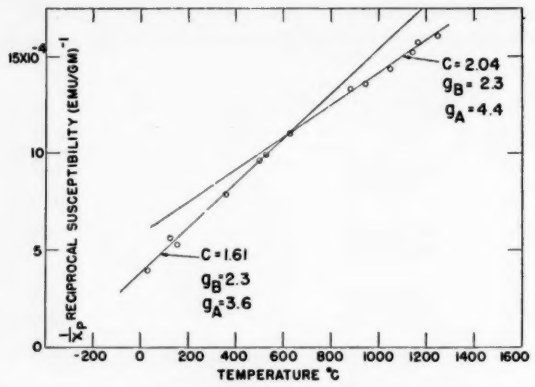

FIG. 5. Reciprocal magnetic susceptibility of $NiOAl_2O_3$ as a function of temperature.

$NiOGa_2O_3$

Since $NiOGa_2O_3$ has been shown to be completely inverted by the x-ray diffraction experiment, the analysis of the susceptibility data (Fig. 4) for this compound should give the g factor for Ni^{++} in octahedral coordination. The value obtained, $g=2.3$, agrees with the values determined previously by Yager *et al.*[14] and Healey[15] from microwave resonance measurements on nickel ferrite.

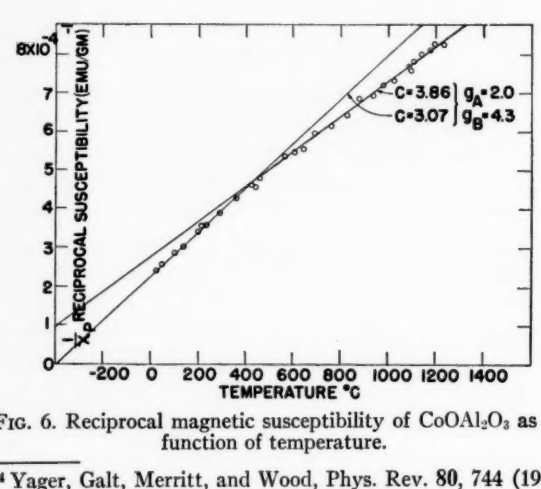

FIG. 6. Reciprocal magnetic susceptibility of $CoOAl_2O_3$ as a function of temperature.

[14] Yager, Galt, Merritt, and Wood, Phys. Rev. **80**, 744 (1950).
[15] D. W. Healy, Jr., Phys. Rev. **86**, 1009 (1952).

$NiOAl_2O_3$

The g value for Ni^{++} in tetrahedral coordination can be obtained for $NiOAl_2O_3$, which is incompletely inverted, from the equation

$$\mu^2_{\text{eff}}=xg_A^2[S(S+1)]+(1-x)g_B^2[S(S+1)], \quad (2)$$

where μ_{eff} is the effective Bohr magneton number, and S the spin quantum number for Ni^{++}. By using $g_B=2.3$, the quenched ion distribution, and the value of μ_{eff} obtained from the high temperature $1/\chi-T$ curve (Fig. 5) a value for g_A of 4.4 is determined. The low temperature slope and annealed distribution gives 3.6 for g_A.

$CoOAl_2O_3$

Co^{++}, like Ni^{++}, has different g values depending on its coordination, but unlike Ni^{++} it is the tetrahedrally coordinated Co^{++} which should have a g value near 2, as given by Van Vleck.[16]

If we assume $g_A=2$ and then use the quenched ionic distribution and the high temperature susceptibility slope (Fig. 6), g_B is 4.30; the annealed distribution and the low temperature slope gives $g_B=4.26$. These are reasonable values for octahedrally coordinated Co^{++} in light of the theoretical and experimental work on various Co compounds done by Abragam and Pryce[17] and Bleaney and Ingram,[18] who obtained g values between 3 and 6.

ACKNOWLEDGMENTS

The authors wish to thank Dr. T. R. McGuire for his help with the susceptibility measurements, and Dr. J. Samuel Smart for many helpful discussions. We are also grateful for the receipt of a copy of Dr. Romeijn's thesis.

[16] J. H. Van Vleck, Phys. Rev. **41**, 208 (1932).
[17] A. Abragam and M. H. L. Pryce, Proc. Roy. Soc. (London) **A206**, 173 (1951).
[18] B. Bleaney and D. J. E. Ingram, Nature **164**, 116 (1949); Proc. Roy. Soc. (London) **A208**, 143 (1951).

Adsorption of Carbon Dioxide on Nickel Single Crystal Surfaces Using a Radiotracer Technique*

J. A. DILLON, JR.,† AND H. E. FARNSWORTH
Brown University, Providence, Rhode Island‡

(Received March 29, 1954)

The adsorption of CO_2 (5.8 percent $C^{14}O_2$) on the (110) and (100) faces of a nickel single crystal has been studied, using an adsorption chamber containing a thin window Geiger counter. Maximum adsorption of CO_2 takes place on adsorbed residual gas layers of optimum thickness rather than on the clean nickel surface. The CO_2-nickel combination has a relatively low rate of adsorption (1.5×10^{11} molecules per minute for each face). The observed equilibrium adsorption values on the (110) and (100) faces were about equal after 54 hours of outgassing at 985°C. After 32 additional hours of heating at 1085°C, the adsorption on the (110) face was twice that on the (100) face. Possible thermal etching of the (110) face makes the reason for this difference uncertain. At equilibrium on the (110) face, the surface coverage is about 2 percent. The equilibrium adsorption on the (100) face decreases linearly by 80 percent as the temperature is increased from 30°C to 110°C.

INTRODUCTION

BECAUSE small amounts of radioactive adsorbates can be detected readily, the use of radiotracers allows the examination of gaseous adsorption on small areas, such as those of smoothly polished solids, and on various faces of metal single crystals. Such a method is important in comparing the surface coverages computed theoretically with the actual areas involved, and in studying the effects of heat treatment of the solid samples prior to adsorption. In those experiments in which powdered samples are used, it is difficult to interpret these effects in terms of the adsorption data. Because sintering occurs when powdered samples are heated at high temperatures, an increase in the adsorption per unit area due to a decrease in the surface contamination may be completely obscured by the resulting decrease in area due to sintering. By using smooth adsorbent surfaces, the effects of sintering can be practically eliminated.

A radiotracer method suitable for the study of gaseous adsorption on metal single crystals has been reported from this laboratory.[1] In order to measure activity after exposure to $C^{14}O_2$, the specimen was removed from the adsorption chamber and placed under an external counter. Exposure of the specimen to the atmosphere between runs introduced the possibility of surface poisoning, and also increased the difficulty of outgassing the specimen after each counting observation.

The object of the present research is the study of the adsorption of carbon dioxide on the (110) and (100) faces of a nickel single crystal in the pressure range from 10^{-6} mm to 10^{-1} mm Hg using an improved radiotracer method. The present technique eliminates the necessity of removing the sample from the vacuum system by employing a counter which is built inside the adsorption chamber.

EXPERIMENTAL APPARATUS

The complete system is shown in the block diagram of Fig. 1. A Geiger counter with a 2 mg/cm² mica window was sealed inside the adsorption chamber.[2] The counter was operated with a counting mixture made of equal partial pressures of Freon-22($CHClF_2$) and argon at a total pressure of 2 cm Hg. Mica was selected for the window material because preliminary tests indicated that CO_2 does not adsorb to any noticeable extent on clean mica in the pressure range used. By means of magnetic controls, the sample could be moved either to the outgassing position, where it could be outgassed by means of electron bombardment, or to the counting position, where its activity after adsorption could be measured. The adsorption chamber was isolated from the adsorbate supply and the pumping lines by metal vacuum values.[3] These valves eliminated

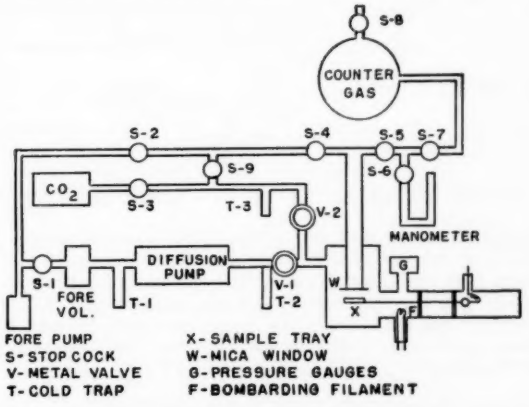

FIG. 1. Block diagram of apparatus.

* Part of a dissertation submitted in partial fulfillment of the requirements for the degree of Doctor of Philosophy at Brown University. Part of this paper was presented at the meeting of the American Physical Society, New York City, January, 1954.

† At the Geophysics Research Directorate, Air Force Cambridge Research Center, July, 1953 to July, 1954.

‡ Assisted in part by U. S. Office of Naval Research.

[1] A. D. Crowell and H. E. Farnsworth, J. Chem. Phys. **19**, 1206 (1951).

[2] J. A. Dillon, Jr., and H. E. Farnsworth, Rev. Sci. Instr. **25**, 96(L), 1954.

[3] D. Alpert, Rev. Sci. Instr. **22**, 536 (1951).

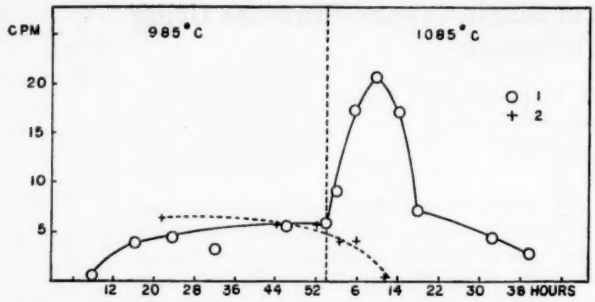

FIG. 2. Activity of (110) nickel single crystal sample as a function of cumulative outgassing time. The adsorption pressure in each case was 3.5×10^{-2} mm Hg, the exposure time was 30 minutes, and the temperature during exposure was 30°C. The second run was made after the crystal had been exposed to the residual gases at 10^{-5} mm Hg for 12 hours. The counting error was ±2 cpm.

any residual gas pressure build up due to desorption from stopcock greases while the adsorption chamber was closed from the pumping lines. The ultimate vacuum attained in this set of experiments was about 7×10^{-8} mm Hg.

Carbon dioxide was generated from $BaCO_3$ by the acid method.[4] The activity of this gas, as specified by Oak Ridge from which the $BaCO_3$ was obtained, was such that 5.8 percent of the molecules were $C^{14}O_2$. The (110) and (100) faces of a nickel single crystal were selected as adsorbents.[5] The two slabs, each of about 2 cm² in area and 1 mm in thickness, were cut from the crystal and then abraded on successively finer grades of metallographic paper, the final grade being 4/0. After polishing the slabs electrolytically to remove the amorphous layer caused by the mechanical working, they were placed, one at a time, in the adsorption chamber, and the following series of tests were made.

EXPERIMENTAL RESULTS

1. Dependence of Adsorption on Outgassing

Outgassing was carried out at a temperature of 985°C and later at 1085°C as measured with an optical

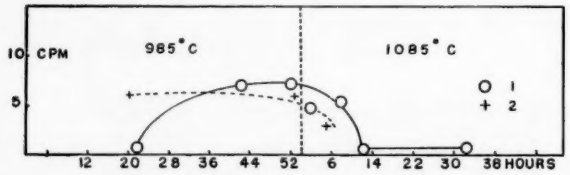

FIG. 3. Activity of (100) nickel single crystal sample as a function of cumulative outgassing time. The adsorption pressure in each case was 3.5×10^{-2} mm Hg, the exposure time was 30 minutes, and the temperature during exposure was 30°C. The second run was made after the crystal had been exposed to the residual gases at 10^{-5} mm Hg for 12 hours. The counting error was ±2 cpm.

[4] Calvin, Heidelberger, Reid, Tolbert, and Yankwich, *Isotopic Carbon* (John Wiley and Sons, Inc., New York, 1949), p. 153.

[5] The nickel single crystal was purchased from Horizons Inc., 2891 East 79th Street, Cleveland, Ohio. Impurities are given as less than 0.003 percent cobalt and 0.1 percent carbon. The crystal was produced in an alumina crucible.

pyrometer, the readings being corrected for emissivity.[6] After definite periods of outgassing, the samples were allowed to cool for one half hour, and the CO_2 was admitted to the adsorption chamber for 30-minute periods at a pressure of 3.5×10^{-2} mm Hg and a temperature of 30°C. Figure 2 shows the resulting activities obtained for the (110) face as a function of outgassing time and temperature. The first detectable activity was noted only after the sample had been outgassed at 985°C for 16 hours. After 52 hours of outgassing, the activity had increased by about 20 percent over the value obtained at 16 hours. At this point the outgassing temperature was raised to 1085°C where appreciable evaporation was observed. The activity increased rapidly over the first 9 hours at this higher temperature, and then it decreased until, at 18 hours, it had reached the same value it had before the temperature increase. From this time until 40 hours the activity decreased slowly. After the final reading, the sample

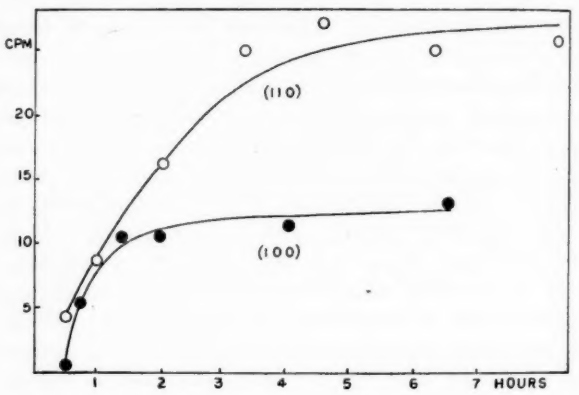

FIG. 4. Activity of the single crystal samples as a function of the exposure time. The adsorption pressure was 3.5×10^{-2} mm Hg, and the exposure temperature was 30°C. The counting error was ±2 cpm.

was outgassed for 15 minutes at 1085°C to remove any residual activity, and was then allowed to stand at a residual gas pressure of 1×10^{-5} mm Hg for about 12 hours. The amounts of adsorption obtained as the sample was again outgassed are shown by the dotted line in Fig. 2. After 22 hours of outgassing at 985°C, the activity had more than doubled over the value obtained after the original outgassing at 1085°C for 40 hours just preceding the exposure to the residual gases. As outgassing was continued at 985°C the measured activity decreased slightly. When the outgassing temperature was again raised to 1085°C, the activity decreased until at 12 hours no activity was detected. The peak obtained in the first run was not observed in these tests.

Figure 3 gives the results obtained when the same outgassing procedure was repeated with the (100) face. When the temperature was raised to 1085°C, the

[6] *International Critical Tables* (McGraw-Hill Book Company, Inc., New York, 1929), Vol. 5, p. 245.

activity decreased rapidly without the presence of a peak as in Fig. 2. The behavior obtained when the sample was allowed to stand for 12 hours at a residual gas pressure of 10^{-5} mm Hg was the same as that noted in the second run of Fig. 2.

2. Dependence of Adsorption on Exposure Time

After 52 hours of outgassing at 985°C, and 32 hours at 1085°C, the samples were exposed to the CO_2 at a pressure of 3.5×10^{-2} mm Hg and a temperature of 30°C for various periods of time. After each run the samples were outgassed at 1085°C for 15 minutes to remove any residual activity. As is shown in Fig. 4, the activity increased with exposure time until an equilibrium value was reached after 80 minutes for the (100) face and 180 minutes for the (110) face.

3. Dependence of Adsorption on Exposure Pressure

After 52 hours of outgassing at 985°C, and 34 hours at 1085°C, the (110) crystal face was exposed to the

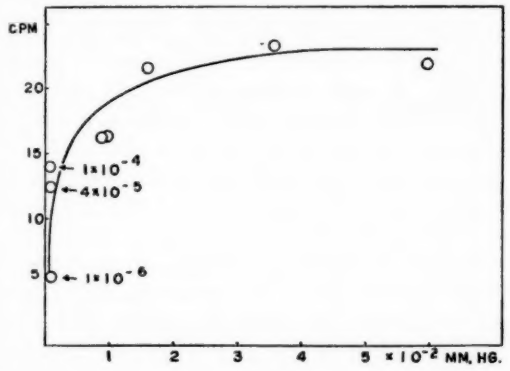

FIG. 5. Activity of the (110) nickel single crystal face as a function of exposure pressure. The exposure time was 3 hours, and the exposure temperature was 30°C. The counting error was ±2 cpm.

CO_2 for three hour periods at 30°C at various pressures from 10^{-6} to 6×10^{-2} mm Hg. After each run the sample was outgassed at 1085°C for 15 minutes to remove any residual activity. The three-hour period was selected so that equilibrium adsorption values would be measured. The results are given in Fig. 5.

4. Dependence of Adsorption on Exposure Temperature

After 52 hours of outgassing at 985°C, and 34 hours at 1085°C, the (100) face was exposed to the CO_2 at a pressure of 3.5×10^{-2} mm Hg for 80-minute periods at various temperatures. The 80-minute period was used so that equilibrium values would be measured. Between runs the crystal was outgassed for 15 minutes at 1085°C, and allowed to cool for 30 minutes before the next exposure. The results, shown in Fig. 6, indicate a linear decrease in the activity as the temperature was increased from 30°C to 110°C.

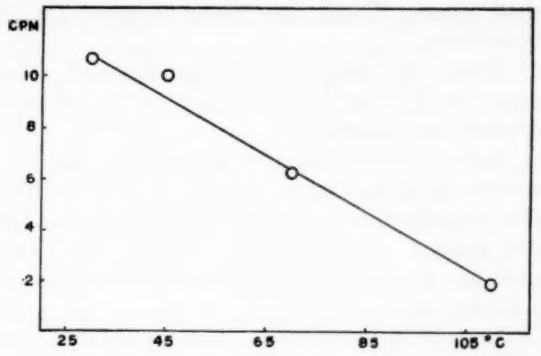

FIG. 6. Activity of the (100) nickel single crystal face as a function of exposure temperature. The adsorption pressure was 3.5×10^{-2} mm Hg, and the exposure temperature was 80 minutes. The counting error was ±2 cpm.

5. Dependence of Adsorption on the Time Elapsed between Outgassing and Exposure to the CO_2

Rather than expose the samples to the CO_2 immediately after the usual 30-minute cooling period following outgassing, they were allowed to remain in a residual gas pressure of about 1×10^{-7} mm Hg for various periods of time. These tests were undertaken to determine the effects of residual gas contamination on the observed adsorption. Following this "standing time," the crystals were exposed to the CO_2 at a pressure of 3.5×10^{-2} mm Hg and a temperature of 30°C. The equilibrium exposure times of 80 and 180 minutes were used for the (100) and (110) faces, respectively. After each run the samples were outgassed at 1085°C for 15 minutes. The results, shown in Fig. 7, show that the amount of adsorption in each case reached a maximum value and then fell off to an apparent equilibrium value as the standing period was increased.

DISCUSSION

The results shown in Fig. 2, 3, and 7 suggest that the maximum adsorption of CO_2 does not take place on the most nearly gas free nickel surface which was obtained but on a critical amount of previously adsorbed

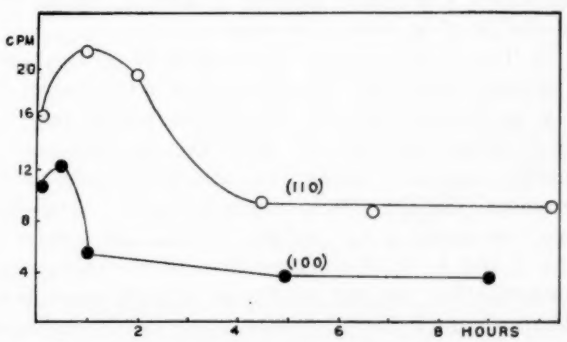

FIG. 7. Activity of the nickel single crystal faces as functions of time elapsed between the end of the normal 30 minute cooling period and exposure to the CO_2. Adsorption pressure was 3.5×10^{-2} mm Hg; exposure temperature was 30°C; exposure time for the (110) face was 180 minutes, and for the (100) face it was 80 minutes. The counting error was ±2 cpm.

residual gases. There are three reasons for this interpretation.

(1) When the samples were first inserted, it was necessary to heat for many hours at 985°C before any adsorption was observed.

As heating continued, the adsorption rose to an apparent equilibrium value. Further heating at 1085°C resulted in a decrease in the observed adsorption. These results suggest that a certain critical condition of residual gas contamination is necessary for maximum CO_2 adsorption.

Electron diffraction studies have shown that amorphous layers persist unless the heating is carried out at temperatures of approximately 600°C for several hours.[7] After heating at 600°C for many hours a single-spaced, simple square array gas structure is observed, and when the temperature is raised to 1100°C the structure becomes a double-spaced, face-centered square array. Heating at 1100°C for many hours does not remove this gas layer from the surface. Field emission studies of nickel surfaces[8] indicate that outgassing for long periods at a high temperature is necessary to remove chemisorbed oxygen from nickel, and that surface carbon can be removed from nickel only by careful oxidation.

A comparison of the present results with those on low-energy electron diffraction suggests that the surface condition (at least for the (100) face of Ni) for maximum adsorption corresponds to a single-spaced square array of residual adsorbate, and that the most nearly gas-free surface is covered by a less dense double-spaced structure.

(2) When the adsorption had reached a low value after long outgassing at the maximum temperature, the samples were exposed to the residual gases for 12 hours. After some additional outgassing at 985°C it was found that the adsorption had increased to a value much higher than that observed just before exposure to the residual gases. Exposure of the sample to residual gas contamination, followed by some heating, apparently restored the surface condition required for appreciable adsorption. Continued heating at 1085°C caused the amount of adsorption to decrease.

(3) The results of Fig. 7 also support the critical contamination suggestion. The adsorption of CO_2 increased to a maximum value as the sample was allowed to stand, before exposure to the CO_2. As the time of standing increased further, the amount of adsorption decreased. The decrease in adsorption as the "standing time" increased is in conformity with the results of Figs. 2 and 3, which indicate that heavy residual gas contamination was not conducive to CO_2 adsorption. The maximum in the adsorption curve can be explained by assuming that the critical amount of residual gas contamination was reached and then exceeded as the standing time increased. Calculations indicated that the 30-minute cooling period was sufficient to return the thin crystal slabs to room temperature after outgassing, so that it is improbable that the maximum can be attributed to an insufficient cooling time. However, because no actual low temperature measuring device was attached to the samples, the temperature effect on the results of Fig. 7 cannot be completely ruled out. Within the limits of the accuracy of the calculations just mentioned, the results of Fig. 7 are in conformity with the experimental evidence discussed in paragraphs 1 and 2 above.

The indication that CO_2 adsorbs on a previously adsorbed layer of residual gases is in conformity with a suggestion made in a discussion of the results obtained in the original experiments of Crowell and Farnsworth.[9] It has also been pointed out that CO_2 adsorbs readily on nickel oxide.[10]

Of several possible explanations for the peak in the outgassing curve of Fig. 2, the most plausible reason is that thermal etching took place. It has been noted that in the case of the (110) face of silver, the surface is unstable under high temperature heating, becoming thermally etched parallel to the more stable (111) and (100) faces.[11] If such etching took place, the increase on the left side of the peak could be due to a cleaning of the surface at the higher temperature (1085°C); the decrease on the right side could be due to the appearance of less active faces. Examination of the crystal face in a beam of light and under the microscope failed to reveal any evidence of thermal etching. X-ray diffraction patterns indicated the crystal face was still (110) after the heat treatment, but these would not give information of the conditions just at the surface. This lack of evidence does not exclude the possibility that thermal etching has taken place. Low-energy electron diffraction studies of the (110) nickel face after high temperature heating should yield conclusive evidence of the stability of this face.

The difference in the equilibrium adsorption values on the (110) and (100) faces does not necessarily indicate that the (110) face is, *per se*, a more active adsorbent than the (100). If the (110) face was thermally etched, there is a possibility that the exposed area increased when the new faces were exposed. It will be noted that the amounts of adsorption obtained in Figs. 2 and 3 after 54 hours of outgassing at 985°C were about equal on the two faces. After 32 additional hours of heating at 1085°C, however, the adsorption on the (110) face was considerably larger than that on the (100) face. The reason for this difference may be either that the (110) face is more difficult to outgas, or that the exposed area of the (110) face after thermal etching was increased.

[7] H. E. Farnsworth, Phys. Rev. **35**, 1131 (1930); R. E. Schlier and H. E. Farnsworth, J. Appl. Phys. (to be published).
[8] R. Gomer, J. Chem. Phys. **21**, 293 (1953).
[9] A. D. Crowell, Am. J. Phys. **20**, 96 (1952).
[10] R. M. Dell and F. S. Stone, Trans. Faraday Soc. **50**, 501 (1954).
[11] H. E. Farnsworth, Phys. Rev. **49**, 598 (1936).

The dependence of adsorption on temperature shown in Fig. 6 is in agreement with the general trend of chemisorption isobars at higher temperatures. The amount of adsorption decreased linearly by about 80 percent as the temperature was increased from 30°C to 110°C.

The low rate of adsorption noted in Fig. 4 suggests that some dissociation of the adsorbed molecules has taken place.[12] If the CO_2 molecules are adsorbed most strongly on previously adsorbed oxygen, a dissociation of the type $CO_2 \rightarrow CO+O$ might be used to explain the long time interval between first exposure and equilibrium. As the adsorbed molecules dissociate, more adsorbed oxygen atoms, and hence more possible adsorption sites, become available for further CO_2 adsorption. When no further sites for oxygen adsorption on the clean nickel are available, equilibrium is attained. A similar mechanism employing carbon as the substratum for CO_2 adsorption may be considered also.

The results of Fig. 5 were fitted quite well to the Langmuir isothermal equation. Attempts to fit the data to the Freundlich, Harkins-Jura, and Williams-Henry equations proved unsuccessful. From a knowledge of the over-all counter efficiency (about 7 percent) and the specific activity of the gas (5.8 percent), it was possible to determine that each count per minute corresponded to about 10^{12} adsorbed CO_2 molecules. The equilibrium value of 23 counts per minute therefore is equivalent to 2.3×10^{13} adsorbed molecules. The observed rate of adsorption is about 1.5×10^{11} molecules per minute for each face.

We wish to acknowledge the receipt of a sample of Freon-22 gas from the E. I. du Pont de Nemours Company, and the assistance in procurement and cutting of thin mica which was provided by Tracerlab, Incorporated.

[12] The possibility of dissociation was suggested by Professor W. W. Russell, Brown University, in a recent discussion.

THE JOURNAL OF CHEMICAL PHYSICS VOLUME 22, NUMBER 9 SEPTEMBER, 1954

Theory of the Spherical Diffusion Flame: The Effect of Atmosphere Depletion

FELIX T. SMITH
Gibbs Memorial Laboratory, Department of Chemistry, Harvard University, Cambridge, Massachusetts

(Received February 8, 1954)

A major uncertainty in the interpretation of data from spherical diffusion flame methods of measuring reaction rates has lain in the difficulty of estimating the effect of depletion of the atmosphere reactant. It is known that the exact treatment of this problem, assuming spherical, purely diffusive flow, leads to a nonlinear ordinary differential equation of the second order. An analytical solution of this equation is presented in a form conveniently applicable to experimental data. The correction is shown to depend on a parameter which is usually small. The solution is applied to the method of temperature pattern measurements, and a modified method of calculating rate constants from experimental data is proposed. The correction to the reaction rate constants previously determined by this method is shown to be small. The use of a wider range of experimental variables than heretofore is made possible.

INTRODUCTION

THE spherical diffusion flame technique for measuring the rate of very fast gas reactions has been widely used since its introduction by Polanyi.[1] The scope of the method has recently been extended by Garvin, Guinn, and Kistiakowsky,[2,3] who determine the pattern of the reaction zone by measuring the steady state temperature pattern, rather than by Polanyi's optical method.

The principle of the experimental method, aside from the method of measurement, is the same in both variants. One reactant, the nozzle reactant, usually accompanied by an inert carrier gas, is allowed to escape at a fixed rate through a small capillary nozzle into the center of a reaction chamber containing a constantly renewed atmosphere of a second reactant, the atmosphere reactant. The pressures and flows are so adjusted that the transport of the reactants in all of the reaction zone beyond a very few nozzle radii from the center is by diffusion, convective flow being negligible by comparison. The nozzle reactant diffuses out through the reaction zone, reacting as it goes, the flow being spherically symmetric and such that the reaction is essentially complete before the walls of the chamber are reached.

The usual equation by means of which a rate constant is determined from the experimental data is derived by assuming spherical symmetry, neglecting convective flow, and assuming constancy of the concentration of the atmosphere reactant throughout the reaction zone. The distortion from spherical symmetry by the jet from the nozzle has recently been discussed by Reed and

[1] Reviews by: M. Polanyi, *Atomic Reactions* (Williams and Wingate, London, 1932); C. E. H. Bawn, Ann. Repts. Chem. Soc. 39, 36 (1942); E. Warhurst, Quart. Revs. (London) 5, 44 (1951).
[2] D. Garvin and G. B. Kistiakowsky, J. Chem. Phys. 20, 105 (1952).
[3] Garvin, Guinn, and Kistiakowsky, Discussions Faraday Soc. (to be published).

Rabinovitch;[4] reliable estimates indicate that both this asymmetry and the convective flow are negligible.[3,4]

The effect of depletion of the atmosphere reactant in the reaction zone has been less amenable to estimation; experimentally it has been necessary to use relatively large concentrations of the atmosphere reactant in an effort to cut down this effect. The extensive experimental investigations of Heller[5] have been of considerable value as a guide to proper experimental conditions, but they were made with the optical flame method principally in view. It has been feared that the atmosphere depletion effect would be comparatively more serious in the method of temperature measurements.[3]

If the atmospheric depletion is to be calculated, the problem leads to a nonlinear differential equation. A solution for a particular case of this equation was obtained by Cvetanović and LeRoy by a laborious numerical computation, but no analytical expression was obtained.[6]

It is the purpose of the present article to present an analytical solution of the spherically symmetric problem with atmosphere depletion but without convective flow, and to explore briefly the conclusions to which this solution leads.

THEORY

In the steady state, neglecting the convective term, the conservation equations for y, the concentration of the nozzle reactant, and z, the concentration of the atmosphere reactant, are

$$D_y\nabla^2 y - kyz = 0, \quad D_z\nabla^2 z - kyz = 0, \tag{1}$$

where D_y, D_z are the diffusion coefficients of the two reactants, and kyz is the reaction rate. Since the inert carrier gas is the predominant constituent of the atmosphere everywhere, and temperatures and pressures vary only slightly throughout the reaction zone, it is permissible to assume that D_y, D_z, and k are constant.

The following change of variables will prove convenient:

$$\rho = cr, \quad \text{where} \quad c^2 = \frac{kz_\infty}{D_y}, \quad m = \frac{kry}{cD_z}, \quad n = \frac{krz}{cD_y}, \tag{2}$$

where z_∞ is the concentration of the atmosphere reactant outside the reaction zone. Assuming spherical symmetry, Eqs. (1) become

$$\frac{d^2m}{d\rho^2} - \frac{mn}{\rho} = 0, \quad \frac{d^2n}{d\rho^2} - \frac{mn}{\rho} = 0. \tag{3}$$

The boundary conditions may be conveniently determined by idealizing the problem to one with a point source of y (plus carrier) at the origin, and allowing the reaction zone to extend to infinity. The first condition is

$$\text{as} \quad r\to\infty, \quad y\to 0, \quad z\to z_\infty. \tag{4}$$

The second condition on y, essentially Garvin and Kistiakowsky's condition[2] expressed in differential form, is established by noting that the point source must introduce y into the system at a rate equal to the experimental flow of y through the nozzle. Thus, if v is the linear rate of flow of the gas in the nozzle, R the nozzle radius, and y_0 the concentration of y in the nozzle mixture

$$\text{as} \quad r\to 0, \quad 4\pi r^2 D_y \frac{dy}{dr} \to -v\cdot\pi R^2\cdot y_0. \tag{5a}$$

We shall also have occasion to use the alternative relation that

$$\text{as} \quad r\to\infty, \quad 4\pi r^2 D_y \frac{dy}{dr} \to 0. \tag{5b}$$

The second condition on z is determined by the fact that its inward flow by diffusion must balance its consumption by reaction plus its loss as it is carried outward by the flow of carrier gas and reaction products ultimately arising from the nozzle. In the case of the ordinary bimolecular exchange reaction, this gives

$$\text{as} \quad r\to\infty,$$

$$4\pi r^2 D_z \frac{dz}{dr} \to v\cdot\pi R^2 y_0 + v\cdot\pi R^2 z_\infty = v\cdot\pi R^2 z_\infty\cdot\beta, \tag{6}$$

where $\beta = 1 + y_0/z_\infty$. In general, β will reflect the stoichiometry of the over-all reaction, as expressed by the change in mole number, Δn.

Changing variables in accordance with (2) and using

$$\alpha = \frac{y_0}{z_\infty}, \quad \beta = 1 + (\Delta n + 1)\frac{y_0}{z_\infty}, \quad \delta = \frac{v}{D_z}\cdot\frac{R^2}{4}\cdot c, \tag{7}$$

we get from (4), (5), and (6),

$$\text{as} \quad \rho\to\infty \begin{cases} \dfrac{m}{\rho}\to 0, & \dfrac{n}{\rho}\to 1 \\ \rho\dfrac{dm}{d\rho} - m \to 0 & \\ \rho\dfrac{dn}{d\rho} - n \to \beta\delta & \end{cases}, \tag{8}$$

and, since $dm/d\rho$ remains finite,

$$\text{as} \quad \rho\to 0, \quad m - \rho\frac{dm}{d\rho} \to m \to \alpha\delta. \tag{9}$$

In the definitions (7), it may sometimes be desirable to use different values of y in α and in β. If consumption of y by back-diffusion of z into the nozzle is important,

[4] J. F. Reed and B. S. Rabinovitch (unpublished manuscript).
[5] W. Heller, Trans. Faraday Soc. (London) **33**, 1566 (1937).
[6] R. J. Cvetanović and D. J. LeRoy, Can. J. Chem. **29**, 597 (1951).

in defining α we should take y_0 as the concentration y in the incoming stream at the nozzle. In Eq. (6), however, the inward flow of z must be such as to replace all the z consumed, whether inside or outside the nozzle, so we should define $\beta=1+(\Delta n+1)y_{-\infty}/z_\infty$, where $y_{-\infty}$ is the initial concentration of y in the system leading to the nozzle.

A relation between m and n may be obtained by taking the difference between Eqs. (3), integrating and applying the condition (8),

$$n=\rho+m-\beta\delta. \tag{10}$$

Substituting in the first equation of (3), we get the nonlinear equation

$$\frac{d^2m}{d\rho^2}=\frac{m}{\rho}(\rho+m-\beta\delta). \tag{11}$$

Taking note of (9), it is convenient to substitute $m/\alpha\delta=\mu$, whence (11) becomes

$$\frac{d^2\mu}{d\rho^2}=\mu\left[1+\delta\left(\frac{\alpha\mu-\beta}{\rho}\right)\right]. \tag{12}$$

Under the ordinary experimental conditions, the parameter δ is quite small. The classical Polanyi approximation is equivalent to neglecting the terms of order δ, whereupon the equation has the solution

$$\mu^{(0)}=e^{-\rho}. \tag{13}$$

Two approaches may be followed to integrate the complete Eq. (12). The solution (13) may be introduced on the right-hand side of (12), and a next approximation may be found by integrating twice and normalizing again to insure that $\mu^{(1)}\to 1$ as $\rho\to 0$. This procedure can be repeated, leading to an iterative relation between successive approximations; the procedure eventually leads to a solution of the form

$$\mu=\mu^{(\infty)}=e^{-\rho}[1+\delta(\alpha F_\alpha-\beta F_\beta)+\delta^2(\alpha^2F_{\alpha\alpha}-\alpha\beta F_{\alpha\beta}+\beta^2F_{\beta\beta})+\cdots], \tag{14}$$

where F_α, F_β, are functions of ρ only, expressed initially in the form of infinite series which may be shown to be convergent.

A simpler approach, however, is to assume that the Eq. (12) has a solution of the form (14). Substituting (14) on both sides of (12), and collecting terms associated with successive powers of δ, α, and β, we get linear equations of standard form

$$F_\alpha''-2F_\alpha'=e^{-\rho}/\rho, \quad F_\beta''-2F_\beta'=1/\rho, \tag{15}$$

$$\left.\begin{aligned} F_{\alpha\alpha}''-2F_{\alpha\alpha}'&=2\frac{e^{-\rho}}{\rho}F_\alpha,\\ F_{\alpha\beta}''-2F_{\alpha\beta}'&=2\frac{e^{-\rho}}{\rho}F_\beta+\frac{1}{\rho}F_\alpha,\\ F_{\beta\beta}''-2F_{\beta\beta}'&=\frac{1}{\rho}F_\beta, \quad \text{etc.}\end{aligned}\right\} \tag{16}$$

To satisfy the boundary conditions, we must have

$$F_\alpha(0)=0, \quad F_\beta(0)=0;$$

and

$$e^{-\rho}F_\alpha(\rho)\to 0, \quad e^{-\rho}F_\beta(\rho)\to 0 \quad \text{as} \quad \rho\to\infty.$$

The appropriate solutions of (15) are

$$\left.\begin{aligned} F_\alpha(\rho)&=-\tfrac{1}{2}[\ln 3+Ei(-\rho)-e^{2\rho}Ei(-3\rho)],\\ F_\beta(\rho)&=-\tfrac{1}{2}[\ln 2\gamma\rho-e^{2\rho}Ei(-2\rho)],\end{aligned}\right\} \tag{17}$$

where $\ln\gamma=0.577216$ is Euler's constant, and

$$Ei(-x)=-\int_x^\infty\frac{e^{-t}}{t}dt$$

is a tabulated function.[7]

The Eqs. (16) may also be solved by standard methods, though the terms on the right-hand side may lead to integrals which cannot readily be expressed in terms of tabulated functions; the integrations may then be performed numerically. Ordinarily, however, it will not be necessary to go beyond the first-order correction (17). While it has not been possible to prove the convergence of the complete solution (14), the equations are of such form that the error committed by stopping at a term of any order in δ appears to be of the order of magnitude of the next succeeding term in the expansion.

The solution for z may be expressed as follows, from Eq. (10),

$$z=z_\infty\left[1+\delta\frac{(\alpha\mu-\beta)}{cr}\right]. \tag{18}$$

Since $\beta>\alpha$, this will be equal to zero at some point $r=r_1$; inside this point the solution for y should be replaced by one for simple diffusion without reaction, so that the corrected solutions become

$$\left.\begin{aligned} y&=\frac{y_0vR^2}{D_y}\cdot\frac{1}{r}\\ z&=0\end{aligned}\right\} r\leqslant r_1$$

$$\left.\begin{aligned} y&=\frac{y_0vR^2}{D_y}\cdot N_1\cdot\frac{e^{-cr}}{r}[1+\alpha\delta F_\alpha(cr)-\beta\delta F_\beta(cr)]\\ z&=z_\infty\left(1+\frac{\delta}{cr}\{N_1\alpha e^{-cr}[1+\alpha\delta F_\alpha(cr)-\beta\delta F_\beta(cr)]-\beta\}\right)\end{aligned}\right\} r\geqslant r_1 \tag{19}$$

where

$$N_1^{-1}=e^{-cr_1}[1+\alpha\delta F_\alpha(cr_1)-\beta\delta F_\beta(cr_1)],$$

[7] Jahnke-Ende, *Tables of Functions*, reprint (Dover Publications, New York, 1945); Mathematical Tables Project, New York, *Tables of Sine, Cosine, and Exponential Integrals* (Washington, D. C., 1940).

and r_1 is determined by $z(r_1)=0$, whence

$$cr_1=\delta(\beta-\alpha)\cong\delta. \tag{20}$$

Since r_1 is thus very small, much less than the nozzle radius in general, and N_1 is therefore very little different from unity, this correction may usually be ignored.

A similar normalizing factor may be desirable in some cases to take account of the fact that depletion of y by reaction is insignificant inside some radius $r_2 \gtrsim R$ because of the effect of the jet in keeping z away from the nozzle. This factor N_2 may be defined as in Eq. (19) by substituting r_2 for r_1; for r_2 the nozzle radius R may be used, or some estimate may be made based on Heller's data.[5]

An alternative treatment of Eq. (12), which might be of value in a case involving large $\beta\delta$, would be to solve the linear equation $d^2\mu_0/d\rho^2=\mu_0(1-\beta\delta/\rho)$, which is easily transformed into an equation of Laguerre type. The nonlinear term $\alpha\delta\mu^2/\rho$ may then be introduced as a perturbation in a manner similar to the above. This approach has not been pursued, since the first-order correction (17) seems accurate enough for most purposes and more convenient for computation.

APPLICATION

The above solution is of a form which is easily applied to experimental data. The concentration of the nozzle reagent is given by the following equation

$$y=\frac{y_0vR^2}{D_y}\cdot\frac{e^{-cr}}{r}[1+\alpha\delta F_\alpha(cr)-\beta\delta F_\beta(cr)+\delta^2(\cdots)]. \tag{21}$$

In this expression, under ordinary experimental conditions, α is considerably less than unity, and β is not much greater than unity. The magnitude of the correction is determined mainly by the parameter $\delta=c\cdot v/D_z\cdot R^2/4$. The value of c is limited to the range 1 to 4 cm^{-1} by the requirement of a convenient reaction zone size.[2,5] The factor v/D_z was recognized to be important by Heller,[5] who recommended use of values in the range 5 to 12 cm^{-1}. Most important is the nozzle radius R. Heller apparently did not study the effect of variation in nozzle size, though it has been considered by Reed and Rabinovitch[4] and by Garvin and Kistiakowsky,[2] who justified the use of v/D_z values somewhat greater than 12 by the fact that they used a nozzle considerably smaller than Heller's. Using $c=4$ cm^{-1}, $v/D_z=12$ cm^{-1}, $R=0.1$ cm, δ becomes 0.12, and terms of higher order in δ may ordinarily be neglected. Garvin and Kistiakowsky used nozzles of radius less than 0.05 cm, so that for their experiments $\delta<0.03$.

The behavior of the functions $F\alpha$ and F_β may be found from Eq. (17). $-F_\alpha$ and $-F_\beta$ are both monotonically increasing functions of ρ starting at 0 when $\rho=0$. $-F_\alpha$ approaches the limit $\frac{1}{2}\ln 3\sim 0.55$, while $-F_\beta$ eventually behaves as $\frac{1}{2}\ln 2\gamma\rho$. The term in F_α therefore gives a negative correction to y, while the F_β term gives a positive one. Since $-F_\beta$ is always greater than $-F_\alpha$, the positive correction always predominates (except possibly at very small r in a case with very large α), as is to be expected.

With a reaction zone less than 5 cm in radius and with $c=4$ cm^{-1}, $-F_\beta<4.3$. Thus, in an extreme case, using $R=0.1$ cm, a maximum correction of about 50 percent in the value of y might be indicated. In the Polanyi type of experiment, this would give a correction of roughly 10 percent in c or about 20 percent in k.

With the thermal method of measurement, the correction is also easily applied. The heat flow equation is

$$\left.\begin{aligned}\kappa\nabla^2T&=-Qkyz\\ \text{or}\qquad \frac{d^2(rT)}{d\rho^2}&=-\frac{Qz_\infty D_z}{\kappa c}\cdot\frac{mn}{\rho}\end{aligned}\right\}. \tag{22}$$

The general solution of this is of the form

$$rT=A\rho+B-\frac{Qz_\infty D_z}{\kappa c}\cdot m, \tag{23a}$$

where m is a solution of Eq. (3), while A and B are determined by the appropriate boundary conditions.[3] Since the quantity measured is a temperature difference, we get, finally

$$\left.\begin{aligned}r\Delta T&=L(1-\mu)-A_0r\\ \text{where}\qquad L&=\frac{Qz_\infty D_z}{\kappa c}\cdot\alpha\delta=\frac{Qy_0vR^2}{4\kappa}\end{aligned}\right\}, \tag{23b}$$

and μ is given by Eq. (14). Following Garvin, Guinn, and Kistiakowsky,[3] $r\Delta T$ may be plotted in arbitrary units against r, and the resulting curve subtracted from the asymptotic straight line represented by $L-A_0r$,

$$L\mu=L-A_0r-(r\Delta T). \tag{24}$$

The logarithms of the resulting differences may be plotted against r, and should be represented by

$$\left.\begin{aligned}\ln(L\mu)&=\ln L+\ln\mu\\ &=\ln L-cr+\ln[1+\alpha\delta F_\alpha(cr)\\ &\qquad -\beta\delta F_\beta(cr)+\cdots]\\ &=\sim\ln L-cr+\alpha\delta F_\alpha(cr)-\beta\delta F_\beta(cr)\cdots,\end{aligned}\right\} \tag{25}$$

where the last form may be used when the correction terms are small. The slope of this curve is given by

$$\frac{d\ln(L\mu)}{dr}=\sim -c[1-\alpha\delta F_\alpha'(cr)+\beta\delta F_\beta'(cr)\cdots], \tag{26}$$

where

$$F_\alpha'(\rho)=e^{2\rho}Ei(-3\rho),\quad F_\beta'(\rho)=e^{2\rho}Ei(-2\rho). \tag{27}$$

The correction terms are seen to be very small in this case: for $cr>1$ and $\delta<0.03$, the correction is less than 1 percent.

The concern of Garvin, Guinn, and Kistiakowsky that

atmospheric depletion might be more serious in the method of temperature patterns than in Polanyi's original optical method is unfounded. In fact, when the same nozzle size and gas flow is assumed, the temperature method is the less sensitive of the two to this effect. The reason for this lies in the fact that the temperature pattern method depends only on the shape of the function μ (on the slope of $\ln\mu$), whereas it is essentially the absolute concentration y that is measured in the optical method. The slope of $\ln\mu$ differs from the slope of $\ln\mu^{(0)}$, the Polanyi function, by an amount which is large only in the region close to the origin (and excluded from experimental measurement) and which declines rapidly toward zero. The deviation between the absolute magnitudes of μ and $\mu^{(0)}$, on the other hand, increases with increasing radius.

DISCUSSION

The solution obtained is a general one which may be used with other boundary conditions than those suggested above. Such a change would involve evaluating the factors $\alpha\delta$ and $\beta\delta$ in terms of the alternative boundary conditions.

It is felt that the boundary conditions (5) and (6), involving the flows of y and z, are more suitable than the use of two-point boundary conditions on the magnitudes of y and z, particularly since the flow conditions introduce in a natural way the physically expected dependence on the factor $v/D_z \cdot R^2$, the ratio of the rate of flow from the nozzle to the rate of inward diffusion of the atmosphere reactant. Proper two-point boundary conditions should give the right magnitudes but would would not reveal the physical origin of the terms $\alpha\delta$ and $\beta\delta$.

There is no inconsistency in taking account of the outward spherical flow in the boundary condition (6) for z, while omitting the corresponding convective term from the differential equations (1). It may be shown that the effect of a spherical convective term in Eqs. (1) will be to introduce a small term in the solution which depends on $\delta/\rho \cdot D_z/D_y$, and which is important only near the nozzle where the solution breaks down in any case because of the jet effect.

The use of two-point boundary conditions on z would be difficult at best. Far from the nozzle, z will be very little less than its value outside the reaction zone, and its depletion very difficult to measure exactly; near the nozzle, the experimentally found reduction of z to very low levels is due largely to the jet effect, and so cannot well be used as a boundary condition with a differential equation from which the convective term has been dropped.

The present calculation shows that, in the absence of the convective term, z would go to zero at a radius r_1 determined by Eq. (20), which in ordinary cases will be distinctly less than R. This agrees with a conclusion of Reed and Rabinovitch.[4] It may be seen that z will be equal to zero at the radius R only when the special and unusual relation exists between the parameters

$$\frac{\delta}{cR} = \frac{v}{D_z} \frac{R}{4} = \frac{1}{\beta - \alpha} \cong 1.$$

If this is kept in mind, it should be possible to compare the results of the computation of Cvetanović and LeRoy,[6] which assumed $z=0$ at $r=R$, with a calculation using the present solution and their initial conditions.

CONCLUSIONS

The present solution shows that the effect of depletion of the atmosphere reactant in relation to its rate of replacement by diffusion is relatively small in the usual experimental conditions. This lends confidence to results previously obtained using the method of spherical diffusion flames, and permits calculation of the correction where it is significant. For example, in the reactions studied by Garvin and Kistiakowsky,[2] the present work indicates that no significant correction is required for this effect, and substantiates their conclusion of the reality of a pressure dependence in the reaction rate constant.

The availability of a simple analytical correction to the Polanyi equation will permit the use of a wider range of experimental conditions. In particular, the use of larger values of the parameter $\alpha = y_0/z_\infty$ suggests itself, the more so as this parameter is associated with the smaller of the correction terms. Alternatively, the use of larger v/D_z ratios and larger nozzle radii might demonstrate the reality of the diffusion effect.

Experimental work in relation to the foregoing theory is under consideration.

ACKNOWLEDGMENTS

I wish to express my thanks to Professor G. B. Kistiakowsky for many fruitful discussions and for arousing my interest in this problem. For many other helpful discussions I wish to thank my associates in the Gibbs Memorial Laboratory, particularly Mr. Richard Williams, who has given much patient advice and information on the experimental method.

This work was performed during tenure of a National Science Foundation Predoctoral Fellowship at Harvard University for the year 1953–1954.

Letters to the Editor

THIS section will accept reports of new work, provided these are terse and contain few figures, and especially few half-tone cuts. The Editorial Board will not hold itself responsible for opinions expressed by the correspondents. Contributions to this section should not exceed 600 words in length and must reach the office of the Editor not later than the 15th of the second month preceding that of the issue in which the Letter is to appear. No proof will be sent to the authors. A publication charge of $10.00 per Letter is made which, when honored, will entitle the Institution to 100 free reprints.

On the Heats of Sublimation and Evaporation of Germanium

RICHARD E. HONIG
RCA Laboratories, Princeton, New Jersey
(Received June 18, 1954)

TO follow up an earlier study[1] of the molecular evaporation of germanium, individual heats of vaporization of the most prominent germanium species have been determined in the neighborhood of the melting point. The mass spectrometer employed in this work has been described previously.[2] The slightly modified ion source is shown in Fig. 1. Indirectly heated graphite crucibles were used to vaporize milligram samples of pure germanium. The crucible temperature was changed in steps and the peaks of interest were studied, one at a time, by recording peak intensity I^+ as a function of crucible heater voltage V_H. Temperature calibration curves were taken with an optical pyrometer in a separate vacuum system before and after each series of runs, and the melting point of germanium (1210°K, determined by Greiner[3]) served to establish an absolute temperature scale. As demonstrated previously,[4] the slopes of the plots $\log(I^+ \times T)$ *vs* $1/T$ represent the desired heats of vaporization, provided the so-called accommodation coefficient is unity.

Table I summarizes the results obtained for the heat of sublimation (near 1150°K) of Ge_1 and for the heats of evaporation (near 1400°K) of Ge_1, Ge_2, Ge_3, and Ge_4, together with the temperature range covered and the number of runs made for each species. All significant values fell within the limits quoted. The

TABLE I. Measured heats of vaporization (in kcal/mole) for the most abundant germanium species.

Species	Number of runs	Heat of vaporization Sublimation L_{1150}	Heat of vaporization Evaporation L_{1400}	Temperature range (°K)
Ge_1	4	89±2		1100–1210
	6		79±2	1210–1500
Ge_2	4		83±3	1350–1500
Ge_3	1		81	1350–1500
Ge_4	2		70	1350–1500

difference between the heats of sublimation and evaporation found for Ge_1 yields directly a value of 10±4 kcal/mole for the heat of fusion, in fair agreement with Greiner's[3] recent direct measurement of 8.1 kcal/mole. By substituting the heats of evaporation measured for Ge_1 and Ge_2 into the well-known energy cycle, one obtains 75 kcal/mole as an estimate for the dissociation energy of the Ge_2 molecule.

In two recently published studies, Searcy[5] measured vapor pressures and a heat of evaporation of germanium by its rate of effusion from a graphite Knudsen cell between 1510 and 1882°K, while Lehovec and co-workers[6] obtained an activation energy from the rates of deposition of germanium at temperatures ranging from 1387 to 1823°K. To effect an exact comparison between these data and the present results, it is necessary to reduce the latter to a "fictitious" total pressure p_f and, based on it, a "fictitious" or apparent heat of evaporation L_f, as defined and used by the author in his recent graphite study.[4] Detailed computations yield an apparent slope of 79 kcal/mole which is indistinguishable from the measured $L(Ge_1)$ because the atomic species Ge_1 predominates and the molecular heats of evaporation do not differ significantly from $L(Ge_1)$. When Searcy's vapor pressure data are plotted *vs* $1/T$,

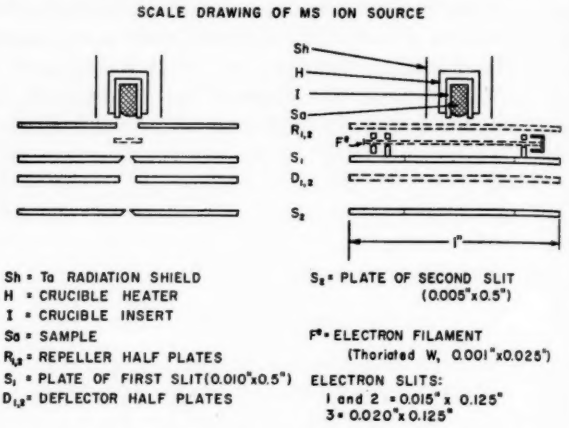

FIG. 1. Scale drawing of mass spectrometer ion source used in this research.

they yield an apparent slope of 85±2 kcal/mole, while Lehovec's deposition data, upon conversion to pressures, give 83±4 kcal/mole. In both cases, the error is based on the scattering of the data. Agreement between these values and the present results is reasonably satisfactory.

Considerable supercooling of liquid germanium samples, observed visually during the temperature calibration runs, was further investigated in the mass spectrometer by going through complete cooling-heating cycles near the melting point. It was found that the liquid could be supercooled to about 1150°K, at which point solidification set in suddenly and the liberated heat of fusion momentarily raised the sample temperature by about 50°K, as indicated by the peak height.

Appearance potentials, I, were measured for the ions Ge_1^+, Ge_2^+, and Ge_3^+ by the critical slope method[7] and compared to the ionization potential of Hg to calibrate the voltage scale. The measured difference between $I(Hg^+)$ and $I(Ge_1^+)$, 2.2_5 v, agrees satisfactorily with the spectroscopic difference (10.44−8.13=2.31 v). The potentials measured for the three germanium species were found to be virtually indistinguishable. This strongly suggests that Ge_2^+ and Ge_3^+ are mainly *parent* ions, deriving from Ge_2 and Ge_3, respectively, and are not fragment ions of larger molecules.

[1] R. E. Honig, J. Chem. Phys. **21**, 573 (1953).
[2] R. E. Honig, Analog. Chem. **25**, 1530 (1953).
[3] E. S. Greiner, J. Metals **4**, A1044 (1952); also private communication.
[4] R. E. Honig, J. Chem. Phys. **22**, 126 (1954).
[5] A. W. Searcy, J. Am. Chem. Soc. **74**, 4789 (1952).
[6] Lehovec, Rosen, MacDonald, and Broder, J. Appl. Phys. **24**, 513 (1953).
[7] R. E. Honig, J. Chem. Phys. **16**, 105 (1948).

Sublimation Studies of Silicon in the Mass Spectrometer

RICHARD E. HONIG
RCA Laboratories, Princeton, New Jersey
(Received June 18, 1954)

TO complete the previously reported vaporization studies of the group IVB elements,[1–3] small samples of pure silicon were sublimed in a 180° mass spectrometer. The experimental setup and procedure were essentially as described in the preceding letter,[3] except that beryllia crucibles were used. The known melt-

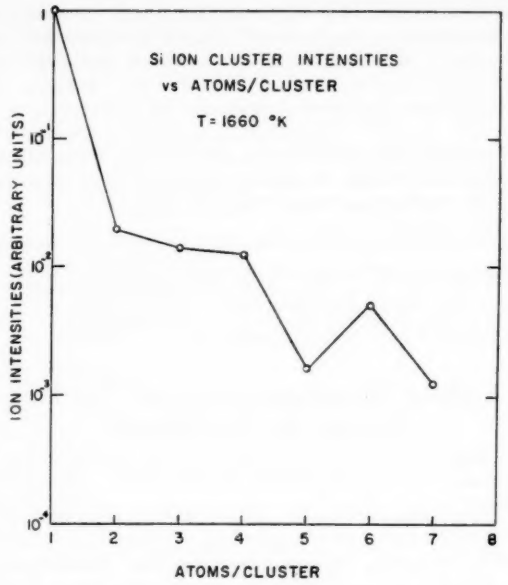

FIG. 1. Typical pattern of silicon ion clusters, obtained at 1660°K. The neutral species subliming were converted into positive ions by bombardment with 47-ev electrons.

ing point of silicon (1688°K, Gayler[4]) served to standardize the temperature scale.

A typical mass spectrum of silicon clusters is shown in Fig. 1. The alternating pattern, made up of positive ions containing from one to seven silicon atoms, is very similar to the pattern obtained previously for the evaporation of liquid germanium.[1] If Si_8^+ clusters exist, their intensity must be less than 5 percent of the Si_7^+ intensity. Large SiO^+ and Be^+ peaks, recorded at the highest temperatures, indicate that a considerable fraction of the sample is lost to the chemical reaction: $Si+BeO \rightarrow SiO+Be$. A search was made for silicon particles emitted as positive or negative ions, but none were found.

Heats of sublimation (at about 1550°K) were determined for the four most prominent species and are presented in Table I,

TABLE I. Measured heats of sublimation (in kcal/mole) for the most abundant silicon species.

Species	Number of runs	Heat of sublimation L_{1550}	Temperature range (°K)
Si_1	11	105 ±12	1450–1600
Si_2	4	135 ±12	1500–1650
Si_3	2	139	1500–1650
Si_4	1	146	1500–1650

which also shows the temperature range covered. The considerable scattering of results, an estimated ±12 kcal/mole, may well be due to the chemical side reaction affecting the vaporizing surface. From the heats of sublimation measured for Si_1 and Si_2 and the well-known energy cycle, one obtains 75 kcal/mole for the dissociation energy of the Si_2 molecule.

All of the more recent literature references concerning the vapor pressure of silicon[5–10] are ultimately based on just two original papers. Ruff and Konschak[11] studied the evaporation of silicon from a SiC crucible between 2160 and 2500°K and measured vapor pressures between 10 and 300 mm Hg by a boiling point method. They obtained widely scattered results, and their $\log p$ *vs* $1/T$ plot, based on the lower-lying points only, shows a slope of 97 kcal/mole. If all their data are given equal weight, a slope of 112 kcal/mole is found (see curve 1, Fig. 2). The results of Baur and Brunner,[12] consisting of three vapor pressure points obtained between 1980 and 2160°K, are plotted as curve 2. As the Al_2O_3 crucible used must have reacted extensively with the sample to yield SiO at these high temperatures, it is quite likely that their pressures are too high. Brewer,[9] assuming silicon vapor to be monatomic, used Ruff and Konschak's and Baur and Brunner's data to compute thermodynamically the results plotted as curve 3.

To compare the present data with the published results, $\log p_t$ has been plotted *vs* $1/T$, where p_t, the total pressure, is defined as the sum of the partial pressures of the different silicon species. The resulting slope, L_t, has no physical significance, yet constitutes a convenient parameter because this is precisely what was measured and plotted by the earlier investigators. Curve 4 shows

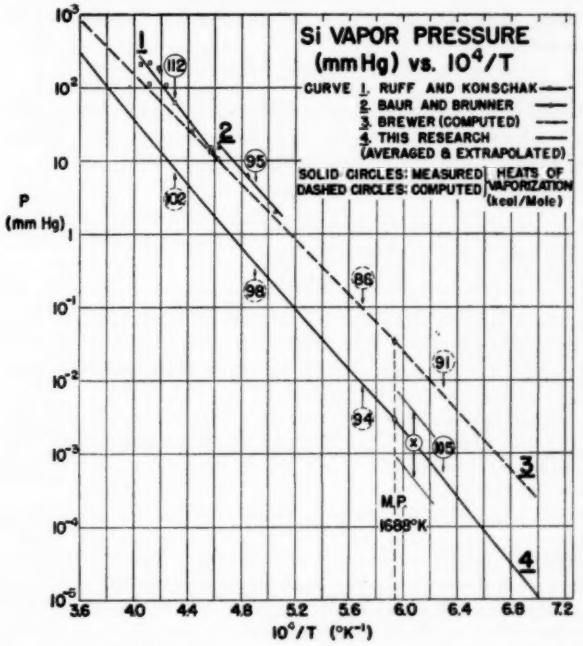

FIG. 2. Comparison of vapor pressure data for silicon. Figures inside the circles indicate heats of vaporization at the temperatures shown. The ordinate of point *x*, curve 4, was determined by comparing, at that temperature, the measured Si_1^+ intensity with the Ge_1^+ peak of a germanium sample intensity with the Ge_1^+ peak of a germanium sample whose vapor pressure was known (reference 5, preceding letter). The dotted lines shown above and below indicate the estimated limits of error.

the present data, taken between 1400 and 1660°K and extrapolated into the high temperature range. Computations were based on the measured heats of sublimation, an atomic heat of fusion of 11 kcal/mole,[13] and the measured concentrations of the individual species. It was assumed that the pattern of silicon ion clusters, measured during a nonequilibrium sublimation, is representative of the concentrations of neutrals evaporating under equilibrium conditions. While the extrapolated region of curve 4 lies about one order of magnitude below curves 1 and 2, their slopes agree fairly well. On the other hand, Brewer's curve 3, which assumes a monatomic vaporization, shows a constant slope that is substantially smaller than all measured values.

[1] R. E. Honig, J. Chem. Phys. **21**, 573 (1953).
[2] R. E. Honig, J. Chem. Phys. **22**, 126 (1954).
[3] R. E. Honig, J. Chem. Phys. **22**, 1610 (1954) (preceding letter).
[4] M. L. V. Gayler, Nature **142**, 478 (1938).
[5] K. K. Kelley, U. S. Bur. Mines Bull. No. 383, pp. 90, 113 (1935).
[6] A. Eucken, Metallwirtschaft **15**, 63 (1936).
[7] R. W. Ditchburn and J. C. Gilmour, Revs. Modern Phys. **13**, 310 (1941).
[8] R. E. Stull, Ind. Eng. Chem. **39**, 540 (1947).
[9] L. Brewer, Paper 3 in *The Chemistry and Metallurgy of Miscellaneous Materials: Thermodynamics*, L. E. Quill, Editor (McGraw-Hill Book Company, Inc., New York, 1950), p. 13.
[10] O. Kubaschewski and E. L. Evans, *Metallurgical Thermochemistry* (Academic Press, Inc., New York, 1951), pp. 281, 303.
[11] O. Ruff and M. Konschak, Z. Elektrochem. **32**, 68 (1926).
[12] E. Baur and R. Brunner, Helv. Chim. Acta **17**, 958 (1934).
[13] O. Kubaschewski *et al.*, Z. Elektrochem. **54**, 275 (1950).

Chemical Kinetics and Equilibrium. The Law of Integral Powers in Kinetics

J. A. CHRISTIANSEN
Physico-Chemical Institute of the University of Copenhagen, Copenhagen, Denmark
(Received November 3, 1954)

THE resulting conclusion of this note is based upon the following three principles: A. Kinetics is more fundamental than (equilibrium-)thermodynamics. Therefore equilibrium conditions must be derived from kinetics. B. The powers in which concentrations (activities) occur in expressions for the velocity of elementary reactions are always integral. C. The principle of microscopic reversibility.

From thermodynamics we know that if a reaction has the stoichiometric equation

$$\Sigma \nu_i M_i = 0$$

where the M's are molecular symbols and the ν's integral positive (left side) or negative (right side) numbers then the necessary and sufficient condition for chemical equilibrium is

$$\Sigma \nu_i \mu_i = 0$$

where the μ's are the chemical potentials.

The condition can also be written

$$p_+ = p_- \tag{1}$$

where the two p's represent the well-known mass action products corresponding to the left and right side, respectively, the powers having their lowest possible integral values, with appropriate constants included in the products.

Kinetics goes further. It states that if the reaction takes place in one step, in other words if its stoichiometric equation also represents its mechanism, the rate s_1 of the reaction in the direction from left to right is

$$s_1 = p_+ - p_- \tag{2}$$

where the powers according to B must be integral. It must be added that if the products contain activities instead of concentrations we must according to Brønsted add a "kinetic activity coefficient" f resulting in the expression $s_1 = f(p_+ - p_-)$. In the following we shall consider for simplicity of presentation only ideal systems, i.e., we shall put f equal to 1, but quite apart from this the equilibrium condition derived from kinetics is identical with (1).

Now it may be that the same reaction in the same solution also takes place through a series of steps. The rate s_2 of this reaction will in most cases be quite different, in magnitude and in form, from s_1. However, we know from C that the condition of equilibrium must be strictly independent of the reaction path. From this it follows that the rate of this second reaction must contain the difference $(p_+ - p_-)$ as a factor, that is, s_2 must be of the form

$$s_2 = F(p_+ - p_-) \tag{3}$$

where F may be a more or less complicated function of the different concentrations. We repeat that p_+ and p_- according to B must contain the concentrations (activities) of the reactants, respectively, the resultants in integral powers.

As recognized for many decades and recently mentioned by C. N. Hinshelwood and co-workers[1] (3) can be used when one wishes to derive information on the concentration dependences of the backward rate of a chemical reaction from its forward rate and the equilibrium condition. M. Manes and co-workers[2] quoted by Frost and Pearson[3] are of the opinion that this procedure is not necessarily permissible. They base this statement on the thermodynamic equilibrium condition which they maintain can be written in the form

$$p_+^q = p_-^q \tag{4}$$

where q may be any number and particularly also a fraction. Now it is a fact that 1^q has several different values if q is a fraction and there are therefore objections against (4). Nevertheless it might be defended if it were not for the fact that kinetics as shown above requires the powers in the equilibrium condition to be integral. Application of A thus restricts the possible values of q in (4) to integers in which case it again follows that the expression for the rate of the reaction must contain the difference $p_+ - p_-$ as a factor.

The authors thanks are due to Martin Kilpatrick, Mary Kilpatrick, and V. K. La Mer for pleasant and helpful discussions before the final preparation of this note.

[1] Gadsby, Hinshelwood, and Sykes, Proc. Roy. Soc. (London) **187**, 129 (1946).
[2] Manes, Hofer, and Weller, J. Chem. Phys. **18**, 1355 (1950).
[3] E. E. Frost and R. G. Pearson, *Kinetics and Mechanism* (John Wiley and Sons, Inc., New York, 1953), p. 178.

Reply to Christiansen's Letter, "Chemical Kinetics and Equilibrium"

MILTON MANES,* L. J. E. HOFER,† AND SOL WELLER‡
(Received November 30, 1953)

THE quoted article by Manes, Hofer, and Weller[1] gives specific examples of rate laws (e.g. Eqs. (25) and (26)) which do not satisfy the equation of Gadsby, Hinshelwood, and Sykes.[2] These rate laws were derived in the usual manner by the method of stationary states, from elementary reactions in which only integral coefficients appeared, and by the use of the Guldberg-Waage mass-action law for all of the *elementary* reactions. These rate laws fulfill all the thermodynamic requirements; the net (observable) reaction rates vanish identically at equilibrium and only at equilibrium, and the direction of the net reaction rate is always consistent with the direction of the thermodynamic displacement. Furthermore, the rate laws do not violate the law of microscopic reversibility. It follows, therefore, that the GHS relation cannot be properly derived as a *necessary* condition, either by the use of thermodynamic restrictions alone (as, for example, in the derivation of GHS) or by the added use of the above-mentioned kinetic restrictions.

Equation (3) of Professor Christiansen's letter[3] is not in contradiction with the conclusions of MHW, unless it necessarily leads to the GHS relation, which, as we shall see, it does not. Christiansen's Eq. (3) can be written as

$$s_2 = r_f - r_b = g_f - g_b = F \cdot (p_+ - p_-), \tag{1}$$

where r_f and r_b are the rates of the forward and reverse reactions; $g_f(=r_f)$ and $g_b(=r_b)$, the corresponding rate functions, including the proper constants; and s_2, F, p_+, and p_- have the same meaning as in Christiansen's letter. Equation (1) defines only the difference between g_f and g_b; it does not yield the relationship, $g_f/g_b = p_+/p_-$, i.e., the equation of GHS. To get this last equation from Eq. (1), it is necessary to satisfy the additional condition that $g_f = F_{p+}$ (or $g_b = F_{p-}$), i.e., that the mathematical manipulations which may be required to bring out $(p_+ - p_-)$ as a factor must preserve the identity of the forward and reverse rates with the positive and negative parts of the resulting equation. This essential condition is not included in Christiansen's derivation. The equation does not exclude, for example, the case where $g_f/g_b = p_+^{\frac{1}{2}}/p_-^{\frac{1}{2}}$. For this case one can write,

$$s_2 = G(p_+^{\frac{1}{2}} - p_-^{\frac{1}{2}}) = F(p_+ - p_-), \tag{2}$$

where $G \equiv F(p_+^{\frac{1}{2}} + p_-^{\frac{1}{2}})$.

It has already been shown[1] that fractional exponents for p_+ and p_- are not excluded by Christiansen's statement B, which applies only to elementary reactions. The statement, in Professor Christiansen's letter, that 1^q has several different values if q is a fraction, is not relevant to the problem. There is only one real value for 1^q, and imaginary solutions are quite freely discarded in conventional thermodynamics. Moreover, fractional coefficients for stoichiometric equations are often and properly used in thermodynamics; there is no unique expression for the equilibrium constant. The present authors maintain that the absolute values of

the coefficients as distinguished from their ratios have physical significance only in the case of the elementary reactions, and that this significance has been scrupulously observed in the MHW article.

One cannot assert at this point that pairs of rate laws not satisfying the GHS relation will necessarily be found. However, no valid grounds have been found to exclude them, either on the basis of thermodynamics or kinetics or both. Therefore, neither retraction nor modification appears to be called for.

* Koppers Company, Inc., Verona Research Center, Verona, Pennsylvania.
† Synthetic Liquid Fuels Research Branch, United States Bureau of Mines, Bruceton, Pennsylvania.
‡ Houdry Process Corporation, Marcus Hook, New Jersey.
[1] Manes, Hofer, and Weller, J. Chem. Phys. **18**, 1355 (1950).
[2] Gadsby, Hinshelwood, and Sykes, Proc. Roy. Soc. (London) **187**, 129 (1946).
[3] J. A. Christiansen, J. Chem. Phys. **22**, 1612 (1954).
Added Note.—Of interest in this connection, although to confine the discussion, not cited for support, are articles by Hollingsworth (J. Chem. Phys. **20**, 921 (1952); **20**, 1649 (1952)) and by Horiuti and co-workers (see, for example, Proc. Japan Acad. **29**, 160 (1953); **29**, 164 (1953)). Hollingsworth considers in detail the consequences of the purely thermodynamic restriction. Horiuti *et al.* consider both thermodynamic and kinetic conditions and examine the question of integral and fractional exponents. We have recently become aware of Horiuti's work, some of which may precede, at least in part, the article of MHW.

Delta Potential Function Model for Electronic Energies in Molecules

ARTHUR A. FROST
Department of Chemistry, Northwestern University, Evanston, Illinois
(Received July 15, 1954)

CONSIDER a one-electron hydrogenlike atom or ion. Let the electron be restricted to motion in one dimension, x, along a line through the nucleus. The Coulombic potential energy of the electron is $V=-Ze^2/|x|$ where Z is the atomic number and e the electronic charge. For convenience in calculation replace this potential function by $V=-g\delta(x)$, which may be thought of as the limiting form of a finite square-well potential with increasing depth and decreasing width such that the product remains finite and equal to g. The Schrödinger equation for this problem is

$$-\frac{\hbar^2}{2m}\frac{d^2\psi}{dx^2}-g\delta(x)\psi=E\psi,$$

and has for its only bound state the simple solution

$$\psi=A\exp(-c|x|)$$

where $c=gm/\hbar^2$ with $E=-g^2m/2\hbar^2$. Now, curiously, if g is set equal to Ze^2, the same coefficient as in the Coulomb potential, $E=-Z^2e^4m/2\hbar^2$, which is the correct energy for the $1s$ state of the atom. Furthermore ψ becomes identical in form with the correct three-dimensional $1s$ wave function along a line through the nucleus.

This simultaneous replacement of the three-dimensional problem by a one-dimensional problem and replacement of the Coulomb potential by a delta function potential makes compensating errors in energy and wave function. It is interesting, then, to consider the possibility of extending this model to diatomic and polyatomic molecules. Such an application is obvious for linear, open-chain, and ring molecules. Extension to branching molecules can easily be handled by choosing an appropriate relation between the derivatives at the branching point.

As the simplest example of a molecular calculation consider the hydrogen molecule-ion. Let the x coordinate be the internuclear axis and $V=-e^2[\delta(x-R/2)+\delta(x+R/2)]$ where R is the internuclear distance. Solution of the Schrödinger equation is easily found in terms of simple exponentials or their linear combinations as hyperbolic functions. On the other hand, a linear combination of atomic orbitals also provides an exact solution if the coefficient c in the exponent is allowed to vary. The effect of a delta function of strength g is to require the fractional change in $d\psi/dx$ at that point to be $-2mg/\hbar^2$. There are two bound states (unless R is too small), symmetric and antisymmetric. The ground-state solution may be expressed as

$$\psi=A\left[\exp\left(-c\left|x-\frac{R}{2}\right|\right)+\exp\left(-c\left|x+\frac{R}{2}\right|\right)\right],$$

where c is determined by

$$c/[1+\exp(-cR)]=me^2/\hbar^2$$

and $E=-\hbar^2c^2/2m$.

This gives an E *versus* R curve of a qualitatively correct form. Although the energy is correct for the separated and united atoms it is too high for intermediate nuclear separations. When a suitably modified internuclear repulsion potential energy such as $(e^2/R)\times\exp(-cR)$ is added, there results a familiar diatomic molecule potential energy function.

Advantages of this model include: (1) Solutions are as easily obtained as are those for the free-electron model. (2) Correct results are obtained for the $1s$ state of the hydrogenlike atoms. (3) Linear combination of atomic orbitals is an exact solution with this model. (4) In contrast to the free-electron model this model will provide ionization energies and also reasonable energies as a function of internuclear distance.

Some disadvantages are: (1) The usual difficulty in handling interelectronic repulsion. Even if this is represented by a positive delta function, no exact solution for two or more electrons in this model is likely. (2) p and d orbitals cannot be represented unless two or more slightly displaced delta functions are used at a nucleus.

Delta function potentials have been previously used for electrons in crystalline lattices[1,2] and for molecules as a correction to the free-electron method.[3–5] A full report of this work will be submitted to this journal shortly. This research was supported by a research grant from the National Science Foundation to Northwestern University.

[1] R. L. Kronig and W. G. Penney, Proc. Roy. Soc. (London) **A130**, 499 (1931).
[2] D. S. Saxon and R. A. Hutner, Philips Research Repts. **4**, 81 (1949).
[3] K. Rüdenberg and R. G. Parr, J. Chem. Phys. **19**, 1268 (1951).
[4] H. Kuhn, Helv. Chim. Acta **34**, 2371 (1951).
[5] Fukui, Nagata, and Yonezawa, J. Chem. Phys. **21**, 186 (1953).

Effects of Internal Motion in the Microwave Spectrum of Methyl Amine*

DAVID R. LIDE, JR.
Mallinckrodt Chemical Laboratory, Harvard University, Cambridge, Massachusetts
(Received July 12, 1954)

THE spectrum of methyl amine in the microwave region is influenced by the rather complicated internal motion which can take place in the molecule. We may expect both a torsional motion of the NH_2 group with respect to the methyl group, similar to that in methyl alcohol, and an inversion of the amino group such as occurs in ammonia. Ivash and Dennison[1] have shown for the methyl alcohol-type molecule that each rotational level of given J, K (where K is the component of total angular momentum along the symmetry axis of the methyl group) is split into four levels, two degenerate and two nondegenerate. In methyl amine the possibility of inversion results in a further doubling of each level, giving a total of eight. Selection rules for the perpendicular dipole component specify that eight lines will result from each

TABLE I. Assigned $\Delta J=\pm1$ lines for methyl amine.

$JK\tau\gamma\rightarrow J'K'\tau'\gamma'$	Observed frequencies (mc) of inversion doublet		Inversion splitting (mc)
5130→4220	23 340.9	17 475.8	5865
5131→4221	36 452.1	30 565.9	5886
5121→4211	28 533.9	19 776.9	8757
5220→6130	23 449.8	29 312.4	5863
5211→6121	13 176.4	21 930.4	8754
5230→6110	29 771.4	...	...
1110→2020	18 348.7	...	...

TABLE II. Inversion doublets of the transition $JK\tau\gamma = J030 \rightarrow J121$ in first excited torsional state.

J	Observed frequencies (mc)	
1	26 728.8	33 631.5
2	26 718.1	33 619.9
3	26 695.4	33 599.1
4	26 655.0	33 563.3
5	26 588.8	33 506.8
6	26 487.1	33 422.3
7	26 339.5	33 302.0
8	26 134.8	33 136.5
9	25 861.2	32 916.8
10	25 507.5	32 634.2

transition $JK \rightarrow J'K'$ which would appear as a single line in the zeroth approximation of a rigid prolate symmetric rotor.

Several communications concerning the microwave spectrum of methyl amine have appeared.[2] We have measured about three hundred lines in the 11 000 to 38 000 mc region, and by analysis of Stark effects and nuclear quadrupole interactions have been able to make specific assignments for twelve lines of the type $\Delta J = \pm 1$. These lines are listed in Table I. The index τ is used to label the torsional state, after Burkhard and Dennison,[3] and γ is zero or one according to whether $J + K_{-1} + K_1$ is even or odd for the asymmetric rotor level in question. Two lines are observed for each transition as a result of the inversion doubling. It should be noted that this inversion splitting changes very little with over-all rotation but is quite sensitive to the torsional state.

The spectrum also includes several series of $\Delta J = 0$ lines. Two of the series have been followed to their convergence points ($J = 1 \rightarrow 1$), which fall at 26 727.8 mc and 33 631.5 mc. The first ten members are given in Table II. These two series are assigned as inversion doublets of the transition $JK\tau\gamma = J030 \rightarrow J121$ in the first excited torsional state, as was suggested by Shimoda, Nishikawa, and Itoh.[2] While the remaining series, which appear to be converging toward the 5-mm region, cannot be definitely assigned, they probably involve the transition $K = 0 \rightarrow 1$ in the torsional ground state.

As a first effort to understand the spectrum, we may take the mean frequencies of the assigned inversion doublets and attempt to fit these "lines" with a model of a simple torsional rotor of the methyl-alcohol type. Following the treatment of Burkhard and Dennison, and using an effective torsional barrier of 632 cm^{-1}, the lines given in Table I have been fitted within a few hundred megacycles. A similar, though probably less reliable calculation on the series of lines in the first excited torsional state gives a barrier of 655 cm^{-1}. It is clear, however, from both experimental and theoretical evidence, that an accurate model for the methyl amine molecule must treat the torsion and the inversion as a composite motion; i.e., an adequate description of the internal motion requires a two-dimensional potential surface. This surface will contain six equivalent minima, and from each of these wells there are two distinct paths by which the system may tunnel into adjacent wells. One of these paths appears to represent a torsional motion of the entire NH_2 group; the other involves a tunneling of only one of the amino hydrogens, while the second hydrogen atom retains its position with respect to the methyl group. The barrier derived above from a crude model in which the inversion was ignored, is presumably related to the potential seen by the system while executing the first type of motion. The observed splittings indicate that the barrier for the second motion is of roughly the same magnitude. It is hoped that a more quantitative analysis of the internal motion can be carried out.

The author expresses his appreciation to Dr. Shimoda, Dr. Nishikawa, and Dr. Itoh for advance communication of their measurements, and to Professor E. Bright Wilson, Jr., for many helpful discussions.

* The research reported in this paper was made possible by support extended Harvard University by the Office of Naval Research under ONR Contract N5ori 76, Task Order V.

[1] Ivash and Dennison, J. Chem. Phys. **21**, 1804 (1953).
[2] D. R. Lide, Jr., J. Chem. Phys. **20**, 1812 (1952); Shimoda and Nishikawa, J. Phys. Soc. Japan **8**, 133, 425 (1953), and private communication.
[3] Burkhard and Dennison, Phys. Rev. **84**, 408 (1951).

Further Evidence for the Existence of the *Gauche*-Form of 1,2-Dichloroethane

SAN-ICHIRO MIZUSHIMA, ICHIRO NAKAGAWA, ISAO ICHISHIMA, AND TATSUO MIYAZAWA
Chemical Laboratory, Faculty of Science, Tokyo University, Hongo, Tokyo, Japan
(Received July 9, 1954)

CONSIDERABLE evidence based on spectroscopic, thermal, and electric measurements has been accumulated to indicate that 1,2-dichloroethane, ClH_2C-CH_2Cl, exists in the *trans*- and the *gauche*-forms in the gaseous and liquid states and only in the *trans*-form in the solid state.[1] The *trans*-form or the more stable form has the symmetry of C_{2h} and the *gauche*-form or the less stable form the symmetry of C_2. Some authors preferred the *cis*-form with the symmetry of C_{2v} to the *gauche*-form,[2] but the papers by Neu and Gwinn[3] and by us[4] have given strong evidence against the existence of the *cis*-form.

We have calculated the normal frequencies of 1,2-dichloroethane as an eight-body problem and could make the assignment of all the observed frequencies.[5] Thus the two strong absorption bands at 880 and 941 cm^{-1} are assigned to the CH_2-rocking vibrations of the *gauche*-molecule. Our normal vibration calculation shows that for all conceivable forms of 1,2-dichloroethane (corresponding to azimuthal angles of internal rotation from 0° to 180°) the CH_2-rocking frequencies fall in the region from 740 to 950 cm^{-1} where no fundamental except for that of the C–Cl stretching vibration at *ca* 750 cm^{-1} can appear in absorption.

The rocking frequencies for the hypothetical *cis*-form have been calculated to be 937 cm^{-1} for A_2 and 742 cm^{-1} for B_2. The latter value differs greatly from the observed value, which difference immediately rules out the possibility of assigning the *cis*-form to the less stable form. However, the fact that we have observed the two strong absorption bands corresponding to the CH_2-rocking frequencies of the less stable form provides conclusive evidence that we do not have the *cis*-form, since A_2 of C_{2v} is not allowed to appear in the absorption by the selection rule. In other words, if the *cis*-form were the less stable form, we would observe only one rocking-vibration band which would disappear in the spectrum of the solid state.

We shall show in a later paper that a similar treatment of the CH_2-rocking frequencies in coordination compounds with ligands of the type of XH_2C-CH_2X leads to the conclusion that the ligand is in the *gauche*-form but definitely not in the *cis*-form. Proof that the ligand is in the *gauche*-form provides conclusive evidence that we have in these compounds a new type of optical isomerism presented in a previous paper.[6]

[1] For the summary see S. Mizushima, *Internal Rotation* (Academic Press, Inc., New York, 1954).
[2] See, e.g., K. W. F. Kohlrausch, *Ramanspektren* (Akademische Verlagsgesellschaft, Leipzig, 1943).
[3] J. T. Neu and W. D. Gwinn, J. Chem. Phys. **18**, 1642 (1950).
[4] Mizushima, Morino, and Shimanouchi, Sci. Papers Inst. Phys. Chem. Research Tokyo, **40**, 87 (1942). Mizushima, Shimanouchi, Nakagawa, and Miyake, J. Chem. Phys. **21**, 215 (1953).
[5] I. Nakagawa, J. Chem. Soc. Japan **74**, 848 (1953); **75**, 178 (1954); I. Nakagawa and S. Mizushima, J. Chem. Phys. **21**, 2195 (1953).
[6] J. V. Quagliano and S. Mizushima, J. Am. Chem. Soc. **75**, 6084 (1953).

Time Lag in the Self-Nucleation

HIROMU WAKESHIMA
The Kobe University of Mercantile Marine, Kobe, Japan
(Received June 16, 1954)

THE stationary Becker-Döring theory of nucleation seems to fail in some cases to predict when the condensation of water vapor will occur in the very rapid expansions in a supersonic flow of moist air. In connection with the solution of this problem the nonsteady Becker-Döring equation for the self-nucleation of a supersaturated vapor was solved by R. F. Probstein[1] under a special simple initial condition. But this condition does not seem to correspond to the actual circumstances of the

experiment. The author has obtained an approximate but more simple and general expression for the nonstationary rate of self-nucleation which will be reported here.

From Zeldovich-Frenkel's general relation[2] satisfied by the number density of embryos $f(g)$,

$$D(g)N(g)\frac{\partial}{\partial g}\left(\frac{f(g)}{N(g)}\right)=-I(g),$$

we have

$$\frac{f(g)}{N(g)}=\int_g^G\frac{I(g)}{D(g)N(g)}dg$$

with

$$N(g)=Ce^{-\Delta\phi/kT}=N(g^*)\exp\{\chi^*/2kT\cdot(g-g^*)^2\},$$

where all notation used is the same as that given in Frenkel's text.[3] As $N(g)$ has a very sharp maximum at $g=g^*$, $D(g)$ in the integral can be replaced by $D(g^*)$ and $I(g)$ by

$$I(g^*)+(\partial I/\partial g)^*(g-g^*)+\tfrac{1}{2}\cdot(\partial^2 I/\partial g^2)^*(g-g^*)^2$$

in approximation. Thus we have

$$\frac{f(g)}{N(g)}=\frac{I(g^*)}{D(g^*)N(g^*)}\int_g^G\left[1+\left(\frac{\partial I}{\partial g}\right)^*\Big/I(g^*)\cdot(g-g^*)+\left(\frac{\partial^2 I}{\partial g^2}\right)^*\Big/2I(g^*)\cdot(g-g^*)^2\right]\exp\left[-\frac{\chi^*}{2kT}(g-g^*)^2\right]dg.$$

The upper and the lower limit of this integral can be replaced by $+\infty$ as well as $-\infty$, because G and g are supposed to be sufficiently distant from g^*. Therefore

$$\frac{f(g)}{N(g)}\doteqdot\frac{I(g^*)}{I_s(g)^*}+\left(\frac{\partial^2 I}{\partial g^2}\right)^*\Big/I_s(g^*)\cdot\frac{kT}{4\chi^*},$$

where $I_s(g^*)$ means the stationary value of $I(g^*)$ corresponding to g^*, i.e., $I_s^*=D(g^*)N(g^*)(\chi^*/2\pi kT)^{\frac{1}{2}}$. The right-hand side of this equation does not depend on g, and as $f(g)/N(g)\doteqdot 1$ for a small g, the following relation can be obtained for the rate of nucleation $I^*\equiv I(g^*)$,

$$I^*-I_s^*=-(\partial^2 I/\partial g^2)^*kT/4\chi^*.$$

Now as $\partial I/\partial g=-\partial f/\partial t$, we have

$$\left(\frac{\partial^2 I}{\partial g^2}\right)^*=-\left\{\frac{\partial}{\partial g}\left(\frac{\partial f}{\partial t}\right)\right\}^*=-\left\{\frac{\partial}{\partial t}\left(\frac{\partial f}{\partial g}\right)\right\}^*\doteqdot-\frac{d}{dt}\left(\frac{\partial f}{\partial g}\right)^*.$$

I can be expressed as

$$-I=D\frac{\partial f}{\partial g}+\frac{1}{kT}D\cdot f\frac{\partial\Delta\phi^3}{\partial g}$$

and the last term of this equation is 0 at $g=g^*$; therefore

$$-I^*=D^*\left(\frac{\partial f}{\partial g}\right)^*.$$

Thus the following relation can be obtained

$$\frac{I^*}{D^*}-\frac{I_s^*}{D^*}=-\frac{d}{dt}\left(\frac{I^*}{D^*}\right)\frac{kT}{4\pi D^*\chi^*}$$

or

$$\frac{dF}{dt}+\phi_*F=\phi_*F_s$$

with $F=I^*/D^*$, $F_s=I_s^*/D^*$, and $\phi_*=4D^*\chi^*/kT$. This equation obviously gives the solution

$$F=e^{-\Phi}\left(\int_{t_0}^t\phi_*F_s e^{\Phi}dt+F_0\right)$$

with

$$\Phi=\int_{t_0}^t\phi_*dt$$

where F_0 denotes the value of F at $t=t_0$. (1) When the degree of supersaturation is changed at $t=0$ from 0 to a given value corresponding to a constant value of I_s^* and ϕ_*, we have $F=F_s(1-e^{-\phi_* t})$. It is interesting to note that this expression is similar to that obtained by the author previously[4] by a more simple treatment. The time corresponding, e.g., to $I^*/I_s^*=1-1/100$ is about $4.6/\phi_*$ and the value of this quantity for the case considered by Probstein,[1] is somewhat smaller, but of the same order of magnitude as compared with that given by him. (2) If we define an "effective time lag" τ_e which satisfies $F_s(t)\equiv F(t+\tau_e)\doteqdot F(t)+(dF/dt)_t\tau_e$, we have $\phi_*\tau_e=1$ or $\tau_e=kT/4D^*\chi^*$. This formula gives a value of about 0.4×10^{-6} sec of τ_e for the same condition as in (1). Therefore it seems likely that the time lag in this sense cannot account for the existing discrepancies between theory and experiment mentioned above. Application of this theory to the problem of so-called "athermal nucleation" proposed by D. Turnbull *et al.*[5] will be given elsewhere later.

[1] R. F. Probstein, J. Chem. Phys. **19**, 619 (1951).
[2] J. Zeldovich, J. Exptl. Theoret. Phys. (USSR) **12**, 525 (1942); J. Frenkel, *Kinetic Theory of Liquids* (Oxford University Press, London, 1946), p. 394.
[3] See reference 2, p. 394.
[4] H. Wakeshima (to be published).
[5] Fisher, Hollomon, and Turnbull, J. Appl. Phys. **19**, 775 (1948).

Vacuum Ultraviolet Absorption Spectra of Iodine and Bromine

NOEL S. BAYLISS, *Chemistry Department, University of Western Australia, Nedlands, Western Australia*
AND
JOHN V. SULLIVAN, *Chemical Physics Section, Division of Industrial Chemistry, Commonwealth Scientific and Industrial Research Organization, Melbourne, Australia*
(Received June 28, 1954)

WE have measured the absorption spectra of iodine and bromine in the gas state and in solution by photographic photometry in the region 2000 A, using a one-meter grating vacuum spectrograph with a dispersion of 22 A/mm.

Table I shows a selection of the values of the molar extinction coefficients.

TABLE I. A selection of ϵ, σ values, and calculated oscillator strengths (f) over the indicated frequency ranges.

Molecule	Type of spectrum	Solvent	ϵ	K	f	Frequency range
Iodine	gas		29 000 130 000 150 000	49 000 51 000 53 000	2.29	46 500 K–54 000 K
Bromine	gas		14 000 22 800 29 000	48 000 51 000 54 000	0.76	47 000 K–54 000 K
Iodine	solution	*n*-heptane	9700 12 000 15 000[a]	50 000 52 000 54 000[a]	0.42	49 500 K–57 000 K
	solution	cyclo-hexane	13 000 14 700 16 200[a]	50 000 52 000 54 000[a]	0.38	49 500 K–56 000 K
Bromine	solution	*n*-heptane	1300 10 000 12 000[a]	50 000 52 000 54 000[a]	0.16	50 000 K–54 000 K

[a] Values of ϵ_{max}, σ_{max}.

Both iodine and bromine solutions have a maximum near 54 000 K; but the breadth of the region of intense absorption and the presence of shoulders on the long wavelength side of the maxima indicate clearly that the solution spectra are complex and consist of several (possibly three) overlapping transitions. There is good agreement for values of ϵ_{max}, σ_{max} between our results and those of Ham, Platt, and McConnell[1] for iodine in *n*-heptane. Our value for the oscillator strength is calculated over a different frequency range from the value $f=0.30$ obtained by these authors.

The gas spectra, for which quantitative extinction values have not been available hitherto, resemble the solution spectra in being apparently complex, and in the absence of observable vibrational

structure. (In order to obtain reasonable exposure times for photographic photometry, we used a relatively wide slit of band width approximately 10 A. Structure such as that of the Cordes bands of I_2 could therefore not be resolved.) Neither gas spectrum reaches its maximum within the frequency range covered by the present measurements. A surprising feature of the gas spectra is that they are between five times (for bromine) and six times (for iodine), as intense as the corresponding solution spectra in the same frequency range (see Table I), whereas solution intensities are generally found to be about equal to or greater than the corresponding gas values.[2,3]

There are two possible alternative explanations either of which is of interest in connection with the theoretical interpretation of halogen spectra and of solvent effects.

(a) There is a large solvent displacement which in solution removes some of the components of the gas spectrum further into the vacuum ultraviolet and out of the region of the present measurements. (b) The solvent perturbation in the present cases is such as to decrease the transition probability in solution.

The problem is being investigated further.

[1] Ham, Platt, and McConnell, J. Chem. Phys. **19**, 1301 (1951).
[2] Lois E. Jacobs and J. R. Platt, J. Chem. Phys. **16**, 1137 (1948).
[3] R. S. Mulliken and C. A. Rieke, Repts. Progr. Phys. **8**, 231 (1941).

On the Entropies of Complex Ions in Aqueous Solution

P. George, G. I. H. Hanania, and D. H. Irvine
Department of Colloid Science, University of Cambridge, Cambridge, England
(Received June 14, 1954)

Cobble[1,2] has recently proposed equations for the empirical calculation of standard partial molal entropies ($\bar{S}^0$) of oxy-anions and complex ions in aqueous solution. Shortly after, however, Connick and Powell[3] showed that the data on 22 oxy-anions could be fitted to within 3.7 eu by a much simpler equation

$$\bar{S}^0 = a - bZ + cn, \tag{1}$$

where a, b, and c are numerical constants, 43.5, 46.5, and 13.0, respectively, Z is the charge, and n the number of charge-bearing ligands. No theoretical justification for counting only charge-bearing oxygen atoms was advanced, and the equation is not directly applicable to complex ions in general (for instance to the amines, where the ligands are neutral molecules).

In our work on cell reactions and complex formation in inorganic and in haemoprotein systems, we have explored the possibility of using Eq. (1) in the modified form

$$\bar{S}^0 = A - BZ + CN, \tag{2}$$

where A, B, and C are numerical constants, but N is the total number of ligands, whatever their nature. The values of A, B, and C thus obtained are given in Table I, the equilibrium constants for successive additions of the ligand being corrected by the usual statistical factors, making every addition and dissociation a bimolecular reaction with only one path rather than several identical paths. The constants for amines were computed from Bjerrum's data[4] on 26 complexes of Ag^+, Cu^{++}, Zn^{++}, Ca^{++}, Co^{++}, and Ni^{++}, and give $\bar{S}^0$ values for these complexes which agree to within 3.4 eu. The data on other complex ions, taken from those listed by Cobble[5] and by Latimer,[6] show the C values to increase with increasing size of the ligand as would be expected. It is also noteworthy that the increment in the value of C per ligand bond is substantially constant for the series ammonia, ethylenediamine and dipyridyl, the triamine and the tetramine. This may be due to restricted rotation in the chelates since CH_3NH_2 has a much larger C value than NH_3. Equation (2) does not fit the 30 recorded values of $\bar{S}^0$ for oxy-anions so well, the mean discrepancy being 7.9 eu compared with 5.0 eu when Eq. (1) is used.

Table I.

Ligand	A	B	C	C (per ligand bond)
Ammonia	44	32	23 ± 2	23 ± 2
Ethylenediamine	...	...	46 ± 3	23 ± 1.5
Diethylenetriamine	...	...	70 ± 4	23 ± 1
Triethylenetetramine	...	...	114 ± 11	28 ± 3
Dipyridyl	−21	3 ± 4[a]	53 ± 2	26.5 ± 1
Methylamine	...	...	41	41
HO and O in oxy-anions	39	40	10	10
Chloride	55	22[a]	7	7
Cyanide	48	52[a]	23	23
Water	78	51	...	...

[a] B has been calculated from data on the cell reactions: $Os(dipy)_3^{++}/Os(dipy)_3^{+++}$, Barnes, Dwyer, and Gyarfas, Trans. Faraday Soc. **48**, 269 (1952); $Fe(dipy)_3^{++}/Fe(dipy)_3^{+++}$, $Ru(dipy)_3^{++}/Ru(dipy)_3^{+++}$, $IrCl_6^{---}/IrCl_6^{--}$, and $Fe(CN)_6^{----}/Fe(CN)_6^{---}$, authors' unpublished results.

Equations (1) and (2) are clearly related to Powell and Latimer's equation[7] for monatomic ions,

$$\bar{S}^0 = \tfrac{3}{2}R\ln M + 37 - \frac{270Z}{(r+x)^2},$$

which reduces to the form "$A-BZ$" if the terms containing the mass M and the radius r (x being a numerical constant) are approximately constant for a series of ions. In fact Eq. (2) accounts reasonably well for the $\bar{S}^0$ values of the monatomic ions Mn^{++}, Fe^{++}, Cu^{++}, Zn^{++}, and Cr^{+++}, Fe^{+++}, and Ga^{+++}, which have similar atomic weights and radii, with $A\simeq78$, $B\simeq51$. Since the contributions to $\bar{S}^0$ from HO, O and probably H_2O are small, $C\simeq10$, the high values of B suggest that there is a more substantial contributions to $\bar{S}^0$ from water molecules outside the primary coordination shell than is the case with the ligands Cl, NH_3, and dipyridyl, which have lower values of B. This could originate from preferential hydrogen bonding between the structurally similar ligand and solvent. The high value of B for CN^- could be attributed to the peripheral N atoms bearing the charge as a result of double bond formation between the metal and the ligand, and the very low value for dipyridyl to complete shielding of the metal ion by the bulky organic ligand.

[1] J. W. Cobble, J. Chem. Phys. **21**, 1443 (1953).
[2] J. W. Cobble, J. Chem. Phys. **21**, 1446 (1953).
[3] R. E. Connick and R. E. Powell, J. Chem. Phys. **21**, 2206 (1953).
[4] J. Bjerrum, *Metal Ammine Formation in Aqueous Solution* (Copenhagen, 1941).
[5] J. W. Cobble, J. Chem. Phys. **21**, 1451 (1953).
[6] W. M. Latimer, *Oxidation Potentials* (Prentice-Hall, Inc., New York, 1952), second edition.
[7] R. E. Powell and W. M. Latimer, J. Chem. Phys. **19**, 1139 (1951).

Assignment of the Intense 'Acene Absorption Systems

D. P. Craig, P. C. Hobbins,* and J. R. Walsh
Department of Physical Chemistry, University of Sydney, Sydney, Australia
(Received June 22, 1954)

In solution anthracene has a very intense absorption at 2500 A ($\epsilon\sim200\,000$) and a weaker one at 2300 A ($\epsilon\sim10\,000$). In the monoclinic crystal as we reported earlier[1] there is a system at 2700 A strongly polarized along the b monoclinic axis and another running to the short-wave side of 2300 A strongly polarized in the ac plane. A further study of the intensities of these crystal systems and an analogous absorptions in tetracene leads us to discard our earlier conjecture[1,2] that there is a simple correspondence between the two systems observed in solution and the two crystal systems. From the intensity differences between crystal and solution spectra it now seems clear that neither crystal system has anything to do with the weak solution system at 2300 A, and we have to explain both crystal systems as arising from the splitting of the single intense solution absorption at 2500 A. Davydov[3] showed that the forces between the two molecules of a unit cell cause the upper states of allowed transitions to split into two oppositely polarized components separated by an energy depending in first approximation on the dipole-dipole interaction. A simple calculation

shows that in an intense transition polarized along the long molecular axis splittings in the other of 10^4 cm^{-1} are possible, with the *b* component lower, but because of the crystal geometry a short axis molecular transition, even if intense, will suffer only a small splitting. The experimental results agree strikingly with expectation for a long axis transition, including a satisfactory agreement in the intensity ratio of the two components, so far as this can be estimated.

The long axis assignment is confirmed by the polarized spectrum of tetracene. Tetracene crystals are triclinic, but the departure from the monoclinic habit is small both in form ($\alpha=98.0°$, $\gamma=92.5°$)[4] and in optical properties: we find for example that the principal polarization directions throughout the quartz ultraviolet do not deviate more than a few degrees from the extinction directions for visible light. We assume that the extinction directions coincide nearly enough with the *a* and *b* crystal axes. We assume also, consistently with the naphthalene and anthracene structures, that the long molecular axis lies closely parallel to the *c* axis, and deduce from the smaller crystal angle β that this axis is more nearly perpendicular to the *ab* plane than in the smaller 'acenes. The crystal spectrum of tetracene corresponding to the intense system observed in solution near 2700 A is entirely consistent with this and with the assignment to a long-axis transition. The crystal absorption shows a weak system, *b* polarized, at 2700 A (weaker than the corresponding anthracene system), and a stronger system beginning near 2200 A, polarized in the *a* direction but overlapped by another strong *b* absorption. The crystal splitting and intensity relationships are again compatible only with a transition polarized along the long molecular axis, which we accordingly assign A_g-B_{3u} both in anthracene and tetracene.

Many authors[5] have reported that strong solution or vapor band systems are greatly weakened in crystal spectra. The explanation of some, and perhaps most, of these is doubtless the same as in anthracene and tetracene: namely that the system is split in the crystal, and a weak component only remains in the wavelength region of the solution absorption. The strong component is displaced either into a less accessible wavelength range, or at least to a region where its connection with the solution system is not apparent.

* Department of Chemistry, University College, London, England.
[1] D. P. Craig and P. C. Hobbins Nature **171**, 566 (1953).
[2] D. P. Craig, Revs. Pure Appl. Chem. **3**, 207 (1953).
[3] A. S. Davydov, J. Exptl. Theoret. Phys. U.S.S.R. **18**, 210 (1948).
[4] J. M. Robertson, *Organic Crystals and Molecules* (Cornell University Press, Ithaca, New York, 1953).
[5] For references see reference 2.

The Stabilization of Methyl Radical*

I. L. Mador†
Applied Physics Laboratory, The Johns Hopkins University, Silver Spring, Maryland
(Received March 31, 1954)

In a number of cases evidence has been presented for the stabilization of free radicals in dilute concentration in rigid media.[1,2] In the present work an attempt has been made to stabilize and obtain the infrared absorption spectrum of the CH_3 radical at liquid helium temperatures. Radicals were produced by photolysis of CH_3I and *x*-radiation and pyrolysis of $Pb(CH_3)_4$.

According to the "cage theory"[3] the efficiency of the photochemical decomposition of liquids or solids will be very low due to reflection of the fragments by the lattice cage, followed by primary recombination. If the absorbed energy is high enough, then the fragments should be able to penetrate the cage and escape from the reaction locus. For CH_3I irradiated at 2537 A it has been shown experimentally[4] that the cage theory is inoperative and the quantum efficiency of the primary act is close to unity.[5]

The samples were introduced as vapors into an optical cell[6] and were generally photolyzed for one or two hours during deposition because of the strong absorption of I_2 relative to that of CH_3I. A Hanovia Sc2537 Hg vapor lamp was used, and the energy of the uncollimated beam falling on the sample was determined as 3.3×10^{17} quanta/cm^2/min with a uranyl oxalate actinometer. For a 0.10 mm thick CH_3I sample which is almost completely absorbing this corresponds to approximately 20 percent decomposition per hour, assuming a quantum yield of unity.

Photolysis of CH_3I at 4°K produced a new absorption band at 1296 cm^{-1}, which is the γ_4 band of CH_4. In a few cases weak bands due to C_2H_4 (949 cm^{-1}), C_2H_6 (818 cm^{-1}) and CH_2I_2 (1029 cm^{-1}) were found. The color by transmitted light was a bright red, though no definite band center could be determined.

On warming after photolysis, in most cases the glassy sample films disintegrated at about 30° or 40°K with pieces observed to strike the outside cell window and then redeposit on the support window to form a yellow-brown translucent film. The phenomenon appeared quite violent on a small scale. In some cases during warmup the films instantaneously changed to a yellow-brown or red-brown color which was characteristic of other photolyses carried out at 77°K.

The x-radiation of $Pb(CH_3)_4$ at 4°K produced CH_4. When the films were subsequently warmed up to about 40°K they instantaneously turned opaque, presumably because of the formation of metallic Pb. $Pb(CH_3)_4$ was pyrolyzed using Xe as a carrier gas and the reaction products frozen out at 4°K. The infrared absorption spectrum could be completely assigned to bands of CH_4, C_2H_6, C_2H_4, and C_3H_8.

Methane is also found as a reaction product in the photolysis of liquid and vapor CH_3I and is attributed to a hot radical mechanism.[4] The photolysis of CH_3I present in about 1 percent concentration in a Xe or N_2 lattice did not result in CH_4 formation. Methylene iodide photolysis was found to produce CH_3I, which is the homologous "hot radical" product.

The disintegration of the films on warmup is interpreted as resulting from exothermic radical recombination reactions. Unphotolyzed films of CH_3I or of CH_3I-CH_4 mixtures warmed up without incident. It is believed that the red color is due to CH_3 and that the brownish color after warmup is due to I_2. The failure to observe any vibrational bands that could be attributed to CH_3 is probably due to an insufficient concentration for infrared determination. The volume swept out by the "hot" CH_3 and I fragments before they are cooled to ambient thermal temperatures may well limit the concentration that may be achieved.

I am indebted to R. S. Quinn for aid in come of the experimental work and to Dr. W. H. Avery for helpful discussions.

* This work was supported by the Bureau of Ordnance, Department of the Navy, under Contract NOrd-7386.
† Present address, Research Division, National Distillers Products Corporation, Cincinnati, Ohio.
[1] G. N. Lewis and D. Lipkin, J. Am. Chem. Soc. **64**, 2801 (1942).
[2] F. O. Rice and M. Freamo, J. Am. Chem. Soc. **73**, 5529 (1951).
[3] J. Franck and E. Rabinowitsch, Trans. Faraday Soc. **30**, 120 (1934).
[4] W. H. Hamill and R. H. Schuler, J. Am. Chem. Soc. **73**, 3466 (1951).
[5] The over-all quantum yield for the photolysis of CH_3I, liquid or vapor, is low for other reasons. See reference 4, and R. D. Schultz and H. A. Taylor, J. Chem. Phys. **18**, 194 (1950).
[6] W. H. Duerig and I. L. Mador, Rev. Sci. Instr. **23**, 421 (1952).

A Statistical Derivation of the B.E.T. Equation

Tominaga Keii
Research Institute for Catalysis, Hokkaido University, Sapporo, Japan
(Received June 28, 1954)

STATISTICAL-MECHANICAL derivations of the B.E.T. equation[1] of multilayer adsorption have been carried out by Hill *et al.*[2] It seems to the writer that those derivations reported are rather cumbersome in spite of the use of statistical mechanics.

In this letter the writer shows that the B.E.T. equation may easily be derived with the use of the grand partition function.

The notations are: *A*—the total number of the adsorbed molecules, X_0—the total number of the surface sites, X_i—the number of adsorbed molecules in the *i*-th layer, s_i—the number of the sur-

face sites housed with i molecules (the area of the i-th layer), $\xi_i-(=\lambda q_i)$, λ-absolute activity of an adsorbed molecule, q_i—partition function of an adsorbed molecule in the i-th layer, $\xi_L-(=\lambda q_L)$, q_L—partition function of the molecule in the liquid state, x—relative pressure, c—(ξ_1/ξ_L) a const.

According to the B.E.T. model of multilayer adsorption, the adsorbed phase may be illustrated as in the figure. Taking the summation of possible number of adsorbed molecules with the columns which constitute the adsorbed phase, the grand partition function is written as

$$\Xi=\sum_{s_0+s_1+\cdots+s_\infty=x_0}\frac{x_0!}{\prod_{i=0}^{\infty}(s_i)!}\xi_1^{s_1}(\xi_1\xi_2)^{s_2}(\xi_1\xi_2\xi_3)^{s_3}\cdots. \tag{1}$$

On the other hand, taking the summation with the layers, we obtain

$$\Xi=\sum_{x_1=0}^{x_0}\frac{x_0!}{(x_0-x_1)!x_1!}\xi_1^{x_1}\sum_{x_2=0}^{x_1}\frac{x_1!}{(x_1-x_2)!x_2!}\xi_2^{x_2}\Sigma\cdots. \tag{2}$$

It is well known that the generating function of the summation (1) is written as

$$\Xi=(1+\xi_1+\xi_1\xi_2+\xi_1\xi_2\xi_3+\cdots)^{x_0}. \tag{3}$$

The summations (2) reduce also to the above form by carrying out the summations successively from right to left.

Specializing (3) with the B.E.T. assumption that $\xi_2=\xi_3=\cdots=\xi_L=x=\xi_1/c$, and using the property of grand partition function, the B.E.T. equation is derived as follows.

$$\Xi=\left(1+\frac{c\xi_L}{1-\xi_L}\right)^{x_0} \tag{4}$$

$$\frac{A}{x_0}=\frac{\xi_L}{x_0}\frac{\partial\ln\Xi}{\partial\xi_L} \tag{5}$$

$$=\frac{cx}{(1-x)(1-x+cx)}. \tag{6}$$

If the possible number of layers were a finite number N, we get as the B.E.T. finite layers equation

$$\Xi=\left(1+c\xi_L\frac{1-\xi_L^{N+1}}{1-\xi_L}\right)^{x_0} \tag{7}$$

$$\frac{A}{x_0}=\frac{cx\{1-(N+1)x^N+Nx^{N+1}\}}{(1-x)(1-x+cx-cx^{N+1})}. \tag{8}$$

The writer wishes to point out that Hüttig's equation[3] has no physical basis. If we carry out the summations of (2) with each layer separately, we obtain

$$\Xi=(1+\xi_1)^{x_0}(1+\xi_2)^{x_1}(1+\xi_3)^{x_2}\cdots \tag{9}$$

from which Hüttig's equation is derived by the same procedure as before. This derivation is, however, clearly incorrect. Applying the relation, $X_i=\xi_i(\partial\ln\Xi/\partial\xi_i)$, to this meaningless equation (9), we obtain a relation, from which Hüttig started,

$$\frac{x_i}{x_{i-1}-x_i}=\xi_i. \tag{10}$$

This relation may be considered as one with the omission of s_{i+1} from a relation of the B.E.T. theory[1] as

$$\frac{x_i-x_{i+1}}{x_{i-1}-x_i}=\xi_i, \tag{11}$$

which is derived from the right form of the grand partition function (3). This procedure to obtain (10) from (11) has been charged by Ross[4] with the neglect of the shielding effect of the $i+1$th layer. However, it is also of no physical meaning since the "shielding" is merely a synonym of "adsorbing" the $i+1$th molecules.

[1] Brunauer, Emmett, and Teller, J. Am. Chem. Soc. **60**, 309 (1938).
[2] T. L. Hill, J. Chem. Phys. **14**, 263 (1946); M. Dole, *ibid.* **16**, 25 (1948).
[3] Hüttig, Monatsh. Chem. **78**, 177 (1948) (quoted by Ross).
[4] Ross, J. Phys. Colloid Chem. **53**, 383 (1949).

The Crystal Structure of Paradichlorobenzene*

BRUCE C. LUTZ
Physics Department, University of Delaware, Newark, Delaware
(Received June 16, 1954)

THE phase change in solid p-$C_6H_4Cl_2$ reported by Dean and Pound[1] has been further investigated. This phase change manifests itself as a discontinuity in the temperature dependence of the pure nuclear quadupole resonance absorption line of the chlorine nucleus which occurs in the region of 35 mc/sec. This resonance line is a transition between energy levels resulting from the interaction of the nuclear quadrupole moment and the field gradient in which it finds itself. The Zeeman splitting of this line is dependent on the angle between the applied magnetic field and the z direction (axis of symmetry of the field gradient) as shown by Kruger.[2] This angular dependence makes it possible to determine the z directions (poles) in the solid crystal. Because of the bonding of the chlorine to the benzene ring this direction corresponds to the C−Cl bond direction. The angle of 76°±2° measured between the two directions in the low temperature phase agrees with those determined by x-ray diffraction data[3] which show two molecules per unit cell.

The investigation of the high temperature phase indicates an ordered state in which the C−Cl bonds are aligned to form a unique direction. All of the crystals examined displayed either a well-defined Zeeman pattern for a single pole or an ill-defined pattern with a suggestion of two poles within a few degrees of each other. Whenever the latter case occurred, the lack of definition and the unusually broad lines indicated a less well-ordered state or an ordered state superimposed on a background of a disordered state. The crystals examined showed no correlation between the direction of the single pole in the high temperature phase and the two in the low temperature phase. The crystals were grown in cylindrical glass tubes and sealed so that they could be immersed in a constant temperature bath. The stability of the high temperature ordered state was poor and must depend sharply on some parameter as yet undetermined.

* Supported in part by the Office of Ordnance Research and the Research Corporation.
[1] C. Dean and R. V. Pound, J. Chem. Phys. **20**, 195 (1952).
[2] H. Kruger, Z. Physik **130**, 371 (1951).
[3] Ralph H. G. Wyckoff, *Crystal Structures* (Interscience Publishers, Inc., New York, 1953), Vol. III, Chap. XIV, p. 5.

Some Detonation Properties of Acetylene Gas

R. E. DUFF, H. T. KNIGHT, AND H. R. WRIGHT
Los Alamos Scientific Laboratory, Los Alamos, New Mexico
(Received June 28, 1954)

IT is the purpose of this letter to describe briefly some interesting and in certain cases anomalous properties of the low-pressure detonation process in acetylene. Heretofore, the lower pressure detonation and combustion limits in gaseous acetylene have been reported to be considerably above one atmosphere;[1-3] and the upper detonation limit in acetylene-oxygen mixtures at one atmosphere has been reported to be 92 percent acetylene.[4] Nevertheless, stable detonation can occur at much lower pressures and at much higher acetylene concentrations. The authors have found that, depending upon the diameter of the detonation tube, 1 to 3 grams of some high explosive such as tetryl will initiate a stable detonation wave in acetylene at an initial pressure of 60 cm Hg. The acetylene used in most of these experiments was free from impurities with the exception of 0.5 percent of nitrogen as determined by mass spectrographic analysis. However, commercial grade acetylene was observed to detonate equally well. The fact that acetylene will detonate at such a low pressure is of considerable significance to the chemical industry, where large quantities of the gas must be stored and handled.

It is a generally accepted rule that the combustion limits of a gas or gas mixture are wider than the detonation limits.[5] The

detonation of acetylene at a pressure well below the combustion limit[3] is believed to be the only known exception to this rule.

The detonation of pure acetylene was observed in tubes several meters long and with internal diameters ranging from 13 mm to 76 mm. In every case the initial part of the wave was observed to spin.[6] The spin-pitch-to-tube-diameter ratio is a linear function of tube diameter ranging from 3.4 in a 76 mm tube to 4.0 in a 13 mm tube. It should be emphasized, however, that this spinning detonation is not stable in tubes smaller than about 40 mm.

For most gaseous mixtures that exhibit spin, the pitch-diameter ratio is very near the constant value of 3.1. This experimental result is in agreement with the mechanical theory of spinning detonation proposed by Fay.[7] If an attempt is made to explain the high values observed in pure acetylene by a straightforward application of the Fay theory in its usual form, it is necessary to assume that γ for the gas in the wake of the detonation wave has impossible values of less than one for most of the waves.

The stability of this detonation process was checked by observations made in very long tubes. In a brass tube 76 mm i.d. and 16 m long the wave propagated in a stable fashion with a velocity of 1870 m/sec along the entire length of the tube. In tubes with an internal diameter of 35 mm or less the wave slows down and stops spinning after a run of several meters. However, the wave does not fail even in tubes as small as 13 mm, but continues to propagate with a constant velocity of about 1500 m/sec. Varying the amount of explosive in the initiator from 1 to 3 grams and lengthening the tube from 16 to 23 m failed to produce any change in this velocity in a 25 mm i.d. tube.

Moving film photographs of the normal reflection of this slow wave at the end of the 25 mm i.d. tube have demonstrated conclusively that a nonluminous shock wave preceeds the luminous zone by a constant distance of about 90 mm. If the assumption is made that the region between the shock front and the luminous zone is a steady-state region; and if the particle velocity of the gas behind the shock is calculated taking account of the temperature variation of the specific heat of acetylene, this result suggests that for this detonation wave the reaction time is about 470 μsec compared with the fractions of microseconds for most detonation processes.

Investigation of these phenomena is continuing. A more detailed account of experimental evidence, results of detonation velocity calculations based on the Chapman-Jouguet theory, and speculations and conclusions concerning the chemical processes responsible for the slow wave will be published.

[1] M. Berthelot and H. L. Le Chatelier, Compt. rend. **129**, 427 (1899).
[2] Jones, Kennedy, Spalan, and Huff, U. S. Bureau of Mines, Report of Investigations **3826** (1945).
[3] J. Echard, Ann. Mines **138**, 15 (1949).
[4] J. Breton, Ann. office natl. combustibles liquides **11**, 487 (1936).
[5] B. Lewis and G. von Elbe, *Combustion Flames and Explosions* (Academic Press, New York, 1951), p. 227.
[6] W. A. Bone and R. P. Fraser, Phil. Trans. Roy. Soc. (London) **A228**, 197 (1929); **A230**, 363 (1932).
[7] J. A. Fay, J. Chem. Phys. **20**, 942 (1952).

On Intermolecular Forces and Crystal Structures of Rare Gases

L. JANSEN AND J. M. DAWSON
Department of Chemistry, University of Maryland, College Park, Maryland
(Received July 12, 1954)

THE relation between the intermolecular potential and the stability of crystal structures of the rare gases has been investigated by several authors. Kihara and Koba[1] extended calculations by Lennard-Jones and Ingham[2] on the stability of cubic structures by comparing a face centered cubic lattice with a structure of hexagonal closest packing. They found that for any value of the parameter s in the inverse s, 6-power potential the hcp is more stable than the fcc form, in contradiction with experimental results for neon, argon, krypton, and xenon. Kihara and Koba repeated the calculations for a Buckingham potential; the result is that for values of the parameter α of the exponential part smaller than 8.765 the fcc lattice is more stable, whereas for values greater than 8.765 the hcp is the preferred structure. However, this limiting value for α is much too low to explain the structures of the rare gases except helium. According to accurate determinations by Mason and Rice[3] the experimental values of α lie between 12.3 (krypton) and 14.5 (neon). Several possible explanations can be given for this discrepancy. Axilrod[4] took into account slight deviations from additivity of the dipole dispersion forces. It was found that this effect favors the slightly less dense fcc lattice, but the difference between fcc and hcp is less than a ten-thousandth of the cohesive energy. Another possibility is that also the Buckingham potential is not accurate enough for the explanation of crystal structures.

TABLE I. Difference in sublimation energy between a face centered cubic and a hexagonal lattice of closest packing, divided by the sublimation energy of the fcc lattice, for different values of the zero-point energy parameter Λ^* and various values of the parameter s in the Lennard-Jones (s,6) potential function.

Λ^*	0	0.1	0.3	0.5	0.7
s	0.10^5	0.10^5	0.10^5	0.10^5	0.10^5
16	−10.1	−10.4	−11.0	−11.5	−11.7
14	−10.3	−10.5	−10.9	−11.9	−12.1
12	−10.0	−10.4	−10.9	−11.5	−12.0
10	−8.8	−9.1	−9.7	−10.3	−10.9
9	−7.8	−8.1	−8.6	−9.1	−9.7
8	−6.2	−6.5	−6.9	−7.4	−7.9
7	−3.8	−4.1	−4.4	−4.8	−5.2

Kihara and Koba neglected the effect of zero-point energy because helium, despite its large zero-point energy, crystallizes in the hcp lattice.[5] Besides the qualitative nature of Kihara's assumption on the effect of zero-point energy, it may be that the limiting value of α is shifted appreciably if zero-point energy is taken into account. We have therefore extended Kihara's calculations by including the zero-point energy of the crystals. Corner's method[6] is used for the evaluation of the zero-point energy. This letter reports on the part of the analysis dealing with the Lennard-Jones (s,6) potential, with s varying from 7 to 16. The expressions for the potential energy and the zero-point energy are, in reduced form, per molecule:

$$\phi_{\text{pot}}/\epsilon=\frac{1}{2(s-6)}\left[6\left(\frac{r_0}{a}\right)^s\cdot C_s-s\left(\frac{r_0}{a}\right)^6\cdot C_6\right]; \tag{1}$$

r_0 is the intermolecular distance for minimum potential $-\epsilon$; a is the nearest neighbor distance in the crystal; C_s, C_6 are crystal sums for the fcc lattice, determined by Lennard-Jones and Ingham[2] and Kihara and Koba.[1]

$$U_{z.p.}/\epsilon=F(s)\Lambda^*\left[s(s-1)\left(\frac{r_0}{a}\right)^{s+2}\cdot C_{s+2}-5s\left(\frac{r_0}{a}\right)^8\cdot C_8\right]^{\frac{1}{2}}, \tag{2}$$

with

$$F(s)=\frac{9}{8}\left(\frac{5}{3}\right)^{\frac{1}{2}}\Big/\{[2\pi^2(s-6)]^{\frac{1}{2}}\cdot(s/6)^{1/(s-6)}\}$$

and

$$\Lambda^*=h/\sigma(m\epsilon)^{\frac{1}{2}}, \tag{3}$$

where σ is the intermolecular distance for zero potential and m is the mass of the molecule. For any value of s, the value of (r_0/a) is found numerically from the equilibrium condition:

$$0=\frac{6s}{s-6}\left[\left(\frac{r_0}{a}\right)^{s-1}\cdot C_s-\left(\frac{r_0}{a}\right)^5\cdot C_6\right]+\frac{F(s)\Lambda^*\left[s(s-1)(s+2)\left(\frac{r_0}{a}\right)^{s+1}-40s\left(\frac{r_0}{a}\right)^7\cdot C_8\right]}{\left[s(s-1)\left(\frac{r_0}{a}\right)^{s+1}\cdot C_{s+2}-5s\left(\frac{r_0}{a}\right)^8\cdot C_8\right]^{\frac{1}{2}}}. \tag{4}$$

For the hexagonal lattice C_s is replaced by H_s, etc. Values for H_s have been determined by Goeppert-Mayer and Kane,[7] and Kihara and Koba.[1] The range $\Lambda^*=0, 0.1, \cdots, 0.7$ covers all rare gases ex-

cept helium. The results of the analysis for the Lennard-Jones (s,6) potential are given in Table I. It is seen that the inclusion of zero-point energy does not change Kihara's conclusion that for any value of s the hcp is more stable than the fcc lattice. A detailed report, including the results for the Buckingham potential, will be published later.

[1] T. Kihara and S. Koba, J. Phys. Soc. Japan **7**, 348 (1952).
[2] J. E. Lennard-Jones and A. E. Ingham, Proc. Roy. Soc. (London) **A107**, 636 (1925).
[3] E. A. Mason and W. E. Rice, J. Chem. Phys. **22**, 843 (1954).
[4] B. M. Axilrod, J. Chem. Phys. **19**, 724 (1951).
[5] T. Kihara, Revs. Modern Phys. **25**, 831 (1953).
[6] J. Corner, Trans. Faraday Soc. **35**, 711 (1939).
[7] M. Goeppert-Mayer and G. Kane, J. Chem. Phys. **8**, 642 (1940).

Influence of Permanent Multipole Interactions on Vibrational Deactivation in Molecular Collisions*

F. W. DE WETTE† AND Z. I. SLAWSKY‡
Department of Chemistry, University of Maryland, College Park, Maryland
(Received June 15, 1954)

IN a previous paper[1] a general outline of the method has been given, which allows the numerical calculation of the vibrational deactivation probabilities in collisions.

This was a generalization of the considerations of Landau and Teller[2] according to which only short range (nonadiabatic) forces are effective in deactivation. As was pointed out in our previous paper, this is not, however, quite correct; the adiabatic interactions have two indirect effects on the transition probabilities: (1) They change the relative motion of the collision partners; (2) They perturb the internal states of the molecules.

Later papers[3–5] have proceeded to numerical calculations without a systematic discussion of the way in which the two types of interaction enter the equations and as a consequence, in what manner the two effects of the long-range (adiabatic) forces appear mathematically. The adiabatic interaction $V^a(\mathbf{r}_a,\mathbf{r}_b,\mathbf{R})$ can be expanded in terms of the internal coordinates of the molecules r_a, r_b (R is the intermolecular distance).

$$V^a(\mathbf{r}_a,\mathbf{r}_b,\mathbf{R}) = V_{\mathrm{I}}{}^a(\mathbf{R}) + V_{\mathrm{II}}{}^a(\mathbf{r}_a,\mathbf{r}_b,\mathbf{R}). \quad (1)$$

$V_{\mathrm{II}}{}^a(\mathbf{r}_a,\mathbf{r}_b,\mathbf{R})$ can be introduced as a perturbation in the internal wave equation of the molecules. This equation can be solved for the perturbed internal eigenfunctions $\chi(\mathbf{r}_a,\mathbf{r}_b,\mathbf{R})$ and the perturbed internal energies $\epsilon(\mathbf{R})$. This expresses the perturbation of the vibrations by the interaction of the two molecules while they are at the fixed distance $\mathbf{R}$, and gives effect II of the long-range forces. $V_{\mathrm{I}}{}^a(\mathbf{R})$ and $V^{na}(\mathbf{r}_a,\mathbf{r}_b,\mathbf{R})$, are then introduced into the full Schrödinger equation, the latter expressing the nonadiabatic interaction. One then proceeds with the usual development for the resultant wave function.

$$\Psi(\mathbf{r}_a,\mathbf{r}_b,\mathbf{R}) = \Sigma_m \chi_m(\mathbf{r}_a,\mathbf{r}_b,\mathbf{R}) F_m(\mathbf{R}). \quad (2)$$

By introducing the wave equations for the modified vibrational wave functions χ_m, as discussed above, multiplying by χ_n and integrating over the internal coordinates—a standard procedure—one obtains sets of differential equations for the F_m which contain, as quasi-potentials: (1) matrix elements of V^{na}, (2) $V_{\mathrm{I}}{}^a$. The latter expresses the effect of the long-range forces on the relative motion of the collision partners (the effect called I before); the elements of V^{na} also influence this motion, but in addition provide the transitions.

An attempt was made to evaluate the adiabatic effect numerically in two cases. The method (in its one dimensional form for head-on collisions) has been applied to collisions of molecules with dipole-dipole ($d-d$) and quadrupole-quadrupole ($q-q$) interactions as the adiabatic interaction. HCl with $d-d$ and CO with $q-q$ interaction have been worked out numerically. It is found that in these cases $V_{\mathrm{II}}{}^a$ is negligible. This simplifies the calculation because only $V_{\mathrm{I}}{}^a$ has to be taken into account. The deactivation probability of HCl is increased by a factor of 4 and that of CO by a factor of 2 as a result of these accelerating interactions. The calculations were made for configurations of the collision partners in which they attract one another.

A more detailed paper on this subject will shortly be submitted for publication in *Physica*.

* Supported by the U. S. Office of Naval Research under contracts Nonr-595 (02) and N6-ORI-215-3. Work under the latter contract was done by one of the authors (F. W. de W.) while he was a visiting lecturer at Brown University, Providence, Rhode Island.
† On leave from the Institute for Theoretical Physics, State University, Utrecht, The Netherlands.
‡ On the staff of the U. S. Naval Ordnance Laboratory, White Oak, Maryland.

[1] Slawsky, de Wette, and de Groot, Nuovo Cimento Suppl. A1, No. 2, Vol. VII, Serie IX (1950).
[2] L. Landau and E. Teller Physik. Z. Sowjetunion **10**, 34 (1936).
[3] Schwartz, Slawsky, and Herzfeld, J. Chem. Phys. **20**, 1591 (1952).
[4] B. Widom and S. H. Bauer, J. Chem. Phys. **21**, 1670 (1953).
[5] R. N. Schwartz and K. F. Herzfeld, J. Chem. Phys. **22**, 767 (1954).

Dichroism of the Crystal of Dicyclopentadienyl-Iron

SHOICHIRO YAMADA, AKITSUGU NAKAHARA, AND RYUTARO TSUCHIDA
Department of Chemistry, Faculty of Science, Osaka University, Nakanoshima, Osaka, Japan
(Received May 11, 1954)

ALTHOUGH the measurement of pleochroism is expected to afford valuable information about the nature of the linkages in dicyclopentadienyl-iron, no paper has been presented on this property. In this letter we report on the dichroism of this compound.

Dicyclopentadienyl-iron was prepared from cyclopentadienyl-magnesium bromide and tris (2, 4-pentanediono) ferriate in orange, monoclinic prisms elongated along the [100]. Quantitative dichroism measurement in the visible and near ultraviolet was performed by Tsuchida-Kobayashi's microscopic method[1] with polarized light having electric vector along and perpendicular to the (100) plane. Based on the crystal analysis,[2] a-absorption (Fig. 1)[3] represents main characteristic of a component absorption

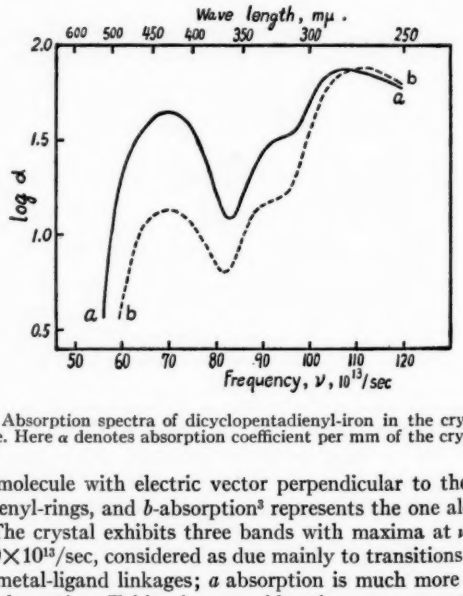

FIG. 1. Absorption spectra of dicyclopentadienyl-iron in the crystalline state. Here α denotes absorption coefficient per mm of the crystal.

of the molecule with electric vector perpendicular to the cyclopentadienyl-rings, and b-absorption[3] represents the one along the rings. The crystal exhibits three bands with maxima at ν 70, 94, and 110×10^{13}/sec, considered as due mainly to transitions related to the metal-ligand linkages; a absorption is much more intense than b absorption. Taking into consideration arrangement of the complexes in the crystal,[2] rough estimation indicates that *for the band at ν 70×10^{13}/sec the absorption with electric vector along the direction combining the iron atom with the centers of the cyclopentadienyl-rings is five and a half times as intense as the absorption with electric vector along the rings.* The above regularity suggests that firm linkage may exist between the iron atom and cyclopentadienyl-rings, π electrons of the rings being considerably involved

in the linkages with the metal. This relation seems to agree with those on planar complexes.[4]

As to the band at ν 110×10¹³/sec, which may be ascribed to transitions in the cyclopentadienyl-rings in co-ordination with the metal,[5] absorption with electric vector along the rings is slightly hypsochromic to that perpendicular to the above. Such tendency is different from that for π-bands of benzene rings[6] and for specific bands of π-electron systems in co-ordination with metal atoms;[4] for both the bands absorption is far bathochromic along the π-electron systems to that perpendicular to the above.[4,6] Therefore, it is supposed that the electronic state of the cyclopentadienyl-rings in dicyclopentadienyl-iron differs from that of the π-electron systems in complexes of a usual type as well as from that of benzene derivatives. Thus as far as dichroism is concerned, dicyclopentadienyl-iron seems to exhibit very little aromatic property.[7] Such behavior of this compound may be understood qualitatively, assuming that the π electrons would be attracted toward the iron atom to form co-ordinate bonds.

The authors wish to express their sincere thanks to Mr. C. Holstein of Firm C. Holstein for a sample of cyclopentadiene, and to Miss I. Föppl (Dipl. Chem.) for her kind interest and valuable help in this work.

[1] R. Tsuchida and M. Kobayashi, *The Colours and the Structures of Metallic Compounds* (Zoshindo, Osaka, 1944), p. 180.
[2] E. O. Fischer and W. Pfab, Z. Naturforsch., **7b**, 377 (1952); J. D. Dunitz and L. E. Orgel, Nature **171**, 121 (1953); P. F. Eiland and R. Pepinsky, J. Am. Chem. Soc. **74**, 4971 (1952).
[3] The *a* and *b* absorptions denote absorptions with electric vector along and perpendicular to the *a* plane of the crystal.
[4] S. Yamada and R. Tsuchida, Bull. Chem. Soc. (Japan) **26**, 489 (1953).
[5] Such a kind of band was previously named "specific band." See R. Tsuchida and M. Kobayashi, Bull. Chem. Soc. (Japan) **13**, 476 (1938).
[6] Tsuchida, Kobayashi, and Nakamoto, J. Chem. Soc. (Japan) **70**, 12 (1949); Scheibe, Hartwig, and Müller, Z. Elektrochem. **49**, 372 (1943).
[7] E. O. Fischer and R. Jira, Z. Naturforsch. **8b**, 1 (1953).

Infrared Evidence for Collagen Structures

G. B. B. M. Sutherland, K. Nolen Tanner,* and D. L. Wood
The Harrison M. Randall Laboratory of Physics, University of Michigan, Ann Arbor, Michigan
(Received July 2, 1954)

A NEW structure for collagen has recently been proposed by Crick[1] consisting of two polypeptide chains wound helically round a common axis. This structure is put forward for the more ordered "interbands" which Bear[2] has suggested contain predominantly the shorter amino acids. Since this model was based solely on x-ray analysis, it is important to consider to what extent infrared data are consistent with the new model.

We have examined the dichroism of collagen (kangaroo-tail tendon) and of oriented gelatin in the range 5000–600 cm⁻¹. Our results are summarized in the second column of Table I. Absorption bands which are more intense when the electric vector is parallel to the fiber axis (or direction of extension, in the case of gelatin) are said to show parallel dichroism (∥), and those which are more intense when the electric vector is perpendicular to the axis are said to show perpendicular dichroism (⊥). Our results agree qualitatively with those reported by Ambrose and Elliott[3] but are more extensive in that we have investigated a very important band at 650 cm⁻¹.

If the Crick model is correct, then the majority of NH bonds lie in planes perpendicular to the fiber axis. Half of the CO bands also lie in these planes, but the other half of the bonds are not perpendicular to the fiber axis. Thus the NH-stretching frequency near 3300 cm⁻¹ should show perpendicular dichroism. The CO-stretching frequency near 1650 cm⁻¹ may also be expected to show perpendicular dichroism but not so marked as that of the 3300 cm⁻¹ band. Both bands do indeed show perpendicular dichroism but the dichroic ratio appears to be higher for the CO than for the NH frequency in contradiction to the values predicted from the Crick model.

A much more serious contradiction occurs in the dichroism of the out-of-plane NH-deformation frequency[4] at 650 cm⁻¹. This

Table I. Dichroism of infrared bands of collagen.

Band center in cm⁻¹	Observed dichroism	Predicted dichroism on Crick model	Interpretation
650	⊥ (weak)	∥	NH deformation out of plane
1550	∥ (weak)	⊥	NH deformation in plane + C−N stretch
1650	⊥	⊥	CO stretching
3300	⊥	⊥	NH stretching
4590	⊥	?	?
4850	∥	⊥	1550+3300 cm⁻¹

should undoubtedly show strong parallel dichroism. In fact, it shows very weak perpendicular dichroism or none at all. A further contradiction occurs when we consider the 1550 cm⁻¹ band which is now generally accepted to be a nonseparable fundamental involving a deformation motion of the NH band in the plane of the peptide link together with a stretching motion of the peptide C−N link.[5] Since this mode of vibration is entirely in the plane of the eight-membered ring (proposed by Crick) it should show marked perpendicular dichroism. It exhibits weak parallel dichroism. Furthermore, the combination band near 4850 cm⁻¹ (which is generally assumed to be the sum of 1550 cm⁻¹ and 3300 cm⁻¹) should also show perpendicular dichroism since both these vibrations take place in planes perpendicular to the fiber axis. It exhibits a definite parallel dichroism.

It would seem therefore that the Crick model is incompatible with the observed dichroism of the infrared spectrum of collagen or oriented gelatin.

The work reported here was supported in part by a grant from the Rockefeller Foundation which is gratefully acknowledged.

* Present address: Naval Ordnance Laboratory, Corona, California.
[1] F. H. C. Crick, J. Chem. Phys. **22**, 347 (1954).
[2] R. S. Bear, Advances in Protein Chem. **7**, 69–160 (1952).
[3] E. J. Ambrose and A. Elliott, Proc. Roy. Soc. (London) **A206**, 206 (1951).
[4] H. K. Kessler and G. B. B. M. Sutherland, J. Chem. Phys. **21**, 570 (1953).
[5] W. C. Price and R. D. B. Fraser, Proc. Roy. Soc. (London) **B141**, 66 (1953).

Methyl Affinities of Aromatic Compounds

M. Levy and M. Szwarc
College of Forestry, State University of New York, Syracuse 10, New York
(Received June 17, 1954)

IT is well known that radicals or free atoms may add to olefinic compounds thus producing new radicals, such a reaction being exemplified by the equation

$$R + CH_2{:}CH_2 \rightarrow R \cdot CH_2 \cdot CH_2. \quad (1)$$

A considerable volume of evidence,[1–5] accumulated during the last few years, indicates that a similar reaction may take place during an interaction between radicals and an aromatic compound, e.g.,

$$R + C_6H_6 \rightarrow R \cdot C_6H_6. \quad (2)$$

Our recent studies[6] have shown that reaction (2) takes place indeed in the interaction between methyl radicals and benzene. The continuation of these investigations led us to a method by which one can determine quantitatively the relative ability with which an aromatic compound captures methyl radicals. We propose the name "methyl affinity" for this particular property of aromatic compounds, and in this communication we are reporting the values of the relative methyl affinities for a number of aromatic compounds.

Our method of determining the methyl affinities is as follows. Methyl radicals are generated by the thermal decomposition of

diacetyl peroxide.* Such a decomposition, carried out in a diluted solution of the peroxide in isooctane, yields carbon dioxide, methane, and ethane in quantities which correspond to the following stoichiometric relation:[6,7]

$$(CH_4+2C_2H_6)/CO_2\approx 1.$$

The addition of an aromatic compound to the solution, decreases the amount of methane formed, without affecting the amount of carbon dioxide formed in the decomposition. It seems, therefore, that the following two competing reactions occur in the latter systems:

$$CH_3+\text{iso-}C_8H_{18}\rightarrow CH_4+\text{iso-}C_8H_{17} \quad (I)$$

$$CH_3+\text{aromatic}\rightarrow CH_4\cdot\text{aromatic}. \quad (II)$$

Denoting by k_I and k_{II} the bimolecular rate constants of reactions I and II, we conclude that

$$k_{II}/k_I=(\text{the amount of } CH_4 \text{ lost})/(\text{amount of } CH_4 \text{ formed})\,(x_{C_8H_{18}}/x_{\text{aromatic}}),$$

where (amount of CH_4 formed) is the amount of methane actually formed in the reaction, (amount of CH_4 lost) is the difference between the amount of methane formed in the absence of an aromatic compound and in its presence, and $x_{C_8H_{18}}/x_{\text{arom}}$ is the molar ratio of iso-octane and the aromatic compound in the solution. We suggest that the ratio k_{II}/k_I may be considered as a measure of the relative methyl affinity of an aromatic compound.

TABLE I.

T°C	Mole % of aromatic in the solution	CH_4/CO_2	k_{II}/k_I	$k_u\cdot 10^5$ sec^{-1}
65°	25% Benzene	0.740	0.26	0.84
65°	50% Benzene	0.605	0.33	0.905
65°	75% Benzene	0.433	0.29	0.96
85°	25% Benzene	0.697	0.45	12.5
85°	50% Benzene	0.582	0.38	13.0
85°	75% Benzene	0.402	0.33	13.3
65°	5% Biphenyl	0.750	1.4	0.76
65°	10% Biphenyl	0.682	1.6	0.77
85°	5% Biphenyl	0.725	2.0	10.4
85°	10% Biphenyl	0.665	1.9	10.3
85°	20% Biphenyl	0.550	1.8	9.8
65°	5% Naphthalene	0.545	9.1	0.81
65°	10% Naphthalene	0.417	9.7	0.82
65°	20% Naphthalene	0.253	10.3	0.87
65°	20% Naphthalene	0.253	10.3	0.85
85°	5% Naphthalene	0.536	9.4	11.8
85°	10% Naphthalene	0.412	8.5	11.0
85°	20% Naphthalene	0.267	8.0	10.5
65°	1.25% Phenanthrene	0.668	16	0.76
65°	2.5% Phenanthrene	0.515	22	0.84
65°	5.0% Phenanthrene	0.413	18	0.83
85°	1.25% Phenanthrene	0.650	19	10.9
85°	2.5% Phenanthrene	0.595	14	10.3
85°	5.0% Phenanthrene	0.420	17	11.3
85°	5.0% Phenanthrene	0.420	17	11.5
85°	0.25% Pyrene	0.727	41	9.1
85°	0.75% Pyrene	0.575	52	9.9
85°	1.00% Pyrene	0.521	53	9.9
65°	0.5% Anthracene	0.275	385	0.93
85°	0.125% Anthracene	0.525	430	12.7
85°	0.25% Anthracene	0.442	326	11.7
85°	0.50% Anthracene	0.313	310	11.7
85°	0.50% Anthracene	0.336	253	10.4
65°	20% Pyridine	0.615	1.2	1.17
65°	30% Pyridine	0.482	1.5	1.41
85°	10% Pyridine	0.730	0.9	12.0
85°	20% Pyridine	0.615	1.2	12.5
85°	30% Pyridine	0.485	1.5	11.5
65°	10% Quinoline	0.327	13.2	0.99
65°	20% Quinoline	0.195	12.5	1.24
65°	30% Quinoline	0.111	14.4	1.39
85°	10% Quinoline	0.357	11.2	11.8
85°	20% Quinoline	0.211	11.2	11.5
85°	30% Quinoline	0.135	11.5	11.4
65°	5% Benzophenone	0.660	4.2	0.79
85°	5% Benzophenone	0.638	4.9	10.6
85°	10% Benzophenone	0.550	4.1	10.4
85°	20% Benzophenone	0.395	4.1	10.8
85°	10% Diphenyl ether	0.725	0.95	9.2
85°	20% Diphenyl ether	0.640	1.0	8.4
85°	30% Diphenyl ether	0.585	0.8	8.2

TABLE II. The relative methyl affinities; benzene taken as unity.

Compound	Relative methyl affinity
Benzene	1
Diphenyl	5
Naphthalene	22
Phenanthrene	42
Pyrene	125
Anthracene	820
Pyridine	3
Quinoline	29
Benzophenone	11
Diphenyl ether	2.5

The results of our experiments are listed in Table I. The ratio CH_4/CO_2 measures the amount of methane formed in the reaction. The amount of methane "lost" is obtained by subtracting the CH_4/CO_2 ratio listed in Table I from the CH_4/CO_2 ratio obtained in the decomposition of diacetyl peroxide proceeding in a pure isooctane. The latter ratio has been found to be 0.805 for 65°C and 0.802 for 85°C.

It is important to notice that the ratio k_{II}/k_I remain approximately constant when the molar percent of the added aromatic compound is varied by a factor 3–4. This constancy of k_{II}/k_I justifies our interpretation of its meaning. To obtain the scale for the relative methyl affinities of aromatic compounds we adopt the following procedure. We define the relative methyl affinity of benzene as unity, and we obtain the relative methyl affinity of any other aromatic compound by dividing the k_{II}/k_I ratio obtained for such a compound by the k_{II}/k_I ratio obtained for benzene. Since the results obtained at 85°C are more reproducible and experimentally more accurate, we average them to obtain the desired data. The results of such computations are listed in Table II.

It seems that the methyl affinity increases with increasing conjugation in an aromatic system. This point is well illustrated by the following data. Diphenyl ether represents essentially two nonconjugated benzene rings and its methyl affinity is approximately twice as high as that of benzene. On the other hand, diphenyl and benzophenone exemplified compounds in which the two benzene rings are conjugated, and indeed their methyl affinities are well above the double value of the benzene methyl affinity. The heterocyclic compounds resemble closely their isocyclic analogs. The methyl affinity of pyridine is similar to that of benzene, and the methyl affinity of quinoline is close to that of naphthalene.

A full account of this investigation will be published later. We thank the National Science Foundation for the financial support of this study.

* It is still an unsettled problem whether the reaction which involves methyl radicals is caused by "free" methyl radicals, or by acetate radicals which are decarboxylated in the course of the reaction. However, the distinction between these two alternatives is relatively unimportant for our present problem.

[1] M. Magat and R. Bonême, Compt. rend. **232**, 1657 (1951).
[2] W. H. Stockmayer and L. H. Peebles, J. Am. Chem. Soc. **75**, 2278 (1953).
[3] E. C. Kooyman and E. Farenhorst, Trans. Faraday Soc. **49**, 58 (1953).
[4] C. S. Marvel and W. S. Anderson, J. Am. Chem. Soc. **75**, 4600 (1953).
[5] F. R. Mayo, J. Am. Chem. Soc. **75**, 6133 (1953).
[6] Levy, Steinberg, and Szwarc, J. Am. Chem. Soc. **76**, 3439 (1954).
[7] M. Levy and M. Szwarc, J. Am. Chem. Soc. (to be published).

Microwave Spectrum of Formic Acid*

RALPH TRAMBARULO AND PAUL M. MOSER
Department of Physics, University of Delaware, Newark, Delaware

(Received July 2, 1954)

THE rotational spectra of HCOOH and HCOOD have been examined in the regions from 21 to 25 and 41 to 50 Kmc with a Stark-modulation spectrometer. Several transitions which have been identified are listed in Table I. Also given are the theoretical values of the transition frequencies in terms of B and C

TABLE I. Formic acid transitions.

Transition	Frequency (Mc) HCOOH	HCOOD	Theoretical frequency
$0_{0,0}\rightarrow 1_{0,1}$	22 471.14[a]	21 732.72 ±0.10	$B+C$
$1_{1,1}\rightarrow 2_{1,2}$	43 301.58 ±0.20	41 672.98 ±0.20	$B+3C$
$1_{0,1}\rightarrow 2_{0,2}$	44 910 ±20	43 421.36 ±0.20	$2B+2C-(B-C)\times(0.75\delta+0.325\delta^2)$
$1_{1,0}\rightarrow 2_{1,1}$	46 582.90 ±0.20	45 257.40 ±0.20	$3B+C$

[a] Measured by J. D. Rogers and D. Williams, Phys. Rev. **83**, 210 (1951).

TABLE II. Spectroscopic constants and moments of inertia.

	B (Mc)	C (Mc)	I_b ($\times 10^{-40}$ g cm^2)[a]	I_c ($\times 10^{-40}$ g cm^2)[a]
HCOOH	12 055.9 ±0.1	10 415.3 ±0.1	69.5851	80.5460
HCOOD	11 762.4 ±0.1	9 970.3 ±0.1	71.3214	84.1410

[a] Constants used for calculations from Gordy, Smith, and Trambarulo, *Microwave Spectroscopy* (John Wiley and Sons, Inc., New York, 1953), p. 298.

and the asymmetry parameter δ if there is no centrifugal distortion.

Values of the spectroscopic parameters and moments of inertia are given in Table II. The asymmetry parameter δ cannot be obtained accurately since it is involved only in a minor way in the $1_{0,1}\rightarrow 2_{0,2}$ transition. Our values of the moments of inertia for HCOOH are in fair agreement with those calculated from the recent electron diffraction results of Karle and Karle,[1] but about seven percent smaller than those obtained from the infrared spectra of Williams.[2]

If formic acid is planar, I_a is the difference between I_c and I_b and, in units of 10^{-40} g cm, has the value 10.961 for HCOOH and 12.820 for HCOOD. A combination of I_a and I_b for these two isotopic species allows the coordinates of the hydroxyl hydrogen to be located in the system of principal axes of HCOOH. This hydrogen atom is located 1.082 A from the "a" axis and 1.014 A from the "b" axis. (In usual spectroscopic notation the "a" axis is that of least moment of inertia. The CH bond lies nearly along the "b" axis.) It is assumed in this calculation that changes in zero-point vibrations can be neglected in going from HCOOH to HCOOD, in addition to planarity of the molecules.

With the information available at present we suggest a tentative model for which the distances are 1.22 A for C=O, 1.34 A for C–O, 0.97 A for O–H, 1.09 A for C–H, and 2.26 A for O– –O; and angles, 121.7° for H–C=O, 124.8° for O–C=O, and 105.5° for C–O–H. Since it is possible to fit other sets of structural constants to the moments of inertia equally well, errors cannot be assigned. However, as Karle and Karle have pointed out, the O– –O distance is extremely sensitive to I_b, and our value should be accurate to about 0.005 A.

This investigation will be extended to higher frequencies which will allow I_a to be found independent of the planarity condition assumed above and also to other isotopic species so that other atoms can be located with more certainty.

* This research was supported by the United States Air Force, through the Office of Scientific Research of the Air Research and Development Command.

[1] I. L. Karle and J. Karle, J. Chem. Phys. **22**, 43 (1954).
[2] V. Z. Williams, J. Chem. Phys. **15**, 232 (1947).

On the Absorption of Nitrobenzene*

ANNELIESE WENZEL†
Department of Physics, Duke University, Durham, North Carolina
(Received June 2, 1954)

NITROBENZENE shows in solution a strong absorption band at 40 000 cm^{-1}, $\epsilon_{max}=8500$ and a much weaker one at 28 600 cm^{-1}, $\epsilon_{max}=100$.[1,2] In the region of 34 500 cm^{-1}, one of the published nitrobenzene curves[1] shows a very slight inflection, which possibly indicates existence of a third transition.[3] Various interpretations have been given for the nitrobenzene spectrum.[1,3] At present it is assumed[2] that the great intensity of the 40 000 cm^{-1} absorption band is due to resonance, whereby supposedly either the weak transition of benzene at 39 000 cm^{-1} or a nitroband is intensified. In continuation of work on biphenyl[4] a new interpretation is given.

The supposed 34 500-cm^{-1} absorption band and the 40 000-cm^{-1} band of nitrobenzene are interpreted to correspond to the 39 000-cm^{-1} and 48 000-cm^{-1} transitions of benzene (called here transitions I and II, see also reference 5). The weak absorption band at 28 600 cm^{-1} is considered to be related to the NO_2 group. Our interpretation assumes that NO_2 substitution has the same effect on the benzene spectrum as substitution by other groups.

The existence of a hidden transition near 34 500 cm^{-1} in the nitrobenzene spectrum is rather convincingly demonstrated by a comparison of the absorption curve of nitrobenzene with the well-known curves of *m*-nitrotoluene,[2,6] *m*-dinitrobenzene,[3,7,8] and *m*-chloronitrobenzene.[1,9] (See Fig. 1.)

Ortho-compounds give similar results. The intensity of the hidden transition can be estimated to be close to $\epsilon=1300$.

We present evidence now that the hidden transition and the 40 000-cm^{-1} transition of nitrobenzene may correspond to transition I and II respectively of benzene. For this purpose the absorption curve of β nitronaphthalene[10] is used. It is known[11] that introduction of the same substituent in benzene and naphthalene (β substitution) produces approximately the same shift of transition I in both cases and increases its intensity to almost the same extent. Transition II of naphthalene, however, shifts only insignificantly by β substitution, even with substituents which cause in benzene a strong shift; neither does it change its intensity much. If NO_2 substitution has the same effect as other substituents then it should be possible to predict from the data of the nitrobenzene curve the data of the β nitronaphthalene curve. NO_2 substitution produces in benzene, using our interpretation, a shift of transition I

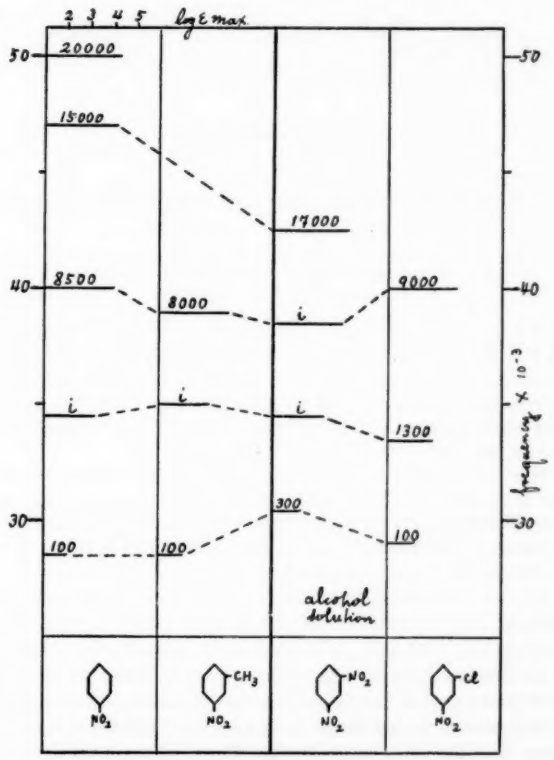

FIG. 1. Spectra of *meta*-derivatives of nitrobenzene. Number above horizontal lines indicates ϵ_{max}, *i* indicates inflection.

of about 4700 cm^{-1}. About the same shift should be found in β nitronaphthalene. Using the data of the naphthalene curve[12] transition I of β nitronaphthalene should occur near 28 600 cm^{-1} with $\epsilon \sim 1300$, and transition II should lie in the vicinity of 36 400 cm^{-1} with $\epsilon \sim 5000$. Actually, an examination of the β nitronaphthalene curve in iso-octane by this author, shows good agreement with these predictions:

Absorption Band A	$\nu_{max} = 29\,200$ cm^{-1}	$\epsilon_{max} = 2500$
Absorption Band B	$\nu_{max}{}^a = 34\,300$ cm^{-1}	$\epsilon_{max}{}^a = 8200$
	$\nu_{max}{}^b = 33\,300$ cm^{-1}	$\epsilon_{max}{}^b = 8000$
	$\nu_{max}{}^c = 33\,100$ cm^{-1}	$\epsilon_{max}{}^c = 8270$.

The absorption curve of *m*-nitro-nitrosobenzene[13] has two weak absorption bands ($\epsilon_{max} \sim 60$), one at 3900 A and one at 7500 A. The first is about where nitrobenzene has a transition of comparable intensity. A similar correspondence exists for the 7500 A band for nitrosobenzene and *m*-nitro-nitrosobenzene. These facts suggest that the weak band of nitrobenzene at 28 600 cm^{-1} (3900 A) is related to the NO_2 group. The weak nitro band is found in many aromatic nitro compounds. β Nitronaphthalene does not show it, and we think that in this case it is hidden. Contradictory statements[6,14,15] as to whether the nitro bands are red shift or blue shift bands should be clarified.

The author wishes to thank Professor Hertha Sponer for her interest and advice, the du Pont Company for the sample of β nitronaphthalene, and Professor S. Mizushima and Professor Y. Nagai, and the Chemical Society of Japan for library facilities.

* This paper presents a continuation of research sponsored by the Office of Naval Research.
† Present address: 31 Shoto-Cho, Shibuya-Ku, Tokyo, Japan.
[1] K. L. Wolf and W. Herold, Z. physik. Chem. **B13**, 201 (1931).
[2] W. G. Brown and H. Reagan, J. Am. Chem. Soc. **69**, 1032 (1947).
[3] G. Kortüm, Z. physik. Chem. **B42**, 39 (1939).
[4] A. Wentzel, J. Chem. Phys. **21**, 403 (1953).
[5] J. R. Platt, J. Chem. Phys. **19**, 101 (1951).
[6] L. Dede and A. Rosenberg, Ber. deut. chem. Ges. **67**, 147 (1934).
[7] P. Fielding and R. W. Le Fèvre, J. Chem. Soc. 2812 (1950).
[8] K. Nakamoto, J. Am. Chem. Soc. **74**, 392 (1952).
[9] G. Förster and J. Wagner, Z. physik. Chem. **B35**, 343 (1937).
[10] H. H. Hodgson and D. E. Hathway, Trans. Faraday Soc. **41**, 115 (1945).
[11] H. G. de Laszlo, Proc. Roy. Soc. (London) **A111**, 355 (1926).
[12] R. A. Friedel and M. Orchin, *Ultraviolet Spectra of Aromatic Compounds* (John Wiley and Sons, Inc., New York), Spectrogram No. 195.
[13] K. Nakamoto, Bull. Chem. Soc. Japan **25**, 255 (1952).
[14] G. Scheibe, Ber. deut. chem. Ges. **59**, 2617 (1926).
[15] H. McConnell, J. Chem. Phys. **20**, 700 (1952).

The Raman Frequency of Liquid Bromine*

H. Stammreich and Roberto Forneris
Department of Physics, Faculdade de Filosofia, Ciências e Letras, University of São Paulo, São Paulo, Brazil
(Received June 23, 1954)

In a previous paper[1] one of the authors has reported some results on the Raman spectrum of gaseous bromine obtained by excitation with helium radiation 5875.6 A. The Raman frequency corresponding to the first vibrational quantum of the Br_2 molecule was found to be $\Delta G_{\frac{1}{2}} = 316.8 \pm 1$ cm^{-1}; Raman shifts corresponding to the first and second overtones were observed.

Since then the luminosity of our Raman excitation arrangement has been improved; and with the aid of the photographic plates with higher sensitivity in the extreme red and near infrared region of the spectrum that are now available, it was possible to attempt to obtain the Raman spectrum of liquid bromine.

Liquid bromine is practically opaque for wavelengths under 7100 A. The transmission of 1 cm layer at 7700 A is about 80 percent; above 8100 A the bromine becomes completely transparent.

As exciting light source we employed a discharge tube filled with pure argon of 3 mm pressure, part of which consisted of 4 mm tubing wound in helicoidal form around the Raman tube. This lamp is of the cold cathode type. Power is supplied by a high-reactance transformer, with an operating voltage of about 1200 volts and with a current of 400 ma. Between the helicoidal part of the discharge tube and the Raman tube, space is provided for refrigeration and for inserting suitable filters that transmit red and infrared radiation.

With an optical arrangement described briefly in a previous paper,[2] and recording the spectra on hypersensitized Kodak IN plates, we obtained in seven minutes the Raman line of Br_2 excited by the 8115.3 A argon line, which is the strongest line in the region of the argon spectrum that interests us here. Exposure times of the order of one hour produce the Raman shifts corresponding to seven exciting argon lines and also the anti-Stokes shifts of the stronger ones.

In view of these relatively short times of exposure we attempted to record the Raman spectrum of liquid bromine with a camera of greater focal length ($f = 84$ cm) in order to measure the Raman shifts with good precision. With this camera we have at 8000 A a reciprocal dispersion of about 91 cm^{-1}/mm; and since the recorded Raman lines of Br_2 are sharp and well defined, the error in our wavelength measurements is not greater than ± 0.4 A.

It seems that this is the first Raman spectrum obtained in the infrared. We therefore think it interesting to reproduce in Fig. 1

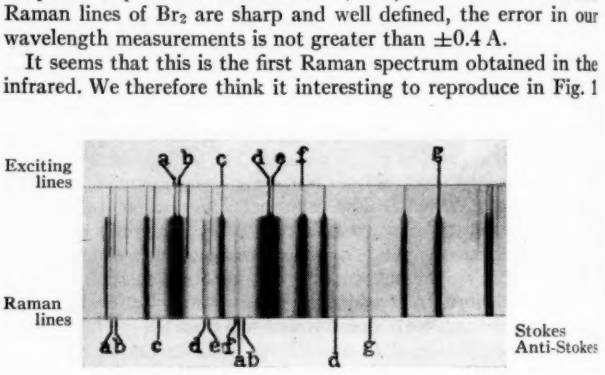

FIG. 1.

Exciting argon lines	A
a	8424.7
b	8408.2
c	8264.5
d	8115.3
e	8103.7
f	8014.8
g	7635.1

Exciting lines and the corresponding Raman lines are designed by the same letters.

one of our spectra obtained by an exposure of 34 hours. Unfortunately some details are lost in the reproduction.

The upper spectrum is an argon-neon spectrum used for the determination of wavelength of the Raman lines of Br_2. The Raman shift was found to be

$$\Delta\nu = 306.1 \pm 0.6 \text{ cm}^{-1}.$$

This value is remarkably low compared with the Raman shift 316.8 cm^{-1} observed by one of us[1] on gaseous bromine and with the value of the fundamental vibrational quantum to be expected from observations on band spectra of Br_2. The Raman frequencies of molecules without permanent electric moment generally show only a very small dependence on the state since intermolecular interactions are weak. In spite of the fact that some work has been done on association phenomena in liquid bromine, little is known on this question.

No overtones were observed in the Raman spectrum of liquid bromine and we believe that the harmonics observed in the previously reported spectrum of gaseous bromine[1] are due to the fact that this spectrum excited by He 5875.6 A represents a transition case from Raman spectrum to a resonance spectrum of the type related by Plumley,[3] who excited bromine vapor at low pressure (0.2 mm) by Hg 5461 A.

* This work has been supported in part by the "Conselho Nacional de Pesquisas, Rio de Janeiro"; the authors are much indebted for the facilities created with the aid of the C. N. Pq.
[1] H. Stammreich, Phys. Rev. **78**, 79 (1950).
[2] H. Stammreich and R. Forneris, J. Chem. Phys. **21**, 944 (1953).
[3] Harold Plumley, Phys. Rev. **43**, 495 (1933).

Errata: Radial Distribution Functions and the Equation of State of Monatomic Fluids

[J. Chem. Phys. 21, 1268 (1953)]

ROBERT W. ZWANZIG, JOHN G. KIRKWOOD, KENNETH F. STRIPP, AND IRWIN OPPENHEIM
Sterling Chemistry Laboratory, Yale University, New Haven, Connecticut

AN error appears in Table V of this article. The experimental value of the isothermal compressibility κ of liquid argon at its normal boiling point is 0.23×10^{-3} (atmos)$^{-1}$ instead of the incorrect value 4.65×10^{-3} (atmos)$^{-1}$ which was presented in this table. The correct compressibility was obtained by an extrapolation to 90°K of the results of van Itterbeek and Verhaegen.[1] The calculated scale factor, $c=1.76$, is also in error. The discrepancy between the calculated compressibility 7.67×10^{-3} (atmos)$^{-1}$ and the experimental value is too great to be adjusted by selecting a value of c close to unity.

The compressibility at liquid densities depends sensitively on the integral $\int_0^\infty x^2[g(x)-1]dx$. The integrand oscillates between positive and negative values out to $x=10$ and is numerically the small difference between large areas alternately above and below the x axis. Therefore, in order to obtain the compressibility with any degree of precision from this integral, the radial distribution function $g(x)$ must be known with greater accuracy than present theoretical or experimental determinations allow.

[1] A. van Itterbeek and L. Verhaegen, Proc. Phys. Soc. (London) **B62**, 800 (1949).

Nitrogen Electronegativity Correction in Free Electron Network Theory

SADHAN BASU
Indian Association for the Cultivation of Science, Calcutta 32, India

(Received July 7, 1954)

IN a previous note[1] it was shown that application of free electron network theory gives close agreement between the calculated and observed wavelengths of absorption in the case of cyanine dyes and diphenylpolyenes. There it was noted that agreement in the latter case was better than that in the former. There may be two reasons for this. Firstly, we assumed that bond length was constant (about 1.41 A) throughout the molecule, which is not correct. This assumption was made in the case of diphenylpolyenes too, but it made no serious error in the calculation. Secondly, the electrons were assumed to move in a uniform potential field in all the segments. Although this assumption is approximately true for a carbon-carbon chain, it cannot be true for a carbon chain containing a nitrogen in conjugation. Since nitrogen is more electronegative than carbon it will introduce a potential well in the uniform potential field of carbon. If we assume that the breadth of the well is 2 bond lengths and the depth is V, then the free electron wave function over the nitrogen atom can be expressed as

$$a'\cos\omega' x+b'\sin\omega' x$$

where

$$\omega'^2=\frac{2ml^2(E+V)}{\hbar^2} \qquad (1)$$

while in the other part of the segment containing only carbon atoms, wave function takes the form

$$a\cos\omega x+b\sin\omega x$$

where

$$\omega^2=\frac{2ml^2E}{\hbar^2}. \qquad (2)$$

From (1) and (2) we get the relation

$$\omega'^2=\omega^2+k^2, \quad k^2=\frac{2ml^2V}{\hbar^2}.$$

From his study on absorption spectra of pyridine, Nakajima[2] found that the value of k^2 must lie between 1 and 2 for a good agreement with the experimental value. We apply free electron network treatment with these modifications to a diphenyl polymethene dye I (Michler's hydroblue) and an Indemine dye II (Bindschedler's green) in which II is obtained from I by replacing the central =CH-group by =N-group

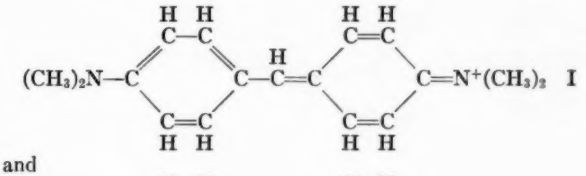

I

and

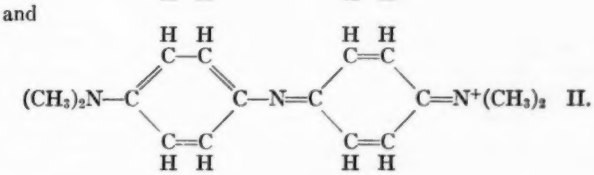

II.

It is evident that unless we apply electronegativity correction for nitrogen, the two dyes should give absorption in the same wavelength region; actually they differ by more than 1000 A. If we apply the modifications stated above we get the following relationship for the allowed energy levels of the two dyes.

For I
$$\cos2\omega=-3\cos6\omega$$
$$\cos3\omega=0$$
$$\sin3\omega=0.$$

For II
$$(\omega'-2\omega)\cos(4\omega-2\omega')=(\omega'+2\omega)\cos(4\omega+2\omega')$$
$$\cos3\omega=0$$
$$\sin3\omega=0.$$

Now if we put $k^2=1.5$ as a first approximation, we get the calculated values for absorption spectra as shown:

	λ(A)	
Dye	Experimental	Calculated
I	6030	5642
II	7250	7368.

It is evident that by applying the electronegativity correction we get better agreement with experimental results although no correction has been applied for terminal nitrogen atom. For the dye I the calculated value is less than the experimental one, while for dye II it is higher. This shows that a value of 1.5 for k^2 is not exact although close to it.

One difficulty in these calculations was that we had to solve the equations (3) and (4) graphically. An error of 1 to 2 percent in evaluating ω introduces 10 to 20 percent error in the calculated energy values. So a better and improved method for solving the secular equations is necessary.

[1] S. Basu, J. Chem. Phys. **22**, 1270 (1954).
[2] Nakajima, Science Repts. Research Insts. Tôhoku Univ. **5**, 98 (1953).

A Quantum-Mechanical Treatment of the Symmetrical Hydrogen Bridge*

A. N. BAKER, JR.†
University of California, Los Angeles, California

(Received July 15, 1954)

THIS is a preliminary report of a theoretical investigation of the variation with oxygen-oxygen distance of the fundamental optical vibration frequency of the hydrogen atom of an O—H···O hydrogen bridge. Experimental investigations of this variation have already been reported.[1,2]

For motions of the hydrogen atom along the join of the two oxygen atoms, we follow Huggins[3] by assuming that the potential

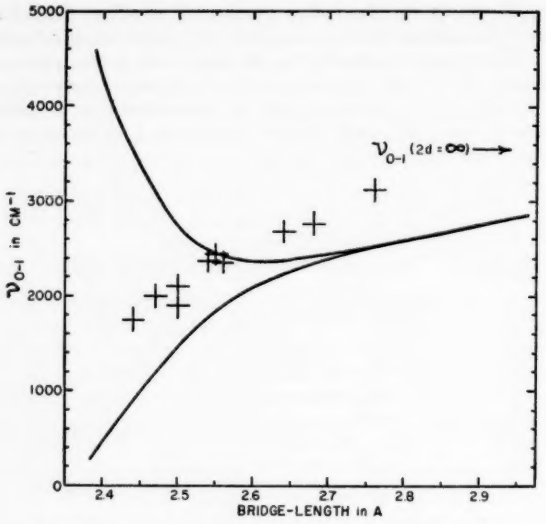

FIG. 1. Fundamental vibration frequencies of a hydrogen bridge.

the hydrogen atom moves in is the sum of two appropriate Morse potentials. By assuming no change in the oxygen-oxygen distance (the bridge length) during a vibration, we can treat the bridge length as a parameter in the calculations. Using the one-dimensional wave equation, we wish to find the energy levels and wave functions corresponding to the assumed potential function. Rather than attempt to obtain an exact solution by straightforward methods,[4] we use an approximation method.

Since the potential function is the sum of two O−H Morse potential functions, we use as zero-order wave functions the normalized sum or difference of the wave functions appropriate to the O−H potential functions.[5] With these, we find that the first-order energy levels are given by

$$H_{ii}=E_i+(1\pm d_i)^{-1}(P_{ii}\pm Q_{ii}),$$

where the plus signs refer to the symmetrical states and the minus signs to the antisymmetrical states. E_i is the ith energy level of a single Morse well; $P_{ii}=\int_{-\infty}^{\infty}\phi_{Li}V_R\phi_{Li}dx$; $Q_{ii}=\int_{-\infty}^{\infty}\phi_{Li}V_L\phi_{Ri}dx$; and $d_i=\int_{-\infty}^{\infty}\phi_{Li}\phi_{Ri}dx$. ϕ_{Li} and V_L are the wave functions and potential associated with the left-hand Morse well and analogously for ϕ_{Ri} and V_R. The P_{ii} are standard gamma-function integrals. The Q_{ii} and d_i are not standard integrals but can be evaluated using the method of saddle-point integration.

From band-spectra measurements of the O−H molecule,[6] we evaluate the parameters of the wave and potential functions. We can then find the values of the energy levels as a function of the bridge length. Since each unperturbed energy level splits into a symmetrical and antisymmetrical level, there are four possible transitions from $i=0$ to $i=1$, two Raman active transitions, and two infrared active transitions. The theoretical frequencies of the infrared transitions are plotted as a function of bridge length in Fig. 1. For comparison the experimental frequencies given by Lord and Merrifield[2] are indicated by the crosses in Fig. 1.

Comparing the experimental frequencies to the theoretical frequencies reveals two facts. First, the calculated results for transitions from $(H_{00})_a$ to $(H_{11})_s$ show the same general trend as the experimental results. The observed frequency *shifts* resulting from the formation of a hydrogen bridge are about 25 percent smaller than the calculated shifts. Second, there seem to be no experimental data for transitions from $(H_{00})_s$ to $(H_{11})_a$.

Considering the first point, if these results were not first-order but complete in themselves, one could conclude that the actual potential function of a hydrogen bridge is different from the assumed potential function. If the actual potential function of the O−H molecule has less curvature than the Morse potential in the region $r>r_0$, then the discrepancy can be explained without dropping the basic assumption concerning the addition of two O−H potentials.

Attention should be paid to the second point in the interpretation of experimental spectra. The present theory predicts that the fundamental vibration spectrum of a hydrogen bridge should consist of a pair of bands of comparable intensity whose separation increases rapidly with decreasing bridge length.

A more complete discussion of the theory including treatments of the transverse vibration frequencies, of the unusual widths of the absorption bands, and of the isotope expansion of hydrogen bridges will be given in a later issue of this journal.

* This paper is abstracted from a portion of a thesis submitted in partial satisfaction of the requirements for the Ph.D. degree in physics at the University of California at Los Angeles.

† Present address: Bell Telephone Laboratories, Inc., Murray Hill, New Jersey.

[1] R. E. Rundle and M. Parasol, J. Chem. Phys. **20**, 1487 (1952).
[2] R. C. Lord and R. E. Merrifield, J. Chem. Phys. **21**, 166 (1953).
[3] M. L. Huggins, J. Phys. Chem. **40**, 723 (1936).
[4] C. E. Nordman and W. N. Lipscomb, J. Chem. Phys. **21**, 2077 (1953).
[5] J. C. Slater, *Quantum Theory of Matter* (McGraw-Hill Book Company, Inc., New York, 1951), p. 107.
[6] G. Herzberg, *Molecular Spectra I* (D. Van Nostrand Company, Inc., New York, 1950), p. 560.

Errata: The Intrinsic Viscosities and Diffusion Constants of Flexible Macromolecules in Solution

[J. Chem. Phys. **16**, 565 (1948)]

JOHN G. KIRKWOOD, *Sterling Chemistry Laboratory, Yale University, New Haven, Connecticut,*

AND

JACOB RISEMAN, *International Resistance Company, Philadelphia, Pennsylvania*

IN this article, the effect of the hydrodynamic interaction of the segments of a polymer chain on the intrinsic viscosity was determined by a function $\varphi(x)$, satisfying the following integral equation:

$$\varphi(x)=f(x)-\lambda\int_{-1}^{+1}\frac{\varphi(t)}{(|x-t|)^{\frac{1}{2}}}dt$$

with

$$\int_{-1}^{+1}f(x)dx=0, \tag{A1}$$

where λ is proportional to the square root of the degree of polymerization. By a justified inversion of order of integration, the last member of this equation was expressed in the form

$$\int_{-1}^{+1}\frac{\varphi(t)}{(|x-t|)^{\frac{1}{2}}}dt=\frac{1}{\pi^{\frac{1}{2}}}\int_{-\infty}^{+\infty}g(x,\beta)d\beta, \tag{A5}$$

where $g(x,\beta)$ satisfies the following differential equation:

$$\frac{\partial^2 g}{\partial x^2}-\beta^4 g=-2\beta^2\varphi. \tag{A6}$$

We wish to call attention to the fact that the solution of (A6)

$$g(x,\beta)=2\sum_{k=-\infty}^{+\infty}\frac{\beta^2\varphi_k}{\pi^2k^2+\beta^4}e^{i\pi kx}$$

presented in (A8) and (A9) is incomplete. To it must be added a linear combination of the solutions $e^{-\beta^2 x}$ and $e^{\beta^2 x}$ of the homogeneous equation in order that (A5) be actually satisfied. When this is done, the analytical solution of (A1) proves to be impracticable.

A numerical solution of (A1) will therefore be undertaken in the near future for the purpose of correcting the function $F(x)$ of Eq. (22) and the constant $\lim_{x\to\infty}\times F(x)$ of Eq. (23). The only important change in the results presented in the paper, which is anticipated, is a correction in the numerical value of this constant. It is hoped that this correction will produce improved agreement between the values of the end-to-end distance of a flexible coil calculated from the intrinsic viscosity and from turbidity and sedimentation constant. It should be pointed out that the results

presented for the translational diffusion constant and semimentation constant of flexible coils remain exact and require no correction.

A similar incompleteness in the solution of the corresponding integral equation for rod-like macromolecules[1] exists and requires correction by numerical integration. However, the analytical solution of the equation, constructed for rods in this paper, becomes asymptotically exact for large degrees of polymerization or large ratios of length to radius. Therefore, the asymptotic results for long rods remain correct here as well as in the paper of Kirkwood and Auer[2] on the viscoelastic properties of rod-like macromolecules.

The authors are indebted to Dr. Bruno Zimm for calling their attention to the necessity for the corrections which are discussed here.

[1] Riseman and Kirkwood, J. Chem. Phys. **18**, 512 (1950).
[2] Kirkwood and Auer, J. Chem. Phys. **19**, 281 (1951).

A Relation Between the Activation Energy for Viscous Flow and the Lennard-Jones (12, 6) Potential Parameter, ϵ/k

C. J. G. RAW
Department of Chemistry and Chemical Technology, University of Natal, Pietermaritzburg, South Africa
(Received June 28, 1954)

THE temperature dependence of the viscosity (η) of a liquid is best represented by the energy of activation for viscous flow, ΔE_{vis}, which is defined as[1]

$$\Delta E_{\text{vis}} = R\frac{d\ln\eta}{d(1/T)},$$

where T is the absolute temperature and R is the molar gas constant. (ΔE_{vis} is obtained experimentally from determinations of η at different temperatures, T.)

Ewell and Eyring[2] have shown that

$$\Delta E_{\text{vis}} = \frac{\Delta E_{\text{vap}}}{n},$$

where ΔE_{vap} is the molar energy of vaporization, and n is a constant. For liquids whose molecules have spherically, or approximately spherically, symmetrical force fields, $n=3$.

Also[1]

$$\Delta E_{\text{vap}} = \Delta H_e - RT_b,$$

where ΔH_e is the latent heat of evaporation at the boiling point, T_b.

By using the Lennard-Jones (12–6) model for the intermolecular potential, it can be shown[3,4] that, for nonpolar liquids with sperically symmetrical molecules,

$$\Delta H_e \approx 14.9\epsilon/k \text{ cal mole}^{-1}$$

and

$$T_b \approx \frac{\epsilon/k}{1.39}$$

where ϵ is the maximum energy of attraction between two molecules and k is Boltzmann's constant.

Thus,

$$\Delta E_{\text{vis}} = \frac{1}{n}(\Delta H_e - RT_b)$$
$$\approx \tfrac{1}{3}\left(14.9 - \frac{R}{1.39}\right)\epsilon/k$$
$$\approx 4.5\epsilon/k \text{ cal mole}^{-1}.$$

This applies, of course, only to normal liquids which have nonpolar, symmetrical molecules and whose intermolecular force field is well represented by the Lennard-Jones model.

In Table I, experimental values[2] of ΔE_{vis} are compared with values calculated from the above relation using tabulated values[5] of ϵ/k (obtained from (i) gas viscosity data, and (ii) second virial coefficients). ΔE_{vis} is given in cal mole^{-1} and ϵ/k in degrees absolute.

TABLE I. Comparison of calculated and experimental values of ΔE_{vis}.

Liquid:	A	N_2	O_2	CO	CH_4
(i) ϵ/k (viscosity)	124	91.46	113.2	110.3	136.5
(ii) ϵ/k (virial)	119.5	95.9	117.5	95.33	142.7
ΔE_{vis} (using (i))	558	412	509	496	615
ΔE_{vis} (using (ii))	538	431	510	429	643
ΔE_{vis} (experimental)	516	449	398	466	719

The discrepancy in the case of oxygen is large, and may be attributed[2] to its paramagnetic properties which make $n=3.5$ rather than 3.0 in the Ewell-Eyring expression. In general, more satisfactory results are obtained by using values of the intermolecular force constant ϵ/k determined from second virial coefficients of gases. The agreement between experimental and calculated values of ΔE_{vis} is satisfactory if the approximations made in obtaining the relation given above are taken into account.

Since ϵ/k is derivable from the temperature dependence of the gas viscosity, it seems that there is some connection between the temperature dependence of the viscosity of the vapor and that of the liquid, notwithstanding the fact that viscous resistance has not the same origin in gases and liquids.

[1] Glasstone, Laidler, and Eyring, *The Theory of Rate Processes* (McGraw-Hill Book Company, Inc., New York, 1941).
[2] Ewell and Eyring, J. Chem. Phys. **5**, 726 (1937).
[3] Fowler and Guggenheim, *Statistical Thermodynamics*, (Cambridge University Press, Cambridge, 1939), pp. 345–350.
[4] Lennard-Jones and Devonshire, Proc. Roy. Soc. (London) **A165**, 1 (1938); **A163**, 53 (1937).
[5] Hirschfelder, Bird, and Spotz, Chem. Revs. **44**, 205 (1949).

Stabilization of Free Radicals from the Decomposition of Hydrazoic Acid*

I. L. MADOR† AND M. C. WILLIAMS
Applied Physics Laboratory, The Johns Hopkins University, Silver Spring, Maryland
(Received March 31, 1954)

IT has been reported by Rice and Freamo[1] that a blue solid may be frozen out at 77°K from the vapor phase decomposition of HN_3. The color was attributed to the NH radical. On warming to 148°K it instantaneously changed to a white solid which at room temperature analyzed for $(NH)n$ with a mass spectrum corresponding to NH_4N_3.

In the present work HN_3 vapor was decomposed by an electric discharge and the products frozen out in different experiments at 4° and at 77°K in an optical cell.[2] The infrared spectrum of the blue solid showed that it contained a substantial portion of undecomposed HN_3. Deposition of HN_3 at 77°K without passage through a discharge gave a clear colorless glass which on warming to 148°K became polycrystalline. Thus, the disappearance of the blue color in this system accompanies the crystallization of the HN_3. After passage through a discharge the low-temperature infrared spectrum of the blue material showed the presence of NH_4N_3, identification being made by comparison with a known sample of NH_4N_3. The intensities of the NH_4N_3 bands were the same on warming above the 148°K transition temperature.

Bands were also observed at 3500 A and 6500 A, the latter being responsible for the blue color. The NH radical in the vapor is known to have a sharp Q branch at 3360 A; the NH_2 radical has a broad band system whose center is at approximately 6300 A.[3] It appears likely that the bands resulting from the HN_3 decomposition are due to these two radicals.

The absorption in the infrared regions of NH stretching and bending vibrations was very intense, and no bands other than those assignable to NH_4N_3 or HN_3 were observed. No absorption was observed corresponding to the N−N stretching mode of N_2H_4. No fine structure could be detected in the 3500 A and

6500 A bands, and after the 148°K transformation both bands disappeared.

In other experiments hydrazoic acid was photolyzed at 2537 A during and after deposition at 4°K and at 77°K. The products were the same as those resulting from the vapor phase decomposition. The quantum yields for the formation of NH_4N_3 indicate it is produced by a chain reaction. The yields of NH_4N_3 were independent of the temperature of irradiation. In different experiments the relative intensities of the 3500 A and 6500 A bands were in different ratios, confirming their assignment as due to different species. The failure to observe any increase in the NH_4N_3 band intensities or any other products above the 148°K transition indicates that the concentrations of the NH and NH_2 radicals stabilized at the lower temperatures are very small.

* This work was supported by the Bureau of Ordnance, Department of the Navy, under Contract NOrd-7386.
† Present address, Research Division, National Distillers Products Corporation, Cincinnati, Ohio.
[1] F. O. Rice and M. Freamo, J. Am. Chem. Soc. **73**, 5529 (1951); **75**, 548 (1953).
[2] W. H. Duerig and I. L. Mador, Rev. Sci. Instr. **23**, 421 (1952).
[3] See G. Herzberg, *Spectra of Diatomic Molecules* (New York, 1950).

Separation and Concentration of Proteins in a *p*H Field Combined with an Electric Field*

ALEXANDER KOLIN
University of Chicago, Chicago, Illinois
(Received July 13, 1954)

THE principle of the method presented below is based on the fact that ions of proteins, as well as of other ampholytes, are positively charged at *p*H values below the isoelectric point and negatively at higher *p*H values. By creating and maintaining a field of varying hydrogen ion concentration in a solution traversed by an electric current, it is possible to make ampholytes converge from both sides toward points at which the *p*H is equal to the isoelectric *p*H of the ampholyte. Such concentration of the ampholyte at its isoelectric point occurs when the current flows in the direction of increasing *p*H in the *p*H field, whereas a diminution in the ampholyte concentration at a point corresponding to its isoelectric *p*H is produced by a current flowing in the direction of diminishing *p*H values. This process may offer a simple and rapid means of identifying and separating different ampholytes, such as proteins, polypeptides, and amino acids in complex mixtures.

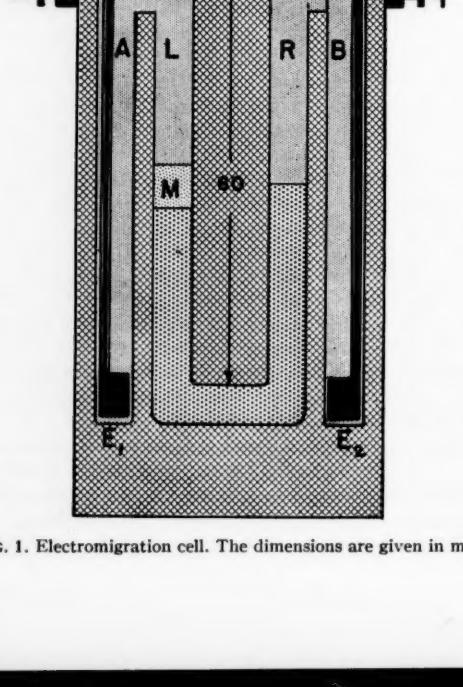

FIG. 1. Electromigration cell. The dimensions are given in mm.

A B C D E
FIG. 2. A, B, C: concentration zone (left arm) and dilution zone (right arm) in hemoglobin solution. D: dilute (left arm) and concentrated (right arm) solutions of hemoglobin in buffer of varying *p*H before passage of current. E: concentration zone (left arm) and dilution zone (right arm) in the hemoglobin solution of D after passage of current.

The effects of concentration, dilution, and separation can be demonstrated rather simply with the cell shown in Fig. 1. A U-shaped channel of square cross section with arms *L* and *R* is milled in a Lucite plate. Next to *L* and *R* are milled the channels *A* and *B* which communicate with *L* and *R*, respectively. They contain the Pt electrodes E_1 and E_2. The U-tube section is filled to about half its height with an acid buffer of *p*H 2.6 which is nearly saturated with sucrose to make it heavier than all the other solutions used. The channels *A* and *B* are filled with a basic buffer of *p*H 9.6,[1] which also fills the upper halves of the U-tube arms *L* and *R*. In the right arm *R* the current flows from the basic buffer toward the acid buffer, whereas in the arm *L* it flows from the acid buffer toward the basic buffer.

Figure 2 illustrates concentration and dilution effects observable with the arrangement of Fig. 1. Hemoglobin (about 1 percent concentration) was dissolved in water and enough glycerol was added to make the density of the solution intermediate between the densities of the acid and basic buffers. This solution was then injected with a pipette between the two buffers to form an intermediate layer *M* (see Fig. 1) in both arms *L* and *R* (Fig. 2A). Figure 2B shows the concentration of hemoglobin in a narrow linear zone in the left arm and the simultaneous dilution in the right arm after a current of 9 ma has been passed for 25 sec. Figure 2C represents the aspect after passage of current for 40 sec. In this fashion, highly concentrated protein samples can be prepared from very dilute solutions.

The concentration of the protein can also be demonstrated by dissolving hemoglobin in the acid and the basic buffers which at first form a sharp boundary as in the arm *R* in Fig. 1. By stirring the boundary, a shallow *p*H gradient is created.[2] Figure 2D shows the arms *L* and *R* after the stirring of the boundary before passing the current and Fig. 2E after a current of 10 ma has been passed for 6 min.

Figure 3 shows the separation of hemoglobin from cytochrome *C* using the same procedure as in connection with Fig. 2A. Figure 3A shows the mixture in the *L* arm before passing the current and Fig. 3B after a current of 8 ma has been passed for 2 min. The lower line corresponds to a brown layer of concentrated hemoglobin and the upper line to an orange layer of cytochrome *C*. The voltage applied to the cell in all of the experiments described above was 220 volts.

Effects described above have also been observed using filter-paper electrophoresis techniques. It is to be expected that the

A B

FIG. 3. Separation of hemoglobin from cytochrome *C*. A: solution before passage of current. B: separated fractions after passage of current. Bottom line: hemoglobin; top line: cytochrome *C*.

effects could also be observed with coarse suspensions of protein-coated material as well as with micro-organisms such as viruses.

The present process is distinct from the conventional electrophoretic separation in that the latter sorts ions according to differences in their mobilities, whereas the former separates them according to their isoelectric *p*H values. It remains to be seen whether or not a general method can be developed for obtaining an "isoelectric spectrum" of a protein mixture whose components could be identified by their isoelectric *p*H rather than electrophoretic mobility.

The theoretical and experimental details of this process will be considered in a later publication.

The author wishes to thank Dr. N. Nicolaides for valuable chemical advice.

* This work has been supported by the Office of Naval Research and by a grant from the Abbott Memorial Fund of the University of Chicago.

[1] We used dilute Michaelis buffers of the following composition: the basic buffer contained 4.85 g of sodium acetate and 7.35 g of barbital sodium per liter of solution. The acid buffer was obtained from the basic buffer by adding to 100 cc of it 75 cc of N/10 HCl and 285 cc of water.

[2] It is noteworthy that with some proteins local laminar concentrations or precipitations are observed before the current is passed. It is to be expected that concentration variations should occur in a nonuniform *p*H field for substances whose solubility and intermolecular forces depend on *p*H. (Note the slight darkening near the center of the left arm in Fig. 2D.)

Dichroism of the Crystal of Diformylhydrazine

SHOICHIRO YAMADA AND RYUTARO TSUCHIDA
Department of Chemistry, Faculty of Science, Osaka University, Nakanoshima, Osaka, Japan

(Received June 28, 1954)

CRYSTAL analysis by Tomiie *et al.*[1] revealed that the crystal of diformylhydrazine, OHC·NH·NH·CHO, consists of the planar molecules which are connected together through intermolecular hydrogen bonds to form layers of giant molecules. The fact that the molecules in the crystal are planar whereas nitrogen usually assumes sp^3-tetrahedral bonds suggests that the linkages around the nitrogen atom in the molecules may involve fairly large π-bond character. The carbon atoms in this molecule also have π electrons available for π bonding, and, therefore, contribution of the structure with conjugated π bonds may be supposed to occur, anisotropy of light absorption, similar to those of π electron systems such as butadiene or benzene rings,[2] being expected.

In order to investigate the above points, we have quantitatively determined absorption spectra with crystals of diformylhydrazine by Tsuchida-Kobayashi's microscopic method[3] in the visible and ultraviolet. The crystals, supplied by Mr. Tomiie, were recrystallized from water. Monoclinic, platy crystals thus obtained had well-developed (110) face, terminated with the $(20\bar{1})$. The measurement was made at room temperature on the (110) with polarized light having its electric vector along the perpendicular to the $(20\bar{1})$. Inspection of the absorption curves (Fig. 1) indicates that

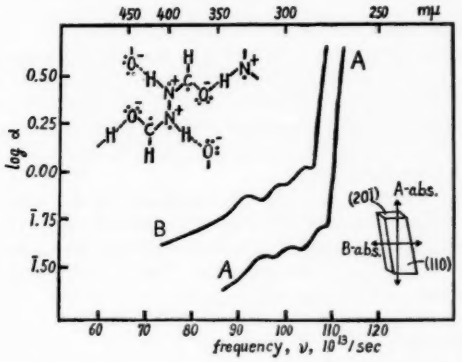

FIG. 1. Absorption spectra of diformylhydrazine in crystalline state.

the structure of the spectrum of diformylhydrazine in crystalline state appears to bear resemblance to that of benzene. The crystal shows two absorption bands, a very weak one at about $90\text{–}105\times10^{13}$/sec, and the other of large intensity at the shorter wavelength. The former, which is not observed with the aqueous solution,[4] may be due to a relatively large contribution of conjugated π bond, and is supposed to be originate principally from transition of π electrons, corresponding to the "π band" at 2600 A of benzene. The latter may tentatively be assumed to correspond to the band at 2100 A of benzene.

For the band at about 100×10^{13}/sec, the *B* absorption[5] is hyperchromic and slightly bathochromic to the *A* absorption:[5] $\alpha_B/\alpha_A{}^6=2$. According to the x-ray analysis,[1] the planes of the molecules are inclined at about 19° to the $(20\bar{1})$. Taking this into account, the following value may approximately be estimated: $\alpha_{\parallel}/\alpha_{\perp}{}^6=$about 2.5. Thus it is concluded that, for the π band of diformylhydrazine in crystalline state, *∥ absorption[6] is much hyperchromic and slightly bathochromic to ⊥ absorption.*[6] This relation is quite similar to that obtained for π-electron systems,[2] and may be explained qualitatively in a similar way.

It is to be noted that the resemblance in the absorption spectrum of diformylhydrazine to benzene seems to support the possible contribution of conjugated π-bond character in the crystal of the compound.

The writers wish to thank Mr. Tomiie for the information on the crystallographic data.

[1] Tomiie, Koo, and Nitta, read before the symposium on structural chemistry, Tokyo, Japan, September, 1952.

[2] Tsuchida, Kobayashi, and Nakamoto, J. Chem. Soc. Japan, **70**, 12 (1949); K. Nakamoto, J. Am. Chem. Soc. **74**, 390 (1952); Scheibe, Hartwig, and Müller, Z. Elektrochem. **49**, 372 (1934).

[3] R. Tsuchida and M. Kobayashi, *The Colours and the Structures of Metallic Compounds* (Zoshindo, Osaka, Japan, 1944), p. 180.

[4] Y. Tomiie (unpublished).

[5] The *A* and *B* absorptions mean the absorption with the electric vector parallel and perpendicular to the $(20\bar{1})$, respectively.

[6] The α_B or α_A denotes absorption coefficient per mm of the crystal with the electric vector parallel or perpendicular to the $(20\bar{1})$, respectively. The subscript ∥ or ⊥ refers to the electric vector parallel or perpendicular to the molecular plane.

Addendum: Critical Temperature and Pressure of Normal Paraffins

YATENDRA PAL VARSHNI
Department of Physics, Allahabad University, Allahabad, India

(Received June 7, 1954)

IN a recent communication Varshni[1] suggested a relationship between the critical temperature and pressure of normal paraffins based on the critical viscosity equations due to Trautz[2] and Grunberg and Nissan.[3] However, there was a serious printing

mistake in the note. While the formula deduced by Varshni was

$$T_c P_c^{\frac{1}{4}} = \text{const}, \quad (1)$$

it was printed as

$$T_c / P_c = \text{const}. \quad (2)$$

The error was corrected in a subsequent erratum.[4]

Meanwhile, Grunberg,[5] not aware of the mistake, criticized the formula (2), which obviously cannot hold. As a matter of fact, T_c/P_c, being proportional to V_c (as $P_c V_c / RT_c = \text{const}$), is additive, and linear relations connecting it with other additive properties like Molar refractivity,[6] number of carbon atoms,[7] Parachor,[8] etc., have been suggested.

Further, Varshni's formula (1) requires both the assumptions that the critical viscosity and the critical density are nearly constant for the normal paraffins (strictly speaking, the assumption is that η_c/ρ_c^3 is constant). Of course, the other formulas proposed by Grunberg are quite correct.

There is one more printing mistake in Varshni's note. Equation (3) should read

$$\eta_c = K\left[\frac{\rho_c^4 T_c^3}{M}\right]^{1/6}$$

and not

$$\eta_c = K\left[\frac{P_c^4 T_c^3}{M}\right]^{1/6}.$$

The author is thankful to Mr. L. Grunberg for pointing out this mistake.[9]

[1] Y. P. Varshni, J. Chem. Phys. **21**, 1400 (1953).
[2] Trautz, Ann. phys. **11**, 190 (1931).
[3] L. Grunberg and A. H. Nissan, Nature **161**, 170 (1948).
[4] Y. P. Varshni, J. Chem. Phys. **22**, 150 (1954).
[5] L. Grunberg, J. Chem. Phys. **22**, 157 (1954).
[6] Guye, J. phys. **9**, 312 (1890); Ann. Chim. **21**, 211 (1890).
[7] Herz, Z. anorg. u. allgem. Chem. **109**, 293 (1920); *ibid.* **11**, 52 (1920); *ibid.* **114**, 150 (1920).
[8] Telang, J. Indian Chem. Soc. **19**, 366 (1942).
[9] L. Grunberg (private communication).

The Polarized Ultraviolet Spectrum of Tetracene Single Crystals by a Photoconductance Method

A. Bree and L. E. Lyons
Department of Physical Chemistry, University of Sydney, Sydney, Australia
(Received May 28, 1954)

SINGLE crystals of some aromatic substances become photoconducting when irradiated with light in an absorbing band.[1] This fact may be used to determine the spectrum in appropriate cases[2] and so to provide a method which we have found simpler and faster than the usual methods of crystal absorption spectroscopy, and which is quantitative in regard to frequency and also, after calibration, to intensity. Without calibration, intensities of two different polarizations may be compared as in the results quoted for tetracene, which are compared with such results as are available from usual methods.[3] In our experiments, linearly polarized parallel light was allowed to fall on the crystal mounted on silica and with two electrodes attached. The conclusion may be drawn that many, and possibly all, of the main features of the usual spectrum are reproduced in the photoconductance curve. Accordingly the results from photoconductance may be used to provide data of value in the interpretation of the relevant optical transitions in terms of frequencies and polarizations, and thus of the symmetry properties of crystal or molecular states. From photoconductance measurements the polarization of the first system is definitely b, in agreement with the absorption result; see Table I. There are no published absorption results for the second and third systems, but at all wavelengths the photocurrent is slightly greater for light polarized near to the b direction. If the two maxima at *ca* 35 700 cm^{-1} (or those at 43 100 cm^{-1}) are components of the same electronic transition, the ratio of the peak currents might indicate that the transition is polarized in the long molecular axis, but in the absence of a detailed knowledge of the crystal structure this is uncertain. The weakness of the second system can in part be explained if the appropriate molecular axis lies close to the direction of light propagation.

TABLE I. Tetracene single crystal: *A*, absorption spectrum.[a] *C*, photoconductance curve.

1st (long wavelength) system				
Maxima ∥b direction, cm^{-1}	*A*	19 235 ±?	20 715	22 320
	C	19 160 ±50	20 750 ±50	22 270 ±300
⊥b	*A*	19 810	21 145	22 545
	C	19 860 ±50	21 190 ±50	22 370 ±400
Splitting between components	*A*	575	430	225
	C	700 ±100	440 ±100	
Ratio of peak currents	*C*	2.9	1.9	1.9
Ratio of oscillator strengths, ∥ to ⊥ (calculated from curves)	*C*	4.5	2.9	
2nd and 3rd systems				
Maxima (∥ and ⊥)	*C*	35 700 ±300	43 100 ±300	
Ratio of peak currents ∥ to (b+12°); ⊥(b+12°)		1.2	1.6	

[a] See reference 3.

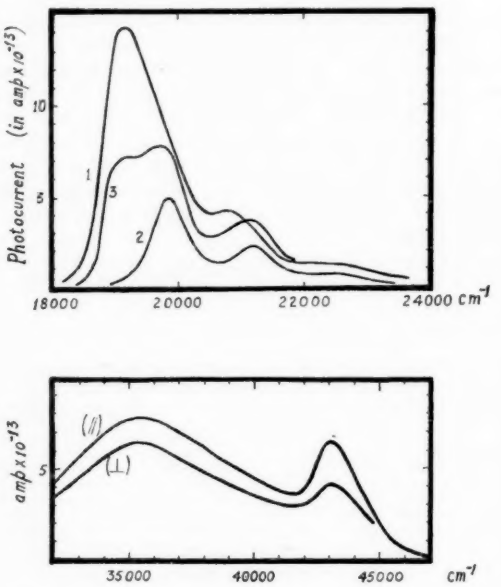

FIG. 1. Photocurrent in tetracene single crystal as a function of frequency, in two ranges of wavelength. Light polarized: 1, ∥b; 2, ⊥b; 3, unpolarized. In lower diagram conditions were different; "∥, ⊥" refer to a direction (b+12°).

The splitting of the first system may be explained on the Davydov theory.[4] The flatness of the curves in the other systems makes the splitting hard to determine.

Photoconductance increases as the series naphthalene, anthracene, tetracene, is ascended (due probably to an increasing ease of reaction with oxygen[5]) and so further members of this series which are sufficiently stable should be able to be investigated in this way.

We are glad to acknowledge the support of the Commonwealth Research Fund and also, in determining the principal absorption directions at low wavelengths, the cooperation of Mr. J. R. Walsh.

[1] Carswell, Ferguson, and Lyons, Nature **173**, 736 (1954).
[2] D. Carswell, J. Chem. Phys. **21**, 1890 (1953); D. Carswell and L. E. Lyons, unpublished.
[3] A. Y. Achis, quoted by A. S. Davydov, Akad. Nauk, Pamyati S. I. Vavilov, 197 (1952).
[4] A. S. Davydov, Zhur. Eksptl. i Teort. Fiz., S.S.S.R. **18**, 210 (1948).
[5] A. Bree and L. E. Lyons (to be published).

Photolysis of Mixtures of Acetone-d_6 and Diethyl Ketone

M. H. J. WIJNEN
Division of Pure Chemistry, National Research Council, Ottawa, Canada
(Received July 9, 1954)

THE photolysis of mixtures of acetone-d_6 and diethyl ketone has been studied over the temperature range 27 to 200°C. If acetone-d_6 and diethyl ketone are photolysed separately, the following reactions have been shown to occur.[1-3]

$$2CD_3 \rightarrow C_2D_6, \quad (1)$$

$$CD_3+CD_3COCD_3 \rightarrow CD_4+CD_2COCD_3 \quad (2)$$

$$2C_2H_5 \rightarrow C_4H_{10}, \quad (3)$$

$$2C_2H_5 \rightarrow C_2H_4+C_2H_6, \quad (4)$$

$$C_2H_5+C_2H_5COC_2H_5 \rightarrow C_2H_6+C_2H_4COC_2H_5, \quad (5)$$

$$C_2H_4COC_2H_5 \rightarrow C_2H_4+CO+C_2H_5. \quad (6)$$

When, as in our case, mixtures of acetone-d_6 and diethyl ketone are photolyzed then, in addition, the following main reactions may be expected to occur.

$$CD_3+C_2H_5COC_2H_5 \rightarrow CD_3H+C_2H_4COC_2H_5, \quad (7)$$

$$CD_3+C_2H_5 \rightarrow C_3H_5D_3, \quad (8)$$

$$CD_3+C_2H_5 \rightarrow CD_3H+C_2H_4, \quad (9)$$

$$C_2H_5+CD_3COCD_3 \rightarrow C_2H_5D+CD_2COCD_3. \quad (10)$$

As expected from the reaction mechanism above, the reaction products are CO, CD_4, CD_3H, C_2D_6, C_2D_5H, C_2H_6, C_2H_4, $C_3H_5D_3$, and C_4H_{10}. The products were separated by fractionated distillation and analyzed by mass spectrometer. Because of overlapping of the ethane spectra, no accurate results could be obtained for C_2H_5D and C_2H_6.

From the reaction mechanism, the following equations may be derived, where R_x means the rate of production of the compound X.

$$\frac{R^2_{C_3H_5D_3}}{R_{C_2D_6}\cdot R_{C_4H_{10}}}=k_8^2/k_1k_3, \quad \text{I}$$

$$\frac{R_{CD_3H}}{R_{C_3H_5D_3}}=k_7/k_2\frac{R_{CD_4}}{R_{C_3H_5D_3}}\cdot\frac{(DK)}{(Ac-d_6)}+k_9/k_8, \quad \text{II}$$

$$\frac{R_{CD_3H}}{R^{\frac{1}{2}}_{C_2D_6}}\cdot\frac{1}{(DK)}=k_7/k_1^{\frac{1}{2}}+k_9/(k_1^{\frac{1}{2}}k_3^{\frac{1}{2}})\frac{R^{\frac{1}{2}}_{C_4H_{10}}}{(DK)}, \quad \text{III}$$

$$\frac{R_{CD_3H}}{R_{CD_4}}\cdot\frac{(Ac-d_6)}{(DK)}=k_7/k_2+k_9/k_2k_3^{\frac{1}{2}}\frac{R^{\frac{1}{2}}_{C_4H_{10}}}{(DK)}. \quad \text{IV}$$

This investigation was carried out mainly to obtain information about reactions (8) and (9). It could, however, be shown at 141°C, where a larger series of experiments was carried out, that the results are correctly expressed by the foregoing equations. By plotting $R_{CD_3H}/R_{C_3H_5D_3}$ against $R_{CD_4}/R_{C_3H_5D_3}\times(DK)/(Ac-d_6)$ we obtained a straight line going within experimental error through the origin. From the slope of this line we obtained $k_7/k_2=56.1$ (141°C). The fact that the line passes within experimental error through the origin indicates that k_9/k_8 is small. At 141°C $R_{CD_3H}/R^{\frac{1}{2}}_{C_2D_6}\times 1/(DK)$ and $R_{CD_3H}/R_{CD_4}\cdot(Ac-d_6)/(DK)$ are independent of $R^{\frac{1}{2}}_{C_4H_{10}}/(DK)$ indicating that $R^{\frac{1}{2}}_{C_4H_{10}}/(DK)$ is small compared to $k_7/k_1^{\frac{1}{2}}$ and k_7/k_2.

From equations IV and V we obtained $k_7/k_1^{\frac{1}{2}}=80\times10^{13}$ cm$^{\frac{3}{2}}$ molecules$^{-\frac{1}{2}}$ sec$^{-\frac{1}{2}}$ at 141°C and $k_7/k_2=57.2$ (141°C), the latter result in good agreement with that obtained by Eq. II.

Equation I indicates that the product $R^2_{C_3H_5D_3}/R_{C_2D_6}\cdot R_{C_4H_{10}}$ is constant, independent of pressures of acetone-d_6 and diethyl ketone. This has been found to be correct, and in Table I we give the average values found for k_8^2/k_1k_3 at the different temperatures of this investigation. Column 2 gives the number of experiments, from which the average values for k_8^2/k_1k_3 are calculated, and column 3 gives the extreme values of $P_{CD_3COCD_3}/P_{C_2H_5COC_2H_5}$ for these experiments.

Since reaction 9 produces CD_3H and C_2H_4 which are also produced by other reactions, it is difficult to obtain quantitative information about this reaction. The fact that within experimental error no intercept was found when plotting $R_{CD_3H}/R_{C_3H_5D_3}$ against $R_{CD_4}/R_{C_3H_5D_3}\cdot(DK)/(Ac-d_6)$ indicates that k_9/k_8 is small. CD H is produced by reactions (9) and (7). At room temperature the amount of CD_3H produced by reaction 7 is small. The ratio $R_{CD_3H}/R_{C_3H_5D_3}$ will therefore give us at room temperature a maximum value for k_8/k_9. The maximum value for $R_{CD_3H}/R_{C_3H_5D_3}$ at room temperature was 0.08, therefore $k_8/k_9<0.08$. If we compare our value of k_8/k_9 with the value $k_4/k_3=0.13\pm0.02$,[4] then there seems no doubt that the rate of disproportionation over recombination is smaller for methyl plus ethyl radicals than for two ethyl radicals.

TABLE I. Values of k_8^2/k_1k_3.

Temperature °C	Number of experiments	P_{Ac}/P_{DK}	k_8^2/k_1k_3
27	8	6.4–1.0	3.4
108	5	5.5–0.4	2.7
141	12	2.8–1.1	3.4
197	7	4.6–0.5	3.4

[1] A. F. Trotman-Dickenson and E. W. R. Steacie, J. Chem. Phys. **18**, 1097 (1950).
[2] M. H. J. Wijnen and E. W. R. Steacie, Can. J. Chem. **29**, 1092 (1951).
[3] Kutschke, Wijnen, and Steacie, J. Am. Chem. Soc. **74**, 714 (1952).
[4] P. Ausloos and E. W. R. Steacie, Bull. soc. chim. Belges. **63**, 87 (1954).

Simultaneous Vibrational Transitions in the Infrared Absorption Spectra of Compressed Gases*

J. FAHRENFORT AND J. A. A. KETELAAR
Laboratory for General and Inorganic Chemistry of the University of Amsterdam, Amsterdam, The Netherlands
(Received June 28, 1954)

IN the course of our investigations on the infrared absorption spectra of compressed gases,[1] we have found that on the addition of nitrogen to carbon dioxide two bands appear, not observed in pure compressed CO_2.

We used an optical path length of 100 cm with a pressure of 20 at of CO_2 and nitrogen added to a total pressure of 75 atmos.

The intensity of these bands at 2994 ± 3 cm^{-1} and at 4670 ± 5 cm^{-1} varies proportionally both with the density of the N_2 and with that of the CO_2.

These facts can most readily be explained only by attributing the new bands of simultaneous transitions in each of the two partners of the CO_2-N_2 collision complex, the CO_2 molecule performing one of its fundamental allowed vibrational transitions at 667.3 cm^{-1} (ν_1) and at 2349.3 cm^{-1} (ν_3), simultaneously with the fundamental vibrational transition of 2330.7 cm^{-1} in the N_2 molecule.

The calculated frequencies of 2998 cm^{-1} and 4680 cm^{-1} show a very good correspondence with the observed values given above.

A further confirmation of the explanation of these bands as due to simultaneous vibrational transitions is gained from the observation of analogous bands in mixtures of carbon dioxide with oxygen and with hydrogen.

We have indeed found a band in 20 at CO_2 and oxygen added to 75 atmos pressure, due to the transition expected at $1554.7(O_2)+2349.3\ (CO_2)=3904$ cm^{-1} observed at 3895 ± 5 cm^{-1}. One band expected at $4160.2(H_2)+2349.3(CO_2)=6509.4$ cm^{-1} was observed at 6505 ± 7 cm^{-1}, already with 10 atmos carbon dioxide and hydrogen added to a total pressure of 27.5 atmos.

Both combinations with the deformation frequency of CO_2

at 667.3 cm^{-1} could not be observed as a consequence of the strong absorption of CO_2 in the corresponding regions.

Our results indicate that simultaneous vibrational transitions arising from collision complexes, as predicted by van Kranendonk,[2] are indeed observed as a quite general phenomenon in pressure induced infrared absorption spectra of mixtures.

In pure gases it will always be difficult to distinguish between the simultaneous transition in a pair of molecules and the corresponding combination frequency (pressure induced transition) in a single molecule.

The appearance of the simultaneous transitions must be primarily ascribed to the polarization of the symmetrical two-atomic molecule by the electric field of the rather large quadrupole moment arising from the partial dipoles present in the CO_2 molecule.

* Research supported by the Section of Molecular Physics III of the F.O.M.

[1] Fahrenfort, de Kluiver, and Babeliowsky, J. phys. (to be published).

[2] J. van Kranendonk, thesis, University of Amsterdam (1952); J. van Kranendonk and R. B. Bird, Physica **17**, 953, 968 (1951).